HOKKAIDO UNIVERSITY

Title	Classification of Multipole in Magnetic Point Group and Exploration of Augmented Odd-Parity Multipole Physics
Author(s)	八城, 愛美; Yatsushiro, Megumi
Degree Grantor	北海道大学
Degree Name	博士(理学)
Dissertation Number	甲第14781号
Issue Date	2022-03-24
DOI	https://doi.org/10.14943/doctoral.k14781
Doc URL	https://hdl.handle.net/2115/88799
Type	doctoral thesis
File Information	Megumi_Yatsushiro.pdf

Hokkaido University Collection of Scholarly and Academic Papers : HUSCAP

Doctoral Dissertation

Classification of Multipole in Magnetic Point Group and Exploration of Augmented Odd-Parity Multipole Physics

(磁気点群のもとでの多極子の分類論と拡張奇パリティ多極子物理の開拓)

Megumi YATSUSHIRO

Graduate School of Science, Hokkaido University

Department of Physics

2022.3

Acknowledgments

I would like to express my deep gratitude to Dr. Satoru Hayami for his generous guidance throughout my bachelor's, master's, and doctoral courses for six years. His continuous support, helpful suggestions, and critical discussions are indispensable for my work. I am glad that I could study under his guidance. I would be grateful to Profs. Takafumi Kita, Hiroshi Amitsuka, and Tatsuya Yanagisawa for their valuable comments in the review process of this dissertation. I also express my sincere thanks to Prof. Hiroaki Kusunose, Dr. Yuki Yanagi, and Mr. Rikuto Oiwa, for the collaboration and the interesting, critical, and fruitful discussion.

I appreciate Prof. Yukitoshi Motome, Drs. Yasuyuki Kato, Shun Okumura, and Mr. Tatsuki Sato for the fruitful discussion of the nonlinear response in Chap. 3. For the multipole physics of CeCoSi discussed in Chap. 4, Profs. Hideki Tou, Hisashi Kotegawa, Hiroshi Tanida, Keisuke Mitsumoto, and Yukihiro Kawamura, Drs. Hiroyuki Hidaka, Masahiro Manago, Yoshihiko Ihara, and the students in J-Material Laboratory in Hokkaido University (especially Messrs. Akinari Koriki and Eikai Hayasaka) gave us important experimental information and opportunities for a fruitful discussion. I sincerely thank all of them and hope for the interesting progress of this material.

In addition, I would like to thank all of the past and present members of Statistical Physics Laboratory in Hokkaido University and Hayami Group in The University of Tokyo, especially Messrs. Takuya Matsumoto, Ryota Yambe, and Kazuki Okigami, and everybody supported my study and life in every situation.

Finally, I would like to thank my precious family (my parents and sister) for understanding my choices in life and always being so supportive.

List of Publications

Papers related to the dissertation

1. M. Yatsushiro and S. Hayami,
   "Odd-Parity Multipoles by Staggered Magnetic Dipole and Electric Quadrupole Orderings in CeCoSi",
   Journal of the Physical Society of Japan **89**, 013703 (2020),
   © 2020 The Physical Society of Japan

2. M. Yatsushiro and S. Hayami,
   "Antisymmetric Spin-Orbit Interaction in a Locally Noncentrosymmetric CeFeSi-type Structure",
   JPS Conference Proceedings **30**, 011151 (2020),
   © 2020 The Physical Society of Japan

3. M. Yatsushiro and S. Hayami,
   "NQR and NMR spectra in odd-parity multipole material CeCoSi",
   Physical Review B **102**, 195147 (2020),
   © 2020 American Physical Society

4. M. Yatsushiro, H. Kusunose, and S. Hayami,
   "Multipole classification in 122 magnetic point groups for unified understanding of multiferroic responses and transport phenomena",
   Physical Review B **104**, 054412 (2021),
   © 2021 American Physical Society

Papers not included in the dissertation

1. S. Hayami, M. Yatsushiro, Y. Yanagi, and H. Kusunose,
   "Classification of atomic-scale multipoles under crystallographic point groups and application to linear response tensors",
   Physical Review B **98**, 165110 (2018),
   © 2018 American Physical Society

2. M. Yatsushiro and S. Hayami,
   "Atomic-Scale Magnetic Toroidal Dipole under Odd-Parity Hybridization",
   Journal of the Physical Society of Japan **88**, 054708 (2019),
   © 2019 The Physical Society of Japan

Contents

Acknowledgments iii

List of Publications v

1 Introduction 1
- 1.1 Multipole in Condensed Matter Physics . . . 1
- 1.2 Four Types of Multipoles . . . 3
- 1.3 Augmented Multipoles . . . 8
  - 1.3.1 Hybrid Multipole . . . 8
  - 1.3.2 Cluster Multipole . . . 9
  - 1.3.3 Bond Multipole . . . 12
  - 1.3.4 k Multipole . . . 13
- 1.4 Multipoles under Point Group Symmetry . . . 15
- 1.5 Relation between Multipole and Field Responses . . . 17
- 1.6 Purpose of This Thesis . . . 20
- 1.7 Organization of This Thesis . . . 20

2 Classification of Multipoles in 122 Magnetic Point Groups 21
- 2.1 Introduction . . . 21
- 2.2 Magnetic Point Group . . . 22
  - 2.2.1 Three Types of Magnetic Point Groups . . . 22
  - 2.2.2 Irreducible Corepresentation of Magnetic Point Group . . . 24
- 2.3 Classification of Multipole . . . 26
- 2.4 Active Multipoles . . . 30
- 2.5 Field Responses . . . 36
  - 2.5.1 Tensor Analysis . . . 38
  - 2.5.2 Linear Response Function . . . 42
  - 2.5.3 Second-Order Nonlinear Response Function . . . 47
- 2.6 Summary . . . 50

3 Nonlinear Transport in Magnetic Toroidal Dipole Ordering 51
- 3.1 Introduction . . . 51
- 3.2 Model . . . 52
  - 3.2.1 Multipole Degrees of Freedom . . . 52
  - 3.2.2 Minimal Two-Band Model . . . 53
  - 3.2.3 Response Functions . . . 54

3.3 Result . . . 56
3.3.1 Band Modulation . . . 56
3.3.2 Second-Order Nonlinear Conductivity . . . 57
3.3.3 Linear Magnetoelectric Effect and Hall Effect . . . 59
3.4 Summary . . . 60

4 Odd-Parity Multipole Order in f-electron Metal CeCoSi 63
4.1 Introduction . . . 63
4.2 Crystalline Electric Field . . . 66
4.3 Multipole Degrees of Freedom . . . 67
4.3.1 Γ_7-Γ_6 Level . . . 68
4.3.2 Γ_7-Γ_7 Level . . . 71
4.4 Analysis Based on the Local Model . . . 71
4.4.1 Model . . . 73
4.4.2 Phase Diagram . . . 73
4.4.3 Susceptibility . . . 78
4.5 Analysis Based on the Itinerant Model . . . 79
4.5.1 Model . . . 80
4.5.2 Zero-Temperature Phase diagram . . . 82
4.5.3 Electronic Band Structure . . . 84
4.5.4 Multiferroic Responses . . . 85
4.6 NQR and NMR in Odd-Parity Multipole Order . . . 88
4.6.1 Electronic Model . . . 88
4.6.2 Hyperfine Field for ^{59}Co Nucleus . . . 91
4.6.3 NQR Spectra . . . 96
4.6.4 [001]-Field NMR Spectra . . . 99
4.6.5 [100]-Field NMR Spectra . . . 101
4.6.6 Spectral Splittings under Odd-parity Multipoles . . . 103
4.7 Summary . . . 104

5 Summary 105

A Multipole Notation under Point Group Symmetry in Crystals 107

B Corepresentation of Nonunitary Group 109
B.1 Corepresentation . . . 109
B.2 Unitary Transformation of Corepresentation . . . 110
B.3 Irreducible Corepresentation (IRREP) . . . 110
B.4 Kronecker Product of IRREP . . . 116

C Tables of Multipole Classification 117
C.1 Gray Point Groups . . . 117
C.2 Black-and-White Point Groups . . . 139

D Laue and Magnetic Laue Groups 169

E Relation between Multipoles and Response Tensors **171**
E.1 Derivation of Multipoles in Response Tensors . . . 171
E.1.1 $\chi^{[1\times1]}$ . . . 171
E.1.2 $\chi^{[0\times2]}$ . . . 172
E.1.3 $\chi^{[1\times2]}$ . . . 172
E.1.4 $\chi^{[0\times3]}$ . . . 173
E.1.5 $\chi^{[1\times3]}$ . . . 173
E.1.6 $\chi^{[2\times2]}$ . . . 176
E.2 Tensor Expression in Hexagonal/Trigonal System . . . 178

F Other NMR Spectra **181**
F.1 Field-Swept NMR Spectra . . . 181
F.2 [110]-Field NMR Spectra . . . 181
F.3 Spectral Splittings for $\Gamma_7^{(1)}$-$\Gamma_7^{(2)}$ Levels . . . 184

Chapter 1

Introduction

1.1 Multipole in Condensed Matter Physics

Multipole, which is a fundamental concept in physics, characterizes the angular dependence of an electromagnetic distribution. It was originally introduced in a series expansion of scalar and vector potentials in classical electromagnetism to describe an arbitrary distribution of sources, such as the electric charge and current, systematically [1, 2]; any electric charge and current distributions are usually described by using the electric and magnetic multipoles. Typical examples of multipole are the electric dipole, magnetic dipole, and electric quadrupole. The electric dipole appears by a polar alignment of positive and negative charges, as shown in Fig. 1.1(a), whose macroscopic alignment gives rise to an electric polarization. The magnetic dipole correspond to a circular electric current known as the Biot-Savart law, as shown in Fig. 1.1(b), which becomes a source of a magnetization. The electric quadrupole in Fig. 1.1(c) describes a symmetric charge configuration consisting of staggered pairs of the electric dipoles. Since the concept of multipole is suitable to analyze any anisotropic angular dependences of electromagnetic objects, it has been used in various fields, such as nuclear physics [3–5], metaphotonics [6–8], colloid science [9, 10], and so on.

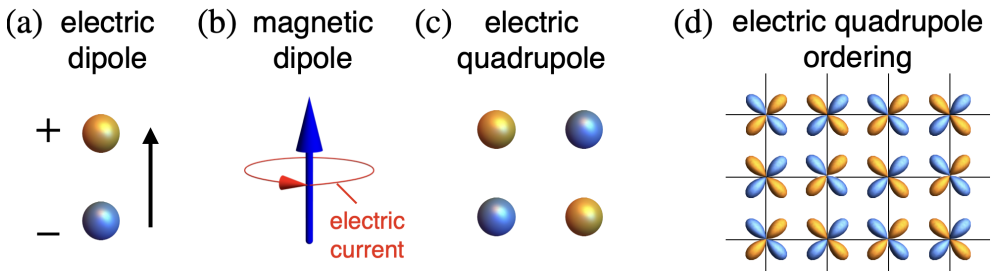

Figure 1.1: (a–c) Schematic pictures of (a) the electric dipole, (b) magnetic dipole, and (c) electric quadrupole. (d) Electric quadrupole ordering in a periodic lattice system.

The concept of multipole can also be used to represent an atomic-scale angular dependence of the wave functions of an electron in quantum mechanics. Notably, the quantum-mechanical operator expressions of atomic-scale multipoles can be applicable to describe various electronic degrees of freedom in solids, such as charge, spin, and orbital. Espe-

cially, it is useful in the situation where there is a mutual entanglement between them by relativistic spin-orbit coupling, crystalline electronic field, electron-electron interaction, and so on, since the multipole expression gives a unified way to describe the electronic degrees of freedom. Indeed, it was shown that the multipole degree of freedom spans the complete set in the Hilbert space for s, p, d, and f electrons without any deficiency [11–13].

The atomic-scale multipole has been used for d- and f-electron systems, since d- and f-orbital electrons tend to be affected by the relativistic spin-orbit coupling and the crystalline electric field owing to their large orbital angular momenta [14–16]. In such a situation, there is a chance of realizing the higher-rank multipole orderings as shown in Fig. 1.1(d), whose electric and magnetic properties are different from the conventional charge and magnetic orderings. The multipole orderings have been found in various materials: electric quadrupole ordering in CeB_6 [17–24], magnetic octupole ordering in NpO_2 [25–30], and electric hexadecapole ordering in $PrRu_4P_{12}$ [31, 32]. Since these higher rank multipoles have no direct coupling to the electric and magnetic fields, an identification of these multipole orderings is quite difficult compared to conventional charge and magnetic orderings. To detect such multipole orderings directly, some microscopic probes, such as the nuclear quadrupole resonance (NQR) and nuclear magnetic resonance (NMR) have been used [17, 22, 24].

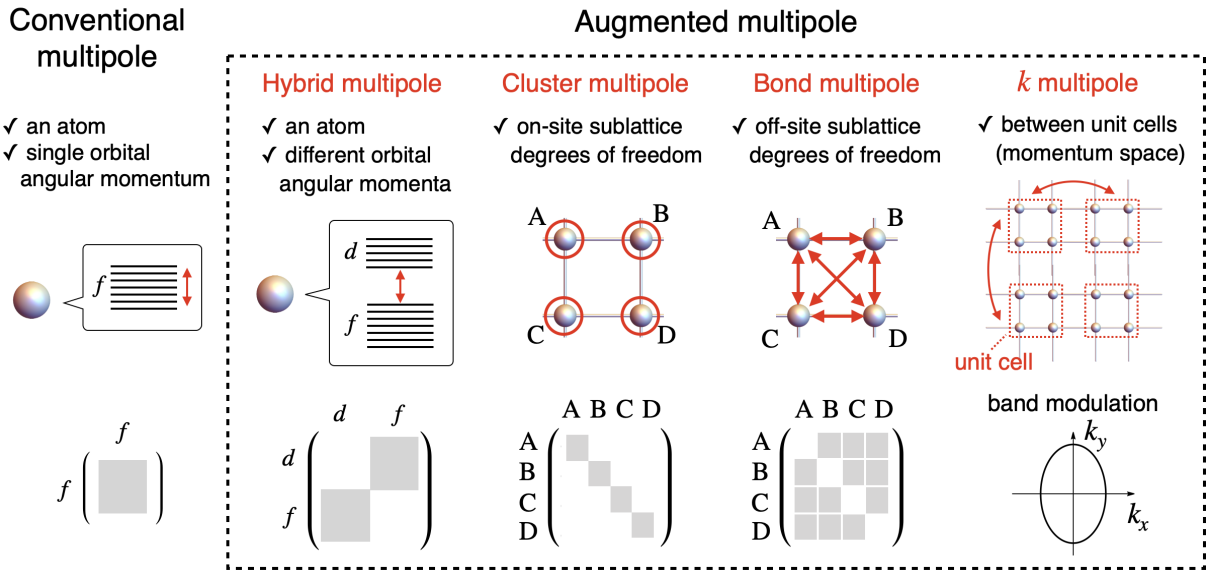

Figure 1.2: Relation of conventional/augmented multipoles and electronic degrees of freedom in solids. The relevant Hilbert space is schematically shown in each bottom panel.

The above multipoles have been usually discussed to describe atomic electronic degrees of freedom in a Hilbert space limited to the orbital space with a single orbital angular momentum as schematically presented in the leftmost panel of Fig. 1.2. They have long been studied in d or f-electron systems, which were denoted as "conventional multipole". Meanwhile, recent studies have extended the concept of multipole to describe the electronic degrees of freedom over different orbitals and sites. For instance, a hybrid multipole has been introduced to describe the atomic interorbital degrees of freedom with

the different orbital angular momenta [12, 13, 33], where the concept of the atomic-scale magnetic toroidal and electric toroidal multipoles has been established. Moreover, the concept of multipole has been extended to describe the electronic degrees of freedom over multi sites: a cluster multipole to describe the on-site sublattice degree of freedom [34, 35] and a bond multipole to describe the off-site sublattice degree of freedom [36, 37] in a cluster. Such a multipole degree of freedom in real space affects the electronic band structure, which leads to the introduction of a k multipole describing the anisotropy in momentum space [37–42]. Collectively, these multipoles are called "augmented multipole", which are summarized in Fig. 1.2 with the schematic illustration of the relevant Hilbert space. Importantly, augmented multipole can describe any electronic degrees of freedom in solids in a classified way, since the multipole degrees of freedom span the symmetry-adapted basis in solids. Moreover, a systematic description by using augmented multipole enables us to explore unconventional electronic order parameters and their related physical properties from the microscopic viewpoint beyond the symmetry argument, as will be discussed in this thesis.

In the remaining part of this section, we briefly review a recent development of augmented multipoles and their physical properties. First, we present the four types of multipoles and their quantum-mechanical operators in Sec. 1.2. After the short review of the conventional atomic multipoles at the end of Sec. 1.2, we introduce augmented multipoles: hybrid multipole, cluster multipole, bond multipole, and k multipole in Sec. 1.3. Finally, we summarize how these multipole degrees of freedom are relevant to the crystallographic symmetry in solids in Sec. 1.4 and physical properties including multiferroic responses in Sec. 1.5. Sections 1.6 and 1.7 are devoted to summarizing the purpose and organization of this thesis, respectively.

1.2 Four Types of Multipoles

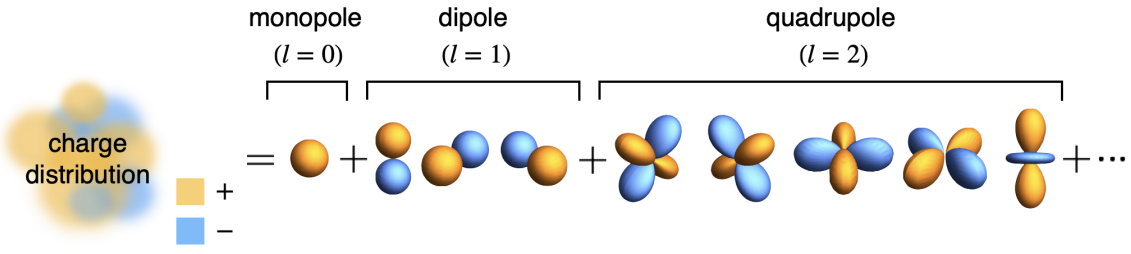

Figure 1.3: Multipole expansion of a source charge for a scalar potential.

We here review classical and quantum-mechanical representations of multipoles [1, 2, 11–13, 43–46]. In classical electromagnetism, multipole moments are introduced to describe a source charge and current distributions of scalar and vector potentials in the multipole expansion, which is schematically shown in Fig. 1.3 [1, 2, 43–46]. Starting from the Maxwell equation for Gaussian-cgs units under the time-independent electric and magnetic field with Coulomb gauge $\boldsymbol{\nabla}\cdot\boldsymbol{A}(\boldsymbol{r})=0$, scalar potential $\phi(\boldsymbol{r})$ and vector

potential $\boldsymbol{A}(\boldsymbol{r})$ satisfy the following Poisson equations:

$$\boldsymbol{\nabla}^2\phi(\boldsymbol{r})=-4\pi\rho_{\rm e}(\boldsymbol{r}), \tag{1.1}$$

$$\boldsymbol{\nabla}^2\boldsymbol{A}(\boldsymbol{r})=-\frac{4\pi}{c}\boldsymbol{j}_{\rm e}(\boldsymbol{r}), \tag{1.2}$$

where c is the speed of light and $\rho_{\rm e}(\boldsymbol{r})$ and $\boldsymbol{j}_{\rm e}(\boldsymbol{r})$ represent a source electric charge $\rho_{\rm e}(\boldsymbol{r})$ and current $\boldsymbol{j}_{\rm e}(\boldsymbol{r})$, respectively. Any angle distributions of $\phi(\boldsymbol{r})$ and $\boldsymbol{A}(\boldsymbol{r})$ can be represented by a superposition of spherical harmonics $Y_{lm}(\hat{\boldsymbol{r}})$ and vector spherical harmonics $\boldsymbol{Y}_{lm}^{(l')}(\hat{\boldsymbol{r}})$ ($\hat{\boldsymbol{r}}=|\boldsymbol{r}|/\boldsymbol{r}$, $-l\leq m\leq l$ and $l'=l,l\pm1$), respectively, where $l^{(\prime)}$ is the azimuthal quantum number and m is the magnetic quantum number[1]. Then, $\phi(\boldsymbol{r})$ and $\boldsymbol{A}(\boldsymbol{r})$, the solutions of the Poisson equations in Eqs. (1.1) and (1.2), are given by

$$\phi(\boldsymbol{r})=\sum_{l=0}^{\infty}\sum_{m=-l}^{l}\sqrt{\frac{4\pi}{2l+1}}Q_{lm}\frac{Y_{lm}(\hat{\boldsymbol{r}})}{r^{l+1}}, \tag{1.4}$$

$$\boldsymbol{A}(\boldsymbol{r})=\sum_{l=0}^{\infty}\sum_{m=-l}^{l}\left[\sqrt{\frac{4\pi(l+1)}{(2l+1)l}}M_{lm}\frac{\boldsymbol{Y}_{lm}^{(l)}(\hat{\boldsymbol{r}})}{ir^{l+1}}-\sqrt{4\pi(l+1)}T_{lm}\frac{\boldsymbol{Y}_{lm}^{(l+1)}(\hat{\boldsymbol{r}})}{r^{l+2}}\right]. \tag{1.5}$$

The coefficient Q_{lm} in Eq. (1.4) represents an electric (E) multipole moment with rank l, which is expressed as

$$Q_{lm}=\int d\boldsymbol{r}\rho_{\rm e}(\boldsymbol{r})O_{lm}(\boldsymbol{r}), \tag{1.6}$$

where $O_{lm}(\boldsymbol{r})=\sqrt{4\pi/(2l+1)}r^lY_{lm}^*(\hat{\boldsymbol{r}})$. Meanwhile, M_{lm} and T_{lm} in Eq. (1.5) represent magnetic (M) and magnetic toroidal (MT) multipole moments, respectively, which are described as

$$M_{lm}=\frac{1}{c(l+1)}\int d\boldsymbol{r}[\boldsymbol{r}\times\boldsymbol{j}_{\rm e}(\boldsymbol{r})]\cdot\boldsymbol{\nabla}O_{lm}(\boldsymbol{r}), \tag{1.7}$$

$$T_{lm}=\frac{1}{c(l+1)}\int d\boldsymbol{r}[\boldsymbol{r}\cdot\boldsymbol{j}_{\rm e}(\boldsymbol{r})]O_{lm}(\boldsymbol{r}). \tag{1.8}$$

MT multipole is sometimes neglected in the multipole expansion in classical electromagnetism as it does not affect a magnetic field. Nevertheless, it is essential to describe a distribution of the vortex-type magnetic field. Such current distributions are only represented by the time-reversal-odd polar quantity that corresponds to the MT multipole

[1]The vector spherical harmonics $\boldsymbol{Y}_{lm}^{(l')}(\hat{\boldsymbol{r}})$ ($l'=l,l\pm1$) are given by using the spherical harmonics $Y_{lm}(\hat{\boldsymbol{r}})$ and an operator $\boldsymbol{l}=-i\boldsymbol{r}\times\boldsymbol{\nabla}$ as follows [11, 43, 44, 47]:

$$\boldsymbol{Y}_{lm}^{(l)}(\hat{\boldsymbol{r}})=\frac{\boldsymbol{l}Y_{lm}(\hat{\boldsymbol{r}})}{\sqrt{l(l+1)}},\ \boldsymbol{Y}_{lm}^{(l+1)}(\hat{\boldsymbol{r}})=-\frac{1}{r}\frac{(l+1)\boldsymbol{r}Y_{lm}(\hat{\boldsymbol{r}})+i\boldsymbol{r}\times[\boldsymbol{l}Y_{lm}(\hat{\boldsymbol{r}})]}{\sqrt{(l+1)(2l+1)}},\ \boldsymbol{Y}_{lm}^{(l-1)}(\hat{\boldsymbol{r}})=\frac{1}{r}\frac{l\boldsymbol{r}Y_{lm}(\hat{\boldsymbol{r}})-i\boldsymbol{r}\times[\boldsymbol{l}Y_{lm}(\hat{\boldsymbol{r}})]}{\sqrt{l(2l+1)}}. \tag{1.3}$$

It is noted that the vector spherical harmonics have several definitions, where $\boldsymbol{Y}_{lm}^{(l')}(\hat{\boldsymbol{r}})$ in Eq. (1.3) do not have the orthogonal relation among $l'=l,l-1$, and $l+1$. The complete orthogonality is satisfied by taking linear combination of $\boldsymbol{Y}_{lm}^{(l)}(\hat{\boldsymbol{r}})$, $\boldsymbol{Y}_{lm}^{(l+1)}(\hat{\boldsymbol{r}})$, and $\boldsymbol{Y}_{lm}^{(l-1)}(\hat{\boldsymbol{r}})$.

T_{lm}, which has different spatial inversion and time-reversal parities from the other two multipoles. Q_{lm}, M_{lm}, and T_{lm} are characterized by $(\mathcal{P},\mathcal{T})=[(-1)^l,+1]$, $[(-1)^{l+1},-1]$, $[(-1)^l,-1]$, respectively, since $O_{lm}(\boldsymbol{r})$ is characterized by the spatial inversion parity $\mathcal{P}=(-1)^l$ and the time-reversal parity $\mathcal{T}=+1$ and $\rho_{\rm e}(\boldsymbol{r})[\boldsymbol{j}_{\rm e}(\boldsymbol{r})]$ is the scalar (polar vector) quantity characterized by $\mathcal{T}=+1(-1)$. In other words, the E multipole corresponds to the time-reversal-even polar tensor, the M multipole corresponds to the time-reversal-odd axial tensor, and the MT multipole corresponds to the time-reversal-odd polar tensor.

In addition, the multipole corresponding to the time-reversal-even axial tensor can be introduced by taking into account the magnetic current density $\boldsymbol{j}_{\rm m}(\boldsymbol{r})$ as a counterpart of $\boldsymbol{j}_{\rm e}(\boldsymbol{r})$ [12, 48, 49]. This fourth multipole is called an electric toroidal (ET) multipole, which is represented as

$$G_{lm}=\frac{1}{c(l+1)}\int d\boldsymbol{r}[\boldsymbol{r}\cdot\boldsymbol{j}_{\rm m}(\boldsymbol{r})]O_{lm}(\boldsymbol{r}), \tag{1.9}$$

with the parities $(\mathcal{P},\mathcal{T})=[(-1)^{l+1},+1]$, since $\boldsymbol{j}_{\rm m}(\boldsymbol{r})$ is the axial vector characterized by $\mathcal{T}=+1$. The spatial inversion and time-reversal parities of four types of multipoles are summarized in Table 1.1. The sources of each multipole are also shown.

Table 1.1: Four types of multipoles and their spatial inversion ($\mathcal{P}$), time-reversal ($\mathcal{T}$), and $\mathcal{PT}$ parities. The relevant sources are also presented.

type	notation	$\mathcal{P}$	$\mathcal{T}$	$\mathcal{PT}$	source
E	Q_{lm}	$(-1)^l$	$+1$	$(-1)^l$	$\rho_{\rm e}$ $(\boldsymbol{j}_{\rm m})$
M	M_{lm}	$(-1)^{l+1}$	-1	$(-1)^l$	$\boldsymbol{j}_{\rm e}$
MT	T_{lm}	$(-1)^l$	-1	$(-1)^{l+1}$	$\boldsymbol{j}_{\rm e}$
ET	G_{lm}	$(-1)^{l+1}$	$+1$	$(-1)^{l+1}$	$\boldsymbol{j}_{\rm m}$

The four types of multipoles constitute a complete set to represent an arbitrary angle dependence of electromagnetic charge and current in terms of spatial inversion and time-reversal symmetries. For example, any vector quantities with different space-time inversion symmetries are described by the E, ET, M, and MT dipoles, as shown in Fig. 1.4(a), where the E dipole is transformed into the ET (MT) dipole by reversing the spatial inversion (time-reversal) parity, while the M dipole is transformed into the MT (ET) dipole by reversing the spatial inversion (time-reversal) parity. This argument holds for the higher-rank multipoles with different rotational symmetries, such as quadrupole ($l=2$), octupole ($l=3$), and so on, since they are described by the anisotropic spatial distribution of the dipole, as shown in Fig. 1.4(b)[2]. In this way, the multipoles up to rank $l\to\infty$ can describe any arbitrary anisotropic charge and current distributions.

Based on Eqs. (1.6)–(1.9), the quantum-mechanical operator expressions of four types

[2]Although E multipole was originally introduced to describe the anisotropic charge distribution $\rho_{\rm e}(\boldsymbol{r})$, it can be used to describe the anisotropic E dipole distribution $\boldsymbol{P}(\boldsymbol{r})$ by using the relation $\rho_{\rm e}(\boldsymbol{r})=-\boldsymbol{\nabla}\cdot\boldsymbol{P}(\boldsymbol{r})$ in Eq. (1.6).

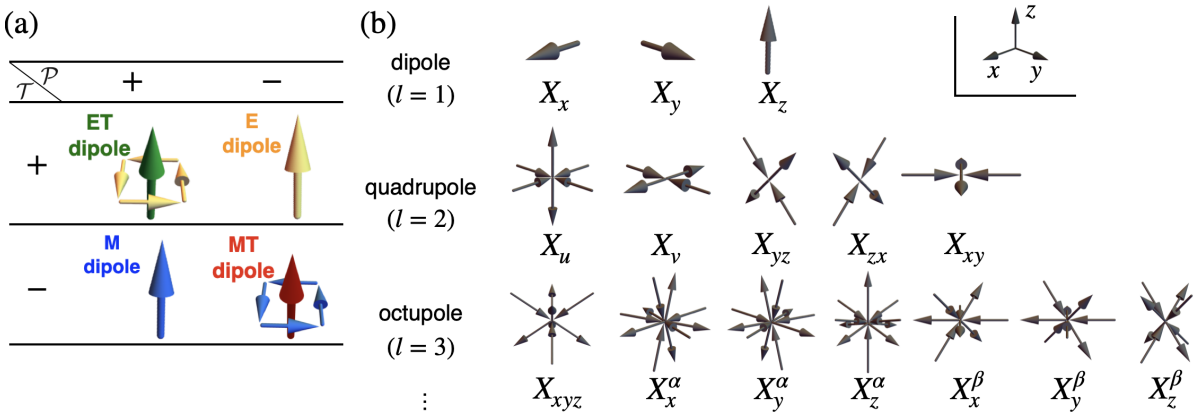

Figure 1.4: (a) Four types of dipoles with different spatial inversion and time-reversal parities: electric (E), magnetic (M), electric toroidal (ET), and magnetic toroidal (MT) dipoles. (b) Dipole distributions up to rank 3. The arrows represent the E, ET, M, or MT dipoles in (a) (X=Q, G, M, or T).

of multipoles are given by [11–13]

$$\hat{Q}_{lm}=-e\sum_i O_{lm}(\boldsymbol{r}_i), \tag{1.10}$$

$$\hat{M}_{lm}=-\mu_{\rm B}\sum_i \boldsymbol{m}_l(\boldsymbol{r}_i)\cdot\boldsymbol{\nabla}O_{lm}(\boldsymbol{r}_i), \tag{1.11}$$

$$\hat{T}_{lm}=-\mu_{\rm B}\sum_i \boldsymbol{t}_l(\boldsymbol{r}_i)\cdot\boldsymbol{\nabla}O_{lm}(\boldsymbol{r}_i), \tag{1.12}$$

$$\hat{G}_{lm}=-e\sum_i\sum_{\alpha\beta}^{x,y,z} g_l^{\alpha\beta}(\boldsymbol{r}_i)\nabla_\alpha\nabla_\beta O_{lm}(\boldsymbol{r}_i), \tag{1.13}$$

where $-e$ and $-\mu_{\rm B}$ are the electron charge and Bohr magneton, respectively, which are taken to be unity hereafter, i.e., $-e, -\mu_{\rm B}\to 1$. $\boldsymbol{m}_l(\boldsymbol{r}_i)$, $\boldsymbol{t}_l(\boldsymbol{r}_i)$, and $g_l^{\alpha\beta}(\boldsymbol{r}_i)$ are the M moment, MT moment, and ET tensor, respectively, which are expressed as

$$\boldsymbol{m}_l(\boldsymbol{r}_i)=\frac{2\boldsymbol{l}_i}{l+1}+\boldsymbol{\sigma}_i, \tag{1.14}$$

$$\boldsymbol{t}_l(\boldsymbol{r}_i)=\frac{\boldsymbol{r}_i}{l+1}\times\left(\frac{2\boldsymbol{l}_i}{l+2}+\boldsymbol{\sigma}_i\right), \tag{1.15}$$

$$g_l^{\alpha\beta}(\boldsymbol{r}_i)=m_l^\alpha(\boldsymbol{r}_i)t_l^\beta(\boldsymbol{r}_i), \tag{1.16}$$

where $\boldsymbol{l}_i$ and $\boldsymbol{\sigma}_i/2$ are the dimensionless orbital and spin angular-momentum operators of an electron at $\boldsymbol{r}_i$, respectively. Similar to the above discussion in the classical representation, these four types of multipoles constitute a complete set to describe an arbitrary electronic degree of freedom, such as the charge, spin, and orbital, in an atomic site [11–13].

In the following discussion for crystallographic systems characterized by a discrete rotational symmetry rather than a continuous rotational symmetry, the real expressions

of O_{lm} are often used [11, 39, 50]. The multipole notation up to the rank 4 is shown as

$$\text{monopole } (l{=}0)\text{: } X_0, \tag{1.17}$$
$$\text{dipole } (l{=}1)\text{: } X_x, X_y, X_z, \tag{1.18}$$
$$\text{quadrupole } (l{=}2)\text{: } X_u, X_v, X_{yz}, X_{zx}, X_{xy}, \tag{1.19}$$
$$\text{octupole } (l{=}3)\text{: } X_{xyz}, X_x^\alpha, X_y^\alpha, X_z^\alpha, X_x^\beta, X_y^\beta, X_z^\beta, \tag{1.20}$$
$$\text{hexadecapole } (l{=}4)\text{: } X_4, X_{4u}, X_{4v}, X_{4x}^\alpha . X_{4y}^\alpha, X_{4z}^\alpha, X_{4x}^\beta, X_{4y}^\beta, X_{4z}^\beta. \tag{1.21}$$

See also Appendix A for their specific expressions.

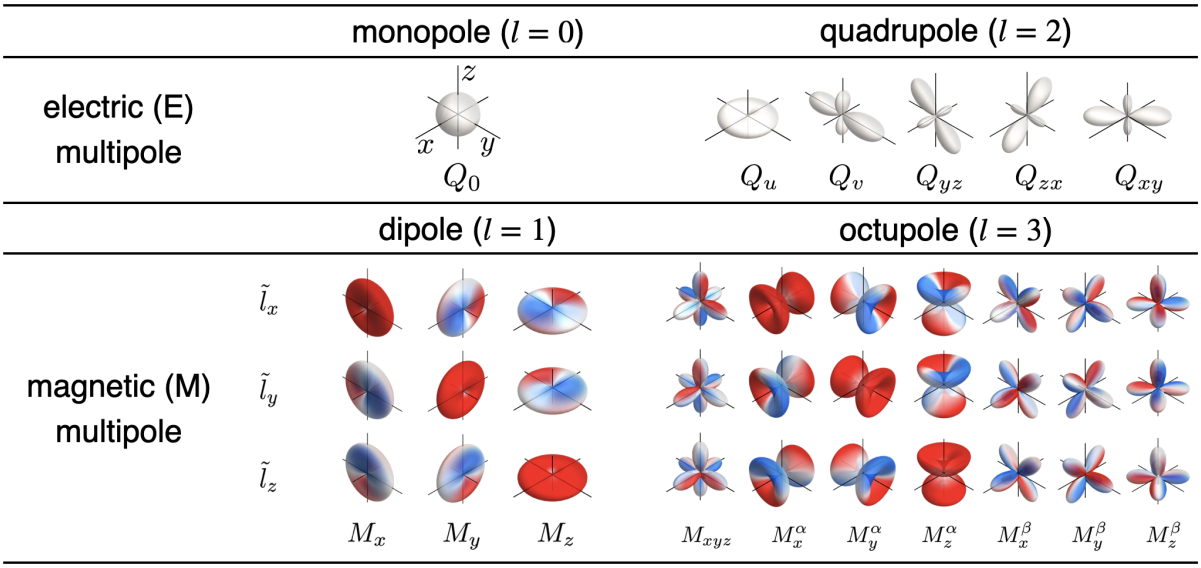

Figure 1.5: Spatial distributions of charge and orbital angular momentum when the expectation value of multipole with rank 0–3 becomes nonzero in the five d-orbital system. The color in the M multipoles represents the spatial distribution of $\tilde{l}_\mu(\boldsymbol{r}){\equiv}{-}l_\mu(\boldsymbol{r})$ $(\mu{=}x, y, z)$, where red (blue) stands for the positive (negative) value.

In quantum-mechanical systems, the types of active multipole degrees of freedom depend on the low-energy Hilbert space. For example, in the situation where only the five d orbitals are relevant with the Hilbert space, following 25 multipoles can be active: E monopole Q_0, M dipoles (M_x, M_y, M_z), E quadrupoles (Q_u, Q_v, Q_{yz}, Q_{zx}, Q_{xy}), M octupoles (M_{xyz}, M_x^α, M_y^α, M_z^α, M_x^β, M_y^β, M_z^β), and E hexadecapoles (Q_4, Q_{4u}, Q_{4v}, Q_{4x}^α, Q_{4y}^α, Q_{4z}^α, Q_{4x}^β, Q_{4y}^β, Q_{4z}^β). These atomic multipoles active within a single orbital angular momentum are referred to as the conventional multipoles in Fig. 1.2. We can evaluate the expectation values of active multipoles by using the d-orbital basis functions. We show the spatial distributions of charge and orbital angular momentum in Eq. (1.6)–(1.9) when each multipole takes a nonzero expectation value in Fig. 1.5. The shape of each wave function in Fig. 1.5 represents the angular dependence of the electronic charge distribution. For example, the charge distribution in the E monopole has the spherical form, while the E quadrupoles have the anisotropic charge distribution satisfying the two-fold rotational symmetry. Besides, the color in M multipoles stands for the spatial distribution of the orbital angular momentum $[\tilde{l}_\mu(\boldsymbol{r}){\equiv}{-}l_\mu(\boldsymbol{r})$ $(\mu{=}x, y, z)]$, where the red and blue describe

the opposite sign, positive and negative, respectively. For instance, the M dipole M_x has the uniform distribution of $\tilde{l}_x$, whereas the other components $\tilde{l}_y$ and $\tilde{l}_z$ have no net value in whole. Meanwhile, the spatial distribution of $\tilde{l}_\mu$ in active M octupoles leads to no net orbital angular momentum, except for $(M_x^\alpha,\ M_y^\alpha,\ M_z^\alpha)$[3]. It is noted that all the conventional multipoles active in the five d-orbital systems have the spatial inversion symmetric electromagnetic distribution, since only even-parity multipoles become active in a Hilbert space spanned by wave functions with a specific spatial-inversion parity.

1.3 Augmented Multipoles

In this section, we briefly introduce the augmented multipoles, which have been used to describe the electronic degrees of freedom in the multi-orbital and multi-sublattice systems that cannot be expressed by conventional multipoles. The augmented multipole is divided into four classes depending on the electronic and site degrees of freedom: the hybrid multipole in the multi-orbital system with different orbital angular momenta in Sec. 1.3.1, the cluster multipole and the bond multipole in the multi-sublattice system in Secs. 1.3.2 and 1.3.3, respectively, and the k multipole in momentum space in Sec. 1.3.4.

1.3.1 Hybrid Multipole

The hybrid multipole has been introduced to describe the atomic interorbital electronic degrees of freedom in the multi-orbital system with different orbital angular momenta, such as the s-p, p-d, d-f, and s-d orbitals [12, 13]. There are two main differences from the conventional multipoles. One is that the hybrid multipole describes the odd-parity multipole without the spatial inversion symmetry. In other words, the hybrid multipole can describe the effect of the parity-mixing hybridization in the absence of the inversion center at the atomic site. The other is that the hybrid multipole describes the ET and MT multipoles, which are not activated in the single d or f-orbital system.

We show an example of the hybrid multipole by considering the s and p_z orbitals. The off-diagonal matrix elements in the Hilbert space spanned by the basis $\{\phi_s, \phi_{p_z}\}$ correspond to the hybrid multipoles. Specifically, the real (imaginary) off-diagonal matrix elements are represented by the odd-parity E dipole Q_z and MT dipole T_z, which are represented by

$$\hat{Q}_z = \begin{pmatrix} 0 & 1 \\ 1 & 0 \end{pmatrix}, \ \hat{T}_z = \begin{pmatrix} 0 & -i \\ i & 0 \end{pmatrix}. \tag{1.22}$$

They have the nonzero expectation values when the s and p_z orbitals are hybridized. In this way, the atomic-scale odd-parity multipoles can be active in the hybridized orbital systems.

A similar discussion holds for other systems; the odd-parity hybrid multipoles (including ET and MT multipoles) can be active in the odd-parity hybridization, while the even-parity hybrid multipoles (including ET and MT multipoles) can be active in the even-parity hybridization. We show the spatial distribution of charge and orbital angular

[3] M_x^α, M_y^α, and M_z^α have a net orbital angular momentum, because active M octupole M_μ^α induces M dipole M_μ.

momentum when each expectation value of multipole takes nonzero in the case of the odd-parity p-d hybridization in Fig. 1.6 and in the case of the even-parity p-f hybridization in Fig. 1.7.

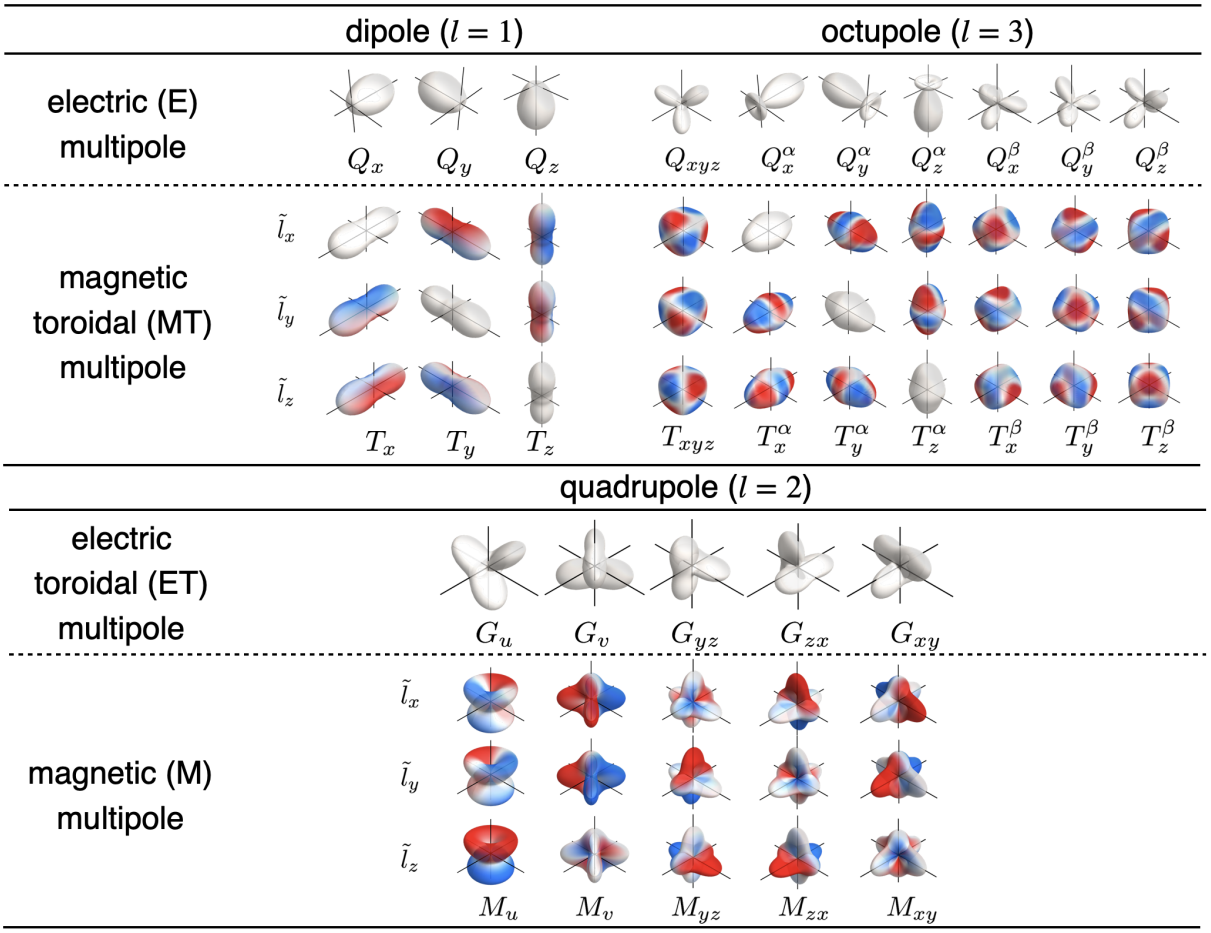

Figure 1.6: Spatial distribution of charge and orbital angular momentum when each expectation value of odd-parity hybrid multipole takes nonzero in the p-d orbital system.

The above hybrid multipole describing the interorbital electronic degrees of freedom becomes important in the lattice structure without the local inversion symmetry [33, 51]. It can also describe interorbital electronic order parameters due to the interorbital Coulomb interaction, such as an excitonic state [52–57].

1.3.2 Cluster Multipole

The cluster multipole can describe the on-site electronic degrees of freedom over several atomic sites in a cluster [16, 34, 35, 58, 59]. The expressions of the cluster multipole can be obtained by substituting $\boldsymbol{r}_i$ in Eqs. (1.10)–(1.13) with the position vector of the ith

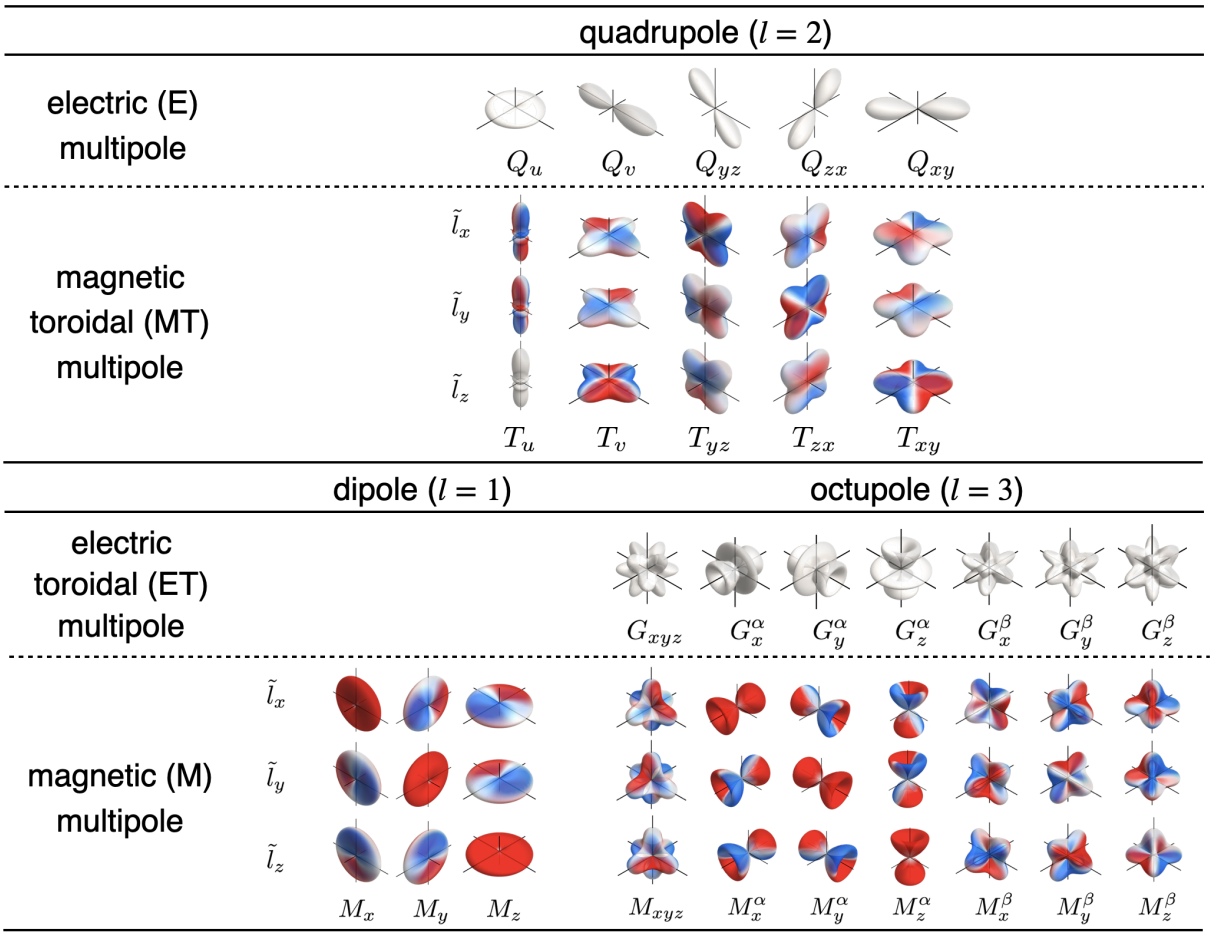

Figure 1.7: Spatial distribution of charge and orbital angular momentum when each expectation value of even-parity hybrid multipole (up to rank 3) takes nonzero in the p-f orbital system.

atom, $\boldsymbol{R}_i$. For example, the cluster E multipole in the N-site cluster is represented by

$$\hat{Q}_{lm}^{(\mathrm{c})}=\sum_{i=1}^{N} q_i O_{lm}(\boldsymbol{R}_i), \tag{1.23}$$

where the superscript (c) represents the cluster multipole and q_i is the charge of the ith atom.

We exemplify the E cluster multipole in a four-sublattice square cluster with q_i=1 for i=1–4. By using Eq. (1.23) from the lower-rank components, four independent E multipoles are obtained as follows:

$$\hat{Q}_0^{(\mathrm{c})}=+q_1+q_2+q_3+q_4, \tag{1.24}$$
$$\hat{Q}_x^{(\mathrm{c})}=-q_1+q_2+q_3-q_4, \tag{1.25}$$
$$\hat{Q}_y^{(\mathrm{c})}=-q_1+q_2-q_3+q_4, \tag{1.26}$$
$$\hat{Q}_{xy}^{(\mathrm{c})}=+q_1+q_2-q_3-q_4, \tag{1.27}$$

where $\boldsymbol{R}_i$ and the schematic charge configurations are illustrated in Fig. 1.8. Among them, the E monopole $\hat{Q}_0^{(\mathrm{c})}$ is characterized by the uniform charge distribution, while the E dipoles $\hat{Q}_x^{(\mathrm{c})}$ and $\hat{Q}_y^{(\mathrm{c})}$ and the E quadrupole $\hat{Q}_{xy}^{(\mathrm{c})}$ are characterized by the anisotropic charge distributions. The corresponding matrix elements for the basis $\{\phi_{i=1}, \phi_2, \phi_3, \phi_4\}$ are given by

$$\hat{Q}_0^{(\mathrm{c})} = \begin{pmatrix} 1 & 0 & 0 & 0 \\ 0 & 1 & 0 & 0 \\ 0 & 0 & 1 & 0 \\ 0 & 0 & 0 & 1 \end{pmatrix}, \ \hat{Q}_x^{(\mathrm{c})} = \begin{pmatrix} -1 & 0 & 0 & 0 \\ 0 & 1 & 0 & 0 \\ 0 & 0 & 1 & 0 \\ 0 & 0 & 0 & -1 \end{pmatrix}, \ \hat{Q}_y^{(\mathrm{c})} = \begin{pmatrix} -1 & 0 & 0 & 0 \\ 0 & 1 & 0 & 0 \\ 0 & 0 & -1 & 0 \\ 0 & 0 & 0 & 1 \end{pmatrix}, \ \hat{Q}_{xy}^{(\mathrm{c})} = \begin{pmatrix} 1 & 0 & 0 & 0 \\ 0 & 1 & 0 & 0 \\ 0 & 0 & -1 & 0 \\ 0 & 0 & 0 & -1 \end{pmatrix}, \tag{1.28}$$

where one finds that any four diagonal matrix elements are spanned by four independent E multipoles.

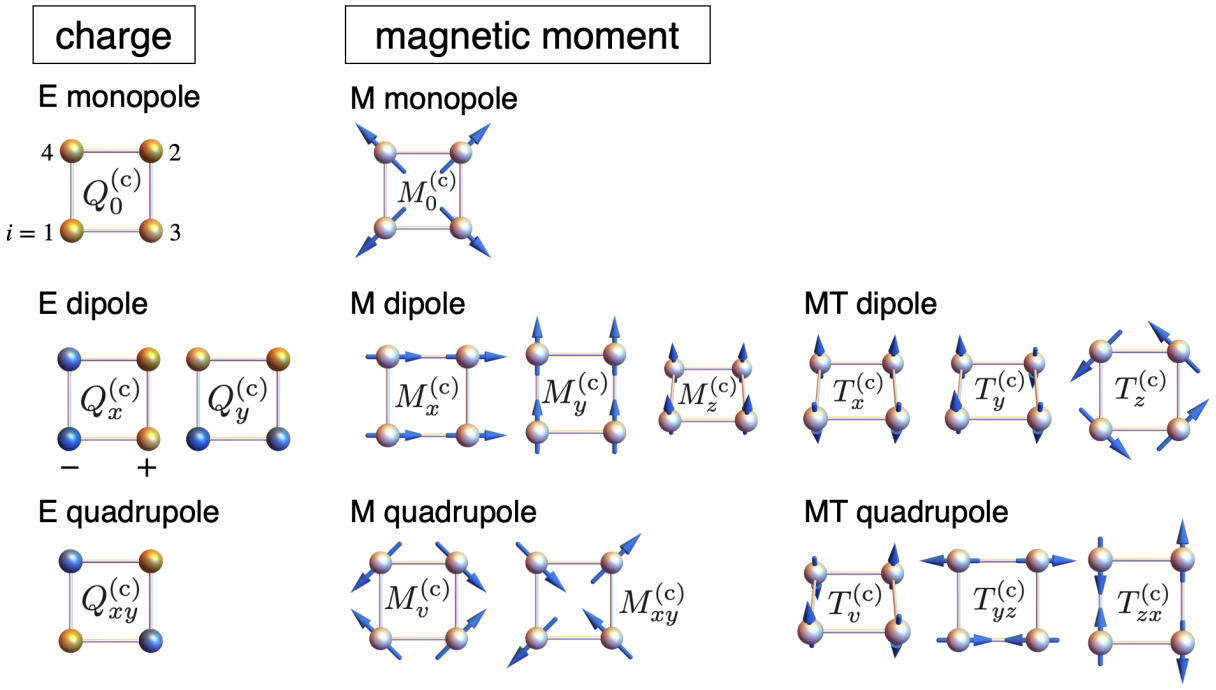

Figure 1.8: Schematic pictures of the cluster multipoles representing the charge and spin configurations in a four-sublattice square cluster.

Similarly, the spin configurations over multi sites can be described by cluster M and MT multipoles, whose expressions are given by [35]

$$\hat{M}_{lm}^{(\mathrm{c})} = \sum_{i=1}^{N} \boldsymbol{\sigma}_i \cdot \boldsymbol{\nabla}_i O_{lm}(\boldsymbol{R}_i), \tag{1.29}$$

$$\hat{T}_{lm}^{(\mathrm{c})} = \frac{1}{l+1} \sum_{i=1}^{N} (\boldsymbol{R}_i \times \boldsymbol{\sigma}_i) \cdot \boldsymbol{\nabla}_i O_{lm}(\boldsymbol{R}_i). \tag{1.30}$$

We show that all the spin configurations in the four-sublattice square cluster, i.e., $3 \times 4 = 12$ spin configurations, are described by the cluster M and MT multipoles in the right panel of Fig. 1.8.

The cluster multipole provides a systematic understanding of the physical phenomena in complicated charge and spin orderings, such as the antiferromagnetic orderings. For example, a cluster M octupole has been used for the understanding of the anomalous Hall effect in Mn_3Sn [34, 60] and the magneto-striction effect [61, 62], the cluster MT dipole for the linear magnetoelectric effect in various antiferromagnetic insulators, e.g., Cr_2O_3 [63], $Ga_{2-x}Fe_xO_3$ [64, 65], $LiCoPO_4$ [66, 67], $Ba_2CoGe_2O_7$ [68], and antiferromagnetic metals, e.g., UNi_4B [69–71] and Ce_3TiBi_5 [72, 73], the cluster M quadrupole for the linear magnetoelectric effect in $Co_4Nb_2O_9$ [74–77] and $KOsO_4$ [78] and the magnetopiezoelectric effect in $Ba_{1-x}K_xMn_2As_2$ [38] and $EuMn_2Bi_2$ [79].

1.3.3 Bond Multipole

The bond multipole describes the bond degrees of freedom over multi sites, i.e., the off-site electronic degrees of freedom in a cluster [37]. Similar to the cluster multipole, the bond E multipole is expressed as

$$\hat{Q}^{(\mathrm{b})}_{lm}=\sum_{ij}^{N_{\mathrm{bond}}} q_{(ij)}O_{lm}(\boldsymbol{R}_{(ij)}), \tag{1.31}$$

where the superscript (b) represents the bond multipole. (ij) stands for the bond between ith and jth atoms with the real value $q_{(ij)}$. $\boldsymbol{R}_{(ij)}$ is the position vector pointing from ith atom to jth atom. N_{bond} is the number of the bonds.

We again consider the four-sublattice square cluster with $q_{(ij)}=1$ to show the correspondence between the bond degree of freedom and the bond E multipoles in Eq. (1.31). The four nearest-neighbor bond degrees of freedom denoted as (b1) and the two next-nearest-neighbor bond degrees of freedom denoted as (b2) are represented by

$$\hat{Q}^{(\mathrm{b1})}_{0}=+q_{(13)}+q_{(32)}+q_{(24)}+q_{(41)}, \tag{1.32}$$
$$\hat{Q}^{(\mathrm{b1})}_{x}=+q_{(32)}-q_{(41)}, \tag{1.33}$$
$$\hat{Q}^{(\mathrm{b1})}_{y}=+q_{(24)}-q_{(13)}, \tag{1.34}$$
$$\hat{Q}^{(\mathrm{b1})}_{v}=-q_{(13)}+q_{(32)}-q_{(24)}+q_{(41)}, \tag{1.35}$$
$$\hat{Q}^{(\mathrm{b2})}_{0}=+q_{(12)}+q_{(34)}, \tag{1.36}$$
$$\hat{Q}^{(\mathrm{b2})}_{xy}=+q_{(12)}-q_{(34)}, \tag{1.37}$$

where each matrix element for the basis $\{\phi_1,\phi_2,\phi_3,\phi_4\}$ is given by

$$\hat{Q}^{(\mathrm{b1})}_{0}=\begin{pmatrix}0&0&1&1\\0&0&1&1\\1&1&0&0\\1&1&0&0\end{pmatrix},\hat{Q}^{(\mathrm{b1})}_{x}=\begin{pmatrix}0&0&0&-1\\0&0&1&0\\0&1&0&0\\-1&0&0&0\end{pmatrix},\hat{Q}^{(\mathrm{b1})}_{y}=\begin{pmatrix}0&0&-1&0\\0&0&0&1\\-1&0&0&0\\0&1&0&0\end{pmatrix},\hat{Q}^{(\mathrm{b1})}_{v}=\begin{pmatrix}0&0&-1&1\\0&0&1&-1\\-1&1&0&0\\1&-1&0&0\end{pmatrix}, \tag{1.38}$$

$$\hat{Q}^{(\mathrm{b2})}_{0}=\begin{pmatrix}0&1&0&0\\1&0&0&0\\0&0&0&1\\0&0&1&0\end{pmatrix},\ \hat{Q}^{(\mathrm{b2})}_{xy}=\begin{pmatrix}0&1&0&0\\1&0&0&0\\0&0&0&-1\\0&0&-1&0\end{pmatrix}. \tag{1.39}$$

The E bond multipoles in the square cluster are shown in Fig. 1.9. The bond E multipoles are useful to describe the real hopping of electrons in terms of multipoles in a systematic way.

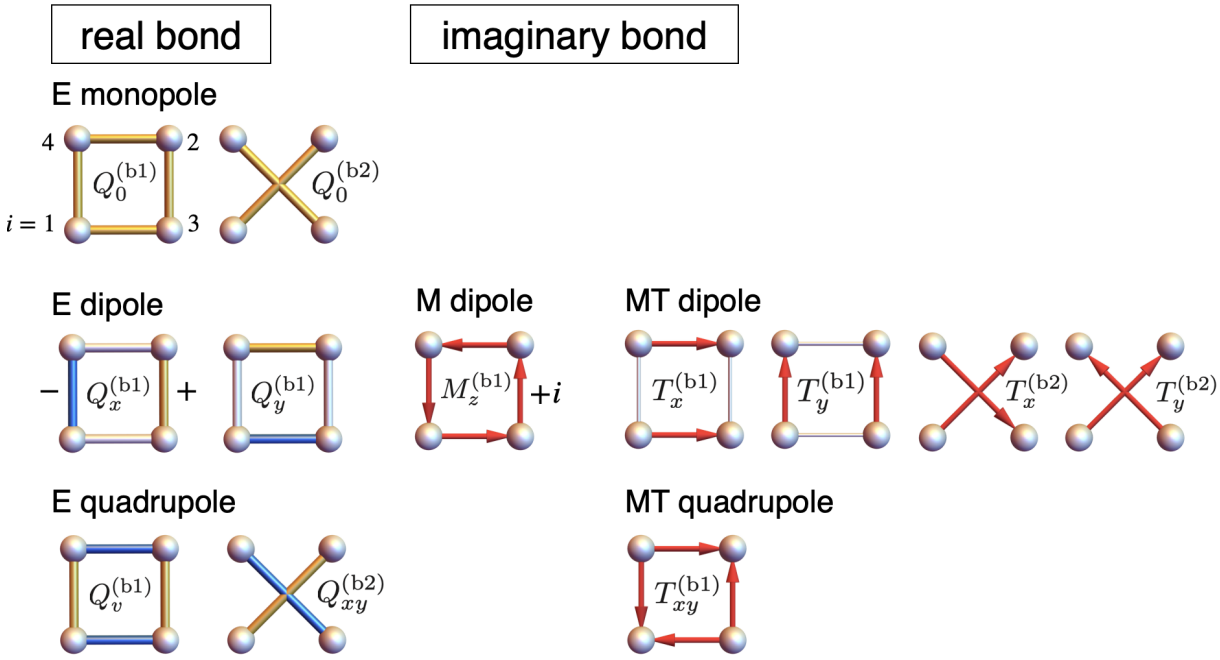

Figure 1.9: Schematic pictures of the bond multipoles in a four-sublattice square cluster.

In a similar way, the imaginary hopping of electrons is described by the bond M and MT multipoles [37], which are given by

$$\hat{M}_{lm}^{(\mathrm{b})}=\sum_{(ij)}^{N_{\mathrm{bond}}}(\boldsymbol{n}_{(ij)}\times\boldsymbol{t}_{(ij)})\cdot\boldsymbol{O}_{lm}(\boldsymbol{R}_{(ij)}), \tag{1.40}$$

$$\hat{T}_{lm}^{(\mathrm{b})}=\sum_{(ij)}^{N_{\mathrm{bond}}}\boldsymbol{t}_{(ij)}\cdot\boldsymbol{O}_{lm}(\boldsymbol{R}_{(ij)}), \tag{1.41}$$

where $\boldsymbol{O}_{lm}(\boldsymbol{r})=\boldsymbol{\nabla}O_{lm}(\boldsymbol{r})$ and $\boldsymbol{n}_{(ij)}=\boldsymbol{R}_{(ij)}/|\boldsymbol{R}_{(ij)}|$. $\boldsymbol{t}_{(ij)}$ is the local MT dipole at the (ij) bond defined as $\boldsymbol{t}_{(ij)}=it_{(ij)}\boldsymbol{n}_{(ij)}$ with the imaginary hopping $it_{(ij)}$. We show the imaginary bond distributions in the square cluster in the right panel of Fig. 1.9, where the red arrow stands for the imaginary hopping with i (imaginary unit).

The bond multipoles are related not only to the hopping in the Hamiltonian but also the bond orders, such as a staggered flux state [80–83] and a loop-current state [36, 37, 84–87]. Furthermore, more exotic bond orders corresponding to the active ET quadrupole have been proposed in the $5d$ spin-orbit-coupled metal $Cd_2Re_2O_7$ [36].

1.3.4 k Multipole

The k multipole describes the anisotropic band deformation and spin splittings in the electronic states. The expressions within the single-band system in the case of $\boldsymbol{k}\to\boldsymbol{0}$ limit

are given by [39]

$$Q_{lm}(\boldsymbol{k})\equiv\begin{cases}\sigma_0 O_{lm}(\boldsymbol{k}) & (l=0,2,4,6,\cdots)\\ (\boldsymbol{k}\times\boldsymbol{\sigma})\cdot\boldsymbol{\nabla}_{\boldsymbol{k}}O_{lm}(\boldsymbol{k}) & (l=1,3,5,\cdots)\end{cases} \tag{1.42}$$

$$T_{lm}(\boldsymbol{k})\equiv\begin{cases}0 & (l=0)\\ (\boldsymbol{k}\times\boldsymbol{\sigma})\cdot\boldsymbol{\nabla}_{\boldsymbol{k}}O_{lm}(\boldsymbol{k}) & (l=2,4,6,\cdots)\\ \sigma_0 O_{lm}(\boldsymbol{k}) & (l=1,3,5,\cdots)\end{cases} \tag{1.43}$$

$$M_{lm}(\boldsymbol{k})\equiv\begin{cases}0 & (l=0,2,4,6,\cdots)\\ \boldsymbol{\sigma}\cdot\boldsymbol{\nabla}_{\boldsymbol{k}}O_{lm}(\boldsymbol{k}) & (l=1,3,5,\cdots)\end{cases} \tag{1.44}$$

$$G_{lm}(\boldsymbol{k})\equiv\begin{cases}\boldsymbol{k}\cdot\boldsymbol{\sigma} & (l=0)\\ \boldsymbol{\sigma}\cdot\boldsymbol{\nabla}_{\boldsymbol{k}}O_{lm}(\boldsymbol{k}) & (l=2,4,6,\cdots)\\ 0 & (l=1,3,5,\cdots)\end{cases} \tag{1.45}$$

where $\boldsymbol{k}$ is the wave vector with parities $(\mathcal{P},\mathcal{T})=(-1,-1)$ and $\boldsymbol{\sigma}$ is the spin with $(\mathcal{P},\mathcal{T})=(+1,-1)$. Although there are no expressions of the rank-0 MT monopole, even-rank M multipoles, and odd-rank ET multipoles in the single-band case, they can be defined in the multi-band case [88].

The k multipoles describe the Hamiltonian in momentum space under a periodic lattice system. A general Hamiltonian in momentum space can be represented as follows:

$$\mathcal{H}=\sum_{\boldsymbol{k}\sigma\sigma'}\left[\varepsilon^{\mathrm{S}}(\boldsymbol{k})\delta_{\sigma\sigma'}+\varepsilon^{\mathrm{A}}(\boldsymbol{k})\delta_{\sigma\sigma'}+f^{\mathrm{S}}_{\sigma\sigma'}(\boldsymbol{k})+f^{\mathrm{A}}_{\sigma\sigma'}(\boldsymbol{k})\right]c^{\dagger}_{\boldsymbol{k}\sigma}c_{\boldsymbol{k}\sigma'}, \tag{1.46}$$

where $c^{\dagger}_{\boldsymbol{k}\sigma}$ ($c_{\boldsymbol{k}\sigma}$) is the creation (annihilation) operator of electron with wave vector $\boldsymbol{k}$ and spin $\sigma=\uparrow,\downarrow$. $\varepsilon^{\mathrm{S}}(\boldsymbol{k})$, $f^{\mathrm{S}}_{\sigma\sigma'}(\boldsymbol{k})$, $\varepsilon^{\mathrm{A}}(\boldsymbol{k})$, and $f^{\mathrm{A}}_{\sigma\sigma'}(\boldsymbol{k})$ has different momentum and spin dependences, which satisfy the following relations for their space-time inversion symmetries as

$$\varepsilon^{\mathrm{S}}(\boldsymbol{k})=\varepsilon^{\mathrm{S}}(-\boldsymbol{k}),\ f^{\mathrm{S}}_{\sigma\sigma'}(\boldsymbol{k})=f^{\mathrm{S}}_{\sigma\sigma'}(-\boldsymbol{k}),\ \varepsilon^{\mathrm{A}}(\boldsymbol{k})=-\varepsilon^{\mathrm{A}}(-\boldsymbol{k}),\ f^{\mathrm{A}}_{\sigma\sigma'}(\boldsymbol{k})=-f^{\mathrm{A}}_{\sigma\sigma'}(-\boldsymbol{k}). \tag{1.47}$$

The band deformation and the spin splittings for these four dispersions are shown in Fig. 1.10(a), where the presence/absence of $\mathcal{P}$, $\mathcal{T}$, and $\mathcal{PT}$ symmetries corresponding to each band deformation and spin splitting is shown. These dispersions are related to the k multipole as

$$\varepsilon^{\mathrm{S}}(\boldsymbol{k})=\sum_{l}^{\mathrm{even}}\sum_{m}Q^{\mathrm{ext}}_{lm}Q_{lm}(\boldsymbol{k}), \tag{1.48}$$

$$\varepsilon^{\mathrm{A}}(\boldsymbol{k})=\sum_{l}^{\mathrm{odd}}\sum_{m}T^{\mathrm{ext}}_{lm}T_{lm}(\boldsymbol{k}), \tag{1.49}$$

$$f^{\mathrm{S}}_{\sigma\sigma'}(\boldsymbol{k})=\sum_{l}^{\mathrm{odd}}\sum_{m}M^{\mathrm{ext}}_{lm}M^{\sigma\sigma'}_{lm}(\boldsymbol{k})+\sum_{l}^{\mathrm{even}}\sum_{m}T^{\mathrm{ext}}_{lm}T^{\sigma\sigma'}_{lm}(\boldsymbol{k}), \tag{1.50}$$

$$f^{\mathrm{A}}_{\sigma\sigma'}(\boldsymbol{k})=\sum_{l}^{\mathrm{even}}\sum_{m}G^{\mathrm{ext}}_{lm}G^{\sigma\sigma'}_{lm}(\boldsymbol{k})+\sum_{l}^{\mathrm{odd}}\sum_{m}Q^{\mathrm{ext}}_{lm}Q^{\sigma\sigma'}_{lm}(\boldsymbol{k}), \tag{1.51}$$

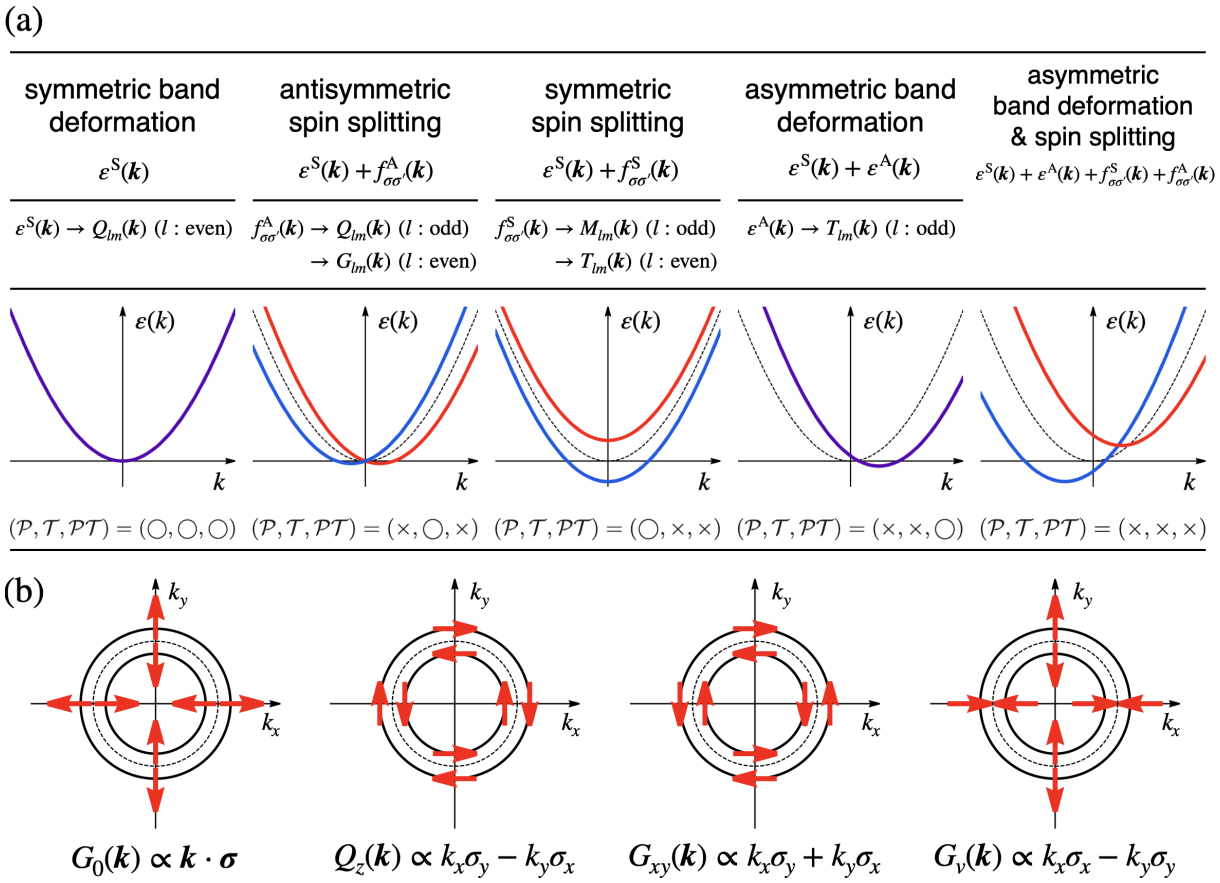

Figure 1.10: (a) Schematic dispersions in the presence of $\varepsilon^{S}(\boldsymbol{k})$, $f^{A}_{\sigma\sigma'}(\boldsymbol{k})$, $f^{S}_{\sigma\sigma'}(\boldsymbol{k})$, and $\varepsilon^{A}(\boldsymbol{k})$. (b) Four examples of the antisymmetric spin splittings induced by odd-parity E/ET multipoles.

where $X^{\rm ext}_{lm}$ (X=Q, M, G, T) is the conjugate field in each multipole. We show the example of $f^{A}_{\sigma\sigma'}(\boldsymbol{k})$ by taking the low-rank E and ET multipoles in Fig. 1.10(b).

In this way, the k multipoles give a systematic way to understand anisotropic band deformations and spin splittings. Such information is useful to engineer desired electronic band structures from the microscopic viewpoint. Indeed, interesting symmetric and antisymmetric spin polarizations in the AFM orderings without the spin-orbit coupling have been proposed based on multipoles [37, 41, 42, 89], e.g., κ-(BETD-TTF)$_2$Cu[N(CN)$_2$]Cl [89, 90] and $Ba_3MnNb_2O_9$ [42, 91].

1.4 Multipoles under Point Group Symmetry

In the previous section, we reviewed that various electronic degrees of freedom, e.g., charge, spin, orbital, sublattice, and bond, can be described by using four types of augmented multipoles. This microscopic description enables us to represent the order parameters with complicated charge or current distribution in a systematic manner. In addition, the concept of augmented multipoles can be applied to any crystallographic point group to understand the physical properties in solids. In this section, we show the classification

of multipoles in crystallographic point group symmetry by using the representation theory. Systematic classification of multipoles gives useful information for the understanding of multiferroic physical phenomena, as discussed in the subsequent section [39, 40].

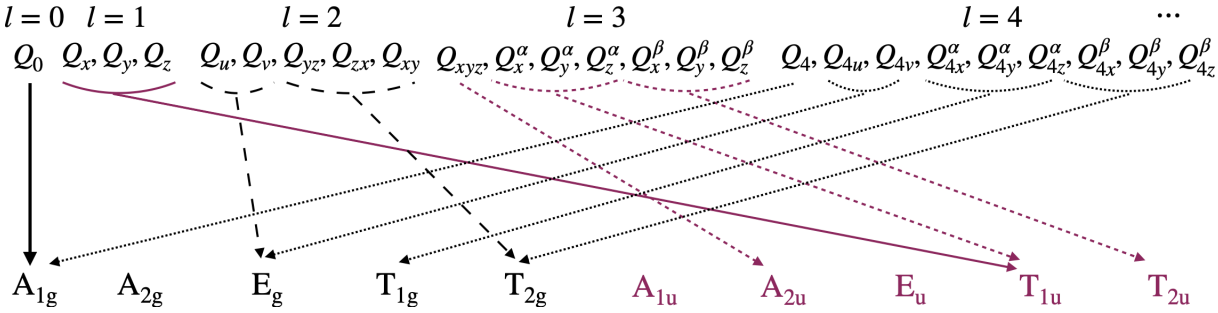

Figure 1.11: Correspondence between E multipoles and irreducible representations in $O_{\rm h}$.

The crystallographic point group is the subgroup of the $O(3)$ group with the 3-dimensional continuous rotation and spatial inversion operations. It means that four types of multipoles, which constitute a complete set of electromagnetic degrees of freedom in the $O(3)$ symmetry[4], are also used as the symmetry-adapted basis in crystallographic point groups.

In the spherical field, rank l corresponds to the index of the $(2l+1)$-dimensional irreducible representation with the rank-l multipole X_{lm} $(X=Q,G,M,T)$ as the basis. When the continuous rotational symmetry is lost and $O(3)$ group is reduced to the crystallographic point group, multipoles are not well classified by rank l and need to use the irreducible representations in the crystallographic point group. For example, we show the irreducible representation of the E multipoles up to rank 4 in cubic $m\bar{3}m$ $(O_{\rm h})$ symmetry in Fig. 1.11, which are denoted as

$$Q_0, Q_4 \in {\rm A_{1g}},\ (Q_u, Q_v), (Q_{4u}, Q_{4v}) \in {\rm E_g}, \tag{1.52}$$

$$(Q^\alpha_{4x}, Q^\alpha_{4y}, Q^\alpha_{4z}) \in {\rm T_{1g}},\ (Q_{yz}, Q_{zx}, Q_{xy}), (Q^\beta_{4x}, Q^\beta_{4y}, Q^\beta_{4z}) \in {\rm T_{2g}}, \tag{1.53}$$

$$Q_{xyz} \in {\rm A_{2u}},\ (Q_x, Q_y, Q_z), (Q^\alpha_x, Q^\alpha_y, Q^\alpha_z) \in {\rm T_{1u}},\ (Q^\beta_x, Q^\beta_y, Q^\beta_z) \in {\rm T_{2u}}. \tag{1.54}$$

One finds that the multipoles with different ranks, e.g., Q_0 and Q_4, belong to the same irreducible representation. In the same way based on the representation theory, one can classify the four types of multipoles under 32 crystallographic point group [39]. For instance, we show the classification of multipoles up to rank 4 in tetragonal $4/mmm$ $(D_{4\rm h})$ symmetry in Table 1.2.

The classification of multipoles has the advantage of obtaining the relevant microscopic electronic degrees of freedom by the symmetry analysis. Let us take an example of a four-sublattice square cluster in Sec. 1.3.2 under $D_{4\rm h}$ symmetry. Since the representation of the four site degrees of freedom is reducible as ${\rm A_{1g}}\oplus{\rm B_{2g}}\oplus{\rm E_u}$ by the symmetry analysis, we map the cluster E multipole onto its irreducible representation by using Table 1.2:

[4]Strictly speaking, four types of multipoles including M and MT multipoles are the basis for the $RO(3)=O(3)\times\{E,\theta\}$ group, where E and θ are the identitical operation and the time-reversal operation, respectively.

Table 1.2: Multipole classification for the irreducible representations (irrep.) in tetragonal $4/mmm$ ($D_{4\mathrm{h}}$) symmetry.

irrep.	E	ET	MT	M
A_{1g}	Q_0, Q_u, Q_4, Q_{4u}	—	T_0, T_u, T_4, T_{4u}	—
A_{2g}	Q^{α}_{4z}	G_z, G^{α}_z	T^{α}_{4z}	M_z, M^{α}_z
B_{1g}	Q_v, Q_{4v}	G_{xyz}	T_v, T_{4v}	M_{xyz}
B_{2g}	Q_{xy}, Q^{β}_{4z}	G^{β}_z	T_{xy}, T^{β}_{4z}	M^{β}_z
E_g	$Q_{yz}, Q^{\alpha}_{4x}, Q^{\beta}_{4x}$	$G_x, G^{\alpha}_x, G^{\beta}_x$	$T_{yz}, T^{\alpha}_{4x}, T^{\beta}_{4x}$	$M_x, M^{\alpha}_x, M^{\beta}_x$
	$Q_{zx}, Q^{\alpha}_{4y}, Q^{\beta}_{4y}$	$G_y, G^{\alpha}_y, G^{\beta}_y$	$T_{zx}, T^{\alpha}_{4y}, T^{\beta}_{4y}$	$M_y, M^{\alpha}_y, M^{\beta}_y$
A_{1u}	—	G_0, G_u, G_4, G_{4u}	—	M_0, M_u, M_4, M_{4u}
A_{2u}	Q_z, Q^{α}_z	G^{α}_{4z}	T_z, T^{α}_z	M^{α}_{4z}
B_{1u}	Q_{xyz}	G_v, G_{4v}	T_{xyz}	M_v, M_{4v}
B_{2u}	Q^{β}_z	G_{xy}, G^{β}_{4z}	T^{β}_z	M_{xy}, M^{β}_{4z}
E_u	$Q_x, Q^{\alpha}_x, Q^{\beta}_x$	$G_{yz}, G^{\alpha}_{4x}, G^{\beta}_{4x}$	$T_x, T^{\alpha}_x, T^{\beta}_x$	$M_{yz}, M^{\alpha}_{4x}, M^{\beta}_{4x}$
	$Q_y, Q^{\alpha}_y, Q^{\beta}_y$	$G_{zx}, G^{\alpha}_{4y}, G^{\beta}_{4y}$	$T_y, T^{\alpha}_y, T^{\beta}_y$	$M_{zx}, M^{\alpha}_{4y}, M^{\beta}_{4y}$

$Q_0 \in A_{1g}$, $Q_{xy} \in B_{2g}$, and $(Q_x, Q_y) \in E_u$. Moreover, when additionally considering the spin degrees of freedom, the irreducible representations of the electronic degrees of freedom are

$$(A_{1g} \oplus B_{2g} \oplus E_u)_{\mathrm{site}} \otimes (E_g \oplus A_{2g})_{\mathrm{spin}} = A_{2g} \oplus B_{1g} \oplus 2E_g \oplus A_{1u} \oplus A_{2u} \oplus B_{1u} \oplus B_{2u} \oplus E_u, \quad (1.55)$$

where $M_z \in A_{2g}$, $T_v \in B_{1g}$, $(M_x, M_y), (T_{yz}, T_{zx}) \in E_g$, $M_0 \in A_{1u}$, $T_z \in A_{2u}$, $M_v \in B_{1u}$, $M_{xy} \in B_{2u}$, and $(T_x, T_y) \in E_u$. In this case, each spin configuration in Fig. 1.8 is obtained based on the projection method in each irreducible representation.

Although the multipole is classified under 32 crystallographic point groups, the consideration about the time-reversal symmetry is lacking. To complete the classification of multipoles, one needs to start from the $RO(3) = O(3) \times \{E, \theta\}$ symmetry with the explicit time-reversal operation θ and classify multipoles under the 122 magnetic point groups. Especially, the classification of multipole is missing in the 58 black-and-white point groups, which are related to a variety of antiferromagnets as summarized in Fig. 1.12[5]. Thus, it is highly desired to formulate a complete classification under the magnetic point group, which becomes a reference to explore interesting physical properties related to the breaking of the time-reversal symmetry, as often found in antiferromagnets.

1.5 Relation between Multipole and Field Responses

In this section, we review the relation between multipoles and the physical property in the crystallographic point group by focusing on the field responses. In general, physical quantities, such as the electric polarization $\boldsymbol{P}$ and magnetization $\boldsymbol{M}$, are induced by

[5]The classification of multipole in 32 gray point groups is straightforwardly obtained from the one in 32 crystallographic point groups with a few exceptions.

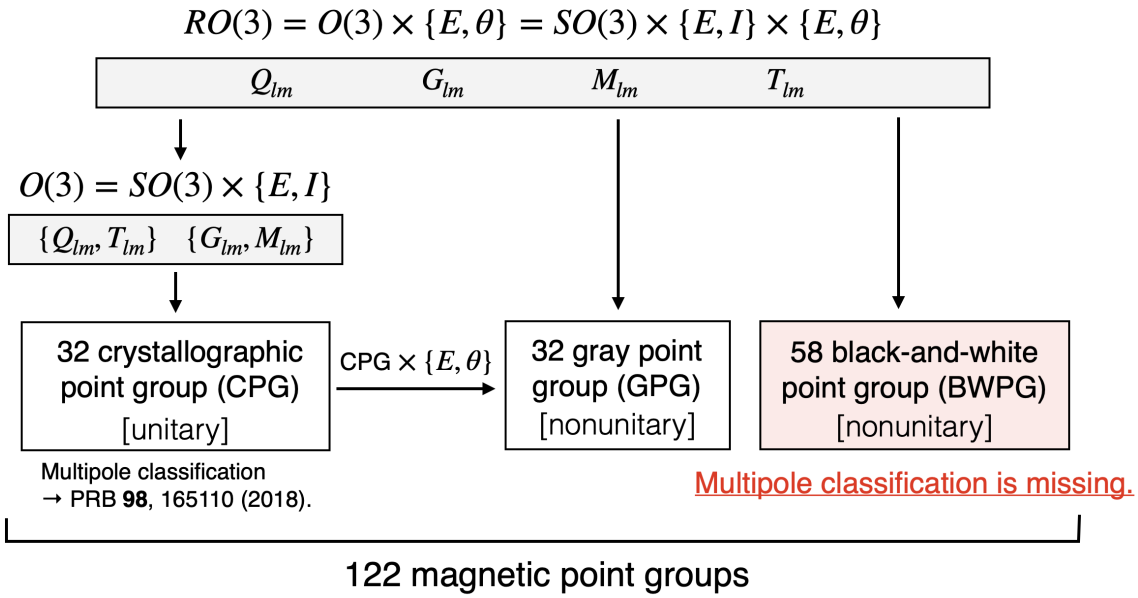

Figure 1.12: Relation between the point groups with the spherical symmetry and magnetic point groups.

corresponding conjugate fields, e.g., the electric field $\boldsymbol{E}(\leftrightarrow \boldsymbol{P})$ and the magnetic field $\boldsymbol{H}(\leftrightarrow \boldsymbol{M})$. However, there are some situations where the physical response is induced by a non-conjugate field under particular symmetry conditions, which is called a multiferroic response (or cross-correlated response). Although possible multiferroic responses have been discussed based on the symmetry analysis [92–95], we here discuss the relevance with the multipoles, since it provides microscopic information to understand the origin of the multiferroic responses based on the electronic degrees of freedom.

For example, a linear magnetoelectric effect, where the magnetization is induced by an electric field, is represented by using the response tensor $\hat{\alpha}$ as follows:

$$\begin{pmatrix} M_x \\ M_y \\ M_z \end{pmatrix} = \begin{pmatrix} \alpha_{xx} & \alpha_{xy} & \alpha_{xz} \\ \alpha_{yx} & \alpha_{yy} & \alpha_{yz} \\ \alpha_{zx} & \alpha_{zy} & \alpha_{zz} \end{pmatrix} \begin{pmatrix} E_x \\ E_y \\ E_z \end{pmatrix}. \tag{1.56}$$

Since $\hat{\alpha}$ is the rank-2 axial tensor with odd time inversion, $\hat{\alpha}$ is related to the 9 multipoles with the same spatial and time-inversion parities: M monopole M_0, MT dipoles (T_x, T_y, T_z), and M quadrupoles $(M_u, M_v, M_{yz}, M_{zx}, M_{xy})$. By using the corresponding tensor components, α^{M_0}, $(\alpha^{T_x}, \alpha^{T_y}, \alpha^{T_z})$, and $(\alpha^{M_u}\alpha^{M_v}, \alpha^{M_{yz}}, \alpha^{M_{zx}}, \alpha^{M_{xy}})$, $\hat{\alpha}$ is represented as

$$\begin{pmatrix} \alpha_{xx} & \alpha_{xy} & \alpha_{xz} \\ \alpha_{yx} & \alpha_{yy} & \alpha_{yz} \\ \alpha_{zx} & \alpha_{zy} & \alpha_{zz} \end{pmatrix} \to \begin{pmatrix} \alpha^{M_0} - \alpha^{M_u} + \alpha^{M_v} & \alpha^{T_z} + \alpha^{M_{xy}} & -\alpha^{T_y} + \alpha^{M_{zx}} \\ -\alpha^{T_z} + \alpha^{M_{xy}} & \alpha^{M_0} - \alpha^{M_u} - \alpha^{M_v} & \alpha^{T_x} + \alpha^{M_{yz}} \\ \alpha^{T_y} + \alpha^{M_{zx}} & -\alpha^{T_x} + \alpha^{M_{yz}} & \alpha^{M_0} + 2\alpha^{M_u} \end{pmatrix}, \tag{1.57}$$

where α^{M_0} is the symmetric component, $\alpha^{T_x}, \alpha^{T_y}, \alpha^{T_z}$ are the antisymmetric components, and $\alpha^{M_u}, \alpha^{M_v}, \alpha^{M_{yz}}, \alpha^{M_{zx}}, \alpha^{M_{xy}}$ are the traceless symmetric components. Since the nonzero response tensor component has a correspondence with the magnetic point group symmetry according to Neumann's principle [92, 96, 97], one can find nonzero

tensor components when the expectation values of the corresponding multipole become nonzero.

It is noted that the magnetoelectric effect can occur in metals even if the time-reversal symmetry is preserved. Such a response is due to the different dissipation process from the magnetoelectric response relevant to the M and MT multipoles in Eq. (1.57). In this case, $\hat{\alpha}$ is related to the ET monopole, E dipoles, and ET quadrupoles as

$$\begin{pmatrix} \alpha^{G_0}-\alpha^{G_u}+\alpha^{G_v} & \alpha^{Q_z}+\alpha^{G_{xy}} & -\alpha^{Q_y}+\alpha^{G_{zx}} \\ -\alpha^{Q_z}+\alpha^{G_{xy}} & \alpha^{G_0}-\alpha^{G_u}-\alpha^{G_v} & \alpha^{Q_x}+\alpha^{G_{yz}} \\ \alpha^{Q_y}+\alpha^{G_{zx}} & -\alpha^{Q_x}+\alpha^{G_{yz}} & \alpha^{G_0}+2\alpha^{G_u} \end{pmatrix}. \tag{1.58}$$

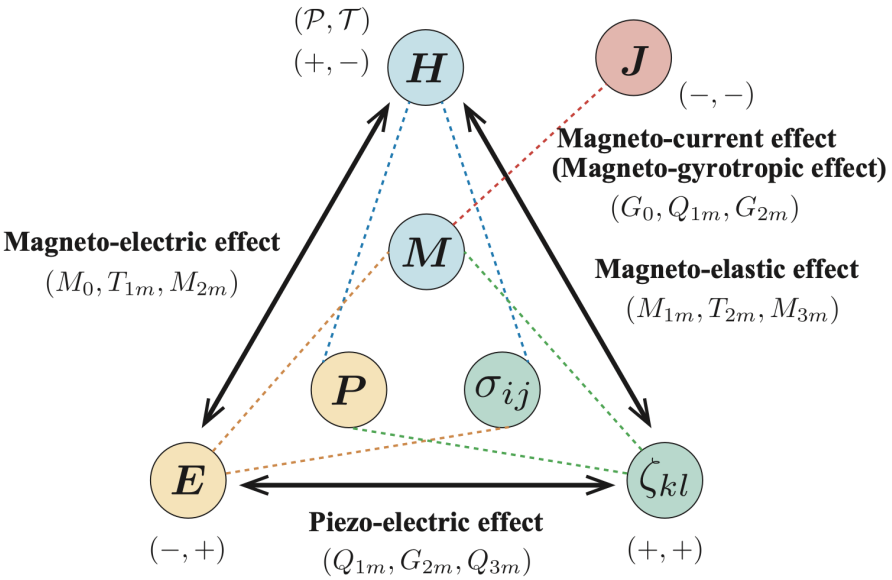

Figure 1.13: Heckmann diagram in Ref. [39]. Essential active multipoles in each multiferroic response are also shown.

The relation between other field responses and active multipoles can be obtained in a similar discussion [39] as shown by the Heckmann diagram in Fig. 1.13, where σ_{ij}, ζ_{kl}, and $\boldsymbol{J}$ stand for the symmetric stress tensor, strain-rotation field, and electric current, respectively. This systematic relation between the field responses and active multipoles gives us comprehensive information about necessary electronic degrees of freedom inducing the field response. In other words, the tensor analysis by using the multipole degrees of freedom gives not only nonzero tensor components from the symmetry viewpoint but also the microscopic origin and the related important model parameters in a systematic way. Such an attempt based on multipole has been developed in recent years, which has uncovered the origin of the anomalous Hall effect without a net magnetization [34, 98], the magnetoelectric effect [58, 74–77, 99, 100], and the magnetic piezoelectric effect [36, 38, 79, 101]. Nevertheless, the discussion has been mainly limited to linear responses. Thus, it is highly desirable to extend the multipole description into a nonlinear response to include the nonreciprocal transport and the nonlinear Hall effect [102, 103] in a systematic way. It is also important to clarify a microscopic essence of the nonlinear physical responses induced by unconventional multipole ordered states with the MT and ET multipoles.

1.6 Purpose of This Thesis

As discussed in the previous sections, the augmented multipole provides a powerful framework to represent the electronic degrees of freedom in solids, e.g., charge, spin, orbital, and sublattice, in a systematic and symmetry-adapted form. Recent studies have developed the concept of multipole to describe not only the conventional multipole orders in d- and f-electron systems but also various electronic states, such as antiferromagnetic ordered states and bond ordered states beyond the symmetry argument [12, 13, 35–37, 39–42]. In particular, the author and her collaborators classified four types of multipoles in all 32 crystallographic point groups [39]. Meanwhile, it is not enough to describe the order parameter and the multipole couplings in the absence of the time-reversal symmetry by the external magnetic field and/or spontaneous magnetic orderings, as discussed in Sec. 1.4. The systematic classification of multipoles to cover such a situation becomes a useful reference to explore further exotic ordered phases and their driven physical phenomena, which will stimulate a future study in both theory and experiment.

The main purpose of this thesis is to establish the classification of multipoles under the 122 magnetic point groups and to open up a new research direction induced by unconventional multipole orderings. For that purpose, we apply the representation theory of the nonunitary groups so as to include the time-reversal symmetry in magnetic point groups. The complete classification of multipoles enables us to analyze the symmetry-adapted order parameters in the magnetic materials, such as antiferromagnetic materials, and to perform the systematic analysis of the physical properties from a microscopic viewpoint. Moreover, we aim at extending the relationship between the multipoles and the response tensors to cover up to the second-order nonlinear responses. We also study the physical phenomena, such as the linear magnetoelectric effect and the nonlinear nonreciprocal transport, under the odd-parity multipole orderings in the absence of the spatial inversion symmetry on the basis of the augmented multipoles. We also aim at providing a microscopic experimental method to detect odd-parity multipoles by the NMR/NQR measurement.

1.7 Organization of This Thesis

This thesis is organized as follows. In Chap. 2, the classification of four types of multipoles in 122 magnetic point groups is shown in a complete way. We also discuss the relation between multipoles and the linear and nonlinear field responses. Based on the systematic classification of multipoles, we explore odd-parity multipole physics by studying the following two systems. One is the MT dipole ordering induced by the collinear AFM ordering on a zigzag chain in Chap. 3. We clarify the microscopic essence of the nonlinear transport under the MT dipole ordering. The second is the odd-parity multipole orderings in the f-electron metal CeCoSi in Chap. 4. We discuss the stability of the odd-parity multipole orderings and their phase transitions by using two effective models so as to reproduce the phase diagram in CeCoSi. We also discuss the multiferroic phenomena and the change of the NQR/NMR spectra in the presence of odd-parity multipoles.

Chapter 2

Classification of Multipoles in 122 Magnetic Point Groups

In this chapter, we show a complete classification of multipoles in 122 magnetic point groups toward a systematic understanding of the physical properties in magnetic materials based on the concept of multipole. The contents in this chapter are based on Ref. [104][1]. This chapter is organized as follows. In Sec. 2.1, we introduce the physical properties in magnetic materials with ferromagnetic and antiferromagnetic spin textures and describe the purpose of the present study. In Sec. 2.2, we briefly give a short review of the three types of magnetic point groups and the representation theory in a nonunitary group. In Sec. 2.3, we perform the classification of multipoles in the 122 magnetic point groups. We discuss the active multipoles belonging to the totally symmetric representation in each magnetic point group in Sec. 2.4. In Sec. 2.5, we clarify the relation between the multipoles and the response tensors by using the symmetry and microscopic analyses based on the Kubo formula. We show the important multipole degrees of freedom to induce linear and second-order nonlinear responses. Section 2.6 summarizes the results of this chapter.

2.1 Introduction

Magnetic orderings such as ferromagnetic (FM) and antiferromagnetic (AFM) orderings provide a fertile field to bring about fascinating phenomena, e.g., the anomalous Hall effect, Kerr effect, Nernst effect [105–108], multiferroicity like the magnetoelectric effect [109–114], nonreciprocal transports [115], and so on. To analyze these physical properties in the FM and AFM materials systematically based on the concept of multipole, one needs to extend the classification of multipoles in the 32 crystallographic point groups [39, 40] to the 122 magnetic point groups, which cover any types of the magnetic orderings [92, 116–120].

For that purpose, we complete the classification of E, M, ET, and MT multipoles by the irreducible representations in all 122 magnetic point groups by using the representation theory for nonunitary magnetic point groups. The established multipole classification enables us to describe any AFM orderings and more exotic orderings, such as nematic, ex-

[1]Tables 2.2, 2.5–2.15, and D.1–D.3 in Appendix D and Figs. 2.1 and 2.2 are reproduced from Ref. [104] (© 2021 by the American Physical Society).

citonic, and loop-current orderings, as ferroic augmented multipole orderings. The present systematic classification is also useful for the understanding of the microscopic essential model parameters relevant to multiferroic physical phenomena, as will be discussed in Chap. 3. We also give a general relation between multipoles and the linear/second-order nonlinear response functions based on the Kubo formula. This systematic study will help the exploration and design of the functional multiferroic materials that can be utilized for future electronics and spintronics devices.

2.2 Magnetic Point Group

Most of the magnetic point groups are nonunitary groups including the antiunitary and antilinear operations accompanied by the time-reversal operation. In such a situation, the representation in the nonunitary point groups is given by a different form from that in the ordinary unitary crystallographic point groups [121]. After classifying the magnetic point groups into the three types in Sec. 2.2.1, we briefly review the representation theory of the magnetic point groups in Sec. 2.2.2.

2.2.1 Three Types of Magnetic Point Groups

The 122 magnetic point groups are classified into the following three types depending on how they include the time-reversal operation θ [122]:

(I) ordinary crystallographic point groups (32),

(II) gray point groups (32),

(III) black-and-white point groups (58),

where the numbers in parentheses are the numbers of magnetic point groups. Type-(I) ordinary crystallographic point group is the unitary point group including no antiunitary operation accompanied by θ. When $\boldsymbol{G}$ represents the type-(I) crystallographic point group, the type-(II) gray point group, $\boldsymbol{M}^{(\mathrm{II})}$, is defined as

$$\boldsymbol{M}^{(\mathrm{II})}=\boldsymbol{G}+\theta\boldsymbol{G}, \tag{2.1}$$

which includes the double elements of $\boldsymbol{G}$. Meanwhile, the type-(III) black-and-white point group, $\boldsymbol{M}^{(\mathrm{III})}$, consists of half of the elements of $\boldsymbol{M}^{(\mathrm{II})}$, which is represented as

$$\boldsymbol{M}^{(\mathrm{III})}=\boldsymbol{H}+\theta(\boldsymbol{G}-\boldsymbol{H}), \tag{2.2}$$

where $\boldsymbol{H}$ is a halving unitary subgroup of $\boldsymbol{G}$. The 58 type-(III) black-and-white point groups are uniquely determined by the combination of $\boldsymbol{G}$ and $\boldsymbol{H}$, as summarized in Table 2.1. Hereafter, we use the primary, secondary, and tertiary axes for the point-group operations as denoted in Table 2.2, unless otherwise mentioned.

Table 2.1: List of 58 black-and-white point groups $\boldsymbol{M}^{(\mathrm{III})}$. $\boldsymbol{H}$ is the unitary subgroup of $\boldsymbol{G}$, which determines $\boldsymbol{M}^{(\mathrm{III})}$. One of the antiunitary operations in $\boldsymbol{M}^{(\mathrm{III})}$, $\mathcal{A}$, and its operation axis/plane are also shown.

	$\boldsymbol{M}^{(\mathrm{III})}$	$\boldsymbol{G}$	$\boldsymbol{H}$	$\mathcal{A}$	axis/plane
cubic	$m'\bar{3}'m'$	$m\bar{3}m$ (O_h)	432 (O)	θI	
	$m'\bar{3}'m$	$m\bar{3}m$ (O_h)	$\bar{4}3m$ (T_d)	θI	
	$m\bar{3}m'$	$m\bar{3}m$ (O_h)	$m\bar{3}$ (T_h)	$\theta C_2'$	[110]
	$4'32'$	432 (O)	23 (T)	$\theta C_2'$	[110]
	$\bar{4}'3m'$	$\bar{4}3m$ (T_d)	23 (T)	$\theta\sigma_d$	$\perp$[110]
	$m'\bar{3}'$	$m\bar{3}$ (T_h)	23 (T)	θI	
hexagonal	$6/m'm'm'$	$6/mmm$ (D_6h)	622 (D_6)	θI	
	$6'/mmm'$	$6/mmm$ (D_6h)	$\bar{6}m2$ (D_3h)	θI	
	$6/m'mm$	$6/mmm$ (D_6h)	$6mm$ (C_6v)	θI	
	$6/mm'm'$	$6/mmm$ (D_6h)	$6/m$ (C_6h)	θC_{2x}	[100]
	$6'/m'mm'$	$6/mmm$ (D_6h)	$\bar{3}m$ (D_3d)	θC_2	[001]
	$62'2'$	622 (D_6)	6 (C_6)	θC_{2x}	[100]
	$6'22'$	622 (D_6)	32 (D_3)	θC_2	[001]
	$\bar{6}m'2'$	$\bar{6}m2$ (D_3h)	$\bar{6}$ (C_3h)	θC_{2y}	[010]
	$\bar{6}'m2'$	$\bar{6}m2$ (D_3h)	$3m$ (C_3v)	$\theta\sigma_h$	$\perp$[001]
	$\bar{6}'m'2$	$\bar{6}m2$ (D_3h)	32 (D_3)	$\theta\sigma_h$	$\perp$[001]
	$6m'm'$	$6mm$ (C_6v)	6 (C_6)	$\theta\sigma_x$	$\perp$[100]
	$6'mm'$	$6mm$ (C_6v)	$3m$ (C_3v)	θC_2	[001]
	$6/m'$	$6/m$ (C_6h)	6 (C_6)	θI	
	$6'/m$	$6/m$ (C_6h)	$\bar{6}$ (C_3h)	θI	
	$6'/m'$	$6/m$ (C_6h)	$\bar{3}$ (S_6)	θC_2	[001]
	$\bar{6}'$	$\bar{6}$ (C_3h)	3 (C_3)	$\theta\sigma_h$	$\perp$[001]
	$6'$	6 (C_6)	3 (C_3)	θC_2	[001]
trigonal	$\bar{3}'m'$	$\bar{3}m$ (D_3d)	32 (D_3)	θI	
	$\bar{3}'m$	$\bar{3}m$ (D_3d)	$3m$ (C_3v)	θI	
	$\bar{3}m'$	$\bar{3}m$ (D_3d)	$\bar{3}$ (S_6)	$\theta C_2'$	[010]
	$32'$	32 (D_3)	3 (C_3)	$\theta C_2'$	[010]
	$3m'$	$3m$ (C_3v)	3 (C_3)	$\theta\sigma_v$	$\perp$[010]
	$\bar{3}'$	$\bar{3}$ (S_6)	3 (C_3)	θI	
tetragonal	$4/m'm'm'$	$4/mmm$ (D_4h)	422 (D_4)	θI	
	$4'/m'm'm$	$4/mmm$ (D_4h)	$\bar{4}2m$ (D_2d)	θI	
	$4/m'mm$	$4/mmm$ (D_4h)	$4mm$ (C_4v)	θI	
	$4/mm'm'$	$4/mmm$ (D_4h)	$4/m$ (C_4h)	$\theta C_2'$	[100]
	$4'/mmm'$	$4/mmm$ (D_4h)	mmm (D_2h)	$\theta C_2''$	[110]
	$42'2'$	422 (D_4)	4 (C_4)	$\theta C_2'$	[100]
	$4'22'$	422 (D_4)	222 (D_2)	$\theta C_2''$	[110]
	$\bar{4}2'm'$	$\bar{4}2m$ (D_2d)	$\bar{4}$ (S_4)	$\theta C_2'$	[100]
	$\bar{4}'2m'$	$\bar{4}2m$ (D_2d)	222 (D_2)	$\theta\sigma_d$	$\perp$[110]
	$\bar{4}'m2'$	$\bar{4}2m$ (D_2d)	$mm2$ (C_2v)	$\theta C_2''$	[110]
	$4m'm'$	$4mm$ (C_4v)	4 (C_4)	$\theta\sigma_v$	$\perp$[100]

(Continue)

	$\boldsymbol{M}^{(\mathrm{III})}$	$\boldsymbol{G}$	$\boldsymbol{H}$	$\mathcal{A}$	axis/plane
	$4'mm'$	$4mm$ ($C_{4\mathrm{v}}$)	$mm2$ ($C_{2\mathrm{v}}$)	$\theta\sigma_d$	$\perp$[110]
	$4'/m'$	$4/m$ ($C_{4\mathrm{h}}$)	$\bar{4}$ (S_4)	θI	
	$4/m'$	$4/m$ ($C_{4\mathrm{h}}$)	4 (C_4)	θI	
	$4'/m$	$4/m$ ($C_{4\mathrm{h}}$)	$2/m$ ($C_{2\mathrm{h}}$)	θC_4	[001]
	$\bar{4}'$	$\bar{4}$ (S_4)	2 (C_2)	$\theta I C_4$	[001]
	$4'$	4 (C_4)	2 (C_2)	θC_4	[001]
orthorhombic	$m'm'm'$	mmm ($D_{2\mathrm{h}}$)	222 (D_2)	θI	
	mmm'	mmm ($D_{2\mathrm{h}}$)	$mm2$ ($C_{2\mathrm{v}}$)	θI	
	$m'm'm$	mmm ($D_{2\mathrm{h}}$)	$2/m$ ($C_{2\mathrm{h}}$)	θC_{2x}	[100]
	$2'2'2$	222 (D_2)	2 (C_2)	θC_{2x}	[100]
	$m'm'2$	$mm2$ ($C_{2\mathrm{v}}$)	2 (C_2)	$\theta\sigma_x$	$\perp$[100]
	$m'm2'$	$mm2$ ($C_{2\mathrm{v}}$)	m ($C_{1\mathrm{h}}$)	θC_{2z}	[001]
monoclinic	$2/m'$	$2/m$ ($C_{2\mathrm{h}}$)	2 (C_2)	θI	
	$2'/m$	$2/m$ ($C_{2\mathrm{h}}$)	m (C_{s})	θI	
	$2'/m'$	$2/m$ ($C_{2\mathrm{h}}$)	$\bar{1}$ (C_{i})	θC_2	[010]
	m'	m (C_{s})	1 (C_1)	$\theta\sigma$	$\perp$[010]
	$2'$	2 (C_2)	1 (C_1)	θC_2	[010]
triclinic	$\bar{1}'$	$\bar{1}$ (C_{i})	1 (C_1)	θI	

Table 2.2: Primary, secondary, and tertiary axes with respect to the symmetry operations in the Cartesian coordinates.

	primary	secondary	tertiary
cubic	$\langle 100\rangle$	$\langle 111\rangle$	$\langle 110\rangle$
tetragonal	[001]	[100]	[110]
orthorhombic	[100]	[010]	[001]
monoclinic	[010]	—	—
triclinic	—	—	—
hexagonal	[001]	[100]	[010]
trigonal	[001]	[010]	—

2.2.2 Irreducible Corepresentation of Magnetic Point Group

The irreducible representation of the type-(I) unitary crystallographic point group has been presented in the previous literatures, e.g., Ref. [123]. On the other hand, the analysis taking into account the antiunitary operation like θ is required to obtain the irreducible representations of the type-(II) and (III) magnetic point groups. Generally, the type-(II) and (III) magnetic point groups in Eqs. (2.1) and (2.2) are represented by using the unitary subgroup $\boldsymbol{G}$ and the antiunitary operation $\mathcal{A}$ as

$$\boldsymbol{M}=\boldsymbol{G}+\mathcal{A}\boldsymbol{G}. \tag{2.3}$$

The time-reversal operation θ is generally chosen as $\mathcal{A}$ in $\boldsymbol{M}^{(\mathrm{II})}$, although $\boldsymbol{M}$ is determined irrespective of the choice of $\mathcal{A}$. One of the choices of $\mathcal{A}$ in $\boldsymbol{M}^{(\mathrm{III})}$ is summarized in Table 2.1.

For the basis set of the irreducible representation Γ with dimension d_Γ in $\boldsymbol{G}$,

$$\langle\psi^\Gamma|=\langle\psi^\Gamma_1,\cdots,\psi^\Gamma_{d_\Gamma}|\,, \tag{2.4}$$

and another set

$$\mathcal{A}\,\langle\psi^\Gamma|\equiv\langle\phi^\Gamma|=\langle\phi^\Gamma_1,\cdots,\phi^\Gamma_{d_\Gamma}|\,, \tag{2.5}$$

the representation in the nonunitary point group in Eq. (2.3) is given as follows [121, 124, 125]:

$$\mathcal{R}\,\langle\psi^\Gamma,\phi^\Gamma|=\langle\psi^\Gamma,\phi^\Gamma|\begin{pmatrix}\Delta^\Gamma(\mathcal{R}) & 0\\ 0 & \left[\Delta^\Gamma(\mathcal{A}^{-1}\mathcal{R}\mathcal{A})\right]^*\end{pmatrix}\equiv\langle\psi^\Gamma,\phi^\Gamma|\,D^\Gamma(\mathcal{R}), \tag{2.6}$$

$$\mathcal{B}\,\langle\psi^\Gamma,\phi^\Gamma|=\langle\psi^\Gamma,\phi^\Gamma|\begin{pmatrix}0 & \Delta^\Gamma(\mathcal{B}\mathcal{A})\\ \left[\Delta^\Gamma(\mathcal{A}^{-1}\mathcal{B})\right]^* & 0\end{pmatrix}\equiv\langle\psi^\Gamma,\phi^\Gamma|\,D^\Gamma(\mathcal{A}), \tag{2.7}$$

where $\mathcal{R}$ ($\mathcal{B}$) represents the (anti)unitary point group operation in $\boldsymbol{M}$ and Δ^Γ is the matrix representation of Γ. The representation $D^\Gamma(\mathcal{R})$ $[D^\Gamma(\mathcal{A})]$ is the matrix representation of the "corepresentation $D\Gamma$".

The corepresentation $D\Gamma$ is classified into three cases:

$$\sum_{\mathcal{B}\in\mathcal{A}\boldsymbol{G}}\chi^\Gamma(\mathcal{B}^2)=\begin{cases}+|\boldsymbol{G}| & :\text{ case (a)},\\ -|\boldsymbol{G}| & :\text{ case (b)},\\ 0 & :\text{ case (c)},\end{cases} \tag{2.8}$$

where $|\boldsymbol{G}|$ is the order of $\boldsymbol{G}$ and $\chi^\Gamma(\mathcal{B}^2)$ is the character with respect to the unitary operation $\mathcal{B}^2$ in Γ [122, 126–130]. In case (a), $\Delta^\Gamma(\mathcal{R})$ and $\left[\Delta^\Gamma(\mathcal{A}^{-1}\mathcal{R}\mathcal{A})\right]^*$ are equivalent and $D\Gamma$ is reducible by using a unitary transformation. The irreducible form of $D\Gamma$ is expressed as

$$D^\Gamma(\mathcal{R})=\begin{pmatrix}\Delta^\Gamma(\mathcal{R}) & 0\\ 0 & \Delta^\Gamma(\mathcal{R})\end{pmatrix}\ \text{for}\ \mathcal{R}\in\boldsymbol{G}, \tag{2.9}$$

$$D^\Gamma(\mathcal{B})=\begin{pmatrix}\Delta^\Gamma(\mathcal{B}\mathcal{A}^{-1})N & 0\\ 0 & -\Delta^\Gamma(\mathcal{B}\mathcal{A}^{-1})N\end{pmatrix}\ \text{for}\ \mathcal{B}\in\mathcal{A}\boldsymbol{G}, \tag{2.10}$$

where N is the unitary matrix satisfying the relation $\Delta^\Gamma(\mathcal{R})=N[\Delta^\Gamma(\mathcal{A}^{-1}\mathcal{R}\mathcal{A})]^*N^{-1}$ [122] (See Appendix B in detail). Hereafter, we denote the irreducible corepresentation (IR-REP) in case (a) characterized by $\Delta^\Gamma(\mathcal{R})$ for $\mathcal{R}$ and $\pm\Delta^\Gamma(\mathcal{B}\mathcal{A}^{-1})N$ for $\mathcal{B}$ as $\Gamma^\pm$, e.g., $\mathrm{A}^\pm_{1\mathrm{g}}$.

On the other hand, $D\Gamma$ in case (b) composed as Eqs. (2.6) and (2.7) is irreducible, but $\Delta^\Gamma(\mathcal{R})$ and $\left[\Delta^\Gamma(\mathcal{A}^{-1}\mathcal{R}\mathcal{A})\right]^*$ are equivalent as well as case (a). In this case, $D\Gamma$ is represented by the unitary transformation as

$$D^\Gamma(\mathcal{R})=\begin{pmatrix}\Delta^\Gamma(\mathcal{R}) & 0\\ 0 & \Delta^\Gamma(\mathcal{R})\end{pmatrix}\ \text{for}\ \mathcal{R}\in\boldsymbol{G}, \tag{2.11}$$

$$D^\Gamma(\mathcal{B})=\begin{pmatrix}0 & -\Delta^\Gamma(\mathcal{B}\mathcal{A}^{-1})N\\ \Delta^\Gamma(\mathcal{B}\mathcal{A}^{-1})N & 0\end{pmatrix}\ \text{for}\ \mathcal{B}\in\mathcal{A}\boldsymbol{G}. \tag{2.12}$$

In case (c), $\Delta^{\Gamma}(\mathcal{R})$ and $\left[\Delta^{\Gamma}(\mathcal{A}^{-1}\mathcal{R}\mathcal{A})\right]^*$ are not equivalent and $D\Gamma$ is irreducible. Then, $D\Gamma$ has the form in Eqs. (2.6) and (2.7)

$$D^{\Gamma}(\mathcal{R})=\begin{pmatrix}\Delta^{\Gamma}(\mathcal{R}) & 0\\ 0 & \left[\Delta^{\Gamma}(\mathcal{A}^{-1}\mathcal{R}\mathcal{A})\right]^*\end{pmatrix} \text{ for } \mathcal{R}\in\boldsymbol{G}, \tag{2.13}$$

$$D^{\Gamma}(\mathcal{B})=\begin{pmatrix}0 & \Delta^{\Gamma}(\mathcal{B}\mathcal{A})\\ \left[\Delta^{\Gamma}(\mathcal{A}^{-1}\mathcal{B})\right]^* & 0\end{pmatrix} \text{ for } \mathcal{B}\in\mathcal{A}\boldsymbol{G}. \tag{2.14}$$

Since $D\Gamma$ in cases (b) and (c) is not block-diagonal with respect to the antiunitary operation $\mathcal{B}$, we denote their corepresentation as Γ for notational simplicity.

Finally, the Kronecker product of the IRREP is defined by using that of the unitary subgroup, whose expression is given by

$$D\Gamma_i\otimes D\Gamma_j=\sum_k d_{ij;k}D\Gamma_k, \tag{2.15}$$

where the coefficient $d_{ij,k}$ is determined by [129, 131]

$$d_{ij,k}=\frac{\frac{1}{|\boldsymbol{G}|}\sum_{\mathcal{R}\in\boldsymbol{G}}\chi^{\Gamma_i}(\mathcal{R})\chi^{\Gamma_j}(\mathcal{R})[\chi^{\Gamma_k}(\mathcal{R})]^*}{\frac{1}{|\boldsymbol{G}|}\sum_{\mathcal{R}\in\boldsymbol{G}}|\chi^{\Gamma_k}(\mathcal{R})|^2}. \tag{2.16}$$

The specific expression of $d_{ij,k}$ in the type-(II) and type-(III) magnetic point groups is presented in Ref. [132]. In Appendix B, we present the details of the representation theory in a nonunitary group.

2.3 Classification of Multipole

By using the IRREP in the previous section, we classify four types of multipoles under 122 magnetic point groups. First, we show the multipole classification in the type-(II) gray point group by taking an example of the cubic gray point group $m\bar{3}m1'$. Since the unitary subgroup $m\bar{3}m$ has 10 irreducible representations: $\mathrm{A}_{1g/u}$, $\mathrm{A}_{2g/u}$, $\mathrm{E}_{g/u}$, $\mathrm{T}_{1g/u}$, and $\mathrm{T}_{2g/u}$, 10 types of corepresentations are constructed in $m\bar{3}m1'$. By using Eq. (2.8), one finds that all of the corepresentations consisting of $\mathrm{A}_{1g/u}$, $\mathrm{A}_{2g/u}$, $\mathrm{E}_{g/u}$, $\mathrm{T}_{1g/u}$, and $\mathrm{T}_{2g/u}$ are classified into case (a). Thus, they are decomposed into two IRREPs, as shown in Table 2.3, by using the unitary matrix N in Ref. [122], such as $\mathrm{A}_{1g}\to\mathrm{A}_{1g}^{\pm}$. The sign in the superscript of IRREPs stands for the parity about the time-reversal operation θ. We show the classification of E, ET, M, and MT multipoles up to rank 4 for the 20 IRREPSs as well as the reduction to the subgroups in Table 2.3. The reduction to each subgroup describes the situation where the ferroic ordering of the multipoles presented in each left column occurs. "P. axis" in Table 2.3 represents the primary axis of the point group operations. For example, the symmetry operations of $4/mm'm'$ with P. axis [001] are represented as

$$\begin{aligned}&E, C_{4z}, C_{4z}^3, C_{4z}^2, \theta C_{2x}', \theta C_{2y}', \theta C_{2[110]}'', \theta C_{2[\bar{1}10]}'',\\ &I, IC_{4z}, IC_{4z}^3, \sigma_{\perp z}, \theta\sigma_{\perp x}, \theta\sigma_{\perp y}, \theta\sigma_{\perp[110]}, \theta\sigma_{\perp[\bar{1}10]},\end{aligned} \tag{2.17}$$

Table 2.3: Irreducible corepresentations (IRREPs) of four types of multipoles: electric (E), electric toroidal (ET), magnetic (M), and magnetic toroidal (MT) multipoles, in the type-(II) gray point group $m\bar{3}m1'$. The character table of the unitary subgroup $m\bar{3}m$ ($O_{\rm h}$) is also shown to clarify the symmetry of each multipole. The IRREPs are obtained from the irreducible representation of the unitary subgroup. The superscript "$\pm$" of IRREP stands for the parity with respect to the antiunitary operation $\mathcal{A}=\theta$.

	E	$6C_4$	$3C_4^2$	$6C_2'$	$8C_3$	I	$6IC_4$	$3\sigma_h$	$6\sigma_d$	$8IC_3$	IRREP	E	ET	MT	M	MPG	P. axis
A_{1g}	1	1	1	1	1	1	1	1	1	1	A_{1g}^+	Q_0, Q_4				$m\bar{3}m1'$	$\langle 100\rangle$
											A_{1g}^-			T_0, T_4		$m\bar{3}m$	$\langle 100\rangle$
A_{2g}	1	−1	1	−1	1	1	−1	1	−1	1	A_{2g}^+		G_{xyz}			$m\bar{3}1'$	$\langle 100\rangle$
											A_{2g}^-				M_{xyz}	$m\bar{3}m'$	$\langle 100\rangle$
E_g	2	0	2	0	−1	2	0	2	0	−1	E_g^+	Q_u, Q_{4u}				$4/mmm1'$	[001]
												Q_v, Q_{4v}				$mmm1'$	[100]
											E_g^-			T_u, T_{4u}		$4/mmm$	[001]
														T_v, T_{4v}		$4'/mmm'$	[001]
T_{1g}	3	1	−1	−1	0	3	1	−1	−1	0	T_{1g}^+	Q_{4x}^α	G_x, G_x^α			$4/m1'$	[100]
												Q_{4y}^α	G_y, G_y^α			$4/m1'$	[010]
												Q_{4z}^α	G_z, G_z^α			$4/m1'$	[001]
											T_{1g}^-			T_{4x}^α	M_x, M_x^α	$4/mm'm'$	[100]
														T_{4y}^α	M_y, M_y^α	$4/mm'm'$	[010]
														T_{4z}^α	M_z, M_z^α	$4/mm'm'$	[001]
T_{2g}	3	−1	−1	1	0	3	−1	−1	1	0	T_{2g}^+	Q_{yz}, Q_{4x}^β	G_x^β			$mmm1'$	[011]
												Q_{zx}, Q_{4y}^β	G_y^β			$mmm1'$	[101]
												Q_{xy}, Q_{4z}^β	G_z^β			$mmm1'$	[110]
											T_{2g}^-			T_{yz}, T_{4x}^β	M_x^β	$4'/mm'm$	[100]
														T_{zx}, T_{4y}^β	M_y^β	$4'/mm'm$	[010]
														T_{xy}, T_{4z}^β	M_z^β	$4'/mm'm$	[001]
A_{1u}	1	1	1	1	1	−1	−1	−1	−1	−1	A_{1u}^+		G_0, G_4			$4321'$	$\langle 100\rangle$
											A_{1u}^-				M_0, M_4	$m'\bar{3}'m'$	$\langle 100\rangle$
A_{2u}	1	−1	1	−1	1	−1	1	−1	1	−1	A_{2u}^+	Q_{xyz}				$\bar{4}3m1'$	$\langle 100\rangle$
											A_{2u}^-			T_{xyz}		$m'\bar{3}'m$	$\langle 100\rangle$
E_u	2	0	2	0	−1	−2	0	−2	0	1	E_u^+		G_u, G_{4u}			$4221'$	[001]
													G_v, G_{4v}			$\bar{4}2m1'$	[001]
											E_u^-				M_u, M_{4u}	$4/m'm'm'$	[001]
															M_v, M_{4v}	$4'/m'm'm$	[001]
T_{1u}	3	1	−1	−1	0	−3	−1	1	1	0	T_{1u}^+	Q_x, Q_x^α	G_{4x}^α			$4mm1'$	[100]
												Q_y, Q_y^α	G_{4y}^α			$4mm1'$	[010]
												Q_z, Q_z^α	G_{4z}^α			$4mm1'$	[001]
											T_{1u}^-			T_x, T_x^α	M_{4x}^α	$4/m'mm$	[100]
														T_y, T_y^α	M_{4y}^α	$4/m'mm$	[010]
														T_z, T_z^α	M_{4z}^α	$4/m'mm$	[001]
T_{2u}	3	−1	−1	1	0	−3	1	1	−1	0	T_{2u}^+	Q_x^β	G_{yz}, G_{4x}^β			$\bar{4}m21'$	[100]
												Q_y^β	G_{zx}, G_{4y}^β			$\bar{4}m21'$	[010]
												Q_z^β	G_{xy}, G_{4z}^β			$\bar{4}m21'$	[001]
											T_{2u}^-			T_x^β	M_{yz}, M_{4x}^β	$4'/m'mm'$	[100]
														T_y^β	M_{zx}, M_{4y}^β	$4'/m'mm'$	[010]
														T_z^β	M_{xy}, M_{4z}^β	$4'/m'mm'$	[001]

where we explicitly denote the operation axis or plane in the subscript. Meanwhile, those of $4/mm'm'$ with P. axis [100] are transformed in cyclic in accordance with the change of

the P. axis as

$$E, C_{4x}, C_{4x}^3, C_{4x}^2, \theta C'_{2y}, \theta C'_{2z}, \theta C''_{2[011]}, \theta C''_{2[0\bar{1}1]},$$
$$I, IC_{4x}, IC_{4x}^3, \sigma_{\perp x}, \theta\sigma_{\perp y}, \theta\sigma_{\perp z}, \theta\sigma_{\perp[011]}, \theta\sigma_{\perp[0\bar{1}1]}. \tag{2.18}$$

We perform a similar procedure to the other 31 type-(I) gray point groups. We present the classification tables of multipoles in the other 31 type-(I) gray point groups in Tables C.1–C.31 in Appendix C.

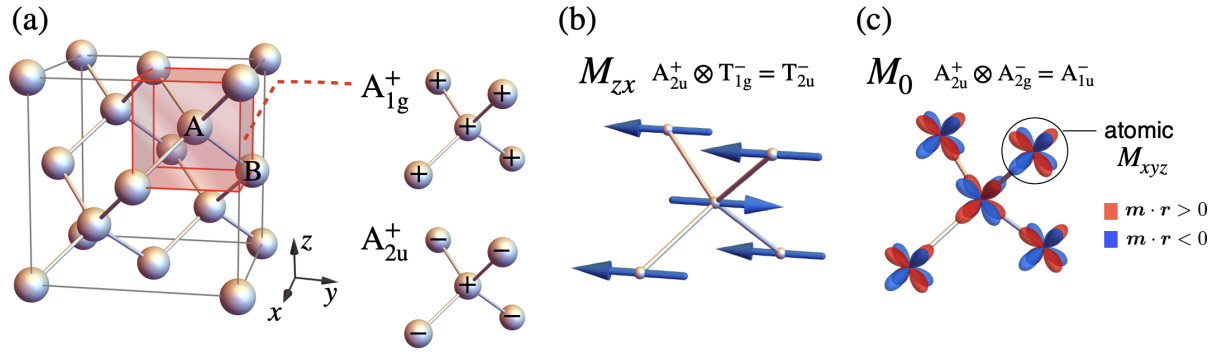

Figure 2.1: (a) Diamond structure with two sublattices A and B (left panel). The IRREPs and the corresponding potential distributions in the two sublattices are shown in the right panel. (b) The staggered M dipole along y axis, which is regarded as the cluster M quadrupole M_{zx}. (c) The staggered xyz-type M octupole, which is regarded as the cluster M monopole M_0. The arrows in (b) represent the spin direction and the color in (c) represents the distribution of the M monopole charge defined by $\boldsymbol{m}\cdot\boldsymbol{r}$.

These tables provide a guide to identifying an electronic order parameter and associated symmetry reduction. For example, we suppose the two-sublattice ordering in the diamond structure in Fig. 2.1(a) with the space group $Fd\bar{3}m$ and the magnetic point group $m\bar{3}m1'$. In the two-sublattice diamond structure, the IRREPs for the sublattice degree of freedom, $\Gamma_{\rm sub}$, are given by

$$\Gamma_{\rm sub}{=}{\rm A}_{1g}^+{\oplus}{\rm A}_{2u}^+, \tag{2.19}$$

where A_{1g}^+ corresponds to the uniform alignment of the scalar variable and A_{2u}^+ corresponds to the staggered one, as shown in the right panel of Fig. 2.1(a). Then, the spin configurations in the two-sublattice diamond structure are characterized by the IRREPs as follows:

$$\Gamma_{\rm sub}{\otimes}\Gamma_{\rm M1}{=}{\rm T}_{1g}^-{\oplus}{\rm T}_{2u}^-, \tag{2.20}$$

where $\Gamma_{\rm M1}(=\mathrm{T}_{1g}^-)$ is the IRREPs for the spin degree of freedom, i.e., the M dipole (M_x, M_y, M_z). In Eq. (2.20), the IRREP T_{1g}^- represents the uniform alignment of the M dipole, i.e., the FM order. On the other hand, the IRREP T_{2u}^-, which corresponds to the staggered magnetic structure shown in Fig. 2.1(b), is regarded as the ferroic ordering of M quadrupole from the Table 2.3[2]. In this way, one can easily identify the multipole

[2]Here and hereafter, we refer the name of the multipole orderings by adopting the lowest-rank multipoles belonging to the same irreducible (co)representation.

order parameters, and then, predict the emergent physical phenomena, as discussed in Sec. 1.5. In the present case of the staggered M dipole orderings in the diamond structure, one expects physical phenomena related to the M quadrupole, e.g., the transverse magnetoelectric effect [78].

The classification in Table 2.3 can be used not only for the FM and AFM orderings but also for the unconventional electronic orderings, such as the spin nematics [133–136], excitonic states [52–57], staggered flux states [80–83], loop-current states [36, 37, 84–87], and other higher-rank multipole orderings [14, 15, 35]. For example, when considering the orderings of the atomic M octupoles ($M_{xyz}, M_x^\alpha, M_y^\alpha, M_z^\alpha, M_x^\beta, M_y^\beta, M_z^\beta$) with the IRREPs $\Gamma_{\rm M3}=\mathrm{A}_{2g}^-\oplus\mathrm{T}_{1g}^-\oplus\mathrm{T}_{2g}^-$ in the diamond structure, the IRREPs corresponding to the two-sublattice orderings are given by

$$\Gamma_{\rm sub}\otimes\Gamma_{\rm M3}=(\mathrm{A}_{2g}^-\oplus\mathrm{T}_{1g}^-\oplus\mathrm{T}_{2g}^-)_{\rm uniform}\oplus(\mathrm{A}_{1u}^-\oplus\mathrm{T}_{1u}^-\oplus\mathrm{T}_{2u}^-)_{\rm staggered}. \tag{2.21}$$

The former (latter) parentheses represent the uniform (staggered) alignment of the M octupoles. From Table 2.3, one can find the corresponding multipole order parameters, e.g., the staggered M_{xyz} ordering with A_{1u}^- is regarded as the M monopole M_0, as schematically shown in Fig. 2.1(c). Then, one expects that the staggered M_{xyz} ordering exhibits physical phenomena driven by M_0, e.g., the longitudinal magnetoelectric effect.

Table 2.4: IRREPs of four types of multipoles in $m'\bar{3}'m'$. The character table of the irreducible representation of the unitary subgroup 432 is also presented. The superscript "±" of IRREP stands for the parity with respect to the antiunitary operation $\mathcal{A}=\theta I$.

	E	$6C_4$	$3C_4^2$	$6C_2'$	$8C_3$	IRREP	E	ET	MT	M	MPG	P. axis
A_1	1	1	1	1	1	A_1^+	Q_0, Q_4			M_0, M_4	$m'\bar{3}'m'$	$\langle 100\rangle$
						A_1^-		G_0, G_4	T_0, T_4		432	$\langle 100\rangle$
A_2	1	−1	1	−1	1	A_2^+		G_{xyz}	T_{xyz}		$m'\bar{3}'$	$\langle 100\rangle$
						A_2^-	Q_{xyz}			M_{xyz}	$\bar{4}'3m'$	$\langle 100\rangle$
E	2	0	2	0	−1	E^+	Q_u, Q_{4u}			M_u, M_{4u}	$4/m'm'm'$	[001]
							Q_v, Q_{4v}			M_v, M_{4v}	$m'm'm'$	[100]
						E^-		G_u, G_{4u}	T_u, T_{4u}		422	[001]
								G_v, G_{4v}	T_v, T_{4v}		$\bar{4}'2m'$	[001]
T_1	3	1	−1	−1	0	T_1^+	Q_{4x}^α	G_x, G_x^α	T_x, T_x^α	M_{4x}^α	$4/m'$	[100]
							Q_{4y}^α	G_y, G_y^α	T_y, T_y^α	M_{4y}^α	$4/m'$	[010]
							Q_{4z}^α	G_z, G_z^α	T_z, T_z^α	M_{4z}^α	$4/m'$	[001]
						T_1^-	Q_x, Q_x^α	G_{4x}^α	T_{4x}^α	M_x, M_x^α	$4m'm'$	[100]
							Q_y, Q_y^α	G_{4y}^α	T_{4y}^α	M_y, M_y^α	$4m'm'$	[010]
							Q_z, Q_z^α	G_{4z}^α	T_{4z}^α	M_z, M_z^α	$4m'm'$	[001]
T_2	3	−1	−1	1	0	T_2^+	Q_{yz}, Q_{4x}^β	G_x^β	T_x^β	M_{yz}, M_{4x}^β	$m'm'm'$	[011]
							Q_{zx}, Q_{4y}^β	G_y^β	T_y^β	M_{zx}, M_{4y}^β	$m'm'm'$	[101]
							Q_{xy}, Q_{4z}^β	G_z^β	T_z^β	M_{xy}, M_{4z}^β	$m'm'm'$	[110]
						T_2^-	Q_x^β	G_{yz}, G_{4x}^β	T_{yz}, T_{4x}^β	M_x^β	$\bar{4}'m'2$	[100]
							Q_y^β	G_{zx}, G_{4y}^β	T_{zx}, T_{4y}^β	M_y^β	$\bar{4}'m'2$	[010]
							Q_z^β	G_{xy}, G_{4z}^β	T_{xy}, T_{4z}^β	M_z^β	$\bar{4}'m'2$	[001]

The multipole classification in type-(III) black-and-white point group is derived by a similar procedure in the case of type-(II) gray point group. We show the result for $m'\bar{3}'m'$ as an example. Since $m'\bar{3}'m'$ consists of the unitary operations in 432 (O) and their combination to the antiunitary operation, e.g., the product of the spatial inversion and

time-reversal operations θI, the IRREPs are obtained by the irreducible representations of 432 as $A_1^{\pm}$, $A_2^{\pm}$, $E^{\pm}$, $T_1^{\pm}$, and $T_2^{\pm}$, where the sign stands for the parity with respect to θI. The multipole classification and reduction groups are summarized in Table 2.4. The classifications for the other 57 type-(III) black-and-white point groups are given in Tables C.32–C.88 in Appendix C.

By using Tables 2.3 and 2.4, we show the correspondence relation of the IRREPs for the group-subgroup relation. For example, the staggered M_{xyz}-type octupole ordering in Fig. 2.1(c) leads to the symmetry reduction as $m\bar{3}m1' \to m'\bar{3}'m'$. In this case, the IRREPs of the parent point group $m\bar{3}m1'$ are read by those of the subgroup $m'\bar{3}'m'$ as follows: $(A_{1g}^{\pm}, A_{1u}^{\mp}) \to A_1^{\pm}$, $(A_{2g}^{\pm}, A_{2u}^{\mp}) \to A_2^{\pm}$, $(E_g^{\pm}, E_u^{\mp}) \to E^{\pm}$, $(T_{1g}^{\pm}, T_{1u}^{\mp}) \to T_1^{\pm}$, $(T_{2g}^{\pm}, T_{2u}^{\mp}) \to T_2^{\pm}$. Since some of the multipoles belong to the same IRREP by the lowering of the symmetry, additional crosscouplings between different multipoles are expected, e.g., the coupling between the MT dipole (T_x, T_y, T_z) and the ET dipole (G_x, G_y, G_z) belonging to the same IRREP T_1^+. The classifications in all 122 magnetic point groups give useful and systematic information about the multipole couplings when the symmetry is lowered by the spontaneous phase transitions and the external fields.

2.4 Active Multipoles

Among the IRREPs, the totally symmetric IRREP represents nonzero multipole moments in the system. As the electronic band structures and the multiferroic properties are closely related to such active multipoles, it is important to show what types of multipoles belong to the totally symmetric IRREP in each magnetic point group. In this section, we present the active multipoles belonging to the totally symmetric IRREP in all 122 magnetic point groups.

We first show the classification of the active multiples in each magnetic point group in terms of the spatial inversion and time-reversal parities in Table 2.5. The E and ET multipoles are active for all the magnetic point groups, while the M and MT multipoles are active only for the type-(I) crystallographic point groups and type-(III) black-and-white point groups without the time-reversal symmetry. The rank and types of the active multipoles depend on the crystallographic symmetry, as will be discussed below.

We start with the discussion of the active multipoles under type-(I) crystallographic point groups, where not only E and ET multipoles but also M and MT multipoles are active because of the time-reversal symmetry ($\mathcal{T}$) breaking. The type of active multipoles depends on the spatial parity, as shown in Table 2.5. In the 11 crystallographic point groups with the spatial inversion symmetry ($\mathcal{P}$): $m\bar{3}m$, $m\bar{3}$, $4/mmm$, $4/m$, mmm, $2/m$, $\bar{1}$, $6/mmm$, $6/m$, $\bar{3}m$, and $\bar{3}$, even-parity E, ET, M, and MT multipoles are active. The specific active multipoles up to rank 4 in each crystallographic point group are shown in Table 2.6. On the other hand, in the 21 noncentrosymmetric crystallographic point groups: 432, $\bar{4}3m$, 23, 422, $\bar{4}2m$, $4mm$, 4, $\bar{4}$, 222, $mm2$, 2, m, 1, 622, $\bar{6}m2$, $6mm$, 6, $\bar{6}$, 32, $3m$, and 3, odd-parity E, ET, M, and MT multipoles become active in addition to the even-parity ones, which are summarized in Table 2.7. It is noted that the same components of Q_{lm} and T_{lm} (G_{lm} and M_{lm}) become active in the type-(I) crystallographic point groups because of the absence of the antiunitary operations accompanied by the time inversion.

Table 2.5: Active multipoles in the crystallographic point group (CPG), gray point group (GPG), and black-and-white point group (BWPG) according to the spatial inversion symmetry ($\mathcal{P}$), time-reversal symmetry ($\mathcal{T}$), and spece-and-time inversion symmetry ($\mathcal{PT}$). "even/odd-parity" represents the spatial inversion parity of multipoles.

type	magnetic point group	$\mathcal{P}$	$\mathcal{T}$	$\mathcal{PT}$	even-parity E, ET	odd-parity E, ET	even-parity MT, M	odd-parity MT, M
(I) CPG	$m\bar{3}m$, $m\bar{3}$, $4/mmm$, $4/m$, mmm, $2/m$, $\bar{1}$, $6/mmm$, $6/m$, $\bar{3}m$, $\bar{3}$	◯	×	×	✓		✓	
	432, $\bar{4}3m$, 23, 422, $\bar{4}2m$, $4mm$, 4, $\bar{4}$, 222, $mm2$, 2, m, 1, 622, $\bar{6}m2$, $6mm$, 6, $\bar{6}$, 32, $3m$, 3	×	×	×	✓	✓	✓	✓
(II) GPG	$m\bar{3}m1'$, $m\bar{3}1'$, $4/mmm1'$, $4/m1'$, $mmm1'$, $2/m1'$, $\bar{1}1'$, $6/mmm1'$, $6/m1'$, $\bar{3}m1'$, $\bar{3}1'$	◯	◯	◯	✓			
	$4321'$, $\bar{4}3m1'$, $231'$, $4221'$, $\bar{4}2m1'$, $4mm1'$, $41'$, $\bar{4}1'$, $2221'$, $mm21'$, $21'$, $m1'$, $11'$, $6221'$, $\bar{6}m21'$, $6mm1'$, $61'$, $\bar{6}1'$, $321'$, $3m1'$, $31'$	×	◯	×	✓	✓		
(III) BWPG	$m\bar{3}m'$, $4/mm'm'$, $4'/mm'm$, $4'/m$, $m'm'm$, $2'/m'$, $6/mm'm'$, $6'/m'mm'$, $6'/m'$, $\bar{3}m'$	◯	×	×	✓		✓	
	$m'\bar{3}'m'$, $m'\bar{3}'m$, $m'\bar{3}'$, $4/m'm'm'$, $4'/m'm'm$, $4/m'mm$, $4'/m'$, $4/m'$, $m'm'm'$, $m'mm$, $2'/m$, $2/m'$, $\bar{1}'$, $6/m'm'm'$, $6'/mmm'$, $6/m'mm$, $6'/m$, $6/m'$, $\bar{3}'m'$, $\bar{3}'m$, $\bar{3}'$	×	×	◯	✓			✓
	$4'32'$, $\bar{4}'3m'$, $42'2'$, $4'22'$, $\bar{4}2'm'$, $\bar{4}'2m'$, $\bar{4}'2'm$, $4m'm'$, $4'm'm$, $4'$, $\bar{4}'$, $2'2'2$, $m'm'2$, $m'm2'$, $2'$, m', $62'2'$, $6'22'$, $\bar{6}m'2'$, $\bar{6}'m'2$, $\bar{6}'m2'$, $6m'm'$, $6'mm'$, $6'$, $\bar{6}'$, $32'$, $3m'$	×	×	×	✓	✓	✓	✓

In the case of the type-(II) gray point groups, no M and MT multipoles become active because of the presence of the time-reversal symmetry [39]. The even-parity E and ET multipoles are active in all the type-(II) gray point groups, while the odd-parity E and ET ones become active in the noncentrosymmetric 21 point groups: $4321'$, $\bar{4}3m1'$, $231'$, $4221'$, $\bar{4}2m1'$, $4mm1'$, $41'$, $\bar{4}1'$, $2221'$, $mm21'$, $21'$, $m1'$, $11'$, $6221'$, $\bar{6}m21'$, $6mm1'$, $61'$, $\bar{6}1'$, $321'$, $3m1'$, and $31'$. The active even-parity E and ET multipoles in the centrosymmetric 11 gray point groups are summarized in Table 2.8, while the E and ET multipoles in the noncentrosymmetric 21 gray point groups are shown in Table 2.9.

In the type-(III) black-and-white point groups, not only E and ET multipoles but also M and MT multipoles become active, similar to the type-(I) crystallographic point groups. In contrast to type-(I) crystallographic point groups, however, the different components of Q_{lm} and T_{lm} (G_{lm} and M_{lm}) become active because of the difference in the symmetry operations, i.e., the product operations of the time-reversal and unitary point-

Table 2.6: Active even-parity E, ET, MT, and M multipoles in the centrosymmetric crystallographic point groups. The triclinic point group $\bar{1}$ ($C_{\rm i}$), in which all the even-parity multipoles are active, is omitted.

	even-parity					even-parity				
	E			ET		MT			M	
	l=0	2	4	1	3	0	2	4	1	3
$m\bar{3}m$ ($O_{\rm h}$)	Q_0		Q_4			T_0		T_4		
$m\bar{3}$ ($T_{\rm h}$)	Q_0		Q_4		G_{xyz}	T_0		T_4		M_{xyz}
$4/mmm$ ($D_{4{\rm h}}$)	Q_0	Q_u	Q_4, Q_{4u}			T_0	T_u	T_4, T_{4u}		
$4/m$ ($C_{4{\rm h}}$)	Q_0	Q_u	$Q_4, Q_{4u}, Q^\alpha_{4z}$	G_z	G^α_z	T_0	T_u	$T_4, T_{4u}, T^\alpha_{4z}$	M_z	M^α_z
mmm ($D_{2{\rm h}}$)	Q_0	Q_u, Q_v	Q_4, Q_{4u}, Q_{4v}		G_{xyz}	T_0	T_u, T_v	T_4, T_{4u}, T_{4v}		M_{xyz}
$2/m$ ($C_{2{\rm h}}$)	Q_0	Q_u, Q_v, Q_{zx}	Q_4, Q_{4u}, Q_{4v}, Q^α_{4y}, Q^β_{4y}	G_y	G_{xyz}, G^α_y, G^β_y	T_0	T_u, T_v, T_{zx}	T_4, T_{4u}, T_{4v}, T^α_{4y}, T^β_{4y}	M_y	M_{xyz}, M^α_y, M^β_y
$6/mmm$ ($D_{6{\rm h}}$)	Q_0	Q_u	Q_{40}			T_0	T_u	T_{40}		
$6/m$ ($C_{6{\rm h}}$)	Q_0	Q_u	Q_{40}	G_z	G^α_z	T_0	T_u	T_{40}	M_z	M^α_z
$\bar{3}m$ ($D_{3{\rm d}}$)	Q_0	Q_u	Q_{40}, Q_{4b}		G_{3b}	T_0	T_u	T_{40}, T_{4b}		M_{3b}
$\bar{3}$ (S_6)	Q_0	Q_u	Q_{40}, Q_{4a}, Q_{4b}	G_z	G^α_z, G_{3a}, G_{3b}	T_0	T_u	T_{40}, T_{4a}, T_{4b}	M_z	M^α_z, M_{3a}, M_{3b}

group operations. The type-(III) black-and-white point groups are classified into three types according to the presence/absence of the $\mathcal{P}$ and $\mathcal{PT}$ symmetries. The first one is the 10 black-and-white point groups with $(\mathcal{P},\mathcal{PT})$=(◯, ×): $m\bar{3}m'$, $4/mm'm'$, $4'/mm'm$, $4'/m$, $m'm'm$, $2'/m'$, $6/mm'm'$, $6'/m'mm'$, $6'/m'$, and $\bar{3}m'$, where the even-parity E, ET, M, and MT multipoles are active, as shown in Table 2.10. The second one is the 21 black-and-white point groups with $(\mathcal{P},\mathcal{PT})$=(×, ◯): $m'\bar{3}'m'$, $m'\bar{3}'m$, $m'\bar{3}'$, $4/m'm'm'$, $4'/m'm'm$, $4/m'mm$, $4'/m'$, $4/m'$, $m'm'm'$, $m'mm$, $2'/m$, $2/m'$, $\bar{1}'$, $6/m'm'm'$, $6'/mmm'$, $6/m'mm$, $6'/m$, $6/m'$, $\bar{3}'m'$, $\bar{3}'m$, and $\bar{3}'$, where the even-parity E and ET multipoles and the odd-parity M and MT multipoles become active, as shown in Table 2.11. The last one is the 27 black-and-white point groups with $(\mathcal{P},\mathcal{PT})$=(×, ×): $4'32'$, $\bar{4}'3m'$, $42'2'$, $4'22'$, $\bar{4}2'm'$, $\bar{4}'2m'$, $\bar{4}'2'm$, $4m'm'$, $4'm'm$, $4'$, $\bar{4}'$, $2'2'2$, $m'm'2$, $m'm2'$, $2'$, m', $62'2'$, $6'22'$, $\bar{6}m'2'$, $\bar{6}'m'2$, $\bar{6}'m2'$, $6m'm'$, $6'mm'$, $6'$, $\bar{6}'$, $32'$, and $3m'$. In this type of black-and-white point groups, all types of the multipoles become active, as summarized in Table 2.12.

Let us remark on the active multipoles from the standpoint of the (magnetic) Laue group, which has been often used for diffraction measurement. The even-parity E and ET multipoles are well classified by 11 Laue groups: $m\bar{3}m$, $m\bar{3}$, $4/mmm$, $4/m$, mmm, $6/mmm$, $6/m$, $\bar{3}m$, $\bar{3}$, $2/m$, and $\bar{1}$, whose correspondence to the magnetic point groups is summarized in Table D.1 in Appendix D. Meanwhile, the even-parity M and MT multipoles are well classified by 32 magnetic Laue groups: $m\bar{3}m1'$, $m\bar{3}1'$, $4/mmm1'$, $4/m1'$, $mmm1'$, $6/mmm1'$, $6/m1'$, $\bar{3}m1'$, $\bar{3}1'$, $2/m1'$, $\bar{1}1'$, $m\bar{3}m$, $m\bar{3}$, $4/mmm$, $4/m$, mmm, $6/mmm$, $6/m$, $\bar{3}m$, $\bar{3}$, $2/m$, $\bar{1}$, $m\bar{3}m'$, $4/mm'm'$, $4'/mm'm$, $4'/m$, $m'm'm$, $6/mm'm'$, $6'/m'mm'$, $6'/m'$, $\bar{3}m'$, and $2'/m'$. The correspondence between the magnetic Laue groups and magnetic point groups is shown in Tables D.2 and D.3 in Appendix D.

Tables 2.6–2.12 are useful to identify the type of the ferroic states with arbitrary multipole moments [137]. For example, the ferroelectric, ferromagnetic, ferrotoroidal, and ferroaxial states correspond to the states with active E dipole Q_i (i=x, y, z), M dipole M_i, MT dipole T_i, and ET dipole G_i, respectively [138–143]. One can easily find all the magnetic point groups to possess these active dipoles from Tables 2.6–2.12 as follows:

Table 2.7: Active E, ET, MT, and M multipoles in the noncentrosymmetric crystallographic point groups. The triclinic point group 1 (C_1), in which all the multipoles are active, is omitted.

	even-parity					odd-parity					even-parity					odd-parity				
	E			ET		E		ET			MT			M		MT		M		
	l=0	2	4	1	3	1	3	0	2	4	0	2	4	1	3	1	3	0	2	4
432 (O)	Q_0		Q_4					G_0		G_4	T_0		T_4					M_0		M_4
$\bar{4}3m$ ($T_{\rm d}$)	Q_0		Q_4				Q_{xyz}				T_0		T_4				T_{xyz}			
23 (T)	Q_0		Q_4		G_{xyz}		Q_{xyz}	G_0		G_4	T_0		T_4		M_{xyz}		T_{xyz}	M_0		M_4
422 (D_4)	Q_0	Q_u	Q_4					G_0	G_u	G_4	T_0	T_u	T_4					M_0	M_u	M_4
			Q_{4u}							G_{4u}			T_{4u}							M_{4u}
$\bar{4}2m$ ($D_{2\rm d}$)	Q_0	Q_u	Q_4				Q_{xyz}		G_v	G_{4v}	T_0	T_u	T_4				T_{xyz}		M_v	M_{4v}
			Q_{4u}										T_{4u}							
$4mm$ ($C_{4\rm v}$)	Q_0	Q_u	Q_4			Q_z	Q_z^α			G_{4z}^α	T_0	T_u	T_4			T_z	T_z^α			M_{4z}^α
			Q_{4u}										T_{4u}							
4 (C_4)	Q_0	Q_u	Q_4	G_z	G_z^α	Q_z	Q_z^α	G_0	G_u	G_4	T_0	T_u	T_4	M_z	M_z^α	T_z	T_z^α	M_0	M_u	M_4
			Q_{4u}							G_{4u}			T_{4u}							M_{4u}
			Q_{4z}^α							G_{4z}^α			T_{4z}^α							M_{4z}^α
$\bar{4}$ (S_4)	Q_0	Q_u	Q_4	G_z	G_z^α		Q_{xyz}		G_v	G_{4v}	T_0	T_u	T_4	M_z	M_z^α		T_{xyz}		M_v	M_{4v}
			Q_{4u}				Q_z^β		G_{xy}	G_{4z}^β			T_{4u}				T_z^β		M_{xy}	M_{4z}^β
			Q_{4z}^α										T_{4z}^α							
222 (D_2)	Q_0	Q_u	Q_4		G_{xyz}		Q_{xyz}	G_0	G_u	G_4	T_0	T_u	T_4		M_{xyz}		T_{xyz}	M_0	M_u	M_4
		Q_v	Q_{4u}						G_v	G_{4u}		T_v	T_{4u}						M_v	M_{4u}
			Q_{4v}							G_{4v}			T_{4v}							M_{4v}
$mm2$ ($C_{2\rm v}$)	Q_0	Q_u	Q_4		G_{xyz}	Q_z	Q_z^α		G_{xy}	G_{4z}^α	T_0	T_u	T_4		M_{xyz}	T_z	T_z^α		M_{xy}	M_{4z}^α
		Q_v	Q_{4u}				Q_z^β			G_{4z}^β		T_v	T_{4u}				T_z^β			M_{4z}^β
			Q_{4v}										T_{4v}							
2 (C_2)	Q_0	Q_u	Q_4	G_y	G_{xyz}	Q_y	Q_{xyz}	G_0	G_u	G_4	T_0	T_u	T_4	M_y	M_{xyz}	T_y	T_{xyz}	M_0	M_u	M_4
		Q_v	Q_{4u}		G_y^α		Q_y^α		G_v	G_{4u}		T_v	T_{4u}		M_y^α		T_y^α		M_v	M_{4u}
		Q_{zx}	Q_{4v}		G_y^β		Q_y^β		G_{zx}	G_{4v}		T_{zx}	T_{4v}		M_y^β		T_y^β		M_{zx}	M_{4v}
			Q_{4y}^α							G_{4y}^α			T_{4y}^α							M_{4y}^α
			Q_{4y}^β							G_{4y}^β			T_{4y}^β							M_{4y}^β
m ($C_{\rm s}$)	Q_0	Q_u	Q_4	G_y	G_{xyz}	Q_z	Q_z^α		G_{xy}	G_{4z}^α	T_0	T_u	T_4	M_y	M_{xyz}	T_z	T_z^α		M_{xy}	M_{4z}^α
		Q_v	Q_{4u}		G_y^α	Q_x	Q_x^α		G_{yz}	G_{4x}^α		T_v	T_{4u}		M_y^α	T_x	T_x^α		M_{yz}	M_{4x}^α
		Q_{zx}	Q_{4v}		G_y^β		Q_z^β			G_{4z}^β		T_{zx}	T_{4v}		M_y^β		T_z^β			M_{4z}^β
			Q_{4y}^α				Q_x^β			G_{4x}^β			T_{4y}^α				T_x^β			M_{4x}^β
			Q_{4y}^β										T_{4y}^β							
622 (D_6)	Q_0	Q_u	Q_{40}					G_0	G_u	G_{40}	T_0	T_u	T_{40}					M_0	M_u	M_{40}
$\bar{6}m2$ ($D_{3\rm h}$)	Q_0	Q_u	Q_{40}				Q_{3b}			G_{4b}	T_0	T_u	T_{40}				T_{3b}			M_{4b}
$6mm$ ($C_{6\rm v}$)	Q_0	Q_u	Q_{40}			Q_z	Q_z^α				T_0	T_u	T_{40}			T_z	T_z^α			
6 (C_6)	Q_0	Q_u	Q_{40}	G_z	G_z^α	Q_z	Q_z^α	G_0	G_u	G_{40}	T_0	T_u	T_{40}	M_z	M_z^α	T_z	T_z^α	M_0	M_u	M_{40}
$\bar{6}$ ($C_{3\rm h}$)	Q_0	Q_u	Q_{40}	G_z	G_z^α		Q_{3a}			G_{4a}	T_0	T_u	T_{40}	M_z	M_z^α		T_{3a}			M_{4a}
							Q_{3b}			G_{4b}							T_{3b}			M_{4b}
32 (D_3)	Q_0	Q_u	Q_{40}		G_{3b}		Q_{3b}	G_0	G_u	G_{40}	T_0	T_u	T_{40}		M_{3b}		T_{3b}	M_0	M_u	M_{40}
			Q_{4b}							G_{4b}			T_{4b}							M_{4b}
$3m$ ($C_{3\rm v}$)	Q_0	Q_u	Q_{40}		G_{3b}	Q_z	Q_{3a}			G_{4a}	T_0	T_u	T_{40}		M_{3b}	T_z	T_{3a}			M_{4a}
			Q_{4b}				Q_z^α						T_{4b}				T_z^α			
3 (C_3)	Q_0	Q_u	Q_{40}	G_z	G_{3a}	Q_z	Q_{3a}	G_0	G_u	G_{40}	T_0	T_u	T_{40}	M_z	M_{3a}	T_z	T_{3a}	M_0	M_u	M_{40}
			Q_{4a}		G_{3b}		Q_{3b}			G_{4a}			T_{4a}		M_{3b}		T_{3b}			M_{4a}
			Q_{4b}		G_z^α		Q_z^α			G_{4b}			T_{4b}		M_z^α		T_z^α			M_{4b}

- E dipole:
  $4mm1'$, $41'$, $mm21'$, $6mm1'$, $61'$, $3m1'$, $31'$, $21'$, $m1'$, $11'$, $4mm$, 4, $mm2$, $6mm$, 6,

Table 2.8: Active even-parity E and ET multipoles in the centrosymmetric gray point groups. The triclinic point group $\bar{1}1'$, in which all the even-parity E and ET multipoles are active, is omitted.

	even-parity				
	E			ET	
	l=0	2	4	1	3
$m\bar{3}m1'$	Q_0		Q_4		
$m\bar{3}1'$	Q_0		Q_4		G_{xyz}
$4/mmm1'$	Q_0	Q_u	Q_4, Q_{4u}		
$4/m1'$	Q_0	Q_u	$Q_4, Q_{4u}, Q^{\alpha}_{4z}$	G_z	G^{α}_z
$mmm1'$	Q_0	Q_u, Q_v	Q_4, Q_{4u}, Q_{4v}		G_{xyz}
$2/m1'$	Q_0	Q_u, Q_v, Q_{zx}	Q_4, Q_{4u}, Q_{4v}, Q^{α}_{4y}, Q^{β}_{4y}	G_y	G_{xyz}, G^{α}_y, G^{β}_y
$6/mmm1'$	Q_0	Q_u	Q_{40}		
$6/m1'$	Q_0	Q_u	Q_{40}	G_z	G^{α}_z
$\bar{3}m1'$	Q_0	Q_u	Q_{40}, Q_{4b}		G_{3b}
$\bar{3}1'$	Q_0	Q_u	Q_{40}, Q_{4a}, Q_{4b}	G_z	G_{3a}, G_{3b}, G^{α}_z

Table 2.9: Active E and ET multipoles in the noncentrosymmetric gray point groups. The triclinic point group $11'$, in which all the E and ET multipoles are active, is omitted.

	even-parity					odd-parity				
	E			ET		E		ET		
	l=0	2	4	1	3	1	3	0	2	4
$4321'$	Q_0		Q_4					G_0		G_4
$\bar{4}3m1'$	Q_0		Q_4				Q_{xyz}			
$231'$	Q_0		Q_4		G_{xyz}		Q_{xyz}	G_0		G_4
$4221'$	Q_0	Q_u	Q_4, Q_{4u}					G_0	G_u	G_4, G_{4u}
$\bar{4}2m1'$	Q_0	Q_u	Q_4, Q_{4u}				Q_{xyz}		G_v	G_{4v}
$4mm1'$	Q_0	Q_u	Q_4, Q_{4u}			Q_z	Q^{α}_z			G^{α}_{4z}
$41'$	Q_0	Q_u	$Q_4, Q_{4u}, Q^{\alpha}_{4z}$	G_z	G^{α}_z	Q_z	Q^{α}_z	G_0	G_u	G_4, G_{4u}, G^{α}_{4z}
$\bar{4}1'$	Q_0	Q_u	$Q_4, Q_{4u}, Q^{\alpha}_{4z}$	G_z	G^{α}_z		Q_{xyz}, Q^{β}_z		G_v, G_{xy}	G_{4v}, G^{β}_{4z}
$2221'$	Q_0	Q_u, Q_v	Q_4, Q_{4u}, Q_{4v}		G_{xyz}		Q_{xyz}	G_0	G_u, G_v	G_4, G_{4u}, G_{4v}
$mm21'$	Q_0	Q_u, Q_v	Q_4, Q_{4u}, Q_{4v}		G_{xyz}	Q_z	Q^{α}_z, Q^{β}_z		G_{xy}	$G^{\alpha}_{4z}, G^{\beta}_{4z}$
$21'$	Q_0	Q_u, Q_v, Q_{zx}	Q_4, Q_{4u}, Q_{4v}, Q^{α}_{4y}, Q^{β}_{4y}	G_y	G_{xyz}, G^{α}_y, G^{β}_y	Q_y	Q_{xyz}, $Q^{\alpha}_y, Q^{\beta}_y$	G_0	G_u, G_v, G_{zx}	G_4, G_{4u}, G_{4v}, G^{α}_{4y}, G^{β}_{4y}
$m1'$	Q_0	Q_u, Q_v, Q_{zx}	Q_4, Q_{4u}, Q_{4v}, Q^{α}_{4y}, Q^{β}_{4y}	G_y	G_{xyz}, G^{α}_y, G^{β}_y	Q_z, Q_x	Q^{α}_z, Q^{α}_x, Q^{β}_z, Q^{β}_x		G_{xy}, G_{yz}	G^{α}_{4z}, G^{α}_{4x}, G^{β}_{4z}, G^{β}_{4x}
$6221'$	Q_0	Q_u	Q_{40}					G_0	G_u	G_{40}
$\bar{6}m21'$	Q_0	Q_u	Q_{40}				Q_{3b}			G_{4b}
$6mm1'$	Q_0	Q_u	Q_{40}			Q_z	Q^{α}_z			
$61'$	Q_0	Q_u	Q_{40}	G_z	G^{α}_z	Q_z	Q^{α}_z	G_0	G_u	G_{40}
$\bar{6}1'$	Q_0	Q_u	Q_{40}	G_z	G^{α}_z		Q_{3a}, Q_{3b}			G_{4a}, G_{4b}
$321'$	Q_0	Q_u	Q_{40}, Q_{4b}		G_{3b}		Q_{3b}	G_0	G_u	G_{40}, G_{4b}
$3m1'$	Q_0	Q_u	Q_{40}, Q_{4b}		G_{3b}	Q_z	Q_{3a}, Q^{α}_z			G_{4a}
$31'$	Q_0	Q_u	Q_{40}, Q_{4a}, Q_{4b}	G_z	G_{3a}, G_{3b}, G^{α}_z	Q_z	Q_{3a}, Q_{3b}, Q^{α}_z	G_0	G_u	G_{40}, G_{4a}, G_{4b}

$3m$, 3, 2, m, 1, $4m'm'$, $4'm'm$, $4'$, $m'm'2$, $m'm2'$, $6m'm'$, $6'mm'$, $6'$, $3m'$, $2'$, m',

- M dipole:
  $4/m$, $\bar{4}$, 4, $6/m$, $\bar{6}$, 6, $\bar{3}$, 3, $\bar{1}$, 1, $2/m$, 2, m, $4/mm'm'$, $42'2'$, $4m'm'$, $\bar{4}2'm'$, $m'm'm$, $2'2'2$, $m'm'2$, $m'm2'$, $6/mm'm'$, $62'2'$, $6m'm'$, $\bar{6}m'2'$, $\bar{3}m'$, $3m'$, $32'$, $2'/m'$, $2'$, m',

Table 2.10: Active even-parity E, ET, MT, and M multipoles in the centrosymmetric black-and-white point groups.

	even-parity					even-parity				
	E			ET		MT			M	
	l=0	2	4	1	3	0	2	4	1	3
$m\bar{3}m'$	Q_0		Q_4							M_{xyz}
$4/mm'm'$	Q_0	Q_u	Q_4, Q_{4u}					T^{α}_{4z}	M_z	M^{α}_z
$4'/mmm'$	Q_0	Q_u	Q_4, Q_{4u}				T_v	T_{4v}		M_{xyz}
$4'/m$	Q_0	Q_u	Q_4, Q_{4u}, Q^{α}_{4z}	G_z	G^{α}_z		T_v, T_{xy}	T_{4v}, T^{β}_{4z}		M_{xyz}, M^{β}_z
$m'm'm$	Q_0	Q_u, Q_v	Q_4, Q_{4u}, Q_{4v}		G_{xyz}		T_{xy}	T^{α}_{4z}, T^{β}_{4z}	M_z	M^{α}_z, M^{β}_z
$2'/m'$	Q_0	Q_u, Q_v, Q_{zx}	Q_4, Q_{4u}, Q_{4v}, Q^{α}_{4y}, Q^{β}_{4y}	G_y	G_{xyz}, G^{α}_y, G^{β}_y		T_{xy}, T_{yz}	T^{α}_{4z}, T^{α}_{4x}, T^{β}_{4z}, T^{β}_{4x}	M_z, M_x	M^{α}_z, M^{α}_x, M^{β}_z, M^{β}_x
$6/mm'm'$	Q_0	Q_u	Q_{40}						M_z	M^{α}_z
$6'/m'mm'$	Q_0	Q_u	Q_{40}					T_{4a}		M_{3a}
$6'/m'$	Q_0	Q_u	Q_{40}	G_z	G^{α}_z			T_{4a}, T_{4b}		M_{3a}, M_{3b}
$\bar{3}m'$	Q_0	Q_u	Q_{40}, Q_{4b}		G_{3b}			T_{4a}	M_z	M_{3a}, M^{α}_z

- MT dipole:
  $4mm$, 4, $mm2$, $6mm$, 6, $3m$, 3, 2, m, 1, $4/m'mm$, $4/m'$, mmm', $6/m'mm$, $6/m'$, $\bar{3}'m$, $\bar{3}'$, $2'/m$, $2/m'$, $\bar{1}'$, $42'2'$, $\bar{4}'2'm$, $\bar{4}'$, $2'2'2$, $m'm2'$, $62'2'$, $\bar{6}'m2'$, $\bar{6}'$, $32'$, m', $2'$,

- ET dipole:
  $4/m1'$, $41'$, $\bar{4}1'$, $6/m1'$, $61'$, $\bar{6}1'$, $\bar{3}1'$, $31'$, $2/m1'$, $21'$, $m1'$, $\bar{1}1'$, $11'$, $4/m$, 4, $\bar{4}$, $6/m$, 6, $\bar{6}$, $\bar{3}$, 3, $2/m$, 2, m, $\bar{1}$, 1, $4'/m'$, $4/m'$, $4'/m$, $4'$, $\bar{4}'$, $6'/m'$, $6/m'$, $6'/m$, $6'$, $\bar{6}'$, $\bar{3}'$, $2'/m'$, $2/m'$, $2'/m$, $2'$, m', $\bar{1}'$.

The above example means that our multipole classification includes the previous classification for the ferroelectric, ferromagnetic, ferrotoroidal, and ferroaxial states based on the symmetry analyses [95, 141, 144–146]. Furthermore, Tables 2.6–2.12 unveil unconventional order parameters other than the dipoles, e.g., E/M/MT/ET quadrupoles and octupoles. Thus, the present classification gives a complete guide to systematically identifying the electronic order parameters.

Tables 2.6–2.12 also enable us to understand a clue of multiferroic phenomena through the couplings between the multipoles at the microscopic level. Let us take an example of the cubic crystal with $m\bar{3}m1'$ symmetry, where the E monopole Q_0 and E hexadecapole Q_4 are active up to rank 4 as shown in Table 2.8. Once the spontaneous symmetry breaking to $m'\bar{3}'m'$ occurs, M monopole M_0 and M hexadecapole M_4 are additionally activated as shown in Table 2.11. In such a situation, there are additional contributions including M_0 and M_4 to the free energy in the form of the multipole coupling between (Q_0, Q_4) and (M_0, M_4). Similarly, one can always perform the Landau free energy expansion in terms of any multipole order parameters systematically by using Tables 2.6–2.12 [11, 13].

Moreover, one can immediately find the additional active multipoles induced by external fields like electric and magnetic fields. For example, when the symmetry is lowered from $m'\bar{3}'m'$ to $4m'm'$ under the magnetic field along the z axis, H_z, the additional active multipoles up to rank 4 are represented by $Q_z, Q_u, Q^{\alpha}_z, Q_{4u}, G^{\alpha}_{4z}, M_z, M_u, M^{\alpha}_z, M_{4u}$, and T^{α}_{4z}, as shown in Table 2.12. Then, there are the additional multipole couplings, which become the source of the field-induced multiferroic phenomena. For example, since Q_z and Q_u, which correspond to the electric polarization P_z and the $(3z^2-r^2)$-type symmet-

Table 2.11: Active even-parity E and ET multipoles and odd-parity MT and M multipoles in the noncentrosymmetric black-and-white point groups with the $\mathcal{PT}$ symmetry. The triclinic point group $\bar{1}'$ is omitted, where all the even-parity E and ET multipoles and odd-parity MT and M multipoles are active.

	even-parity					odd-parity				
	E			ET		MT		M		
	l=0	2	4	1	3	1	3	0	2	4
$m'\bar{3}'m'$	Q_0		Q_4					M_0		M_4
$m'\bar{3}'m$	Q_0		Q_4				T_{xyz}			
$m'\bar{3}'$	Q_0		Q_4		G_{zyz}		T_{xyz}	M_0		M_4
$4/m'm'm'$	Q_0	Q_u	Q_4, Q_{4u}					M_0	M_u	M_4, M_{4u}
$4'/m'm'm$	Q_0	Q_u	Q_4, Q_{4u}				T_{xyz}		M_v	M_{4v}
$4/m'mm$	Q_0	Q_u	Q_4, Q_{4u}			T_z	T_z^α			M_{4z}^α
$4'/m'$	Q_0	Q_u	Q_4, Q_{4u}, Q_{4z}^α	G_z	G_z^α		T_{xyz}, T_z^β		M_v, M_{xy}	M_{4v}, M_{4z}^β
$4/m'$	Q_0	Q_u	Q_4, Q_{4u}, Q_{4z}^α	G_z	G_z^α	T_z	T_z^α	M_0	M_u	M_4, M_{4u}, M_{4z}^α
mmm'	Q_0	Q_u, Q_v	Q_4, Q_{4u}, Q_{4v}		G_{xyz}	T_z	T_z^α, T_z^β		M_{xy}	M_{4z}^α, M_{4z}^β
$m'm'm'$	Q_0	Q_u, Q_v	Q_4, Q_{4u}, Q_{4v}		G_{xyz}		T_{xyz}	M_0	M_u, M_v	M_4, M_{4u}, M_{4v}
$2'/m$	Q_0	Q_u, Q_v, Q_{zx}	Q_4, Q_{4u}, Q_{4v}, Q_{4y}^α, Q_{4y}^β	G_y	G_{xyz}, G_y^α, G_y^β	T_z, T_x	T_z^α, T_x^α, T_z^β, T_x^β		M_{xy}, M_{yz}	M_{4z}^α, M_{4x}^α, M_{4z}^β, M_{4x}^β
$2/m'$	Q_0	Q_u, Q_v, Q_{zx}	Q_4, Q_{4u}, Q_{4v}, Q_{4y}^α, Q_{4y}^β	G_y	G_{xyz}, G_y^α, G_y^β	T_y	T_{xyz}, T_y^α, T_y^β	M_0	M_u, M_v, M_{zx}	M_4, M_{4u}, M_{4v}, M_{4y}^α, M_{4y}^β
$6/m'm'm'$	Q_0	Q_u	Q_{40}					M_0	M_u	M_{40}
$6'/mmm'$	Q_0	Q_u	Q_{40}				T_{3b}			M_{4b}
$6/m'mm$	Q_0	Q_u	Q_{40}			T_z	T_z^α			
$6'/m$	Q_0	Q_u	Q_{40}	G_z	G_z^α		T_{3a}, T_{3b}			M_{4a}, M_{4b}
$6/m'$	Q_0	Q_u	Q_{40}	G_z	G_z^α	T_z	T_z^α	M_0	M_u	M_{40}
$\bar{3}'m'$	Q_0	Q_u	Q_{40}, Q_{4b}		G_{3b}		T_{3b}	M_0	M_u	M_{40}, M_{4b}
$\bar{3}'m$	Q_0	Q_u	Q_{40}, Q_{4b}		G_{3b}	T_z	T_{3a}, T_z^α			M_{4a}
$\bar{3}'$	Q_0	Q_u	Q_{40}, Q_{4a}, Q_{4b}	G_z	G_z^α, G_{3a}, G_{3b}	T_z	T_z^α, T_{3a}, T_{3b}	M_0	M_u	M_{40}, M_{4a}, M_{4b}

ric strain ε_u, respectively, become active, one expects that the magnetoelectric coupling $H_z P_z$ and magnetoelastic coupling $H_z \varepsilon_u$ appear in the free energy expansion.

In addition, our result can be used when constructing the so-called hyperfine coupling to investigate the field dependence of NQR/NMR spectra, which will be discussed in Sec. 4.6 [147]. Besides, such multipole couplings in each magnetic point group are also related to the band modulations [37, 41, 42, 88] and field responses [39, 40, 148].

2.5 Field Responses

According to Neumann's principle, macroscopic physical responses are determined by the crystallographic point group symmetry [96, 97]. This statement is generalized to magnetic point groups; macroscopic responses in magnets, such as the linear magnetoelectric effect, the Hall effect, and the nonlinear transport, are determined by the magnetic point group

Table 2.12: Active multipoles in the noncentrosymmetric black-and-white point groups without the $\mathcal{PT}$ symmetry.

	even-parity					odd-parity					even-parity					odd-parity				
	E			ET		E		ET			MT			M		MT		M		
	l=0	2	4	1	3	1	3	0	2	4	0	2	4	1	3	1	3	0	2	4
$\bar{4}'3m'$	Q_0		Q_4				Q_{xyz}								M_{xyz}			M_0		M_4
			Q_{4u}							G_{4u}										
$4'32'$	Q_0		Q_4					G_0		G_4					M_{xyz}		T_{xyz}			
			Q_{4u}							G_{4u}										
$42'2'$	Q_0	Q_u	Q_4					G_0	G_u	G_4			T^α_{4z}	M_z	M^α_z	T_z	T^α_z			M^α_{4z}
			Q_{4u}							G_{4u}										
$4'22'$	Q_0	Q_u	Q_4					G_0	G_u	G_4		T_v	T_{4v}		M_{xyz}		T_{xyz}		M_v	M_{4v}
			Q_{4u}							G_{4u}										
$\bar{4}2'm'$	Q_0	Q_u	Q_4				Q_{xyz}		G_v	G_{4v}			T^α_{4z}	M_z	M^α_z		T^β_z		M_{xy}	M^β_{4z}
			Q_{4u}																	
$\bar{4}'2m'$	Q_0	Q_u	Q_4				Q_{xyz}		G_v	G_{4v}		T_v	T_{4v}		M_{xyz}			M_0	M_u	M_4
			Q_{4u}																	M_{4u}
$\bar{4}'m2'$	Q_0	Q_u	Q_4				Q^β_z		G_{xy}	G^β_{4z}		T_v	T_{4v}		M_{xyz}	T_z	T^α_z			M^α_{4z}
			Q_{4u}																	
$4m'm'$	Q_0	Q_u	Q_4			Q_z	Q^α_z			G^α_{4z}			T^α_{4z}	M_z	M^α_z			M_0	M_u	M_4
			Q_{4u}																	M_{4u}
$4'mm'$	Q_0	Q_u	Q_4			Q_z	Q^α_z			G^α_{4z}		T_v	T_{4v}		M_{xyz}		T^β_z		M_{xy}	M^β_{4z}
			Q_{4u}																	
$4'$	Q_0	Q_u	Q_4	G_z	G^α_z	Q_z	Q^α_z	G_0	G_u	G_4		T_v	T_{4v}		M_{xyz}		T_{xyz}		M_v	M_{4v}
			Q_{4u}							G_{4u}		T_{xy}	T^β_{4z}		M^β_z		T^β_z		M_{xy}	M^β_{4z}
			Q^α_{4z}							G^α_{4z}										
$\bar{4}'$	Q_0	Q_u	Q_4	G_z	G^α_z		Q_{xyz}		G_v	G_{4v}		T_v	T_{4v}		M_{xyz}	T_z	T^α_z	M_0	M_u	M_4
			Q_{4u}				Q^β_z		G_{xy}	G^β_{4z}		T_{xy}	T^β_{4z}		M^β_z					M_{4u}
			Q^α_{4z}																	M^α_{4z}
$2'2'2$	Q_0	Q_u	Q_4		G_{xyz}		Q_{xyz}	G_0	G_u	G_4		T_{xy}	T^α_{4z}	M_z	M^α_z	T_z	T^α_z		M_{xy}	M^α_{4z}
		Q_v	Q_{4u}						G_v	G_{4u}			T^β_{4z}		M^β_z		T^β_z			M^β_{4z}
			Q_{4v}							G_{4v}										
$m'm2'$	Q_0	Q_u	Q_4		G_{xyz}	Q_z	Q^α_z		G_{xy}	G^α_{4z}		T_{zx}	T^α_{4y}	M_y	M^α_y	T_x	T^α_x		M_{yz}	M^α_{4x}
		Q_v	Q_{4u}				Q^β_z			G^β_{4z}			T^β_{4y}		M^β_y		T^β_x			M^β_{4x}
			Q_{4v}																	
$m'm'2$	Q_0	Q_u	Q_4		G_{xyz}	Q_z	Q^α_z		G_{xy}	G^α_{4z}		T_{xy}	T^α_{4z}	M_z	M^α_z		T_{xyz}	M_0	M_u	M_4
		Q_v	Q_{4u}				Q^β_z			G^β_{4z}			T^β_{4z}		M^β_z				M_v	M_{4u}
			Q_{4v}																	M_{4v}
m'	Q_0	Q_u	Q_4	G_y	G_{xyz}	Q_z	Q^α_z		G_{xy}	G^α_{4z}		T_{xy}	T^α_{4z}	M_z	M^α_z	T_y	T_{xyz}	M_0	M_u	M_4
		Q_v	Q_{4u}		G^α_y	Q_x	Q^α_x		G_{yz}	G^α_{4x}		T_{yz}	T^α_{4x}	M_x	M^α_x		T^α_y		M_v	M_{4u}
		Q_{zx}	Q_{4v}		G^β_y		Q^β_z			G^β_{4z}			T^β_{4z}		M^β_z		T^β_y		M_{zx}	M_{4v}
			Q^α_{4y}, Q^β_{4y}				Q^β_x			G^β_{4x}			T^β_{4x}		M^β_x					M^α_{4y}, M^β_{4y}
$2'$	Q_0	Q_u	Q_4	G_y	G_{xyz}	Q_y	Q_{xyz}	G_0	G_u	G_4		T_{xy}	T^α_{4z}	M_z	M^α_z	T_z	T^α_z		M_{xy}	M^α_{4z}
		Q_v	Q_{4u}		G^α_y		Q^α_y		G_v	G_{4u}		T_{yz}	T^α_{4x}	M_x	M^α_x	T_x	T^α_x		M_{yz}	M^α_{4x}
		Q_{zx}	Q_{4v}		G^β_y		Q^β_y		G_{zx}	G_{4v}			T^β_{4z}		M^β_z		T^β_z			M^β_{4z}
			Q^α_{4y}, Q^β_{4y}							G^α_{4y}, G^β_{4y}			T^β_{4x}		M^β_x		T^β_x			M^β_{4x}
$62'2'$	Q_0	Q_u	Q_{40}					G_0	G_u	G_{40}				M_z	M^α_z	T_z	T^α_z			
$6'22'$	Q_0	Q_u	Q_{40}					G_0	G_u	G_{40}			T_{4a}		M_{3a}		T_{3a}			M_{4a}
$\bar{6}m'2'$	Q_0	Q_u	Q_{40}				Q_{3b}			G_{4b}				M_z	M^α_z		T_{3a}			M_{4a}
$\bar{6}'m'2$	Q_0	Q_u	Q_{40}				Q_{3b}			G_{4b}			T_{4b}		M_{3b}			M_0	M_u	M_{40}
$\bar{6}'m2'$	Q_0	Q_u	Q_{40}				Q_{3b}			G_{4b}			T_{4a}		M_{3a}	T_z	T^α_z			
$6m'm'$	Q_0	Q_u	Q_{40}			Q_z	Q^α_z							M_z	M^α_z			M_0	M_u	M_{40}
$6'mm'$	Q_0	Q_u	Q_{40}			Q_z	Q^α_z						T_{4a}		M_{3a}		T_{3b}			M_{4b}
$6'$	Q_0	Q_u	Q_{40}	G_z	G^α_z	Q_z	Q^α_z	G_0	G_u	G_{40}			T_{4a}		M_{3a}		T_{3a}			M_{4a}
													T_{4b}		M_{3b}		T_{3b}			M_{4b}
$\bar{6}'$	Q_0	Q_u	Q_{40}	G_z	G^α_z		Q_{3a}			G_{4a}			T_{4a}		M_{3a}	T_z	T^α_z	M_0	M_u	M_{40}
							Q_{3b}			G_{4b}			T_{4b}		M_{3b}					
$3m'$	Q_0	Q_u	Q_{40}		G_{3b}	Q_z	Q_{3a}			G_{4a}			T_{4a}	M_z	M_{3a}		T_{3b}	M_0	M_u	M_{40}
			Q_{4b}				Q^α_z								M^α_z					M_{4b}
$32'$	Q_0	Q_u	Q_{40}		G_{3b}		Q_{3b}	G_0	G_u	G_{40}			T_{4a}	M_z	M_{3a}	T_z	T_{3a}			M_{4a}
			Q_{4b}							G_{4b}					M^α_z		T^α_z			

symmetry [92–95, 149–159].

In this section, we present a relation between the physical response tensors and active multipoles in magnetic point groups toward the understanding of the microscopic essence in addition to the symmetry for the responses in the magnetic materials [148]. In the following in this section, we first show the symmetry analysis of the response tensors and the relation to multipoles in Sec. 2.5.1. Then, we discuss the role of the antiunitary operation on the response function and how it relates the active multipoles by analyzing the linear and second-order nonlinear Kubo formula in Secs. 2.5.2 and 2.5.3, respectively.

2.5.1 Tensor Analysis

We show the relation between the response tensor components and multipoles based on the point group symmetry. The response tensor $\chi^{[n_B\times n_F]}$ is defined as

$$B^{[n_B]}=\chi^{[n_B\times n_F]}F^{[n_F]}, \tag{2.22}$$

where $B^{[n_B]}$ and $F^{[n_F]}$ are the rank-n_B output response and the rank-n_F external input field, respectively, which are typically represented by the electric, magnetic, elastic, and their product degrees of freedom. For example, $F^{[n_F]}$ represents the electric field $\boldsymbol{E}$, the magnetic field $\boldsymbol{H}$, the (symmetric) stress $\boldsymbol{\tau}$ and their combination, while $B^{[n_B]}$ represents the electric polarization $\boldsymbol{P}$, the magnetization $\boldsymbol{M}$, the symmetric strain $\varepsilon_{ij}=(\partial_i u_j+\partial_j u_i)/2$, and the rotation $\boldsymbol{\omega}=(\boldsymbol{\nabla}\times\boldsymbol{u})/2$ where $\boldsymbol{u}$ is the displacement vector[3]. $B^{[n_B]}$ also represents quantities for the transport phenomena, such as the electric (thermal) current $\boldsymbol{J}$ ($\boldsymbol{J}^{\mathrm{Q}}$) and the spin current $J^{\mathrm{s}}_{ij}=\sigma_i J_j$. Each external field and response have the correspondence to the multipoles, e.g., electric field $\boldsymbol{E}\leftrightarrow$ E dipole and symmetric strain $\boldsymbol{\varepsilon}\leftrightarrow$ E monopole and E quadrupole. The relation between the input field/output response and multipoles is summarized in Table 2.13, where the upper (lower) panel stands for the correspondence between the external field (response) and multipole.

In accordance with the spatial inversion parities of $B^{[n_B]}$ and $F^{[n_F]}$, $\chi^{[n_B\times n_F]}$ represents a polar or axial tensor; $\chi^{[n_B\times n_F]}$ is the polar (axial) tensor with the parity

$$\mathcal{P}=(-1)^{n_B+n_F}\ [\mathcal{P}=(-1)^{n_B+n_F+1}]. \tag{2.23}$$

In the following, we show the correspondence between multipoles and rank-1–4 tensor components in Secs. 2.5.1–2.5.1, respectively. See also Appendix E for details of the derivation. Here, we mainly focus on the response tensors in cubic, tetragonal, orthorhombic, monoclinic, and triclinic systems, and show those in hexagonal and trigonal systems in Appendix E.2.

Rank-1 tensor

The rank-1 response tensor $\chi^{[0\times 1]}$ for the scalar response $B^{[0]}=(B)$ with $n_B=0$ and vector field $F^{[1]}=(F_x,F_y,F_z)$ with $n_F=1$ is related with the dipole (X_x,X_y,X_z) as

$$\chi^{[0\times 1]}=\begin{pmatrix}X_x & X_y & X_z\end{pmatrix}, \tag{2.24}$$

[3]It is noted that $\boldsymbol{\omega}$ in the long-wavelength limit does not contribute to the free energy, since it corresponds to a uniform rotation of the crystal.

Table 2.13: Correspondence of the external fields and the responses to the multipoles. The spatial inversion parity of the external field or the response is shown in the column of $\mathcal{P}$. In the column of multipole, X_{lm} (l=0, 1, 2) means the rank-l multipole (X=Q, G, M, T).

n_F	$\mathcal{P}$	external field	multipole
1	+	magnetic field $\boldsymbol{H}$	M dipole (M_{1m})
	−	electric field $\boldsymbol{E}$	E dipole (Q_{1m})
2	+	(symmetric) stress $\boldsymbol{\tau}$	E monopole (Q_0)
			E quadrupole (Q_{2m})
n_B		response	
1	+	magnetization $\boldsymbol{M}$	M dipole (M_{1m})
		rotation $\boldsymbol{\omega}$	ET dipole (G_{1m})
	−	electric polarization $\boldsymbol{P}$	E dipole (Q_{1m})
		electric (thermal) current $\boldsymbol{J}$($\boldsymbol{J}^{\mathrm{Q}}$)	MT dipole (T_{1m})
2	+	symmetric strain $\boldsymbol{\varepsilon}$	E monopole (Q_0)
			E quadrupole (Q_{2m})
	−	spin current $\boldsymbol{J}^{\mathrm{s}}$	ET monopole (G_0)
			E dipole (Q_{1m})
			ET quadrupole (G_{2m})

where X stands for the polar multipoles (Q or T) [axial multipoles (G or M)] when $\chi^{[0\times1]}$ is the polar (axial) tensor. The dipoles X_x, X_y, and X_z in Eq. (2.24) is X_i=$\chi^{[0\times1]}_{0;i}$ (i=x, y, z). The response tensor $\chi^{[1\times0]}$ is obtained by transposing $\chi^{[0\times1]}$, which is expressed by the same type of multipole as $\chi^{[0\times1]}$.

The electrocaloric (magnetocaloric) effect where the entropy variation ΔS is induced by the electric field (the magnetic field) as ΔS=$\sum_i p_i E_i$ (ΔS=$\sum_i q_i H_i$), is described by one of the rank-1 polar (axial) response tensors. As ΔS corresponds to E monopole (Q_0), the tensor component of p_i (q_i) is described by the E dipole (Q_x, Q_y, Q_z) or MT dipole (T_x, T_y, T_z) [the ET dipole (G_x, G_y, G_z) or M dipole (M_x, M_y, M_z)]. Here and hereafter in Sec. 2.5.1, we do not distinguish the multipoles with the opposite time-reversal parity for simplicity, which depends on the microscopic process in the presence/absence of the dissipation, which will be discussed in Secs. 2.5.2 and 2.5.3.

Rank-2 tensor

We consider two types of rank-2 tensors, $\chi^{[1\times1]}$ and $\chi^{[0\times2]}$. $\chi^{[1\times1]}$ is the response tensor for $B^{[1]}$=(B_x, B_y, B_z) and $F^{[1]}$=(F_x, F_y, F_z), which is related to the rank-0 to 2 multipoles as monopole X_0, dipole (Y_x, Y_y, Y_z), and quadrupole $(X_u, X_v, X_{yz}, X_{zx}, X_{xy})$. The tensor component of $\chi^{[1\times1]}$ is given by

$$\chi^{[1\times1]}=\begin{pmatrix} X_0-X_u+X_v & X_{xy}+Y_z & X_{zx}-Y_y \\ X_{xy}-Y_z & X_0-X_u-X_v & X_{yz}+Y_x \\ X_{zx}+Y_y & X_{yz}-Y_x & X_0+2X_u \end{pmatrix}, \tag{2.25}$$

where X=Q or T (G or M) and Y=G or M (Q or T) for the polar (axial) tensor. See also Appendix E.1.1 for details. When $\chi^{[1\times1]}$ is a polar tensor, such as the magnetic suscepti-

bility tensor for $F^{[1]}=\boldsymbol{H}$ and $B^{[1]}=\boldsymbol{M}$, the dielectric susceptibility tensor for $F^{[1]}=\boldsymbol{E}$ and $B^{[1]}=\boldsymbol{P}$, and the electric conductivity tensor for $F^{[1]}=\boldsymbol{E}$ and $B^{[1]}=\boldsymbol{J}$, the corresponding multipoles are the E (MT) monopole and E (MT) quadrupoles for X and ET (M) dipoles for Y. Meanwhile, when $\chi^{[1\times1]}$ is an axial tensor, such as the magnetoelectric tensor for $F^{[1]}=\boldsymbol{E}$ and $B^{[1]}=\boldsymbol{M}$ or $F^{[1]}=\boldsymbol{H}$ and $B^{[1]}=\boldsymbol{P}$, the ET (M) monopole and ET (M) quadrupoles for X and E (MT) dipoles for Y are relevant.

$\chi^{[0\times2]}$ is another rank-2 tensor for $B^{[0]}=(B)$ and $F^{[2]}=(F_{xx},F_{yy},F_{zz},F_{yz},F_{zx},F_{xy})$ where $F_{ij}=F_{ji}$. As $F^{[2]}$ is decomposed into the monopole and quadrupole components, the tensor component of $\chi^{[0\times2]}$ is given by

$$\chi^{[0\times2]}=\begin{pmatrix} X_0-X_u+X_v \\ X_0-X_u-X_v \\ X_0+2X_u \\ X_{yz} \\ X_{zx} \\ X_{xy} \end{pmatrix}^{\mathrm{T}}. \tag{2.26}$$

Thus, the active monopole and quadrupole contribute to $\chi^{[0\times2]}$. See Appendix E.1.2 for details. For example, the piezocaloric tensor for $F^{[2]}=\boldsymbol{\tau}$ and $B^{[0]}=\Delta S$ corresponds to $\chi^{[0\times2]}$, where the E (MT) monopole and quadrupole are relevant. The multipole expression of $\chi^{[2\times0]}$ is obtained by transposing $\chi^{[0\times2]}$.

Rank-3 tensor

We consider two types of rank-3 tensors, $\chi^{[1\times2]}$ and $\chi^{[0\times3]}$. $\chi^{[1\times2]}$ is the rank-3 tensor for $B^{[1]}=(B_x,B_y,B_z)$ and $F^{[2]}=(F_{xx},F_{yy},F_{zz},F_{yz},F_{zx},F_{xy})$, which is expressed by dipole (X_x,X_y,X_z), quadrupole $(Y_u,Y_v,Y_{yz},Y_{zx},Y_{xy})$, and octupole $(X_{xyz},X_x^\alpha,X_y^\alpha,X_z^\alpha,X_x^\beta,X_y^\beta,X_z^\beta)$ as

$$\chi^{[1\times2]}=\begin{pmatrix} 3X_x+2X_x^\alpha & 2(X_y'-Y_{zx})+X_y-X_y^\alpha-X_y^\beta & 2(X_z'+Y_{xy})+X_z-X_z^\alpha+X_z^\beta \\ 2(X_x'+Y_{yz})+X_x-X_x^\alpha+X_x^\beta & 3X_y+2X_y^\alpha & 2(X_z'-Y_{xy})+X_z-X_z^\alpha-X_z^\beta \\ 2(X_x'-Y_{yz})+X_x-X_x^\alpha-X_x^\beta & 2(X_y'+Y_{zx})+X_y-X_y^\alpha+X_y^\beta & 3X_z+2X_z^\alpha \\ Y_u+Y_v+X_{xyz} & -X_z'+Y_{xy}+X_z-X_z^\alpha-X_z^\beta & -X_y'-Y_{zx}+X_y-X_y^\alpha+X_y^\beta \\ -X_z'-Y_{xy}+X_z-X_z^\alpha+X_z^\beta & -Y_u+Y_v+X_{xyz} & -X_x'+Y_{yz}+X_x-X_x^\alpha-X_x^\beta \\ -X_y'+Y_{zx}+X_y-X_y^\alpha-X_y^\beta & -X_x'-Y_{yz}+X_x-X_x^\alpha+X_x^\beta & -2Y_v+X_{xyz} \end{pmatrix}^{\mathrm{T}}. \tag{2.27}$$

It is noted that both X_i and X_i' $(i=x,y,z)$ stand for the dipole but they are independent with each other. See Appendix E.1.3 for details. $\chi^{[1\times2]}$ is polar for the piezoelectric tensor $(F^{[2]}=\boldsymbol{\tau},B^{[1]}=\boldsymbol{P})$ and second-order nonlinear conductivity $(F_{ij}^{[2]}=E_iE_j,B^{[1]}=\boldsymbol{J})$ where $X=Q$ or T and $Y=G$ or M, while it is axial for the piezomagnetic tensor $(F^{[2]}=\boldsymbol{\tau},B^{[1]}=\boldsymbol{M})$ where $X=G$ or M and $Y=Q$ or T. The multipole expression of the tensor $\chi^{[2\times1]}$, e.g., the spin conductivity tensor $(F^{[1]}=\boldsymbol{E},B^{[2]}=\boldsymbol{J}^{\mathrm{s}})$, is obtained by transposing $\chi^{[1\times2]}$.

$\chi^{[0\times3]}$ is another rank-3 response tensor for the rank-0 response $B^{[0]}=(B)$ and rank-3 field $F^{[3]}=(F_{xxx},F_{yyy},F_{zzz},F_{yyz},F_{zzx},F_{xxy},F_{yzz},F_{zxx},F_{xyy},F_{xyz})$ where $F_{ijk}=F_{jik}=F_{ikj}$. As $F^{[3]}$ itself is decomposed into the dipole and octupole components, $\chi^{[0\times3]}$ is also related

to them, which is shown as

$$\chi^{[0\times3]}=\begin{pmatrix} 3X_x+2X_x^\alpha \\ 3X_y+2X_y^\alpha \\ 3X_z+2X_z^\alpha \\ X_z-X_z^\alpha-X_z^\beta \\ X_x-X_x^\alpha-X_x^\beta \\ X_y-X_y^\alpha-X_y^\beta \\ X_y-X_y^\alpha+X_y^\beta \\ X_z-X_z^\alpha+X_z^\beta \\ X_x-X_x^\alpha+X_x^\beta \\ X_{xyz} \end{pmatrix}^{\mathrm{T}}. \tag{2.28}$$

See Appendix E.1.4 for details. $\chi^{[0\times3]}$, such as the third-order electrocaloric effect, is relevant with $X=Q$ or $T(G$ or $M)$ for the polar (axial) tensor. The multipole expression of $\chi^{[3\times0]}$ is obtained by transposing $\chi^{[0\times3]}$.

Rank-4 tensor

We consider two types of rank-4 tensors, $\chi^{[1\times3]}$ and $\chi^{[2\times2]}$. $\chi^{[1\times3]}$ is the rank-4 response tensor for $B^{[1]}=(B_x,B_y,B_z)$ and $F^{[3]}=(F_{xxx},F_{yyy},F_{zzz},F_{yyz},F_{zzx},F_{xxy},F_{yzz},F_{zxx},F_{xyy},F_{xyz})$ where $F_{ijk}=F_{jik}=F_{ikj}$. The relevant multipoles are ones with rank 0–4: monopole X_0, dipole (Y_x,Y_y,Y_z), quadrupole $(X_u,X_v,X_{yz},X_{zx},X_{xy})$, octupole $(Y_{xyz},Y_x^\alpha,Y_y^\alpha,Y_z^\alpha,Y_x^\beta,Y_y^\beta,Y_z^\beta)$, and hexadecapole $(X_4,X_{4u},X_{4v},X_{4x}^\alpha,X_{4y}^\alpha,X_{4z}^\alpha,X_{4x}^\beta,X_{4y}^\beta,X_{4z}^\beta)$. The tensor component of $\chi^{[1\times3]}$ is given by

$$\chi^{[1\times3]}=\begin{pmatrix} 3(X_0-\tilde{X}_u+\tilde{X}_v)+2X_4-X_{4u}+X_{4v} & 3(-Y_z-\tilde{X}_{xy}+Y_z^\alpha-Y_z^\beta)+X_{4z}^\alpha-X_{4z}^\beta & 3(Y_y-\tilde{X}_{zx}-Y_y^\alpha-Y_y^\beta)-X_{4y}^\alpha-X_{4y}^\beta \\ 3(Y_z-\tilde{X}_{xy}-Y_z^\alpha-Y_z^\beta)-X_{4z}^\alpha-X_{4z}^\beta & 3(X_0-\tilde{X}_u-\tilde{X}_v)+2X_4-X_{4u}-X_{4v} & 3(-Y_x-\tilde{X}_{yz}+Y_x^\alpha-Y_x^\beta)+X_{4x}^\alpha-X_{4x}^\beta \\ 3(-Y_y-\tilde{X}_{zx}+Y_y^\alpha-Y_y^\beta)+X_{4y}^\alpha-X_{4y}^\beta & 3(Y_x-\tilde{X}_{yz}-Y_x^\alpha-Y_x^\beta)-X_{4x}^\alpha-X_{4x}^\beta & 3(X_0+2\tilde{X}_u)+2X_4+2X_{4u} \\ -Y_y-\tilde{X}_{zx}-4Y_y^\alpha+2Y_y^\beta+2X_{4y}^\beta & Y_x+\tilde{X}'_{yz}-Y_x^\alpha+Y_x^\beta+X_{4x}^\alpha-X_{4x}^\beta & X_0+\tilde{X}''_u-5X_v-Y_{xyz}-X_4-X_{4u}+X_{4v} \\ X_0+\tilde{X}'_u-\tilde{X}'_v-Y_{xyz}-X_4-X_{4u}-X_{4v} & -Y_z-\tilde{X}_{xy}-4Y_z^\alpha+2Y_z^\beta+2X_{4z}^\beta & Y_y+\tilde{X}'_{zx}-Y_y^\alpha+Y_y^\beta+X_{4y}^\alpha-X_{4y}^\beta \\ Y_z+\tilde{X}'_{xy}-Y_z^\alpha+Y_z^\beta+X_{4z}^\alpha-X_{4z}^\beta & X_0-\tilde{X}_u+\tilde{X}''_v-Y_{xyz}-X_4+2X_{4u} & -Y_x-\tilde{X}_{yz}-4Y_x^\alpha+2Y_x^\beta+2X_{4x}^\beta \\ Y_z-\tilde{X}_{xy}+4Y_z^\alpha+2Y_z^\beta+2X_{4z}^\beta & X_0+\tilde{X}'_u+\tilde{X}'_v+Y_{xyz}-X_4-X_{4u}+X_{4v} & -Y_x+\tilde{X}'_{yz}+Y_x^\alpha+Y_x^\beta-X_{4x}^\alpha-X_{4x}^\beta \\ -Y_y+\tilde{X}'_{zx}+Y_y^\alpha+Y_y^\beta-X_{4y}^\alpha-X_{4y}^\beta & Y_x-\tilde{X}_{yz}+4Y_x^\alpha+2Y_x^\beta+2X_{4x}^\beta & X_0+\tilde{X}''_u+5X_v+Y_{xyz}-X_4-X_{4u}-X_{4v} \\ X_0-\tilde{X}_u-\tilde{X}''_v+Y_{xyz}-X_4+2X_{4u} & -Y_z+\tilde{X}'_{xy}+Y_z^\alpha+Y_z^\beta-X_{4z}^\alpha-X_{4z}^\beta & Y_y-\tilde{X}_{zx}+4Y_y^\alpha+2Y_y^\beta+2X_{4y}^\beta \\ 5X_{yz}-2Y_x^\beta+2X_{4x}^\beta & 5X_{zx}-2Y_y^\beta+2X_{4y}^\beta & 5X_{xy}-2Y_z^\beta+2X_{4z}^\beta \end{pmatrix}^{\mathrm{T}}. \tag{2.29}$$

Note that $(\tilde{X}_u,\tilde{X}'_u,\tilde{X}''_u)$, $(\tilde{X}_v,\tilde{X}'_v,\tilde{X}''_v)$, and $(\tilde{X}_{yz},\tilde{X}'_{yz})$ (cyclic) are introduced to express the two independent quadrupoles. See Appendix E.1.5 for details. $\chi^{[1\times3]}$ corresponds to the response tensors, such as the third-order nonlinear electric conductivity. The relevant multipoles are $X=Q$ or T and $Y=G$ or M for the polar tensor, while those are $X=G$ or M and $Y=Q$ or T for the axial tensor. The multipole expression of $\chi^{[3\times1]}$ is obtained by transposing $\chi^{[1\times3]}$.

$\chi^{[2\times2]}$ is another rank-4 tensor for $B^{[2]}=(B_{xx},B_{yy},B_{zz},B_{yz},B_{zx},B_{xy})$ where $B_{ij}=B_{ji}$ and $F^{[2]}=(F_{xx},F_{yy},F_{zz},F_{yz},F_{zx},F_{xy})$ where $F_{ij}=F_{ji}$. The tensor component of $\chi^{[2\times2]}$ is

related to the rank 0–4 multipoles, which is given by

$$\chi^{[2\times2]}=\begin{pmatrix}\chi_{ll} & \chi_{lt}\\ \chi_{tl} & \chi_{tt}\end{pmatrix}, \tag{2.30}$$

$$\chi_{ll}=\begin{pmatrix}\tilde{X}_0+\tilde{X}_u+\tilde{X}_v+2X_4-X_{4u}+X_{4v} & \tilde{X}'_0+\tilde{X}'_u-2X_v^{(-)}+X_{xyz}-X_4+2X_{4u} & \tilde{X}'_0+\tilde{X}_u^{(+)}+\tilde{X}_v^{(-)}-X_{xyz}-X_{4uv+}\\ \tilde{X}'_0+\tilde{X}'_u+2X_v^{(-)}-X_{xyz}-X_4+2X_{4u} & \tilde{X}_0+\tilde{X}_u-\tilde{X}_v+2X_4-X_{4u}-X_{4v} & \tilde{X}'_0+\tilde{X}_u^{(+)}-\tilde{X}_v^{(-)}+X_{xyz}-X_{4uv-}\\ \tilde{X}'_0+\tilde{X}_u^{(-)}+\tilde{X}_v^{(+)}+X_{xyz}-X_{4uv+} & \tilde{X}'_0+\tilde{X}_u^{(-)}-\tilde{X}_v^{(+)}-X_{xyz}-X_{4uv-} & \tilde{X}_0-2\tilde{X}_u+2X_4+2X_{4u}\end{pmatrix}, \tag{2.31}$$

$$\chi_{lt}=\begin{pmatrix}\tilde{X}_{yz}^{(+)}-2Y_x^\beta+2X_{4x}^\beta & -2Y_y+\tilde{X}_{zx}^{\prime(+)}+Y_y^\alpha+Y_y^\beta-X_{4y}^\alpha-X_{4y}^\beta & 2Y_z+\tilde{X}_{xy}^{\prime(+)}-Y_z^\alpha+Y_z^\beta+X_{4z}^\alpha-X_{4z}^\beta\\ 2Y_x+\tilde{X}_{yz}^{\prime(+)}-Y_x^\alpha+Y_x^\beta+X_{4x}^\alpha-X_{4x}^\beta & \tilde{X}_{zx}^{(+)}-2Y_y^\beta+2X_{4y}^\beta & -2Y_z+\tilde{X}_{xy}^{\prime(+)}+Y_z^\alpha+Y_z^\beta-X_{4z}^\alpha-X_{4z}^\beta\\ -2Y_x+\tilde{X}_{yz}^{\prime(+)}+Y_x^\alpha+Y_x^\beta-X_{4x}^\alpha-X_{4x}^\beta & 2Y_y+\tilde{X}_{zx}^{\prime(+)}-Y_y^\alpha+Y_y^\beta+X_{4y}^\alpha-X_{4y}^\beta & \tilde{X}_{xy}^{(+)}-2Y_z^\beta+2X_{4z}^\beta\end{pmatrix}, \tag{2.32}$$

$$\chi_{tl}=\begin{pmatrix}\tilde{X}_{yz}^{(-)}+2Y_x^\beta+2X_{4x}^\beta & -2Y_x+\tilde{X}_{yz}^{\prime(-)}+Y_x^\alpha-Y_x^\beta+X_{4x}^\alpha-X_{4x}^\beta & 2Y_x+\tilde{X}_{yz}^{\prime(-)}-Y_x^\alpha-Y_x^\beta-X_{4x}^\alpha-X_{4x}^\beta\\ 2Y_y+\tilde{X}_{zx}^{\prime(-)}-Y_y^\alpha-Y_y^\beta-X_{4y}^\alpha-X_{4y}^\beta & \tilde{X}_{zx}^{(-)}+2Y_y^\beta+2X_{4y}^\beta & -2Y_y+\tilde{X}_{zx}^{\prime(-)}+Y_y^\alpha-Y_y^\beta+X_{4y}^\alpha-X_{4y}^\beta\\ -2Y_z+\tilde{X}_{xy}^{\prime(-)}+Y_z^\alpha-Y_z^\beta+X_{4z}^\alpha-X_{4z}^\beta & 2Y_z+\tilde{X}_{xy}^{\prime(-)}-Y_z^\alpha-Y_z^\beta-X_{4z}^\alpha-X_{4z}^\beta & \tilde{X}_{xy}^{(-)}+2Y_z^\beta+2X_{4z}^\beta\end{pmatrix}, \tag{2.33}$$

$$\chi_{tt}=\begin{pmatrix}3X_0+3X_u-3X_v-X_{4uv-} & -Y_z+3X_{xy}-2Y_z^\alpha+2X_{4z}^\beta & Y_y+3X_{zx}+2Y_y^\alpha+2X_{4y}^\beta\\ Y_z+3X_{xy}+2Y_z^\alpha+2X_{4z}^\beta & 3X_0+3X_u+3X_v-X_{4uv+} & -Y_x+3X_{yz}-2Y_x^\alpha+2X_{4x}^\beta\\ -Y_y+3X_{zx}-2Y_y^\alpha+2X_{4y}^\beta & Y_x+3X_{yz}+2Y_x^\alpha+2X_{4x}^\beta & 3X_0-6X_u-X_4+2X_{4u}\end{pmatrix}, \tag{2.34}$$

where $X_{4uv\pm}=X_4+X_{4u}\pm X_{4v}$. We also introduce $(\tilde{X}_0,\tilde{X}'_0)$, $(\tilde{X}_u,\tilde{X}_u^{(\pm)},\tilde{X}'_u)$, $(\tilde{X}_v,\tilde{X}_v^{(\pm)})$, and $(\tilde{X}_{yz}^{(\pm)},\tilde{X}_{yz}^{\prime(\pm)})$ (cyclic) for notational simplicity. See Appendix E.1.6 for details. $\chi^{[2\times2]}$ represents the rank-4 tensor, such as the elastic stiffness tensor and magneto-Seebeck tensor, which is related to the multipoles $X=Q$ or T and $Y=G$ or M for the polar tensor and to $X=G$ or M and $Y=Q$ or T for the axial tensor.

2.5.2 Linear Response Function

The multipoles with the opposite time-reversal parities, E and MT (ET and M), are not completely distinguished by the above analyses based on the point group symmetry. For the equilibrium physical properties, the relation between the time-reversal parities of the response tensor and corresponding multipoles are determined by the time-reversal parities of the input field and output response [92, 93], e.g., the linear magnetoelectric tensor in an insulator is the time-reversal odd tensor with the relation to the M and MT multipoles. Meanwhile, the restriction for the transport tensor by the time-reversal symmetry is not so simple as mentioned in Sec. 1.5 and has been investigated by using the Onsager's reciprocal relations [149, 153, 154] and the Kubo formula [150, 156–158]; the time-reversal property of the transport tensor is determined by the microscopic dissipation processes. Thus, we demonstrate the relation of the multipoles and response tensors by considering the dissipation processes based on the Kubo formula [38, 39].

When we consider the external perturbation Hamiltonian $\mathcal{H}_{\rm ext}=-\sum_j \hat{A}_j F_j(t)$, where $F_j(t)=\int_{-\infty}^{\infty}\frac{d\omega}{2\pi}F_{j,\omega}e^{-i\omega t+\delta t}$ is the jth component of an external field for $\delta>0$, the linear complex susceptibility $\chi_{i;j}(\omega)$ satisfies the relation

$$\langle\hat{B}_{i,\omega}\rangle=\int_{-\infty}^{\infty}\frac{d\omega'}{2\pi}\delta(\omega-\omega')\chi_{i;j}(\omega')F_{j,\omega'}. \tag{2.35}$$

$\langle\hat{B}_{i,\omega}\rangle$ is the expectation value of the ω component of $\hat{B}_i$. Considering the uniform external field with the wave vector $\boldsymbol{q}\to\boldsymbol{0}$, and then taking the static limit $\omega\to0$, the linear response function for the periodic system is represented as

$$\begin{aligned}\chi_{i;j}&\equiv\chi_{i;j}(\omega\to0)\\&=-\frac{i\hbar}{V}\sum_{\boldsymbol{k}nm}\frac{f[\varepsilon_n(\boldsymbol{k})]-f[\varepsilon_m(\boldsymbol{k})]}{\varepsilon_n(\boldsymbol{k})-\varepsilon_m(\boldsymbol{k})}\frac{B^{nm}_{i\boldsymbol{k}}\dot{A}^{mn}_{j\boldsymbol{k}}}{i\hbar\delta+\varepsilon_n(\boldsymbol{k})-\varepsilon_m(\boldsymbol{k})},\end{aligned} \tag{2.36}$$

where $\dot{A}=dA/dt$. $X^{nm}_{\boldsymbol{k}}\equiv\langle n\boldsymbol{k}|\hat{X}|m\boldsymbol{k}\rangle$ is the matrix element between the Bloch states $|n\boldsymbol{k}\rangle$ and $|m\boldsymbol{k}\rangle$ with the band indices n and m, respectively, and the wave vector $\boldsymbol{k}$. $f[\varepsilon_n(\boldsymbol{k})]$ is the Fermi distribution function with the eigenenergy $\varepsilon_n(\boldsymbol{k})$ of the eigenstate $|n\boldsymbol{k}\rangle$. V, $\hbar$, and δ are the system volume, the reduced Planck constant, and the broadening factor, respectively. We here assume the relaxation-time approximation and mimic the constant $1/\delta$ as the relaxation time. $\chi_{i;j}$ can be decomposed as

$$\chi_{i;j}=\chi^{(\rm J)}_{i;j}+\chi^{(\rm E)}_{i;j}, \tag{2.37}$$

$$\chi^{(\rm J)}_{i;j}=-\frac{\hbar^2\delta}{V}\sum_{\boldsymbol{k}nm}\frac{f[\varepsilon_n(\boldsymbol{k})]-f[\varepsilon_m(\boldsymbol{k})]}{\varepsilon_n(\boldsymbol{k})-\varepsilon_m(\boldsymbol{k})}\frac{B^{nm}_{i\boldsymbol{k}}\dot{A}^{mn}_{j\boldsymbol{k}}}{(\hbar\delta)^2+[\varepsilon_n(\boldsymbol{k})-\varepsilon_m(\boldsymbol{k})]^2}, \tag{2.38}$$

$$\chi^{(\rm E)}_{i;j}=-\frac{i\hbar}{V}\sum_{\boldsymbol{k}nm}^{\neq}\frac{f[\varepsilon_n(\boldsymbol{k})]-f[\varepsilon_m(\boldsymbol{k})]}{(\hbar\delta)^2+[\varepsilon_n(\boldsymbol{k})-\varepsilon_m(\boldsymbol{k})]^2}B^{nm}_{i\boldsymbol{k}}\dot{A}^{mn}_{j\boldsymbol{k}}, \tag{2.39}$$

where $\chi^{(\rm J)}_{i;j}$ includes the intraband (dissipative) contribution proportional to $1/\delta$, while $\chi^{(\rm E)}_{i;j}$ is the interband (nondissipative) one, which remains finite in the clean limit of $\delta\to0$.

$\chi^{(\rm J)}$ and $\chi^{(\rm E)}$ have the opposite time-reversal property [38, 39]. When the time-reversal symmetry is preserved, they are transformed as

$$\chi^{(\rm J)}_{i;j}=-t_{B_i}t_{A_j}\chi^{(\rm J)}_{i;j},\ \chi^{(\rm E)}_{i;j}=t_{B_i}t_{A_j}\chi^{(\rm E)}_{i;j}, \tag{2.40}$$

where $X^{nm}_{\boldsymbol{k}}=t_X X^{\bar{m}\bar{n}}_{-\boldsymbol{k}}$ for $t_X=\pm1$ ($X=A_j,B_i$). The $\bar{n}$th band stands for the time-reversal partner of the nth band. Equation (2.40) means that $\chi^{(\rm J)}_{i;j}$ [$\chi^{(\rm E)}_{i;j}$] can be finite when $t_{B_i}t_{A_j}=-1(+1)$. In other words, $\chi^{(\rm J)}_{i;j}$ [$\chi^{(\rm E)}_{i;j}$] becomes nonzero when the M and MT (E and ET) multipoles are active for $t_{B_i}t_{A_j}=+1$, while $\chi^{(\rm J)}_{i;j}$ [$\chi^{(\rm E)}_{i;j}$] becomes nonzero when the E and ET (M and MT) multipoles are active for $t_{B_i}t_{A_j}=-1$. The multipoles contributing to $\chi^{(\rm J)}_{i;j}$ and $\chi^{(\rm E)}_{i;j}$ are summarized in Table 2.14.

It is noted that the similar argument holds for the static isothermal susceptibility such as the magnetic susceptibility, which is obtained by $\omega\to0$ and then $\boldsymbol{q}\to\boldsymbol{0}$ for $\chi_{i;j}(\omega)$

Table 2.14: Correspondence between the linear response functions $\chi^{(\mathrm{J,E})}$ and multipoles X_{lm} (l=1–4, X=Q, G, T, M). Nonzero $\chi^{(\mathrm{J,E})}$ is indicated by the checkmark(✓). In the rightmost column, the parentheses represent the corresponding multipoles to the response B and the external field F (See also Table 2.13). Only the corresponding multipoles are shown in the absence of the familiar response.

rank		$t_{B_i}t_{A_j}$		multipole	$(\mathcal{P},\mathcal{T},\mathcal{PT})$= $(\bigcirc,\bigcirc,\bigcirc)$	$(\times,\bigcirc,\times)$	$(\bigcirc,\times,\times)$	$(\times,\times,\bigcirc)$	$(\times,\times,\times)$	examples ($B\leftrightarrow F$)
1	polar	+1	$\chi^{(\mathrm{J})}$	T_{1m}				✓	✓	electrocaloric tensor
			$\chi^{(\mathrm{E})}$	Q_{1m}		✓			✓	($Q_0\leftrightarrow Q_{1m}$)
		−1	$\chi^{(\mathrm{J})}$	Q_{1m}		✓			✓	toroidalcaloric tensor
			$\chi^{(\mathrm{E})}$	T_{1m}				✓	✓	($Q_0\leftrightarrow T_{1m}$)
	axial	+1	$\chi^{(\mathrm{J})}$	M_{1m}			✓		✓	
			$\chi^{(\mathrm{E})}$	G_{1m}	✓	✓	✓	✓	✓	($Q_0\leftrightarrow G_{1m}$)
		−1	$\chi^{(\mathrm{J})}$	G_{1m}	✓	✓	✓	✓	✓	magnetocaloric tensor
			$\chi^{(\mathrm{E})}$	M_{1m}			✓		✓	($Q_0\leftrightarrow M_{1m}$)
2	polar	+1	$\chi^{(\mathrm{J})}$	T_0, M_{1m}, T_{2m}			✓		✓	magnetic susceptibility
			$\chi^{(\mathrm{E})}$	Q_0, G_{1m}, Q_{2m}	✓	✓	✓	✓	✓	($M_{1m}\leftrightarrow M_{1m}$)
		−1	$\chi^{(\mathrm{J})}$	Q_0, G_{1m}, Q_{2m}	✓	✓	✓	✓	✓	electric conductivity
			$\chi^{(\mathrm{E})}$	T_0, M_{1m}, T_{2m}			✓		✓	($T_{1m}\leftrightarrow E_{1m}$)
	axial	+1	$\chi^{(\mathrm{J})}$	M_0, T_{1m}, M_{2m}				✓	✓	
			$\chi^{(\mathrm{E})}$	G_0, Q_{1m}, G_{2m}		✓			✓	($T_{1m}\leftrightarrow M_{1m}$)
		−1	$\chi^{(\mathrm{J})}$	G_0, Q_{1m}, G_{2m}		✓			✓	magnetoelectric tensor
			$\chi^{(\mathrm{E})}$	M_0, T_{1m}, M_{2m}				✓	✓	($M_{1m}\leftrightarrow E_{1m}$)
3	polar	+1	$\chi^{(\mathrm{J})}$	T_{1m}, M_{2m}, T_{3m}				✓	✓	piezoelectric tensor
			$\chi^{(\mathrm{E})}$	Q_{1m}, G_{2m}, Q_{3m}		✓			✓	($Q_{1m}\leftrightarrow Q_0, Q_{2m}$)
		−1	$\chi^{(\mathrm{J})}$	Q_{1m}, G_{2m}, Q_{3m}		✓			✓	
			$\chi^{(\mathrm{E})}$	T_{1m}, M_{2m}, T_{3m}				✓	✓	($T_{1m}\leftrightarrow Q_0, Q_{2m}$)
	axial	+1	$\chi^{(\mathrm{J})}$	M_{1m}, T_{2m}, M_{3m}			✓		✓	spin conductivity
			$\chi^{(\mathrm{E})}$	G_{1m}, Q_{2m}, G_{3m}	✓	✓	✓	✓	✓	($G_0, Q_{1m}, G_{2m}\leftrightarrow Q_{1m}$)
		−1	$\chi^{(\mathrm{J})}$	G_{1m}, Q_{2m}, G_{3m}	✓	✓	✓	✓	✓	piezomagnetic tensor
			$\chi^{(\mathrm{E})}$	M_{1m}, T_{2m}, M_{3m}			✓		✓	($M_{1m}\leftrightarrow Q_0, Q_{2m}$)
4	polar	+1	$\chi^{(\mathrm{J})}$	$T_0, M_{1m}, T_{2m}, M_{3m}, T_{4m}$			✓		✓	elastic stiffness tensor ($Q_0, Q_{2m}\leftrightarrow Q_0, Q_{2m}$)
			$\chi^{(\mathrm{E})}$	$Q_0, G_{1m}, Q_{2m}, G_{3m}, Q_{4m}$	✓	✓	✓	✓	✓	
		−1	$\chi^{(\mathrm{J})}$	$Q_0, G_{1m}, Q_{2m}, G_{3m}, Q_{4m}$	✓	✓	✓	✓	✓	($T_0, T_{2m}\leftrightarrow Q_0, Q_{2m}$)
			$\chi^{(\mathrm{E})}$	$T_0, M_{1m}, T_{2m}, M_{3m}, T_{4m}$			✓		✓	
	axial	+1	$\chi^{(\mathrm{J})}$	$M_0, T_{1m}, M_{2m}, T_{3m}, M_{4m}$				✓	✓	($G_0, G_{2m}\leftrightarrow Q_0, Q_{2m}$)
			$\chi^{(\mathrm{E})}$	$G_0, Q_{1m}, G_{2m}, Q_{3m}, G_{4m}$		✓			✓	
		−1	$\chi^{(\mathrm{J})}$	$G_0, Q_{1m}, G_{2m}, Q_{3m}, G_{4m}$		✓			✓	($M_0, M_{2m}\leftrightarrow Q_0, Q_{2m}$)
			$\chi^{(\mathrm{E})}$	$M_0, T_{1m}, M_{2m}, T_{3m}, M_{4m}$				✓	✓	

in Eq. (2.35) in the non-degenerate system. The general form of the static isothermal

susceptibility $\chi^T_{i;j}$ is given by

$$\chi^T_{i;j}=\beta\sum_{nm}^{=} w_n B^{nm}_i A^{mn}_j+\sum_{nm}^{\neq}\frac{w_m-w_n}{E_n-E_m}B^{nm}_i A^{mn}_j, \tag{2.41}$$

where $\beta=1/k_{\rm B}T$, w_n is the Boltzmann weight of eigenstate n, and the notation $=$ $(\neq)$ stands for the summation taken over $E_n=E_m$ $(E_n\neq E_m)$. The first term corresponds to the Curie term in the degenerate system. From the viewpoint of the time-reversal symmetry, both terms of $\chi^T_{i;j}$ satisfy the relation $\chi^T_{i;j}=t_B t_A \chi^T_{i;j}$, which is the same as that of $\chi^{\rm (E)}_{i;j}$ in Eq. (2.40).

In the following, let us discuss $\chi^{\rm (J)}_{i;j}$ and $\chi^{\rm (E)}_{i;j}$ by taking an example. We consider the uniform and staggered magnetic orderings with magnetic moments along the z axis in the diamond structure in Secs. 2.5.2 and 2.5.2, respectively.

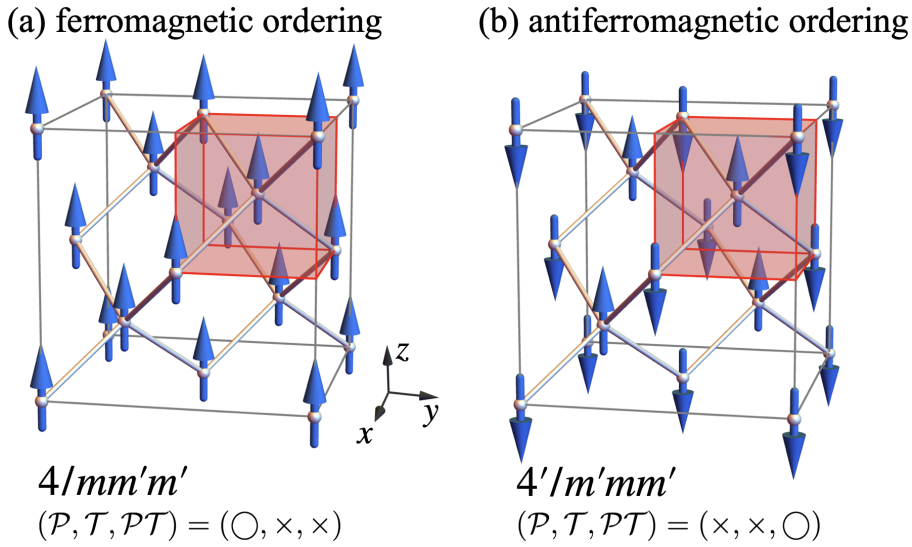

Figure 2.2: (a) Ferromagnetic ordering and (b) antiferromagnetic ordering in the diamond structure. (a) is characterized by $4/mm'm'$ with the spatial inversion symmetry ($\mathcal{P}$), whereas (b) is represented by $4'/m'mm'$ with the spatial inversion and time-reversal symmetry ($\mathcal{PT}$).

$\mathcal{P}$-symmetric magnetic structure

The uniform magnetic structure in the $\mathrm{T}^-_{1\rm g}$ representation of $m\bar{3}m1'$ as illustrated in Fig. 2.2(a) reduces the symmetry to the $\mathcal{P}$-symmetric $4/mm'm'$. From Table 2.10, one can find that the active multipoles up to rank 4 are the even-parity E multipoles Q_0 (monopole), Q_u (quadrupole), Q_4, Q_{4u} (hexadecapole), even-parity M multipoles M_z (dipole), M^α_z (octupole), and even-parity MT multipole T^α_{4z} (hexadecapole). Thus, the physical responses related to these active multipoles are expected to occur, such as the magnetocaloric response, electric conductivity including the Hall effect, and piezomagnetic response from Table 2.14.

For example, the electric conductivity tensor $J_i=\sum_j \sigma_{i;j}E_j$ is given by

$$\sigma_{i;j}=-\frac{i\hbar}{V}\sum_{\boldsymbol{k}nm}\frac{f[\varepsilon_n(\boldsymbol{k})]-f[\varepsilon_m(\boldsymbol{k})]}{\varepsilon_n(\boldsymbol{k})-\varepsilon_m(\boldsymbol{k})}\frac{J^{nm}_{i\boldsymbol{k}}J^{mn}_{j\boldsymbol{k}}}{i\hbar\delta+\varepsilon_n(\boldsymbol{k})-\varepsilon_m(\boldsymbol{k})}, \tag{2.42}$$

which is decomposed into the dissipative part $\sigma^{(\mathrm{J})}_{i;j}$ and the non-dissipative part $\sigma^{(\mathrm{E})}_{i;j}$ as

$$\sigma_{i;j}=\sigma^{(\mathrm{J})}_{i;j}+\sigma^{(\mathrm{E})}_{i;j}, \tag{2.43}$$

$$\sigma^{(\mathrm{J})}_{i;j}=-\frac{\hbar^2\delta}{V}\sum_{\boldsymbol{k}nm}\frac{f[\varepsilon_n(\boldsymbol{k})]-f[\varepsilon_m(\boldsymbol{k})]}{\varepsilon_n(\boldsymbol{k})-\varepsilon_m(\boldsymbol{k})}\frac{J^{nm}_{i\boldsymbol{k}}J^{mn}_{j\boldsymbol{k}}}{(\hbar\delta)^2+[\varepsilon_n(\boldsymbol{k})-\varepsilon_m(\boldsymbol{k})]^2}, \tag{2.44}$$

$$\sigma^{(\mathrm{E})}_{i;j}=-\frac{i\hbar}{V}\sum_{\boldsymbol{k}nm}^{\neq}\frac{f[\varepsilon_n(\boldsymbol{k})]-f[\varepsilon_m(\boldsymbol{k})]}{(\hbar\delta)^2+[\varepsilon_n(\boldsymbol{k})-\varepsilon_m(\boldsymbol{k})]^2}J^{nm}_{i\boldsymbol{k}}J^{mn}_{j\boldsymbol{k}}, \tag{2.45}$$

where $\sigma^{(\mathrm{J})}_{i;j}$ corresponds to the symmetric tensor component, whereas $\sigma^{(\mathrm{E})}_{i;j}$ corresponds to the antisymmetric tensor component. From Table 2.14, each component is related to the multipoles as follows:

$$\sigma^{(\mathrm{J})}\leftrightarrow\begin{pmatrix}Q_0-Q_u+Q_v & Q_{xy} & Q_{zx}\\ Q_{xy} & Q_0-Q_u-Q_v & Q_{yz}\\ Q_{zx} & Q_{yz} & Q_0+2Q_u\end{pmatrix},\ \sigma^{(\mathrm{E})}\leftrightarrow\begin{pmatrix}0 & M_z & -M_y\\ -M_z & 0 & M_x\\ M_y & -M_x & 0\end{pmatrix}. \tag{2.46}$$

By applying the active multipoles in the $\mathcal{P}$-symmetric $4/mm'm'$, the electric conductivity tensor in the FM ordering in Fig. 2.2(a) is given as

$$\sigma^{(\mathrm{J})}\leftrightarrow\begin{pmatrix}Q_0-Q_u & 0 & 0\\ 0 & Q_0-Q_u & 0\\ 0 & 0 & Q_0+2Q_u\end{pmatrix},\ \sigma^{(\mathrm{E})}\leftrightarrow\begin{pmatrix}0 & M_z & 0\\ -M_z & 0 & 0\\ 0 & 0 & 0\end{pmatrix}. \tag{2.47}$$

Thus, one expects that the system exhibits the anisotropic electric conductivity along the xy and z directions and the anomalous Hall effect in the xy plane.

Let us take another example by considering the piezomagnetic effect where $M_i=\sum_{jk}\Lambda_{i;jk}\tau_{jk}$. In a similar way, the tensor component in Fig. 2.2(a) is given by

$$\Lambda^{(\mathrm{E})}=\begin{pmatrix}0 & 0 & \Lambda^{(\mathrm{E})}_{z;xx}\\ 0 & 0 & \Lambda^{(\mathrm{E})}_{z;xx}\\ 0 & 0 & \Lambda^{(\mathrm{E})}_{z;zz}\\ 0 & \Lambda^{(\mathrm{E})}_{y;yz} & 0\\ \Lambda^{(\mathrm{E})}_{y;yz} & 0 & 0\\ 0 & 0 & 0\end{pmatrix}^{\mathrm{T}}\leftrightarrow\begin{pmatrix}0 & 0 & 2M'_z+M_z-M^\alpha_z\\ 0 & 0 & 2M'_z+M_z-M^\alpha_z\\ 0 & 0 & 3M_z+2M^\alpha_z\\ 0 & -M'_z+M_z-M^\alpha_z & 0\\ -M'_z+M_z-M^\alpha_z & 0 & 0\\ 0 & 0 & 0\end{pmatrix}^{\mathrm{T}}. \tag{2.48}$$

by using Eq. (E.49). We here omit $\Lambda^{(\mathrm{J})}$ by taking $\delta\to 0$.

$\mathcal{PT}$-symmetric magnetic structure

The staggered magnetic structure belonging to the $\mathrm{T}_{2\mathrm{u}}^{-}$ representation in Fig. 2.2(b) is characterized by the $\mathcal{PT}$-symmetric $4'/m'mm'$. In this case, the odd-parity M multipoles M_{xy} (quadrupole), M_{4z}^{β} (hexadecapole), and odd-parity MT multipole T_z^{β} (octupole) become active in addition to the even-parity E multipoles Q_0, Q_u, Q_4, and Q_{4u}, which are obtained by appropriately replacing the mirror plane of $4'/m'm'm$ in Table 2.11. The active odd-parity M and MT multipoles become sources of induceing the multiferroic responses such as the magnetoelectric effect and the piezoelectric effect in Table 2.14.

For example, the magnetoelectric tensor $\alpha_{i;j}$ is given by

$$\alpha^{(\mathrm{E})}=\begin{pmatrix} 0 & \alpha_{x;y}^{(\mathrm{E})} & 0 \\ \alpha_{x;y}^{(\mathrm{E})} & 0 & 0 \\ 0 & 0 & 0 \end{pmatrix} \leftrightarrow \begin{pmatrix} 0 & M_{xy} & 0 \\ M_{xy} & 0 & 0 \\ 0 & 0 & 0 \end{pmatrix}. \tag{2.49}$$

It is noted that $\alpha^{(\mathrm{J})}=0$, as no odd-parity E and ET multipoles are active under the $\mathcal{PT}$ symmetric magnetic point group $4'/m'm'm$.

Meanwhile, in the inverse piezoelectric response, the response tensor $d_{ij;k}$ for $\varepsilon_{ij}=\sum_k d_{ij;k}E_k$ [38, 79] is described by M_{xy} and T_z^{β} as

$$d^{(\mathrm{J})}=\begin{pmatrix} 0 & 0 & d_{xx;x} \\ 0 & 0 & -d_{xx;x} \\ 0 & 0 & 0 \\ 0 & d_{yz;y} & 0 \\ -d_{yz;y} & 0 & 0 \\ 0 & 0 & 0 \end{pmatrix} \leftrightarrow \begin{pmatrix} 0 & 0 & 2M_{xy}+T_z^{\beta} \\ 0 & 0 & -2M_{xy}-T_z^{\beta} \\ 0 & 0 & 0 \\ 0 & M_{xy}-T_z^{\beta} & 0 \\ -M_{xy}+T_z^{\beta} & 0 & 0 \\ 0 & 0 & 0 \end{pmatrix}. \tag{2.50}$$

Similar to $\alpha_{i;j}$, $d_{ij;k}^{(\mathrm{E})}=0$ owing to the lack of odd-parity E and ET multipoles.

2.5.3 Second-Order Nonlinear Response Function

In a similar way to the linear response tensor $\chi_{i;j}$, we discuss the relation between active multipoles and the second-order nonlinear response tensor $\chi_{i;jk}$ based on the Kubo formula [160]. The nonlinear complex susceptibility $\chi_{i;jk}(\omega',\omega'')$ satisfies the relation

$$\langle \hat{B}_{i,\omega}\rangle=\int_{-\infty}^{\infty}\int_{-\infty}^{\infty}\frac{d\omega'}{2\pi}\frac{d\omega''}{2\pi}\chi_{i;jk}(\omega',\omega'')F_{j,\omega'}F_{k,\omega''}\delta(\omega-\omega'-\omega''), \tag{2.51}$$

where $\chi_{i;jk}(\omega',\omega'')$ is represented as

$$\chi_{i;jk}(\omega',\omega'')=\frac{1}{2}\left(\frac{1}{i\hbar}\right)^2\int_0^{\infty}\int_0^{\infty}dt'dt''\,\mathrm{Tr}\left[\hat{B}_i[\hat{A}_j(-t'),[\hat{A}_k(-t'-t''),\rho_0]]\right] \times e^{i(\omega'+\omega'')t'-2\delta t'}e^{i\omega''t''-\delta t''}+(j,\omega')\leftrightarrow(k,\omega''), \tag{2.52}$$

where $\hat{X}(t)$ is the Heisenberg representation of an operator $\hat{X}$. ρ_0 is the density matrix for the nonperturbative state, whose matrix element is represented by the Fermi distribution function $f(\varepsilon_n)$ as $[\rho_0]_{nm}=f(\varepsilon_n)\delta_{nm}$. When we suppose $\hat{A}$ as the well-defined operator in a

periodic system, i.e., the matrix element of $\hat{A}$ includes no differential operator with respect to the wave vector, the nonlinear response function in the static limit ($\boldsymbol{q}\to\boldsymbol{0}$, $\omega\to 0$) is given as follows.

$$\begin{aligned}\chi_{i;jk}\equiv&\chi_{i;jk}(0,0)\\ =&\frac{1}{2}\frac{1}{V}\sum_{\boldsymbol{k}}\sum_{lmn}\frac{B^{nm}_{i\boldsymbol{k}}\left(A^{ml}_{j\boldsymbol{k}}A^{ln}_{k\boldsymbol{k}}+A^{ml}_{k\boldsymbol{k}}A^{ln}_{j\boldsymbol{k}}\right)}{\varepsilon_n(\boldsymbol{k})-\varepsilon_m(\boldsymbol{k})+2i\hbar\delta}\left\{\frac{f[\varepsilon_n(\boldsymbol{k})]-f[\varepsilon_l(\boldsymbol{k})]}{\varepsilon_n(\boldsymbol{k})-\varepsilon_l(\boldsymbol{k})+i\hbar\delta}-\frac{f[\varepsilon_l(\boldsymbol{k})]-f[\varepsilon_m(\boldsymbol{k})]}{\varepsilon_l(\boldsymbol{k})-\varepsilon_m(\boldsymbol{k})+i\hbar\delta}\right\}.\end{aligned} \tag{2.53}$$

The nonlinear response function is also decomposed into the two parts with different time-reversal properties as

$$\chi_{i;jk}=\chi^{(\mathrm{Re})}_{i;jk}+\chi^{(\mathrm{Im})}_{i;jk}, \tag{2.54}$$

where

$$\begin{aligned}\chi^{(\mathrm{Re})}_{i;jk}\equiv&\frac{1}{V}\sum_{\boldsymbol{k}lmn}\frac{\mathrm{Re}\left(B^{nm}_{i\boldsymbol{k}}A^{ml}_{j\boldsymbol{k}}A^{ln}_{k\boldsymbol{k}}\right)[\varepsilon_n(\boldsymbol{k})-\varepsilon_m(\boldsymbol{k})]}{[\varepsilon_n(\boldsymbol{k})-\varepsilon_m(\boldsymbol{k})]^2+(2\hbar\delta)^2}\\ &\times\left(\frac{\{f[\varepsilon_n(\boldsymbol{k})]-f[\varepsilon_l(\boldsymbol{k})]\}[\varepsilon_n(\boldsymbol{k})-\varepsilon_l(\boldsymbol{k})]}{[\varepsilon_n(\boldsymbol{k})-\varepsilon_l(\boldsymbol{k})]^2+(\hbar\delta)^2}-\frac{\{f[\varepsilon_l(\boldsymbol{k})]-f[\varepsilon_m(\boldsymbol{k})]\}[\varepsilon_l(\boldsymbol{k})-\varepsilon_m(\boldsymbol{k})]}{[\varepsilon_l(\boldsymbol{k})-\varepsilon_m(\boldsymbol{k})]^2+(\hbar\delta)^2}\right)\\ &-\frac{2\hbar^2\delta^2}{V}\sum_{\boldsymbol{k}lmn}\frac{\mathrm{Re}\left(B^{nm}_{i\boldsymbol{k}}A^{ml}_{j\boldsymbol{k}}A^{ln}_{k\boldsymbol{k}}\right)}{[\varepsilon_n(\boldsymbol{k})-\varepsilon_m(\boldsymbol{k})]^2+(2\hbar\delta)^2}\left\{\frac{f[\varepsilon_n(\boldsymbol{k})]-f[\varepsilon_l(\boldsymbol{k})]}{[\varepsilon_n(\boldsymbol{k})-\varepsilon_l(\boldsymbol{k})]^2+(\hbar\delta)^2}-\frac{f[\varepsilon_l(\boldsymbol{k})]-f[\varepsilon_m(\boldsymbol{k})]}{[\varepsilon_l(\boldsymbol{k})-\varepsilon_m(\boldsymbol{k})]^2+(\hbar\delta)^2}\right\},\end{aligned} \tag{2.55}$$

$$\begin{aligned}\chi^{(\mathrm{Im})}_{i;jk}\equiv&\frac{\hbar\delta}{V}\sum_{\boldsymbol{k}lmn}\frac{\mathrm{Im}\left(B^{nm}_{i\boldsymbol{k}}A^{ml}_{j\boldsymbol{k}}A^{ln}_{k\boldsymbol{k}}\right)[\varepsilon_n(\boldsymbol{k})-\varepsilon_m(\boldsymbol{k})]}{[\varepsilon_n(\boldsymbol{k})-\varepsilon_m(\boldsymbol{k})]^2+(2\hbar\delta)^2}\left\{\frac{f[\varepsilon_n(\boldsymbol{k})]-f[\varepsilon_l(\boldsymbol{k})]}{[\varepsilon_n(\boldsymbol{k})-\varepsilon_l(\boldsymbol{k})]^2+(\hbar\delta)^2}-\frac{f[\varepsilon_l(\boldsymbol{k})]-f[\varepsilon_m(\boldsymbol{k})]}{[\varepsilon_l(\boldsymbol{k})-\varepsilon_m(\boldsymbol{k})]^2+(\hbar\delta)^2}\right\}\\ &+\frac{2\hbar\delta}{V}\sum_{\boldsymbol{k}lmn}\frac{\mathrm{Im}\left(B^{nm}_{i\boldsymbol{k}}A^{ml}_{j\boldsymbol{k}}A^{ln}_{k\boldsymbol{k}}\right)}{[\varepsilon_n(\boldsymbol{k})-\varepsilon_m(\boldsymbol{k})]^2+(2\hbar\delta)^2}\\ &\times\left(\frac{\{f[\varepsilon_n(\boldsymbol{k})]-f[\varepsilon_l(\boldsymbol{k})]\}[\varepsilon_n(\boldsymbol{k})-\varepsilon_l(\boldsymbol{k})]}{[\varepsilon_n(\boldsymbol{k})-\varepsilon_l(\boldsymbol{k})]^2+(\hbar\delta)^2}-\frac{\{f[\varepsilon_l(\boldsymbol{k})]-f[\varepsilon_m(\boldsymbol{k})]\}[\varepsilon_l(\boldsymbol{k})-\varepsilon_m(\boldsymbol{k})]}{[\varepsilon_l(\boldsymbol{k})-\varepsilon_m(\boldsymbol{k})]^2+(\hbar\delta)^2}\right).\end{aligned} \tag{2.56}$$

In contrast to the linear response tensor $\chi_{i;j}$, there are complicated intraband and interband processes in both $\chi^{(\mathrm{Re})}_{i;jk}$ and $\chi^{(\mathrm{Im})}_{i;jk}$. It is noted that the nonlinear response function for the electric field in the length gauge needs rederivation by applying $\hat{A}=-e\hat{r}$ ($\hat{r}$: position operator) in Eq. (2.52), since the matrix element of $\hat{r}$ in a periodic system includes differential operator of $\boldsymbol{k}$[4].

$\chi^{(\mathrm{Re})}_{i;jk}$ and $\chi^{(\mathrm{Im})}_{i;jk}$ show the following relations in the presence of the time-reversal symmetry:

$$\chi^{(\mathrm{Re})}_{i;jk}=t_{B_i}t_{A_j}t_{A_k}\chi^{(\mathrm{Re})}_{i;jk},\quad \chi^{(\mathrm{Im})}_{i;jk}=-t_{B_i}t_{A_j}t_{A_k}\chi^{(\mathrm{Im})}_{i;jk}. \tag{2.57}$$

[4]For example, the second-order nonlinear conductivity is obtained by applying $\hat{B}=-e\hat{v}$ ($\hat{v}$: velocity operator) and $\hat{A}=-e\hat{r}$, where its functional form is consistent to the $\omega\to 0$ limit of the second-order nonlinear optical conductivity [161–164]. The second-order nonlinear conductivity has the following δ dependences in the clean limit: δ^{-2} and δ^0 with the time-inversion odd property of $\chi^{(\mathrm{Re})}_{i;jk}$ for the Drude and intrinsic terms, respectively, and δ^{-1} with the time-inversion even property of $\chi^{(\mathrm{Im})}_{i;jk}$ for the Berry curvature dipole term [102].

Equation (2.57) indicates that $\chi^{(\mathrm{Re})}_{i;jk}$ and $\chi^{(\mathrm{Im})}_{i;jk}$ are represented by E and ET (M and MT) multipoles and the M and MT (E and ET) multipoles, respectively, for $t_{B_i}t_{A_j}t_{A_k}=+1(-1)$. The multipoles relevant to the nonlinear response tensors are summarized in Table 2.15. In the following, we show the correspondence between the nonlinear responses and multipoles by considering again the FM and AFM orderings in the diamond structure in Figs. 2.2(a) and 2.2(b).

Table 2.15: Correspondence between the second-order nonlinear response functions $\chi^{(\mathrm{Re,Im})}$ and multipoles. Nonzero $\chi^{(\mathrm{Re,Im})}$ is shown by the checkmark (✓).

rank		$t_{B_i}t_{A_j}t_{A_k}$		multipole	$(\mathcal{P},\mathcal{T},\mathcal{PT})=$ $(\bigcirc,\bigcirc,\bigcirc)$	$(\times,\bigcirc,\times)$	$(\bigcirc,\times,\times)$	$(\times,\times,\bigcirc)$	$(\times,\times,\times)$	examples $(B\leftrightarrow F)$
3	polar	$+1$	$\chi^{(\mathrm{Im})}$	T_{1m},M_{2m},T_{3m}				✓	✓	
			$\chi^{(\mathrm{Re})}$	Q_{1m},G_{2m},Q_{3m}		✓			✓	$(Q_{1m}\leftrightarrow Q_0,Q_{2m})$
		-1	$\chi^{(\mathrm{Im})}$	Q_{1m},G_{2m},Q_{3m}		✓			✓	electric conductivity
			$\chi^{(\mathrm{Re})}$	T_{1m},M_{2m},T_{3m}				✓	✓	$(T_{1m}\leftrightarrow Q_0,Q_{2m})$
	axial	$+1$	$\chi^{(\mathrm{Im})}$	M_{1m},T_{2m},M_{3m}			✓		✓	Nernst effect tensor
			$\chi^{(\mathrm{Re})}$	G_{1m},Q_{2m},G_{3m}	✓	✓	✓	✓	✓	$(T_{1m}\leftrightarrow M_0,M_{2m})$
		-1	$\chi^{(\mathrm{Im})}$	G_{1m},Q_{2m},G_{3m}	✓	✓	✓	✓	✓	magnetoelectric tensor
			$\chi^{(\mathrm{Re})}$	M_{1m},T_{2m},M_{3m}			✓		✓	$(M_{1m}\leftrightarrow Q_0,Q_{2m})$
4	polar	$+1$	$\chi^{(\mathrm{Im})}$	$T_0,M_{1m},T_{2m},M_{3m},T_{4m}$			✓		✓	electric striction tensor $(Q_0,Q_{2m}\leftrightarrow Q_0,Q_{2m})$
			$\chi^{(\mathrm{Re})}$	$Q_0,G_{1m},Q_{2m},G_{3m},Q_{4m}$	✓	✓	✓	✓	✓	
		-1	$\chi^{(\mathrm{Im})}$	$Q_0,G_{1m},Q_{2m},G_{3m},Q_{4m}$	✓	✓	✓	✓	✓	$(Q_0,Q_{2m}\leftrightarrow T_0,T_{2m})$
			$\chi^{(\mathrm{Re})}$	$T_0,M_{1m},T_{2m},M_{3m},T_{4m}$			✓		✓	
	axial	$+1$	$\chi^{(\mathrm{Im})}$	$M_0,T_{1m},M_{2m},T_{3m},M_{4m}$				✓	✓	$(Q_0,Q_{2m}\leftrightarrow G_0,G_{2m})$
			$\chi^{(\mathrm{Re})}$	$G_0,Q_{1m},G_{2m},Q_{3m},G_{4m}$		✓			✓	
		-1	$\chi^{(\mathrm{Im})}$	$G_0,Q_{1m},G_{2m},Q_{3m},G_{4m}$		✓			✓	$(Q_0,Q_{2m}\leftrightarrow M_0,M_{2m})$
			$\chi^{(\mathrm{Re})}$	$M_0,T_{1m},M_{2m},T_{3m},M_{4m}$				✓	✓	

$\mathcal{P}$-symmetric magnetic structure

In the $\mathcal{P}$-symmetric FM structure in Fig. 2.2(a), the nonlinear responses, such as the Nernst effect and the second-order nonlinear magnetoelectric effect, are expected. In the case of the nonlinear magnetoelectric effect $M_i=\sum_{jk}\alpha_{i;jk}E_jE_k$, the tensor $\alpha^{(\mathrm{Re})}_{i;jk}$ becomes nonzero in the presence of the even-parity M and MT multipoles in Table 2.15. Since M_z and M_z^α are active in the $4/mm'm'$ symmetry, the tensor component of $\alpha^{(\mathrm{Re})}_{i;jk}$ is represented

by

$$\alpha^{(\mathrm{Re})}=\begin{pmatrix} 0 & 0 & \alpha^{(\mathrm{E})}_{z;xx} \\ 0 & 0 & \alpha^{(\mathrm{E})}_{z;xx} \\ 0 & 0 & \alpha^{(\mathrm{E})}_{z;zz} \\ 0 & \alpha^{(\mathrm{E})}_{y;yz} & 0 \\ \alpha^{(\mathrm{E})}_{y;yz} & 0 & 0 \\ 0 & 0 & 0 \end{pmatrix}^{\mathrm{T}} \leftrightarrow \begin{pmatrix} 0 & 0 & 2M'_z+M_z-M^\alpha_z \\ 0 & 0 & 2M'_z+M_z-M^\alpha_z \\ 0 & 0 & 3M_z+2M^\alpha_z \\ 0 & -M'_z+M_z-M^\alpha_z & 0 \\ -M'_z+M_z-M^\alpha_z & 0 & 0 \\ 0 & 0 & 0 \end{pmatrix}^{\mathrm{T}}. \tag{2.58}$$

where there are three independent matrix elements in $\alpha^{(\mathrm{Re})}$.

$\mathcal{PT}$-symmetric magnetic structure

In the AFM ordering with the $4'/m'mm'$ symmetry in Fig. 2.2(b), the second-order nonlinear conductivity, $\sigma_{i;jk}$, for $J_i=\sum_{jk}\sigma_{i;jk}E_jE_k$ becomes nonzero, which reflects the lack of the spatial inversion symmetry. Among the two parts $\sigma^{(\mathrm{Re})}_{i;jk}$ and $\sigma^{(\mathrm{Im})}_{i;jk}$, $\sigma^{(\mathrm{Re})}_{i;jk}$ becomes nonzero in the presence of the odd-parity M and MT multipoles. The finite tensor component of $\sigma^{(\mathrm{Re})}_{i;jk}$ is shown as

$$\sigma^{(\mathrm{Re})}=\begin{pmatrix} 0 & 0 & \sigma^{(\mathrm{Re})}_{x;xx} \\ 0 & 0 & -\sigma^{(\mathrm{Re})}_{x;xx} \\ 0 & 0 & 0 \\ 0 & \sigma^{(\mathrm{Re})}_{y;zy} & 0 \\ -\sigma^{(\mathrm{Re})}_{y;zy} & 0 & 0 \\ 0 & 0 & 0 \end{pmatrix}^{\mathrm{T}} \leftrightarrow \begin{pmatrix} 0 & 0 & 2M_{xy}+T^\beta_z \\ 0 & 0 & -2M_{xy}-T^\beta_z \\ 0 & 0 & 0 \\ 0 & M_{xy}-T^\beta_z & 0 \\ -M_{xy}+T^\beta_z & 0 & 0 \\ 0 & 0 & 0 \end{pmatrix}. \tag{2.59}$$

Thus, the nonlinear conductivity, which is known as the nonlinear Drude and the intrinsic terms, is expected in the AFM structure in Fig. 2.2(b) [102].

2.6 Summary

In summary, we have completed the classification of multipoles in the 122 magnetic point groups by extending the classification to the nonunitary groups with the antiunitary operations accompanied by the time-reversal operation. The present classification gives the systematic way to identify the symmetry-adapted electronic order parameters not only in the AFM orderings but also in unconventional nematic, chiral, excitonic, loop-current, and anisotropic bond ordered states. Moreover, we have also clarified the relation between the multipoles and field responses to cover the second-order nonlinear response in addition to the linear response in the previous studies [38, 39], which gives us an intuitive understanding of the multiferroic phenomena and nonlinear transports based on the microscopic multipole couplings. The present comprehensive study will help the exploration of the further exotic physical phenomena induced by the unconventional higher-rank multipoles, such as MT quadrupole and octupole, and the functional magnetic materials in cooperation with the material database like MAGNDATA [165].

Chapter 3

Nonlinear Transport in Magnetic Toroidal Dipole Ordering

In this chapter, we investigate the microscopic essential model parameters of the nonlinear transport property in the collinear AFM ordering with the MT dipole moment, which is called the MT dipole ordering. The present chapter is based on Ref. [166].

This chapter is organized as follows. Section 3.1 describes the introduction of the MT dipole physics. In Sec. 3.2, we show the electronic multipole degrees of freedom activated in the tight-binding model on the two-sublattice zigzag chain. We also present the response functions for the linear magnetoelectric effect, Hall effect, and second-order nonlinear conductivity. We discuss the conditions to cause the linear and nonlinear responses under the MT dipole ordering based on the microscopic model calculations. We show the essential model parameters in each response. Sec. 3.4 is devoted to the summary in this chapter.

3.1 Introduction

An MT dipole, which is one of the odd-parity multipoles in the absence of the spatial inversion and time-reversal symmetries, has attracted much attention as it induces various multiferroic phenomena like the magnetoelectric effect [58, 113, 167, 168] and nonreciprocal transport properties [103, 115, 169, 170]. Among them, the magnetoelectric effect in the MT dipole orderings has been observed in the AFM insulators, e.g., Cr_2O_3 [63], $Ga_{2-x}Fe_xO_3$ [64, 65], $LiCoPO_4$ [66, 67], and $Ba_2CoGe_2O_7$ [68], and in the AFM metals, e.g., UNi_4B [69–71] and Ce_3TiBi_5 [72, 73]. Theoretically, such a magnetoelectric effect has been analyzed by using the linear response theory [69, 99, 171–176]. Meanwhile, there are still few studies on the nonlinear transports [104, 170, 177, 178]. Especially, its microscopic understanding beyond the symmetry argument has not been fully understood. One of the remaining problems is the lacking of the understanding of the essential model parameters to induce the nonlinear transport. It is also important to understand how the MT dipole plays a role in the nonlinear transport.

By performing the symmetry analysis and model calculation with the use of the second-order nonlinear Kubo formula, we elucidate the microscopic essential model parameters for the second-order nonlinear conductivity in the MT orderings with the $\mathcal{PT}$ symmetry.

Based on the analysis of a minimal model on a two-dimensionally-stacked zigzag chain, we show that an effective coupling between the MT dipole and the antisymmetric spin-orbit interaction (ASOI) plays an essential role in inducing the longitudinal and transverse components of the nonlinear conductivity. Moreover, we find that the nonlinear conductivities are highly enhanced near the transition temperature in the case that the AFM molecular field is comparable to the ASOI in a multi-band system. We also discuss the difference between the transverse nonlinear conductivity and the linear magnetoelectric coefficient on the basis of the microscopic model parameters.

3.2 Model

We show the multipole degrees of freedom in a two-sublattice unit cell on a zigzag chain from the symmetry viewpoint in Sec. 3.2.1. Then, we present a minimal two-band tight-binding model in Sec. 3.2.2 and outline the linear and second-order nonlinear response functions in Sec. 3.2.3.

3.2.1 Multipole Degrees of Freedom

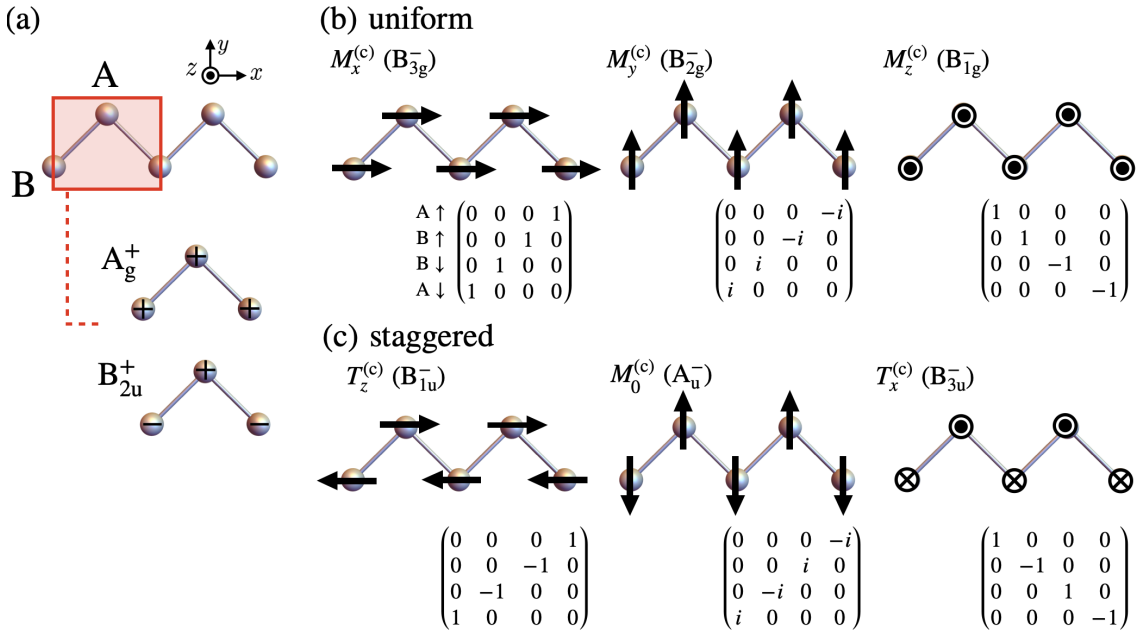

Figure 3.1: (a) Zigzag chain with two sublattices A and B. The IRREPs and the corresponding potential distributions are also shown below. (b,c) Magnetic structures of the (b) uniform and (c) staggered alignments. The corresponding IRREPs, cluster multipoles, and their matrix elements in the 4×4 Hilbert space spanned by the spin and sublattice degrees of freedom are also shown.

We describe the six degrees of freedom consisting of the three spin components and two sublattices by the symmetry-adapted cluster multipoles. The zigzag structure has the orthorhombic symmetry $mmm1'$, where the corepresentation of the sublattice degrees of freedom $\Gamma_{\rm sub}$ is decomposed into two IRREPs as $\Gamma_{\rm sub}=A_g^+\oplus B_{2u}^+$. The former (latter)

corresponds to the uniform (staggered) potential configuration on the sublattices A and B as shown in Fig. 3.1(a). Since M dipole degrees of freedom have the symmetry $\Gamma_{\rm MD}=\mathrm{B}_{1g}^{-}\oplus\mathrm{B}_{2g}^{-}\oplus\mathrm{B}_{3g}^{-}$ from Table C.24, the IRREPs of the magnetic structure with the ordering vector $\boldsymbol{q}=\boldsymbol{0}$ are obtained as follows:

$$\Gamma_{\rm sub}\otimes\Gamma_{\rm MD}=(\mathrm{B}_{1g}^{-}\oplus\mathrm{B}_{2g}^{-}\oplus\mathrm{B}_{3g}^{-})_{\rm uniform}\oplus(\mathrm{B}_{1u}^{-}\oplus\mathrm{A}_{u}^{-}\oplus\mathrm{B}_{3u}^{-})_{\rm staggered}. \tag{3.1}$$

The former three components $\mathrm{B}_{1g}^{-}\oplus\mathrm{B}_{2g}^{-}\oplus\mathrm{B}_{3g}^{-}$ stand for the ferromagnetic structures [Fig. 3.1(b)], which corresponds to the active cluster-type M dipoles: $M_x^{(\rm c)}$, $M_y^{(\rm c)}$, and $M_z^{(\rm c)}$. Meanwhile, the latter three components $\mathrm{B}_{1u}^{-}\oplus\mathrm{A}_{u}^{-}\oplus\mathrm{B}_{3u}^{-}$ are the collinear AFM structures [Fig. 3.1(c)]. From Table C.24, their corresponding multipoles are the MT dipoles $T_x^{(\rm c)}$ and $T_z^{(\rm c)}$ for B_{3u}^{-} and B_{1u}^{-}, respectively, and M monopole $M_0^{(\rm c)}$ for A_{u}^{-}. In the following discussion, we focus on the MT dipole $T_x^{(\rm c)}$ and examine the relevant nonlinear and multiferroic responses induced by $T_x^{(\rm c)}$. The following discussion is straightforwardly applied to another MT dipole $T_z^{(\rm c)}$.

3.2.2 Minimal Two-Band Model

To examine the microscopic essence of the nonlinear conductivity in the presence of the MT dipole in a solid, we consider a minimal two-band model where the zigzag chain along the x direction [Fig. 3.2(a)] is stacked along the z direction [Fig. 3.2(b)].

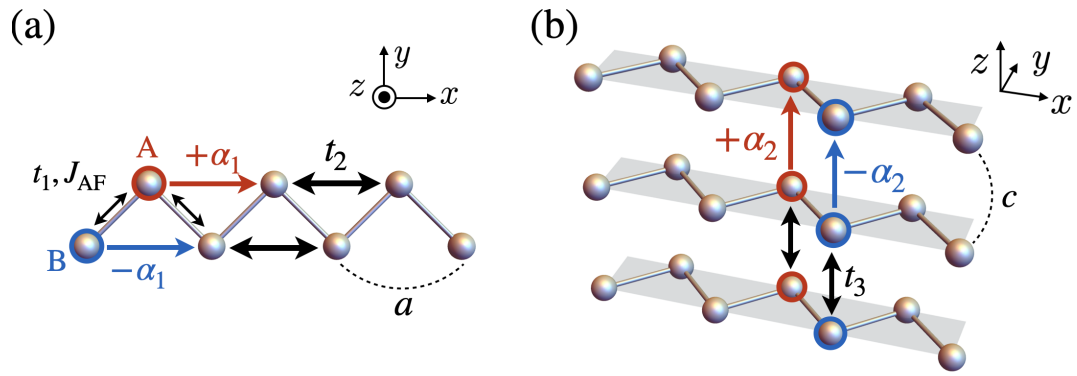

Figure 3.2: (a,b) Schematic pictures of (a) a two-sublattice zigzag chain and (b) its stacking along the z direction.

The tight-binding Hamiltonian is given by

$$\mathcal{H}=\mathcal{H}_{\rm hop}^{\rm AB}+\mathcal{H}_{\rm hop}+\mathcal{H}_{\rm ASOI}+\mathcal{H}_{\rm int}, \tag{3.2}$$

$$\mathcal{H}_{\rm hop}^{\rm AB}=\sum_{\boldsymbol{k}}\sum_{\sigma}\left[\varepsilon^{\rm AB}(\boldsymbol{k})c_{\boldsymbol{k}\mathrm{A}\sigma}^{\dagger}c_{\boldsymbol{k}\mathrm{B}\sigma}+\mathrm{H.c.}\right], \tag{3.3}$$

$$\mathcal{H}_{\rm hop}=\sum_{\boldsymbol{k}}\sum_{\sigma}\varepsilon(\boldsymbol{k})(c_{\boldsymbol{k}\mathrm{A}\sigma}^{\dagger}c_{\boldsymbol{k}\mathrm{A}\sigma}+c_{\boldsymbol{k}\mathrm{B}\sigma}^{\dagger}c_{\boldsymbol{k}\mathrm{B}\sigma}), \tag{3.4}$$

$$\mathcal{H}_{\rm ASOI}=\sum_{\boldsymbol{k}}\sum_{\sigma\sigma'}\boldsymbol{g}(\boldsymbol{k})\cdot\boldsymbol{\sigma}^{\sigma\sigma'}(c_{\boldsymbol{k}\mathrm{A}\sigma}^{\dagger}c_{\boldsymbol{k}\mathrm{A}\sigma'}-c_{\boldsymbol{k}\mathrm{B}\sigma}^{\dagger}c_{\boldsymbol{k}\mathrm{B}\sigma'}), \tag{3.5}$$

$$\mathcal{H}_{\rm int}=J_{\rm AF}\sum_{\langle ij\rangle}\hat{M}_{i\mathrm{A}}^{z}\hat{M}_{j\mathrm{B}}^{z}, \tag{3.6}$$

where $c^\dagger_{\boldsymbol{k}l\sigma}$ ($c_{\boldsymbol{k}l\sigma}$) is the creation (annihilation) operator of electrons at wave vector $\boldsymbol{k}$, sublattice l=A, B, and spin $\sigma=\uparrow,\downarrow$. The hopping Hamiltonian $\mathcal{H}^{\rm AB}_{\rm hop}$ in Eq. (3.3) includes the nearest-neighbor hopping between A and B sublattices as $\varepsilon^{\rm AB}(\boldsymbol{k})=-2t_1\cos(k_xa/2)$, while $\mathcal{H}_{\rm hop}$ includes the hoppings within the same sublattices along the x and z directions as $\varepsilon(\boldsymbol{k})=-2t_2\cos(k_xa)-2t_3\cos(k_zc)$. $\mathcal{H}_{\rm ASOI}$ in Eq. (3.5) represents the ASOI that arises from the relativistic spin-orbit coupling as $\boldsymbol{g}(\boldsymbol{k})=[-\alpha_2\sin(k_zc),0,\alpha_1\sin(k_xa)]$. The ASOI in Eq. (3.5) has the sublattice-dependent staggered form satisfying the global inversion symmetry [171, 179]. $\mathcal{H}_{\rm int}$ in Eq. (3.6) represents the Ising-type AFM exchange interaction of the nearest-neighbor A-B bond with $J_{\rm AF}>0$ where $\hat{M}^z_{i{\rm A(B)}}=\sum_{\sigma\sigma'}c^\dagger_{i{\rm A(B)}\sigma}\sigma^z_{\sigma\sigma'}c_{i{\rm A(B)}\sigma'}$ is the z component of the M dipole operator and $c^\dagger_{il\sigma}$ and $c_{il\sigma}$ are the Fourier transforms of $c^\dagger_{\boldsymbol{k}l\sigma}$ and $c_{\boldsymbol{k}l\sigma}$, respectively. We adopt the Hartree-type mean-field decoupling as

$$J_{\rm AF}\sum_{\langle ij\rangle}\hat{M}^z_{i\rm A}\hat{M}^z_{j\rm B}\to\tilde{J}_{\rm AF}\sum_i\left(\langle\hat{M}^z_{\rm A}\rangle\,\hat{M}^z_{i\rm B}+\langle\hat{M}^z_{\rm B}\rangle\,\hat{M}^z_{i\rm A}-\langle\hat{M}^z_{\rm A}\rangle\,\langle\hat{M}^z_{\rm B}\rangle\right), \tag{3.7}$$

where $\langle\cdots\rangle$ represents the statistical average and $\tilde{J}_{\rm AF}=2J_{\rm AF}$ is the renormalized coupling constant considering the two nearest-neighbor atomic sites. As presented in Sec. 3.2.1, the staggered AFM moment along the z direction in the present system is equivalent to the uniform cluster MT dipole along the x direction, $T^{\rm MF}_x\equiv(\langle\hat{M}^z_{\rm A}\rangle-\langle\hat{M}^z_{\rm B}\rangle)/2$ [180], where the superscript MF is used instead of (c) to explicitly represent the mean-field value in the following.

3.2.3 Response Functions

The magnetic point group symmetry is reduced from $mmm1'$ to $m'mm$ in the presence of $T^{\rm MF}_x$ from Table C.24. In the magnetic point group $m'mm$, the following even-parity E and ET multipoles and odd-parity M and MT multipoles within rank 0–3 belong to the totally symmetric IRREP:

$$Q_0, Q_u, Q_v, G_{xyz}, T_x, T^\alpha_x, T^\beta_x, M_{yz}, \tag{3.8}$$

as shown in Table 2.11. Due to the presence of the odd-parity multipoles like $T_x, T^\alpha_x, T^\beta_x$, and M_{yz}, the second-order nonlinear electric conductivity tensor is expected as follows:

$$\sigma^{\rm (Re)}=\begin{pmatrix}\sigma_{xxx}&0&0\\ \sigma_{xyy}&0&0\\ \sigma_{xzz}&0&0\\ 0&0&0\\ 0&0&\sigma_{zzx}\\ 0&\sigma_{yxy}&0\end{pmatrix}^{\rm T} \tag{3.9}$$

$$\leftrightarrow\begin{pmatrix}3T_x+2T^\alpha_x&0&0\\ 2(T'_x+M_{yz})+T_x-T^\alpha_x+T^\beta_x&0&0\\ 2(T'_x-M_{yz})+T_x-T^\alpha_x-T^\beta_x&0&0\\ 0&0&0\\ 0&0&-T'_x+M_{yz}+T_x-T^\alpha_x-T^\beta_x\\ 0&-T'_x-M_{yz}+T_x-T^\alpha_x+T^\beta_x&0\end{pmatrix}^{\rm T}, \tag{3.10}$$

where $\sigma^{(\mathrm{Re})}$ includes the Drude-type intraband term and the intrinsic-type interband term within the relaxation time approximation as mentioned in Sec. 2.5[1]. The former Drude-type term is represented by the MT dipoles and octupoles as

$$\sigma^{(\mathrm{D})}=\begin{pmatrix} \sigma^{(\mathrm{D})}_{xxx} & 0 & 0 \\ \sigma^{(\mathrm{D})}_{xyy} & 0 & 0 \\ \sigma^{(\mathrm{D})}_{xzz} & 0 & 0 \\ 0 & 0 & 0 \\ 0 & 0 & \sigma^{(\mathrm{D})}_{zzx} \\ 0 & \sigma^{(\mathrm{D})}_{yxy} & 0 \end{pmatrix}^{\mathrm{T}} \leftrightarrow \begin{pmatrix} 3T_x+2T_x^\alpha & 0 & 0 \\ T_x-T_x^\alpha+T_x^\beta & 0 & 0 \\ T_x-T_x^\alpha-T_x^\beta & 0 & 0 \\ 0 & 0 & 0 \\ 0 & 0 & T_x-T_x^\alpha-T_x^\beta \\ 0 & T_x-T_x^\alpha+T_x^\beta & 0 \end{pmatrix}^{\mathrm{T}}, \tag{3.12}$$

while the latter intrinsic-type term is expressed by the MT dipoles and M quadrupoles as

$$\sigma^{(\mathrm{int})}=\begin{pmatrix} 0 & 0 & 0 \\ \sigma^{(\mathrm{int})}_{xyy} & 0 & 0 \\ \sigma^{(\mathrm{int})}_{xzz} & 0 & 0 \\ 0 & 0 & 0 \\ 0 & 0 & \sigma^{(\mathrm{int})}_{zzx} \\ 0 & \sigma^{(\mathrm{int})}_{yxy} & 0 \end{pmatrix}^{\mathrm{T}} \leftrightarrow \begin{pmatrix} 0 & 0 & 0 \\ 2(T_x+M_{yz}) & 0 & 0 \\ 2(T_x-M_{yz}) & 0 & 0 \\ 0 & 0 & 0 \\ 0 & 0 & -T_x+M_{yz} \\ 0 & -T_x-M_{yz} & 0 \end{pmatrix}^{\mathrm{T}}. \tag{3.13}$$

Among them, we consider the Drude-type intraband contribution with the dissipation δ^{-2} by supposing the clean limit. The expression representing the Drude-type intraband contribution eventually coincides with that obtained by the Boltzmann formalism [102, 170, 181], which is given as follows:

$$\sigma^{(\mathrm{D})}_{\mu\nu\lambda}=\frac{e^3\tau^2}{\hbar^3}\frac{1}{V}\sum_{\boldsymbol{k}}\sum_{n}\frac{\partial^2\varepsilon_n(\boldsymbol{k})}{\partial k_\mu\partial k_\nu}\frac{\partial\varepsilon_n(\boldsymbol{k})}{\partial k_\lambda}\frac{\partial f[\varepsilon_n(\boldsymbol{k})]}{\partial\varepsilon_n(\boldsymbol{k})}, \tag{3.14}$$

where $e(>0)$, $\tau(=1/\delta)$, and V are the electron charge, relaxation time, and the system volume, respectively. Among the nonlinear components in Eq. (3.12), $\sigma^{(\mathrm{D})}_{xyy}$ and $\sigma^{(\mathrm{D})}_{yxy}$ vanish owing to $k_y=0$ in the present two-dimensional system. Moreover, $\sigma^{(\mathrm{D})}_{xzz}=\sigma^{(\mathrm{D})}_{zzx}$ is satisfied as shown in Eq. (3.12). Hence, the present system has two independent components: the longitudinal $\sigma^{(\mathrm{D})}_{xxx}$ and transverse $\sigma^{(\mathrm{D})}_{xzz}$. Hereafter, we omit the superscript of $\sigma^{(\mathrm{D})}_{\mu\nu\lambda}$ and use the scaled $\sigma_{\mu\nu\lambda}$ as $\bar{\sigma}_{\mu\nu\lambda}=\sigma_{\mu\nu\lambda}/(e^3\tau^2\hbar^{-3})$.

[1]The Drude-type and intrinsic-type terms have different symmetry with respect to the permutation of the input and output directions; the former is totally symmetric and the latter is asymmetric. By considering such a difference, the multipole expression of $\sigma^{(\mathrm{Re})}$ can be decomposed into the Drude-type part $\sigma^{(\mathrm{D})}$ and the intrinsic-type part $\sigma^{(\mathrm{int})}$ as follows:

$$\sigma^{(\mathrm{D})}=\begin{pmatrix} 3T_x+2T_x^\alpha & T_y-T_y^\alpha-T_y^\beta & T_z-T_z^\alpha+T_z^\beta \\ T_x-T_x^\alpha+T_x^\beta & 3T_y+2T_y^\alpha & T_z-T_z^\alpha-T_z^\beta \\ T_x-T_x^\alpha-T_x^\beta & T_y-T_y^\alpha+T_y^\beta & 3T_z+2T_z^\alpha \\ T_{xyz} & T_z-T_z^\alpha-T_z^\beta & T_y-T_y^\alpha+T_y^\beta \\ T_z-T_z^\alpha+T_z^\beta & T_{xyz} & T_x-T_x^\alpha-T_x^\beta \\ T_y-T_y^\alpha-T_y^\beta & T_x-T_x^\alpha+T_x^\beta & T_{xyz} \end{pmatrix}^{\mathrm{T}}, \quad \sigma^{(\mathrm{int})}=\begin{pmatrix} 0 & 2(T_y-M_{zx}) & 2(T_z+M_{xy}) \\ 2(T_x+M_{yz}) & 0 & 2(T_z-M_{xy}) \\ 2(T_x-M_{yz}) & 2(T_y+M_{zx}) & 0 \\ M_u+M_v & -T_z+M_{xy} & -T_y-M_{zx} \\ -T_z-M_{xy} & -M_u+M_v & -T_x+M_{yz} \\ -T_y+M_{zx} & -T_x-M_{yz} & -2M_v \end{pmatrix}^{\mathrm{T}}. \tag{3.11}$$

For later convenience, we show the expressions of two quantities, the linear magnetoelectric coefficient α_{yz} and the linear Hall coefficient σ_{xz}, both of which are calculated by the linear response theory:

$$\alpha_{yz}=\frac{eg\mu_{\rm B}\hbar}{2Vi}\sum_{\boldsymbol{k}}\sum_{n\neq m}\frac{f[\varepsilon_n(\boldsymbol{k})]-f[\varepsilon_m(\boldsymbol{k})]}{[\varepsilon_n(\boldsymbol{k})-\varepsilon_m(\boldsymbol{k})]^2+(\hbar\delta)^2}\sigma_{y\boldsymbol{k}}^{nm}v_{z\boldsymbol{k}}^{mn}, \tag{3.15}$$

$$\sigma_{xz}=\frac{e^2\hbar}{Vi}\sum_{\boldsymbol{k}}\sum_{n\neq m}\frac{f[\varepsilon_n(\boldsymbol{k})]-f[\varepsilon_m(\boldsymbol{k})]}{[\varepsilon_n(\boldsymbol{k})-\varepsilon_m(\boldsymbol{k})]^2+(\hbar\delta)^2}v_{x\boldsymbol{k}}^{nm}v_{z\boldsymbol{k}}^{mn}. \tag{3.16}$$

In Eq. (3.15), $g(=2)$ and $\mu_{\rm B}$ are the g factor and Bohr magneton, respectively. $\sigma_{y\boldsymbol{k}}^{nm}=\langle n\boldsymbol{k}|\sigma_y|m\boldsymbol{k}\rangle$ and $v_{z\boldsymbol{k}}^{mn}=\langle m\boldsymbol{k}|v_{z\boldsymbol{k}}|n\boldsymbol{k}\rangle$ are the matrix elements of spin σ_y and the velocity $v_{z\boldsymbol{k}}=\partial\mathcal{H}/(\hbar\partial k_z)$ for the eigenstate $|n\boldsymbol{k}\rangle$. The interband process is important in both tensors. We use the scaled $\bar{\alpha}_{yz}=\alpha_{yz}/(e\mu_{\rm B}\hbar)$ and $\bar{\sigma}_{xz}=\sigma_{xz}/(e^2\hbar H_y)$.

3.3 Result

In this section, we discuss the microscopic essential model parameters for the physical properties in the MT dipole ordering by analyzing the minimal model presented in Sec. 3.2.2. The numerical results of the band modulation, nonlinear conductivity, and the linear magnetoelectric effect are discussed in Secs. 3.3.1, 3.3.2, and 3.3.3, respectively. We set the model parameters as $(t_1,t_2,t_3,J_{\rm AF})=(0.1,1,0.5,2.5)$, electron filling as 1/5, and the lattice constant as $a=c=1$ in the following discussion; t_2 is set as the energy unit.

3.3.1 Band Modulation

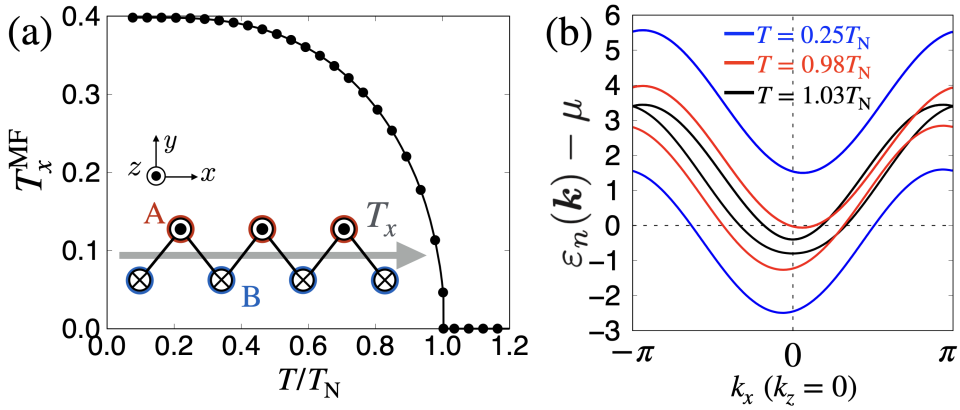

Figure 3.3: (a) The temperature (T) dependence of the MT dipole $T_x^{\rm MF}$ at $\alpha_1=0.4$ and $\alpha_2=0.1$. The MT dipole ordering along the x direction T_x is shown in the inset. (b) The energy bands measured from the chemical potential μ at $k_z=0$ for three temperatures.

First, we show the T dependence of $T_x^{\rm MF}$ at $\alpha_1=0.4$ and $\alpha_2=0.1$ in Fig. 3.3(a), where $T_x^{\rm MF}$ is self-consistently determined within the mean-field calculations for the two-sublattice unit cell by taking over 200^2 grid points in the Brillouin zone. $T_x^{\rm MF}$ becomes

nonzero below the transition temperature $T_{\rm N}$ and saturates below $T{\simeq}0.2T_{\rm N}$. Almost the same behavior is obtained for $\alpha_1, \alpha_2 {\lesssim} 0.5$.

As discussed in Sec. 1.3.4, the asymmetric band deformation is induced by the MT dipole. In fact, Fig. 3.3(b) shows the asymmetric band deformation along the k_x direction when $T_x^{\rm MF}{\neq}0$ [171, 180]. This asymmetric band modulation is understood from the effective coupling between $T_x^{\rm MF}$ and the ASOI α_1. We explicitly write down the band dispersion $\varepsilon_{\pm}(\boldsymbol{k})$ as

$$\varepsilon_{\pm}(\boldsymbol{k}){=}\varepsilon(\boldsymbol{k}){\pm}X(\boldsymbol{k}) \text{ with } X(\boldsymbol{k}){=}\sqrt{(\alpha_1 \sin k_x{-}\tilde{T}_x^{\rm MF})^2{+}\alpha_2^2 \sin^2 k_z{+}4t_1^2 \cos^2 \frac{k_x}{2}}, \quad (3.17)$$

where $\tilde{T}_x^{\rm MF}{=}\tilde{J}_{\rm AF}T_x^{\rm MF}$. The double degeneracy of $\varepsilon_{\pm}(\boldsymbol{k})$ is due to the $\mathcal{PT}$ symmetry. The factor $(\alpha_1 \sin k_x{-}\tilde{T}_x^{\rm MF})^2$ includes the coupling between $\tilde{T}_x^{\rm MF}$ and α_1 with the odd function of k_x, which clearly corresponds to the microscopic origin of the antisymmetric band modulation. This asymmetric band modulation becomes a source of the nonlinear transport as discussed in the subsequent section.

3.3.2 Second-Order Nonlinear Conductivity

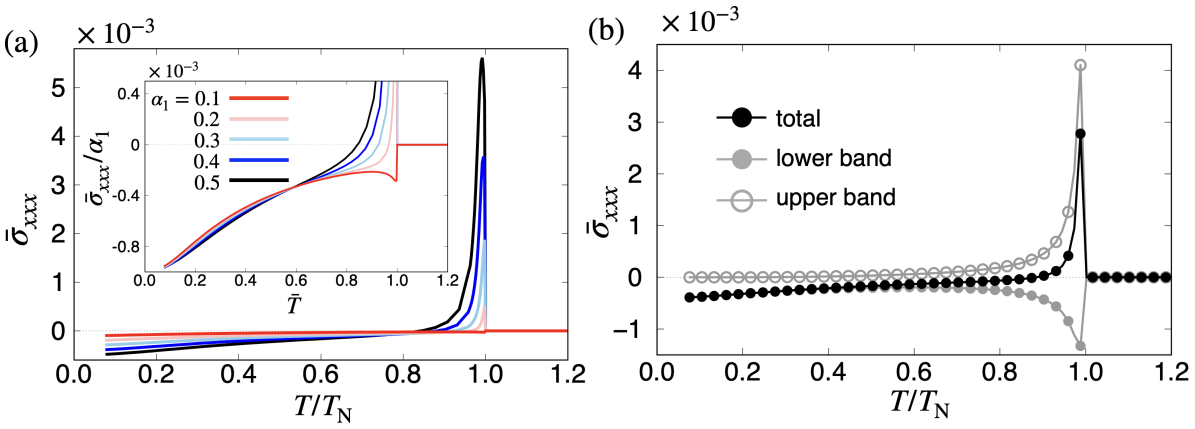

Figure 3.4: (a) The longitudinal second-order conductivity $\bar{\sigma}_{xxx}$ for $\alpha_1{=}0.1$–0.5 as a function of T at $\alpha_2{=}0.1$. The inset shows $\bar{\sigma}_{xxx}/\alpha_1$. (b) The upper- and lower-band contributions to $\bar{\sigma}_{xxx}$ at $\alpha_1{=}0.4$.

We discuss the longitudinal nonlinear conductivity $\bar{\sigma}_{xxx}$. Figure 3.4(a) shows $\bar{\sigma}_{xxx}$ as a function of T for various $\alpha_1{=}0.1$–0.5 at $\alpha_2{=}0.1$. The T dependence for different α_1 shows a qualitatively similar behavior; $\bar{\sigma}_{xxx}$ is highly enhanced just below $T{=}T_{\rm N}$, and shows maximum with a decrease of T. While further decreasing T, $\bar{\sigma}_{xxx}$ shows the sign change, and then reaches a negative value at the lowest T.

The nonzero σ_{xxx} is closely related to the formation of the asymmetric band structure under $T_x^{\rm MF}{\neq}0$. As the asymmetric band modulation is caused by the coupling between $\tilde{T}_x^{\rm MF}$ and α_1, they are indispensable for nonzero σ_{xxx}. In fact, $\bar{\sigma}_{xxx}$ vanishes for $\alpha_1{=}0$. Furthermore, the numerical result in the inset of Fig. 3.4(a) shows that $\bar{\sigma}_{xxx}$ is well scaled by $\bar{\sigma}_{xxx}/\alpha_1$ at low temperatures $T{\lesssim}0.7T_{\rm N}$.

Meanwhile, $\bar{\sigma}_{xxx}$ is not scaled by α_1 for $0.7{\lesssim}T/T_{\rm N}{\leq}1$, where $\bar{\sigma}_{xxx}$ is drastically enhanced. This is attributed to the rapid increase of $\tilde{T}_x^{\rm MF}$ and resultant drastic change of

the electronic band structure near the Fermi level. As σ_{xxx} in Eq. (3.14) includes the factors $\partial^2\varepsilon_n(\boldsymbol{k})/\partial k_x^2$ and $\partial\varepsilon_n(\boldsymbol{k})/\partial k_x$, the small $X(\boldsymbol{k})$ appearing in the denominator of $\partial^2\varepsilon_n(\boldsymbol{k})/\partial k_x^2$ and $\partial\varepsilon_n(\boldsymbol{k})/\partial k_x$ gives a dominant contribution. When considering the small order parameter compared to the ASOI, i.e., $\tilde{T}_x^{\rm MF}\lesssim\alpha_1$, $X(\boldsymbol{k})$ can become small when the Fermi wavenumber $k_x^{\rm F}$ satisfies $\tilde{T}_x^{\rm MF}\simeq\alpha_1\sin k_x^{\rm F}$, which results in a large enhancement of $\bar{\sigma}_{xxx}$. Such an enhancement is remarkable when the upper and lower bands are closely located in the paramagnetic state as shown in Fig. 3.3(b), which can be realized for small t_1=0.1 and α_2=0.1. In short, there are two conditions for the realization of large $\bar{\sigma}_{xxx}$; One is the large essential model parameters, such as α_1, $T_x^{\rm MF}$, and $J_{\rm AF}$, and the other is to satisfy $\tilde{T}_x^{\rm MF}\simeq\alpha_1\sin k_x^{\rm F}$ when there is a drastic change of the band structure by the MTD ordering in a multi-band system. These conditions might be experimentally controlled by electron/hole doping and temperature.

The sign change of $\bar{\sigma}_{xxx}$ in T dependence is owing to the multiband effect. As shown in Fig. 3.3(b), the band bottom is shifted in the opposite direction for the upper and lower bands, which means that the opposite sign of the coupling $\alpha_1\tilde{T}_x^{\rm MF}$ results in the opposite contribution to $\bar{\sigma}_{xxx}$. This is demonstrated by decomposing $\bar{\sigma}_{xxx}$ into the upper- and lower-band contributions, as shown in Fig. 3.4(b). The results indicate that the dominant contribution of $\bar{\sigma}_{xxx}$ arises from the upper band for $0.9\lesssim T/T_{\rm N}\leq 1$, while that arises from the lower band for $T/T_{\rm N}\lesssim 0.9$. The suppression of the upper-band contribution for low T is because it becomes away from the Fermi level by the development of $T_x^{\rm MF}$.

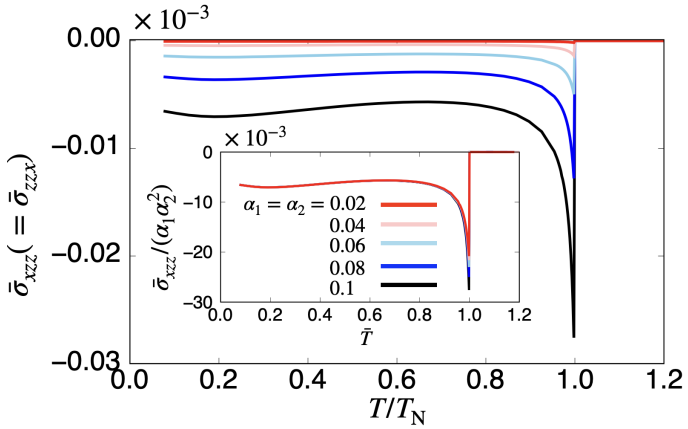

Figure 3.5: The transverse second-order nonlinear conductivity $\bar{\sigma}_{xzz}$ for several α_1 and α_2 while keeping α_1=α_2. The inset represents $\bar{\sigma}_{zxx}/(\alpha_1\alpha_2^2)$.

Next, let us discuss the transverse nonlinear conductivity $\bar{\sigma}_{xzz}$. Figure 3.5 shows the T dependence of $\bar{\sigma}_{xzz}$ for $0.02\leq\alpha_1,\alpha_2\leq 0.1$ with α_1=α_2. The behavior of $\bar{\sigma}_{xzz}$ against T is similar to $\bar{\sigma}_{xxx}$ except for the sign change; $\bar{\sigma}_{xzz}$ becomes nonzero below $T_{\rm N}$ and shows the maximum just below $T_{\rm N}$. While decreasing T, $\bar{\sigma}_{xzz}$ is suppressed and shows an almost constant value.

Similar to σ_{xxx}, the origin of nonzero σ_{xzz} is the asymmetric band modulation under $T_x^{\rm MF}\neq 0$ via the effective coupling $\tilde{T}_x^{\rm MF}\alpha_1$. Besides, we find another contribution from α_2 for nonzero σ_{xzz} in contrast to σ_{xxx}. This additional parameter dependence is owing to an additional symmetry between k_z and $k_z+\pi$ for α_2=0, which gives the opposite-sign contribution to σ_{xzz} so that totally σ_{xzz}=0. As shown in the inset of Fig. 3.5, $\bar{\sigma}_{xzz}$ is well

scaled by $\alpha_1\alpha_2^2$.

3.3.3 Linear Magnetoelectric Effect and Hall Effect

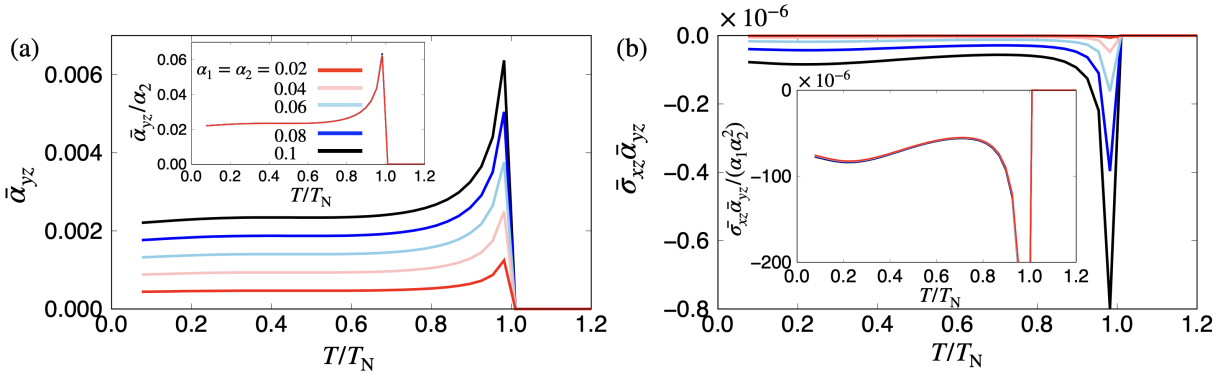

Figure 3.6: (a) The magnetoelectric coefficient $\bar{\alpha}_{yz}$ and (b) the quantity $\bar{\sigma}_{xz}\bar{\alpha}_{yz}$ with the same parameters as Fig. 3.5. $\bar{\sigma}_{xz}$ is calculated by supposing the small magnetic field H_y=0.01. The insets of (a) and (b) represent $\bar{\alpha}_{yz}/\alpha_2$ and $\bar{\sigma}_{xz}\bar{\alpha}_{yz}/(\alpha_1\alpha_2^2)$, respectively.

We also present another MT-moment-driven phenomena, the magnetoelectric response, and compare the temperature and essential model parameter dependences between the nonlinear conductivity and the linear magnetoelectric effect. Figure 3.6(a) shows the T dependence of $\bar{\alpha}_{yz}$ for $0.02 \leq \alpha_1, \alpha_2 \leq 0.1$ with $\alpha_1 = \alpha_2$, whose behavior is similar to the transverse nonlinear conductivity σ_{xzz} in Fig. 3.5 except for the sign. $\bar{\alpha}_{yz}$ is nonzero even if $\alpha_1 = 0$ that is different from the nonlinear conductivities, whereas α_2 and $\tilde{T}_x^{\mathrm{MF}}$ are essential to obtain the finite $\bar{\alpha}_{yz}$. As shown in the inset of Fig. 3.6(a), $\bar{\alpha}_{yz}$ is well scaled as $\bar{\alpha}_{yz}/\alpha_2$ for small α_2.

Moreover, it is noteworthy to comment on the relation between the transverse nonlinear conductivity and a combination of the linear magnetoelectric and Hall coefficients, since the nonlinear transverse transport in the $\mathcal{PT}$-symmetric AFMs can be understood as the Hall transport driven by the induced magnetization through the linear magnetoelectric response at the phenomenological level [69, 169].

We show the T dependence of $\bar{\sigma}_{xz}\bar{\alpha}_{yz}$ in Fig. 3.6(b) for the same parameters in Fig. 3.5. The small magnetic field H_y=0.01 is introduced to mimic the induced magnetization via α_{yz}. Compared to the results in Fig. 3.5, one finds the resemblance between the T dependences of $\bar{\sigma}_{xzz}$ and $\bar{\sigma}_{xz}\bar{\alpha}_{yz}$, both of which are scaled by $\alpha_1\alpha_2^2$. A good qualitative correspondence in these responses indicates that the interpretation of dividing subsequent two linear processes for nonlinear conductivity is reasonable in the present model. The overall quantitative difference $\bar{\sigma}_{xz}\bar{\alpha}_{yz}/\bar{\sigma}_{xzz} \sim 10^{-2}$ may be ascribed to the magnitude of the used internal magnetic field (H_y=0.01) that should be replaced by the true internal field. However, it is hard to estimate it quantitatively.

The above results clearly depend on the fact that the essential model parameters are common in σ_{xzz} and $\sigma_{xz}\alpha_{yz}$. However, such a correspondence does not always hold by introducing other model parameters. For example, we take into account the interlayer hopping between sublattices A and B as shown in Fig. 3.7(a), which changes $\varepsilon^{\mathrm{AB}}(\boldsymbol{k})$ in Eq. (3.3) as $-2t_1 \cos(k_x a/2) \to -2[t_1 + 2t_4 \cos(k_z c)] \cos(k_x a/2)$. Figures 3.7(b) and 3.7(c)

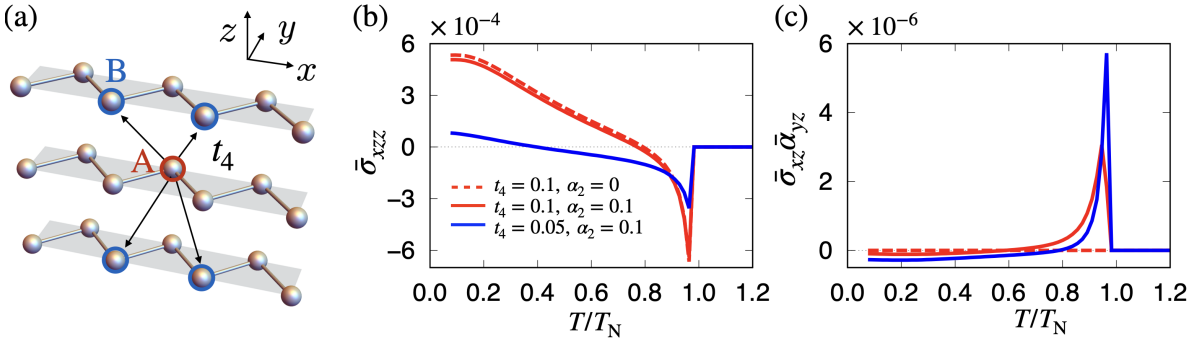

Figure 3.7: (a) Schematic picture of the interlayer hopping t_4 between A and B sublattices. (b,c) The T dependences of (b) $\bar{\sigma}_{xzz}$ and (c) $\bar{\sigma}_{xz}\bar{\alpha}_{yz}$ for $(t_4, \alpha_2)=(0.1, 0)$, $(0.1, 0.1)$, and $(0.05, 0.1)$.

show $\bar{\sigma}_{xzz}$ and $\bar{\sigma}_{xz}\bar{\alpha}_{yz}$ as functions of T, respectively, for t_4=0.1, 0.05 and α_2=0, 0.1, where α_1=0.4 is used. As shown by the red dashed line in Fig. 3.7(b), $\bar{\sigma}_{xzz}$ still remains nonzero even for α_2=0, while $\bar{\sigma}_{xz}\bar{\alpha}_{yz}$ in Fig. 3.7(c) vanishes. Furthermore, the nonzero t_4 enhances $\bar{\sigma}_{xzz}$, while it suppresses $\bar{\sigma}_{xz}\bar{\alpha}_{yz}$ while increasing t_4. This is because the essential model parameters are different for σ_{xzz} and $\sigma_{xz}\alpha_{yz}$. Indeed, in the presence of t_4 and α_2, the essential model parameter of σ_{xzz} is represented by using the coefficients, c and c', as $\alpha_1\tilde{T}_x^{\rm MF}(c\alpha_2^2 t_2 + c' t_4)$, which clearly shows that σ_{xzz} has the additional contribution from t_4 and does not vanish for α_2=0. On the other hand, the essential model parameters of σ_{xz} and α_{yz} does not show the change from $\sigma_{xz}\to\alpha_1\alpha_2 H_y$ and $\alpha_{yz}\to\alpha_2\tilde{T}_x^{\rm MF}$, respectively; the hopping t_4 is not the essential model parameter for σ_{xz} and α_{yz}. Thus, there is no simple relation between them in this set of the model parameters.

Finally, we discuss the order estimate of the nonlinear conductivity for α_1=0.5 and α_2=0.1 by the ratio $\sigma_{xxx}/(\sigma_{xx})^2$ with being independent of the relaxation time in the clean limit. By putting the typical values as $a\sim$0.5 [nm] and $|t_2|$=0.2 eV, we obtain $\sigma_{xxx}/(\sigma_{xx})^2\sim 10^{-3}\hbar a^2 e^{-1}|t_2|^{-1}\sim 10^{-18}$ [m^3 A^{-1}] for $T\to 0$ and 10^{-17} [m^3 A^{-1}] near $T_{\rm N}$, which is comparable to the value in the 2D nonmagnetic Rashba system under the magnetic field [181]. Further enhancement can be achieved by tuning the model parameters and electron filling.

3.4 Summary

In summary, we investigated the microscopic essential parameters for the second-order nonlinear conductivity due to the MT dipole in the collinear AFM metal. Based on the nonlinear Kubo formula in the clean limit, we found that the effective coupling between the ASOI and the MT dipole is the essence to induce the nonlinear conductivity. By analyzing both the longitudinal and transverse components of the nonlinear conductivity while changing the ASOI and the temperature, we showed that their large enhancement can be achieved near the transition temperature, provided that the AFM molecular field is comparable to the ASOI. Moreover, we also showed that the physical phenomena characterized by the same essential model parameters exhibit a similar temperature dependence by comparing the linear magnetoelectric and Hall coefficients with the transverse nonlin-

ear conductivity.

The similar analysis to extract essential model parameters can be applied to any MT dipole orderings in the zigzag structure, e.g., $CeRu_2Al_{10}$ [182, 183], Ce_3TiBi_5 [72, 73], and α-$YbAl_{1-x}Mn_xB_4$ [184], and other ferrotoroidal metals/semiconductors with the locally noncentrosymmetric crystal structures, such as Mn_2Au [178, 185], RB_4 (R=Dy, Er) [186, 187], CuMnAs [177, 188, 189], PrMnSbO [190], NdMnAsO [191], and $X_yFe_{2-x}Se_2$ (X=K, Tl, Rb) [192–194], once the model Hamiltonian is constructed. The measurements and comparison of the linear magnetoelectric effect and the nonlinear conductivity for these materials are also useful to obtain the microscopic information of the electronic state.

Chapter 4

Odd-Parity Multipole Order in f-electron Metal CeCoSi

We investigate the stability of the odd-parity multipole order and its multiferroic responses in the f-electron metal CeCoSi. We also study a way of detecting odd-parity multipole orderings by the NQR/NMR measurement. The study in this chapter includes the contents of Refs. [101, 147, 195][1]. This chapter is organized as follows. In Sec. 4.1, we briefly review the recent experimental results of the f-electron metal CeCoSi and present the motivation of this study. We show the crystalline electric field level of the Ce ion in Sec. 4.2 and present potential multipole order parameters in Sec. 4.3. We examine the stability of the odd-parity multipole orderings, finite-temperature phase transitions, and the physical properties by using an effective local model in Sec. 4.4. We also analyze the stability and current-induced multiferroic responses in the presence of the odd-parity multipoles based on an effective itinerant model in Sec. 4.5. In Sec. 4.6, we formulate the theory of the NQR and NMR spectra to identify the odd-parity multipole orderings. We summarize this chapter in Sec. 4.7.

4.1 Introduction

First, we give a short review of the crystal structure and the experimental results of the ordered states in the f-electron metal CeCoSi [196–205]. CeCoSi has the CeFeSi-type tetragonal crystal structure ($P4/nmm$, D_{4h}^7, No. 129) presented in Fig. 4.1(a), where the Ce and Si atoms are located at $2c$ sites with point group symmetry $4mm$ (C_{4v}), whereas the Co atom is at $2a$ site with $\bar{4}m2$ (D_{2d}) [206]. A unit cell includes two Ce ions denoted as $\mathrm{Ce_A}$ and $\mathrm{Ce_B}$ as shown in Fig. 4.1(a). Although the local inversion symmetry is lacking at all atomic sites, the inversion center exists between two Ce sites, which is illustrated in Fig. 4.1(b). The lattice constants are a=0.4057 nm and c=0.6987 nm determined by the x-ray diffraction measurement [200]. The crystalline electric field (CEF) ground state for

[1]Table 4.5 and Figs. 4.9 and 4.11 are reproduced from Ref. [101] (© (2020) The Physical Society of Japan).
Figure 4.10 is reproduced from Ref. [195] (© (2020) The Physical Society of Japan).
Tables 4.2, 4.6–4.9, and F.1 in Appendix F and Figs. 4.12–4.15, F.1, and F.2 are reproduced from Ref. [147] (© 2020 by the American Physical Society).

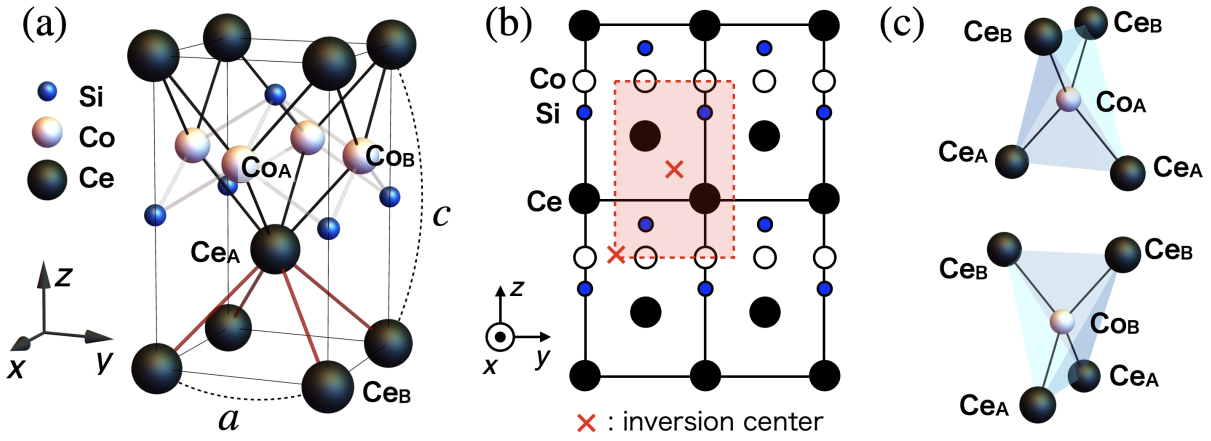

Figure 4.1: (a) Tetragonal crystal structure of CeCoSi in a unit cell with the lattice constants a and c. The nearest-neighbor Ce-Ce, Ce-Co, and Co-Si bonds are represented by red, black, and gray solid lines, respectively. The rectangle represents a unit cell. (b) Crystal structure viewed from the x axis. The red rectangle shows the unit cell where the inversion centers are located at the center and vertices of the unit cell. (c) Co_A (top) and Co_B (bottom) sites surrounded by the Ce tetrahedron.

the Ce site was suggested to be the Γ_7 Kramers doublet and the first and second excited levels are separated by around 100 K and 150 K, respectively [198–200, 202].

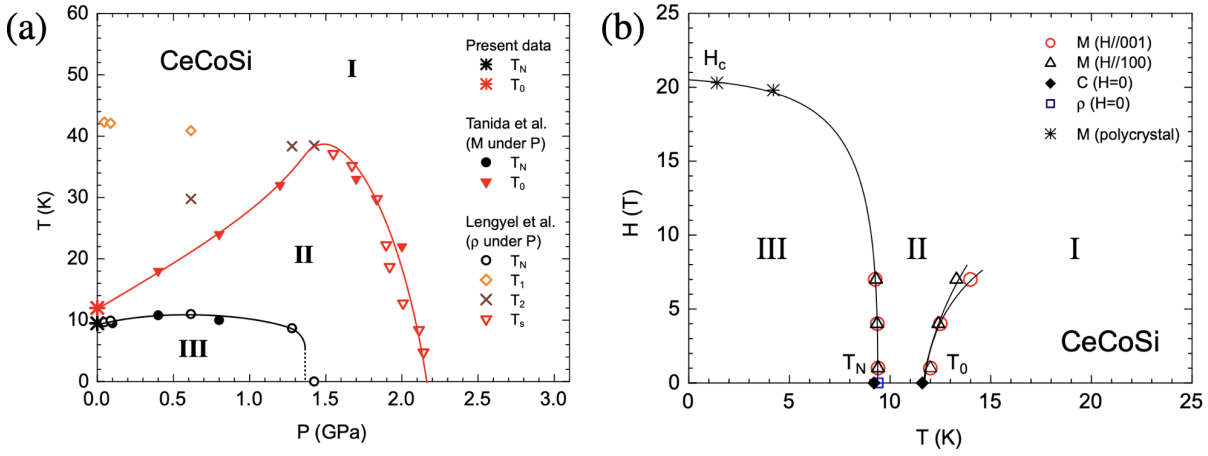

Figure 4.2: (a) The temperature-pressure and (b) magnetic-field-temperature phase diagrams in Ref. [200]. "Present data", " Tanida et al.", and "Lengyel et al." in (a) stand for the data of Refs. [200], [199], and [198], respectively. (Reproduced with permission from Ref. [200]. © (2019) The Physical Society of Japan.)

From the measurements of the specific heat, electrical resistivity, and magnetization, the physical properties in the low-temperature region have been investigated and clarified the existence of two types of ordered phases. They are denoted as "II phase" and "III phase" in the temperature-pressure (T-P) phase diagram [Fig. 4.2(a)] and the magnetic-field-temperature (H-T) phase diagram [Fig. 4.2(b)], where "I phase" is the paramagnetic phase without showing any electronic orderings [198–200].

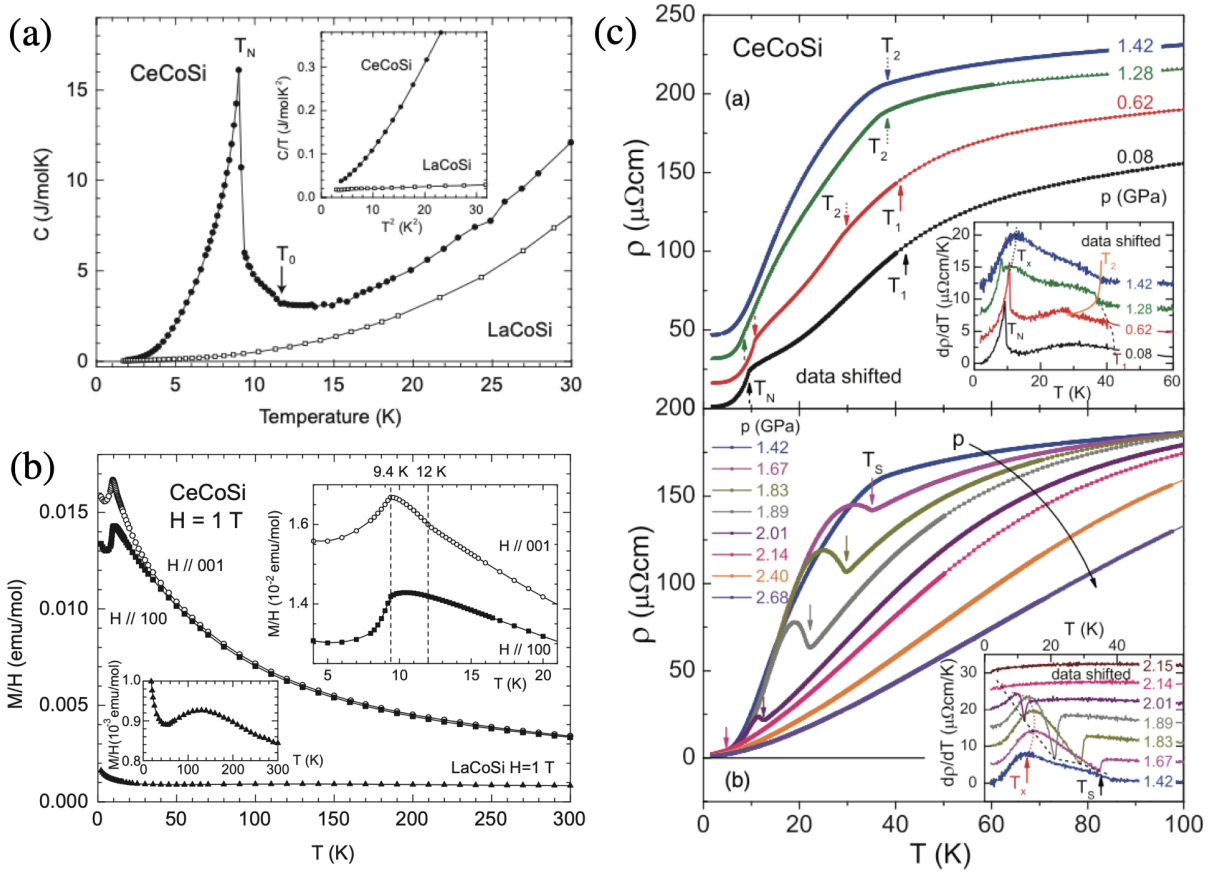

Figure 4.3: (a) Specific heat and (b) magnetization of CeCoSi and LaCoSi single crystals. (Reproduced with permission from Ref. [200]. © (2019) The Physical Society of Japan.) (c) Electric resistivity of CeCoSi polycrystal under pressure [198]. (Reprinted figure with permission from Ref. [198] © 2013 by the American Physical Society.)

The low-temperature III phase was identified as the AFM phase with the transition temperature $T_{\rm N}$∼9.5 K under ambient pressure. At $T_{\rm N}$, the specific heat shows a sharp anomaly [197, 198, 200, 202] [Fig. 4.3(a)], the magnetization has a cusp-like anomaly [Fig. 4.3(b)] [197–200], and electric resistivity shows a clear kink [197–200, 203]. Under pressure, the III phase disappears around P∼1.3 GPa after the slight change of the transition temperature as shown in Fig. 4.2(a). The neutron diffraction measurement under ambient pressure for the polycrystal indicated that the magnetic structure in the III phase is the staggered AFM structure along the [100] direction as shown in Fig. 4.4(a) [202].

Meanwhile, the II phase under ambient pressure shows the second-order phase transition at T_0∼12 K. One can recognize the slight anomaly at T_0 in the heat capacity and magnetization in Figs. 4.3(a) and 4.3(b), while no clear anomaly appears in the electric conductivity [200]. This phase is referred to as "pressure induced ordered phase (PIOP)", because it was originally observed only under pressure in a polycrystal. Subsequently, it was observed under ambient pressure in the single crystal [200]. The II phase is strongly enhanced by the hydrostatic pressure; the transition temperature T_0 reaches T_0∼40 K at P∼1.5 GPa as shown in Fig. 4.2(a). In such a pressured region, a clear cusp-like anomaly appears in the electric resistivity as shown in Fig. 4.3(c) [198, 199], which suggests the

existence of the superzone gap in the Fermi surface due to the antiferroic electronic orderings. By applying further pressure, the II phase is suppressed and disappears around $P{\sim}2.2$ GPa. In a magnetic field, the transition temperature of the II phase is enhanced as shown in Fig. 4.2(b); such magnetic-field dependence has been often recognized as the onset of the antiferroquadrupole (AFQ) ordering, as found in CeB_6 [207–209]. Moreover, the II phase was confirmed to be nonmagnetic from the NQR measurement for the ^{59}Co nuclear surrounded by the four nearest-neighbor Ce ions as shown in Fig. 4.1(c) [205]; it suggested that the II phase is higher-rank E multipole ordered phases in the $4f$ electron at Ce ion. The existence of the II phase has been also confirmed by the NMR spectra with the clear splitting below T_0 [Fig. 4.4].

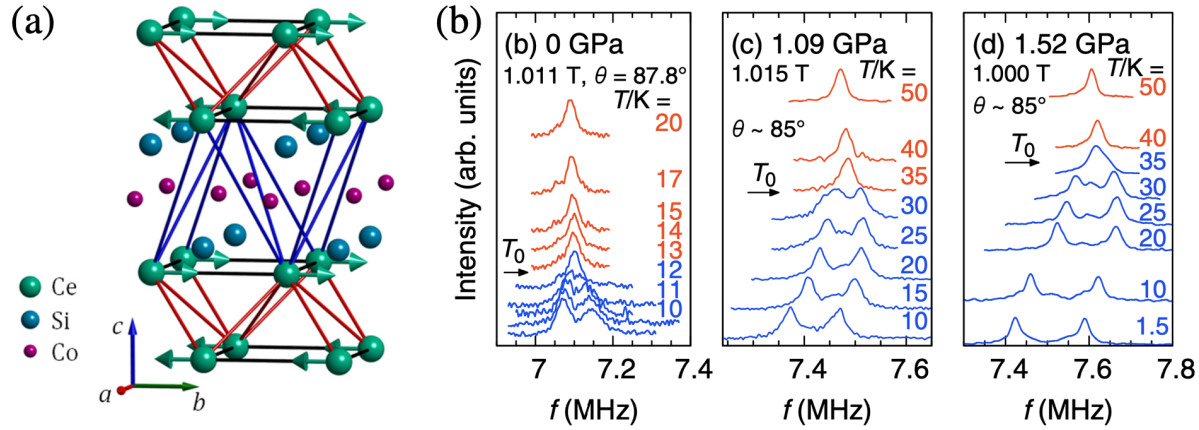

Figure 4.4: (a) Magnetic structure in the III phase determined by the neutron powder diffraction [202]. (b) NMR spectra under the magnetic field slightly tilted from the [100] direction. (Reproduced with permission from Ref. [205]. © (2021) The Physical Society of Japan.)

The II and III phases might show interesting multiferroic phenomena from the viewpoint of the odd-parity multipole physics. It is because the antiferroic orderings with the ordering vector $\boldsymbol{q}=\boldsymbol{0}$ in the locally noncentrosymmetric structure, which have been suggested by the experiments, break the global inversion symmetry and induce the cluster odd-parity multipoles. They become a source of the multiferroic responses, e.g., magnetoelectric and elastic-electric effects. Especially, the cluster odd-parity multipole order consisting of the atomic AFQ moment, which has been expected in the II phase, corresponds to the unconventional augmented ET quadrupole and/or E dipole order. Thus, it is important to investigate a microscopic origin of the odd-parity multipole orderings and their related multiferroic responses from the microscopic viewpoint. Moreover, it is desirable to establish a method of identifying the odd-parity multipole order parameter by using microscopic measurement like the NQR and NMR measurements beyond the conventional even-parity one [17, 22, 24].

4.2 Crystalline Electric Field

We discuss the CEF Hamiltonian and the basis wave function of $4f$ electron with f^1 configuration in the Ce^{3+} ion. The tetragonal CEF Hamiltonian at Ce site with C_{4v}

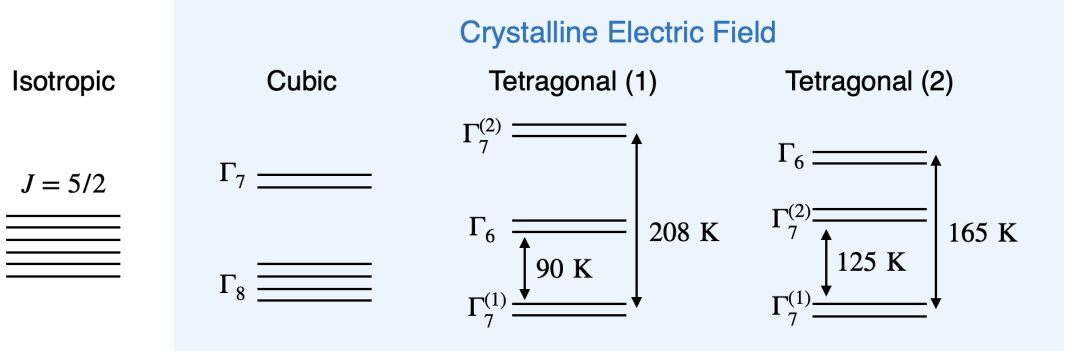

Figure 4.5: The level splittings of $J{=}5/2$ multiplet in the cubic and tetragonal CEFs. The CEF parameters $(B_{20}, B_{40}, B_{44}){=}(-0.95, -0.14, 3.8)$ K are used for "Tetragonal (1)", whereas $(B_{20}, B_{40}, B_{44}){=}(-1.26, 0.487, 1.36)$ K are used for "Tetragonal (2)".

symmetry is given as

$$\mathcal{H}_{\rm CEF}{=}B_{20}\hat{O}_{20}{+}B_{40}\hat{O}_{40}{+}B_{44}\hat{O}_{44}^{\rm (c)}, \tag{4.1}$$

where B_{lm} and $\hat{O}_{lm}$ are the CEF parameter and Stevens operator [50], respectively. Here we omit the B_{60} and B_{64} terms by supposing the $J{=}5/2$ basis. We also omit the contribution of the local hybridization between d and f orbitals. In the CEF Hamiltonian in Eq. (4.1), the sixfold $J{=}5/2$ basis split into one Γ_6 level and two Γ_7 levels. The eigen energies of Γ_6 and Γ_7 levels, E_{Γ_6} and $E_{\Gamma_7^{(1,2)}}$, are given by

$$E_{\Gamma_6}{=}{-}8B_{20}{+}120B_{40}, \tag{4.2}$$

$$E_{\Gamma_7^{(1)}}{=}4B_{20}{-}60B_{40}{-}6\sqrt{(B_{20}{+}20B_{40})^2{+}20B_{44}^2}, \tag{4.3}$$

$$E_{\Gamma_7^{(2)}}{=}4B_{20}{-}60B_{40}{+}6\sqrt{(B_{20}{+}20B_{40})^2{+}20B_{44}^2}, \tag{4.4}$$

whose wave functions are represented as

$$|\Gamma_6, \uparrow\downarrow\rangle{=}\left|\pm\frac{1}{2}\right\rangle,\ |\Gamma_7^{(i)}, \uparrow\downarrow\rangle{=}c_1^{(i)}\left|\pm\frac{5}{2}\right\rangle{+}c_2^{(i)}\left|\mp\frac{3}{2}\right\rangle\ (i{=}1,2), \tag{4.5}$$

where $c_1^{(i)}$ and $c_2^{(i)}$ $(i{=}1,2)$ are the linear combination coefficients determined by B_{20}, B_{40}, and B_{44}. Two types of CEF parameters are proposed from experiments: $(B_{20}, B_{40}, B_{44}){=}(-0.95, -0.14, 3.8)$ K [210] and $(B_{20}, B_{40}, B_{44}){=}(-1.26, 0.487, 1.36)$ K [202]. The former CEF parameter gives the Γ_7 ground state and the Γ_6 first excited state with 90 K level splitting denoted as "Tetragonal (1)" in Fig. 4.5, whereas the latter leads to the Γ_7 ground and first excited states with 125 K level splitting denoted as "Tetragonal (2)" in Fig. 4.5.

4.3 Multipole Degrees of Freedom

In the Kramers doublet, the electronic degrees of freedom are usually expressed as E monopole (charge) and M dipole ones. It means that the active higher-rank multipole

degrees of freedom, which might be a source of the AFQ order suggested for the II phase in CeCoSi, appear only in the interorbital degrees of freedom between the CEF ground state and the CEF excited state. Although the CEF excited levels are relatively separated from the ground state, there is a chance of interorbital multipole orderings as found in CeTe [208]. In the following, we focus on the possibility of the multipole orderings by considering the four low-energy levels consisting of the CEF ground state and the first excited state.

In this section, we present the atomic multipoles activated in the low-energy Γ_7-Γ_6 levels in Tetragonal (1) and $\Gamma_7^{(1)}$-$\Gamma_7^{(2)}$ levels in Tetragonal (2) in Secs. 4.3.1 and 4.3.2, respectively. We also show the correspondence to the cluster multipoles in a unit cell within the two sublattice degrees of freedom.

4.3.1 Γ_7-Γ_6 Level

We show the multipole degrees of freedom in the Γ_7-Γ_6 subspace. By calculating each matrix element by using Eqs. (1.10) and (1.11)[2], we obtain the 16 multipole degrees of freedom as follows: E monopole Q_0, M dipole (M_x, M_y, M_z), E quadrupole (Q_u, Q_v, Q_{yz}, Q_{zx}, Q_{xy}), and M octupole (M_{xyz}, M_x^α, M_y^α, M_z^α, M_x^β, M_y^β, M_z^β). Among them, the multipoles activated in the intraorbital space are the E monopole and M dipoles: $\hat{Q}_0{=}\sigma_0\tau_0$, $\hat{M}_\mu$ ($\mu{=}x,y$) is represented by a linear combination of $\tau_0\sigma_\mu$, $\tau_z\sigma_\mu$, and $\tau_x\sigma_\mu$, and $\hat{M}_z$ is represented by a linear combination of $\tau_0\sigma_z$ and $\tau_z\sigma_z$ by using the identity matrix σ_0 (τ_0) and the Pauli matrix σ_μ (τ_μ) ($\mu{=}x,y,z$) in quasi-spin (Γ_7-Γ_6) space. It is noted that the M dipole M_x (M_y) includes the interorbital component represented by $\tau_x\sigma_x$ ($\tau_x\sigma_y$). Besides, there are further four types of intraorbital multipole degrees of freedom due to the consideration of the two orbitals, an E quadrupole and three M octupoles: the E quadrupole $\hat{Q}_u$ is represented by a linear combination of $\tau_0\sigma_0$ and $\tau_z\sigma_0$, M octupole $\hat{M}_\mu^\alpha$ ($\mu{=}x,y$) is represented by a linear combination of $\tau_0\sigma_\mu$, $\tau_z\sigma_\mu$, and $\tau_x\sigma_\mu$, and $\hat{M}_z^\alpha$ is represented by a linear combination of $\tau_0\sigma_z$ and $\tau_z\sigma_z$. Note that $\hat{M}_x^\alpha$ and $\hat{M}_y^\alpha$ include the interorbital component as well as the M dipoles $\hat{M}_x$ and $\hat{M}_y$.

Meanwhile, there are eight types of interorbital degrees of freedom between the Γ_7 and Γ_6 orbitals: the four E quadrupoles and four M octupoles. Their matrix elements are given as $\hat{Q}_v{=}\frac{1}{2}\tau_x\sigma_0$, $\hat{Q}_{xy}{=}\frac{1}{2}\tau_y\sigma_z$, and $(\hat{Q}_{yz},\hat{Q}_{zx}){=}\frac{1}{2}(\tau_y\sigma_x,\tau_y\sigma_y)$ for the E quadrupoles, and $M_{xyz}{=}\frac{1}{2}\tau_y\sigma_0$ and $M_z^\beta{=}\frac{1}{2}\tau_x\sigma_z$ for the M octupoles. Besides, the other two M octupoles $\hat{M}_\mu^\beta$ ($\mu{=}x,y$) are represented by a linear combination of $\tau_0\sigma_\mu$, $\tau_z\sigma_\mu$, and $\tau_x\sigma_\mu$, which include the intraorbital contributions as well as the M dipoles $\hat{M}_x$ and $\hat{M}_y$. Each matrix element and the linear combination coefficients calculated for the Tetragonal (1) are summarized in Table 4.1. In the table, we also present the higher-rank multipoles composed from the same matrix elements, which have the different linear combination coefficients.

By taking into account the two sublattice degrees of freedom in Fig. 4.1(a), the cluster multipole expressions are obtained. Under the symmetry $4/mmm1'$, the sublattice degrees of freedom is decomposed into the IRREPs $\Gamma_{\rm sub}{=}\mathrm{A}_{1\rm g}^+{\oplus}\mathrm{A}_{2\rm u}^+$, where $\mathrm{A}_{1\rm g}^+$ represents the uniform potential configuration, while $\mathrm{A}_{2\rm u}^+$ describes the staggered one. By taking the direct product of $\Gamma_{\rm sub}$ and the IRREPs of the atomic multipoles $Q_0, Q_u{\in}\mathrm{A}_{1\rm g}^+$, $Q_v{\in}\mathrm{B}_{1\rm g}^+$, $Q_{xy}{\in}\mathrm{B}_{2\rm g}^+$, $(Q_{yz},Q_{zx}){\in}\mathrm{E}_{\rm g}^+$, $M_z, M_z^\alpha{\in}\mathrm{A}_{2\rm g}^-$, $M_{xyz}{\in}\mathrm{B}_{1\rm g}^-$, $M_z^\beta{\in}\mathrm{B}_{2\rm g}^-$, (M_x,M_y), (M_x^α,M_y^α), $(M_x^\beta,M_y^\beta){\in}\mathrm{E}_{\rm g}^-$

[2]The same result is obtained by using the spherical tensor operators [11].

Table 4.1: Multipole degrees of freedom activated in the Γ_7-Γ_6 subspace and their expressions. Each expression is normalized to satisfy $\mathrm{Tr}[XX^\dagger]=1$. The linear combination coefficients in the Tetragonal (1) with $(B_{20}, B_{40}, B_{44})=(-0.95, -0.14, 3.8)$ and the relevant higher-rank multipoles are also shown.

multipole	matrix	linear combination coefficient	higher rank
M_x	$c_1^x\tau_0\sigma_x+c_2^x\tau_z\sigma_x+c_3^x\tau_x\sigma_x$	$(c_1^x, c_2^x, c_3^x)=(0.064, -0.41, -0.28)$	$M_{5x}^{\alpha_1}, M_{5x}^{\alpha_2}, M_{5x}^{\beta}$
M_y	$c_1^y\tau_0\sigma_y+c_2^y\tau_z\sigma_y+c_3^y\tau_x\sigma_y$	$(c_1^y, c_2^y, c_3^y)=(0.064, -0.41, 0.28)$	$M_{5y}^{\alpha_1}, M_{5y}^{\alpha_2}, M_{5y}^{\beta}$
M_z	$c_1^z\tau_0\sigma_z+c_2^z\tau_z\sigma_z$	$(c_1^z, c_2^z)=(0.48, 0.14)$	$M_{5z}^{\alpha_1}, M_{5z}^{\alpha_2}$
Q_u	$c_1^u\tau_0\sigma_0+c_2^u\tau_z\sigma_0$	$(c_1^u, c_2^u)=(-0.1, 0.49)$	Q_4, Q_{4u}
Q_v	$\frac{1}{2}\tau_x\sigma_0$		Q_{4v}
Q_{xy}	$\frac{1}{2}\tau_y\sigma_z$		Q_{4z}^{β}
Q_{yz}	$\frac{1}{2}\tau_y\sigma_x$		$Q_{4x}^{\alpha}, Q_{4x}^{\beta}$
Q_{zx}	$\frac{1}{2}\tau_y\sigma_y$		$Q_{4y}^{\alpha}, Q_{4y}^{\beta}$
M_{xyz}	$\frac{1}{2}\tau_y\sigma_0$		M_{5v}
M_x^{α}	$c_1^{x\alpha}\tau_0\sigma_x+c_2^{x\alpha}\tau_z\sigma_x+c_3^{x\alpha}\tau_x\sigma_x$	$(c_1^{x\alpha}, c_2^{x\alpha}, c_3^{x\alpha})=(0.42, 0.11, 0.25)$	
M_y^{α}	$c_1^{y\alpha}\tau_0\sigma_y+c_2^{y\alpha}\tau_z\sigma_y+c_3^{y\alpha}\tau_x\sigma_y$	$(c_1^{y\alpha}, c_2^{y\alpha}, c_3^{y\alpha})=(0.42, 0.11, -0.25)$	
M_z^{α}	$c_1^{z\alpha}\tau_0\sigma_z+c_2^{z\alpha}\tau_z\sigma_z$	$(c_1^{z\alpha}, c_2^{z\alpha})=(0.09, 0.49)$	
M_x^{β}	$c_1^{x\beta}\tau_0\sigma_x+c_2^{x\beta}\tau_z\sigma_x+c_3^{x\beta}\tau_x\sigma_x$	$(c_1^{x\beta}, c_2^{x\beta}, c_3^{x\beta})=(0.35, -0.062, -0.35)$	
M_y^{β}	$c_1^{y\beta}\tau_0\sigma_y+c_2^{y\beta}\tau_z\sigma_y+c_3^{y\beta}\tau_x\sigma_y$	$(c_1^{y\beta}, c_2^{y\beta}, c_3^{y\beta})=(-0.35, 0.062, -0.35)$	
M_z^{β}	$\frac{1}{2}\tau_x\sigma_z$		M_{5z}^{β}

from Table C.17, the IRREPs of the cluster multipoles are given as follows:

$$\begin{aligned}&(\mathrm{A}_{1\mathrm{g}}^{+}\oplus\mathrm{A}_{2\mathrm{u}}^{+})\otimes(2\mathrm{A}_{1\mathrm{g}}^{+}\oplus\mathrm{B}_{1\mathrm{g}}^{+}\oplus\mathrm{B}_{2\mathrm{g}}^{+}\oplus\mathrm{E}_{\mathrm{g}}^{+}\oplus2\mathrm{A}_{2\mathrm{g}}^{-}\oplus\mathrm{B}_{1\mathrm{g}}^{-}\oplus\mathrm{B}_{2\mathrm{g}}^{-}\oplus3\mathrm{E}_{\mathrm{g}}^{-})\\&=(2\mathrm{A}_{1\mathrm{g}}^{+}\oplus\mathrm{B}_{1\mathrm{g}}^{+}\oplus\mathrm{B}_{2\mathrm{g}}^{+}\oplus\mathrm{E}_{\mathrm{g}}^{+}\oplus2\mathrm{A}_{2\mathrm{g}}^{-}\oplus\mathrm{B}_{1\mathrm{g}}^{-}\oplus\mathrm{B}_{2\mathrm{g}}^{-}\oplus3\mathrm{E}_{\mathrm{g}}^{-})_{\text{uniform}}\\&\quad\oplus(2\mathrm{A}_{2\mathrm{u}}^{+}\oplus\mathrm{B}_{1\mathrm{u}}^{+}\oplus\mathrm{B}_{2\mathrm{u}}^{+}\oplus\mathrm{E}_{\mathrm{u}}^{+}\oplus2\mathrm{A}_{1\mathrm{u}}^{-}\oplus\mathrm{B}_{1\mathrm{u}}^{-}\oplus\mathrm{B}_{2\mathrm{u}}^{-}\oplus3\mathrm{E}_{\mathrm{u}}^{-})_{\text{staggered}},\end{aligned}\tag{4.6}$$

where the subscript "uniform (staggered)" means the IRREPs with the uniform (staggered) configuration of the atomic multipoles. By using Table C.17, the corresponding multipoles and their IRREPs are obtained, as summarized in Table 4.2[3], where the IRREP

[3]The total M dipole is defined as $\hat{M}_{\mu}^{\mathrm{tot}}=\tau_0\sigma_{\mu}+\tau_x\sigma_{\mu}$ for $\mu=x,y$ and $\hat{M}_{z}^{\mathrm{tot}}=\tau_0\sigma_z$ so as to eliminate the

of each multipole in a magnetic field is also shown.

Table 4.2: Cluster multipoles (CMP) consisting of the (a) uniform and (b) staggered configurations of atomic multipoles in the Γ_7-Γ_6 levels. The IRREPs of each CMP in a magnetic field are also shown for the magnetic field along the [001] direction ($\boldsymbol{H}\parallel$ [001]) with symmetry $4/mm'm'$, the [100] direction ($\boldsymbol{H}\parallel$[100]) with symmetry $mm'm'$, and the [110] direction ($\boldsymbol{H}\parallel$[110]) with symmetry $mm'm'$. The sign of IRREP in each magnetic point group symmetry means that the parity for the time-reversal operation θ in $4/mmm1'$, $\theta C'_{2x}$ in $4/mm'm'$, and θC_{2z} in $mm'm'$. The cluster multipoles in the parentheses are used for $\boldsymbol{H}\parallel$[110].

type of CMP		definition	$\boldsymbol{H}=\boldsymbol{0}$ $4/mmm1'$	$\boldsymbol{H}\parallel$[001] $4/mm'm'$	$\boldsymbol{H}\parallel$[100] $mm'm'$	$\boldsymbol{H}\parallel$[110] $mm'm'$
(a) uniform						
E monopole	$\hat{Q}_0^{(\mathrm{c})}$	$\hat{Q}_{0,\mathrm{A}}+\hat{Q}_{0,\mathrm{B}}$	$\mathrm{A}_{1\mathrm{g}}^+$	$\mathrm{A}_{\mathrm{g}}^+$	$\mathrm{A}_{\mathrm{g}}^+$	$\mathrm{A}_{\mathrm{g}}^+$
M dipole	$\hat{M}_x^{(\mathrm{c})}$ $(\hat{M}_x^{(\mathrm{c})}+\hat{M}_y^{(\mathrm{c})})$	$\hat{M}_{x,\mathrm{A}}^{\mathrm{tot}}+\hat{M}_{x,\mathrm{B}}^{\mathrm{tot}}$	$\mathrm{E}_{\mathrm{g}}^-$	$\mathrm{E}_{\mathrm{g}}^-$	$\mathrm{A}_{\mathrm{g}}^+$	$\mathrm{A}_{\mathrm{g}}^+$
	$\hat{M}_y^{(\mathrm{c})}$ $(\hat{M}_x^{(\mathrm{c})}-\hat{M}_y^{(\mathrm{c})})$	$\hat{M}_{y,\mathrm{A}}^{\mathrm{tot}}+\hat{M}_{y,\mathrm{B}}^{\mathrm{tot}}$			$\mathrm{B}_{\mathrm{g}}^+$	$\mathrm{B}_{\mathrm{g}}^+$
	$\hat{M}_z^{(\mathrm{c})}$	$\hat{M}_{z,\mathrm{A}}^{\mathrm{tot}}+\hat{M}_{z,\mathrm{B}}^{\mathrm{tot}}$	$\mathrm{A}_{2\mathrm{g}}^-$	$\mathrm{A}_{\mathrm{g}}^+$	$\mathrm{B}_{\mathrm{g}}^-$	$\mathrm{B}_{\mathrm{g}}^-$
E quadrupole	$\hat{Q}_u^{(\mathrm{c})}$	$\hat{Q}_{u,\mathrm{A}}+\hat{Q}_{u,\mathrm{B}}$	$\mathrm{A}_{1\mathrm{g}}^+$	$\mathrm{A}_{\mathrm{g}}^+$	$\mathrm{A}_{\mathrm{g}}^+$	$\mathrm{A}_{\mathrm{g}}^+$
	$\hat{Q}_v^{(\mathrm{c})}$	$\hat{Q}_{v,\mathrm{A}}+\hat{Q}_{v,\mathrm{B}}$	$\mathrm{B}_{1\mathrm{g}}^+$	$\mathrm{B}_{\mathrm{g}}^+$	$\mathrm{A}_{\mathrm{g}}^+$	$\mathrm{B}_{\mathrm{g}}^+$
	$\hat{Q}_{yz}^{(\mathrm{c})}$ $(\hat{Q}_{yz}^{(\mathrm{c})}+\hat{Q}_{zx}^{(\mathrm{c})})$	$\hat{Q}_{yz,\mathrm{A}}+\hat{Q}_{yz,\mathrm{B}}$	$\mathrm{E}_{\mathrm{g}}^+$	$\mathrm{E}_{\mathrm{g}}^+$	$\mathrm{A}_{\mathrm{g}}^-$	$\mathrm{B}_{\mathrm{g}}^-$
	$\hat{Q}_{zx}^{(\mathrm{c})}$ $(\hat{Q}_{yz}^{(\mathrm{c})}-\hat{Q}_{zx}^{(\mathrm{c})})$	$\hat{Q}_{zx,\mathrm{A}}+\hat{Q}_{zx,\mathrm{B}}$			$\mathrm{B}_{\mathrm{g}}^-$	$\mathrm{A}_{\mathrm{g}}^-$
	$\hat{Q}_{xy}^{(\mathrm{c})}$	$\hat{Q}_{xy,\mathrm{A}}+\hat{Q}_{xy,\mathrm{B}}$	$\mathrm{B}_{2\mathrm{g}}^+$	$\mathrm{B}_{\mathrm{g}}^-$	$\mathrm{B}_{\mathrm{g}}^+$	$\mathrm{A}_{\mathrm{g}}^+$
M octupole	$\hat{M}_{xyz}^{(\mathrm{c})}$	$\hat{M}_{xyz,\mathrm{A}}+\hat{M}_{xyz,\mathrm{B}}$	$\mathrm{B}_{1\mathrm{g}}^-$	$\mathrm{B}_{\mathrm{g}}^-$	$\mathrm{A}_{\mathrm{g}}^-$	$\mathrm{B}_{\mathrm{g}}^-$
	$\hat{M}_z^{\beta(\mathrm{c})}$	$\hat{M}_{z,\mathrm{A}}^{\beta}+\hat{M}_{z,\mathrm{B}}^{\beta}$	$\mathrm{B}_{2\mathrm{g}}^-$	$\mathrm{B}_{\mathrm{g}}^+$	$\mathrm{B}_{\mathrm{g}}^-$	$\mathrm{A}_{\mathrm{g}}^-$
(b) staggered						
E dipole	$\hat{Q}_z^{(\mathrm{c})}$	$\hat{Q}_{0,\mathrm{A}}-\hat{Q}_{0,\mathrm{B}}$	$\mathrm{A}_{2\mathrm{u}}^+$	$\mathrm{A}_{\mathrm{u}}^+$	$\mathrm{B}_{\mathrm{u}}^+$	$\mathrm{B}_{\mathrm{u}}^+$
MT dipole	$\hat{T}_y^{(\mathrm{c})}$ $(\hat{T}_x^{(\mathrm{c})}+\hat{T}_x^{(\mathrm{c})})$	$\hat{M}_{x,\mathrm{A}}^{\mathrm{tot}}-\hat{M}_{x,\mathrm{B}}^{\mathrm{tot}}$	$\mathrm{E}_{\mathrm{u}}^-$	$\mathrm{E}_{\mathrm{u}}^-$	$\mathrm{B}_{\mathrm{u}}^+$	$\mathrm{A}_{\mathrm{u}}^+$
	$-\hat{T}_x^{(\mathrm{c})}$ $(-\hat{T}_x^{(\mathrm{c})}+\hat{T}_x^{(\mathrm{c})})$	$\hat{M}_{y,\mathrm{A}}^{\mathrm{tot}}-\hat{M}_{y,\mathrm{B}}^{\mathrm{tot}}$			$\mathrm{A}_{\mathrm{u}}^+$	$\mathrm{B}_{\mathrm{u}}^+$
M monopole	$\hat{M}_0^{(\mathrm{c})}$	$\hat{M}_{z,\mathrm{A}}^{\mathrm{tot}}-\hat{M}_{z,\mathrm{B}}^{\mathrm{tot}}$	$\mathrm{A}_{1\mathrm{u}}^-$	$\mathrm{A}_{\mathrm{u}}^+$	$\mathrm{A}_{\mathrm{u}}^-$	$\mathrm{A}_{\mathrm{u}}^-$
E dipole	$\hat{Q}_z^{(\mathrm{c})}$	$\hat{Q}_{u,\mathrm{A}}-\hat{Q}_{u,\mathrm{B}}$	$\mathrm{A}_{2\mathrm{u}}^+$	$\mathrm{A}_{\mathrm{u}}^+$	$\mathrm{B}_{\mathrm{u}}^+$	$\mathrm{B}_{\mathrm{u}}^+$
ET quadrupole	$\hat{G}_{xy}^{(\mathrm{c})}$	$\hat{Q}_{v,\mathrm{A}}-\hat{Q}_{v,\mathrm{B}}$	$\mathrm{B}_{2\mathrm{u}}^+$	$\mathrm{B}_{\mathrm{u}}^+$	$\mathrm{B}_{\mathrm{u}}^+$	$\mathrm{A}_{\mathrm{u}}^+$
E dipole	$\hat{Q}_y^{(\mathrm{c})}$ $(\hat{Q}_x^{(\mathrm{c})}+\hat{Q}_y^{(\mathrm{c})})$	$\hat{Q}_{yz,\mathrm{A}}-\hat{Q}_{yz,\mathrm{B}}$	$\mathrm{E}_{\mathrm{u}}^+$	$\mathrm{E}_{\mathrm{u}}^+$	$\mathrm{B}_{\mathrm{u}}^-$	$\mathrm{A}_{\mathrm{u}}^-$
	$\hat{Q}_x^{(\mathrm{c})}$ $(-\hat{Q}_x^{(\mathrm{c})}+\hat{Q}_y^{(\mathrm{c})})$	$\hat{Q}_{zx,\mathrm{A}}-\hat{Q}_{zx,\mathrm{B}}$			$\mathrm{A}_{\mathrm{u}}^-$	$\mathrm{B}_{\mathrm{u}}^-$
ET quadrupole	$\hat{G}_v^{(\mathrm{c})}$	$\hat{Q}_{xy,\mathrm{A}}-\hat{Q}_{xy,\mathrm{B}}$	$\mathrm{B}_{1\mathrm{u}}^+$	$\mathrm{B}_{\mathrm{u}}^-$	$\mathrm{A}_{\mathrm{u}}^+$	$\mathrm{B}_{\mathrm{u}}^+$
M quadrupole	$\hat{M}_{xy}^{(\mathrm{c})}$	$\hat{M}_{xyz,\mathrm{A}}-\hat{M}_{xyz,\mathrm{B}}$	$\mathrm{B}_{2\mathrm{u}}^-$	$\mathrm{B}_{\mathrm{u}}^-$	$\mathrm{B}_{\mathrm{u}}^-$	$\mathrm{A}_{\mathrm{u}}^-$
	$\hat{M}_v^{(\mathrm{c})}$	$\hat{M}_{z,\mathrm{A}}^{\beta}-\hat{M}_{z,\mathrm{B}}^{\beta}$	$\mathrm{B}_{1\mathrm{u}}^-$	$\mathrm{B}_{\mathrm{u}}^+$	$\mathrm{A}_{\mathrm{u}}^-$	$\mathrm{B}_{\mathrm{u}}^-$

component of the M octupole belonging to the same IRREP.

4.3.2 Γ_7-Γ_7 Level

We show the atomic multipole degrees of freedom activated in $\Gamma_7^{(1)}$-$\Gamma_7^{(2)}$ space corresponding to Tetragonal (2) in Fig. 4.5. The atomic multipoles and their matrix elements are summarized in Table 4.3. There are several differences from the result in the Γ_7-Γ_6 subspace; M dipole M_z has the interorbital component, E quadrupoles Q_v and Q_{xy} and M octupoles M_{xyz} and M_z^β are lacking, and the E hexadecapole Q_{4z}^α and M triacontadipole M_{5u} can be active as the independent multipole degrees of freedom. Similarly, we present the cluster multipoles consisting of two atomic sites in the unit cell in Table 4.4.

Table 4.3: Multipole degrees of freedom activated in the low-energy $\Gamma_7^{(1)}$-$\Gamma_7^{(2)}$ subspace in the Tetragonal (2) with $(B_{20}, B_{40}, B_{44})=(-1.26, 0.487, 1.36)$.

multipole	matrix	linear combination coefficient	higher rank
M_x	$c_1^x\tau_0\sigma_x+c_2^x\tau_z\sigma_x+c_3^x\tau_x\sigma_x$	$(c_1^x, c_2^x, c_3^x)=(0, -0.29, -0.41)$	$M_{5x}^{\alpha_1}, M_{5x}^{\alpha_2}, M_{5x}^{\beta}$
M_y	$c_1^y\tau_0\sigma_y+c_2^y\tau_z\sigma_y+c_3^y\tau_x\sigma_y$	$(c_1^y, c_2^y, c_3^y)=(0, 0.29, 0.41)$	$M_{5y}^{\alpha_1}, M_{5y}^{\alpha_2}, M_{5y}^{\beta}$
M_z	$c_1^z\tau_0\sigma_z+c_2^z\tau_z\sigma_z+c_3^z\tau_x\sigma_z$	$(c_1^z, c_2^z, c_3^z)=(-0.12, 0.39, -0.28)$	$M_{5z}^{\alpha_1}, M_{5z}^{\alpha_2}$
Q_u	$c_1^u\tau_0\sigma_0+c_2^u\tau_z\sigma_0+c_3^u\tau_x\sigma_0$	$(c_1^u, c_2^u, c_3^u)=(0.28, -0.34, 0.24)$	Q_4, Q_{4u}
Q_{yz}	$\frac{1}{2}\tau_y\sigma_x$		$Q_{4x}^\alpha, Q_{4x}^\beta$
Q_{zx}	$\frac{1}{2}\tau_y\sigma_y$		$Q_{4y}^\alpha, Q_{4y}^\beta$
M_x^α	$c_1^{x\alpha}\tau_0\sigma_x+c_2^{x\alpha}\tau_z\sigma_x+c_3^{x\alpha}\tau_x\sigma_x$	$(c_1^{x\alpha}, c_2^{x\alpha}, c_3^{x\alpha})=(0.26, 0.41, 0.13)$	
M_y^α	$c_1^{y\alpha}\tau_0\sigma_y+c_2^{y\alpha}\tau_z\sigma_y+c_3^{y\alpha}\tau_x\sigma_y$	$(c_1^{y\alpha}, c_2^{y\alpha}, c_3^{y\alpha})=(-0.26, -0.41, -0.13)$	
M_z^α	$c_1^{z\alpha}\tau_0\sigma_z+c_2^{z\alpha}\tau_z\sigma_z+c_3^{z\alpha}\tau_x\sigma_z$	$(c_1^{z\alpha}, c_2^{z\alpha}, c_3^{z\alpha})=(-0.49, -0.065, 0.048)$	
M_x^β	$c_1^{x\beta}\tau_0\sigma_x+c_2^{x\beta}\tau_z\sigma_x+c_3^{x\beta}\tau_x\sigma_x$	$(c_1^{x\beta}, c_2^{x\beta}, c_3^{x\beta})=(-0.189, 0.093, 0.454)$	
M_y^β	$c_1^{y\beta}\tau_0\sigma_y+c_2^{y\beta}\tau_z\sigma_y+c_3^{y\beta}\tau_x\sigma_y$	$(c_1^{y\beta}, c_2^{y\beta}, c_3^{y\beta})=(-0.189, 0.093, 0.454)$	
Q_{4z}^α	$\frac{1}{2}\tau_y\sigma_z$		
M_{5u}	$\frac{1}{2}\tau_y\sigma_0$		

4.4 Analysis Based on the Local Model

We investigate the stability and the physical property in the AFQ and AFM phases in the presence of the large CEF splitting by using the self-consistent mean-field calculation for the local model to clarify when the AFQ and AFM phase transitions are possible.

Table 4.4: Cluster multipoles (CMP) consisting of the (a) uniform and (b) staggered configurations of atomic multipoles in the $\Gamma_7^{(1)}$-$\Gamma_7^{(2)}$ levels.

type of CMP		definition	$\boldsymbol{H}=\boldsymbol{0}$ $4/mmm1'$	$\boldsymbol{H}\parallel[001]$ $4/mm'm'$	$\boldsymbol{H}\parallel[100]$ $mm'm'$	$\boldsymbol{H}\parallel[110]$ $mm'm'$
(a) uniform						
E monopole	$\hat{Q}_0^{(\mathrm{c})}$	$\hat{Q}_{0,\mathrm{A}}+\hat{Q}_{0,\mathrm{B}}$	$\mathrm{A}_{1\mathrm{g}}^{+}$	$\mathrm{A}_{\mathrm{g}}^{+}$	$\mathrm{A}_{\mathrm{g}}^{+}$	$\mathrm{A}_{\mathrm{g}}^{+}$
M dipole	$\hat{M}_x^{(\mathrm{c})}$ $(\hat{M}_x^{(\mathrm{c})}+\hat{M}_y^{(\mathrm{c})})$	$\hat{M}_{x,\mathrm{A}}^{\mathrm{tot}}+\hat{M}_{x,\mathrm{B}}^{\mathrm{tot}}$	$\mathrm{E}_{\mathrm{g}}^{-}$	$\mathrm{E}_{\mathrm{g}}^{-}$	$\mathrm{A}_{\mathrm{g}}^{+}$	$\mathrm{A}_{\mathrm{g}}^{+}$
	$\hat{M}_y^{(\mathrm{c})}$ $(\hat{M}_x^{(\mathrm{c})}-\hat{M}_y^{(\mathrm{c})})$	$\hat{M}_{y,\mathrm{A}}^{\mathrm{tot}}+\hat{M}_{y,\mathrm{B}}^{\mathrm{tot}}$			$\mathrm{B}_{\mathrm{g}}^{+}$	$\mathrm{B}_{\mathrm{g}}^{+}$
	$\hat{M}_z^{(\mathrm{c})}$	$\hat{M}_{z,\mathrm{A}}^{\mathrm{tot}}+\hat{M}_{z,\mathrm{B}}^{\mathrm{tot}}$	$\mathrm{A}_{2\mathrm{g}}^{-}$	$\mathrm{A}_{\mathrm{g}}^{+}$	$\mathrm{B}_{\mathrm{g}}^{-}$	$\mathrm{B}_{\mathrm{g}}^{-}$
E quadrupole	$\hat{Q}_u^{(\mathrm{c})}$	$\hat{Q}_{u,\mathrm{A}}+\hat{Q}_{u,\mathrm{B}}$	$\mathrm{A}_{1\mathrm{g}}^{+}$	$\mathrm{A}_{\mathrm{g}}^{+}$	$\mathrm{A}_{\mathrm{g}}^{+}$	$\mathrm{A}_{\mathrm{g}}^{+}$
	$\hat{Q}_{yz}^{(\mathrm{c})}$ $(\hat{Q}_{yz}^{(\mathrm{c})}+\hat{Q}_{zx}^{(\mathrm{c})})$	$\hat{Q}_{yz,\mathrm{A}}+\hat{Q}_{yz,\mathrm{B}}$	$\mathrm{E}_{\mathrm{g}}^{+}$	$\mathrm{E}_{\mathrm{g}}^{+}$	$\mathrm{A}_{\mathrm{g}}^{-}$	$\mathrm{B}_{\mathrm{g}}^{-}$
	$\hat{Q}_{zx}^{(\mathrm{c})}$ $(\hat{Q}_{yz}^{(\mathrm{c})}-\hat{Q}_{zx}^{(\mathrm{c})})$	$\hat{Q}_{zx,\mathrm{A}}+\hat{Q}_{zx,\mathrm{B}}$			$\mathrm{B}_{\mathrm{g}}^{-}$	$\mathrm{A}_{\mathrm{g}}^{-}$
E hexadecapole	$\hat{Q}_{4z}^{\alpha(\mathrm{c})}$	$\hat{Q}_{4z,\mathrm{A}}^{\alpha}+\hat{Q}_{4z,\mathrm{B}}^{\alpha}$	$\mathrm{A}_{2\mathrm{g}}^{+}$	$\mathrm{A}_{\mathrm{g}}^{-}$	$\mathrm{B}_{\mathrm{g}}^{+}$	$\mathrm{B}_{\mathrm{g}}^{+}$
M triacontadipole	$\hat{M}_{5u}^{(\mathrm{c})}$	$\hat{M}_{5u,\mathrm{A}}+\hat{M}_{5u,\mathrm{B}}$	$\mathrm{A}_{1\mathrm{g}}^{-}$	$\mathrm{A}_{\mathrm{g}}^{-}$	$\mathrm{A}_{\mathrm{g}}^{-}$	$\mathrm{A}_{\mathrm{g}}^{-}$
(b) staggered						
E dipole	$\hat{Q}_z^{(\mathrm{c})}$	$\hat{Q}_{0,\mathrm{A}}-\hat{Q}_{0,\mathrm{B}}$	$\mathrm{A}_{2\mathrm{u}}^{+}$	$\mathrm{A}_{\mathrm{u}}^{+}$	$\mathrm{B}_{\mathrm{u}}^{+}$	$\mathrm{B}_{\mathrm{u}}^{+}$
MT dipole	$\hat{T}_y^{(\mathrm{c})}$ $(\hat{T}_x^{(\mathrm{c})}+\hat{T}_x^{(\mathrm{c})})$	$\hat{M}_{x,\mathrm{A}}^{\mathrm{tot}}-\hat{M}_{x,\mathrm{B}}^{\mathrm{tot}}$	$\mathrm{E}_{\mathrm{u}}^{-}$	$\mathrm{E}_{\mathrm{u}}^{-}$	$\mathrm{B}_{\mathrm{u}}^{+}$	$\mathrm{A}_{\mathrm{u}}^{+}$
	$-\hat{T}_x^{(\mathrm{c})}$ $(-\hat{T}_x^{(\mathrm{c})}+\hat{T}_x^{(\mathrm{c})})$	$\hat{M}_{y,\mathrm{A}}^{\mathrm{tot}}-\hat{M}_{y,\mathrm{B}}^{\mathrm{tot}}$			$\mathrm{A}_{\mathrm{u}}^{+}$	$\mathrm{B}_{\mathrm{u}}^{+}$
M monopole	$\hat{M}_0^{(\mathrm{c})}$	$\hat{M}_{z,\mathrm{A}}^{\mathrm{tot}}-\hat{M}_{z,\mathrm{B}}^{\mathrm{tot}}$	$\mathrm{A}_{1\mathrm{u}}^{-}$	$\mathrm{A}_{\mathrm{u}}^{+}$	$\mathrm{A}_{\mathrm{u}}^{-}$	$\mathrm{A}_{\mathrm{u}}^{-}$
E dipole	$\hat{Q}_y^{(\mathrm{c})}$ $(\hat{Q}_x^{(\mathrm{c})}+\hat{Q}_y^{(\mathrm{c})})$	$\hat{Q}_{yz,\mathrm{A}}-\hat{Q}_{yz,\mathrm{B}}$	$\mathrm{E}_{\mathrm{u}}^{+}$	$\mathrm{E}_{\mathrm{u}}^{+}$	$\mathrm{B}_{\mathrm{u}}^{-}$	$\mathrm{A}_{\mathrm{u}}^{-}$
	$\hat{Q}_x^{(\mathrm{c})}$ $(-\hat{Q}_x^{(\mathrm{c})}+\hat{Q}_y^{(\mathrm{c})})$	$\hat{Q}_{zx,\mathrm{A}}-\hat{Q}_{zx,\mathrm{B}}$			$\mathrm{A}_{\mathrm{u}}^{-}$	$\mathrm{B}_{\mathrm{u}}^{-}$
ET quadrupole	$\hat{G}_u^{(\mathrm{c})}$	$\hat{Q}_{4z,\mathrm{A}}^{\alpha}-\hat{Q}_{4z,\mathrm{B}}^{\alpha}$	$\mathrm{A}_{1\mathrm{u}}^{+}$	$\mathrm{A}_{\mathrm{u}}^{+}$	$\mathrm{A}_{\mathrm{u}}^{+}$	$\mathrm{A}_{\mathrm{u}}^{+}$
MT dipole	$\hat{T}_z^{(\mathrm{c})}$	$\hat{M}_{5u,\mathrm{A}}-\hat{M}_{5u,\mathrm{B}}$	$\mathrm{A}_{2\mathrm{u}}^{-}$	$\mathrm{A}_{\mathrm{u}}^{+}$	$\mathrm{B}_{\mathrm{u}}^{-}$	$\mathrm{B}_{\mathrm{u}}^{-}$

In the following discussion, we use the Γ_7-Γ_6 level scheme for the CEF parameter of Tetragonal (1), although one can also analyze the case for the $\Gamma_7^{(1)}$-$\Gamma_7^{(2)}$ level scheme as well.

In Sec. 4.4.1, we show the effective local model including the CEF level splitting and multipole-multipole interactions. We discuss the stability of the multipole ordered states and their finite-temperature phase transitions in Sec. 4.4.2 and magnetic and quadrupole susceptibilities in Sec. 4.4.3.

4.4.1 Model

We consider an effective local model, which includes the CEF level splitting, the Zeeman term, and the multipole-multipole interaction. The model Hamiltonian is given as follows:

$$\mathcal{H}=\mathcal{H}_{\rm CEF}+\mathcal{H}_{\rm Zeeman}+\mathcal{H}_{\rm int}, \tag{4.7}$$

$$\mathcal{H}_{\rm CEF}=\Delta\sum_{R}\sum_{i={\rm A,B}}\sum_{\sigma=\uparrow,\downarrow} f^{\dagger}_{Ri\Gamma_6\sigma}f_{Ri\Gamma_6\sigma} \tag{4.8}$$

$$\mathcal{H}_{\rm Zeeman}=-g\mu_{\rm B}\sum_{R}\sum_{i={\rm A,B}}\boldsymbol{H}\cdot\hat{\boldsymbol{J}}_{Ri}, \tag{4.9}$$

$$\begin{aligned}\mathcal{H}_{\rm int}=D\sum_{\langle r,s\rangle}^{\rm n.n.}\Big[&\delta_u\hat{Q}_{u,r}\hat{Q}_{u,s}+\delta_v\hat{Q}_{v,r}\hat{Q}_{v,s}+\delta_{\rm E^+}(\hat{Q}_{yz,r}\hat{Q}_{yz,s}+\hat{Q}_{zx,r}\hat{Q}_{zx,s})+\delta_{xy}\hat{Q}_{xy,r}\hat{Q}_{xy,s}\\&+\delta_{\rm E^-}(\hat{M}_{x,r}\hat{M}_{x,s}+\hat{M}_{y,r}\hat{M}_{y,s})+\delta_z\hat{M}_{z,r}\hat{M}_{z,s}\\&+\delta_{xyz}\hat{M}_{xyz,r}\hat{M}_{xyz,s}+\delta_{\rm E^-_{3\alpha}}(\hat{M}^{\alpha}_{x,r}\hat{M}^{\alpha}_{x,s}+\hat{M}^{\alpha}_{y,r}\hat{M}^{\alpha}_{y,s})+\delta_{z\alpha}\hat{M}^{\alpha}_{z,r}\hat{M}^{\alpha}_{z,s}\\&+\delta_{\rm E^-_{3\beta}}(\hat{M}^{\beta}_{x,r}\hat{M}^{\beta}_{x,s}+\hat{M}^{\beta}_{y,r}\hat{M}^{\beta}_{y,s})+\delta_{z\beta}\hat{M}^{\beta}_{z,r}\hat{M}^{\beta}_{z,s}\Big],\end{aligned} \tag{4.10}$$

where $f^{\dagger}_{Ri\Gamma_6\sigma}$ ($f_{Ri\Gamma_6\sigma}$) and $\hat{\boldsymbol{J}}_{Ri}$ are the creation (annihilation) operator of the f electron with the quasi spin $\sigma=\uparrow,\downarrow$ in the Γ_6 level and the total angular momentum, respectively, at the sublattice $i={\rm A,B}$ in the Rth unit cell. $\hat{X}_r\equiv\hat{X}_{Ri}=\sum_{ll'}\sum_{\sigma\sigma'}f^{\dagger}_{Ril\sigma}\hat{X}^{ll'}_{\sigma\sigma'}f_{Ril'\sigma'}$ ($X=Q_u$, Q_v, Q_{yz}, Q_{zx}, Q_{xy}, M_x, M_y, M_z, M_{xyz}, M^{α}_x, M^{α}_y, M^{α}_z, M^{β}_x, M^{β}_y, M^{β}_z) is the normalized multipole operator at rth atomic site, where $\hat{X}^{ll'}_{\sigma\sigma'}$ is the matrix element for the orbital $l,l'=\Gamma_7,\Gamma_6$ and quasi spin $\sigma,\sigma'=\uparrow,\downarrow$ shown in Table 4.1. The first term $\mathcal{H}_{\rm CEF}$ in Eq. (4.7) is the CEF level splitting, where Δ is calculated from the CEF Hamiltonian in Eq. (4.1) as $\Delta\sim$90 K. The second term $\mathcal{H}_{\rm Zeeman}$ in Eq. (4.7) is the Zeeman term, where g is the g factor with the value $g=6/7$ and the Bohr magneton $\mu_{\rm B}$ is set as $\mu_{\rm B}\to\mu_{\rm B}/k_{\rm B}=0.67$ [K/T]. The Boltzmann factor $k_{\rm B}$ is set as 1 in the following. The last term $\mathcal{H}_{\rm int}$ in Eq. (4.7) is the antiferroic multipole-multipole interaction term ($D>0$), where the summation is taken for the eight neighbor $\rm Ce_A$ and $\rm Ce_B$ sites, $\langle r,s\rangle$. δ_X stands for the weight of the multipole-multipole interaction ($0\le\delta_X\le1$). $\mathcal{H}_{\rm int}$ is derived based on the symmetry analysis[4].

By applying the Hartree approximation for $\mathcal{H}_{\rm int}$ as

$$D\sum_{\langle r,s\rangle}^{\rm n.n.}\delta_X\hat{X}_r\hat{X}_s\to Dz\sum_{R=1}^{N}\delta_X(\langle\hat{X}_{\rm A}\rangle\,\hat{X}_{R\rm B}+\langle\hat{X}_{\rm B}\rangle\,\hat{X}_{R\rm A}-\langle\hat{X}_{\rm A}\rangle\,\langle\hat{X}_{\rm B}\rangle), \tag{4.11}$$

the mean-field Hamiltonian is obtained. We take into account the interaction to the upper-nearest-neighbor four sites and lower-nearest-neighbor four sites [See also Fig. 4.1(a)] as a mean field and set $z=8$. We set $\bar{D}\equiv Dz$ in the following discussion.

4.4.2 Phase Diagram

We investigate the stability of the AFM and AFQ phases by using the two-sublattice self-consistent mean-field calculation for the local model in Eq. (4.7). We suppose that the

[4]We omit the coupling between different types of multipoles, such as M_x and M^{α}_x, for simplicity, while it is allowed from the symmetry viewpoint.

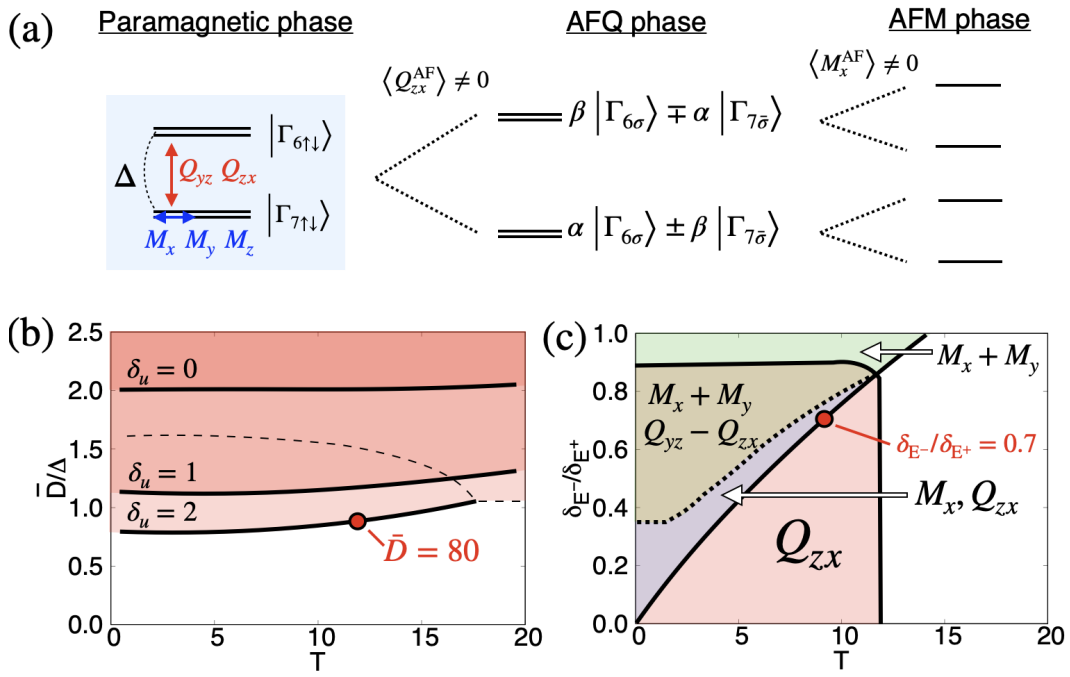

Figure 4.6: (a) Schematic picture of the low-energy four levels in the paramagnetic phase (left), AFQ phase (middle), and AFM phase (right). The basis functions are also shown except for the AFM phase, where α and β are the linear combination coefficients and $\bar{\sigma}=-\sigma$. (b) The phase diagram while changings the temperature (T) and interaction $\bar{D}$ in the absence of the AFM interaction. For δ_u=0, 1, and 2, the AFQ ordering is stabilized in the colored region above each bold line. The broken line describes the transition from the Q_{zx}(or Q_{yz})-type AFQ order to the Q_u-type AFQ order when increasing $\bar{D}$ for δ_u=2. Other nonzero parameters are δ_{E^+}=1 and δ_v=0.8. (c) The phase diagram when T and the ratio $\delta_{E^-}/\delta_{E^+}$ change, where the antiferroic order parameters in each phase are presented.

in-plane AFM order, which is suggested by the neutron diffraction of CeCoSi [202], and the Q_{yz}- or Q_{zx}-type AFQ order by setting δ_z=0.3δ_{E^-}, δ_{E^+}=1, and δ_v=0.8 in the present calculation. Other interaction parameters are set 0 except for δ_u and δ_{E^-} in the following. Although the order parameters and the relevant multipoles have not been identified yet in the II phase, we discuss a case of the Q_{yz}-or Q_{zx}-type AFQ orderings breaking the tetragonal symmetry, whose symmetry violation has been recently implied by the x-ray diffraction measurement [211].

First, we examine the multipole interaction to stabilize the AFM and AFQ phases in a zero magnetic field. In the paramagnetic phase without any electronic orderings, two CEF levels are separated by Δ as shown in the left panel of Fig. 4.6(a). When the effect of the multipole-multipole interaction $\bar{D}$ is taken into account, the interorbital AFQ ordering becomes possible. In the presence of the AFQ ordering, the mixing of Γ_7 and Γ_6 levels occurs like the middle panel of Fig. 4.6(a), where the two-fold degeneracy remains due to the time-reversal symmetry. Temperature (T) and $\bar{D}$ required to stabilize the Q_{yz}- or Q_{zx}-type AFQ order are shown in Fig. 4.6(b) for three δ_u=0, 1, and 2, where we set the AFM interaction δ_{E^-}=0. In the colored region above the bold line, AFQ ordered

state is stabilized for each δ_u. For δ_u=0, the large value $\bar{D}\sim 2\Delta$ is needed to stabilize the AFQ state, which is consistent with the theoretical study on the cubic system with the Γ_7 ground state[5] [212]. Meanwhile, nonzero δ_u suppresses the critical value of $\bar{D}$ to stabilize the AFQ phase as shown in Fig. 4.6(b). It is because the δ_u term renormalizes the CEF splitting effectively through the development of the ferroic Q_u moment. It is noted that the suppression of the CEF splitting depends on the temperature, as the ferroic Q_u moment depends on the temperature. In the following discussion, we use δ_u=2 and $\bar{D}$=80, which gives a similar transition temperature to that of the II phase observed in CeCoSi.

Next, we introduce the AFM interaction to describe the AFQ-AFM phase transition observed in CeCoSi. The introduction of δ_{E^-} replaces the AFQ ground state with the AFM ground state owing to the lifting of the Kramers degeneracy as shown in the right panel of Fig. 4.6(a). Figure 4.6(c) shows the phase diagram while changing T and the ratio of the AFM and AFQ interaction, δ_{E^-} and δ_{E^+}. The solid (dotted) line means the second-order (first-order) phase transition. For the small $\delta_{\mathrm{E}^-}/\delta_{\mathrm{E}^+}\lesssim 0.35$, decreasing T leads to the $Q_{zx}(Q_{yz})$-type AFQ ordering, followed by the $M_x(M_y)$-type AFM ordering accompanied by the $Q_{zx}(Q_{yz})$-type AFQ moment. In $0.35\lesssim\delta_{\mathrm{E}^-}/\delta_{\mathrm{E}^+}\lesssim 0.9$, the AFM phase shows further first-order phase transition to the $(M_x+M_y)[(M_x-M_y)]$-type AFM ordering with the $(Q_{yz}-Q_{zx})[(Q_{yz}+Q_{zx})]$-type AFQ moment. There are two differences in these two AFM phases; one is the in-plane anisotropy between [100] and [110] directions, and the other is the difference in angle relative to the AFQ moment. Especially, the latter difference results in the different symmetry between two types of AFM phases. For large $\delta_{\mathrm{E}^-}/\delta_{\mathrm{E}^+}\gtrsim 0.9$, only the AFM phase appears without the AFQ phase. In the end, the result in the region $\delta_{\mathrm{E}^-}/\delta_{\mathrm{E}^+}\lesssim 0.9$ might correspond the situation observed in CeCoSi; AFQ and AFM phases appear while changing the temperature. We set $\delta_{\mathrm{E}^-}=0.7\delta_{\mathrm{E}^+}$ in the following calculation.

We also investigate the AFQ and AFM phases in a magnetic field. Figures 4.7(a) and 4.7(b) are the phase diagrams against the magnetic field (H) and T, where the Zeeman field in Eq. (4.7) is directed along the [001] and [100] directions. The solid (dotted) line represents the phase boundary characterized by the second-order (first-order) phase transition. The filled square (T_0), filled circle (T_{N}), and empty circle (T'_{N}) in a zero magnetic field stand for the AFQ transition temperature, AFM transition temperature, and phase transition between two types of AFM states, respectively.

In the [001] magnetic field, the $Q_{zx}(Q_{yz})$-type AFQ order is stabilized even in the high-field region. The magnetic point group symmetry is $2'm'm$ ($m'2'm$) as presented in the parentheses in Fig. 4.7(a). The transition temperature of the AFQ phase is almost the same when applying the [001] magnetic field. The transition at T_{N} in a zero magnetic field disappears in the [001] magnetic field because of the same symmetry to the AFQ phase, although the broad peak structure remains in the T derivative of the magnetization and heat capacity, which is presented by the dashed thin line in Fig. 4.7(a). On the other hand, the low-temperature AFM phase, which has the $(M_x+M_y)[(M_x-M_y)]$-type AFM moment and the $(Q_{yz}-Q_{zx})[(Q_{yz}+Q_{zx})]$-type AFQ moment in a zero magnetic field, has the symmetry m and remains in the [001] magnetic field as presented in Fig. 4.7(a). By applying the magnetic field, these vertically coupled AFM and AFQ moments rotate in

[5]It is noted that the present study uses the normalized multipole moment unlike Ref. [212].

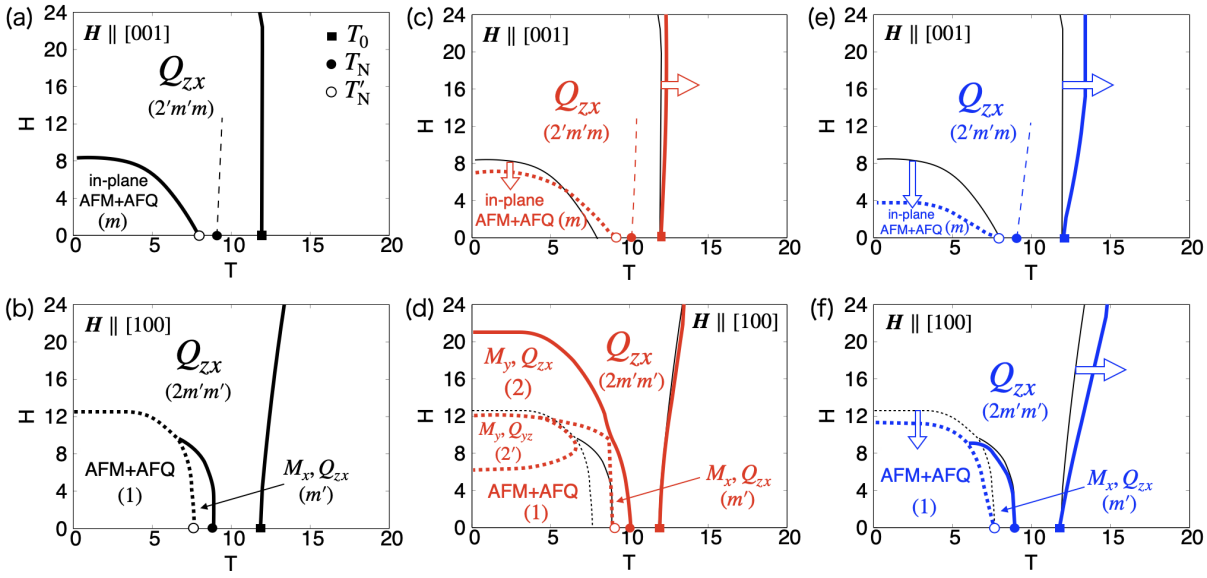

Figure 4.7: (a–f) H-T phase diagrams in the (a,c,e) [001] and (b,d,f) [100] magnetic fields. In addition to the effect of the Zeeman coupling in (a) and (b), the magnetic octupole interaction $\delta_{\mathrm{E}^-_{3\beta}}$ is additionally considered in (c) and (d), and the effective multipole coupling between the FM and AFQ moments is considered in (e) and (f). The solid (dotted) line stands for the second-order (first-order) phase transition. The dashed thin line in the [001] magnetic field represents the minimum in the T derivative of the magnetization [see the main text in the details]. The phase boundaries in (a)[(b)] is shown by the thin black lines in (c) and (e) [(d) and (f)] for reference.

the xy plane and reach the parallel coupled $M_x(M_y)$-type AFM and $Q_{zx}(Q_{yz})$-type AFQ moment, which means the phase transition to the AFQ phase.

The phase diagram in the [100] magnetic field in Fig. 4.7(b) shows that the Q_{zx}-type AFQ ordering is similar to the result in the [001] magnetic field (Note that Q_{yz}-type AFQ has higher energy owing to the orthorhombic symmetry in the [100] magnetic field). Different from the [001] magnetic field, the AFQ transition temperature shows a slight enhancement by the magnetic field, whose difference might be attributed to the difference of the matrix elements of $\hat{J}_{x(y)}$ and $\hat{J}_z$ determined by the CEF parameters. In the low-temperature region under the [100] magnetic field, two types of the AFM phases survive as shown in Fig. 4.7(b): one with the symmetry m' and the other with the symmetry 1.

The present result shows that the AFQ and AFM phases remain stable in the magnetic field, which is consistent with that observed in CeCoSi [Fig. 4.2(b)]. Meanwhile, there are several differences between them; one of the difference is the slope of the phase boundary between the AFQ and paramagnetic states by introducing the magnetic field. In other words, the present result shows that there are no almost change in the phase boundaries, whereas the AFQ transition temperature is enhanced by the magnetic fields especially for the [001] direction in experiments.

To explain the behavior of the phase boundary between the AFQ and paramagnetic states, we consider two scenarios. First, we additionally introduce the antiferroic octupole (AFO) interaction, which describes an effective coupling between the FM and AFQ mo-

ments [23]. We show the modified phase diagram in the presence of $\delta_{\mathrm{E}^-_{3\beta}}$=0.5 in the [001] and [100] magnetic fields in Figs. 4.7(c) and 4.7(d), respectively[6]. In the [001] magnetic field, the AFO interaction slightly increases the AFQ transition temperature as shown in Fig. 4.7(c). Meanwhile, it suppresses the critical field of the AFM phase. This is because $\delta_{\mathrm{E}^-_{3\beta}}$ affects the stability of the in-plane AFM phase due to the same symmetry of M^{β}_{μ} and M_{μ} (μ=x, y).

In the [100] magnetic field, $\delta_{\mathrm{E}^-_{3\beta}}$ hardly affects the phase boundary of the AFQ phase, since M^{β}_{μ} (μ=x, y) has a different symmetry from the coupling between the ferroic M_x moment and the antiferroic Q_{zx} moment. Meanwhile, the octupole interaction changes the AFM phase drastically, which leads to additional three phases with different AFM and AFQ moments. The symmetry in each AFM phase is presented in Fig. 4.7(d). In summary, the AFO interaction for the present AFQ order is not sufficient to reproduce the behavior of the phase boundaries in CeCoSi.

The second scenario is that an effective coupling between the M dipole and AFQ moments in the presence of the magnetic field. We introduce the additional effective coupling for the [001] magnetic field with the Q_{zx}-type AFQ moment within the mean-field level

$$\mathcal{H}^{\mathrm{eff}}_{[001]}=\bar{D}\sum_{R}\delta'_{[001]}\Big[(\langle\hat{M}_{z,\mathrm{A}}\rangle+\langle\hat{M}_{z,\mathrm{B}}\rangle)(\hat{Q}_{zx,R\mathrm{A}}-\hat{Q}_{zx,R\mathrm{B}})+(\langle\hat{Q}_{zx,\mathrm{A}}\rangle-\langle\hat{Q}_{zx,\mathrm{B}}\rangle)(\hat{M}_{zR,\mathrm{A}}+\hat{M}_{zR,\mathrm{B}})$$
$$-(\langle\hat{M}_{z,\mathrm{A}}\rangle+\langle\hat{M}_{z,\mathrm{B}}\rangle)(\langle\hat{Q}_{zx,\mathrm{A}}\rangle-\langle\hat{Q}_{zx,\mathrm{B}}\rangle)\Big], \tag{4.12}$$

where $\langle\hat{M}_{z,\mathrm{A}}\rangle+\langle\hat{M}_{z,\mathrm{B}}\rangle$ and $\langle\hat{Q}_{zx,\mathrm{A}}\rangle-\langle\hat{Q}_{zx,\mathrm{B}}\rangle$ are the FM and the AFQ moments, respectively. Figure 4.7(e) represents the phase diagram in the [001] magnetic field for $\delta'_{[001]}$=-0.005. The result shows that the direct coupling between the FM and AFQ moments in Eq. (4.12) leads to the strong enhancement of the AFQ transition temperature by the magnetic field. Meanwhile, the critical field of the AFM phase tends to be suppressed as well as that in the presence of the AFO interaction.

Meanwhile, in the [100] magnetic field, we consider a different type of the effective coupling as

$$\mathcal{H}^{\mathrm{eff}}_{[100]}=\bar{D}\sum_{R}\delta'_{[100]}\Big[(\langle\hat{M}_{x,\mathrm{A}}\rangle+\langle\hat{M}_{x,\mathrm{B}}\rangle)(\hat{Q}_{zx,R\mathrm{A}}-\hat{Q}_{zx,R\mathrm{B}})+(\langle\hat{Q}_{zx,\mathrm{A}}\rangle-\langle\hat{Q}_{zx,\mathrm{B}}\rangle)(\hat{M}_{xR,\mathrm{A}}+\hat{M}_{xR,\mathrm{B}})$$
$$-(\langle\hat{M}_{x,\mathrm{A}}\rangle+\langle\hat{M}_{x,\mathrm{B}}\rangle)(\langle\hat{Q}_{zx,\mathrm{A}}\rangle-\langle\hat{Q}_{zx,\mathrm{B}}\rangle)\Big]. \tag{4.13}$$

The phase diagram for $\delta'_{[100]}$=-0.005 is shown in Fig. 4.7(f). The result shows that the phase boundary between the AFQ and paramagnetic phases moves to the high-temperature side with an increase of the magnetic field. The AFM phase shows a modulation, where the critical field between the AFM and AFQ is slightly suppressed, in the presence of the effective coupling in Eq. (4.13). Thus, the effective coupling induced under the magnetic field is one of the important factors to reproduce the H dependence of the AFQ transition temperature observed in CeCoSi.

[6]We neglected $\delta_{\mathrm{E}^-_{3\alpha}}$, which corresponds to another AFO interaction, as it mainly changes the AFM phase boundary rather than the AFQ one.

4.4.3 Susceptibility

We investigate behaviors of the magnetic and quadrupole susceptibilities under the multipole orderings while changing the temperature. We calculate the magnetic and quadrupole susceptibilities by using the following isothermal susceptibility

$$\chi_X(T)=2\sum_{nm} w_n \frac{\left|\langle n|\hat{X}|m\rangle\right|^2}{E_m-E_n}+\frac{1}{k_{\rm B}T}\left[\sum_n w_n \langle n|\hat{X}|n\rangle^2-\left(\sum_n w_n \langle n|\hat{X}|n\rangle\right)^2\right], \quad (4.14)$$

where $|n\rangle$ is the electronic state with the eigenenergy E_n and $w_n=e^{-\frac{E_n}{k_{\rm B}T}}$ is the Boltzmann weight of the eigenstate n. For magnetic and quadrupole susceptibilities, $\chi^{\rm D}_\mu$ $(\mu=x,y,z)$ and $\chi^{\rm Q}_\nu$ $(\nu=u,v,yz,zx,xy)$, we set $\hat{X}=g\mu_{\rm B}\hat{J}_{\mu,i}$ $(i={\rm A,B})$ and $\hat{Q}_{\nu,i}$, respectively. In the following, we show the susceptibilities in the total two-sublattice system.

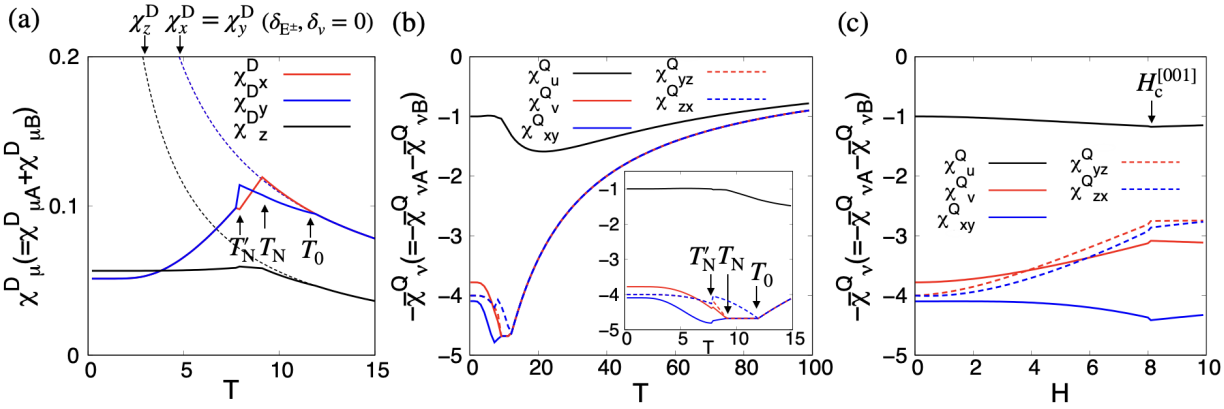

Figure 4.8: (a,b) T dependences of the (a) magnetic and (b) quadrupole susceptibilities at a zero magnetic field. (c) H dependence of the quadrupole susceptibility in the [001] magnetic field.

First, we discuss the magnetic susceptibility $\chi^{\rm D}_\mu$ $(\mu=x,y,z)$ in Fig. 4.8(a). The magnetic susceptibilities without any electronic ordered phases for $\delta_{\rm E^\pm}=\delta_v=0$ are also shown by the broken lines for reference. $\chi^{\rm D}_\mu$ shows the slight anomaly at the Q_{zx}-type AFQ transition temperature T_0; $\chi^{\rm D}_x$ shows a little upturn from the paramagnetic phase, whereas $\chi^{\rm D}_y$ and $\chi^{\rm D}_z$ show the down-turn modulation below T_0. At the transition temperature $T_{\rm N}$ to the M_x-type AFM order, $\chi^{\rm D}_x$ shows a cusp-like anomaly as the conventional AFM order, while $\chi^{\rm D}_y$ shows almost no anomaly and $\chi^{\rm D}_z$ has the almost constant value below $T_{\rm N}$. Below $T'_{\rm N}$, $\chi^{\rm D}_x=\chi^{\rm D}_y$ due to transition from the AFM order along the [100] direction to that along the [110] direction.

We focus on the behavior of $\chi^{\rm D}_\mu$ below T_0. The up- or down-turn behavior of $\chi^{\rm D}_\mu$ depends on the magnitude of the effective M dipole within the ground-state Kramers doublet. To demonstrate that, we calculate a quantity of ${\rm Tr}[M^2_\mu]_{\rm AFQ}-{\rm Tr}[M^2_\mu]_{\rm para}$, where ${\rm Tr}[M^2_\mu]_{\rm AFQ}$ is calculated for the Kramers doublet with nonzero but small Q_{zx} moment and

$\mathrm{Tr}[M_\mu^2]_{\mathrm{para}}$ is for the CEF ground state. It is approximately given by

$$\mathrm{Tr}[M_x^2]_{\mathrm{AFQ}}-\mathrm{Tr}[M_x^2]_{\mathrm{para}}=\frac{2[(c_3^x)^2-c_1^x(c_1^x+c_2^x)]}{\Delta^2}q_{zx}^2+O(q_{zx}^4), \tag{4.15}$$

$$\mathrm{Tr}[M_y^2]_{\mathrm{AFQ}}-\mathrm{Tr}[M_y^2]_{\mathrm{para}}=-\frac{2c_2^y(c_1^y+c_2^y)}{\Delta^2}q_{zx}^2+O(q_{zx}^4), \tag{4.16}$$

$$\mathrm{Tr}[M_z^2]_{\mathrm{AFQ}}-\mathrm{Tr}[M_z^2]_{\mathrm{para}}=\frac{2[(c_3^z)^2-c_1^z(c_1^z+c_2^z)]}{\Delta^2}q_{zx}^2+O(q_{zx}^4), \tag{4.17}$$

where $q_{zx}=\bar{D}\delta_{\mathrm{E}^+}Q_{zx}$. As the present CEF parameters in Table 4.1 give $(c_3^x)^2-c_1^x(c_1^x+c_2^x)>0$, $c_2^y(c_1^y+c_2^y)<0$, and $(c_3^z)^2-c_1^z(c_1^z+c_2^z)<0$, the up-turn behavior appears in χ_x^{D} and the down-turn behavior appears in χ_y^{D} and χ_z^{D}, as shown in Fig. 4.8(a). This result indicates that the behavior of the magnetic susceptibility in the AFQ orderings gives information about the CEF and the AFQ order parameter.

Besides, we also discuss the quadrupole susceptibility χ_ν^{Q}. Figure 4.8(b) shows the quadrupole suceptibility $-\bar{\chi}_\nu^{\mathrm{Q}}$ scaled as $\bar{\chi}_u^{\mathrm{Q}}=1$ at $T=0.2$, in a zero magnetic field. The low-temperature region is presented in the inset of Figure 4.8(b). All χ_ν^{Q} components show the softening with decreasing T in the paramagnetic phase. In spite of the large CEF splitting, their modulation in the AFQ ordered phase is similar to that seen in the conventional AFQ ordered systems like CeB_6 [21]; χ_{zx}^{Q} shows a cusp-like anomaly at T_0 and upturns with decreasing T, while χ_v^{Q}, χ_{yz}^{Q}, and χ_{xy}^{Q} show almost constant values. In the AFM phases, these four components mostly show the up-turn behavior with decreasing T, although χ_{xy}^{Q} slightly decreases between T_{N} and T_{N}'. On the other hand, χ_u^{Q} shows a broad peak around $T\sim15$, which roughly corresponds to half of the effective CEF splitting described by $\Delta^{\mathrm{eff}}\sim\Delta-\bar{D}\delta_u\langle\hat{Q}_{u,\mathrm{A(B)}}\rangle\sim30$ K. While decreasing T, χ_u^{Q} shows anomaly at the AFM transition temperature and reaches the constant value.

Moreover, we investigate the behavior of χ^{Q} in a magnetic field by focusing on the region below T_{N}. We here do not consider the octupole interaction and the effective coupling discussed in the previous section, since they do not give a qualitative difference. Figure 4.8(c) shows the χ_ν^{Q} in the [001] magnetic field at $T=2$, where $H_{\mathrm{c}}^{[001]}$ is the critical field of the AFM phase. χ_{yz}^{Q} and χ_{zx}^{Q} split by the magnetic field with the hardening, χ_v^{Q} also shows the hardening, and χ_{xy}^{Q} shows the softening. Such various behaviors are due to the rotation of the AFM and AFQ moments when increasing the magnetic field as mentioned in the previous section. In other words, since the $(Q_{yz}-Q_{zx})[(Q_{yz}+Q_{zx})]$-type AFQ moment is rotated to the Q_{zx}(or Q_{yz})-type one, χ_{yz}^{Q} and χ_{zx}^{Q} show the split and different behaviors of χ_{xy}^{Q} and χ_v^{Q}. Thus, the quadrupole susceptibility in a magnetic field provides information about the coupling between the AFM and AFQ moments.

4.5 Analysis Based on the Itinerant Model

We investigate the multiferroic responses expected in the odd-parity multipole orderings induced by the AFM and AFQ moments by using the itinerant model. In the present section, we suppose the Γ_7-Γ_6 level scheme similar to the local model in the previous section.

In Sec. 4.5.1, we present the effective tight-binding model with the multipole-multipole interaction. By using the effective itinerant model, we investigate the stability of the

multipole orderings at zero temperature in Sec. 4.5.2, the band modulation due to the odd-parity multipole ordering in Sec. 4.5.3, and the multiferroic responses in Sec. 4.5.4.

4.5.1 Model

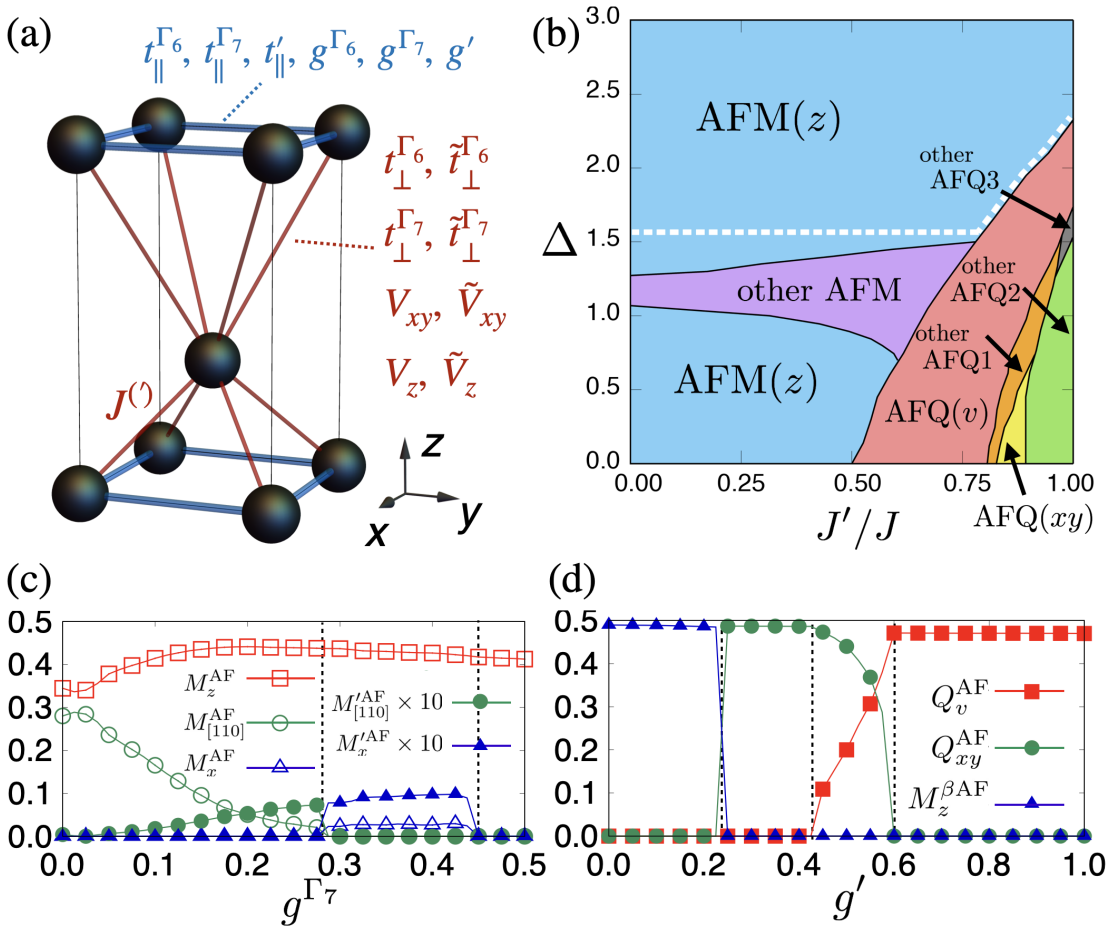

Figure 4.9: (a) Schematic picture presenting the bond with hopping and multipole-multipole interaction. (b) The ground-state phase diagram obtained from the self-consistent mean-field calculations at $g^{\Gamma_6}=-0.4$, $g^{\Gamma_7}=0.5$, and $g'=0.8$. AFM(z) represents the AFM phase with staggered M moments along the z direction. AFQ(v) and AFQ(xy) stand for the Q_v and Q_{xy}-type AFQ phases, respectively. Other AFM and other AFQ1, 2, 3 are the AFM and AFQ phases characterized by more than one order parameter. The phases are metallic (insulating) in the region below (above) the white dashed line. (c) The intraorbital ASOI dependence of the AFM moments at $J'/J=0.2$, $\Delta=1$, $g'=0.8$, and $g^{\Gamma_6}=-0.8g^{\Gamma_7}$. (d) The interorbital ASOI dependence of the interorbital multipole moments at $J'/J=0.7$, $\Delta=0.5$, $g^{\Gamma_6}=-0.4$, and $g^{\Gamma_7}=0.5$.

We investigate a tight-binding model constructed by considering two f orbitals at Ce ions and a d orbital at Co ions and taking into account the atomic spin-orbit coupling, CEF level splitting, f-f hopping, and d-f hybridization [195]. By tracing out the d-orbital degree of freedom, an effective Hamiltonian with the multipole-multipole interaction is

given by

$$\begin{aligned}\mathcal{H}=&\Delta\sum_{\boldsymbol{k}}\sum_{\sigma}\sum_{i}f^{\dagger}_{\boldsymbol{k}i\Gamma_6\sigma}f_{\boldsymbol{k}i\Gamma_6\sigma}+\sum_{\boldsymbol{k}}\sum_{\sigma}\sum_{\mu,\nu}^{0,x,y,z}\sum_{i,j}\sum_{l,m}[\varepsilon_{\mu\nu}(\boldsymbol{k})\rho_{\mu}\tau_{\nu}]^{lm}_{ij}f^{\dagger}_{\boldsymbol{k}il\sigma}f_{\boldsymbol{k}jm\sigma}\\&+\sum_{\boldsymbol{k}}\sum_{\sigma,\sigma'}\sum_{\mu,\nu}\sum_{i,j}\sum_{l,m}\left\{\left[\boldsymbol{g}_{\mu\nu}(\boldsymbol{k})-\boldsymbol{h}_{\mu\nu}(\boldsymbol{k})\right]\rho_{\mu}\tau_{\nu}\right\}^{lm}_{ij}\cdot\boldsymbol{\sigma}^{\sigma\sigma'}f^{\dagger}_{\boldsymbol{k}il\sigma}f_{\boldsymbol{k}jm\sigma'}\\&+\sum_{\langle r,s\rangle}\left[J\left(\hat{\boldsymbol{M}}^{\Gamma_6}_{r}\cdot\hat{\boldsymbol{M}}^{\Gamma_6}_{s}+\hat{\boldsymbol{M}}^{\Gamma_7}_{r}\cdot\hat{\boldsymbol{M}}^{\Gamma_7}_{s}\right)+J'\hat{\boldsymbol{X}}_{r}\cdot\hat{\boldsymbol{X}}_{s}\right],\end{aligned}\tag{4.18}$$

where $f^{\dagger}_{\boldsymbol{k}il\sigma}$ ($f_{\boldsymbol{k}il\sigma}$) is a creation (annihilation) operator of an electron with the wave vector $\boldsymbol{k}$, sublattice i= A, B, orbital l=Γ_6,Γ_7, and quasi-spin σ=$\uparrow,\downarrow$. ρ_{μ} (μ=$0,x,y,z$) is the Pauli matrix in sublattice spaces. The first term in Eq. (4.18) is the CEF level splitting between the Γ_6 and Γ_7 levels. The second term is the symmetry-allowed hopping term; the intraorbital hoppings, $\varepsilon_{00}(\boldsymbol{k})$ and $\varepsilon_{0z}(\boldsymbol{k})$, and the interorbital hopping, $\varepsilon_{0x}(\boldsymbol{k})$, between the same sublattices, and the intraorbital hoppings, $\varepsilon_{x0}(\boldsymbol{k}),\varepsilon_{xz}(\boldsymbol{k}),\varepsilon_{y0}(\boldsymbol{k})$, and $\varepsilon_{yz}(\boldsymbol{k})$, between the different sublattices. By setting the positions of $\mathrm{Ce_A}$ and $\mathrm{Ce_B}$ as $(a/2,a/2,c/2-\theta)$ and $(0,0,0)$ with the lattice constants a and c, and using the notations $\varepsilon_{\mu l}(\boldsymbol{k})$≡$[\varepsilon_{\mu 0}(\boldsymbol{k})+p(l)\varepsilon_{\mu z}(\boldsymbol{k})]/2$ where $p(l)$=$+1(-1)$ for l=Γ_7 (Γ_6), each $\varepsilon_{\mu\nu}(\boldsymbol{k})$ is given by

$$\varepsilon_{0l}(\boldsymbol{k})=t^{l}_{\parallel}(\cos k_x a+\cos k_y a),\tag{4.19}$$

$$\varepsilon_{0x}(\boldsymbol{k})=t'_{\parallel}(\cos k_x a-\cos k_y a),\tag{4.20}$$

$$\varepsilon_{xl}(\boldsymbol{k})=\left(t^{l}_{\perp}\cos\frac{k_z c}{2}\cos k_z\theta+\tilde{t}^{l}_{\perp}\sin\frac{k_z c}{2}\sin k_z\theta\right)\cos\frac{k_x a}{2}\cos\frac{k_y a}{2},\tag{4.21}$$

$$\varepsilon_{yl}(\boldsymbol{k})=\left(t^{l}_{\perp}\cos\frac{k_z c}{2}\sin k_z\theta-\tilde{t}^{l}_{\perp}\sin\frac{k_z c}{2}\cos k_z\theta\right)\cos\frac{k_x a}{2}\cos\frac{k_y a}{2}.\tag{4.22}$$

The third term in Eq. (4.18) is the spin-dependent hopping term originating from the atomic spin-orbit coupling. The antisymmetric contribution $\boldsymbol{g}_{\mu\nu}(\boldsymbol{k})$ with respect to $\boldsymbol{k}$ corresponds to the ASOI, which includes the intraorbital contributions, $\boldsymbol{g}_{z0}(\boldsymbol{k})$ and $\boldsymbol{g}_{zz}(\boldsymbol{k})$, and the interorbital contribution, $\boldsymbol{g}_{zx}(\boldsymbol{k})$, between the same sublattices, which are represented by

$$\boldsymbol{g}_{zl}(\boldsymbol{k})=g^{l}(-\sin k_y a,\sin k_x a,0),\tag{4.23}$$

$$\boldsymbol{g}_{zx}(\boldsymbol{k})=g'(-\sin k_y a,-\sin k_x a,0),\tag{4.24}$$

where $\boldsymbol{g}_{zl}(\boldsymbol{k})$≡$[\boldsymbol{g}_{z0}(\boldsymbol{k})+p(l)\boldsymbol{g}_{zz}(\boldsymbol{k})]/2$. It is noted that the only staggered component of the ASOI appears in the presence of the global inversion symmetry. The ASOI is microscopically derived from the off-site hybridization with the Co $3d$ electrons and the atomic spin-orbit coupling. Meanwhile, the symmetric spin-dependent hoppings between the different sublattices with the different orbitals, are represented by $\boldsymbol{h}_{xy}(\boldsymbol{k})$=

$\{\mathrm{Im}[h_x(\boldsymbol{k})], \mathrm{Im}[h_y(\boldsymbol{k})], -\mathrm{Re}[h_z(\boldsymbol{k})]\}$ and $\boldsymbol{h}_{yy}(\boldsymbol{k})=\{\mathrm{Re}[h_x(\boldsymbol{k})], \mathrm{Re}[h_y(\boldsymbol{k})], \mathrm{Im}[h_z(\boldsymbol{k})]\}$, where

$$h_x(\boldsymbol{k})=\left(V_{xy}\cos\frac{k_zc}{2}+i\tilde{V}_{xy}\sin\frac{k_zc}{2}\right)e^{-i\theta k_z}\cos\frac{k_xa}{2}\sin\frac{k_ya}{2}, \tag{4.25}$$

$$h_y(\boldsymbol{k})=\left(V_{xy}\cos\frac{k_zc}{2}+i\tilde{V}_{xy}\sin\frac{k_zc}{2}\right)e^{-i\theta k_z}\sin\frac{k_xa}{2}\cos\frac{k_ya}{2}, \tag{4.26}$$

$$h_z(\boldsymbol{k})=\left(V_z\cos\frac{k_zc}{2}+i\tilde{V}_z\sin\frac{k_zc}{2}\right)e^{-i\theta k_z}\sin\frac{k_xa}{2}\sin\frac{k_ya}{2}. \tag{4.27}$$

The fourth term in Eq. (4.18) represents the effective antiferroic interactions between the intraorbital multipoles $J>0$ and interorbital multipoles $J'>0$. The summation is taken for the four nearest-neighbor A and B sites $\langle r,s\rangle$, as shown in Fig. 4.9(a). $\hat{\boldsymbol{M}}_r^l=\frac{1}{2}\sum_{\sigma\sigma'}\boldsymbol{\sigma}^{\sigma\sigma'}f_{rl\sigma}^\dagger f_{rl\sigma'}$ $(l=\Gamma_6,\Gamma_7)$ and $\hat{X}_r=\sum_{lm}\sum_{\sigma\sigma'}(\hat{X})_{\sigma\sigma'}^{lm}f_{rl\sigma}^\dagger f_{rm\sigma'}$ are the M dipole and the eight interorbital multipoles[7] at site r, respectively, where $f_{rl\sigma}^\dagger$ $(f_{rl\sigma})$ is the Fourier transform of $f_{\boldsymbol{k}il\sigma}^\dagger$ $(f_{\boldsymbol{k}il\sigma})$. We adopt the isotropic exchange interactions J and J', which are introduced to mimic the strong intraorbital and interorbital Coulomb interaction without the spin-orbit coupling [213]. The intraorbital interaction J favors the AFM ordering, while the interorbital interaction J' favors the antiferroic interorbital multipole orderings, such as the AFQ ordering. We note that the intraorbital states with $(\hat{M}_x,\hat{M}_y,\hat{M}_z)$ and interorbital states with $(\hat{Q}_v,\hat{Q}_{xy},\hat{Q}_{yz},\hat{Q}_{zx},\hat{M}_{xyz},\hat{M}_z^\beta,\hat{M}_x',\hat{M}_y')$ are degenerate within the J and J' terms, respectively. Such a degeneracy is lifted by considering the effect of the staggered ASOIs in Eqs. (4.23) and (4.24), as will be shown below.

Before we discuss the multiferroic responses, we investigate the ground-state phase diagram of the itinerant model in Eq. (4.18) by the self-consistent mean-field calculations. We use the Hartree approximation for the two-body terms and consider supercells consisting of 80^3 copies of the two sublattices under the periodic boundary conditions. The numerical error of the self-consistent calculations is less than 10^{-4}. We adopt the f^1 configuration, i.e., the 1/4 filling, and set parameters $t_\parallel^{\Gamma_6}=0.8, t_\parallel^{\Gamma_7}=1$, $t_\parallel'=0.1$, $t_\perp^{\Gamma_6}=t_\perp^{\Gamma_7}=0.15$, $\tilde{t}_\perp^{\Gamma_6}=\tilde{t}_\perp^{\Gamma_7}=0.05$, $V_{xy}=0.15$, $\tilde{V}_{xy}=0.05$, $V_z=0.3$, $\tilde{V}_z=0.1$, $J=2.5$, and $c/a=1.4$. We set $\theta=0$. Although θ is finite in CeCoSi, the effect of nonzero θ is taken into account for the hopping and interaction parameters along the z direction.

4.5.2 Zero-Temperature Phase diagram

Figure 4.9(b) shows the ground-state phase diagram by changing J'/J and Δ for $g^{\Gamma_6}=-0.4$, $g^{\Gamma_7}=0.5$, and $g'=0.8$. For large Δ where the Γ_6 level is well-separated from the CEF ground state Γ_7, the intraorbital multipole instability occurs and the AFM state is stabilized through the intraorbital interaction J. In a large portion of the AFM regions, the M moments are along the z direction, where we denote the phase as AFM(z). This phase is accompanied by the M quadrupole M_u, as shown in Table 4.2. In the phase diagram, another AFM phase denoted as "other AFM" is realized around $0.8\lesssim\Delta\lesssim1.4$,

[7] As the matrix representation $\hat{X}$, we use E quadrupoles $\hat{Q}_v=\frac{1}{2}\tau_x\sigma_0$, $\hat{Q}_{xy}=-\frac{1}{2}\tau_y\sigma_z$, and $(\hat{Q}_{yz},\hat{Q}_{zx})=-\frac{1}{2}(\tau_y\sigma_x,\tau_y\sigma_y)$, M dipoles $(\hat{M}_x',\hat{M}_y')=\frac{1}{2}(\tau_x\sigma_x,-\tau_x\sigma_y)$, and M octupoles $\hat{M}_{xyz}=-\frac{1}{2}\tau_y\sigma_0$ and $\hat{M}_z^\beta=\tau_x\sigma_z$ based on Table 4.1, where M octupoles $M_\mu^{\alpha,\beta}$ $(\mu=x,y)$ is considered as the interorbital component of the M dipole for simplicity.

where the staggered M dipole moments are tilted from the z direction. The obtained AFM phases for $\Delta \lesssim 1.56$ are metallic, whereas the AFM(z) phase for $\Delta \gtrsim 1.56$ is insulating.

The magnetic anisotropy in the AFM phases results from the interplay between two types of ASOIs in the present itinerant model. Especially, the AFM(z) state stabilized in the insulating region for large Δ is presumably owing to the intraorbital ASOI. Note that a similar tendency is obtained in magnetic insulators in the strongly correlated regime where the effective out-of-plane anisotropic interaction appears [214]. In the metallic region, although the effective interaction by the ASOIs is affected by the band structure and can be more complicated, the mean-field results indicate that the intraorbital ASOI tends to stabilize the AFM(z) state, whereas the interorbital ASOI, whose effect becomes important for large J'/J, tends to stabilize the other AFM state with the in-plane moments, as discussed below.

The AFM states are replaced with the AFQ states by decreasing Δ and increasing J'/J with a finite jump of order parameters. The stabilization of the nonmagnetic AFQ state at $T=0$ resembles the situation realized in the high-pressure region of the II phase in CeCoSi [Fig. 4.2(a)], which did not realize in the local model calculation in the previous section. The dominant AFQ instability in Fig. 4.9(b) is the Q_v channel with the ET quadrupole G_{xy}. The other AFQ states denoted as AFQ(xy) and other AFQ1, 2, 3 in $J'/J \gtrsim 0.8$ are characterized by the staggered orders of Q_{xy}, and linear combinations of (Q_{xy}, Q_v), (Q_{xy}, M_{xyz}), and $(Q_v, Q_{xy}, M_{xyz}, M_z^\beta)$, respectively. The stability of the interorbital orders depends on the two types of ASOIs and the interorbital hopping. All the AFQ phases are metallic in the present calculation.

To examine the effect of the ASOI on the AFM(z) state obtained in Fig. 4.9(b), we show the intraorbital staggered ASOI g^{Γ_7} dependence of the staggered AFM moments while keeping $g^{\Gamma_6} = -0.8 g^{\Gamma_7}$ at $J'/J=0.2$, $\Delta=1$, and $g'=0.8$ in Fig. 4.9(c). We compute the μ component of the AFM moment $M_\mu^{\rm AF} \equiv [(M_\mu^{\Gamma_6 {\rm AF}})^2 + (M_\mu^{\Gamma_7 {\rm AF}})^2]^{1/2}$ for $\mu = x, y, z$ and $M_{[110]}^{\rm AF} = [(M_x^{\rm AF})^2 + (M_y^{\rm AF})^2]^{1/2}$ where the staggered component of multipoles X is defined as $X^{\rm AF} = (X_{\rm A} - X_{\rm B})/2$. It is noted that there is also interorbital contribution $M_{x(y)}^{\prime {\rm AF}}$ for the in-plane moments.

In Fig. 4.9(c), the AFM(z) phase is stabilized at $g^{\Gamma_7}=0.5$, as shown in Fig. 4.9(b). While decreasing g^{Γ_7}, $\boldsymbol{M}^{\rm AF}$ is tilted from the z axis toward the [100] direction for $g^{\Gamma_7} \lesssim 0.45$, although $M_z^{\rm AF}$ is larger than $M_{x(y)}^{\rm AF}$ and $M_{x(y)}^{\prime {\rm AF}}$. The appearance of $M_{x(y)}^{\rm AF}$ and $M_{x(y)}^{\prime {\rm AF}}$ corresponds to the emergence of the MT dipole $T_y(T_x)$ as shown in Table 4.2. With a further decrease of g^{Γ_7}, the in-plane moment direction changes from the [100] to [110] direction at $g^{\Gamma_7} \sim 0.275$. Then, $M_{[110]}^{\rm AF}$ increases while decreasing g^{Γ_7} and becomes comparable to $M_z^{\rm AF}$ at $g^{\Gamma_7}=0$, whereas $M_{[110]}^{\prime {\rm AF}}$ is suppressed when decreasing g^{Γ_7}. The result indicates that the intraorbital ASOI favors the AFM(z) state. On the other hand, it also indicates that the AFM state with the in-plane magnetic moments, such as the other AFM state, can be stabilized by the interorbital ASOI [33, 180].

Next, we show the effect of the interorbital ASOI g' on the AFQ(v) state at $J'/J=0.7$, $\Delta=0.5$, $g^{\Gamma_7}=0.5$, and $g^{\Gamma_6}=-0.4$. Figure 4.9(d) shows that four interorbital states are stabilized while changing g'. The AFQ(v) phase is stabilized for $0.6 \lesssim g' \lesssim 1$, the other AFQ1 phase is stabilized for $0.425 \lesssim g' \lesssim 0.6$, the AFQ($xy$) phase is stabilized for $0.225 \lesssim g' \lesssim 0.425$, and the staggered M_z^β phase appears for $0 \lesssim g' \lesssim 0.225$. From the numerical result, the interorbital ASOI g' tends to favor the AFQ(v) state. On the other hand,

the stability of the AFQ(xy) and the staggered M_z^β states for small g' depends on the intraorbital ASOI g^{Γ_6} and g^{Γ_7} and the interorbital hopping $t'_\parallel$. The large g^{Γ_7} and g^{Γ_6} tend to favor the AFQ(xy) state for small g', while $t'_\parallel$ tends to stabilize the M_z^β state. Thus, the stability of the interorbital phases is mainly related to g', g^{Γ_6}, g^{Γ_7}, and $t'_\parallel$[8].

4.5.3 Electronic Band Structure

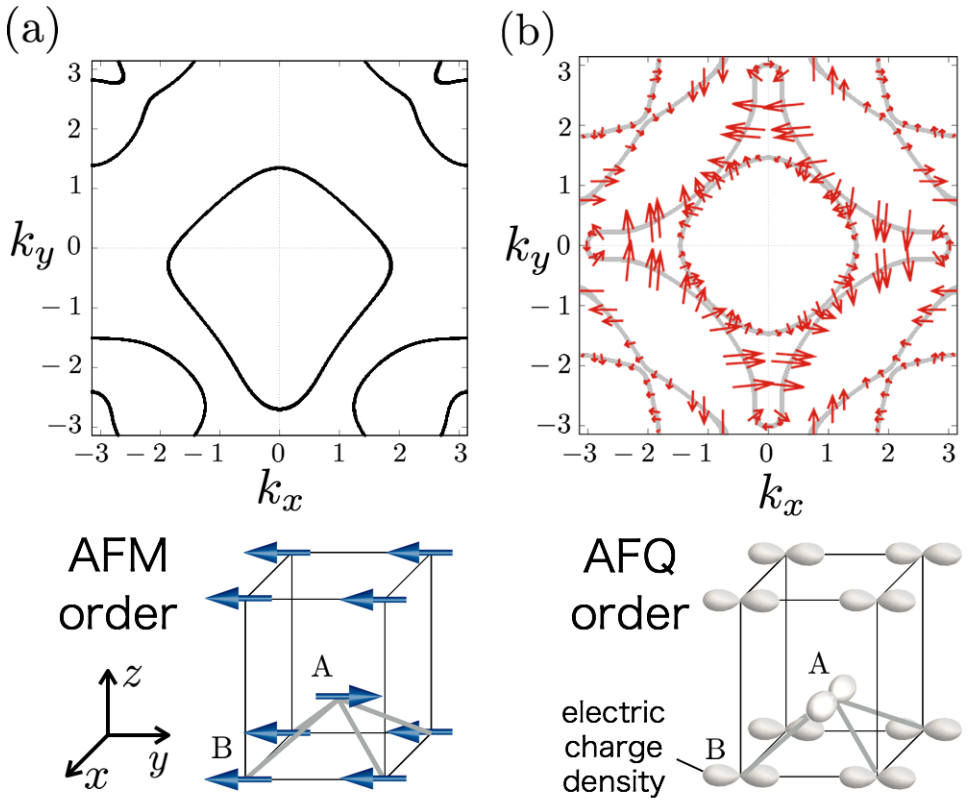

Figure 4.10: (Upper panel) The Fermi surfaces in the k_x-k_y plane at k_z=0 in (a) the staggered AFM ordering for $H_{\rm AFM}$=1 and $H_{\rm AFQ}$=0 and (b) the staggered AFQ ordering for $H_{\rm AFM}$=0 and $H_{\rm AFQ}$=1. See the text for other parameters. In (b), the red arrows represent the in-plane spin polarizations at each $\boldsymbol{k}$. (Lower panel) Schematic pictures of (a) the AFM ordering with the moments along the x direction and (b) the Q_v-type AFQ ordering.

We discuss the electronic band structure in the odd-parity multipole orderings by using the tight-binding model in Eq. (4.18). Although the effect of the staggered ASOI is hidden in the paramagnetic state because of the global inversion symmetry, asymmetric band modulations occur in the presence of the AFM and AFQ orderings due to the appearance of the net ASOIs. For example, we suppose the AFM state with the staggered moments

[8]To stabilize the antiferroic states of (M'_x, M'_y) and/or (Q_{yz}, Q_{zx}) in the present model, factors other than the intraorbital and interorbital ASOIs will be important, since two types of ASOIs those phases do not give the energy gain in these states, which can be inferred from the effective Hamiltonian in the strongly correlated limit (not shown).

along the x direction and the AFQ state with the Q_v component. We introduce the mean-field Hamiltonian instead of the multipole-multipole interaction term in Eq. (4.18) to mimic the staggered AFM and AFQ states as

$$\mathcal{H}=-H_{\rm AFM}\sum_{\boldsymbol{k}}\left(\hat{M}^{\Gamma_7}_{x,\boldsymbol{k}\rm A}-\hat{M}^{\Gamma_7}_{x,\boldsymbol{k}\rm B}\right)-H_{\rm AFQ}\sum_{\boldsymbol{k}}\left(\hat{Q}_{v,\boldsymbol{k}\rm A}-\hat{Q}_{v,\boldsymbol{k}\rm B}\right), \tag{4.28}$$

where $\hat{M}^{\Gamma_7}_{x,\boldsymbol{k}i}=f^\dagger_{\boldsymbol{k}i\Gamma_7\uparrow}f_{\boldsymbol{k}i\Gamma_7\downarrow}+f^\dagger_{\boldsymbol{k}i\Gamma_7\downarrow}f_{\boldsymbol{k}i\Gamma_7\uparrow}$ is the x component of the M dipole operator in the Γ_7 orbital with the wave number $\boldsymbol{k}$ and sublattice i=A and B and $\hat{Q}_{v,\boldsymbol{k}i}=\sum_\sigma(f^\dagger_{\boldsymbol{k}i\Gamma_6\sigma}f_{\boldsymbol{k}i\Gamma_7\sigma}+f^\dagger_{\boldsymbol{k}i\Gamma_7\sigma}f_{\boldsymbol{k}i\Gamma_6\sigma})$ is the Q_v-type E quadrupole operator with the wave number $\boldsymbol{k}$ and sublattice i=A and B. $H_{\rm AFM}$ and $H_{\rm AFQ}$ are the magnitudes of the mean fields in the staggered AFM and AFQ orders, respectively. We set the hopping parameters in Eqs. (4.19)–(4.27) as used in Sec. 4.5.2 and set $g^{\Gamma_6}=-0.4$, $g^{\Gamma_7}=0.5$, $g'=0.8$, $\Delta^f=1$, and $J=J'=0$. We consider the quarter-filling case (f^1 configuration).

The upper panel of Fig. 4.10(a) shows the Fermi surface in the k_x-k_y plane at $k_z=0$ for $H_{\rm AFM}=1$ and $H_{\rm AFQ}=0$ in the staggered AFM state. The schematic picture of the AFM state is shown in the lower panel in Fig. 4.10(a). The result clearly shows that the Fermi surface in the AFM state is asymmetric along the k_y direction, while it is symmetric in the absence of $\boldsymbol{g}^l(\boldsymbol{k})$ and $\boldsymbol{g}'(\boldsymbol{k})$. This indicates that the interplay between the staggered ASOI and the staggered AFM molecular field leads to the asymmetric band deformation, which is regarded as the emergence of the odd-parity MT dipoles [69, 171].

On the other hand, the Fermi surface in the k_x-k_y plane at $k_z=0$ for $H_{\rm AFM}=0$ and $H_{\rm AFQ}=1$ in the AFQ state is shown in the upper panel in Fig. 4.10(b). The lower panel of Fig. 4.10(b) shows the schematic picture of the AFQ state. The Fermi surface shows the momentum-dependent antisymmetric spin splitting with the form of $k_x\sigma_y+k_y\sigma_x$, which corresponds to the emergence of the odd-parity ET quadrupoles with the xy component [36]. This spin-splitting band structure also vanishes in the absence of the ASOIs.

4.5.4 Multiferroic Responses

We discuss the magnetoelectric effect and elastic-electric effect, under the AFM and AFQ phases with the odd-parity multipole moments. After presenting the nonzero tensor components by the symmetry analysis, we discuss the T dependence of the magnetoelectric tensor for two types of odd-parity multipole phases.

Symmetry analysis

We show the nonzero components of the magnetoelectric ($\alpha_{\mu\nu}$) and elastic-electric ($d_{\mu\nu}$) tensors in each antiferroic multipole phase. We summarize the nonzero tensor components in Table 4.5, where the superscripts (J) and (E) represent the intraotbital and interorbital (dissipative and non-dissipative) components of the linear response function.

Response function

To investigate the multiferroic responses, we use the linear response function given by

$$\chi_{\mu\nu}=\frac{e\hbar}{Vi}\sum_{\boldsymbol{k}}\sum_{nm}\frac{f[\varepsilon_n(\boldsymbol{k})]-f[\varepsilon_m(\boldsymbol{k})]}{[\varepsilon_n(\boldsymbol{k})-\varepsilon_m(\boldsymbol{k})][\varepsilon_n(\boldsymbol{k})-\varepsilon_m(\boldsymbol{k})+i\hbar\delta]}X^{pq}_{\mu\boldsymbol{k}}v^{qp}_{\nu\boldsymbol{k}}=\chi^{(\rm J)}_{\mu\nu}+\chi^{(\rm E)}_{\mu\nu}, \tag{4.29}$$

Table 4.5: Nonzero components of the magnetoelectric ($\alpha_{\mu\nu}$) and elastic-electric ($d_{\mu\nu}$) tensors in each antiferroic multipole (MP) phase. The magnetic point groups (MPG) and the odd-parity multipoles (OPMP) are also shown.

MPG	MP	OPMP	$\alpha_{\mu\nu}$	$d_{\mu\nu}$
$\bar{4}m21'$	$\hat{Q}_v$	G_{xy}	$\alpha^{(\mathrm{J})}_{yx}=\alpha^{(\mathrm{J})}_{xy}$	$d^{(\mathrm{E})}_{zxx}=-d^{(\mathrm{E})}_{yzy}, d^{(\mathrm{E})}_{vz}$
$\bar{4}2m1'$	$\hat{Q}_{xy}$	G_v	$\alpha^{(\mathrm{J})}_{xx}=-\alpha^{(\mathrm{J})}_{yy}$	$d^{(\mathrm{E})}_{yzx}=d^{(\mathrm{E})}_{zxy}, d^{(\mathrm{E})}_{xyz}$
$mm21'$	$\hat{Q}_{yz}$	Q_y	$\alpha^{(\mathrm{J})}_{zx}, \alpha^{(\mathrm{J})}_{xz}$	$d^{(\mathrm{E})}_{xyx}, d^{(\mathrm{E})}_{uy}, d^{(\mathrm{E})}_{vy}, d^{(\mathrm{E})}_{yzz}$
$mm21'$	$\hat{Q}_{zx}$	Q_x	$\alpha^{(\mathrm{J})}_{zy}, \alpha^{(\mathrm{J})}_{yz}$	$d^{(\mathrm{E})}_{ux}, d^{(\mathrm{E})}_{vx}, d^{(\mathrm{E})}_{xyy}, d^{(\mathrm{E})}_{zxz}$
$mm'm$	$\hat{M}_x$	T_y	$\alpha^{(\mathrm{E})}_{zx}, \alpha^{(\mathrm{E})}_{xz}$	$d^{(\mathrm{J})}_{xyx}, d^{(\mathrm{J})}_{uy}, d^{(\mathrm{J})}_{vy}, d^{(\mathrm{J})}_{yzz}$
$m'mm$	$\hat{M}_y$	T_x	$\alpha^{(\mathrm{E})}_{zy}, \alpha^{(\mathrm{E})}_{yz}$	$d^{(\mathrm{J})}_{ux}, d^{(\mathrm{J})}_{vx}, d^{(\mathrm{J})}_{xyy}, d^{(\mathrm{J})}_{zxx}$
$4/m'm'm'$	$\hat{M}_z$	M_u	$\alpha^{(\mathrm{E})}_{xx}=\alpha^{(\mathrm{E})}_{yy}, \alpha^{(\mathrm{E})}_{zz}$	$d^{(\mathrm{J})}_{yzx}=-d^{(\mathrm{J})}_{zxy}$
$4'/m'mm'$	$\hat{M}_{xyz}$	M_{xy}	$\alpha^{(\mathrm{E})}_{yx}=\alpha^{(\mathrm{E})}_{xy}$	$d^{(\mathrm{J})}_{zxx}=-d^{(\mathrm{J})}_{yzx}, d^{(\mathrm{J})}_{vz}$
$4'/m'm'm$	$\hat{M}^{\beta}_z$	M_v	$\alpha^{(\mathrm{E})}_{xx}=-\alpha^{(\mathrm{E})}_{yy}$	$d^{(\mathrm{J})}_{yzx}=d^{(\mathrm{J})}_{zxy}, d^{(\mathrm{J})}_{xyz}$

where we take $e=\hbar=1$ and $\delta=0.1$. $X^{pq}_{\mu\boldsymbol{k}}=\langle p\boldsymbol{k}|\hat{X}_\mu|q\boldsymbol{k}\rangle$ and $v^{pq}_{\nu\boldsymbol{k}}=\langle p\boldsymbol{k}|\hat{v}_{\nu\boldsymbol{k}}|q\boldsymbol{k}\rangle$ are the matrix elements of the multipole $\hat{X}_\mu$ and velocity $\hat{v}_{\mu\boldsymbol{k}}=\partial\hat{\mathcal{H}}/(\hbar\partial k_\mu)$. When $\hat{X}_\mu$ is the M dipole $\hat{M}_\mu$, $\chi_{\mu\nu}$ corresponds to the magnetoelectric tensor $\alpha_{\mu\nu}$, where the magnetization M_μ is induced by the electric field E_ν for $\mu,\nu=x,y,z$. Note that the magnetoelectric tensor $\alpha_{\mu\nu}$ consists of three contributions of $\alpha^{(\Gamma_6)}_{\mu\nu}$, $\alpha^{(\Gamma_7)}_{\mu\nu}$, and $\alpha'_{\mu\nu}$, as there are three types of magnetizations $M^{\Gamma_6}_\mu$, $M^{\Gamma_7}_\mu$, and M'_μ as shown in Sec. 4.5.1. On the other hand, when $\hat{X}_\mu$ is the E quadrupole $\hat{Q}_\mu$, $\chi_{\mu\nu}$ corresponds to the elastic-electric (inverse piezo-electric) tensor $d_{\mu\nu}$, where the symmetric distortion ϵ_μ ($\mu=u,v,yz,zx,xy$) is induced by E_ν.

Numerical calculation

We discuss the behavior of the magnetoelectric tensor $\alpha_{\mu\nu}$ in the AFM(z) and AFQ(v) states in detail by using the self-consistent mean-field solution. Figure 4.11(a) shows $\alpha^{(\mathrm{E})}_{xx}$ as a function of T in the AFM(z) phase with the M quadrupole M_u (finite $\alpha^{(\mathrm{E})}_{xx}=\alpha^{(\mathrm{E})}_{yy}$ and $\alpha^{(\mathrm{E})}_{zz}$) at $J'/J=0.2$, $\Delta=1$, $g^{\Gamma_6}=-0.4$, $g^{\Gamma_7}=0.5$, and $g'=0.8$[9]. $\alpha^{(\mathrm{E})}_{xx}$ becomes nonzero below the AFM transition temperature $T_{\mathrm{N}}\simeq0.77$ and decreases for $0.69\lesssim T\lesssim0.75$ after showing the peak structure at $T\simeq0.75$. While further decreasing T, $\alpha^{(\mathrm{E})}_{xx}$ grows and becomes the largest at the lowest T. The complicated temperature dependence of $\alpha^{(\mathrm{E})}_{xx}$ is due to the orbital degree of freedom. Its qualitative behavior is characterized by each component $\alpha^{(\mathrm{E},\Gamma_6)}_{xx}$, $\alpha^{(\mathrm{E},\Gamma_7)}_{xx}$, and $\alpha'^{(\mathrm{E})}_{xx}$, as also plotted in Fig. 4.11(a). $\alpha^{(\mathrm{E},\Gamma_7)}_{xx}$ increases with onset of M^{AF}_z in the inset of Fig. 4.11(a), since M^{AF}_z mainly consists of the M dipole moment in the Γ_7 orbital. On the other hand, as a further increase of M^{AF}_z leads to the large energy gap between the up- and down-spin bands of the Γ_7 orbital, $\alpha^{(\mathrm{E},\Gamma_7)}_{xx}$ decreases and the interorbital contribution, $\alpha'^{(\mathrm{E})}_{xx}$, becomes dominant for $T\lesssim0.69$. It means that the interorbital M'_x activated in Γ_6-Γ_7 space is significant for the large magnetoelectric response in this multi-orbital system. The typical magnitude of the magnetoelectric tensor

[9]We here omit the result of $\alpha^{(\mathrm{E})}_{zz}$, as the magnitude of $\alpha^{(\mathrm{E})}_{zz}$ is smaller than that of $\alpha^{(\mathrm{E})}_{xx}$ by the order of 10^{-2} because of the low conductivity in the z direction.

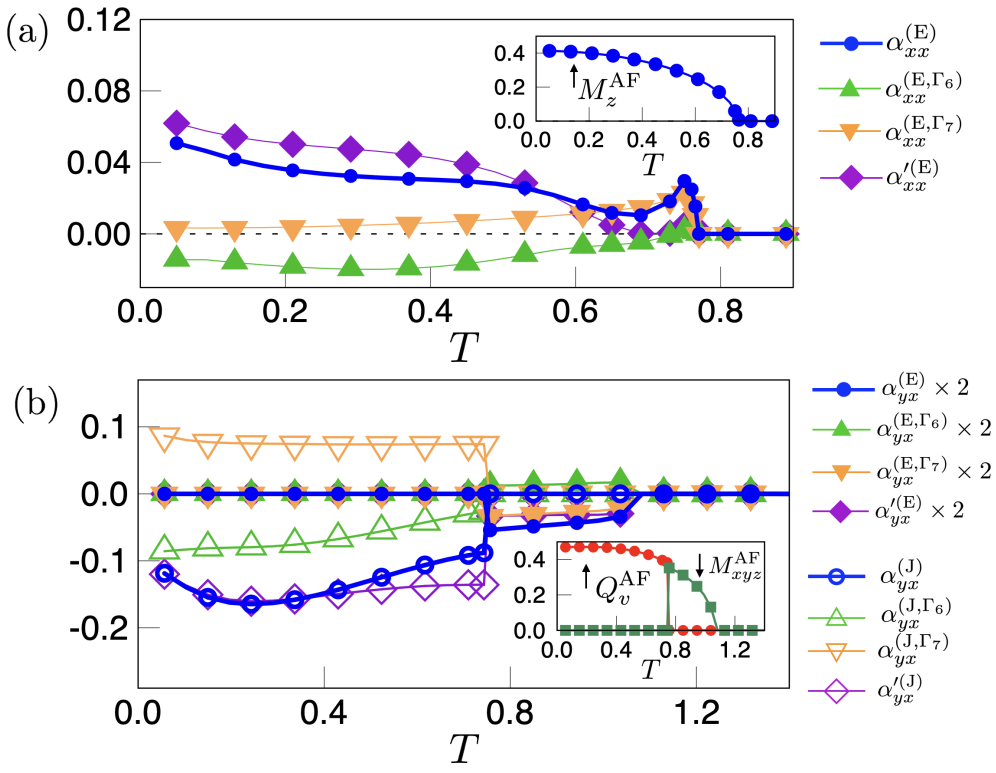

Figure 4.11: (a,b) Temperature (T) dependences of magnetoelectric tensors in (a) the AFM(z) state at J'/J=0.2 and Δ=1 and (b) the AFQ(v) state at J'/J=0.7 and Δ=0.5. The insets of the (a) and (b) stand for the T dependences of the order parameters. Other model parameters are fixed at g^{Γ_6}=−0.4, g^{Γ_7}=0.5, and g'=0.8.

is estimated as $\sim 10^{-1}|t_{\parallel}^{\Gamma_7}|^{-1}$ ps m^{-1} in the unit of $|t_{\parallel}^{\Gamma_7}|$ eV.

We show nonzero α_{yx} in the AFQ(v) phase in Fig. 4.11(b) in addition to the order parameter $Q_v^{\rm AF}$ in the inset of Fig. 4.11(b) at J'/J=0.7, Δ=0.5, g^{Γ_6}=−0.4, g^{Γ_7}=0.5, and g'=0.8. We find the finite-temperature phase transition between AFQ(v) state and the AFO state with $M_{xyz}^{\rm AF}$ at $T_0 \sim 0.75$. From the symmetry in Table 4.5, in the former AFQ state, odd-parity G_{xy} induces $\alpha_{yx}^{\rm (J)}=\alpha_{xy}^{\rm (J)}$, while M_{xy} in the AFO state shows $\alpha_{yx}^{\rm (E)}=\alpha_{xy}^{\rm (E)}$.

In the AFQ(v) state in Fig. 4.11(b), the amplitude of $\alpha_{yx}^{\rm (J)}$ increases from the lowest T and it shows the peak at $T \sim 0.25$, where $Q_v^{\rm AF}$ reaches almost full saturation. While further increasing T, $|\alpha_{yx}^{\rm (J)}|$ gradually decreases and jumps at the phase boundary with the AFO state. The temperature dependence of $\alpha_{yx}^{\rm (J)}$ reflects the electronic state around the Fermi surface, since the intraband contribution is dominant. For $\alpha_{yx}^{\rm (J)}$ in the AFQ(v) state, the interorbital component $\alpha_{yx}^{\prime\rm (J)}$ becomes dominant, while $\alpha_{yx}^{\rm (J,\Gamma_6)}$ and $\alpha_{yx}^{\rm (J,\Gamma_7)}$ almost cancel with each other, which also shows that the interorbital component $\alpha_{yx}^{\prime\rm (J)}$ is significant in this multi-orbital system. The typical magnitude of $\alpha_{yx}^{\rm (J)}$ in the AFQ(v) state is estimated as $\sim 10^{-1}|t_{\parallel}^{\Gamma_7}|^{-1}\delta^{-1}$ ps m^{-1} for $|t_{\parallel}^{\Gamma_7}|$ eV and the broadening factor δ s^{-1}. On the other hand, the electric conductivity is obtained as $10^{-3}\delta^{-1}$ $\mu\Omega^{-1}$cm^{-1}, which implies $\delta \sim 10^{-2}$-10^{-1} from the comparison with the experimental data [200]. Therefore, a large magnetoelectric response might be expected in CeCoSi.

4.6 NQR and NMR in Odd-Parity Multipole Order

In this section, we theoretically study NQR and NMR spectra in the presence of odd-parity multipoles orderings, which will be useful to identify the unknown odd-parity order parameters in the II phase of CeCoSi.

We introduce the effective electronic model for the $4f$ electron at the Ce ion in Sec. 4.6.1. We show the hyperfine coupling between the nuclear spin at the Co atom and the electronic multipole at the Ce ion in Sec. 4.6.2. By using the hyperfine Hamiltonian, we calculate the NQR and [001]-and [100]-field NMR spectra in the presence of the odd-parity multipole orderings in Secs. 4.6.3, 4.6.4, and 4.6.5, respectively. We present the correspondence between the NQR/NMR spectra and the odd-parity multipole orderings in Sec. 4.6.6.

4.6.1 Electronic Model

We consider an effective multipole mean field to examine a hyperfine field on ^{59}Co nucleus. We here introduce a local Hamiltonian for Ce electron at the phenomenological level to incorporate the effect of odd-parity multipoles. The Hamiltonian for i=A, B sublattice is given by

$$\mathcal{H}_{\mathrm{Ce}_i}=\Delta\sum_{\sigma} f^{\dagger}_{i\Gamma_6\sigma}f_{i\Gamma_6\sigma}-\boldsymbol{H}^{(\mathrm{el})}\cdot\hat{\boldsymbol{M}}_i\mp\sum_{X} h^{\mathrm{s}}_X\hat{X}_i. \tag{4.30}$$

The first term is the CEF level splitting and set Δ=0.5 in the following calculation. The second term in Eq. (4.30) is the Zeeman term for the external field $\boldsymbol{H}^{(\mathrm{el})}\equiv\mu_{\mathrm{B}}\boldsymbol{H}$ coupled with the M dipoles $\boldsymbol{M}=(M_x,M_y,M_z)$. We take the linear combination of intraorbital components $\hat{M}^{\Gamma_6}_{\mu}$, $\hat{M}^{\Gamma_7}_{\mu}$ and interorbital component $\hat{M}'_{\mu}$ as $\hat{M}_{\mu}\equiv(\hat{M}^{\Gamma_7}_{\mu}+\delta^{\Gamma_6}\hat{M}^{\Gamma_6}_{\mu}\pm\delta'\hat{M}'_{\mu})$ [the sign is +(−) for $\mu=x(y)$] and $\hat{M}_z\equiv(\hat{M}^{\Gamma_7}_{z}+\delta^{\Gamma_6}\hat{M}^{\Gamma_6}_{z})$. The parameters δ^{Γ_6} and δ' are introduced to represent the difference of the magnetic susceptibility per different orbitals and are taken to be $(\delta^{\Gamma_6},\delta')=(1/4,1/2)$ for simplicity[10]. The last term in Eq. (4.30) represents the multipolar mean fields leading to the multipole orderings with $\langle\hat{X}_i\rangle\neq0$, which mimic the interaction terms in Eqs. (4.10) and (4.18), where $\hat{X}_i$ is the multipole operator at the ith site defined in the same way in Sec. 4.5.1. Besides, we redefine the E quadrupole operator as $\hat{Q}_u=\frac{1}{2}\sigma_0\tau_z$. They originate from the mean-field decoupling for the intraorbital and interorbital Coulomb interaction terms [15]; the multipoles activated in a Γ_6 or Γ_7 level are relevant with the intraorbital Coulomb interaction, while those activated between the Γ_6 and Γ_7 levels are relevant with the interorbital Coulomb interaction, as discussed in Sec. 4.5.2. As we focus on the cluster multipoles induced by the staggered electronic orderings, we adopt the negative (positive) sign for the A (B) sublattice.

In the following discussion, we mainly consider three types of staggered orderings: M_x-type AFM, Q_u-type AFQ, and Q_v-type AFQ states, whose schematics are shown in Figs. 4.12(a)–4.12(c), respectively. This is because the neutron diffraction has indicated

[10]Note that δ^{Γ_6} and δ' depend on the spin-orbit coupling and the CEF parameters as shown in Table 4.1. In addition, we avoid the situation where some multipole moments, such as $Q_{yz},Q_{zx},Q_{xy},M_{xyz},T_x,T_y,M_u$, and M_{xy}, vanish by taking specific values, $\delta^{\Gamma_6}=\delta'=1$, in the Q_u-type AFQ state for the magnetic field in the plane normal to the $[\bar{1}10]$ direction.

the M_x-type AFM state [202]. On the other hand, as the order parameter of the II phase is still controversial, we discuss two types of AFQ states as an example; one is the Q_u-type AFQ state and the other is the Q_v-type AFQ state. For completeness, we also investigate other antiferroic multipole ordered states and the results are summarized in Sec. 4.6.6.

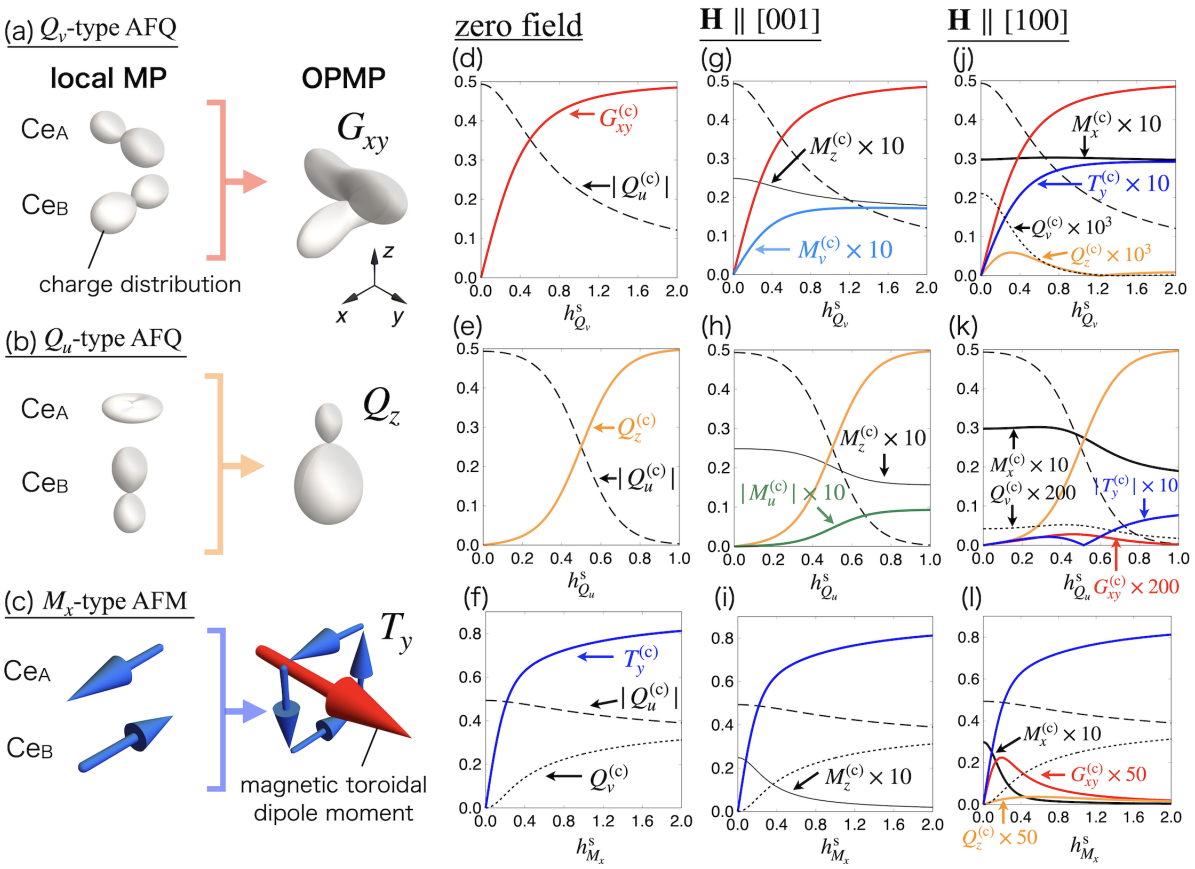

Figure 4.12: (a–c) Schematics of local multipoles (MP) and cluster odd-parity multipoles (OPMP) in the (a) Q_v-type AFQ, (b) Q_u-type AFQ, and (c) M_x-type AFM states. The shape of the pictures in (a) and (b) represents the charge distribution. The blue and red arrows in (c) represent the M dipole and MT dipole moments, respectively. (d–l) The staggered mean field dependences of multipoles under (d–f) zero magnetic field, (g–i) magnetic field $\boldsymbol{H}\parallel[001]$ and (j–l) $\boldsymbol{H}\parallel[100]$. The data represent those in (d,g,j) Q_v-type AFQ, (e,h,k) Q_u-type AFQ, and (f,i,l) M_x-type AFM states, respectively. Black solid and dashed lines represent the even-parity multipole moments, whereas colored solid lines are odd-parity multipole moments.

We show the behavior of the electronic multipole moments induced by the staggered mean field with and without the external magnetic field. We evaluate the thermal expectation value of the multipole moments $X\equiv\langle\hat{X}\rangle=\sum_n\langle n|\hat{X}|n\rangle\exp(-\beta E_n)/Z$, where $|n\rangle$ (n=1–8) is the eigenstate with energy E_n of the total Hamiltonian $\mathcal{H}_{\mathrm{Ce_A}}+\mathcal{H}_{\mathrm{Ce_B}}$, and Z is a partition function. We set the inverse temperature β=10, which corresponds to T/Δ=0.2.

Figures 4.12(d)–4.12(f) show all the nonzero multipole moments at zero magnetic field as a function of the staggered fields $h^{\mathrm{s}}_{Q_v}$, $h^{\mathrm{s}}_{Q_u}$, and $h^{\mathrm{s}}_{M_x}$, respectively, where the definition

of the cluster multipoles is given in Table 4.2. It is noted that $Q_u^{(c)}$ becomes nonzero irrespective of types of order parameters due to nonzero Δ in Eq. (4.30). When the mean fields h_X^s turn on, the corresponding cluster odd-parity multipole moments $X^{(c)}$ become nonzero.

The results in the Q_v- and Q_u-type AFQ ordered states are shown in Figs. 4.12(d) and 4.12(e), respectively. The odd-parity ET quadrupole $G_{xy}^{(c)}$ is induced in the Q_v-type AFQ ordering, while the odd-parity E dipole $Q_z^{(c)}$ is induced in the Q_u-type AFQ ordering. The mean-field dependence of the odd-parity moments are different from each other: $G_{xy}^{(c)}$ roughly increases as a function of $h_{Q_v}^s$, whereas $Q_z^{(c)}$ increases as a function of $(h_{Q_u}^s)^3$ in the small h_X^s region. This is attributed to the nature of the odd-parity order parameters, which is understood from the perturbation expansion for large Δ.

The power expansion of the multipole moments is given as follows

$$\hat{X}^{(c)}=X_A-X_B=a_X^{(1)}(h_X^s)+a_X^{(3)}(h_X^s)^3+\cdots, \tag{4.31}$$

where $\hat{X}^{(c)}=G_{xy}^{(c)}(Q_z^{(c)})$ for $X=Q_v(Q_u)$. $a_X^{(n)}$ are the coefficients, which depend on the CEF level splitting Δ. It is noted that the even order of h_X^s does not appear due to the different parity with respect to the spatial inversion symmetry.

For large Δ, by treating the mean-field term in Eq. (4.30) perturbatively, the basis function at Ce_i site in the Q_v-type AFQ state changes into

$$\tilde{\phi}_{\Gamma_7\sigma,i}=\frac{1}{N}\left(\phi_{\Gamma_7\sigma,i}\pm\frac{h_{Q_v}^s}{2\Delta}\phi_{\Gamma_6\sigma,i}\right), \tag{4.32}$$

where the sign $+(-)$ is taken for $i=$A(B) and N is the normalization factor. $\sigma=\uparrow,\downarrow$ is the quasi spin. Then, $G_{xy}^{(c)}$ is obtained as

$$G_{xy}^{(c)}=\frac{1}{N}\frac{h_{Q_v}^s}{2\Delta}=\left[1+\left(\frac{h_{Q_v}^s}{2\Delta}\right)^2\right]^{-\frac{1}{2}}\frac{h_{Q_v}^s}{2\Delta}\sim\frac{1}{2\Delta}h_{Q_v}^s-\left(\frac{1}{2\Delta}\right)^3(h_{Q_v}^s)^3. \tag{4.33}$$

As $a_{Q_v}^{(1)}(=\frac{1}{2\Delta})\gg a_{Q_v}^{(3)}[=(\frac{1}{2\Delta})^3]$ is satisfied for $h_{Q_v}^s/\Delta\ll 1$, there is a linear dependence of $G_{xy}^{(c)}$ in Fig. 4.12(d).

On the other hand, in the Q_u-type AFQ state, $Q_z^{(c)}$ becomes zero for large Δ, which means that

$$Q_z^{(c)}=0\ (\Delta>h_{Q_u}^s), \tag{4.34}$$

$$Q_z^{(c)}=1\ (\Delta<h_{Q_u}^s). \tag{4.35}$$

Thus, the onset of $Q_z^{(c)}$ for small $h_{Q_u}^s$ in Fig. 4.12(e) is owing to the finite temperature effect. Numerically, the opposite relation ($a_{Q_u}^{(1)}\ll a_{Q_u}^{(3)}$) to the Q_u-type AFQ ordered case is obtained for large Δ; $a_{Q_u}^{(1)}\sim 10^{-2}a_{Q_u}^{(3)}$ for $\Delta=0.5$ and $\beta=10$. This implies that $Q_z^{(c)}$ increases as a function of $(h_{Q_u}^s)^3$ in the small $h_{Q_u}^s$ region in Fig. 4.12(e).

According to the development of $G_{xy}^{(c)}$ or $Q_z^{(c)}$, $Q_u^{(c)}$ is suppressed in both AFQ states in different ways. In the case of the Q_v-type AFQ ordered state, $Q_u^{(c)}$ is suppressed as

$(h^{\rm s}_{Q_v})^2$, while it is suppressed as $(h^{\rm s}_{Q_u})^4$ in the Q_u-type AFQ state. The different mean-field dependences of the multipole moments give different multipole-field dependences of the NQR and NMR frequency shifts, as discussed in Secs. 4.6.3, 4.6.4, and 4.6.5.

Figure 4.12(f) shows the result in the M_x-type AFM state with the odd-parity MT dipole moment $T_y^{(\rm c)}$. The mean-field dependence of $T_y^{(\rm c)}$ is similar to that in the Q_v-type AFQ ordering in Fig. 4.12(d). As a different point, the additional even-parity E quadrupole $Q_v^{(\rm c)}$ is induced in the AFM state due to the breaking of the fourfold rotational symmetry.

Next, we discuss the effect of the magnetic field, whose magnitude is set to be $|\boldsymbol{H}^{(\rm el)}|$=0.01. The results are shown in Figs. 4.12(g)–4.12(i) in the case of the [001] field and in Figs. 4.12(j)–4.12(l) in the case of the [100] field. There are two important observations under the magnetic field. The first one is that additional multipole moments other than the M dipole moments $\boldsymbol{M}^{(\rm c)}$ are induced according to the lowering of the magnetic point group symmetry by the magnetic field. For example, in the Q_v-type AFQ state, M quadrupole moment $M_v^{(\rm c)}$ becomes nonzero for the field along the [001] direction in Fig. 4.12(g), while nonzero $Q_v^{(\rm c)}$, $Q_z^{(\rm c)}$, and $T_y^{(\rm c)}$ are induced for that along the [100] direction in Fig. 4.12(j). The second one is that the additional multipole moments induced by the magnetic field are much smaller than primary odd-parity multipole moments, which indicates that the additional multipoles lead to the small quantitative change in the NQR and NMR spectra. We summarize the active multipole moments induced by the AFQ and AFM orderings at zero and nonzero fields in Table 4.6. The obtained results are consistent with those given by the symmetry analysis.

Table 4.6: Multipole moments induced in the Q_v-type AFQ, Q_u-type AFQ, and M_x-type AFM ordered states as well as the paramagnetic (para) state. For nonzero fields, additional multipoles induced by $\boldsymbol{H}$ are shown.

$\boldsymbol{H}$	para	Q_v-type AFQ	Q_u-type AFQ	M_x-type AFM
zero	$Q_u^{(\rm c)}$	$G_{xy}^{(\rm c)}$	$Q_z^{(\rm c)}$	$T_y^{(\rm c)}$, $Q_v^{(\rm c)}$
$\parallel$[001]	$M_z^{(\rm c)}$	$M_v^{(\rm c)}$	$M_u^{(\rm c)}$	—
$\parallel$[100]	$M_x^{(\rm c)}$, $Q_v^{(\rm c)}$	$Q_z^{(\rm c)}$, $T_y^{(\rm c)}$	$G_{xy}^{(\rm c)}$, $T_y^{(\rm c)}$	$Q_z^{(\rm c)}$, $G_{xy}^{(\rm c)}$

4.6.2 Hyperfine Field for ^{59}Co Nucleus

The hyperfine field Hamiltonian up to the second order of the nuclear spin with $I \geq 1$ is given by [215]

$$\mathcal{H} = -\gamma\hbar \boldsymbol{H}\cdot\hat{\boldsymbol{I}} + \frac{e^2qQ}{4I(2I-1)}\left[3\hat{I}_Z^2 - \hat{I}^2 + \eta\left(\hat{I}_X^2 - \hat{I}_Y^2\right)\right], \tag{4.36}$$

where γ represents gyromagnetic ratio. $\hat{\boldsymbol{I}}=(\hat{I}_X, \hat{I}_Y, \hat{I}_Z)$ is the nuclear spin operator with respect to the principal axes of the local electric-field gradient at Co nuclear site, (X, Y, Z).

The magnitude of $\hat{\boldsymbol{I}}$ is given as I=7/2 for ^{59}Co nucleus. The first term is the Zeeman coupling term. The second term describes the nuclear quadrupole interaction; e is the

electric charge, q is the electric-field gradient parameter, Q is the nuclear E quadrupole moment, and η is the anisotropic parameter. The amplitudes of $\boldsymbol{H}$, q, and η depend on electronic multipole moments at neighboring four Ce sites [Fig. 4.1(c)] as well as the external magnetic field and CEF potential. When we define $\boldsymbol{H}^{(\mathrm{n})}\equiv\gamma\hbar\boldsymbol{H}$, the energy scale of the nuclear system is compared with that of the electronic system as $\boldsymbol{H}^{(\mathrm{n})}/\boldsymbol{H}^{(\mathrm{el})}\sim10^{-4}$. We rewrite the Hamiltonian in Eq. (4.36) in terms of the crystallographic axes coordinate (x,y,z) [see also Fig. 4.1(a)] as

$$\mathcal{H}=\boldsymbol{C}\cdot\hat{\boldsymbol{I}}+C_u\hat{I}_u+C_v\hat{I}_v+C_{yz}\hat{I}_{yz}+C_{zx}\hat{I}_{zx}+C_{xy}\hat{I}_{xy}, \tag{4.37}$$

where

$$\hat{I}_u=\frac{1}{2}\left(3\hat{I}_z^2-\hat{I}^2\right),\ \hat{I}_v=\frac{\sqrt{3}}{2}\left(\hat{I}_x^2-\hat{I}_y^2\right), \tag{4.38}$$

$$\hat{I}_{yz}=\frac{\sqrt{3}}{2}\left(\hat{I}_y\hat{I}_z+\hat{I}_z\hat{I}_y\right),\ \hat{I}_{zx}=\frac{\sqrt{3}}{2}\left(\hat{I}_z\hat{I}_x+\hat{I}_x\hat{I}_z\right),\ \hat{I}_{xy}=\frac{\sqrt{3}}{2}\left(\hat{I}_x\hat{I}_y+\hat{I}_y\hat{I}_x\right). \tag{4.39}$$

The coupling constants for the effective magnetic field and electric-field gradient are parameterized as $\boldsymbol{C}=(C_x,C_y,C_z)$ and $(C_u,C_v,C_{yz},C_{zx},C_{xy})$, respectively. Among them, $C_\mu(\mu=x,y,z)$ includes two contributions from the external field $H_\mu^{(\mathrm{n})}$ and the internal dipole field C_μ^{el} from the electronic multipoles as

$$C_\mu=-\boldsymbol{H}^{(\mathrm{n})}+C_\mu^{\mathrm{el}}, \tag{4.40}$$

whereas C_ν $(\nu=u,v,yz,zx,xy)$ consists of two contributions from the CEF potential C_ν^{CF} and the internal quadrupole field C_ν^{el} from the electronic multipoles as

$$C_\nu=C_\nu^{\mathrm{CF}}+C_\nu^{\mathrm{el}}. \tag{4.41}$$

In Eqs. (4.40) and (4.41), C_μ^{el} and C_ν^{el} depend on types of multipole orderings, which become nonzero through the effective hyperfine coupling between the electronic multipoles and nuclear spins or quadrupoles.

In the following sections, we focus on the multipole contributions to the effective hyperfine field by setting $C_\nu^{\mathrm{CF}}=0$ for simplicity[11]. We show an effective Hamiltonian for Co nucleus under multipole fields from Ce sites at zero magnetic field and at finite magnetic fields.

At a zero magnetic field

Before discussing the effect of odd-parity multipoles, we start from the hyperfine field in the paramagnetic state. In the paramagnetic state at a zero magnetic field, only E quadrupole $Q_u^{(\mathrm{c})}$ becomes finite among electronic multipoles, which corresponds to the second term in Eq. (4.37), as shown in Table 4.6. The nuclear Hamiltonian at single Co site is given by

$$\mathcal{H}_{\mathrm{para}}=C_u^{\mathrm{el}}\hat{I}_u\equiv c_u^{\mathrm{e}}Q_u^{(\mathrm{c})}\hat{I}_u, \tag{4.42}$$

[11]The following result does not change for nonzero C_ν^{CF} in the present model.

where the coupling constant $C_u^{\rm el}$ is represented by the product of the hyperfine coupling constant $c_u^{\rm e}$ and the thermal average of the cluster E quadrupole $Q_u^{\rm (c)}$, $C_u^{\rm el}=c_u^{\rm e}Q_u^{\rm (c)}$. Here and hereafter, the superscript and subscript in $c_\mu^{\rm p}$ represent the even- or odd-parity (p=e or o) multipoles and type of the coupled nuclear multipoles ($\mu=x,y,z,u,v,yz,zx,xy$), respectively.

The other terms in Eq. (4.37) become nonzero once the electronic multipole orderings occur, i.e., for nonzero $h_X^{\rm s}$ in Eq. (4.30). One can derive the effective hyperfine field in the multipole orderings on the basis of magnetic point group symmetry, as it consists of the coupling terms belonging to the totally symmetric representation under $\bar{4}m21'$. We display the IRREPs of the cluster multipoles and nuclear multipoles in Table 4.7.

The general form of the effective hyperfine field in the odd-parity multipole orders is given by

$$\mathcal{H}^{\rm o}_{\rm order}=c_z^{\rm o}M_v^{\rm (c)}\hat{I}_z+c_{x,y}^{\rm o}\left(T_y^{\rm (c)}\hat{I}_x+T_x^{\rm (c)}\hat{I}_y\right)+c_u^{\rm o}G_{xy}^{\rm (c)}\hat{I}_u+c_v^{\rm o}Q_z^{\rm (c)}\hat{I}_v+c_{yz,zx}^{\rm o}\left(Q_y^{\rm (c)}\hat{I}_{yz}-Q_x^{\rm (c)}\hat{I}_{zx}\right), \tag{4.43}$$

$$\mathcal{H}^{\rm e}_{\rm order}=c_z^{\rm e}M_z^{\rm (c)}\hat{I}_z+c_{x,y}^{\rm e}\left(M_x^{\rm (c)}\hat{I}_x+M_y^{\rm (c)}\hat{I}_y\right)+c_{xy}^{\rm e}Q_{xy}^{\rm (c)}\hat{I}_{xy}+c_v^{\rm e}Q_v^{\rm (c)}\hat{I}_v+c_{yz,zx}^{\rm e}\left(Q_{yz}^{\rm (c)}\hat{I}_{yz}+Q_{zx}^{\rm (c)}\hat{I}_{zx}\right), \tag{4.44}$$

where $\mathcal{H}^{\rm o}_{\rm order}$ ($\mathcal{H}^{\rm e}_{\rm order}$) stands for the hyperfine field in the presence of odd(even)-parity multipoles. Interestingly, the effective hyperfine field includes the coupling between electronic odd-parity multipoles and nuclear even-parity multipoles owing to the lack of the local inversion symmetry at the Co site. The hyperfine fields in Eqs. (4.42)–(4.44) are summarized in Table 4.8(a).

In CeCoSi, there are two Co ions in the unit cell, which are connected by the fourfold rotation. As the sign of the odd-parity CEF at two Co ions is opposite, while that of the even-parity one is same, the total nuclear Hamiltonian in a unit cell is given by

$$\mathcal{H}_{\rm Co}=\mathcal{H}_{\rm Co_A}+\mathcal{H}_{\rm Co_B}, \tag{4.45}$$

$$\mathcal{H}_{\rm Co_A}=\mathcal{H}_{\rm para}+\mathcal{H}^{\rm o}_{\rm order}+\mathcal{H}^{\rm e}_{\rm order}, \tag{4.46}$$

$$\mathcal{H}_{\rm Co_B}=\mathcal{H}_{\rm para}-\mathcal{H}^{\rm o}_{\rm order}+\mathcal{H}^{\rm e}_{\rm order}. \tag{4.47}$$

The different sign of $\mathcal{H}^{\rm o}_{\rm order}$ for the different sublattices is an important outcome of odd-parity multipoles. In other words, the presence of the sublattice-dependent splitting of the resonant spectrum corresponds to the emergent odd-parity multipoles within the $\boldsymbol{q}=\boldsymbol{0}$ orders, as shown in Secs. 4.6.3, 4.6.4, and 4.6.5.

At a magnetic field

At an external magnetic field, a Zeeman term is taken into account, which is given by

$$\mathcal{H}_{\rm Zeeman}=-\boldsymbol{H}^{\rm (n)}\cdot\hat{\boldsymbol{I}}. \tag{4.48}$$

Although the Zeeman term induces the M dipole contribution, it also induces additional electronic multipole contributions according to the lowering of the symmetry.

Table 4.7: IRREPs of nuclear multipoles (NMP) and electronic cluster multipoles (CMP) in the local symmetry of the Co site under zero and nonzero magnetic fields $\boldsymbol{H}$. $X_{\pm}\equiv X_x \pm nX_y$ and $X_{2\pm}\equiv X_{yz}\pm nX_{zx}$ for $X=I, Q^{(\mathrm{c})}, M^{(\mathrm{c})}, T^{(\mathrm{c})}$. $n=i(1)$ for $\bar{4}m'2'$ ($2'22'$, $2'$). For $\boldsymbol{H}_{\parallel[001]}$, the multipoles in the square brackets are also activated. The superscript $\pm$ of the irreducible representation is the parity with respect to the antiunitary operation (even: $+$, odd: $-$). The unitary subgroup of each magnetic point group is also shown in the parentheses. The axes of the twofold rotation C_2 of $2'22'$ and $\mathcal{T}C_2$ of $2'$ under $\boldsymbol{H}_{\perp[001]}$ ($\boldsymbol{H}_{\perp[\bar{1}10]}$) are along to the [110] and [001] ([$\bar{1}$10]), respectively. The mirror plane in m' is normal to the [010] direction.

magnetic field		—	$\boldsymbol{H}_{\parallel[001]}$	$\boldsymbol{H}_{\parallel[100]}$	$\boldsymbol{H}_{\parallel[110]}$	$\boldsymbol{H}_{\perp[001]}$	$\boldsymbol{H}_{\perp[010]}$	$\boldsymbol{H}_{\perp[\bar{1}10]}$
		$\bar{4}m21'$	$\bar{4}m'2'$	$2'mm'$	$2'22'$	$2'$	m'	$2'$
NMP	CMP	($\bar{4}m2$)	($\bar{4}$)	(m)	(2)	(1)	(1)	(1)
I_u	$Q_u^{(\mathrm{c})}$, $G_{xy}^{(\mathrm{c})}$	A_1^+	A^+	A'^+	A^+	A^+	A^+	A^+
—	$G_v^{(\mathrm{c})}$	A_2^+	A^-	A''^+	B^-	A^+	A^-	A^-
I_{xy}	$Q_{xy}^{(\mathrm{c})}$	B_1^+	B^+	A''^+	A^+	A^+	A^-	A^+
I_v	$Q_v^{(\mathrm{c})}$, $Q_z^{(\mathrm{c})}$	B_2^+	B^-	A'^+	B^-	A^+	A^+	A^-
I_{yz}	$Q_{yz}^{(\mathrm{c})}$	E^+	—	A'^-	—	A^-	A^-	—
I_{zx}	$Q_{zx}^{(\mathrm{c})}$		—	A''^-	—	A^-	A^+	—
—	$Q_x^{(\mathrm{c})}$	E^+	—	A''^-	—	A^-	A^+	—
—	$Q_y^{(\mathrm{c})}$		—	A'^-	—	A^-	A^-	—
I_{2+}	$Q_{2+}^{(\mathrm{c})}$ $[iQ_+^{(\mathrm{c})}]$	—	$\mathrm{E}^{(2)+}$	—	B^+	A^-	—	A^+
I_{2-}	$Q_{2-}^{(\mathrm{c})}$ $[iQ_-^{(\mathrm{c})}]$	—	$\mathrm{E}^{(1)+}$	—	A^-	A^-	—	A^-
$[iI_{2+}]$	$Q_+^{(\mathrm{c})}$ $[iQ_{2+}^{(\mathrm{c})}]$	—	$\mathrm{E}^{(2)-}$	—	A^-	A^-	—	A^-
$[iI_{2-}]$	$Q_-^{(\mathrm{c})}$ $[iQ_{2-}^{(\mathrm{c})}]$	—	$\mathrm{E}^{(1)-}$	—	B^+	A^-	—	A^+
—	$M_{xy}^{(\mathrm{c})}$	A_1^-	A^-	A'^-	A^-	A^-	A^-	A^-
I_z	$M_z^{(\mathrm{c})}$, $M_v^{(\mathrm{c})}$	A_2^-	A^+	A''^-	B^+	A^-	A^+	A^+
—	$M_z^{\beta(\mathrm{c})}$, $M_u^{(\mathrm{c})}$	B_1^-	B^-	A''^-	A^-	A^-	A^+	A^-
—	$M_{xyz}^{(\mathrm{c})}$	B_2^-	B^+	A'^-	B^+	A^-	A^-	A^+
I_x	$M_x^{(\mathrm{c})}$	E^-	—	A'^+	—	A^+	A^+	—
I_y	$M_y^{(\mathrm{c})}$		—	A''^+	—	A^+	A^-	—
—	$T_x^{(\mathrm{c})}$	E^-	—	A''^+	—	A^+	A^-	—
—	$T_y^{(\mathrm{c})}$		—	A'^+	—	A^+	A^+	—
I_+	$M_+^{(\mathrm{c})}$ $[iT_-^{(\mathrm{c})}]$	—	$\mathrm{E}^{(1)-}$	—	A^+	A^+	—	A^+
I_-	$M_-^{(\mathrm{c})}$ $[iT_+^{(\mathrm{c})}]$	—	$\mathrm{E}^{(2)-}$	—	B^-	A^+	—	A^-
$[iI_-]$	$T_+^{(\mathrm{c})}$ $[iM_-^{(\mathrm{c})}]$	—	$\mathrm{E}^{(2)+}$	—	A^+	A^+	—	A^+
$[iI_+]$	$T_-^{(\mathrm{c})}$ $[iM_+^{(\mathrm{c})}]$	—	$\mathrm{E}^{(1)+}$	—	B^-	A^+	—	A^-

By considering the magnetic field along the [001] direction, additional hyperfine field

Table 4.8: (a) Hyperfine field at zero magnetic field. (b,c) Additional hyperfine field terms in the magnetic field along the (b) [001] and (c) [100] directions. The coupling constants are real.

(a) zero magnetic field

	$C_x^{\rm el}$	$C_y^{\rm el}$	$C_z^{\rm el}$	$C_u^{\rm el}$	$C_v^{\rm el}$	$C_{yz}^{\rm el}$	$C_{zx}^{\rm el}$	$C_{xy}^{\rm el}$
$\mathcal{H}_{\rm para}$	—	—	—	$c_u^{\rm e}Q_u^{(\rm c)}$	—	—	—	—
$\mathcal{H}_{\rm order}^{\rm o}$	$c_{x,y}^{\rm o}T_y^{(\rm c)}$	$c_{x,y}^{\rm o}T_x^{(\rm c)}$	$c_z^{\rm o}M_v^{(\rm c)}$	$c_u^{\rm o}G_{xy}^{(\rm c)}$	$c_v^{\rm o}Q_z^{(\rm c)}$	$c_{yz,zx}^{\rm o}Q_y^{(\rm c)}$	$-c_{yz,zx}^{\rm o}Q_x^{(\rm c)}$	—
$\mathcal{H}_{\rm order}^{\rm e}$	$c_{x,y}^{\rm e}M_x^{(\rm c)}$	$c_{x,y}^{\rm e}M_y^{(\rm c)}$	$c_z^{\rm e}M_z^{(\rm c)}$	—	$c_v^{\rm e}Q_v^{(\rm c)}$	$c_{yz,zx}^{\rm e}Q_{yz}^{(\rm c)}$	$c_{yz,zx}^{\rm e}Q_{zx}^{(\rm c)}$	$c_{xy}^{\rm e}Q_{xy}^{(\rm c)}$

(b) [001] magnetic field

	$C_x^{\rm el}$	$C_y^{\rm el}$	$C_z^{\rm el}$	$C_u^{\rm el}$	$C_v^{\rm el}$	$C_{yz}^{\rm el}$	$C_{zx}^{\rm el}$	$C_{xy}^{\rm el}$
$\tilde{\mathcal{H}}_{\rm para}^{[001]}$	—	—	$\tilde{c}_z^{\rm e}Q_u^{(\rm c)}$	$\tilde{c}_u^{\rm e}M_z^{(\rm c)}$	—	—	—	—
$\tilde{\mathcal{H}}_{\rm order}^{\rm o[001]}$	$\tilde{c}_{x,y}^{\rm o}Q_x^{(\rm c)}$	$-\tilde{c}_{x,y}^{\rm o}Q_y^{(\rm c)}$	$\tilde{c}_z^{\rm o}G_{xy}^{(\rm c)}$	$\tilde{c}_u^{\rm o}M_v^{(\rm c)}$	$\tilde{c}_v^{\rm o}M_u^{(\rm c)}$	$\tilde{c}_{yz,zx}^{\rm o}T_x^{(\rm c)}$	$\tilde{c}_{yz,zx}^{\rm o}T_y^{(\rm c)}$	—
$\tilde{\mathcal{H}}_{\rm order}^{\rm e[001]}$	$\tilde{c}_{x,y}^{\rm e}Q_{zx}^{(\rm c)}$	$\tilde{c}_{x,y}^{\rm e}Q_{yz}^{(\rm c)}$	—	—	$\tilde{c}_v^{\rm e}M_z^{\beta(\rm c)}$	$\tilde{c}_{yz,zx}^{\rm e}M_y^{(\rm c)}$	$\tilde{c}_{yz,zx}^{\rm e}M_x^{(\rm c)}$	$\tilde{c}_{xy}^{\rm e}M_{xyz}^{(\rm c)}$

(c) [100] magnetic field

	$C_x^{\rm el}$	$C_y^{\rm el}$	$C_z^{\rm el}$
$\tilde{\mathcal{H}}_{\rm para}^{[100]}$	$\tilde{c}_x^{\rm e,1}Q_u^{(\rm c)}+\tilde{c}_x^{\rm e,2}Q_v^{(\rm c)}$	—	—
$\tilde{\mathcal{H}}_{\rm order}^{\rm o[100]}$	$\tilde{c}_x^{\rm o,1}Q_z^{(\rm c)}+\tilde{c}_x^{\rm o,2}G_{xy}^{(\rm c)}$	$\tilde{c}_y^{\rm o,1}G_v^{(\rm c)}+\tilde{c}_y^{\rm o,2}T_x^{(\rm c)}$	$\tilde{c}_z^{\rm o,1}Q_x^{(\rm c)}+\tilde{c}_z^{\rm o,2}M_u^{(\rm c)}$
$\tilde{\mathcal{H}}_{\rm order}^{\rm e[100]}$	—	$\tilde{c}_y^{\rm e,1}Q_{xy}^{(\rm c)}+\tilde{c}_y^{\rm e,2}M_y^{(\rm c)}$	$\tilde{c}_z^{\rm e,1}Q_{zx}^{(\rm c)}+\tilde{c}_z^{\rm e,2}M_z^{\beta(\rm c)}$

	$C_u^{\rm el}$	$C_v^{\rm el}$	$C_{yz}^{\rm el}$	$C_{zx}^{\rm el}$	$C_{xy}^{\rm el}$
$\tilde{\mathcal{H}}_{\rm para}^{[100]}$	$\tilde{c}_u^{\rm e,1}Q_v^{(\rm c)}+\tilde{c}_u^{\rm e,2}M_x^{(\rm c)}$	$\tilde{c}_v^{\rm e,1}Q_u^{(\rm c)}+\tilde{c}_v^{\rm e,2}M_x^{(\rm c)}$	—	—	—
$\tilde{\mathcal{H}}_{\rm order}^{\rm o[100]}$	$\tilde{c}_u^{\rm o,1}Q_z^{(\rm c)}+\tilde{c}_u^{\rm o,2}T_y^{(\rm c)}$	$\tilde{c}_v^{\rm o,1}G_{xy}^{(\rm c)}+\tilde{c}_v^{\rm o,2}T_y^{(\rm c)}$	$\tilde{c}_{yz}^{\rm o,1}Q_y^{(\rm c)}+\tilde{c}_{yz}^{\rm o,2}M_{xy}^{(\rm c)}$	$\tilde{c}_{zx}^{\rm o,1}M_u^{(\rm c)}+\tilde{c}_{zx}^{\rm o,2}M_v^{(\rm c)}$	$\tilde{c}_{xy}^{\rm o,1}G_v^{(\rm c)}+\tilde{c}_{xy}^{\rm o,2}T_x^{(\rm c)}$
$\tilde{\mathcal{H}}_{\rm order}^{\rm e[100]}$	—	—	$\tilde{c}_{yz}^{\rm e,1}Q_{yz}^{(\rm c)}+\tilde{c}_{yz}^{\rm e,2}M_{xyz}^{(\rm c)}$	$\tilde{c}_{zx}^{\rm e,1}M_z^{(\rm c)}+\tilde{c}_{zx}^{\rm e,2}M_z^{\beta(\rm c)}$	$\tilde{c}_{xy}^{\rm e}M_y^{(\rm c)}$

terms appear as follow.

$$\tilde{\mathcal{H}}_{\rm para}^{[001]}=\tilde{c}_z^{\rm e}Q_u^{(\rm c)}\hat{I}_z+\tilde{c}_u^{\rm e}M_z^{(\rm c)}\hat{I}_u, \tag{4.49}$$

$$\begin{aligned}\tilde{\mathcal{H}}_{\rm order}^{\rm o[001]}=&\tilde{c}_z^{\rm o}G_{xy}^{(\rm c)}\hat{I}_z+\tilde{c}_{x,y}^{\rm o}\left(Q_x^{(\rm c)}\hat{I}_x-Q_y^{(\rm c)}\hat{I}_y\right)\\&+\tilde{c}_u^{\rm o}M_v^{(\rm c)}\hat{I}_u+\tilde{c}_v^{\rm o}M_u^{(\rm c)}\hat{I}_v+\tilde{c}_{yz,zx}^{\rm o}\left(T_x^{(\rm c)}\hat{I}_{yz}+T_y^{(\rm c)}\hat{I}_{zx}\right),\end{aligned} \tag{4.50}$$

$$\begin{aligned}\tilde{\mathcal{H}}_{\rm order}^{\rm e[001]}=&\tilde{c}_{x,y}^{\rm e}\left(Q_{zx}^{(\rm c)}\hat{I}_x+Q_{yz}^{(\rm c)}\hat{I}_y\right)\\&+\tilde{c}_{xy}^{\rm e}M_{xyz}^{(\rm c)}\hat{I}_{xy}+\tilde{c}_v^{\rm e}M_z^{\beta(\rm c)}\hat{I}_v+\tilde{c}_{yz,zx}^{\rm e}\left(M_y^{(\rm c)}\hat{I}_{yz}+M_x^{(\rm c)}\hat{I}_{zx}\right),\end{aligned} \tag{4.51}$$

where $\tilde{\mathcal{H}}_{\rm para}^{[001]}$ is the additional hyperfine field induced by the magnetic field in the paramagnetic state, while $\tilde{\mathcal{H}}_{\rm order}^{\rm o[001]}$ ($\tilde{\mathcal{H}}_{\rm order}^{\rm e[001]}$) is the additional hyperfine field in the presence of the odd(even)-parity multipole orderings. $\tilde{c}_\mu^p$ (p=e or o, μ=u, v, yz, zx, xy) is a magnetic-field dependent coupling constant, which vanishes without the magnetic field.

The appearance of various multipole contributions in Eqs. (4.49)–(4.51) is due to the reduction of the local symmetry at Co site $\bar{4}m21' \to \bar{4}m'2'$. Reflecting the breaking of the time-reversal symmetry, the effective couplings between electronic and nuclear multipoles with opposite time-reversal parity appear as discussed in Sec. 2.4. In other words, the E (M) multipole at Ce site is coupled with the nuclear dipole (quadrupole) at Co site. From the microscopic viewpoint, such a coupling originates from the M multipoles with spatially anisotropic distributions, such as M octupole, which are described by the coupling between the anisotropic charge distribution and M dipole moment [22, 216]. For instance, in the case of the Q_v-type ordering under the magnetic field along the [001] direction, the M quadrupole $M_v^{(\mathrm{c})}$ with time-reversal odd is induced as shown in Fig. 4.12(g). Since $M_v^{(\mathrm{c})}$ belongs to the same IRREP A^+ as I_u with time-reversal even under the magnetic point group $\bar{4}m'2'$ from Table 4.7, the field-induced $M_v^{(\mathrm{c})}$ affects the $3z^2-r^2$-type charge distribution and results in the effective coupling between $M_v^{(\mathrm{c})}$ and I_u.

Similarly, the additional hyperfine fields in the [100] magnetic field are given by

$$\tilde{\mathcal{H}}^{[100]}_{\mathrm{para}} = \left(\tilde{c}^{\mathrm{e},1}_x Q^{(\mathrm{c})}_u + \tilde{c}^{\mathrm{e},2}_x Q^{(\mathrm{c})}_v\right)\hat{I}_x + \left(\tilde{c}^{\mathrm{e},1}_u Q^{(\mathrm{c})}_v + \tilde{c}^{\mathrm{e},2}_u M^{(\mathrm{c})}_x\right)\hat{I}_u + \left(\tilde{c}^{\mathrm{e},1}_v Q^{(\mathrm{c})}_u + \tilde{c}^{\mathrm{e},2}_v M^{(\mathrm{c})}_x\right)\hat{I}_v, \tag{4.52}$$

$$\begin{aligned}\tilde{\mathcal{H}}^{\mathrm{o}[100]}_{\mathrm{order}} = {} & \left(\tilde{c}^{\mathrm{o},1}_x Q^{(\mathrm{c})}_z + \tilde{c}^{\mathrm{o},2}_x G^{(\mathrm{c})}_{xy}\right)\hat{I}_x + \left(\tilde{c}^{\mathrm{o},1}_y G^{(\mathrm{c})}_v + \tilde{c}^{\mathrm{o},2}_y T^{(\mathrm{c})}_x\right)\hat{I}_y + \left(\tilde{c}^{\mathrm{o},1}_z Q^{(\mathrm{c})}_x + \tilde{c}^{\mathrm{o},2}_z M^{(\mathrm{c})}_u\right)\hat{I}_z \\ & + \left(\tilde{c}^{\mathrm{o},1}_u Q^{(\mathrm{c})}_z + \tilde{c}^{\mathrm{o},2}_u T^{(\mathrm{c})}_y\right)\hat{I}_u + \left(\tilde{c}^{\mathrm{o},1}_v G^{(\mathrm{c})}_{xy} + \tilde{c}^{\mathrm{o},2}_v T^{(\mathrm{c})}_y\right)\hat{I}_v \\ & + \left(\tilde{c}^{\mathrm{o},1}_{yz} Q^{(\mathrm{c})}_y + \tilde{c}^{\mathrm{o},2}_{yz} M^{(\mathrm{c})}_{xy}\right)\hat{I}_{yz} + \left(\tilde{c}^{\mathrm{o},1}_{zx} M^{(\mathrm{c})}_u + \tilde{c}^{\mathrm{o},2}_{zx} M^{(\mathrm{c})}_v\right)\hat{I}_{zx} + \left(\tilde{c}^{\mathrm{o},1}_{xy} G^{(\mathrm{c})}_v + \tilde{c}^{\mathrm{o},2}_{xy} T^{(\mathrm{c})}_x\right)\hat{I}_{xy},\end{aligned} \tag{4.53}$$

$$\begin{aligned}\tilde{\mathcal{H}}^{\mathrm{e}[100]}_{\mathrm{order}} = {} & \left(\tilde{c}^{\mathrm{e},1}_y Q^{(\mathrm{c})}_{xy} + \tilde{c}^{\mathrm{e},2}_y M^{(\mathrm{c})}_y\right)\hat{I}_y + \left(\tilde{c}^{\mathrm{e},1}_z Q^{(\mathrm{c})}_{zx} + \tilde{c}^{\mathrm{e},2}_z M^{\beta(\mathrm{c})}_z\right)\hat{I}_z \\ & + \left(\tilde{c}^{\mathrm{e},1}_{yz} Q^{(\mathrm{c})}_{yz} + \tilde{c}^{\mathrm{e},2}_{yz} M^{(\mathrm{c})}_{xyz}\right)\hat{I}_{yz} + \left(\tilde{c}^{\mathrm{e},1}_{zx} M^{(\mathrm{c})}_z + \tilde{c}^{\mathrm{e},2}_{zx} M^{\beta(\mathrm{c})}_z\right)\hat{I}_{zx} + \tilde{c}^{\mathrm{e}}_{xy} M^{(\mathrm{c})}_y \hat{I}_{xy},\end{aligned} \tag{4.54}$$

where the local symmetry at Co site reduces as $\bar{4}m21' \to 2'mm'$. For in-plane fields, the $\hat{I}_v$ term additionally contributes to $\tilde{\mathcal{H}}^{[100]}_{\mathrm{para}}$ due to the breaking of the fourfold improper rotational symmetry.

The additional hyperfine field Hamiltonian at the external magnetic field is summarized in Tables 4.8(b) and 4.8(c). One can obtain the hyperfine field Hamiltonian for other field directions by using the IRREPs in Table 4.7.

In the end, the total Hamiltonian in a unit cell under the magnetic field is given by

$$\mathcal{H}_{\mathrm{Co}} = \mathcal{H}_{\mathrm{Co_A}} + \mathcal{H}_{\mathrm{Co_B}} + \tilde{\mathcal{H}}_{\mathrm{Co_A}} + \tilde{\mathcal{H}}_{\mathrm{Co_B}}, \tag{4.55}$$

$$\mathcal{H}_{\mathrm{Co_A}} = \mathcal{H}_{\mathrm{Zeeman}} + \mathcal{H}_{\mathrm{para}} + \mathcal{H}^{\mathrm{o}}_{\mathrm{order}} + \mathcal{H}^{\mathrm{e}}_{\mathrm{order}}, \tag{4.56}$$

$$\mathcal{H}_{\mathrm{Co_B}} = \mathcal{H}_{\mathrm{Zeeman}} + \mathcal{H}_{\mathrm{para}} - \mathcal{H}^{\mathrm{o}}_{\mathrm{order}} + \mathcal{H}^{\mathrm{e}}_{\mathrm{order}}, \tag{4.57}$$

$$\tilde{\mathcal{H}}_{\mathrm{Co_A}} = \tilde{\mathcal{H}}_{\mathrm{para}} + \tilde{\mathcal{H}}^{\mathrm{o}}_{\mathrm{order}} + \tilde{\mathcal{H}}^{\mathrm{e}}_{\mathrm{order}}, \tag{4.58}$$

$$\tilde{\mathcal{H}}_{\mathrm{Co_B}} = \tilde{\mathcal{H}}_{\mathrm{para}} - \tilde{\mathcal{H}}^{\mathrm{o}}_{\mathrm{order}} + \tilde{\mathcal{H}}^{\mathrm{e}}_{\mathrm{order}}. \tag{4.59}$$

We use above nuclear Hamiltonian $\mathcal{H}_{\mathrm{Co}}$ to examine the NMR spectra in the odd-parity multipole orderings in the following sections.

4.6.3 NQR Spectra

We examine how odd-parity multipole moments affect the NQR spectrum. In the paramagnetic state, the nuclear Hamiltonian given by Eq. (4.45) leads to three NQR frequencies, $f = \nu_{\mathrm{Q}}$, $2\nu_{\mathrm{Q}}$, and $3\nu_{\mathrm{Q}}$, where $\hbar\nu_{\mathrm{Q}} = 3c^{\mathrm{e}}_u Q^{(\mathrm{c})}_u$. We take $\nu_{\mathrm{Q}} = 1$ as the frequency unit.

In the following, we show the resonance frequencies in odd-parity multipole orderings: the Q_v-type AFQ state with $G_{xy}^{(\mathrm{c})}$, the Q_u-type AFQ state with $Q_z^{(\mathrm{c})}$, and the M_x-type AFM state with $T_y^{(\mathrm{c})}$. In the calculations, we set the coupling constant in Eqs. (4.42) and (4.43) as $c_u^{\mathrm{e}}{=}c_{\mathrm{Q}}$, which is estimated from the NQR frequency in Ref. [205] as $c_{\mathrm{Q}}{=}0.13$ when setting $\gamma\hbar{=}1$, while the coupling constants are set to be c for the primary-induced multipoles and to be c' for the secondary-induce multipoles as the unknown model parameters for simplicity.

Staggered Q_v-type AFQ

We discuss the NQR spectrum in the staggered Q_v-type AFQ state, where the effective nuclear Hamiltonian is represented by considering the finite electronic multipoles in Eqs. (4.42)–(4.44) as

$$\mathcal{H}_{\mathrm{Co_{A/B}}}{=}\left(c_{\mathrm{Q}}Q_u^{(\mathrm{c})}{\pm}cG_{xy}^{(\mathrm{c})}\right)\hat{I}_u. \tag{4.60}$$

The positive (negative) sign in the second term corresponds to $\mathcal{H}_{\mathrm{Co_A}}$ ($\mathcal{H}_{\mathrm{Co_B}}$).

The NQR frequencies of $\mathrm{Co_A}$ and $\mathrm{Co_B}$ sites as a function of $G_{xy}^{(\mathrm{c})}$ with fixed $c{=}0.02$ are shown in Fig. 4.13(a). The color scale in Fig. 4.13 shows the intensity of the NQR spectrum, which is calculated by the magnitude of the matrix element of I_x between different nuclear state i and j at $\mathrm{Co_{A(B)}}$ site, $\left|\hat{I}^{ij}_{x,\mathrm{A(B)}}\right|^2{\equiv}\left|\langle i|\hat{I}_{x,\mathrm{A(B)}}|j\rangle\right|^2$, where $\hat{I}_\mu$ ($\mu{=}x,y,z$) represents the normalized I_μ satisfying $\mathrm{Tr}[\hat{I}_\mu\hat{I}_\mu^\dagger]{=}1$.

The result shows that the NQR frequencies for $\mathrm{Co_A}$ and $\mathrm{Co_B}$ have different values and show the spectral splittings and shift in the Q_v-type AFQ state. The sublattice-dependent splitting is owing to the effective coupling between $G_{xy}^{(\mathrm{c})}$ and I_u with different signs for different sublattices. In other words, the odd-parity multipole moment $G_{xy}^{(\mathrm{c})}$ in Eq. (4.60) plays a significant role in splitting of the NQR frequencies. In fact, the splittings of the NQR frequencies are proportional to $G_{xy}^{(\mathrm{c})}$. On the other hand, the shift of the frequency to smaller f is due to the decrease of dominant $c_{\mathrm{Q}}Q_u^{(\mathrm{c})}$ ($c_{\mathrm{Q}}{\gg}c$) term in Eq. (4.60) by the suppression of $Q_u^{(\mathrm{c})}$ while increasing $G_{xy}^{(\mathrm{c})}$ as shown in Fig. 4.12(d).

It is noted that it might be difficult to detect the splitting due to the odd-parity multipoles even for a saturated multipole moment $G_{xy}^{(\mathrm{c})}{\sim}0.5$ when the coupling constant c is small, since the splittings are proportional to $cG_{xy}^{(\mathrm{c})}$.

Staggered Q_u-type AFQ

In the staggered Q_u-type AFQ state with $Q_z^{(\mathrm{c})}$, the effective nuclear Hamiltonians of $\mathrm{Co_A}$ and $\mathrm{Co_B}$ are represented by

$$\mathcal{H}_{\mathrm{Co_{A/B}}}{=}c_{\mathrm{Q}}Q_u^{(\mathrm{c})}\hat{I}_u{\pm}cQ_z^{(\mathrm{c})}\hat{I}_v. \tag{4.61}$$

The NQR spectrum for the coupling constant $c{=}0.02$ is shown in Fig. 4.13(b). In contrast to the result in the Q_v-type AFQ state, there is no splitting in the NQR spectrum. This is because the different sign of $Q_z^{(\mathrm{c})}$ in Eq. (4.61) is not relevant to the splitting, which is consistent with the symmetry argument that there is no linear coupling between $Q_z^{(\mathrm{c})}$

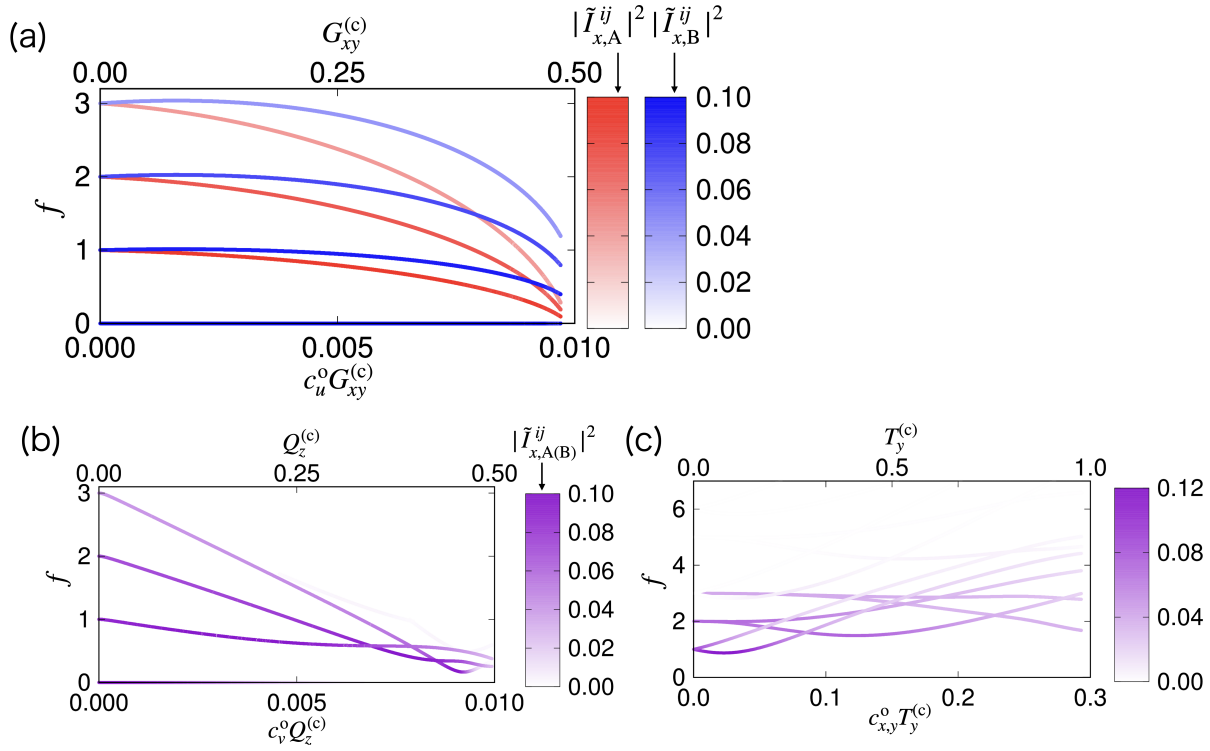

Figure 4.13: The odd-parity multipole (upper scale) and its hyperfine field (lower scale) dependences of the NQR frequency f in the staggered (a) Q_v-type AFQ, (b) Q_u-type AFQ, and (c) M_x-type AFM states. The coupling constants c_u^o, c_v^o, and $c_{x,y}^o$ are set as $c_u^o{=}c_v^o{=}c{=}0.02$ in the AFQ states and $c_{x,y}^o{=}c{=}0.3$ in the AFM state. Other coupling constants are set to be $c'{=}0.02$. As an intensity of the spectrum, $\left|\hat{I}_{x,\mathrm{A(B)}}^{ij}\right|^2$ is shown by the counter plot in red (blue) for $\mathrm{Co_A}$ ($\mathrm{Co_B}$) site. When the spectra from $\mathrm{Co_A}$ and $\mathrm{Co_B}$ are equivalent, their intensities are shown by violet.

and $Q_u^{(c)}$ in the free energy expansion at Co site. In the end, nonzero $Q_z^{(c)}$ just affects the spectral shift.

In addition to the splitting, the difference is found in the odd-parity multipole dependence of the frequency shift. The frequencies in the Q_u-type AFQ state in Fig. 4.13(b) decrease with increasing $Q_z^{(c)}$ faster than those in the Q_v-type AFQ state in Fig. 4.13(a). This is understood from the different dependences on the multipole moments as discussed in Sec. 4.6.1; $Q_u^{(c)}$ in the Q_u-type AFQ state decreases by $\sim[Q_z^{(c)}]^{4/3}$, while that in the Q_v-type AFQ state decreases by $\sim[G_{xy}^{(c)}]^2$.

Staggered M_x-type AFM

In the staggered M_x-type AFM state, the nuclear Hamiltonian is represented by

$$\mathcal{H}_{\mathrm{Co_{A/B}}}=\pm cT_y^{(c)}\hat{I}_x+c_{\mathrm{Q}}Q_u^{(c)}\hat{I}_u+c'Q_v^{(c)}\hat{I}_v. \tag{4.62}$$

It is noted that nuclear dipole contribution in the M_x-type AFM appears even without the net magnetization nor the magnetic field.

Figure 4.13(c) shows the NQR spectrum for the coupling constants c=0.3 and c'=0.02 in the M_x-type AFM state, where c is estimated from the magnitude of the internal magnetic field in Ref. [205]. The NQR frequencies are split into seven due to the contribution from the internal magnetic field arising from the first term in Eq. (4.62). Meanwhile, the NQR frequencies for Co_A and Co_B sites are the same, which indicates that there is no sublattice-dependent splitting in the presence of the odd-parity $T_y^{(c)}$. This means that $T_y^{(c)}$ does not linearly couple with $Q_u^{(c)}$ in the free energy expansion, which is consistent with the symmetry argument. Thus, it is difficult to conclude the presence of $T_y^{(c)}$ only from the seven splittings in Fig. 4.13(c). In fact, the NQR spectra split into seven can be obtained in the even-parity M dipole order, such as $M_x^{(c)}$, in Table 4.2.

4.6.4 [001]-Field NMR Spectra

In this section, we discuss the [001]-field NMR spectra in the odd-parity multipole orderings. We set $\gamma\hbar$=1 and $|\boldsymbol{H}^{(n)}|$=1 in the following. The coupling constants are set as c_u^e=c_Q=0.13 as well as that in NQR in Sec. 4.6.3. The other coupling constants are set to be c for the primary-induced multipoles and to be c' for the secondary-induced multipoles for simplicity. The field-swept spectra are shown in Appendix F.1. We discuss the NMR spectra in the paramagnetic state, Q_v-type AFQ state, Q_u-type AFQ state, and M_x-type AFM state.

Paramagnetic state

In the paramagnetic state at the [001] magnetic field, $\boldsymbol{H}^{(n)}=(0,0,H_z^{(n)})$, the effective nuclear Hamiltonian is represented by

$$\mathcal{H}_{Co_{A/B}}=\left(-H_z^{(n)}+c'M_z^{(c)}\right)\hat{I}_z+c_Q Q_u^{(c)}\hat{I}_u, \tag{4.63}$$

$$\hat{\mathcal{H}}_{Co_{A/B}}=c'Q_u^{(c)}\hat{I}_z+c'M_z^{(c)}\hat{I}_u. \tag{4.64}$$

The first term in Eq. (4.63) includes the Zeeman term from the external magnetic field. The sum of the external magnetic field and the hyperfine field in Eqs. (4.63) and (4.64) results in the seven spectral peaks separated by the same interval in the NMR measurement.

Staggered Q_v-type AFQ

In the Q_v-type AFQ state, the effective nuclear Hamiltonian is obtained as

$$\mathcal{H}_{Co_{A/B}}=\left(-H_z^{(n)}+c'M_z^{(c)}\right)\hat{I}_z+\left(c_Q Q_u^{(c)}\pm cG_{xy}^{(c)}\right)\hat{I}_u, \tag{4.65}$$

$$\hat{\mathcal{H}}_{Co_{A/B}}=c'\left(Q_u^{(c)}\pm G_{xy}^{(c)}\pm M_v^{(c)}\right)\hat{I}_z+c'\left(M_z^{(c)}\pm M_v^{(c)}\right)\hat{I}_u. \tag{4.66}$$

The frequency-swept NMR spectrum for c=c'=0.02 is shown in Fig. 4.14(a), where the color scale represents the intensity of the [001]-field NMR spectrum. Figure 4.14(a) shows that $G_{xy}^{(c)}$ leads to sublattice-dependent spectral splittings due to the different frequencies of Co_A and Co_B as well as the result in NQR. The NMR spectrum is mainly determined by the following dominant contributions: Zeeman term, $c_Q Q_u^{(c)}$ term, and primarily induced

$G_{xy}^{(c)}$ terms. The spectral splittings originate from the odd-parity multipoles $G_{xy}^{(c)}$ and $M_v^{(c)}$ which are coupled with $Q_u^{(c)}$ and $M_z^{(c)}$, though the contribution from $M_v^{(c)}$ is much smaller than that of $G_{xy}^{(c)}$, as discussed in Sec. 4.6.1. Additionally, each spectrum is shifted by $[G_{xy}^{(c)}]^2$.

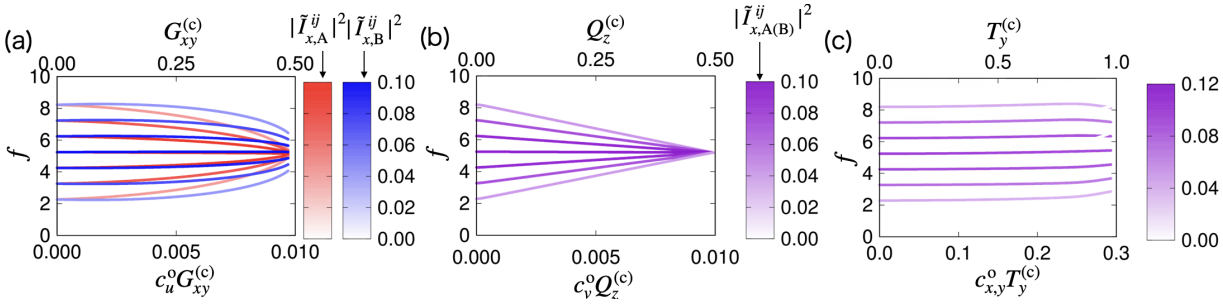

Figure 4.14: (a–c) The odd-parity multipole dependences of the NMR frequency f under the [001] magnetic field. The data are for the (a) Q_v-type AFQ, (b) Q_u-type AFQ, and (c) M_x-type AFM states. The color scales represent the intensities with $\left|\hat{I}_{x,\mathrm{A(B)}}^{ij}\right|^2$. The coupling constants are set as $c_u^o=c_v^o=c=0.02$ in the AFQ states and $c_{x,y}^o=c=0.3$ in the AFM state. Other coupling constants are set to be $c'=0.02$.

Staggered Q_u-type AFQ

In the Q_u-type AFQ state, the effective nuclear Hamiltonian is described as

$$\mathcal{H}_{\mathrm{Co_{A/B}}}=\left(-H_z^{(n)}+c'M_z^{(c)}\right)\hat{I}_z+c_{\mathrm{Q}}Q_u^{(c)}\hat{I}_u\pm cQ_z^{(c)}\hat{I}_v, \tag{4.67}$$

$$\hat{\mathcal{H}}_{\mathrm{Co_{A/B}}}=c'Q_u^{(c)}\hat{I}_z+c'M_z^{(c)}\hat{I}_u\pm c'M_u^{(c)}\hat{I}_v. \tag{4.68}$$

The NMR spectrum for $c=c'=0.02$ is shown in Fig. 4.14(b). The seven frequencies have no additional split for both Co sites, since the induced odd-parity multipoles, $Q_z^{(c)}$ and $M_u^{(c)}$, in the ordered state do not couple with $Q_u^{(c)}$ or $M_z^{(c)}$. Meanwhile, each frequency is shifted by $[Q_z^{(c)}]^{4/3}$, which is understood by the behavior of $Q_u^{(c)}$, as discussed in Sec. 4.6.3.

For full-saturated $Q_z^{(c)}=0.5$, all the NMR frequencies become $f\sim5.2$, which corresponds to the frequency only in the external magnetic field. This is because $Q_u^{(c)}$ in the CEF term vanishes for $Q_z^{(c)}=0.5$, as shown in Fig. 4.12(h).

Staggered M_x-type AFM

In the M_x-type AFM state, the effective nuclear Hamiltonian for the Co nucleus is represented as

$$\mathcal{H}_{\mathrm{Co_{A/B}}}=\left(-H_z^{(n)}+c'M_z^{(c)}\right)\hat{I}_z\pm c'T_y^{(c)}\hat{I}_x+c_{\mathrm{Q}}Q_u^{(c)}\hat{I}_u+cQ_v^{(c)}\hat{I}_v, \tag{4.69}$$

$$\hat{\mathcal{H}}_{\mathrm{Co_{A/B}}}=c'Q_u^{(c)}\hat{I}_z+c'M_z^{(c)}\hat{I}_u\pm c'T_y^{(c)}\hat{I}_{zx}. \tag{4.70}$$

The NMR spectra for $c=0.3$ and $c'=0.02$ is shown in Fig. 4.14(c). The spectra show no sublattice-dependent splitting, which is similar to those in NQR spectra in Sec. 4.6.3,

as $T_y^{(\mathrm{c})}$ does not couple with $Q_u^{(\mathrm{c})}$ or $M_z^{(\mathrm{c})}$. The shift of the resonance frequency against $T_y^{(\mathrm{c})}$ is small compared to that in the Q_u-type AFQ state in Fig. 4.14(b), which reflects the different behavior of $Q_u^{(\mathrm{c})}$, as shown in Fig. 4.12(i).

4.6.5 [100]-Field NMR Spectra

We show the [100]-field NMR spectrum in the paramagnetic state, Q_v-type AFQ state, Q_u-type AFQ state, and M_x-type AFM state.

Paramagnetic state

In the paramagnetic state at the [100] magnetic field, the effective nuclear Hamiltonian at Co nucleus is represented by

$$\mathcal{H}_{\mathrm{Co_{A/B}}} = \left(-H_x^{(\mathrm{n})} + c' M_x^{(\mathrm{c})}\right) \hat{I}_x + c_{\mathrm{Q}} Q_u^{(\mathrm{c})} \hat{I}_u + c' Q_v^{(\mathrm{c})} \hat{I}_v. \tag{4.71}$$

$$\hat{\mathcal{H}}_{\mathrm{Co_{A/B}}} = c' \left(Q_u^{(\mathrm{c})} + Q_v^{(\mathrm{c})}\right) \hat{I}_x + c' \left(Q_v^{(\mathrm{c})} + M_x^{(\mathrm{c})}\right) \hat{I}_u + c' \left(Q_u^{(\mathrm{c})} + M_x^{(\mathrm{c})}\right) \hat{I}_v. \tag{4.72}$$

The nuclear Hamiltonian in Eqs. (4.71) and (4.72) leads to the seven spectra similar to those at the [001] magnetic field. However, the intervals between the resonance frequencies are not equivalent, since the magnetic field normal to the z axis leads to the emergence of $Q_v^{(\mathrm{c})}$.

Staggered Q_v-type AFQ

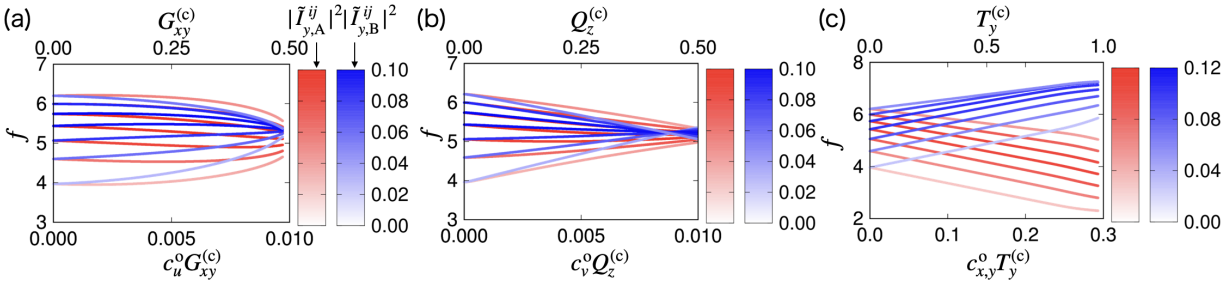

Figure 4.15: (a–c) The odd-parity multipole dependences of the NMR frequency f under the [100] magnetic field. The data are for the (a) Q_v-type AFQ, (b) Q_u-type AFQ, and (c) M_x-type AFM states. The color scales represent the intensities with $\left|\hat{I}_{y,\mathrm{A(B)}}^{ij}\right|^2$. The coupling constants are set as $c_u^{\mathrm{o}}=c_v^{\mathrm{o}}=c=0.02$ in the AFQ states and $c_{x,y}^{\mathrm{o}}=c=0.3$ in the AFM state. Other coupling constants are set to be $c'=0.02$.

In the Q_v-type AFQ state, the effective nuclear Hamiltonian is described as

$$\mathcal{H}_{\mathrm{Co_{A/B}}} = \left(-H_x^{(\mathrm{n})} + c' M_x^{(\mathrm{c})}\right) \hat{I}_x + \left(c_{\mathrm{Q}} Q_u^{(\mathrm{c})} \pm c G_{xy}^{(\mathrm{c})}\right) \hat{I}_u + c' Q_v^{(\mathrm{c})} \hat{I}_v, \tag{4.73}$$

$$\begin{aligned}\hat{\mathcal{H}}_{\mathrm{Co_{A/B}}} = {} & \left[c' \left(Q_u^{(\mathrm{c})} + Q_v^{(\mathrm{c})} \pm Q_z^{(\mathrm{c})} \pm G_{xy}^{(\mathrm{c})}\right) \pm c'_{\mathrm{M}} T_y^{(\mathrm{c})}\right] \hat{I}_x \\ & + c' \left(Q_v^{(\mathrm{c})} + M_x^{(\mathrm{c})} \pm Q_z^{(\mathrm{c})} \pm T_y^{(\mathrm{c})}\right) \hat{I}_u + c' \left(Q_u^{(\mathrm{c})} + M_x^{(\mathrm{c})} \pm Q_z^{(\mathrm{c})} \pm G_{xy}^{(\mathrm{c})} \pm T_y^{(\mathrm{c})}\right) \hat{I}_v.\end{aligned} \tag{4.74}$$

Figure 4.15(a) shows the [100]-field NMR spectra for $c{=}c'{=}0.02, c'_{\rm M}{=}0.3$, where the color scale represents the intensity of the NMR spectra. The result indicates that sublattice-dependent spectral splitting occurs as well as the results in NQR and [001]-field NMR. Also in the [100]-field NMR, the spectrum is mainly determined by the following dominant contributions: Zeeman term, $c_{\rm Q}Q_u^{(\rm c)}$ term, and primarily induced $G_{xy}^{(\rm c)}$ terms. In other words, among the odd-parity multipoles, $G_{xy}^{(\rm c)}$, $Q_z^{(\rm c)}$, and $T_y^{(\rm c)}$, the important contribution comes from $G_{xy}^{(\rm c)}$, since the magnitudes of $Q_z^{(\rm c)}$ and $T_y^{(\rm c)}$ are much smaller than that of $G_{xy}^{(\rm c)}$, as shown in Fig. 4.12(j). Meanwhile, the shift of the spectra is dominated by $Q_u^{(\rm c)}$.

Staggered Q_u-type AFQ

The effective nuclear Hamiltonian in the Q_u-type AFQ state is

$$\mathcal{H}_{\rm Co_{A/B}} = \left(-H_x^{(\rm n)} + c' M_x^{(\rm c)}\right) \hat{I}_x + c_{\rm Q} Q_u^{(\rm c)} \hat{I}_u + \left(c' Q_v^{(\rm c)} \pm c Q_z^{(\rm c)}\right) \hat{I}_v, \tag{4.75}$$

$$\begin{aligned}\hat{\mathcal{H}}_{\rm Co_{A/B}} = &\left[c' \left(Q_u^{(\rm c)} + Q_v^{(\rm c)} \pm Q_z^{(\rm c)} \pm G_{xy}^{(\rm c)}\right) \pm c'_{\rm M} T_y^{(\rm c)}\right] \hat{I}_x \\ &+ c' \left(Q_v^{(\rm c)} + M_x^{(\rm c)} \pm G_{xy}^{(\rm c)} \pm Q_z^{(\rm c)} \pm T_y^{(\rm c)}\right) \hat{I}_u + c' \left(Q_u^{(\rm c)} + M_x^{(\rm c)} \pm G_{xy}^{(\rm c)} \pm T_y^{(\rm c)}\right) \hat{I}_v,\end{aligned} \tag{4.76}$$

which is the same as that in the Q_v-type AFQ state in Eqs. (4.73) and (4.74), as the magnetic point group symmetry under the magnetic field is the same as $2'mm'$ with each other. Thus, in contrast to the results for the NQR [Sec. 4.6.3] and [001]-field NMR [Sec. 4.6.4], the sublattice-dependent splittings occur under the [100] magnetic field as shown in the NMR spectra for $c{=}c'{=}0.02, c'_{\rm M}{=}0.3$ in Fig. 4.15(b).

However, the mean-field dependence of the spectra is different from that in the Q_v-type AFQ state, since the magnitude of $Q_z^{(\rm c)}$ is much larger than that of other multipoles. Especially, the spectral shift reflects the different mean-field dependence of $Q_u^{(\rm c)}$, as already discussed in Sec. 4.6.3.

Staggered M_x-type AFM

The nuclear Hamiltonian in the M_x-type AFM state is

$$\mathcal{H}_{\rm Co_{A/B}} = \left(-H_x^{(\rm n)} + c' M_x^{(\rm c)} \pm c T_y^{(\rm c)}\right) \hat{I}_x + c_{\rm Q} Q_u^{(\rm c)} \hat{I}_u + c' Q_v^{(\rm c)} \hat{I}_v, \tag{4.77}$$

$$\begin{aligned}\hat{\mathcal{H}}_{\rm Co_{A/B}} = &c' \left(Q_u^{(\rm c)} + Q_v^{(\rm c)} \pm Q_z^{(\rm c)} \pm G_{xy}^{(\rm c)}\right) \hat{I}_x \\ &+ c' \left(Q_v^{(\rm c)} + M_x^{(\rm c)} \pm G_{xy}^{(\rm c)} \pm Q_z^{(\rm c)} \pm T_y^{(\rm c)}\right) \hat{I}_u + c' \left(Q_u^{(\rm c)} + M_x^{(\rm c)} \pm G_{xy}^{(\rm c)} \pm Q_z^{(\rm c)} \pm T_y^{(\rm c)}\right) \hat{I}_v,\end{aligned} \tag{4.78}$$

where the same multipoles appear in the two AFQ states in Eqs. (4.73)–(4.76), since the magnetic point group symmetry under the [100] magnetic field reduces to $2'mm'$ also in this case. Thus, the sublattice-dependent NMR splittings occur, which is similar to those in the AFQ states. However, the dominant odd-parity multipole to induce the spectral splitting is given by $T_y^{(\rm c)}$. The [100]-field NMR spectra for $c{=}0.3$ and $c'{=}0.02$ is shown in Fig. 4.15(c).

4.6.6 Spectral Splittings under Odd-parity Multipoles

So far, we have focused on the NQR and NMR spectra in the two AFQ and the AFM ordered states under the magnetic fields along the [001] and [100] directions as well as the zero magnetic field. In a similar way, possible NQR and NMR splittings in other odd-parity multipole orderings under any field directions can be calculated. We show the presence or absence of the sublattice-dependent NQR and NMR splittings for the other candidate odd-parity multipole orders in CeCoSi, which are expected from the low-energy two CEF levels. The present analysis is applicable once the phase transition occurs in the magnetic field unless the second excited levels are involved in the phase transition. It is noted that our analysis can be extended to other electronic orderings in the Γ_7-Γ_6 level scheme and the $\Gamma_7^{(1)}$-$\Gamma_7^{(2)}$ level scheme, where the latter is discussed in Appendix F.3.

The present results for the Γ_7-Γ_6 level scheme are summarized in Table 4.9. We list the other candidates; two AFM states, three AFQ states, and two AFO states. We also include the results in the Q_v- and Q_u-type AFQ states and the M_x-type AFM state discussed in Secs. 4.6.3, 4.6.4, and 4.6.5 under the other magnetic-field directions. The table exhibits when the sublattice-dependent spectral splittings occur in the presence of odd-parity multipoles.

For example, in the AFQ phase, the NMR measurement in the $zx(yz)$-plane magnetic field is useful to identify the odd-parity multipole order parameter; the sublattice-dependent splittings which always appear when the magnetic field direction is rotated in the $zx(yz)$-plane indicate the emergence of $G_{xy}^{(\mathrm{c})}$. Meanwhile, in the AFM phase, the sublattice-dependent splittings under the magnetic field along the x direction will indicate the presence of $T_y^{(\mathrm{c})}$. In this way, as the different spectral splittings are found in the different odd-parity multipole orderings depending on the magnetic field directions, the detailed investigation of the field angle dependence enables us to identify the order parameter in CeCoSi.

Table 4.9: The sublattice-dependent NQR and NMR splittings in the AFM, AFQ, and AFO states under the six field directions [001], [100], [110], $\perp$[001], $\perp$[010], and $\perp$[$\bar{1}$10]. The local multipoles (LMP) at Ce site and cluster odd-parity multipoles (OPMP) are shown in second and third columns, respectively. The mark ✓ represents the presence of the sublattice-dependent splittings.

			NQR	NMR					
	LMP	OPMP	—	$\boldsymbol{H}_{\parallel[001]}$	$\boldsymbol{H}_{\parallel[100]}$	$\boldsymbol{H}_{\parallel[110]}$	$\boldsymbol{H}_{\perp[001]}$	$\boldsymbol{H}_{\perp[010]}$	$\boldsymbol{H}_{\perp[\bar{1}10]}$
AFM	M_x	T_y	—	—	✓	✓	✓	✓	✓
	M_y	T_x	—	—	—	✓	✓	—	✓
	M_z	M_u	—	—	—	—	—	✓	—
AFQ	Q_u	Q_z	—	—	✓	—	✓	✓	—
	Q_v	G_{xy}	✓	✓	✓	✓	✓	✓	✓
	Q_{xy}	G_v	—	—	—	—	✓	—	—
	Q_{yz}	Q_y	—	—	—	—	—	—	✓
	Q_{zx}	Q_x	—	—	—	—	—	✓	✓
AFO	M_{xyz}	M_{xy}	—	—	—	—	—	—	—
	M_z^β	M_v	—	✓	—	—	—	✓	✓

4.7 Summary

We investigated the odd-parity multipole orderings that corresponds to the staggered multipole orderings in the f electron metal CeCoSi with the locally noncentrosymmetric crystal structure. We examined three different models to investigate the finite-temperature phase transition, multiferroic properties, and NQR/NMR spectra.

First, we examined the relation between the AFM and AFQ ordered states and the odd-parity multipole moment. By using the self-consistent mean-field calculation for the effective local model, we clarified the important interaction parameters to stabilize the AFM and AFQ phases while changing the temperature. We showed that the interorbital AFQ ordering is possible by the relatively small interaction even in the case of the large CEF level splitting when taking into account the effect of the multipole interaction for the $(3z^2-r^2)$-type E quadrupole. We also discussed the behaviors of the magnetic susceptibility and the quadrupole susceptibility. We showed that the magnetic susceptibility is closely related to the AFQ order parameter and CEF, while the quadrupole susceptibility in a magnetic field is related to the coupling between the AFM and AFQ moments.

Second, we examined the itinerant model to investigate the stability of the multipole orderings at the zero temperature and the multiferroic responses. Different from the local model, we showed that the itinerant model can realize the nonmagnetic AFQ ground state, which might correspond to the situation in the high-pressure region of CeCoSi. Moreover, it was clarified that the types of the AFM and interorbital higher-rank multipole phases are mainly related to the two types of ASOIs and the interorbital hoppings. We also investigated the band modulation and the multiferroic responses in the presence of the odd-parity multipole orderings. Especially, we discussed the temperature dependence of the magnetoelectric coefficients with the complicated T dependence, which originates from the multi-orbital effect.

Third, we investigated the NQR and NMR spectra in the presence of the odd-parity multipole orderings. We introduced the hyperfine field Hamiltonian based on the symmetry analysis for the zero magnetic field, [001] magnetic field, and [100] magnetic field, and calculated them under the odd-parity multipole orderings. As a result, we clarified that the odd-parity multipole leads to the sublattice-dependent spectral splitting of the NQR and NMR. As the presence/absence of the spectral splittings depends on the odd-parity order parameter and the direction of the magnetic field, the present results provide information for the identification of the unknown order parameter in CeCoSi.

Although the present study focused on the odd-parity multipole order of the specific material CeCoSi, the theoretical results, such as the stability of the multipole orderings in the presence of the large CEF level splitting, multiferroic responses in the multi-orbital system with the unconventional odd-parity multipole order, and the way to identify the odd-parity multipole order parameter by the NMR measurement, can be applicable to other materials hosting odd-parity multipoles. Thus, the result will be useful to explore for future exploration of functional materials in the absence of the spatial inversion symmetry.

Chapter 5

Summary

In this dissertation, we have investigated multipole physics in condensed matter physics. We already gave a summary of the results in each chapter. We here conclude this dissertation by wrapping up the main results from a broader viewpoint.

In Chap. 2, we completed the classification of multipoles in the 122 magnetic point groups. We systematically classified four types of multipoles, i.e., electric, magnetic, electric toroidal, and magnetic toroidal multipoles, based on the representation theory in a nonunitary group. The symmetry-adapted four types of multipoles can express any electronic degrees of freedom including not only atomic-scale ones, such as the charge, spin, and orbital, but also sublattice one. Thus, the present classification of multipoles will enable us to understand electronic order parameters, entanglement among the charge, spin, and orbital, multiferroic phenomena, and transport properties in a systematic way. Especially, the multipole description in the magnetic point groups including the antiunitary operations accompanied by the time-inversion operation becomes a powerful tool when clarifying microscopic essences for various physical phenomena in magnetic materials with the complicated magnetic structures and exotic higher-rank multipole structures. Indeed, we uncovered the parity-violating physical phenomena based on the multipole concept in Chaps. 3 and 4.

In Chap. 3, we investigated the second-order nonlinear transport in the magnetic toroidal dipole ordering with an emphasis on the necessary model parameters to induce the nonlinear transport. By analyzing the staggered antiferromagnetic ordering with the magnetic toroidal dipole on a two-dimensional zigzag chain, we obtained the important antisymmetric spin-orbit interaction and hopping parameters for the second-order nonlinear transport in the ferrotoroidal metal/semiconductor. We also showed that a large enhancement of the nonlinear conductivity can occur near the transition temperature in a multi-band system.

In Chap. 4, we investigated one of the candidate materials to host odd-parity multipoles, CeCoSi. We discussed the potential odd-parity multipoles in the antiferromagnetic and antiferroquadrupole ordered phases from the viewpoint of both local and itinerant models. By analyzing the local model, we constructed the finite-temperature phase diagram by the self-consistent mean-field calculation, which gave the similar result to the experimental one in the low-pressure region. We gave a physical interpretation of the interorbital multipole ordering in the presence of the large crystalline-electric-field splitting by considering the multipole-multipole interaction. Meanwhile, in the itinerant model,

we showed that not only the antiferromagnetic ordering but also the antiferroquadrupole ordering can be stabilized even in the ground state, which might explain the emergent antiferroquadrupole ordering in the high-pressure region of CeCoSi. We also investigated the multiferroic response driven by the odd-parity multipole orderings by focusing on the importance of the interorbital degree of freedom. Furthermore, we developed the theory of the NQR and NMR spectra in order to microscopically detect the odd-parity multipole orderings.

For future work, there is the further exploration of multiferroic responses and linear/nonlinear transport properties in terms of the unconventional order parameters, e.g., magnetic toroidal quadrupole and octupole, by the systematic analysis based on the present multipole classification. It might open the way to use various functional materials with antiferromagnetic states and the unconventional spin, orbital, and current ordered states for the novel electronics and spintronics devices. Meanwhile, the theoretical study on the multipole orderings in CeCoSi also remains several issues to explain the experimental result. For example, the high critical magnetic field in the temperature-field phase diagram and the behavior of the magnetization depending on the higher-order magnetic field. To examine them, the theoretical analysis taking into account the additional effect beyond the present effective mean-field model will be necessary.

Appendix A

Multipole Notation under Point Group Symmetry in Crystals

We adopt the real expressions of $O_{lm}(\boldsymbol{r})$, which are given by [50]

$$O_{l0}^{(\mathrm{c})}(\boldsymbol{r}) \equiv O_{l0}(\boldsymbol{r}), \tag{A.1}$$

$$O_{lm}^{(\mathrm{c})}(\boldsymbol{r}) \equiv \frac{(-1)^m}{\sqrt{2}}[O_{lm}(\boldsymbol{r}) + O_{lm}^*(\boldsymbol{r})], \tag{A.2}$$

$$O_{lm}^{(\mathrm{s})}(\boldsymbol{r}) \equiv i\frac{(-1)^m}{\sqrt{2}}[O_{lm}(\boldsymbol{r}) - O_{lm}^*(\boldsymbol{r})]. \tag{A.3}$$

We use the linear combination of $O_{lm}^{(\mathrm{c})}(\boldsymbol{r})$ and $O_{lm}^{(\mathrm{s})}(\boldsymbol{r})$ for the expressions of multipoles in crystallographic systems.

The cubic harmonics are used for the cubic groups and its subgroups, where $O_{lm}(\boldsymbol{r})$ up to rank 4 is represented as follows. The rank-0 monopole is

$$O_0 = 1, \tag{A.4}$$

the rank-1 dipole is

$$(O_x, O_y, O_z) = (x, y, z), \tag{A.5}$$

the rank-2 quadrupole is

$$O_u = \frac{1}{2}(3z^2 - r^2), \tag{A.6}$$

$$O_v = \frac{\sqrt{3}}{2}(x^2 - y^2), \tag{A.7}$$

$$(O_{yz}, O_{zx}, O_{xy}) = \sqrt{3}(yz, zx, xy), \tag{A.8}$$

the rank-3 octupole is

$$O_{xyz} = \sqrt{15}xyz, \tag{A.9}$$

$$\left(O_x^\alpha, O_y^\alpha, O_z^\alpha\right) = \frac{1}{2}\left(x(5x^2 - 3r^2), y(5y^2 - 3r^2), z(5z^2 - 3r^2)\right), \tag{A.10}$$

$$\left(O_x^\beta, O_y^\beta, O_z^\beta\right) = \frac{\sqrt{15}}{2}\left(x(y^2 - z^2), y(z^2 - x^2), z(x^2 - y^2)\right), \tag{A.11}$$

and the rank-4 hexadecapole is

$$O_4 = \frac{5\sqrt{21}}{12}\left(x^4+y^4+z^4-\frac{3}{5}r^4\right), \tag{A.12}$$

$$O_{4u} = \frac{7\sqrt{15}}{6}\left[z^4-\frac{x^4+y^4}{2}-\frac{3}{7}r^2(3z^2-r^2)\right], \tag{A.13}$$

$$O_{4v} = \frac{7\sqrt{5}}{4}\left[x^4-y^4-\frac{6}{7}r^2(x^2-y^2)\right], \tag{A.14}$$

$$\left(O^\alpha_{4x}, O^\alpha_{4y}, O^\alpha_{4z}\right) = \frac{\sqrt{35}}{2}\left(yz(y^2-z^2), zx(z^2-x^2), xy(x^2-y^2)\right), \tag{A.15}$$

$$\left(O^\beta_{4x}, O^\beta_{4y}, O^\beta_{4z}\right) = \frac{\sqrt{5}}{2}\left(yz(7x^2-r^2), zx(7y^2-r^2), xy(7z^2-r^2)\right), \tag{A.16}$$

where we denote $O_{lm}(\boldsymbol{r}) \to O_{lm}$ for notational simplicity.

For the hexagonal and trigonal groups, we adopt different notations for four rank-3 octupoles O^α_x, O^α_y, O^β_x, and O^β_y in Eqs. (A.10) and (A.11) and all the rank-4 hexadecapoles in Eqs. (A.12)–(A.16) by

$$O_{3a} = \frac{\sqrt{10}}{4}x(x^2-3y^2), \tag{A.17}$$

$$O_{3b} = \frac{\sqrt{10}}{4}y(3x^2-y^2), \tag{A.18}$$

$$(O_{3u}, O_{3v}) = \frac{\sqrt{6}}{4}\left(x(5z^2-r^2), y(5z^2-r^2)\right), \tag{A.19}$$

and

$$O_{40} = \frac{1}{8}(35z^4-30z^2r^2+3r^4), \tag{A.20}$$

$$O_{4a} = \frac{\sqrt{70}}{4}yz(3x^2-y^2), \tag{A.21}$$

$$O_{4b} = \frac{\sqrt{70}}{4}zx(x^2-3y^2), \tag{A.22}$$

$$(O^\alpha_{4u}, O^\alpha_{4v}) = \frac{\sqrt{10}}{4}\left(zx(7z^2-3r^2), yz(7z^2-3r^2)\right), \tag{A.23}$$

$$\left(O^{\beta 1}_{4u}, O^{\beta 1}_{4v}\right) = \frac{\sqrt{35}}{8}\left(x^4-6x^2y^2+y^4, 4xy(x^2-y^2)\right), \tag{A.24}$$

$$\left(O^{\beta 2}_{4u}, O^{\beta 2}_{4v}\right) = \frac{\sqrt{5}}{4}\left((x^2-y^2)(7z^2-r^2), 2xy(7z^2-r^2)\right), \tag{A.25}$$

with the use of the tesseral harmonics.

Appendix B

Corepresentation of Nonunitary Group

We review the representation theory of nonunitary groups to use the irreducible representation in type-(II) and type-(III) nonunitary magnetic point groups [121, 122, 124–127, 129, 130]. In Sec. B.1, we introduce the corepresentation of a nonunitary group in detail. After presenting the unitary transformation of the corepresentation in Sec. B.2, we show the irreducible corepresentation in Sec. B.3. In Sec. B.4, the Kronecker product of the irreducible corepresentation is briefly reviewed.

B.1 Corepresentation

A nonunitary group $\boldsymbol{M}$ is expressed as

$$\boldsymbol{M}=\boldsymbol{G}+\mathcal{A}\boldsymbol{G}, \tag{B.1}$$

where $\boldsymbol{G}$ is the unitary subgroup and $\mathcal{A}$ is the antiunitary operation. When $\boldsymbol{M}$ is a type-(II) [(III)] magnetic point group, $\boldsymbol{G}$ is a crystallographic point group and $\mathcal{A}$ is the time-reversal operation (combination of the time-inversion and unitary crystallographic point group operations). For the basis set of the irreducible representation Γ in $\boldsymbol{G}$ with dimension d_Γ

$$\langle\psi^\Gamma|=\langle\psi^\Gamma_1,\cdots,\psi^\Gamma_{d_\Gamma}|\,, \tag{B.2}$$

and another set obtained as

$$\mathcal{A}\,\langle\psi^\Gamma|=\langle\phi^\Gamma|=\langle\phi^\Gamma_1,\cdots,\phi^\Gamma_{d_\Gamma}|\,, \tag{B.3}$$

the representations with respect to a unitary operation $\mathcal{R}\in\boldsymbol{G}$ are given as

$$\mathcal{R}\,\langle\psi^\Gamma|=\langle\psi^\Gamma|\,\Delta^\Gamma(\mathcal{R}), \tag{B.4}$$

$$\mathcal{R}\,\langle\phi^\Gamma|=\mathcal{A}(\mathcal{A}^{-1}\mathcal{R}\mathcal{A})\,\langle\psi^\Gamma|=\mathcal{A}\,\langle\psi^\Gamma|\,\Delta^\Gamma(\mathcal{A}^{-1}\mathcal{R}\mathcal{A})=\langle\phi^\Gamma|\,[\Delta^\Gamma(\mathcal{A}^{-1}\mathcal{R}\mathcal{A})]^*, \tag{B.5}$$

respectively. Meanwhile, an antiunitary operation $\mathcal{B}=\mathcal{A}\mathcal{R}$ ($\mathcal{B}\in\mathcal{A}\boldsymbol{G}$) for $\langle\psi^\Gamma|$ and $\langle\phi^\Gamma|$ are represented as

$$\mathcal{B}\,\langle\psi^\Gamma|=\mathcal{A}\mathcal{R}\,\langle\psi^\Gamma|=\mathcal{A}\,\langle\psi^\Gamma|\,\Delta^\Gamma(\mathcal{R})=\langle\phi^\Gamma|\,[\Delta^\Gamma(\mathcal{A}^{-1}\mathcal{B})]^*, \tag{B.6}$$

$$\mathcal{B}\,\langle\phi^\Gamma|=\mathcal{B}\mathcal{A}\,\langle\psi^\Gamma|=\langle\psi^\Gamma|\,\Delta^\Gamma(\mathcal{B}\mathcal{A}). \tag{B.7}$$

Thus, a unitary operation $\mathcal{R}$ and an antiunitary operation $\mathcal{B}$ for the set basis $\langle\psi^\Gamma, \phi^\Gamma|$ are represented by the following unitary matrices $D^\Gamma(\mathcal{R})$ and $D^\Gamma(\mathcal{B})$, which satisfy

$$\mathcal{R}\,\langle\psi^\Gamma, \phi^\Gamma| = \langle\psi^\Gamma, \phi^\Gamma| \begin{pmatrix} \Delta^\Gamma(\mathcal{R}) & 0 \\ 0 & \left[\Delta^\Gamma(\mathcal{A}^{-1}\mathcal{R}\mathcal{A})\right]^* \end{pmatrix} \equiv \langle\psi^\Gamma, \phi^\Gamma|\, D^\Gamma(\mathcal{R}) \quad \text{for } \mathcal{R}\in\boldsymbol{G}, \tag{B.8}$$

$$\mathcal{B}\,\langle\psi^\Gamma, \phi^\Gamma| = \langle\psi^\Gamma, \phi^\Gamma| \begin{pmatrix} 0 & \Delta^\Gamma(\mathcal{B}\mathcal{A}) \\ \left[\Delta^\Gamma(\mathcal{A}^{-1}\mathcal{B})\right]^* & 0 \end{pmatrix} \equiv \langle\psi^\Gamma, \phi^\Gamma|\, D^\Gamma(\mathcal{B}) \quad \text{for } \mathcal{B}\in\mathcal{A}\boldsymbol{G}, \tag{B.9}$$

respectively. Such a representation composed for the basis set $\langle\psi^\Gamma, \phi^\Gamma|$, which will be denoted as $D\Gamma$ in the following discussion, is called "corepresentation". From Eqs. (B.8) and (B.9), $D\Gamma$ satisfies the following relations for $\mathcal{R}, \mathcal{S}\in\boldsymbol{G}$, $\mathcal{B}, \mathcal{C}\in\mathcal{A}\boldsymbol{G}$:

$$D^\Gamma(\mathcal{R})D^\Gamma(\mathcal{S}) = D^\Gamma(\mathcal{R}\mathcal{S}), \tag{B.10}$$

$$D^\Gamma(\mathcal{R})D^\Gamma(\mathcal{B}) = D^\Gamma(\mathcal{R}\mathcal{S}), \tag{B.11}$$

$$D^\Gamma(\mathcal{B})[D^\Gamma(\mathcal{R})]^* = D^\Gamma(\mathcal{B}\mathcal{R}), \tag{B.12}$$

$$D^\Gamma(\mathcal{B})[D^\Gamma(\mathcal{C})]^* = D^\Gamma(\mathcal{B}\mathcal{C}). \tag{B.13}$$

B.2 Unitary Transformation of Corepresentation

We show a unitary transformation of a corepresentation. For a unitary matrix U which transforms basis $\langle\psi^\Gamma, \phi^\Gamma|$ as

$$\langle\psi'^\Gamma, \phi'^\Gamma| = \langle\psi^\Gamma, \phi^\Gamma|\, U, \tag{B.14}$$

the corepresentation $D\Gamma$ is transformed as

$$D'^\Gamma(\mathcal{R}) = U^{-1}D^\Gamma(\mathcal{R})U, \tag{B.15}$$

$$D'^\Gamma(\mathcal{B}) = U^{-1}D^\Gamma(\mathcal{B})U^*, \tag{B.16}$$

where $\mathcal{R}\in\boldsymbol{G}$, $\mathcal{B}\in\mathcal{A}\boldsymbol{G}$. Above relations are derived as follows:

$$\mathcal{R}\,\langle\psi'^\Gamma, \phi'^\Gamma| \equiv \langle\psi'^\Gamma, \phi'^\Gamma|\, D'^\Gamma(\mathcal{R}) = \mathcal{R}\,\langle\psi^\Gamma, \phi^\Gamma|\, U = \langle\psi^\Gamma, \phi^\Gamma|\, D^\Gamma(\mathcal{R})U, \tag{B.17}$$

$$\mathcal{B}\,\langle\psi'^\Gamma, \phi'^\Gamma| \equiv \langle\psi'^\Gamma, \phi'^\Gamma|\, D'^\Gamma(\mathcal{B}) = \mathcal{B}\,\langle\psi^\Gamma, \phi^\Gamma|\, U = \langle\psi^\Gamma, \phi^\Gamma|\, D^\Gamma(\mathcal{B})U^*. \tag{B.18}$$

Thus, there is an equivalent corepresentation when the unitary matrix U satisfying Eqs. (B.15) and (B.16) exists.

B.3 Irreducible Corepresentation (IRREP)

The derivation of an irreducible corepresentation (IRREP) is shown with the use of a unitary transformation. By assuming that the corepresentation $D\Gamma$ is reducible by the unitary matrix $U^{-1} = \begin{pmatrix} a & b \\ c & d \end{pmatrix}$, $D\Gamma$ satisfies the relation

$$\begin{pmatrix} a & b \\ c & d \end{pmatrix} \begin{pmatrix} \Delta^\Gamma(\mathcal{R}) & 0 \\ 0 & \left[\Delta^\Gamma(\mathcal{A}^{-1}\mathcal{R}\mathcal{A})\right]^* \end{pmatrix} = \begin{pmatrix} X(\mathcal{R}) & 0 \\ 0 & Y(\mathcal{R}) \end{pmatrix} \begin{pmatrix} a & b \\ c & d \end{pmatrix}, \tag{B.19}$$

where $X(\mathcal{R})$ and $Y(\mathcal{R})$ are equivalent to $\Delta^{\Gamma}(\mathcal{R})$ and $\left[\Delta^{\Gamma}(\mathcal{A}^{-1}\mathcal{R}\mathcal{A})\right]^{*}$, respectively. The respective matrix elements have the following relations

$$a\Delta^{\Gamma}(\mathcal{R})=X(\mathcal{R})a, \tag{B.20}$$
$$b\left[\Delta^{\Gamma}(\mathcal{A}^{-1}\mathcal{R}\mathcal{A})\right]^{*}=X(\mathcal{R})b, \tag{B.21}$$
$$c\Delta^{\Gamma}(\mathcal{R})=Y(\mathcal{R})c, \tag{B.22}$$
$$d\left[\Delta^{\Gamma}(\mathcal{A}^{-1}\mathcal{R}\mathcal{A})\right]^{*}=Y(\mathcal{R})d, \tag{B.23}$$

which result in

$$a^{-1}b\left[\Delta^{\Gamma}(\mathcal{A}^{-1}\mathcal{R}\mathcal{A})\right]^{*}=\Delta^{\Gamma}(\mathcal{R})a^{-1}b, \tag{B.24}$$
$$c^{-1}d\left[\Delta^{\Gamma}(\mathcal{A}^{-1}\mathcal{R}\mathcal{A})\right]^{*}=\Delta^{\Gamma}(\mathcal{R})c^{-1}d. \tag{B.25}$$

To clarify when the unitary matrix satisfying Eqs. (B.24) and (B.25) block-diagonalizes the corepresentation $D\Gamma$ for all components in a nonunitary group, we examine two cases; $\Delta^{\Gamma}(\mathcal{R})$ and $\left[\Delta^{\Gamma}(\mathcal{A}^{-1}\mathcal{R}\mathcal{A})\right]^{*}$ are equivalent or not equivalent.

First, we examine the case when $\Delta^{\Gamma}(\mathcal{R})$ and $\left[\Delta^{\Gamma}(\mathcal{A}^{-1}\mathcal{R}\mathcal{A})\right]^{*}$ are not equivalent. From Schur's lemma (1), matrices a, b, c, and d satisfy[1]

$$a^{-1}b=c^{-1}d=0, \tag{B.26}$$
$$\therefore\ b=c=0, \tag{B.27}$$

which results in

$$U^{-1}=\begin{pmatrix} a & 0 \\ 0 & d \end{pmatrix}. \tag{B.28}$$

The unitary matrix U in Eq. (B.28) cannot block-diagonalize the corepresentation matrix with respect to the antiunitary operation

$$D^{\Gamma}(\mathcal{B})=\begin{pmatrix} 0 & \Delta^{\Gamma}(\mathcal{B}\mathcal{A}) \\ \left[\Delta^{\Gamma}(\mathcal{A}^{-1}\mathcal{B})\right]^{*} & 0 \end{pmatrix}. \tag{B.29}$$

It means that the corepresetation $D\Gamma$ is irreducible when $\Delta^{\Gamma}(\mathcal{R})$ and $\left[\Delta^{\Gamma}(\mathcal{A}^{-1}\mathcal{R}\mathcal{A})\right]^{*}$ are not equivalent.

Next, we present the case when $\Delta^{\Gamma}(\mathcal{R})$ and $\left[\Delta^{\Gamma}(\mathcal{A}^{-1}\mathcal{R}\mathcal{A})\right]^{*}$ are equivalent. In this case, the unitary matrix N satisfying

$$\Delta^{\Gamma}(\mathcal{R})=N\left[\Delta^{\Gamma}(\mathcal{A}^{-1}\mathcal{R}\mathcal{A})\right]^{*}N^{-1}, \tag{B.30}$$

exists as Eqs. (B.24) and (B.25). By a unitary matrix $U=\begin{pmatrix} I & 0 \\ 0 & N \end{pmatrix}$, $D^{\Gamma}(\mathcal{R})$ is transformed as

$$\begin{aligned} D'^{\Gamma}(\mathcal{R})\equiv U^{-1}D^{\Gamma}(\mathcal{R})U&=\begin{pmatrix} I & 0 \\ 0 & N \end{pmatrix}\begin{pmatrix} \Delta^{\Gamma}(\mathcal{R}) & 0 \\ 0 & \left[\Delta^{\Gamma}(\mathcal{A}^{-1}\mathcal{R}\mathcal{A})\right]^{*} \end{pmatrix}\begin{pmatrix} I & 0 \\ 0 & N^{-1} \end{pmatrix} \\ &=\begin{pmatrix} \Delta^{\Gamma}(\mathcal{R}) & 0 \\ 0 & \Delta^{\Gamma}(\mathcal{R}) \end{pmatrix}, \end{aligned} \tag{B.31}$$

[1] $a, d\neq 0$, as we set $X(\mathcal{R})$ and $Y(\mathcal{R})$ are the equivalent representations of $\Delta^{\Gamma}(\mathcal{R})$ and $\left[\Delta^{\Gamma}(\mathcal{A}^{-1}\mathcal{R}\mathcal{A})\right]^{*}$, respectively.

where I is the identity matrix. Meanwhile, the corepresentation with respect to an antiunitary operation $\mathcal{A}$ is transformed by U as follows:

$$D'^{\Gamma}(\mathcal{A}) \equiv U^{-1} D^{\Gamma}(\mathcal{A}) U^{*} = \begin{pmatrix} I & 0 \\ 0 & N \end{pmatrix} \begin{pmatrix} 0 & \Delta^{\Gamma}(\mathcal{A}^2) \\ I & 0 \end{pmatrix} \begin{pmatrix} I & 0 \\ 0 & [N^{-1}]^{*} \end{pmatrix} = \begin{pmatrix} 0 & \Delta^{\Gamma}(\mathcal{A}^2)[N^{-1}]^{*} \\ N & 0 \end{pmatrix}. \tag{B.32}$$

Further decomposition of $D'^{\Gamma}(\mathcal{A})$ into IRREP needs the unitary matrix that keeps $D'^{\Gamma}(\mathcal{R})$ in the block-diagonalized form and block-diagonalizes $D'^{\Gamma}(\mathcal{A})$. Such a unitary matrix denoted as V is required to be commutative with $D'^{\Gamma}(\mathcal{R})$. When we set $V^{-1} = \begin{pmatrix} \alpha & \beta \\ \gamma & \delta \end{pmatrix}$, the following relation

$$V^{-1} D'^{\Gamma}(\mathcal{R}) = D'^{\Gamma}(\mathcal{R}) V^{-1}, \tag{B.33}$$

is satisfied, i.e.,

$$\begin{pmatrix} \alpha\Delta^{\Gamma}(\mathcal{R}) & \beta\Delta^{\Gamma}(\mathcal{R}) \\ \gamma\Delta^{\Gamma}(\mathcal{R}) & \delta\Delta^{\Gamma}(\mathcal{R}) \end{pmatrix} = \begin{pmatrix} \Delta^{\Gamma}(\mathcal{R})\alpha & \Delta^{\Gamma}(\mathcal{R})\beta \\ \Delta^{\Gamma}(\mathcal{R})\gamma & \Delta^{\Gamma}(\mathcal{R})\delta \end{pmatrix}. \tag{B.34}$$

Since $\Delta^{\Gamma}(\mathcal{R})$ is the irreducible representation of the unitary group $\boldsymbol{G}$, matrices α, β, γ, and λ can be represented by using complex numbers κ, μ, ν, ρ as $\alpha = \kappa I$, $\beta = \mu I$, $\gamma = \nu I$, $\lambda = \rho I$ because of Schur's lemma (2). By using V, the corepresentation $D'^{\Gamma}(\mathcal{A})$ can be transformed as

$$\begin{aligned} D''^{\Gamma}(\mathcal{A}) \equiv V^{-1} D'^{\Gamma}(\mathcal{A}) V^{*} &= \begin{pmatrix} \kappa I & \mu I \\ \nu I & \rho I \end{pmatrix} \begin{pmatrix} 0 & \Delta^{\Gamma}(\mathcal{A}^2)[N^{-1}]^{*} \\ N & 0 \end{pmatrix} \begin{pmatrix} \kappa I & \nu I \\ \mu I & \rho I \end{pmatrix}, \\ &= \begin{pmatrix} \kappa\mu(\Delta^{\Gamma}(\mathcal{A}^2)[N^{-1}]^{*} + N) & \kappa\rho\Delta^{\Gamma}(\mathcal{A}^2)[N^{-1}]^{*} + \mu\nu N \\ \mu\nu\Delta^{\Gamma}(\mathcal{A}^2)[N^{-1}]^{*} + \kappa\rho N & \nu\rho(\Delta^{\Gamma}(\mathcal{A}^2)[N^{-1}]^{*} + N) \end{pmatrix}. \end{aligned} \tag{B.35}$$

In order to obtain the block-diagonalized $D''^{\Gamma}(\mathcal{A})$ in Eq. (B.35), the following relations need to be satisfied.

$$\kappa\rho\Delta^{\Gamma}(\mathcal{A}^2)[N^{-1}]^{*} + \mu\nu N = 0, \tag{B.36}$$

$$\mu\nu\Delta^{\Gamma}(\mathcal{A}^2)[N^{-1}]^{*} + \kappa\rho N = 0, \tag{B.37}$$

i.e.,

$$[(\mu\nu)^2 - (\rho\kappa)^2] = 0. \tag{B.38}$$

In addition, μ, ν, ρ, and κ have the further restriction $\mu\nu \neq \rho\kappa$ when $D''^{\Gamma}(\mathcal{A})$ is block-diagonalized, since the unitary matrix V satisfies $\det[V^{-1}] \neq 0$. It results in

$$\mu\nu = -\rho\kappa. \tag{B.39}$$

When we set $\kappa = \mu = \rho = 1/\sqrt{2}$ and $\nu = -1/\sqrt{2}$, the relations in Eq. (B.39) is satisfied and $D''^{\Gamma}(\mathcal{A})$ is block-diagonalized as follows:

$$\begin{aligned} D''^{\Gamma}(\mathcal{A}) &= \frac{1}{2} \begin{pmatrix} \Delta^{\Gamma}(\mathcal{A}^2)[N^{-1}]^{*} + N & 0 \\ 0 & -(\Delta^{\Gamma}(\mathcal{A}^2)[N^{-1}]^{*} + N) \end{pmatrix} \\ &= \begin{pmatrix} N & 0 \\ 0 & -N \end{pmatrix}, \end{aligned} \tag{B.40}$$

where we used Eq. (B.36). Thus, the corepresentation matrix for $\mathcal{B}\in\mathcal{A}\boldsymbol{G}$ is block-diagonalized as

$$D''^{\Gamma}(\mathcal{B})=D''^{\Gamma}(\mathcal{B}\mathcal{A}^{-1})D''^{\Gamma}(\mathcal{A})=\begin{pmatrix}\Delta^{\Gamma}(\mathcal{B}\mathcal{A}^{-1}) & 0\\ 0 & \Delta^{\Gamma}(\mathcal{B}\mathcal{A}^{-1})\end{pmatrix}\begin{pmatrix}N & 0\\ 0 & -N\end{pmatrix}$$
$$=\begin{pmatrix}\Delta^{\Gamma}(\mathcal{B}\mathcal{A}^{-1})N & 0\\ 0 & -\Delta^{\Gamma}(\mathcal{B}\mathcal{A}^{-1})N\end{pmatrix}. \tag{B.41}$$

Meanwhile, above block-diagonalization is not always possible even if $\Delta^{\Gamma}(\mathcal{A}^2)$ and $\left[\Delta^{\Gamma}(\mathcal{A}^{-1}\mathcal{R}\mathcal{A})\right]^*$ are quivalent. Whether $D'^{\Gamma}(\mathcal{B})$ can be block-diagonalized or not is determined by whether the unitary matrix N satisfies

$$NN^*=\Delta^{\Gamma}(\mathcal{A}^2), \tag{B.42}$$

from Eqs. (B.36) and (B.39), while $NN^*=\pm\Delta^{\Gamma}(\mathcal{A}^2)$ is possible for the equivalent $\Delta^{\Gamma}(\mathcal{A}^2)$ and $\left[\Delta^{\Gamma}(\mathcal{A}^{-1}\mathcal{R}\mathcal{A})\right]^*$[2]. When $D'^{\Gamma}(\mathcal{B})$ cannot be block-diagonalized because of $NN^*=-\Delta^{\Gamma}(\mathcal{A}^2)$, which is given as

$$D'^{\Gamma}(\mathcal{B})=D'^{\Gamma}(\mathcal{B}\mathcal{A}^{-1})D'^{\Gamma}(\mathcal{A})=\begin{pmatrix}\Delta^{\Gamma}(\mathcal{B}\mathcal{A}^{-1}) & 0\\ 0 & \Delta^{\Gamma}(\mathcal{B}\mathcal{A}^{-1})\end{pmatrix}\begin{pmatrix}0 & \Delta^{\Gamma}(\mathcal{A}^2)[N^{-1}]^*\\ N & 0\end{pmatrix}$$
$$=\begin{pmatrix}\Delta^{\Gamma}(\mathcal{B}\mathcal{A}^{-1}) & 0\\ 0 & \Delta^{\Gamma}(\mathcal{B}\mathcal{A}^{-1})\end{pmatrix}\begin{pmatrix}0 & -N\\ N & 0\end{pmatrix}$$
$$=\begin{pmatrix}0 & -\Delta^{\Gamma}(\mathcal{B}\mathcal{A}^{-1})N\\ \Delta^{\Gamma}(\mathcal{B}\mathcal{A}^{-1})N & 0\end{pmatrix}. \tag{B.50}$$

In summary, the corepresentation $D\Gamma$ in a nonunitary group $\boldsymbol{M}=\boldsymbol{G}+\mathcal{A}\boldsymbol{G}$ obtained by the irreducible representation Γ in $\boldsymbol{G}$ is classified into three cases (a)–(c):

[2]When $\Delta^{\Gamma}(\mathcal{A}^2)$ and $\left[\Delta^{\Gamma}(\mathcal{A}^{-1}\mathcal{R}\mathcal{A})\right]^*$ are equivalent,

$$\Delta^{\Gamma}(\mathcal{R})=N\left[\Delta^{\Gamma}(\mathcal{A}^{-1}\mathcal{R}\mathcal{A})\right]^*N^{-1}=N\left[N\left[\Delta^{\Gamma}(\mathcal{A}^{-1}\mathcal{A}^{-1}\mathcal{R}\mathcal{A}\mathcal{A})\right]^*N^{-1}\right]^*N^{-1} \tag{B.43}$$
$$=\left(NN^*[\Delta^{\Gamma}(\mathcal{A}^2)]^{-1}\right)\Delta^{\Gamma}(\mathcal{R})\left(\Delta^{\Gamma}(\mathcal{A}^2)[N^{-1}]^*N^{-1}\right). \tag{B.44}$$

Thus, Schur's lemma (2) leads to

$$NN^*[\Delta^{\Gamma}(\mathcal{A}^2)]^{-1}=\lambda I, \tag{B.45}$$
$$\therefore\ \Delta^{\Gamma}(\mathcal{A}^2)=\frac{NN^*}{\lambda}, \tag{B.46}$$

where λ is a complex number. Moreover, by setting $\mathcal{R}=\mathcal{A}^2$ in $\Delta^{\Gamma}(\mathcal{R})=N\left[\Delta^{\Gamma}(\mathcal{A}^{-1}\mathcal{R}\mathcal{A})\right]^*N^{-1}$, we obtain the relation

$$\Delta^{\Gamma}(\mathcal{A}^2)=N[\Delta^{\Gamma}(\mathcal{A}^2)]^*N^{-1}, \tag{B.47}$$

which results in

$$\frac{NN^*}{\lambda}=\Delta^{\Gamma}(\mathcal{A}^2)=N[\Delta^{\Gamma}(\mathcal{A}^2)]^*N^{-1}=\frac{NN^*NN^{-1}}{\lambda^*}=\frac{NN^*}{\lambda^*}, \tag{B.48}$$

i.e., $\lambda=\lambda^*$. In addition, $\lambda=\pm1$, since $|\lambda|=1$ for the unitary matrices N and $\Delta^{\Gamma}(\mathcal{A}^2)$. Therefore,

$$NN^*=\pm\Delta^{\Gamma}(\mathcal{A}^2). \tag{B.49}$$

(a) The irreducible representation matrix $\Delta^{\Gamma}(\mathcal{R})$ is equivalent to $[\Delta^{\Gamma}(\mathcal{A}^{-1}\mathcal{R}\mathcal{A})]^*$. In addition, the unitary matrix N satisfying

$$\Delta^{\Gamma}(\mathcal{R})=N[\Delta^{\Gamma}(\mathcal{A}^{-1}\mathcal{R}\mathcal{A})]^*N^{-1}, \tag{B.51}$$

has the relation with $\Delta^{\Gamma}(\mathcal{A}^2)$ as

$$NN^*=\Delta^{\Gamma}(\mathcal{A}^2). \tag{B.52}$$

In this case, the corepresentation matrix composed from $\Delta^{\Gamma}(\mathcal{R})$ ($\mathcal{R}\in\boldsymbol{G}$) can be block-diagonalized as $D''^{\Gamma}(\mathcal{R})=V^{-1}U^{-1}D^{\Gamma}(\mathcal{R})UV$ and $D''^{\Gamma}(\mathcal{B})=V^{-1}U^{-1}D^{\Gamma}(\mathcal{B})U^*V^*$ by the unitary matrices

$$U^{-1}=\begin{pmatrix} I & 0 \\ 0 & N \end{pmatrix},\ V^{-1}=\frac{1}{\sqrt{2}}\begin{pmatrix} I & I \\ -I & I \end{pmatrix}. \tag{B.53}$$

It results in the two IRREPs $D\Gamma^+$ and $D\Gamma^-$

$$D\Gamma^+\to\Delta^{\Gamma}(\mathcal{R}) \text{ for } \mathcal{R}\in\boldsymbol{G},\ +\Delta^{\Gamma}(\mathcal{B}\mathcal{A}^{-1})N \text{ for } \mathcal{R}\in\mathcal{A}\boldsymbol{G}, \tag{B.54}$$

$$D\Gamma^-\to\Delta^{\Gamma}(\mathcal{R}) \text{ for } \mathcal{R}\in\boldsymbol{G},\ -\Delta^{\Gamma}(\mathcal{B}\mathcal{A}^{-1})N \text{ for } \mathcal{R}\in\mathcal{A}\boldsymbol{G}. \tag{B.55}$$

(b) The irreducible representation matrix $\Delta^{\Gamma}(\mathcal{R})$ is equivalent to $[\Delta^{\Gamma}(\mathcal{A}^{-1}\mathcal{R}\mathcal{A})]^*$. In addition, the unitary matrix N satisfies

$$\Delta^{\Gamma}(\mathcal{R})=N[\Delta^{\Gamma}(\mathcal{A}^{-1}\mathcal{R}\mathcal{A})]^*N^{-1}. \tag{B.56}$$

It follows the relation

$$NN^*=-\Delta^{\Gamma}(\mathcal{A}^2). \tag{B.57}$$

In this case, the corepresentation is already irreducible. Meanwhile, the matrix representation can be transformed into the form which explicitly presents the equivalence between $\Delta^{\Gamma}(\mathcal{R})$ and $[\Delta^{\Gamma}(\mathcal{A}^{-1}\mathcal{R}\mathcal{A})]^*$ by the unitary matrix U. Thus, one IRREP $D\Gamma$ is obtained as follows:

$$D\Gamma\to\begin{pmatrix} \Delta^{\Gamma}(\mathcal{R}) & 0 \\ 0 & \Delta^{\Gamma}(\mathcal{R}) \end{pmatrix} \text{ for } \mathcal{R}\in\boldsymbol{G},\ \begin{pmatrix} 0 & -\Delta^{\Gamma}(\mathcal{B}\mathcal{A}^{-1})N \\ \Delta^{\Gamma}(\mathcal{B}\mathcal{A}^{-1})N & 0 \end{pmatrix} \text{ for } \mathcal{R}\in\mathcal{A}\boldsymbol{G}. \tag{B.58}$$

(c) The irreducible representation matrix $\Delta^{\Gamma}(\mathcal{R})$ is not equivalent to $[\Delta^{\Gamma}(\mathcal{A}^{-1}\mathcal{R}\mathcal{A})]^*$. In this case, the corepresentation $D\Gamma$ is already irreducible, whose representation matrix is described as

$$D\Gamma\to\begin{pmatrix} \Delta^{\Gamma}(\mathcal{R}) & 0 \\ 0 & \left[\Delta^{\Gamma}(\mathcal{A}^{-1}\mathcal{R}\mathcal{A})\right]^* \end{pmatrix} \text{ for } \mathcal{R}\in\boldsymbol{G},\ \begin{pmatrix} 0 & \Delta^{\Gamma}(\mathcal{B}\mathcal{A}) \\ \left[\Delta^{\Gamma}(\mathcal{A}^{-1}\mathcal{B})\right]^* & 0 \end{pmatrix} \text{ for } \mathcal{R}\in\mathcal{A}\boldsymbol{G}. \tag{B.59}$$

Finally, we show the way to examine in which cases a corepresentation is classified by using the character. Generally,

$$\begin{aligned}\sum_{\mathcal{B}\in\mathcal{A}\boldsymbol{G}}\Delta^{\Gamma}(\mathcal{B}^2)_{rr}&=\sum_{\mathcal{R}\in\boldsymbol{G}}\Delta^{\Gamma}(\mathcal{A}\mathcal{R}\mathcal{A}\mathcal{R})_{rr}\\&=\sum_{\mathcal{R}\in\boldsymbol{G}}\Delta^{\Gamma}(\mathcal{A}^2\mathcal{A}^{-1}\mathcal{R}\mathcal{A}\mathcal{R})_{rr}\\&=\sum_{\mathcal{R}\in\boldsymbol{G}}\Delta^{\Gamma}(\mathcal{A}^2)_{rs}\Delta^{\Gamma}(\mathcal{A}^{-1}\mathcal{R}\mathcal{A})_{st}\Delta^{\Gamma}(\mathcal{R})_{tr},\end{aligned}\tag{B.60}$$

for $\mathcal{B}\in\mathcal{A}\boldsymbol{G}$. For equivalent $\Delta^{\Gamma}(\mathcal{R})$ and $[\Delta^{\Gamma}(\mathcal{A}^{-1}\mathcal{R}\mathcal{A})]^*$ [case (a) or (b)],

$$\begin{aligned}\sum_{\mathcal{B}\in\mathcal{A}\boldsymbol{G}}\Delta^{\Gamma}(\mathcal{B}^2)_{rr}&=\sum_{\mathcal{R}\in\boldsymbol{G}}\Delta^{\Gamma}(\mathcal{A}^2)_{rs}[N_{sp}^{-1}\Delta^{\Gamma}(\mathcal{R})_{pq}N_{qt}]^*\Delta^{\Gamma}(\mathcal{R})_{tr}\\&=\Delta^{\Gamma}(\mathcal{A}^2)_{rs}[N_{sp}^{-1}]^*[N_{qt}]^*\sum_{\mathcal{R}\in\boldsymbol{G}}[\Delta^{\Gamma}(\mathcal{R})_{pq}]^*\Delta^{\Gamma}(\mathcal{R})_{tr}.\end{aligned}\tag{B.61}$$

By using the orthogonal relation for the irreducible representation in a unitary group,

$$\sum_{\mathcal{R}\in\boldsymbol{G}}\Delta^{\Gamma}(\mathcal{R})_{rl}[\Delta^{\tilde{\Gamma}}(\mathcal{R})]^*_{sm}=\frac{|\boldsymbol{G}|}{d^{\Gamma}}\delta_{\Gamma\tilde{\Gamma}}\delta_{rs}\delta_{lm},\tag{B.62}$$

where $|\boldsymbol{G}|$ is the order of $\boldsymbol{G}$,

$$\begin{aligned}\sum_{\mathcal{B}\in\mathcal{A}\boldsymbol{G}}\Delta(\mathcal{B}^2)_{rr}&=\Delta^{\Gamma}(\mathcal{A}^2)_{rs}[N_{sp}^{-1}]^*[N_{qt}]^*\frac{|\boldsymbol{G}|}{d^{\Gamma}}\delta_{pt}\delta_{qr}\\&=\frac{|\boldsymbol{G}|}{d^{\Gamma}}\Delta^{\Gamma}(\mathcal{A}^2)_{rs}[N_{st}^{-1}]^*[N_{rt}]^*\\&=\frac{|\boldsymbol{G}|}{d^{\Gamma}}\Delta^{\Gamma}(\mathcal{A}^2)_{rs}[N_{rt}]^*N_{ts}.\end{aligned}\tag{B.63}$$

Since the relation $[N_{rt}]^*N_{ts}=\pm[\Delta^{\Gamma}(\mathcal{A}^2)_{rs}]^*=\pm\Delta^{\Gamma}(-\mathcal{A}^2)_{sr}$ is satisfied for cases (a)(positive sign) and (b)(negative sign), respectively,

$$\begin{aligned}\sum_{\mathcal{B}\in\mathcal{A}\boldsymbol{G}}\Delta(\mathcal{B}^2)_{rr}&=\pm\frac{|\boldsymbol{G}|}{d^{\Gamma}}\Delta^{\Gamma}(\mathcal{A}^2)_{rs}\Delta^{\Gamma}(-\mathcal{A}^2)_{sr}\\&=\pm\frac{|\boldsymbol{G}|}{d^{\Gamma}}\Delta^{\Gamma}(\mathcal{E})_{rr},\\&=\pm|\boldsymbol{G}|.\end{aligned}\tag{B.64}$$

Here, $\mathcal{E}$ is the identical operation.

In case (c), $\sum_{\mathcal{B}\in\mathcal{A}\boldsymbol{G}}\Delta^{\Gamma}(\mathcal{B}^2)_{rr}=0$ in Eq. (B.60) because of the orthogonality between inequivalent representations $\Delta^{\Gamma}(\mathcal{A}^{-1}\mathcal{R}\mathcal{A})$ and $\Delta^{\Gamma}(\mathcal{R})$.

Therefore, one can examine three cases as

$$\sum_{\mathcal{B}\in\mathcal{A}\boldsymbol{G}}\chi^{\Gamma}(\mathcal{B}^2)=\begin{cases}+|\boldsymbol{G}| & :\text{case (a)},\\ -|\boldsymbol{G}| & :\text{case (b)},\\ 0 & :\text{case (c)}.\end{cases}\tag{B.65}$$

B.4 Kronecker Product of IRREP

We present the Kronecker product between IRREPs. The Kronecker product between irreducible representations Γ_i and Γ_j in a unitary group can be decomposed as

$$\Gamma_i \otimes \Gamma_j = \sum_k c_{ij,k} \Gamma_k, \tag{B.66}$$

where the Clebsch–Gordan coefficient $c_{ij,k}$ is represented by the character in Γ_i, $\psi^{\Gamma_i}(\mathcal{R}) = \mathrm{Tr}[\Delta^{\Gamma}(\mathcal{R})]$, as

$$c_{ij,k} = \frac{1}{|\boldsymbol{G}|} \sum_{\mathcal{R} \in \boldsymbol{G}} \psi^{\Gamma_i}(\mathcal{R}) \psi^{\Gamma_j}(\mathcal{R}) [\psi^{\Gamma_k}(\mathcal{R})]^*. \tag{B.67}$$

In the same manner, the Kronecker product between IRREPs $D\Gamma_i$ and $D\Gamma_j$ consisting of Γ_i and Γ_j can be decomposed as

$$D\Gamma_i \otimes D\Gamma_j = \sum_k d_{ij,k} D\Gamma_k. \tag{B.68}$$

The coefficient $d_{ij,k}$ is given by the relation among $\psi^{\Gamma_i}(\mathcal{R})$, $\psi^{\Gamma_j}(\mathcal{R})$, and $\psi^{\Gamma_k}(\mathcal{R})$, since IRREPs in a nonunitary group are uniquely determined by the unitary subgroup.

As IRREPs $D^{\Gamma_k}(\mathcal{R})$ include the same (different) multiple irreducible representations for case (b) [(c)], the character of IRREP, $\chi^{\Gamma}(\mathcal{R})$, satisfies the relation as

$$\chi^{\Gamma}(\mathcal{R}) = \mathrm{Tr}[D^{\Gamma}(\mathcal{R})] = \begin{cases} \mathrm{Tr}[\Delta^{\Gamma}(\mathcal{R})] = \psi^{\Gamma}(\mathcal{R}) & : \text{case (a)}, \\ \mathrm{Tr}[\Delta^{\Gamma}(\mathcal{R})] + \mathrm{Tr}[\Delta^{\Gamma}(\mathcal{R})] = 2\psi^{\Gamma}(\mathcal{R}) & : \text{case (b)}, \\ \mathrm{Tr}[\Delta^{\Gamma}(\mathcal{R})] + \mathrm{Tr}\{[\Delta^{\Gamma}(\mathcal{A}^{-1}\mathcal{R}\mathcal{A})]^*\} = \psi^{\Gamma}(\mathcal{R}) + \psi^{\bar{\Gamma}}(\mathcal{R}) & : \text{case (c)}, \end{cases} \tag{B.69}$$

i.e.,

$$\frac{1}{|\boldsymbol{G}|} \sum_{\mathcal{R} \in \boldsymbol{G}} |\chi^{\Gamma_k}(\mathcal{R})|^2 = \begin{cases} 1 & : \text{case (a)}, \\ 4 & : \text{case (b)}, \\ 2 & : \text{case (c)}. \end{cases} \tag{B.70}$$

We set $\left[\Delta^{\Gamma}(\mathcal{A}^{-1}\mathcal{R}\mathcal{A})\right]^* \equiv \Delta^{\bar{\Gamma}}(\mathcal{R})$ in Eq. (B.69). By generalizing Eq. (B.67) in the consideration of the relation in Eq. (B.70), the coefficient $d_{ij,k}$ can be obtained as [129, 131]

$$d_{ij,k} = \frac{\frac{1}{|\boldsymbol{G}|} \sum_{\mathcal{R} \in \boldsymbol{G}} \chi^{\Gamma_i}(\mathcal{R}) \chi^{\Gamma_j}(\mathcal{R}) [\chi^{\Gamma_k}(\mathcal{R})]^*}{\frac{1}{|\boldsymbol{G}|} \sum_{\mathcal{R} \in \boldsymbol{G}} |\chi^{\Gamma_k}(\mathcal{R})|^2}. \tag{B.71}$$

Since the character of IRREP, $\chi^{\Gamma}(\mathcal{R})$, is relevant to ψ^{Γ}, $d_{ij,k}$ also can be represented by the Clebsch–Gordan coefficient $c_{ij,k}$, whose general relation is summarized in the previous literatures, e.g., Ref. [129]. In addition, the specific decomposition of the Kronecker product for black-and-white point groups is given in Ref. [132].

Appendix C

Tables of Multipole Classification

The multipole classification for 32 gray point groups is summarized in Table 2.3 in Sec. 2.3 and Tables C.1–C.31 in Sec. C.1. Meanwhile, the classification of 58 black-and-white point groups is summarized in Table 2.4 in Sec. 2.3 and Tables C.32–C.88 in Sec. C.2.

C.1 Gray Point Groups

Table C.1: Irreducible corepresentations (IRREPs) of four types of multipoles: electric (E), electric toroidal (ET), magnetic (M), and magnetic toroidal (MT) multipoles, in the type-(II) gray point group $4321'$. The character table of the unitary subgroup 432 (O) is also shown to represent the symmetry of each multipole. The IRREPs are obtained from the irreducible representations of the unitary subgroup. The superscript "$\pm$" of IRREP stands for the parity with respect to the antiunitary operation $\mathcal{A}=\theta$.

	E	$6C_4$	$3C_4^2$	$6C_2'$	$8C_3$	IRREP	E	ET	MT	M	MPG	P. axis
A_1	1	1	1	1	1	A_1^+	Q_0, Q_4	G_0, G_4			$4321'$	$\langle 100\rangle$
						A_1^-			T_0, T_4	M_0, M_4	432	$\langle 100\rangle$
A_2	1	-1	1	-1	1	A_2^+	Q_{xyz}	G_{xyz}			$231'$	$\langle 100\rangle$
						A_2^-			T_{xyz}	M_{xyz}	$4'32'$	$\langle 100\rangle$
E	2	0	2	0	-1	E^+	Q_u, Q_{4u}	G_u, G_{4u}			$4221'$	[001]
							Q_v, Q_{4v}	G_v, G_{4v}			$2221'$	[100]
						E^-			T_u, T_{4u}	M_u, M_{4u}	422	[001]
									T_v, T_{4v}	M_v, M_{4v}	$4'22'$	[001]
T_1	3	1	-1	-1	0	T_1^+	$Q_x, Q_x^\alpha, Q_{4x}^\alpha$	$G_x, G_x^\alpha, G_{4x}^\alpha$			$41'$	[100]
							$Q_y, Q_y^\alpha, Q_{4y}^\alpha$	$G_y, G_y^\alpha, G_{4y}^\alpha$			$41'$	[010]
							$Q_z, Q_z^\alpha, Q_{4z}^\alpha$	$G_z, G_z^\alpha, G_{4z}^\alpha$			$41'$	[001]
						T_1^-			$T_x, T_x^\alpha, T_{4x}^\alpha$	$M_x, M_x^\alpha, M_{4x}^\alpha$	$42'2'$	[100]
									$T_y, T_y^\alpha, T_{4y}^\alpha$	$M_y, M_y^\alpha, M_{4y}^\alpha$	$42'2'$	[010]
									$T_z, T_z^\alpha, T_{4z}^\alpha$	$M_z, M_z^\alpha, M_{4z}^\alpha$	$42'2'$	[001]
T_2	3	-1	-1	1	0	T_2^+	$Q_{yz}, Q_x^\beta, Q_{4x}^\beta$	$G_{yz}, G_x^\beta, G_{4x}^\beta$			$2221'$	[011]
							$Q_{zx}, Q_y^\beta, Q_{4y}^\beta$	$G_{zx}, G_y^\beta, G_{4y}^\beta$			$2221'$	[101]
							$Q_{xy}, Q_z^\beta, Q_{4z}^\beta$	$G_{xy}, G_z^\beta, G_{4z}^\beta$			$2221'$	[110]
						T_2^-			$T_{yz}, T_x^\beta, T_{4x}^\beta$	$M_{yz}, M_x^\beta, M_{4x}^\beta$	$4'2'2$	[100]
									$T_{zx}, T_y^\beta, T_{4y}^\beta$	$M_{zx}, M_y^\beta, M_{4y}^\beta$	$4'2'2$	[010]
									$T_{xy}, T_z^\beta, T_{4z}^\beta$	$M_{xy}, M_z^\beta, M_{4z}^\beta$	$4'2'2$	[001]

Table C.2: IRREPs of four types of multipoles in $\bar{4}3m1'$. The superscript "±" of IRREP stands for the parity with respect to the antiunitary operation $\mathcal{A}=\theta$.

E	$6IC_4$	$3C_4^2$	$6\sigma_d$	$8C_3$	IRREP	E	ET	MT	M	MPG	P. axis
A_1 1	1	1	1	1	A_1^+	Q_0, Q_{xyz}, Q_4				$\bar{4}3m1'$	$\langle 100\rangle$
					A_1^-			T_0, T_{xyz}, T_4		$\bar{4}3m$	$\langle 100\rangle$
A_2 1	−1	1	−1	1	A_2^+		G_0, G_{xyz}, G_4			$231'$	$\langle 100\rangle$
					A_2^-				M_0, M_{xyz}, M_4	$\bar{4}'3m'$	$\langle 100\rangle$
E 2	0	2	0	−1	E^+	Q_u, Q_{4u}	G_v, G_{4v}			$\bar{4}2m1'$	[001]
						Q_v, Q_{4v}	G_u, G_{4u}			$2221'$	[100]
					E^-			T_u, T_{4u}	M_v, M_{4v}	$\bar{4}2m$	[001]
								T_v, T_{4v}	M_u, M_{4u}	$\bar{4}'2m'$	[001]
T_1 3	1	−1	−1	0	T_1^+	Q_x^β, Q_{4x}^α	$G_x, G_{yz}, G_x^\alpha, G_{4x}^\beta$			$\bar{4}1'$	[100]
						Q_y^β, Q_{4y}^α	$G_y, G_{zx}, G_y^\alpha, G_{4y}^\beta$			$\bar{4}1'$	[010]
						Q_z^β, Q_{4z}^α	$G_z, G_{xy}, G_z^\alpha, G_{4z}^\beta$			$\bar{4}1'$	[001]
					T_1^-			T_x^β, T_{4x}^α	$M_x, M_{yz}, M_x^\alpha, M_{4x}^\beta$	$\bar{4}2'm'$	[100]
								T_y^β, T_{4y}^α	$M_y, M_{zx}, M_y^\alpha, M_{4y}^\beta$	$\bar{4}2'm'$	[010]
								T_z^β, T_{4z}^α	$M_z, M_{xy}, M_z^\alpha, M_{4z}^\beta$	$\bar{4}2'm'$	[001]
T_2 3	−1	−1	1	0	T_2^+	$Q_x, Q_{yz}, Q_x^\alpha, Q_{4x}^\beta$	G_x^β, G_{4x}^α			$mm21'$	[011]
						$Q_y, Q_{zx}, Q_y^\alpha, Q_{4y}^\beta$	G_y^β, G_{4y}^α			$mm21'$	[101]
						$Q_z, Q_{xy}, Q_z^\alpha, Q_{4z}^\beta$	G_z^β, G_{4z}^α			$mm21'$	[110]
					T_2^-			$T_x, T_{yz}, T_x^\alpha, T_{4x}^\beta$	M_x^β, M_{4x}^α	$\bar{4}'2'm$	[100]
								$T_y, T_{zx}, T_y^\alpha, T_{4y}^\beta$	M_y^β, M_{4y}^α	$\bar{4}'2'm$	[010]
								$T_z, T_{xy}, T_z^\alpha, T_{4z}^\beta$	M_z^β, M_{4z}^α	$\bar{4}'2'm$	[001]

Table C.3: IRREPs of four types of multipoles in $m\bar{3}1'$. The superscript "±" of case-(a) IRREP stands for the parity with respect to the antiunitary operation $\mathcal{A}=\theta$. $\mathrm{E_{g/u}}$ without superscript is the case-(c) IRREP.

E	$3C_2$	$4C_3$	$4C_3^2$	I	$3\sigma_h$	$4IC_3$	$4IC_3^2$	IRREP	E	ET	MT	M	MPG	P. axis
$\mathrm{A_g}$ 1	1	1	1	1	1	1	1	$\mathrm{A_g^+}$	Q_0, Q_4	G_{xyz}			$m\bar{3}1'$	$\langle 100\rangle$
								$\mathrm{A_g^-}$			T_0, T_4	M_{xyz}	$m\bar{3}$	$\langle 100\rangle$
$\mathrm{E_g}$ 1	1	ω	ω^2	1	1	ω	ω^2	$\mathrm{E_g}$	Q_u, Q_{4u}				$mmm1'$	[100]
1	1	ω^2	ω	1	1	ω^2	ω		Q_v, Q_{4v}				$mmm1'$	[100]
											T_u, T_{4u}		mmm	[100]
											T_v, T_{4v}		mmm	[100]
$\mathrm{T_g}$ 3	−1	0	0	3	−1	0	0	$\mathrm{T_g^+}$	$Q_{yz}, Q_{4x}^\alpha, Q_{4x}^\beta$	$G_x, G_x^\alpha, G_x^\beta$			$2/m1'$	[100]
									$Q_{zx}, Q_{4y}^\alpha, Q_{4y}^\beta$	$G_y, G_y^\alpha, G_y^\beta$			$2/m1'$	[010]
									$Q_{xy}, Q_{4z}^\alpha, Q_{4z}^\beta$	$G_z, G_z^\alpha, G_z^\beta$			$2/m1'$	[001]
								$\mathrm{T_g^-}$			$T_{yz}, T_{4x}^\alpha, T_{4x}^\beta$	$M_x, M_x^\alpha, M_x^\beta$	$mm'm'$	[100]
											$T_{zx}, T_{4y}^\alpha, T_{4y}^\beta$	$M_y, M_y^\alpha, M_y^\beta$	$m'mm'$	[100]
											$T_{xy}, T_{4z}^\alpha, T_{4z}^\beta$	$M_z, M_z^\alpha, M_z^\beta$	$m'm'm$	[100]
$\mathrm{A_u}$ 1	1	1	1	−1	−1	−1	−1	$\mathrm{A_u^+}$	Q_{xyz}	G_0, G_4			$231'$	$\langle 100\rangle$
								$\mathrm{A_u^-}$			T_{xyz}	M_0, M_4	$m'\bar{3}'$	$\langle 100\rangle$
$\mathrm{E_u}$ 1	1	ω	ω^2	−1	−1	$-\omega$	$-\omega^2$	$\mathrm{E_u}$		G_u, G_{4u}			$2221'$	[100]
1	1	ω^2	ω	−1	−1	$-\omega^2$	$-\omega$			G_v, G_{4v}			$2221'$	[100]
												M_u, M_{4u}	$m'm'm'$	[100]
												M_v, M_{4v}	$m'm'm'$	[100]
$\mathrm{T_u}$ 3	−1	0	0	−3	1	0	0	$\mathrm{T_u^+}$	$Q_x, Q_x^\alpha, Q_x^\beta$	$G_{yz}, G_{4x}^\alpha, G_{4x}^\beta$			$2mm1'$	[100]
									$Q_y, Q_y^\alpha, Q_y^\beta$	$G_{zx}, G_{4y}^\alpha, G_{4y}^\beta$			$m2m1'$	[100]
									$Q_z, Q_z^\alpha, Q_z^\beta$	$G_{xy}, G_{4z}^\alpha, G_{4z}^\beta$			$mm21'$	[100]
								$\mathrm{T_u^-}$			$T_x, T_x^\alpha, T_x^\beta$	$M_{yz}, M_{4x}^\alpha, M_{4x}^\beta$	$m'mm$	[100]
											$T_y, T_y^\alpha, T_y^\beta$	$M_{zx}, M_{4y}^\alpha, M_{4y}^\beta$	$mm'm$	[100]
											$T_z, T_z^\alpha, T_z^\beta$	$M_{xy}, M_{4z}^\alpha, M_{4z}^\beta$	mmm'	[100]

ω=exp($-2\pi i/3$)

Table C.4: IRREPs of four types of multipoles $231'$. The superscript "$\pm$" of IRREP stands for the parity with respect to the antiunitary operation $\mathcal{A}=\theta$.

	E	$3C_2$	$4C_3$	$4C_3^2$	IRREP	E	ET	MT	M	MPG	P. axis
A	1	1	1	1	A^+	Q_0, Q_{xyz}, Q_4	G_0, G_{xyz}, G_4			$231'$	$\langle 100\rangle$
					A^-			T_0, T_{xyz}, T_4	M_0, M_{xyz}, M_4	23	$\langle 100\rangle$
E	1	1	ω	ω^2	E	Q_u, Q_{4u}	G_u, G_{4u}			$2221'$	[100]
	1	1	ω^2	ω		Q_v, Q_{4v}	G_v, G_{4v}			$2221'$	[100]
								T_u, T_{4u}	M_u, M_{4u}	222	[100]
								T_v, T_{4v}	M_v, M_{4v}	222	[100]
T	3	-1	0	0	T^+	$Q_x, Q_{yz},$ $Q_x^\alpha, Q_x^\beta, Q_{4x}^\alpha, Q_{4x}^\beta$	$G_x, G_{yz},$ $G_x^\alpha, G_x^\beta, G_{4x}^\alpha, G_{4x}^\beta$			$21'$	[100]
						$Q_y, Q_{zx},$ $Q_y^\alpha, Q_y^\beta, Q_{4y}^\alpha, Q_{4y}^\beta$	$G_y, G_{zx},$ $G_y^\alpha, G_y^\beta, G_{4y}^\alpha, G_{4y}^\beta$			$21'$	[010]
						$Q_z, Q_{xy},$ $Q_z^\alpha, Q_z^\beta, Q_{4z}^\alpha, Q_{4z}^\beta$	$G_z, G_{xy},$ $G_z^\alpha, G_z^\beta, G_{4z}^\alpha, G_{4z}^\beta$			$21'$	[001]
					T^-			$T_x, T_{yz},$ $T_x^\alpha, T_x^\beta, T_{4x}^\alpha, T_{4x}^\beta$	$M_x, M_{yz},$ $M_x^\alpha, M_x^\beta, M_{4x}^\alpha, M_{4x}^\beta$	$22'2'$	[100]
								$T_y, T_{zx},$ $T_y^\alpha, T_y^\beta, T_{4y}^\alpha, T_{4y}^\beta$	$M_y, M_{zx},$ $M_y^\alpha, M_y^\beta, M_{4y}^\alpha, M_{4y}^\beta$	$2'22'$	[100]
								$T_z, T_{xy},$ $T_z^\alpha, T_z^\beta, T_{4z}^\alpha, T_{4z}^\beta$	$M_z, M_{xy},$ $M_z^\alpha, M_z^\beta, M_{4z}^\alpha, M_{4z}^\beta$	$2'2'2$	[100]

$\omega=\exp(-2\pi i/3)$

Table C.5: IRREPs of four types of multipoles in $6/mmm1'$. The superscript "±" of IRREP stands for the parity with respect to the antiunitary operation $\mathcal{A}=\theta$.

E	$2C_6$	$2C_3$	C_2	$3C_{2x}$	$3C_{2y}$	I	$2IC_6$	$2IC_3$	σ_h	$3\sigma_x$	$3\sigma_y$	IRREP	E	ET	MT	M	MPG	P. axis
A_{1g} 1	1	1	1	1	1	1	1	1	1	1	1	A^+_{1g}	Q_0, Q_u, Q_{40}				$6/mmm1'$	[001]
												A^-_{1g}			T_0, T_u, T_{40}		$6/mmm$	[001]
A_{2g} 1	1	1	1	−1	−1	1	1	1	1	−1	−1	A^+_{2g}		G_z, G^α_z			$6/m1'$	[001]
												A^-_{2g}				M_z, M^α_z	$6/mm'm'$	[001]
B_{1g} 1	−1	1	−1	1	−1	1	−1	1	−1	1	−1	B^+_{1g}	Q_{4a}	G_{3a}			$\bar{3}m1'$	[001]
												B^-_{1g}			T_{4a}	M_{3a}	$6'/m'mm'$	[001]
B_{2g} 1	−1	1	−1	−1	1	1	−1	1	−1	−1	1	B^+_{2g}	Q_{4b}	G_{3b}			$\bar{3}m1'$	[001]
												B^-_{2g}			T_{4b}	M_{3b}	$6'/m'm'm$	[001]
E_{1g} 2	1	−1	−2	0	0	2	1	−1	−2	0	0	E^+_{1g}	Q_{yz}, Q^α_{4v}	G_x, G_{3u}			$2/m1'$	[100]
													Q_{zx}, Q^α_{4u}	G_y, G_{3v}			$2/m1'$	[010]
												E^-_{1g}			T_{yz}, T^α_{4v}	M_x, M_{3u}	$mm'm'$	[100]
															T_{zx}, T^α_{4u}	M_y, M_{3v}	$m'mm'$	[100]
E_{2g} 2	−1	−1	2	0	0	2	−1	−1	2	0	0	E^+_{2g}	$Q_v, Q^{\beta1}_{4u}, Q^{\beta2}_{4u}$	G_{xyz}			$mmm1'$	[100]
													$Q_{xy}, Q^{\beta1}_{4v}, Q^{\beta2}_{4v}$	G^β_z			$2/m1'$	[001]
												E^-_{2g}			$T_v, T^{\beta1}_{4u}, T^{\beta2}_{4u}$	M_{xyz}	mmm	[100]
															$T_{xy}, T^{\beta1}_{4v}, T^{\beta2}_{4v}$	M^β_z	$m'm'm$	[100]
A_{1u} 1	1	1	1	1	1	−1	−1	−1	−1	−1	−1	A^+_{1u}		G_0, G_u, G_{40}			$6221'$	[001]
												A^-_{1u}				M_0, M_u, M_{40}	$6/m'm'm'$	[001]
A_{2u} 1	1	1	1	−1	−1	−1	−1	−1	−1	1	1	A^+_{2u}	Q_z, Q^α_z				$6mm1'$	[001]
												A^-_{2u}			T_z, T^α_z		$6/m'mm$	[001]
B_{1u} 1	−1	1	−1	1	−1	−1	1	−1	1	−1	1	B^+_{1u}	Q_{3a}	G_{4a}			$\bar{6}2m1'$	[001]
												B^-_{1u}			T_{3a}	M_{4a}	$6'/mm'm$	[001]
B_{2u} 1	−1	1	−1	−1	1	−1	1	−1	1	1	−1	B^+_{2u}	Q_{3b}	G_{4b}			$\bar{6}m21'$	[001]
												B^-_{2u}			T_{3b}	M_{4b}	$6'/mmm'$	[001]
E_{1u} 2	1	−1	−2	0	0	−2	−1	1	2	0	0	E^+_{1u}	Q_x, Q_{3u}	G_{yz}, G^α_{4v}			$2mm1'$	[100]
													Q_y, Q_{3v}	G_{zx}, G^α_{4u}			$m2m1'$	[100]
												E^-_{1u}			T_x, T_{3u}	M_{yz}, M^α_{4v}	$m'mm$	[100]
															T_y, T_{3v}	M_{zx}, M^α_{4u}	$mm'm$	[100]
E_{2u} 2	−1	−1	2	0	0	−2	1	1	−2	0	0	E^+_{2u}	Q_{xyz}	$G_v, G^{\beta1}_{4u}, G^{\beta2}_{4u}$			$2221'$	[100]
													Q^β_z	$G_{xy}, G^{\beta1}_{4v}, G^{\beta2}_{4v}$			$mm21'$	[100]
												E^-_{2u}			T_{xyz}	$M_v, M^{\beta1}_{4u}, M^{\beta2}_{4u}$	$m'm'm'$	[100]
															T^β_z	$M_{xy}, M^{\beta1}_{4v}, M^{\beta2}_{4v}$	mmm'	[100]

[1]We partially revised the classification from Ref. [104] to follow the standard character table of D_{3h}.

Table C.6: IRREPs of four types of multipoles in $6221'$. The superscript "$\pm$" of IRREP stands for the parity with respect to the antiunitary operation $\mathcal{A}=\theta$.

	E	$2C_6$	$2C_3$	C_2	$3C_{2x}$	$3C_{2y}$	IRREP	E	ET	MT	M	MPG	P. axis
A_1	1	1	1	1	1	1	A_1^+	Q_0, Q_u, Q_{40}	G_0, G_u, G_{40}			$6221'$	[001]
							A_1^-			T_0, T_u, T_{40}	M_0, M_u, M_{40}	622	[001]
A_2	1	1	1	1	-1	-1	A_2^+	Q_z, Q_z^α	G_z, G_z^α			$61'$	[001]
							A_2^-			T_z, T_z^α	M_z, M_z^α	$62'2'$	[001]
B_1	1	-1	1	-1	1	-1	B_1^+	Q_{3a}, Q_{4a}	G_{3a}, G_{4a}			$321'$	[001]
							B_1^-			T_{3a}, T_{4a}	M_{3a}, M_{4a}	$6'22'$	[001]
B_2	1	-1	1	-1	-1	1	B_2^+	Q_{3b}, Q_{4b}	G_{3b}, G_{4b}			$321'$	[001]
							B_2^-			T_{3b}, T_{4b}	M_{3b}, M_{4b}	$6'2'2$	[001]
E_1	2	1	-1	-2	0	0	E_1^+	$Q_x, Q_{yz},$ Q_{3u}, Q_{4v}^α	$G_x, G_{yz},$ G_{3u}, G_{4v}^α			$21'$	[100]
								$Q_y, Q_{zx},$ Q_{3v}, Q_{4u}^α	$G_y, G_{zx},$ G_{3v}, G_{4u}^α			$21'$	[010]
							E_1^-			$T_x, T_{yz},$ T_{3u}, T_{4v}^α	$M_x, M_{yz},$ M_{3u}, M_{4v}^α	$22'2'$	[100]
										$T_y, T_{zx},$ T_{3v}, T_{4u}^α	$M_y, M_{zx},$ M_{3v}, M_{4u}^α	$2'22'$	[100]
E_2	2	-1	-1	2	0	0	E_2^+	$Q_v, Q_{xyz},$ $Q_{4u}^{\beta 1}, Q_{4u}^{\beta 2}$	$G_v, G_{xyz},$ $G_{4u}^{\beta 1}, G_{4u}^{\beta 2}$			$2221'$	[100]
								$Q_{xy}, Q_z^\beta,$ $Q_{4v}^{\beta 1}, Q_{4v}^{\beta 2}$	$G_{xy}, G_z^\beta,$ $G_{4v}^{\beta 1}, G_{4v}^{\beta 2}$			$21'$	[001]
							E_2^-			$T_v, T_{xyz},$ $T_{4u}^{\beta 1}, T_{4u}^{\beta 2}$	$M_v, M_{xyz},$ $M_{4u}^{\beta 1}, M_{4u}^{\beta 2}$	222	[100]
										$T_{xy}, T_z^\beta,$ $T_{4v}^{\beta 1}, T_{4v}^{\beta 2}$	$M_{xy}, M_z^\beta,$ $M_{4v}^{\beta 1}, M_{4v}^{\beta 2}$	$2'2'2$	[100]

Table C.7: IRREPs of four types of multipoles in $6mm1'$. The superscript "$\pm$" of IRREP stands for the parity with respect to the antiunitary operation $\mathcal{A}=\theta$.

	E	$2C_6$	$2C_3$	C_2	$3\sigma_y$	$3\sigma_x$	IRREP	E	ET	MT	M	MPG	P. axis
A_1	1	1	1	1	1	1	A_1^+	$Q_0, Q_z, Q_u, Q_z^\alpha, Q_{40}$				$6mm1'$	[001]
							A_1^-			$T_0, T_z, T_u, T_z^\alpha, T_{40}$		$6mm$	[001]
A_2	1	1	1	1	-1	-1	A_2^+		$G_0, G_z, G_u, G_z^\alpha, G_{40}$			$61'$	[001]
							A_2^-				$M_0, M_z, M_u, M_z^\alpha, M_{40}$	$6m'm'$	[001]
B_1	1	-1	1	-1	1	-1	B_1^+	Q_{3b}, Q_{4a}	G_{3a}, G_{4b}			$3m1'$	[001]
							B_1^-			T_{3b}, T_{4a}	M_{3a}, M_{4b}	$6'm'm$	[001]
B_2	1	-1	1	-1	-1	1	B_2^+	Q_{3a}, Q_{4b}	G_{3b}, G_{4a}			$3m1'$	[001]
							B_2^-			T_{3a}, T_{4b}	M_{3b}, M_{4a}	$6'mm'$	[001]
E_1	2	1	-1	-2	0	0	E_1^+	$Q_y, Q_{yz}, Q_{3v}, Q_{4v}^\alpha$	$G_x, G_{zx}, G_{3u}, G_{4u}^\alpha$			$m1'$	[100]
								$Q_x, Q_{zx}, Q_{3u}, Q_{4u}^\alpha$	$G_y, G_{yz}, G_{3v}, G_{4v}^\alpha$			$m1'$	[010]
							E_1^-			$T_y, T_{yz}, T_{3v}, T_{4v}^\alpha$	$M_x, M_{zx}, M_{3u}, M_{4u}^\alpha$	$mm'2'$	[100]
										$T_x, T_{zx}, T_{3u}, T_{4u}^\alpha$	$M_y, M_{yz}, M_{3v}, M_{4v}^\alpha$	$m'm2'$	[100]
E_2	2	-1	-1	2	0	0	E_2^+	$Q_v, Q_z^\beta, Q_{4u}^{\beta 1}, Q_{4u}^{\beta 2}$	$G_{xy}, G_{xyz}, G_{4v}^{\beta 1}, G_{4v}^{\beta 2}$			$mm21'$	[100]
								$Q_{xy}, Q_{xyz}, Q_{4v}^{\beta 1}, Q_{4v}^{\beta 2}$	$G_v, G_z^\beta, G_{4u}^{\beta 1}, G_{4u}^{\beta 2}$			$21'$	[001]
							E_2^-			$T_v, T_z^\beta, T_{4u}^{\beta 1}, T_{4u}^{\beta 2}$	$M_{xy}, M_{xyz}, M_{4v}^{\beta 1}, M_{4v}^{\beta 2}$	$mm2$	[100]
										$T_{xy}, T_{xyz}, T_{4v}^{\beta 1}, T_{4v}^{\beta 2}$	$M_v, M_z^\beta, M_{4u}^{\beta 1}, M_{4u}^{\beta 2}$	$m'm'2$	[100]

Table C.8: IRREPs of four types of multipoles in $\bar{6}m21'$[1]. The superscript "±" of IRREP stands for the parity with respect to the antiunitary operation $\mathcal{A}=\theta$.

E	$2IC_6$	$2C_3$	σ_h	$3C_{2y}$	$3\sigma_x$	IRREP	E	ET	MT	M	MPG	P. axis
A_1' 1	1	1	1	1	1	$A_1'^+$	Q_0, Q_u, Q_{3b}, Q_{40}	G_{4b}			$\bar{6}m21'$	[001]
						$A_1'^-$			T_0, T_u, T_{3b}, T_{40}	M_{4b}	$\bar{6}m2$	[001]
A_2' 1	1	1	1	−1	−1	$A_2'^+$	Q_{3a}	G_z, G_z^α, G_{4a}			$\bar{6}1'$	[001]
						$A_2'^-$			T_{3a}	M_z, M_z^α, M_{4a}	$\bar{6}m'2'$	[001]
A_1'' 1	−1	1	−1	1	−1	$A_1''^+$	Q_{4b}	G_0, G_u, G_{3b}, G_{40}			$321'$	[001]
						$A_1''^-$			T_{4b}	M_0, M_u, M_{3b}, M_{40}	$\bar{6}'m'2$	[001]
A_2'' 1	−1	1	−1	−1	1	$A_2''^+$	Q_z, Q_z^α, Q_{4a}	G_{3a}			$3m1'$	[001]
						$A_2''^-$			T_z, T_z^α, T_{4a}	M_{3a}	$\bar{6}'m2'$	[001]
E'' 2	1	−1	−2	0	0	E''^+	$Q_{yz}, Q_z^\beta, Q_{4v}^\alpha$	$G_x, G_{xy}, G_{3u}, G_{4v}^{\beta 1}, G_{4v}^{\beta 2}$			$m1'$	[100]
							$Q_{zx}, Q_{xyz}, Q_{4u}^\alpha$	$G_y, G_v, G_{3v}, G_{4u}^{\beta 1}, G_{4u}^{\beta 2}$			$21'$	[010]
						E''^-			$T_{yz}, T_z^\beta, T_{4v}^\alpha$	$M_x, M_{xy}, M_{3u}, M_{4v}^{\beta 1}, M_{4v}^{\beta 2}$	$m2'm'$	[100]
									$T_{zx}, T_{xyz}, T_{4u}^\alpha$	$M_y, M_v, M_{3v}, M_{4u}^{\beta 1}, M_{4u}^{\beta 2}$	$m'2m'$	[100]
E' 2	−1	−1	2	0	0	E'^+	Q_y, Q_v, Q_{3v} $Q_{4u}^{\beta 1}, Q_{4u}^{\beta 2}$	$G_{zx}, G_{xyz}, G_{4u}^\alpha$			$m2m1'$	[100]
							Q_x, Q_{xy}, Q_{3u} $Q_{4v}^{\beta 1}, Q_{4v}^{\beta 2}$	$G_{yz}, G_z^\beta, G_{4v}^\alpha$			$m1'$	[001]
						E'^-			T_y, T_v, T_{3v} $T_{4u}^{\beta 1}, T_{4u}^{\beta 2}$	$M_{zx}, M_{xyz}, M_{4u}^\alpha$	$m2m$	[100]
									T_x, T_{xy}, T_{3u} $T_{4v}^{\beta 1}, T_{4v}^{\beta 2}$	$M_{yz}, M_z^\beta, M_{4v}^\alpha$	$m'2'm$	[100]

Table C.9: IRREPs of four types of multipoles in $6/m1'$. The superscript "$\pm$" of IRREP stands for the parity with respect to the antiunitary operation $\mathcal{A}=\theta$.

	E	C_6	C_3	C_2	C_3^2	C_6^5	I	IC_6	IC_3	σ_h	IC_3^2	IC_6^5	IRREP	E	ET	MT	M	MPG	P. axis
A_g	1	1	1	1	1	1	1	1	1	1	1	1	A_g^+	Q_0, Q_u, Q_{40}	G_z, G_z^α			$6/m1'$	[001]
													A_g^-			T_0, T_u, T_{40}	M_z, M_z^α	$6/m$	[001]
B_g	1	−1	1	−1	1	−1	1	−1	1	−1	1	−1	B_g^+	Q_{4a}, Q_{4b}	G_{3a}, G_{3b}			$\bar{3}1'$	[001]
													B_g^-			T_{4a}, T_{4b}	M_{3a}, M_{3b}	$6'/m'$	[001]
E_{1g}	1	$-\omega$	ω^2	−1	ω	$-\omega^2$	1	$-\omega$	ω^2	−1	ω	$-\omega^2$	E_{1g}	Q_{yz}, Q_{4v}^α	G_x, G_{3u}			$\bar{1}1'$	—
	1	$-\omega^2$	ω	−1	ω^2	$-\omega$	1	$-\omega^2$	ω	−1	ω^2	$-\omega$		Q_{zx}, Q_{4u}^α	G_y, G_{3v}			$\bar{1}1'$	—
																T_{yz}, T_{4v}^α	M_x, M_{3u}	$2'/m'$	[001]
																T_{zx}, T_{4u}^α	M_y, M_{3v}	$2'/m'$	[001]
E_{2g}	1	ω	ω^2	1	ω	ω^2	1	ω	ω^2	1	ω	ω^2	E_{2g}	$Q_v, Q_{4u}^{\beta1}, Q_{4u}^{\beta2}$	G_{xyz}			$2/m1'$	[001]
	1	ω^2	ω	1	ω^2	ω	1	ω^2	ω	1	ω^2	ω		$Q_{xy}, Q_{4v}^{\beta1}, Q_{4v}^{\beta2}$	G_z^β			$2/m1'$	[001]
																$T_v, T_{4u}^{\beta1}, T_{4u}^{\beta2}$	M_{xyz}	$2/m$	[001]
																$T_{xy}, T_{4v}^{\beta1}, T_{4v}^{\beta2}$	M_z^β	$2/m$	[001]
A_u	1	1	1	1	1	1	−1	−1	−1	−1	−1	−1	A_u^+	Q_z, Q_z^α	G_0, G_u, G_{40}			$61'$	[001]
													A_u^-			T_z, T_z^α	M_0, M_u, M_{40}	$6/m'$	[001]
B_u	1	−1	1	−1	1	−1	−1	1	−1	1	−1	1	B_u^+	Q_{3a}, Q_{3b}	G_{4a}, G_{4b}			$\bar{6}1'$	[001]
													B_u^-			T_{3a}, T_{3b}	M_{4a}, M_{4b}	$6'/m$	[001]
E_{1u}	1	$-\omega$	ω^2	−1	ω	$-\omega^2$	−1	ω	$-\omega^2$	1	$-\omega$	ω^2	E_{1u}	Q_x, Q_{3u}	G_{yz}, G_{4v}^α			$m1'$	[001]
	1	$-\omega^2$	ω	−1	ω^2	$-\omega$	−1	ω^2	$-\omega$	1	$-\omega^2$	ω		Q_y, Q_{3v}	G_{zx}, G_{4u}^α			$m1'$	[001]
																T_x, T_{3u}	M_{yz}, M_{4v}^α	$2'/m$	[001]
																T_y, T_{3v}	M_{zx}, M_{4u}^α	$2'/m$	[001]
E_{2u}	1	ω	ω^2	1	ω	ω^2	−1	$-\omega$	$-\omega^2$	−1	$-\omega$	$-\omega^2$	E_{2u}	Q_{xyz}	$G_v, G_{4u}^{\beta1}, G_{4u}^{\beta2}$			$21'$	[001]
	1	ω^2	ω	1	ω^2	ω	−1	$-\omega^2$	$-\omega$	−1	$-\omega^2$	$-\omega$		Q_z^β	$G_{xy}, G_{4v}^{\beta1}, G_{4v}^{\beta2}$			$21'$	[001]
																T_{xyz}	$M_v, M_{4u}^{\beta1}, M_{4u}^{\beta2}$	$2/m'$	[001]
																T_z^β	$M_{xy}, M_{4v}^{\beta1}, M_{4v}^{\beta2}$	$2/m'$	[001]

ω=exp($-2\pi i/3$)

Table C.10: IRREPs of four types of multipoles in $61'$. The superscript "$\pm$" of IRREP stands for the parity with respect to the antiunitary operation $\mathcal{A}=\theta$.

	E	C_6	C_3	C_2	C_3^2	C_6^5	IRREP	E	ET	MT	M	MPG	P. axis
A	1	1	1	1	1	1	A^+	$Q_0, Q_z, Q_u,$ Q_z^α, Q_{40}	$G_0, G_z, G_u,$ G_z^α, G_{40}			$61'$	[001]
							A^-			$T_0, T_z, T_u,$ T_z^α, T_{40}	$M_0, M_z, M_u,$ M_z^α, M_{40}	6	[001]
B	1	-1	1	-1	1	-1	B^+	$Q_{3a}, Q_{3b},$ Q_{4a}, Q_{4b}	$G_{3a}, G_{3b},$ G_{4a}, G_{4b}			$31'$	[001]
							B^-			$T_{3a}, T_{3b},$ T_{4a}, T_{4b}	$M_{3a}, M_{3b},$ M_{4a}, M_{4b}	$6'$	[001]
E_1	1	$-\omega$	ω^2	-1	ω	$-\omega^2$	E_1	$Q_x, Q_{yz},$ Q_{3u}, Q_{4v}^α	$G_x, G_{yz},$ G_{3u}, G_{4v}^α			$11'$	—
	1	$-\omega^2$	ω	-1	ω^2	$-\omega$		$Q_y, Q_{zx},$ Q_{3v}, Q_{4u}^α	$G_y, G_{zx},$ G_{3v}, G_{4u}^α			$11'$	—
										$T_x, T_{yz},$ T_{3u}, T_{4v}^α	$M_x, M_{yz},$ M_{3u}, M_{4v}^α	$2'$	[001]
										$T_y, T_{zx},$ T_{3v}, T_{4u}^α	$M_y, M_{zx},$ M_{3v}, M_{4u}^α	$2'$	[001]
E_2	1	ω	ω^2	1	ω	ω^2	E_2	$Q_v, Q_{xyz},$ $Q_{4u}^{\beta 1}, Q_{4u}^{\beta 2}$	$G_v, G_{xyz},$ $G_{4u}^{\beta 1}, G_{4u}^{\beta 2}$			$21'$	[001]
	1	ω^2	ω	1	ω^2	ω		$Q_{xy}, Q_z^\beta,$ $Q_{4v}^{\beta 1}, Q_{4v}^{\beta 2}$	$G_{xy}, G_z^\beta,$ $G_{4v}^{\beta 1}, G_{4v}^{\beta 2}$			$21'$	[001]
										$T_v, T_{xyz},$ $T_{4u}^{\beta 1}, T_{4u}^{\beta 2}$	$M_v, M_{xyz},$ $M_{4u}^{\beta 1}, M_{4u}^{\beta 2}$	2	[001]
										$T_{xy}, T_z^\beta,$ $T_{4v}^{\beta 1}, T_{4v}^{\beta 2}$	$M_{xy}, M_z^\beta,$ $M_{4v}^{\beta 1}, M_{4v}^{\beta 2}$	2	[001]

$\omega=\exp(-2\pi i/3)$

Table C.11: IRREPs of four types of multipoles in $\bar{6}1'$. The superscript "±" of IRREP stands for the parity with respect to the antiunitary operation $\mathcal{A}=\theta$.

E	IC_6	C_3	σ_h	C_3^2	IC_6^5	IRREP	E	ET	MT	M	MPG	P. axis
A′ 1	1	1	1	1	1	A′$^+$	$Q_0, Q_u,$ Q_{3a}, Q_{3b}, Q_{40}	$G_z, G_z^\alpha,$ G_{4a}, G_{4b}			$\bar{6}1'$	[001]
						A′$^-$			$T_0, T_u,$ T_{3a}, T_{3b}, T_{40}	$M_z, M_z^\alpha,$ M_{4a}, M_{4b}	$\bar{6}$	[001]
A″ 1	−1	1	−1	1	−1	A″$^+$	$Q_z, Q_z^\alpha,$ Q_{4a}, Q_{4b}	$G_0, G_u,$ G_{3a}, G_{3b}, G_{40}			$31'$	[001]
						A″$^-$			$T_z, T_z^\alpha,$ T_{4a}, T_{4b}	$M_0, M_u,$ M_{3a}, M_{3b}, M_{40}	$\bar{6}'$	[001]
E′ 1	ω	ω^2	1	ω	ω^2	E′	$Q_x, Q_v, Q_{3u},$ $Q_{4u}^{\beta1}, Q_{4u}^{\beta2}$	$G_{yz}, G_{xyz}, G_{4v}^\alpha$			$m1'$	[001]
1	ω^2	ω	1	ω^2	ω		$Q_y, Q_{xy}, Q_{3v},$ $Q_{4v}^{\beta1}, Q_{4v}^{\beta2}$	$G_{zx}, G_z^\beta, G_{4u}^\alpha$			$m1'$	[001]
									$T_x, T_v, T_{3u},$ $T_{4u}^{\beta1}, T_{4u}^{\beta2}$	$M_{yz}, M_{xyz}, M_{4v}^\alpha$	m	[001]
									$T_y, T_{xy}, T_{3v},$ $T_{4v}^{\beta1}, T_{4v}^{\beta2}$	$M_{zx}, M_z^\beta, M_{4u}^\alpha$	m	[001]
E″ 1	$-\omega$	ω^2	−1	ω	$-\omega^2$	E″	$Q_{yz}, Q_{xyz}, Q_{4v}^\alpha$	$G_x, G_v, G_{3u},$ $G_{4u}^{\beta1}, G_{4u}^{\beta2}$			$11'$	—
1	$-\omega^2$	ω	−1	ω^2	$-\omega$		$Q_{zx}, Q_z^\beta, Q_{4u}^\alpha$	$G_y, G_{xy}, G_{3v},$ $G_{4v}^{\beta1}, G_{4v}^{\beta2}$			$11'$	—
									$T_{yz}, T_{xyz}, T_{4v}^\alpha$	$M_x, M_v, M_{3u},$ $M_{4u}^{\beta1}, M_{4u}^{\beta2}$	m'	[001]
									$T_{zx}, T_z^\beta, T_{4u}^\alpha$	$M_y, M_{xy}, M_{3v},$ $M_{4v}^{\beta1}, M_{4v}^{\beta2}$	m'	[001]

ω=exp$(-2\pi i/3)$

Table C.12: IRREPs of four types of multipoles in $\bar{3}m1'$. The superscript "±" of IRREP stands for the parity with respect to the antiunitary operation $\mathcal{A}=\theta$.

	E	$2C_3$	$3C_{2y}$	I	$2IC_3$	$3\sigma_y$	IRREP	E	ET	MT	M	MPG	P. axis
A_{1g}	1	1	1	1	1	1	A_{1g}^+	$Q_0, Q_u,$ Q_{40}, Q_{4b}	G_{3b}			$\bar{3}m1'$	[001]
							A_{1g}^-			$T_0, T_u,$ T_{40}, T_{4b}	M_{3b}	$\bar{3}m$	[001]
A_{2g}	1	1	−1	1	1	−1	A_{2g}^+	Q_{4a}	G_z, G_z^α, G_{3a}			$\bar{3}1'$	[001]
							A_{2g}^-			T_{4a}	M_z, M_z^α, M_{3a}	$\bar{3}m'$	[001]
E_g	2	−1	0	2	−1	0	E_g^+	$Q_{yz}, Q_{xy},$ $Q_{4v}^\alpha, Q_{4v}^{\beta 1}, Q_{4v}^{\beta 2}$	G_x, G_{3u}, G_z^β			$\bar{1}1'$	—
								$Q_{zx}, Q_v,$ $Q_{4u}^\alpha, Q_{4u}^{\beta 1}, Q_{4u}^{\beta 2}$	G_y, G_{3v}, G_{xyz}			$2/m1'$	[010]
							E_g^-			$T_{yz}, T_{xy},$ $T_{4v}^\alpha, T_{4v}^{\beta 1}, T_{4v}^{\beta 2}$	M_x, M_{3u}, M_z^β	$2'/m'$	[010]
										$T_{zx}, T_v,$ $T_{4u}^\alpha, T_{4u}^{\beta 1}, T_{4u}^{\beta 2}$	M_y, M_{3v}, M_{xyz}	$2/m$	[010]
A_{1u}	1	1	1	−1	−1	−1	A_{1u}^+	Q_{3b}	$G_0, G_u,$ G_{40}, G_{4b}			$321'$	[001]
							A_{1u}^-			T_{3b}	$M_0, M_u,$ M_{40}, M_{4b}	$\bar{3}'m'$	[001]
A_{2u}	1	1	−1	−1	−1	1	A_{2u}^+	Q_z, Q_z^α, Q_{3a}	G_{4a}			$3m1'$	[001]
							A_{2u}^-			T_z, T_z^α, T_{3a}	M_{4a}	$\bar{3}'m$	[001]
E_u	2	−1	0	−2	1	0	E_u^+	Q_x, Q_{3u}, Q_z^β	$G_{yz}, G_{xy},$ $G_{4v}^\alpha, G_{4v}^{\beta 1}, G_{4v}^{\beta 2}$			$m1'$	[010]
								Q_y, Q_{3v}, Q_{xyz}	$G_{zx}, G_v,$ $G_{4u}^\alpha, G_{4u}^{\beta 1}, G_{4u}^{\beta 2}$			$21'$	[010]
							E_u^-			T_x, T_{3u}, T_z^β	$M_{yz}, M_{xy},$ $M_{4v}^\alpha, M_{4v}^{\beta 1}, M_{4v}^{\beta 2}$	$2'/m$	[010]
										T_y, T_{3v}, T_{xyz}	$M_{zx}, M_v,$ $M_{4u}^\alpha, M_{4u}^{\beta 1}, M_{4u}^{\beta 2}$	$2/m'$	[010]

Table C.13: IRREPs of four types of multipoles in $321'$. The superscript "±" of IRREP stands for the parity with respect to the antiunitary operation $\mathcal{A}=\theta$.

	E	$2C_3$	$3C_{2y}$	IRREP	E	ET	MT	M	MPG	P. axis
A_1	1	1	1	A_1^+	$Q_0, Q_u, Q_{3b},$ Q_{40}, Q_{4b}	$G_0, G_u, G_{3b},$ G_{40}, G_{4b}			$321'$	[001]
				A_1^-			$T_0, T_u, T_{3b},$ T_{40}, T_{4b}	$M_0, M_u, M_{3b},$ M_{40}, M_{4b}	32	[001]
A_2	1	1	−1	A_2^+	$Q_z, Q_z^\alpha, Q_{3a}, Q_{4a}$	$G_z, G_z^\alpha, G_{3a}, G_{4a}$			$31'$	[001]
				A_2^-			$T_z, T_z^\alpha, T_{3a}, T_{4a}$	$M_z, M_z^\alpha, M_{3a}, M_{4a}$	$32'$	[001]
E	2	−1	0	E^+	$Q_x, Q_{yz}, Q_{xy}, Q_{3u},$ $Q_z^\beta, Q_{4v}^\alpha, Q_{4v}^{\beta 1}, Q_{4v}^{\beta 2}$	$G_x, G_{yz}, G_{xy}, G_{3u},$ $G_z^\beta, G_{4v}^\alpha, G_{4v}^{\beta 1}, G_{4v}^{\beta 2}$			$11'$	—
					$Q_y, Q_{zx}, Q_v, Q_{3v},$ $Q_{xyz}, Q_{4u}^\alpha, Q_{4u}^{\beta 1}, Q_{4u}^{\beta 2}$	$G_y, G_{zx}, G_v, G_{3v},$ $G_{xyz}, G_{4u}^\alpha, G_{4u}^{\beta 1}, G_{4u}^{\beta 2}$			$21'$	[010]
				E^-			$T_x, T_{yz}, T_{xy}, T_{3u},$ $T_z^\beta, T_{4v}^\alpha, T_{4v}^{\beta 1}, T_{4v}^{\beta 2}$	$M_x, M_{yz}, M_{xy}, M_{3u},$ $M_z^\beta, M_{4v}^\alpha, M_{4v}^{\beta 1}, M_{4v}^{\beta 2}$	$2'$	[010]
							$T_y, T_{zx}, T_v, T_{3v},$ $T_{xyz}, T_{4u}^\alpha, T_{4u}^{\beta 1}, T_{4u}^{\beta 2}$	$M_y, M_{zx}, M_v, M_{3v},$ $M_{xyz}, M_{4u}^\alpha, M_{4u}^{\beta 1}, M_{4u}^{\beta 2}$	2	[010]

Table C.14: IRREPs of four types of multipoles in $3m1'$. The superscript "±" of IRREP stands for the parity with respect to the antiunitary operation $\mathcal{A}=\theta$.

E	$2C_3$	$3\sigma_y$	IRREP	E	ET	MT	M	MPG	P. axis
1	1	1	A_1^+	$Q_0, Q_z, Q_u, Q_z^\alpha, Q_{3a}, Q_{40}, Q_{4b}$	G_{3b}, G_{4a}			$3m1'$	[001]
			A_1^-			$T_0, T_z, T_u, T_z^\alpha, T_{3a}, T_{40}, T_{4b}$	M_{3b}, M_{4a}	$3m$	[001]
1	1	−1	A_2^+	Q_{3b}, Q_{4a}	$G_0, G_z, G_u, G_z^\alpha, G_{3a}, G_{40}, G_{4b}$			$31'$	[001]
			A_2^-			T_{3b}, T_{4a}	$M_0, M_z, M_u, M_z^\alpha, M_{3a}, M_{40}, M_{4b}$	$3m'$	[001]
2	−1	0	E^+	$Q_y, Q_{yz}, Q_{xy}, Q_{3v}, Q_{xyz}, Q_{4v}^\alpha, Q_{4v}^{\beta1}, Q_{4v}^{\beta2}$	$G_x, G_{zx}, G_v, G_{3u}, G_z^\beta, G_{4u}^\alpha, G_{4u}^{\beta1}, G_{4u}^{\beta2}$			$11'$	—
				$Q_x, Q_{zx}, Q_v, Q_{3u}, Q_z^\beta, Q_{4u}^\alpha, Q_{4u}^{\beta1}, Q_{4u}^{\beta2}$	$G_y, G_{yz}, G_{xy}, G_{3v}, G_{xyz}, G_{4v}^\alpha, G_{4v}^{\beta1}, G_{4v}^{\beta2}$			$m1'$	[010]
			E^-			$T_y, T_{yz}, T_{xy}, T_{3v}, T_{xyz}, T_{4v}^\alpha, T_{4v}^{\beta1}, T_{4v}^{\beta2}$	$M_x, M_{zx}, M_v, M_{3u}, M_z^\beta, M_{4u}^\alpha, M_{4u}^{\beta1}, M_{4u}^{\beta2}$	m'	[010]
						$T_x, T_{zx}, T_v, T_{3u}, T_z^\beta, T_{4u}^\alpha, T_{4u}^{\beta1}, T_{4u}^{\beta2}$	$M_y, M_{yz}, M_{xy}, M_{3v}, M_{xyz}, M_{4v}^\alpha, M_{4v}^{\beta1}, M_{4v}^{\beta2}$	m	[010]

Table C.15: IRREPs of four types of multipoles in $\bar{3}1'$. The superscript "±" of IRREP stands for the parity with respect to the antiunitary operation $\mathcal{A}=\theta$.

E	C_3	C_3^2	I	IC_3	IC_3^2	IRREP	E	ET	MT	M	MPG	P. axis
1	1	1	1	1	1	A_g^+	$Q_0, Q_u, Q_{40}, Q_{4a}, Q_{4b}$	$G_z, G_z^\alpha, G_{3a}, G_{3b}$			$\bar{3}1'$	[001]
						A_g^-			$T_0, T_u, T_{40}, T_{4a}, T_{4b}$	$M_z, M_z^\alpha, M_{3a}, M_{3b}$	$\bar{3}$	[001]
1	ω	ω^2	1	ω	ω^2	E_g	$Q_{yz}, Q_{xy}, Q_{4v}^\alpha, Q_{4v}^{\beta1}, Q_{4v}^{\beta2}$	G_x, G_{3u}, G_z^β			$\bar{1}1'$	—
1	ω^2	ω	1	ω^2	ω		$Q_{zx}, Q_v, Q_{4u}^\alpha, Q_{4u}^{\beta1}, Q_{4u}^{\beta2}$	G_y, G_{3v}, G_{xyz}			$\bar{1}1'$	—
									$T_{yz}, T_{xy}, T_{4v}^\alpha, T_{4v}^{\beta1}, T_{4v}^{\beta2}$	M_x, M_{3u}, M_z^β	$\bar{1}$	—
									$T_{zx}, T_v, T_{4u}^\alpha, T_{4u}^{\beta1}, T_{4u}^{\beta2}$	M_y, M_{3v}, M_{xyz}	$\bar{1}$	—
1	1	1	−1	−1	−1	A_u^+	$Q_z, Q_z^\alpha, Q_{3a}, Q_{3b}$	$G_0, G_u, G_{40}, G_{4a}, G_{4b}$			$31'$	[001]
						A_u^-			$T_z, T_z^\alpha, T_{3a}, T_{3b}$	$M_0, M_u, M_{40}, M_{4a}, M_{4b}$	$\bar{3}'$	[001]
1	ω	ω^2	−1	$-\omega$	$-\omega^2$	E_u	Q_x, Q_{3u}, Q_z^β	$G_{yz}, G_{xy}, G_{4v}^\alpha, G_{4v}^{\beta1}, G_{4v}^{\beta2}$			$11'$	—
1	ω^2	ω	−1	$-\omega^2$	$-\omega$		Q_y, Q_{3v}, Q_{xyz}	$G_{zx}, G_v, G_{4u}^\alpha, G_{4u}^{\beta1}, G_{4u}^{\beta2}$			$11'$	—
									T_x, T_{3u}, T_z^β	$M_{yz}, M_{xy}, M_{4v}^\alpha, M_{4v}^{\beta1}, M_{4v}^{\beta2}$	$\bar{1}'$	—
									T_y, T_{3v}, T_{xyz}	$M_{zx}, M_v, M_{4u}^\alpha, M_{4u}^{\beta1}, M_{4u}^{\beta2}$	$\bar{1}'$	—

ω=exp($-2\pi i/3$)

Table C.16: IRREPs of four types of multipoles in $31'$. The superscript "$\pm$" of IRREP stands for the parity with respect to the antiunitary operation $\mathcal{A}=\theta$.

$E\ C_3\ C_3^2$	IRREP	E	ET	MT	M	MPG	P. axis
A 1 1 1	A^+	$Q_0, Q_z, Q_u,$ $Q_z^\alpha, Q_{3a}, Q_{3b},$ Q_{40}, Q_{4a}, Q_{4b}	$G_0, G_z, G_u,$ $G_z^\alpha, G_{3a}, G_{3b},$ G_{40}, G_{4a}, G_{4b}			$31'$	[001]
	A^-			$T_0, T_z, T_u,$ $T_z^\alpha, T_{3a}, T_{3b},$ T_{40}, T_{4a}, T_{4b}	$M_0, M_z, M_u,$ $M_z^\alpha, M_{3a}, M_{3b},$ M_{40}, M_{4a}, M_{4b}	3	[001]
E 1 ω ω^2 1 ω^2 ω	E	$Q_x, Q_{yz}, Q_{xy}, Q_{3u},$ $Q_z^\beta, Q_{4v}^\alpha, Q_{4v}^{\beta 1}, Q_{4v}^{\beta 2}$	$G_x, G_{yz}, G_{xy}, G_{3u},$ $G_z^\beta, G_{4v}^\alpha, G_{4v}^{\beta 1}, G_{4v}^{\beta 2}$			$11'$	—
		$Q_y, Q_{zx}, Q_v, Q_{3v},$ $Q_{xyz}, Q_{4u}^\alpha, Q_{4u}^{\beta 1}, Q_{4u}^{\beta 2}$	$G_y, G_{zx}, G_v, G_{3v},$ $G_{xyz}, G_{4u}^\alpha, G_{4u}^{\beta 1}, G_{4u}^{\beta 2}$			$11'$	—
				$T_x, T_{yz}, T_{xy}, T_{3u},$ $T_z^\beta, T_{4v}^\alpha, T_{4v}^{\beta 1}, T_{4v}^{\beta 2}$	$M_x, M_{yz}, M_{xy}, M_{3u},$ $M_z^\beta, M_{4v}^\alpha, M_{4v}^{\beta 1}, M_{4v}^{\beta 2}$	1	—
				$T_y, T_{zx}, T_v, T_{3v},$ $T_{xyz}, T_{4u}^\alpha, T_{4u}^{\beta 1}, T_{4u}^{\beta 2}$	$M_y, M_{zx}, M_v, M_{3v},$ $M_{xyz}, M_{4u}^\alpha, M_{4u}^{\beta 1}, M_{4u}^{\beta 2}$	1	—

$\omega=\exp(-2\pi i/3)$

Table C.17: IRREPs of four types of multipoles in $4/mmm1'$. The superscript "±" of IRREP stands for the parity with respect to the antiunitary operation $\mathcal{A}=\theta$.

	E	$2C_4$	C_4^2	$2C_2'$	$2C_2''$	I	$2IC_4$	σ_h	$2\sigma_v$	$2\sigma_d$	IRREP	E	ET	MT	M	MPG	P. axis
A_{1g}	1	1	1	1	1	1	1	1	1	1	A_{1g}^+	$Q_0, Q_u,$ Q_4, Q_{4u}				$4/mmm1'$	[001]
											A_{1g}^-			$T_0, T_u,$ T_4, T_{4u}		$4/mmm$	[001]
A_{2g}	1	1	1	−1	−1	1	1	1	−1	−1	A_{2g}^+	Q_{4z}^α	G_z, G_z^α			$4/m1'$	[001]
											A_{2g}^-			T_{4z}^α	M_z, M_z^α	$4/mm'm'$	[001]
B_{1g}	1	−1	1	1	−1	1	−1	1	1	−1	B_{1g}^+	Q_v, Q_{4v}	G_{xyz}			$mmm1'$	[100]
											B_{1g}^-			T_v, T_{4v}	M_{xyz}	$4'/mmm'$	[001]
B_{2g}	1	−1	1	−1	1	1	−1	1	−1	1	B_{2g}^+	Q_{xy}, Q_{4z}^β	G_z^β			$mmm1'$	[110]
											B_{2g}^-			T_{xy}, T_{4z}^β	M_z^β	$4'/mm'm$	[001]
E_g	2	0	−2	0	0	2	0	−2	0	0	E_g^+	$Q_{yz},$ $Q_{4x}^\alpha, Q_{4x}^\beta$	$G_x,$ G_x^α, G_x^β			$2/m1'$	[100]
												$Q_{zx},$ $Q_{4y}^\alpha, Q_{4y}^\beta$	$G_y,$ G_y^α, G_y^β			$2/m1'$	[010]
											E_g^-			$T_{yz},$ $T_{4x}^\alpha, T_{4x}^\beta$	$M_x,$ M_x^α, M_x^β	$mm'm'$	[100]
														$T_{zx},$ $T_{4y}^\alpha, T_{4y}^\beta$	$M_y,$ M_y^α, M_y^β	$m'mm'$	[100]
A_{1u}	1	1	1	1	1	−1	−1	−1	−1	−1	A_{1u}^+		$G_0, G_u,$ G_4, G_{4u}			$4221'$	[001]
											A_{1u}^-				$M_0, M_u,$ M_4, M_{4u}	$4/m'm'm'$	[001]
A_{2u}	1	1	1	−1	−1	−1	−1	−1	1	1	A_{2u}^+	Q_z, Q_z^α	G_{4z}^α			$4mm1'$	[001]
											A_{2u}^-			T_z, T_z^α	M_{4z}^α	$4/m'mm$	[001]
B_{1u}	1	−1	1	1	−1	−1	1	−1	−1	1	B_{1u}^+	Q_{xyz}	G_v, G_{4v}			$\bar{4}2m1'$	[001]
											B_{1u}^-			T_{xyz}	M_v, M_{4v}	$4'/m'm'm$	[001]
B_{2u}	1	−1	1	−1	1	−1	1	−1	1	−1	B_{2u}^+	Q_z^β	G_{xy}, G_{4z}^β			$\bar{4}m21'$	[001]
											B_{2u}^-			T_z^β	M_{xy}, M_{4z}^β	$4'/m'mm'$	[001]
E_u	2	0	−2	0	0	−2	0	2	0	0	E_u^+	$Q_x,$ Q_x^α, Q_x^β	$G_{yz},$ $G_{4x}^\alpha, G_{4x}^\beta$			$2mm1'$	[100]
												$Q_y,$ Q_y^α, Q_y^β	$G_{zx},$ $G_{4y}^\alpha, G_{4y}^\beta$			$m2m1'$	[100]
											E_u^-			$T_x,$ T_x^α, T_x^β	$M_{yz},$ $M_{4x}^\alpha, M_{4x}^\beta$	$m'mm$	[100]
														$T_y,$ T_y^α, T_y^β	$M_{zx},$ $M_{4y}^\alpha, M_{4y}^\beta$	$mm'm$	[100]

Table C.18: IRREPs of four types of multipoles in $4221'$. The superscript "$\pm$" of IRREP stands for the parity with respect to the antiunitary operation $\mathcal{A}=\theta$.

E	$2C_4$	C_4^2	$2C_2'$	$2C_2''$	IRREP	E	ET	MT	M	MPG	P. axis
1	1	1	1	1	A_1^+	Q_0, Q_u, Q_4, Q_{4u}	G_0, G_u, G_4, G_{4u}			$4221'$	[001]
					A_1^-			T_0, T_u, T_4, T_{4u}	M_0, M_u, M_4, M_{4u}	422	[001]
1	1	1	-1	-1	A_2^+	$Q_z, Q_z^\alpha, Q_{4z}^\alpha$	$G_z, G_z^\alpha, G_{4z}^\alpha$			$41'$	[001]
					A_2^-			$T_z, T_z^\alpha, T_{4z}^\alpha$	$M_z, M_z^\alpha, M_{4z}^\alpha$	$42'2'$	[001]
1	-1	1	1	-1	B_1^+	Q_v, Q_{xyz}, Q_{4v}	G_v, G_{xyz}, G_{4v}			$2221'$	[100]
					B_1^-			T_v, T_{xyz}, T_{4v}	M_v, M_{xyz}, M_{4v}	$4'22'$	[001]
1	-1	1	-1	1	B_2^+	$Q_{xy}, Q_z^\beta, Q_{4z}^\beta$	$G_{xy}, G_z^\beta, G_{4z}^\beta$			$2221'$	[110]
					B_2^-			$T_{xy}, T_z^\beta, T_{4z}^\beta$	$M_{xy}, M_z^\beta, M_{4z}^\beta$	$4'2'2$	[001]
2	0	-2	0	0	E^+	$Q_x, Q_{yz},$ $Q_x^\alpha, Q_x^\beta, Q_{4x}^\alpha, Q_{4x}^\beta$	$G_x, G_{yz},$ $G_x^\alpha, G_x^\beta, G_{4x}^\alpha, G_{4x}^\beta$			$21'$	[100]
						$Q_y, Q_{zx},$ $Q_y^\alpha, Q_y^\beta, Q_{4y}^\alpha, Q_{4y}^\beta$	$G_y, G_{zx},$ $G_y^\alpha, G_y^\beta, G_{4y}^\alpha, G_{4y}^\beta$			$21'$	[010]
					E^-			$T_x, T_{yz},$ $T_x^\alpha, T_x^\beta, T_{4x}^\alpha, T_{4x}^\beta$	$M_x, M_{yz},$ $M_x^\alpha, M_x^\beta, M_{4x}^\alpha, M_{4x}^\beta$	$22'2'$	[100]
								$T_y, T_{zx},$ $T_y^\alpha, T_y^\beta, T_{4y}^\alpha, T_{4y}^\beta$	$M_y, M_{zx},$ $M_y^\alpha, M_y^\beta, M_{4y}^\alpha, M_{4y}^\beta$	$2'22'$	[100]

Table C.19: IRREPs of four types of multipoles in $4mm1'$. The superscript "$\pm$" of IRREP stands for the parity with respect to the antiunitary operation $\mathcal{A}=\theta$.

E	$2C_4$	C_4^2	$2\sigma_v$	$2\sigma_d$	IRREP	E	ET	MT	M	MPG	P. axis
1	1	1	1	1	A_1^+	$Q_0, Q_z, Q_u,$ Q_z^α, Q_4, Q_{4u}	G_{4z}^α			$4mm1'$	[001]
					A_1^-			$T_0, T_z, T_u,$ T_z^α, T_4, T_{4u}	M_{4z}^α	$4mm$	[001]
1	1	1	-1	-1	A_2^+	Q_{4z}^α	$G_0, G_z, G_u,$ G_z^α, G_4, G_{4u}			$41'$	[001]
					A_2^-			T_{4z}^α	$M_0, M_z, M_u,$ M_z^α, M_4, M_{4u}	$4m'm'$	[001]
1	-1	1	1	-1	B_1^+	Q_v, Q_z^β, Q_{4v}	$G_{xy}, G_{xyz}, G_{4z}^\beta$			$mm21'$	[100]
					B_1^-			T_v, T_z^β, T_{4v}	$M_{xy}, M_{xyz}, M_{4z}^\beta$	$4'mm'$	[001]
1	-1	1	-1	1	B_2^+	$Q_{xy}, Q_{xyz}, Q_{4z}^\beta$	G_v, G_z^β, G_{4v}			$mm21'$	[110]
					B_2^-			$T_{xy}, T_{xyz}, T_{4z}^\beta$	M_v, M_z^β, M_{4v}	$4'm'm$	[001]
2	0	-2	0	0	E^+	$Q_y, Q_{yz},$ $Q_y^\alpha, Q_y^\beta, Q_{4x}^\alpha, Q_{4x}^\beta$	$G_x, G_{zx},$ $G_x^\alpha, G_x^\beta, G_{4y}^\alpha, G_{4y}^\beta$			$m1'$	[100]
						$Q_x, Q_{zx},$ $Q_x^\alpha, Q_x^\beta, Q_{4y}^\alpha, Q_{4y}^\beta$	$G_y, G_{yz},$ $G_y^\alpha, G_y^\beta, G_{4x}^\alpha, G_{4x}^\beta$			$m1'$	[010]
					E^-			$T_y, T_{yz},$ $T_y^\alpha, T_y^\beta, T_{4x}^\alpha, T_{4x}^\beta$	$M_x, M_{zx},$ $M_x^\alpha, M_x^\beta, M_{4y}^\alpha, M_{4y}^\beta$	$mm'2'$	[100]
								$T_x, T_{zx},$ $T_x^\alpha, T_x^\beta, T_{4y}^\alpha, T_{4y}^\beta$	$M_y, M_{yz},$ $M_y^\alpha, M_y^\beta, M_{4x}^\alpha, M_{4x}^\beta$	$m'm2'$	[100]

Table C.20: IRREPs of four types of multipoles in $\bar{4}2m1'$. The superscript "±" of IRREP stands for the parity with respect to the antiunitary operation $\mathcal{A}=\theta$.

E	$2IC_4$	C_4^2	$2C_2'$	$2\sigma_d$	IRREP	E	ET	MT	M	MPG	P. axis
A_1 1	1	1	1	1	A_1^+	$Q_0, Q_u,$ Q_{xyz}, Q_4, Q_{4u}	G_v, G_{4v}			$\bar{4}2m1'$	[001]
					A_1^-			$T_0, T_u,$ T_{xyz}, T_4, T_{4u}	M_v, M_{4v}	$\bar{4}2m$	[001]
A_2 1	1	1	−1	−1	A_2^+	Q_z^β, Q_{4z}^α	$G_z, G_{xy}, G_z^\alpha, G_{4z}^\beta$			$\bar{4}1'$	[001]
					A_2^-			T_z^β, T_{4z}^α	$M_z, M_{xy}, M_z^\alpha, M_{4z}^\beta$	$\bar{4}2'm'$	[001]
B_1 1	−1	1	1	−1	B_1^+	Q_v, Q_{4v}	$G_0, G_u,$ G_{xyz}, G_4, G_{4u}			$2221'$	[100]
					B_1^-			T_v, T_{4v}	$M_0, M_u,$ M_{xyz}, M_4, M_{4u}	$\bar{4}'2m'$	[001]
B_2 1	−1	1	−1	1	B_2^+	$Q_z, Q_{xy}, Q_z^\alpha, Q_{4z}^\beta$	G_z^β, G_{4z}^α			$mm21'$	[110]
					B_2^-			$T_z, T_{xy}, T_z^\alpha, T_{4z}^\beta$	M_z^β, M_{4z}^α	$\bar{4}'2'm$	[001]
E 2	0	−2	0	0	E^+	$Q_x, Q_{yz},$ $Q_x^\alpha, Q_x^\beta, Q_{4x}^\alpha, Q_{4x}^\beta$	$G_x, G_{yz},$ $G_x^\alpha, G_x^\beta, G_{4x}^\alpha, G_{4x}^\beta$			$21'$	[100]
						$Q_y, Q_{zx},$ $Q_y^\alpha, Q_y^\beta, Q_{4y}^\alpha, Q_{4y}^\beta$	$G_y, G_{zx},$ $G_y^\alpha, G_y^\beta, G_{4y}^\alpha, G_{4y}^\beta$			$21'$	[010]
					E^-			$T_x, T_{yz},$ $T_x^\alpha, T_x^\beta, T_{4x}^\alpha, T_{4x}^\beta$	$M_x, M_{yz},$ $M_x^\alpha, M_x^\beta, M_{4x}^\alpha, M_{4x}^\beta$	$22'2'$	[100]
								$T_y, T_{zx},$ $T_y^\alpha, T_y^\beta, T_{4y}^\alpha, T_{4y}^\beta$	$M_y, M_{zx},$ $M_y^\alpha, M_y^\beta, M_{4y}^\alpha, M_{4y}^\beta$	$2'22'$	[100]

Table C.21: IRREPs of four types of multipoles in $4/m1'$. The superscript "±" of IRREP stands for the parity with respect to the antiunitary operation $\mathcal{A}=\theta$.

E	C_4	C_4^2	C_4^3	I	$2IC_4$	σ_h	IC_4^3	IRREP	E	ET	MT	M	MPG	P. axis
A_g 1	1	1	1	1	1	1	1	A_g^+	$Q_0, Q_u,$ $Q_4, Q_{4u}, Q_{4z}^\alpha$	G_z, G_z^α			$4/m1'$	[001]
								A_g^-			$T_0, T_u,$ $T_4, T_{4u}, T_{4z}^\alpha$	M_z, M_z^α	$4/m$	[001]
B_g 1	−1	1	−1	1	−1	1	−1	B_g^+	$Q_v, Q_{xy},$ Q_{4v}, Q_{4z}^β	G_{xyz}, G_z^β			$2/m1'$	[001]
								B_g^-			$T_v, T_{xy},$ T_{4v}, T_{4z}^β	M_{xyz}, M_z^β	$4'/m$	[001]
E_g 1	$-i$	−1	i	1	$-i$	−1	i	E_g	$Q_{yz}, Q_{4x}^\alpha, Q_{4x}^\beta$	$G_x, G_x^\alpha, G_x^\beta$			$\bar{1}1'$	—
1	i	−1	$-i$	1	i	−1	$-i$		$Q_{zx}, Q_{4y}^\alpha, Q_{4y}^\beta$	$G_y, G_y^\alpha, G_y^\beta$			$\bar{1}1'$	—
											$T_{yz}, T_{4x}^\alpha, T_{4x}^\beta$	$M_x, M_x^\alpha, M_x^\beta$	$2'/m'$	[001]
											$T_{zx}, T_{4y}^\alpha, T_{4y}^\beta$	$M_y, M_y^\alpha, M_y^\beta$	$2'/m'$	[001]
A_u 1	1	1	1	−1	−1	−1	−1	A_u^+	Q_z, Q_z^α	$G_0, G_u,$ $G_4, G_{4u}, G_{4z}^\alpha$			$41'$	[001]
								A_u^-			T_z, T_z^α	$M_0, M_u,$ $M_4, M_{4u}, M_{4z}^\alpha$	$4/m'$	[001]
B_u 1	−1	1	−1	−1	1	−1	1	B_u^+	Q_{xyz}, Q_z^β	$G_v, G_{xy},$ G_{4v}, G_{4z}^β			$\bar{4}1'$	[001]
								B_u^-			T_{xyz}, T_z^β	$M_v, M_{xy},$ M_{4v}, M_{4z}^β	$4'/m'$	[001]
E_u 1	$-i$	−1	i	−1	i	1	$-i$	E_u	$Q_x, Q_x^\alpha, Q_x^\beta$	$G_{yz}, G_{4x}^\alpha, G_{4x}^\beta$			$m1'$	[001]
1	i	−1	$-i$	−1	$-i$	1	i		$Q_y, Q_y^\alpha, Q_y^\beta$	$G_{zx}, G_{4y}^\alpha, G_{4y}^\beta$			$m1'$	[001]
											$T_x, T_x^\alpha, T_x^\beta$	$M_{yz}, M_{4x}^\alpha, M_{4x}^\beta$	$2'/m$	[001]
											$T_y, T_y^\alpha, T_y^\beta$	$M_{zx}, M_{4y}^\alpha, M_{4y}^\beta$	$2'/m$	[001]

Table C.22: IRREPs of four types of multipoles in $41'$. The superscript "$\pm$" of IRREP stands for the parity with respect to the antiunitary operation $\mathcal{A}=\theta$.

E	C_4	C_4^2	C_4^3	IRREP	E	ET	MT	M	MPG	P. axis
1	1	1	1	A^+	$Q_0, Q_z, Q_u, Q_z^\alpha, Q_4, Q_{4u}, Q_{4z}^\alpha$	$G_0, G_z, G_u, G_z^\alpha, G_4, G_{4u}, G_{4z}^\alpha$			$41'$	[001]
				A^-			$T_0, T_z, T_u, T_z^\alpha, T_4, T_{4u}, T_{4z}^\alpha$	$M_0, M_z, M_u, M_z^\alpha, M_4, M_{4u}, M_{4z}^\alpha$	4	[001]
1	-1	1	-1	B^+	$Q_v, Q_{xy}, Q_{xyz}, Q_z^\beta, Q_{4v}, Q_{4z}^\beta$	$G_v, G_{xy}, G_{xyz}, G_z^\beta, G_{4v}, G_{4z}^\beta$			$21'$	[001]
				B^-			$T_v, T_{xy}, T_{xyz}, T_z^\beta, T_{4v}, T_{4z}^\beta$	$M_v, M_{xy}, M_{xyz}, M_z^\beta, M_{4v}, M_{4z}^\beta$	$4'$	[001]
1	$-i$	-1	i	E	$Q_x, Q_{yz}, Q_x^\alpha, Q_x^\beta, Q_{4x}^\alpha, Q_{4x}^\beta$	$G_x, G_{yz}, G_x^\alpha, G_x^\beta, G_{4x}^\alpha, G_{4x}^\beta$			$11'$	—
1	i	-1	$-i$		$Q_y, Q_{zx}, Q_y^\alpha, Q_y^\beta, Q_{4y}^\alpha, Q_{4y}^\beta$	$G_y, G_{zx}, G_y^\alpha, G_y^\beta, G_{4y}^\alpha, G_{4y}^\beta$			$11'$	—
							$T_x, T_{yz}, T_x^\alpha, T_x^\beta, T_{4x}^\alpha, T_{4x}^\beta$	$M_x, M_{yz}, M_x^\alpha, M_x^\beta, M_{4x}^\alpha, M_{4x}^\beta$	$2'$	[001]
							$T_y, T_{zx}, T_y^\alpha, T_y^\beta, T_{4y}^\alpha, T_{4y}^\beta$	$M_y, M_{zx}, M_y^\alpha, M_y^\beta, M_{4y}^\alpha, M_{4y}^\beta$	$2'$	[001]

Table C.23: IRREPs of four types of multipoles in $\bar{4}1'$. The superscript "$\pm$" of IRREP stands for the parity with respect to the antiunitary operation $\mathcal{A}=\theta$.

E	IC_4	C_4^2	IC_4^3	IRREP	E	ET	MT	M	MPG	P. axis
1	1	1	1	A^+	$Q_0, Q_u, Q_{xyz}, Q_z^\beta, Q_4, Q_{4u}, Q_{4z}^\alpha$	$G_z, G_v, G_{xy}, G_z^\alpha, G_{4v}, G_{4z}^\beta$			$\bar{4}1'$	[001]
				A^-			$T_0, T_u, T_{xyz}, T_z^\beta, T_4, T_{4u}, T_{4z}^\alpha$	$M_z, M_v, M_{xy}, M_z^\alpha, M_{4v}, M_{4z}^\beta$	$\bar{4}$	[001]
1	-1	1	-1	B^+	$Q_z, Q_v, Q_{xy}, Q_z^\alpha, Q_{4v}, Q_{4z}^\beta$	$G_0, G_u, G_{xyz}, G_z^\beta, G_4, G_{4u}, G_{4z}^\alpha$			$21'$	[001]
				B^-			$T_z, T_v, T_{xy}, T_z^\alpha, T_{4v}, T_{4z}^\beta$	$M_0, M_u, M_{xyz}, M_z^\beta, M_4, M_{4u}, M_{4z}^\alpha$	$\bar{4}'$	[001]
1	$-i$	-1	i	E	$Q_x, Q_{yz}, Q_x^\alpha, Q_x^\beta, Q_{4x}^\alpha, Q_{4x}^\beta$	$G_x, G_{yz}, G_x^\alpha, G_x^\beta, G_{4x}^\alpha, G_{4x}^\beta$			$11'$	—
1	i	-1	$-i$		$Q_y, Q_{zx}, Q_y^\alpha, Q_y^\beta, Q_{4y}^\alpha, Q_{4y}^\beta$	$G_y, G_{zx}, G_y^\alpha, G_y^\beta, G_{4y}^\alpha, G_{4y}^\beta$			$11'$	—
							$T_x, T_{yz}, T_x^\alpha, T_x^\beta, T_{4x}^\alpha, T_{4x}^\beta$	$M_x, M_{yz}, M_x^\alpha, M_x^\beta, M_{4x}^\alpha, M_{4x}^\beta$	$2'$	[001]
							$T_y, T_{zx}, T_y^\alpha, T_y^\beta, T_{4y}^\alpha, T_{4y}^\beta$	$M_y, M_{zx}, M_y^\alpha, M_y^\beta, M_{4y}^\alpha, M_{4y}^\beta$	$2'$	[001]

Table C.24: IRREPs of four types of multipoles in $mmm1'$. The superscript "±" of IRREP stands for the parity with respect to the antiunitary operation $\mathcal{A}=\theta$.

E	C_{2z}	C_{2y}	C_{2x}	I	σ_z	σ_y	σ_x	IRREP	E	ET	MT	M	MPG	P. axis
A_g 1	1	1	1	1	1	1	1	A_g^+	$Q_0, Q_u, Q_v,$ Q_4, Q_{4u}, Q_{4v}	G_{xyz}			$mmm1'$	[100]
								A_g^-			$T_0, T_u, T_v,$ T_4, T_{4u}, T_{4v}	M_{xyz}	mmm	[100]
B_{1g} 1	1	−1	−1	1	1	−1	−1	B_{1g}^+	$Q_{xy}, Q_{4z}^\alpha, Q_{4z}^\beta$	$G_z, G_z^\alpha, G_z^\beta$			$2/m1'$	[001]
								B_{1g}^-			$T_{xy}, T_{4z}^\alpha, T_{4z}^\beta$	$M_z, M_z^\alpha, M_z^\beta$	$m'm'm$	[100]
B_{2g} 1	−1	1	−1	1	−1	1	−1	B_{2g}^+	$Q_{zx}, Q_{4y}^\alpha, Q_{4y}^\beta$	$G_y, G_y^\alpha, G_y^\beta$			$2/m1'$	[010]
								B_{2g}^-			$T_{zx}, T_{4y}^\alpha, T_{4y}^\beta$	$M_y, M_y^\alpha, M_y^\beta$	$m'mm'$	[100]
B_{3g} 1	−1	−1	1	1	−1	−1	1	B_{3g}^+	$Q_{yz}, Q_{4x}^\alpha, Q_{4x}^\beta$	$G_x, G_x^\alpha, G_x^\beta$			$2/m1'$	[100]
								B_{3g}^-			$T_{yz}, T_{4x}^\alpha, T_{4x}^\beta$	$M_x, M_x^\alpha, M_x^\beta$	$mm'm'$	[100]
A_u 1	1	1	1	−1	−1	−1	−1	A_u^+	Q_{xyz}	$G_0, G_u, G_v,$ G_4, G_{4u}, G_{4v}			$2221'$	[100]
								A_u^-			T_{xyz}	$M_0, M_u, M_v,$ M_4, M_{4u}, M_{4v}	$m'm'm'$	[100]
B_{1u} 1	1	−1	−1	−1	−1	1	1	B_{1u}^+	$Q_z, Q_z^\alpha, Q_z^\beta$	$G_{xy}, G_{4z}^\alpha, G_{4z}^\beta$			$mm21'$	[100]
								B_{1u}^-			$T_z, T_z^\alpha, T_z^\beta$	$M_{xy}, M_{4z}^\alpha, M_{4z}^\beta$	mmm'	[100]
B_{2u} 1	−1	1	−1	−1	1	−1	1	B_{2u}^+	$Q_y, Q_y^\alpha, Q_y^\beta$	$G_{zx}, G_{4y}^\alpha, G_{4y}^\beta$			$m2m1'$	[100]
								B_{2u}^-			$T_y, T_y^\alpha, T_y^\beta$	$M_{zx}, M_{4y}^\alpha, M_{4y}^\beta$	$mm'm$	[100]
B_{3u} 1	−1	−1	1	−1	1	1	−1	B_{3u}^+	$Q_x, Q_x^\alpha, Q_x^\beta$	$G_{yz}, G_{4x}^\alpha, G_{4x}^\beta$			$2mm1'$	[100]
								B_{3u}^-			$T_x, T_x^\alpha, T_x^\beta$	$M_{yz}, M_{4x}^\alpha, M_{4x}^\beta$	$m'mm$	[100]

Table C.25: IRREPs of four types of multipoles in $2221'$. The superscript "±" of IRREP stands for the parity with respect to the antiunitary operation $\mathcal{A}=\theta$.

E	C_{2z}	C_{2y}	C_{2x}	IRREP	E	ET	MT	M	MPG	P. axis
A 1	1	1	1	A^+	$Q_0, Q_u, Q_v, Q_{xyz},$ Q_4, Q_{4u}, Q_{4v}	$G_0, G_u, G_v, G_{xyz},$ G_4, G_{4u}, G_{4v}			$2221'$	[100]
				A^-			$T_0, T_u, T_v, T_{xyz},$ T_4, T_{4u}, T_{4v}	$M_0, M_u, M_v, M_{xyz},$ M_4, M_{4u}, M_{4v}	222	[100]
B_1 1	1	−1	−1	B_1^+	$Q_z, Q_{xy},$ $Q_z^\alpha, Q_z^\beta, Q_{4z}^\alpha, Q_{4z}^\beta$	$G_z, G_{xy},$ $G_z^\alpha, G_z^\beta, G_{4z}^\alpha, G_{4z}^\beta$			$21'$	[001]
				B_1^-			$T_z, T_{xy},$ $T_z^\alpha, T_z^\beta, T_{4z}^\alpha, T_{4z}^\beta$	$M_z, M_{xy},$ $M_z^\alpha, M_z^\beta, M_{4z}^\alpha, M_{4z}^\beta$	$2'2'2$	[100]
B_2 1	−1	1	−1	B_2^+	$Q_y, Q_{zx},$ $Q_y^\alpha, Q_y^\beta, Q_{4y}^\alpha, Q_{4y}^\beta$	$G_y, G_{zx},$ $G_y^\alpha, G_y^\beta, G_{4y}^\alpha, G_{4y}^\beta$			$21'$	[010]
				B_2^-			$T_y, T_{zx},$ $T_y^\alpha, T_y^\beta, T_{4y}^\alpha, T_{4y}^\beta$	$M_y, M_{zx},$ $M_y^\alpha, M_y^\beta, M_{4y}^\alpha, M_{4y}^\beta$	$2'22'$	[100]
B_3 1	−1	−1	1	B_3^+	$Q_x, Q_{yz},$ $Q_x^\alpha, Q_x^\beta, Q_{4x}^\alpha, Q_{4x}^\beta$	$G_x, G_{yz},$ $G_x^\alpha, G_x^\beta, G_{4x}^\alpha, G_{4x}^\beta$			$21'$	[100]
				B_3^-			$T_x, T_{yz},$ $T_x^\alpha, T_x^\beta, T_{4x}^\alpha, T_{4x}^\beta$	$M_x, M_{yz},$ $M_x^\alpha, M_x^\beta, M_{4x}^\alpha, M_{4x}^\beta$	$22'2'$	[100]

Table C.26: IRREPs of four types of multipoles in $mm21'$. The superscript "±" of IRREP stands for the parity with respect to the antiunitary operation $\mathcal{A}=\theta$.

E	C_{2z}	σ_y	σ_x	IRREP	E	ET	MT	M	MPG	P. axis
1	1	1	1	A_1^+	$Q_0, Q_z, Q_u, Q_v, Q_z^\alpha, Q_z^\beta, Q_4, Q_{4u}, Q_{4v}$	$G_{xy}, G_{xyz}, G_{4z}^\alpha, G_{4z}^\beta$			$mm21'$	[100]
				A_1^-			$T_0, T_z, T_u, T_v, T_z^\alpha, T_z^\beta, T_4, T_{4u}, T_{4v}$	$M_{xy}, M_{xyz}, M_{4z}^\alpha, M_{4z}^\beta$	$mm2$	[100]
1	1	−1	−1	A_2^+	$Q_{xy}, Q_{xyz}, Q_{4z}^\alpha, Q_{4z}^\beta$	$G_0, G_z, G_u, G_v, G_z^\alpha, G_z^\beta, G_4, G_{4u}, G_{4v}$			$21'$	[001]
				A_2^-			$T_{xy}, T_{xyz}, T_{4z}^\alpha, T_{4z}^\beta$	$M_0, M_z, M_u, M_v, M_z^\alpha, M_z^\beta, M_4, M_{4u}, M_{4v}$	$m'm'2$	[001]
1	−1	1	−1	B_1^+	$Q_x, Q_{zx}, Q_x^\alpha, Q_x^\beta, Q_{4y}^\alpha, Q_{4y}^\beta$	$G_y, G_{yz}, G_y^\alpha, G_y^\beta, G_{4x}^\alpha, G_{4x}^\beta$			$m1'$	[010]
				B_1^-			$T_x, T_{zx}, T_x^\alpha, T_x^\beta, T_{4y}^\alpha, T_{4y}^\beta$	$M_y, M_{yz}, M_y^\alpha, M_y^\beta, M_{4x}^\alpha, M_{4x}^\beta$	$m'm2'$	[100]
1	−1	−1	1	B_2^+	$Q_y, Q_{yz}, Q_y^\alpha, Q_y^\beta, Q_{4x}^\alpha, Q_{4x}^\beta$	$G_x, G_{zx}, G_x^\alpha, G_x^\beta, G_{4y}^\alpha, G_{4y}^\beta$			$m1'$	[100]
				B_2^-			$T_y, T_{yz}, T_y^\alpha, T_y^\beta, T_{4x}^\alpha, T_{4x}^\beta$	$M_x, M_{zx}, M_x^\alpha, M_x^\beta, M_{4y}^\alpha, M_{4y}^\beta$	$mm'2'$	[100]

Table C.27: IRREPs of four types of multipoles in $2/m1'$. The superscript "±" of IRREP stands for the parity with respect to the antiunitary operation $\mathcal{A}=\theta$.

E	C_{2y}	I	σ_y	IRREP	E	ET	MT	M	MPG	P. axis
1	1	1	1	A_g^+	$Q_0, Q_u, Q_v, Q_{zx}, Q_4, Q_{4u}, Q_{4v}, Q_{4y}^\alpha, Q_{4y}^\beta$	$G_y, G_{xyz}, G_y^\alpha, G_y^\beta$			$2/m1'$	[010]
				A_g^-			$T_0, T_u, T_v, T_{zx}, T_4, T_{4u}, T_{4v}, T_{4y}^\alpha, T_{4y}^\beta$	$M_y, M_{xyz}, M_y^\alpha, M_y^\beta$	$2/m$	[010]
1	−1	1	−1	B_g^+	$Q_{yz}, Q_{xy}, Q_{4x}^\alpha, Q_{4z}^\alpha, Q_{4x}^\beta, Q_{4z}^\beta$	$G_x, G_z, G_x^\alpha, G_z^\alpha, G_x^\beta, G_z^\beta$			$\bar{1}1'$	—
				B_g^-			$T_{yz}, T_{xy}, T_{4x}^\alpha, T_{4z}^\alpha, T_{4x}^\beta, T_{4z}^\beta$	$M_x, M_z, M_x^\alpha, M_z^\alpha, M_x^\beta, M_z^\beta$	$2'/m'$	[010]
1	1	−1	−1	A_u^+	$Q_y, Q_{xyz}, Q_y^\alpha, Q_y^\beta$	$G_0, G_u, G_v, G_{zx}, G_4, G_{4u}, G_{4v}, G_{4y}^\alpha, G_{4y}^\beta$			$21'$	[010]
				A_u^-			$T_y, T_{xyz}, T_y^\alpha, T_y^\beta$	$M_0, M_u, M_v, M_{zx}, M_4, M_{4u}, M_{4v}, M_{4y}^\alpha, M_{4y}^\beta$	$2/m'$	[010]
1	−1	−1	1	B_u^+	$Q_x, Q_z, Q_x^\alpha, Q_z^\alpha, Q_x^\beta, Q_z^\beta$	$G_{yz}, G_{xy}, G_{4x}^\alpha, G_{4z}^\alpha, G_{4x}^\beta, G_{4z}^\beta$			$m1'$	[010]
				B_u^-			$T_x, T_z, T_x^\alpha, T_z^\alpha, T_x^\beta, T_z^\beta$	$M_{yz}, M_{xy}, M_{4x}^\alpha, M_{4z}^\alpha, M_{4x}^\beta, M_{4z}^\beta$	$2'/m$	[010]

Table C.28: IRREPs of four types of multipoles in $21'$. The superscript "$\pm$" of IRREP stands for the parity with respect to the antiunitary operation $\mathcal{A}=\theta$.

E	C_{2y}	IRREP	E	ET	MT	M	MPG	P. axis
A	1	A$^+$	$Q_0, Q_y, Q_u, Q_v, Q_{zx}, Q_{xyz}, Q_y^\alpha, Q_y^\beta, Q_4, Q_{4u}, Q_{4v}, Q_{4y}^\alpha, Q_{4y}^\beta$	$G_0, G_y, G_u, G_v, G_{zx}, G_{xyz}, G_y^\alpha, G_y^\beta, G_4, G_{4u}, G_{4v}, G_{4y}^\alpha, G_{4y}^\beta$			$21'$	[010]
		A$^-$			$T_0, T_y, T_u, T_v, T_{zx}, T_{xyz}, T_y^\alpha, T_y^\beta, T_4, T_{4u}, T_{4v}, T_{4y}^\alpha, T_{4y}^\beta$	$M_0, M_y, M_u, M_v, M_{zx}, M_{xyz}, M_y^\alpha, M_y^\beta, M_4, M_{4u}, M_{4v}, M_{4y}^\alpha, M_{4y}^\beta$	2	[010]
B	1	B$^+$	$Q_x, Q_z, Q_{yz}, Q_{xy}, Q_x^\alpha, Q_z^\alpha, Q_x^\beta, Q_z^\beta, Q_{4x}^\alpha, Q_{4z}^\alpha, Q_{4x}^\beta, Q_{4z}^\beta$	$G_x, G_z, G_{yz}, G_{xy}, G_x^\alpha, G_z^\alpha, G_x^\beta, G_z^\beta, G_{4x}^\alpha, G_{4z}^\alpha, G_{4x}^\beta, G_{4z}^\beta$			$11'$	—
		B$^-$			$T_x, T_z, T_{yz}, T_{xy}, T_x^\alpha, T_z^\alpha, T_x^\beta, T_z^\beta, T_{4x}^\alpha, T_{4z}^\alpha, T_{4x}^\beta, T_{4z}^\beta$	$M_x, M_z, M_{yz}, M_{xy}, M_x^\alpha, M_z^\alpha, M_x^\beta, M_z^\beta, M_{4x}^\alpha, M_{4z}^\alpha, M_{4x}^\beta, M_{4z}^\beta$	$2'$	[010]

Table C.29: IRREPs of four types of multipoles in $m1'$. The superscript "$\pm$" of IRREP stands for the parity with respect to the antiunitary operation $\mathcal{A}=\theta$.

E	σ_y	IRREP	E	ET	MT	M	MPG	P. axis
A$'$	1	A$'^+$	$Q_0, Q_x, Q_z, Q_u, Q_v, Q_{zx}, Q_x^\alpha, Q_z^\alpha, Q_x^\beta, Q_z^\beta, Q_4, Q_{4u}, Q_{4v}, Q_{4y}^\alpha, Q_{4y}^\beta$	$G_y, G_{yz}, G_{xy}, G_{xyz}, G_y^\alpha, G_y^\beta, G_{4x}^\alpha, G_{4z}^\alpha, G_{4x}^\beta, G_{4z}^\beta$			$m1'$	[010]
		A$'^-$			$T_0, T_x, T_z, T_u, T_v, T_{zx}, T_x^\alpha, T_z^\alpha, T_x^\beta, T_z^\beta, T_4, T_{4u}, T_{4v}, T_{4y}^\alpha, T_{4y}^\beta$	$M_y, M_{yz}, M_{xy}, M_{xyz}, M_y^\alpha, M_y^\beta, M_{4x}^\alpha, M_{4z}^\alpha, M_{4x}^\beta, M_{4z}^\beta$	m	[010]
A$''$	-1	A$''^+$	$Q_y, Q_{yz}, Q_{xy}, Q_{xyz}, Q_y^\alpha, Q_y^\beta, Q_{4x}^\alpha, Q_{4z}^\alpha, Q_{4x}^\beta, Q_{4z}^\beta$	$G_0, G_x, G_z, G_u, G_v, G_{zx}, G_x^\alpha, G_z^\alpha, G_x^\beta, G_z^\beta, G_4, G_{4u}, G_{4v}, G_{4y}^\alpha, G_{4y}^\beta$			$11'$	—
		A$''^-$			$T_y, T_{yz}, T_{xy}, T_{xyz}, T_y^\alpha, T_y^\beta, T_{4x}^\alpha, T_{4z}^\alpha, T_{4x}^\beta, T_{4z}^\beta$	$M_0, M_x, M_z, M_u, M_v, M_{zx}, M_x^\alpha, M_z^\alpha, M_x^\beta, M_z^\beta, M_4, M_{4u}, M_{4v}, M_{4y}^\alpha, M_{4y}^\beta$	m'	[010]

Table C.30: IRREPs of four types of multipoles in $\bar{1}1'$. The superscript "±" of IRREP stands for the parity with respect to the antiunitary operation $\mathcal{A}=\theta$.

	E	I	IRREP	E	ET	MT	M	MPG	P. axis
A_g	1	1	A_g^+	$Q_0, Q_u, Q_v,$ $Q_{yz}, Q_{zx}, Q_{xy},$ $Q_4, Q_{4u}, Q_{4v},$ $Q^\alpha_{4x}, Q^\alpha_{4y}, Q^\alpha_{4z},$ $Q^\beta_{4x}, Q^\beta_{4y}, Q^\beta_{4z}$	$G_x, G_y, G_z,$ $G_{xyz},$ $G^\alpha_x, G^\alpha_y, G^\alpha_z,$ $G^\beta_x, G^\beta_y, G^\beta_z$			$\bar{1}1'$	—
			A_g^-			$T_0, T_u, T_v,$ $T_{yz}, T_{zx}, T_{xy},$ $T_4, T_{4u}, T_{4v},$ $T^\alpha_{4x}, T^\alpha_{4y}, T^\alpha_{4z},$ $T^\beta_{4x}, T^\beta_{4y}, T^\beta_{4z}$	$M_x, M_y, M_z,$ $M_{xyz},$ $M^\alpha_x, M^\alpha_y, M^\alpha_z,$ $M^\beta_x, M^\beta_y, M^\beta_z$	$\bar{1}$	—
A_u	1	-1	A_u^+	$Q_x, Q_y, Q_z,$ $Q_{xyz},$ $Q^\alpha_x, Q^\alpha_y, Q^\alpha_z,$ $Q^\beta_x, Q^\beta_y, Q^\beta_z$	$G_0, G_u, G_v,$ $G_{yz}, G_{zx}, G_{xy},$ $G_4, G_{4u}, G_{4v},$ $G^\alpha_{4x}, G^\alpha_{4y}, G^\alpha_{4z},$ $G^\beta_{4x}, G^\beta_{4y}, G^\beta_{4z}$			$11'$	—
			A_u^-			$T_x, T_y, T_z,$ $T_{xyz},$ $T^\alpha_x, T^\alpha_y, T^\alpha_z,$ $T^\beta_x, T^\beta_y, T^\beta_z$	$M_0, M_u, M_v,$ $M_{yz}, M_{zx}, M_{xy},$ $M_4, M_{4u}, M_{4v},$ $M^\alpha_{4x}, M^\alpha_{4y}, M^\alpha_{4z},$ $M^\beta_{4x}, M^\beta_{4y}, M^\beta_{4z}$	$\bar{1}'$	—

Table C.31: IRREPs of four types of multipoles in $11'$. The superscript "±" of IRREP stands for the parity with respect to the antiunitary operation $\mathcal{A}=\theta$.

E	IRREP	E	ET	MT	M	MPG	P. axis
A 1	A^+	$Q_0, Q_x, Q_y, Q_z,$ $Q_u, Q_v, Q_{yz}, Q_{zx}, Q_{xy},$ $Q_{xyz}, Q^\alpha_x, Q^\alpha_y, Q^\alpha_z,$ $Q^\beta_x, Q^\beta_y, Q^\beta_z,$ $Q_4, Q_{4u}, Q_{4v},$ $Q^\alpha_{4x}, Q^\alpha_{4y}, Q^\alpha_{4z},$ $Q^\beta_{4x}, Q^\beta_{4y}, Q^\beta_{4z}$	$G_0, G_x, G_y, G_z,$ $G_u, G_v, G_{yz}, G_{zx}, G_{xy},$ $G_{xyz}, G^\alpha_x, G^\alpha_y, G^\alpha_z,$ $G^\beta_x, G^\beta_y, G^\beta_z,$ $G_4, G_{4u}, G_{4v},$ $G^\alpha_{4x}, G^\alpha_{4y}, G^\alpha_{4z},$ $G^\beta_{4x}, G^\beta_{4y}, G^\beta_{4z}$			$11'$	—
	A^-			$T_0, T_x, T_y, T_z,$ $T_u, T_v, T_{yz}, T_{zx}, T_{xy},$ $T_{xyz}, T^\alpha_x, T^\alpha_y, T^\alpha_z,$ $T^\beta_x, T^\beta_y, T^\beta_z,$ $T_4, T_{4u}, T_{4v},$ $T^\alpha_{4x}, T^\alpha_{4y}, T^\alpha_{4z},$ $T^\beta_{4x}, T^\beta_{4y}, T^\beta_{4z}$	$M_0, M_x, M_y, M_z,$ $M_u, M_v, M_{yz}, M_{zx}, M_{xy},$ $M_{xyz}, M^\alpha_x, M^\alpha_y, M^\alpha_z,$ $M^\beta_x, M^\beta_y, M^\beta_z,$ $M_4, M_{4u}, M_{4v},$ $M^\alpha_{4x}, M^\alpha_{4y}, M^\alpha_{4z},$ $M^\beta_{4x}, M^\beta_{4y}, M^\beta_{4z}$	1	—

C.2 Black-and-White Point Groups

Table C.32: IRREPs of four types of multipoles in $m'\bar{3}'m$. The superscript "±" of IRREP stands for the parity with respect to the antiunitary operation $\mathcal{A}=\theta I$.

	E	$6IC_4$	$3C_4^2$	$6\sigma_d$	$8C_3$	IRREP	E	ET	MT	M	MPG	P. axis
A_1	1	1	1	1	1	A_1^+	Q_0, Q_4		T_{xyz}		$m'\bar{3}'m$	$\langle 100\rangle$
						A_1^-	Q_{xyz}		T_0, T_4		$\bar{4}3m$	$\langle 100\rangle$
A_2	1	−1	1	−1	1	A_2^+		G_{xyz}		M_0, M_4	$m'\bar{3}'$	$\langle 100\rangle$
						A_2^-		G_0, G_4		M_{xyz}	$4'32'$	$\langle 100\rangle$
E	2	0	2	0	−1	E^+	Q_u, Q_{4u}			M_v, M_{4v}	$4'/m'm'm$	[001]
							Q_v, Q_{4v}			M_u, M_{4u}	$m'm'm'$	[100]
						E^-		G_v, G_{4v}	T_u, T_{4u}		$\bar{4}2m$	[001]
								G_u, G_{4u}	T_v, T_{4v}		$4'22'$	[001]
T_1	3	1	−1	−1	0	T_1^+	Q_{4x}^α	G_x, G_x^α	T_x^β	M_{yz}, M_{4x}^β	$4'/m'$	[100]
							Q_{4y}^α	G_y, G_y^α	T_y^β	M_{zx}, M_{4y}^β	$4'/m'$	[010]
							Q_{4z}^α	G_z, G_z^α	T_z^β	M_{xy}, M_{4z}^β	$4'/m'$	[001]
						T_1^-	Q_x^β	G_{yz}, G_{4x}^β	T_{4x}^α	M_x, M_x^α	$\bar{4}m'2'$	[100]
							Q_y^β	G_{zx}, G_{4y}^β	T_{4y}^α	M_y, M_y^α	$\bar{4}m'2'$	[010]
							Q_z^β	G_{xy}, G_{4z}^β	T_{4z}^α	M_z, M_z^α	$\bar{4}m'2'$	[001]
T_2	3	−1	−1	1	0	T_2^+	Q_{yz}, Q_{4x}^β	G_x^β	T_x, T_x^α	M_{4x}^α	mmm'	[011]
							Q_{zx}, Q_{4y}^β	G_y^β	T_y, T_y^α	M_{4y}^α	mmm'	[101]
							Q_{xy}, Q_{4z}^β	G_z^β	T_z, T_z^α	M_{4z}^α	mmm'	[110]
						T_2^-	Q_x, Q_x^α	G_{4x}^α	T_{yz}, T_{4x}^β	M_x^β	$4'm'm$	[100]
							Q_y, Q_y^α	G_{4y}^α	T_{zx}, T_{4y}^β	M_y^β	$4'm'm$	[010]
							Q_z, Q_z^α	G_{4z}^α	T_{xy}, T_{4z}^β	M_z^β	$4'm'm$	[001]

Table C.33: IRREPs of four types of multipoles in $m\bar{3}m'$. The superscript "±" of IRREP stands for the parity with respect to the antiunitary operation $\mathcal{A}=\theta C_2'$ (about [110] axis). The basis of case-(a) IRREP $\mathrm{E}_{\mathrm{g/u}}^{(1,2)\pm}$ consists of the linear combination of the multipoles shown in the right side of a close brace.

	E	$3C_2$	$4C_3$	$4C_3^2$	I	$3\sigma_h$	$4IC_3$	$4IC_3^2$	IRREP	E	ET	MT	M	MPG	P. axis
$\mathrm{A_g}$	1	1	1	1	1	1	1	1	$\mathrm{A_g^+}$	Q_0, Q_4			M_{xyz}	$m\bar{3}m'$	$\langle 100\rangle$
									$\mathrm{A_g^-}$		G_{xyz}	T_0, T_4		$m\bar{3}$	$\langle 100\rangle$
$\mathrm{E_g}$	1	1	ω	ω^2	1	1	ω	ω^2	$\mathrm{E_g^{(1)+}}$ }	Q_u, Q_{4u}				$4'/mmm'$	[001]
	1	1	ω^2	ω	1	1	ω^2	ω	$\mathrm{E_g^{(2)+}}$ }	Q_v, Q_{4v}				mmm	[100]
									$\mathrm{E_g^{(1)-}}$ }			T_u, T_{4u}		mmm	[100]
									$\mathrm{E_g^{(2)-}}$ }			T_v, T_{4v}		$4'/mmm'$	[001]
$\mathrm{T_g}$	3	−1	0	0	3	−1	0	0	$\mathrm{T_g^+}$	Q_{4x}^α	G_x, G_x^α	T_{yz}, T_{4x}^β	M_x^β	$4'/m$	[100]
										Q_{4y}^α	G_y, G_y^α	T_{zx}, T_{4y}^β	M_y^β	$4'/m$	[010]
										Q_{4z}^α	G_z, G_z^α	T_{xy}, T_{4z}^β	M_z^β	$4'/m$	[001]
									$\mathrm{T_g^-}$	Q_{yz}, Q_{4x}^β	G_x^β	T_{4x}^α	M_x, M_x^α	$m'm'm$	[011]
										Q_{zx}, Q_{4y}^β	G_y^β	T_{4y}^α	M_y, M_y^α	$m'm'm$	[101]
										Q_{xy}, Q_{4z}^β	G_z^β	T_{4z}^α	M_z, M_z^α	$m'm'm$	[110]
$\mathrm{A_u}$	1	1	1	1	−1	−1	−1	−1	$\mathrm{A_u^+}$		G_0, G_4	T_{xyz}		$4'32'$	$\langle 100\rangle$
									$\mathrm{A_u^-}$	Q_{xyz}			M_0, M_4	$\bar{4}'3m'$	$\langle 100\rangle$
$\mathrm{E_u}$	1	1	ω	ω^2	−1	−1	$-\omega$	$-\omega^2$	$\mathrm{E_u^{(1)+}}$ }		G_u, G_{4u}			$4'22'$	[001]
	1	1	ω^2	ω	−1	−1	$-\omega^2$	$-\omega$	$\mathrm{E_u^{(2)+}}$ }		G_v, G_{4v}			$\bar{4}'2m'$	[001]
									$\mathrm{E_u^{(1)-}}$ }				M_u, M_{4u}	$\bar{4}'2m'$	[001]
									$\mathrm{E_u^{(2)-}}$ }				M_v, M_{4v}	$4'22'$	[001]
$\mathrm{T_u}$	3	−1	0	0	−3	1	0	0	$\mathrm{T_u^+}$	Q_x, Q_x^α	G_{4x}^α	T_x^β	M_{yz}, M_{4x}^β	$4'mm'$	[100]
										Q_y, Q_y^α	G_{4y}^α	T_y^β	M_{zx}, M_{4y}^β	$4'mm'$	[010]
										Q_z, Q_z^α	G_{4z}^α	T_z^β	M_{xy}, M_{4z}^β	$4'mm'$	[001]
									$\mathrm{T_u^-}$	Q_x^β	G_{yz}, G_{4x}^β	T_x, T_x^α	M_{4x}^α	$\bar{4}'m2'$	[100]
										Q_y^β	G_{zx}, G_{4y}^β	T_y, T_y^α	M_{4y}^α	$\bar{4}'m2'$	[010]
										Q_z^β	G_{xy}, G_{4z}^β	T_z, T_z^α	M_{4z}^α	$\bar{4}'m2'$	[001]

ω=exp($-2\pi i/3$)

Table C.34: IRREPs of four types of multipoles $4'32'$. The superscript "±" of IRREP stands for the parity with respect to the antiunitary operation $\mathcal{A}=\theta C_2'$ (about [110] axis).

	E	$3C_2$	$4C_3$	$4C_3^2$	IRREP	E	ET	MT	M	MPG	P. axis
A	1	1	1	1	$\mathrm{A^+}$	Q_0, Q_4	G_0, G_4	T_{xyz}	M_{xyz}	$4'32'$	$\langle 100\rangle$
					$\mathrm{A^-}$	Q_{xyz}	G_{xyz}	T_0, T_4	M_0, M_4	23	$\langle 100\rangle$
E	1	1	ω	ω^2	$\mathrm{E^{(1)+}}$ }	Q_u, Q_{4u}	G_u, G_{4u}			$4'22'$	[001]
	1	1	ω^2	ω	$\mathrm{E^{(2)+}}$ }	Q_v, Q_{4v}	G_v, G_{4v}			222	[100]
					$\mathrm{E^{(1)-}}$ }			T_u, T_{4u}	M_u, M_{4u}	222	[100]
					$\mathrm{E^{(2)-}}$ }			T_v, T_{4v}	M_v, M_{4v}	$4'22'$	[001]
T	3	−1	0	0	$\mathrm{T^+}$	$Q_x, Q_x^\alpha, Q_{4x}^\alpha$	$G_x, G_x^\alpha, G_{4x}^\alpha$	$T_{yz}, T_x^\beta, T_{4x}^\beta$	$M_{yz}, M_x^\beta, M_{4x}^\beta$	$4'$	[100]
						$Q_y, Q_y^\alpha, Q_{4y}^\alpha$	$G_y, G_y^\alpha, G_{4y}^\alpha$	$T_{zx}, T_y^\beta, T_{4y}^\beta$	$M_{zx}, M_y^\beta, M_{4y}^\beta$	$4'$	[010]
						$Q_z, Q_z^\alpha, Q_{4z}^\alpha$	$G_z, G_z^\alpha, G_{4z}^\alpha$	$T_{xy}, T_z^\beta, T_{4z}^\beta$	$M_{xy}, M_z^\beta, M_{4z}^\beta$	$4'$	[001]
					$\mathrm{T^-}$	$Q_{yz}, Q_x^\beta, Q_{4x}^\beta$	$G_{yz}, G_x^\beta, G_{4x}^\beta$	$T_x, T_x^\alpha, T_{4x}^\alpha$	$M_x, M_x^\alpha, M_{4x}^\alpha$	$2'2'2$	[011]
						$Q_{zx}, Q_y^\beta, Q_{4y}^\beta$	$G_{zx}, G_y^\beta, G_{4y}^\beta$	$T_y, T_y^\alpha, T_{4y}^\alpha$	$M_y, M_y^\alpha, M_{4y}^\alpha$	$2'2'2$	[101]
						$Q_{xy}, Q_z^\beta, Q_{4z}^\beta$	$G_{xy}, G_z^\beta, G_{4z}^\beta$	$T_z, T_z^\alpha, T_{4z}^\alpha$	$M_z, M_z^\alpha, M_{4z}^\alpha$	$2'2'2$	[110]

ω=exp($-2\pi i/3$)

Table C.35: IRREPs of four types of multipoles $\bar{4}'3m'$. The superscript "±" of IRREP stands for the parity with respect to the antiunitary operation $\mathcal{A}=\theta\sigma_d$ (normal to the [110] direction).

	E	$3C_2$	$4C_3$	$4C_3^2$	IRREP	E	ET	MT	M	MPG	P. axis
A	1	1	1	1	A^+	Q_0, Q_{xyz}, Q_4			M_0, M_{xyz}, M_4	$\bar{4}'3m'$	$\langle 100\rangle$
					A^-		G_0, G_{xyz}, G_4	T_0, T_{xyz}, T_4		23	$\langle 100\rangle$
E	1	1	ω	ω^2	$E^{(1)+}$	Q_u, Q_{4u}			M_u, M_{4u}	$\bar{4}'2m'$	[001]
	1	1	ω^2	ω	$E^{(2)+}$	Q_v, Q_{4v}			M_v, M_{4v}	222	[100]
					$E^{(1)-}$		G_u, G_{4u}	T_u, T_{4u}		222	[100]
					$E^{(2)-}$		G_v, G_{4v}	T_v, T_{4v}		$\bar{4}'2m'$	[001]
T	3	−1	0	0	T^+	Q_x^β, Q_{4x}^α	$G_x, G_{yz}, G_x^\alpha, G_{4x}^\beta$	$T_x, T_{yz}, T_x^\alpha, T_{4x}^\beta$	M_x^β, M_{4x}^α	$\bar{4}'$	[100]
						Q_y^β, Q_{4y}^α	$G_y, G_{zx}, G_y^\alpha, G_{4y}^\beta$	$T_y, T_{zx}, T_y^\alpha, T_{4y}^\beta$	M_y^β, M_{4y}^α	$\bar{4}'$	[010]
						Q_z^β, Q_{4z}^α	$G_z, G_{xy}, G_z^\alpha, G_{4z}^\beta$	$T_z, T_{xy}, T_z^\alpha, T_{4z}^\beta$	M_z^β, M_{4z}^α	$\bar{4}'$	[001]
					T^-	$Q_x, Q_{yz}, Q_x^\alpha, Q_{4x}^\beta$	G_x^β, G_{4x}^α	T_x^β, T_{4x}^α	$M_x, M_{yz}, M_x^\alpha, M_{4x}^\beta$	$m'm'2$	[011]
						$Q_y, Q_{zx}, Q_y^\alpha, Q_{4y}^\beta$	G_y^β, G_{4y}^α	T_y^β, T_{4y}^α	$M_y, M_{zx}, M_y^\alpha, M_{4y}^\beta$	$m'm'2$	[101]
						$Q_z, Q_{xy}, Q_z^\alpha, Q_{4z}^\beta$	G_z^β, G_{4z}^α	T_z^β, T_{4z}^α	$M_z, M_{xy}, M_z^\alpha, M_{4z}^\beta$	$m'm'2$	[110]

$\omega=\exp(-2\pi i/3)$

Table C.36: IRREPs of four types of multipoles $m'\bar{3}'$. The superscript "±" of IRREP stands for the parity with respect to the antiunitary operation $\mathcal{A}=\theta I$.

	E	$3C_2$	$4C_3$	$4C_3^2$	IRREP	E	ET	MT	M	MPG	P. axis
A	1	1	1	1	A^+	Q_0, Q_4	G_{xyz}	T_{xyz}	M_0, M_4	$m'\bar{3}'$	$\langle 100\rangle$
					A^-	Q_{xyz}	G_0, G_4	T_0, T_4	M_{xyz}	23	$\langle 100\rangle$
E	1	1	ω	ω^2	E	Q_u, Q_{4u}			M_u, M_{4u}	$m'm'm'$	[100]
	1	1	ω^2	ω		Q_v, Q_{4v}			M_v, M_{4v}	$m'm'm'$	[100]
							G_u, G_{4u}	T_u, T_{4u}		222	[100]
							G_v, G_{4v}	T_v, T_{4v}		222	[100]
T	3	−1	0	0	T^+	$Q_{yz}, Q_{4x}^\alpha, Q_{4x}^\beta$	$G_x, G_x^\alpha, G_x^\beta$	$T_x, T_x^\alpha, T_x^\beta$	$M_{yz}, M_{4x}^\alpha, M_{4x}^\beta$	$2/m'$	[100]
						$Q_{zx}, Q_{4y}^\alpha, Q_{4y}^\beta$	$G_y, G_y^\alpha, G_y^\beta$	$T_y, T_y^\alpha, T_y^\beta$	$M_{zx}, M_{4y}^\alpha, M_{4y}^\beta$	$2/m'$	[010]
						$Q_{xy}, Q_{4z}^\alpha, Q_{4z}^\beta$	$G_z, G_z^\alpha, G_z^\beta$	$T_z, T_z^\alpha, T_z^\beta$	$M_{xy}, M_{4z}^\alpha, M_{4z}^\beta$	$2/m'$	[001]
					T^-	$Q_x, Q_x^\alpha, Q_x^\beta$	$G_{yz}, G_{4x}^\alpha, G_{4x}^\beta$	$T_{yz}, T_{4x}^\alpha, T_{4x}^\beta$	$M_x, M_x^\alpha, M_x^\beta$	$2m'm'$	[100]
						$Q_y, Q_y^\alpha, Q_y^\beta$	$G_{zx}, G_{4y}^\alpha, G_{4y}^\beta$	$T_{zx}, T_{4y}^\alpha, T_{4y}^\beta$	$M_y, M_y^\alpha, M_y^\beta$	$m'2m'$	[100]
						$Q_z, Q_z^\alpha, Q_z^\beta$	$G_{xy}, G_{4z}^\alpha, G_{4z}^\beta$	$T_{xy}, T_{4z}^\alpha, T_{4z}^\beta$	$M_z, M_z^\alpha, M_z^\beta$	$m'm'2$	[100]

$\omega=\exp(-2\pi i/3)$

Table C.37: IRREPs of four types of multipoles in $6/m'm'm'$. The superscript "±" of IRREP stands for the parity with respect to the antiunitary operation $\mathcal{A}=\theta I$.

	E	$2C_6$	$2C_3$	C_2	$3C_{2x}$	$3C_{2y}$	IRREP	E	ET	MT	M	MPG	P. axis
A_1	1	1	1	1	1	1	A_1^+	Q_0, Q_u, Q_{40}			M_0, M_u, M_{40}	$6/m'm'm'$	[001]
							A_1^-		G_0, G_u, G_{40}	T_0, T_u, T_{40}		622	[001]
A_2	1	1	1	1	−1	−1	A_2^+		G_z, G_z^α	T_z, T_z^α		$6/m'$	[001]
							A_2^-	Q_z, Q_z^α			M_z, M_z^α	$6m'm'$	[001]
B_1	1	−1	1	−1	1	−1	B_1^+	Q_{4a}	G_{3a}	T_{3a}	M_{4a}	$\bar{3}'m'$	[001]
							B_1^-	Q_{3a}	G_{4a}	T_{4a}	M_{3a}	$\bar{6}'2m'$	[001]
B_2	1	−1	1	−1	−1	1	B_2^+	Q_{4b}	G_{3b}	T_{3b}	M_{4b}	$\bar{3}'m'$	[001]
							B_2^-	Q_{3b}	G_{4b}	T_{4b}	M_{3b}	$\bar{6}'m'2$	[001]
E_1	2	1	−1	−2	0	0	E_1^+	Q_{yz}, Q_{4v}^α	G_x, G_{3u}	T_x, T_{3u}	M_{yz}, M_{4v}^α	$2/m'$	[100]
								Q_{zx}, Q_{4u}^α	G_y, G_{3v}	T_y, T_{3v}	M_{zx}, M_{4u}^α	$2/m'$	[010]
							E_1^-	Q_x, Q_{3u}	G_{yz}, G_{4v}^α	T_{yz}, T_{4v}^α	M_x, M_{3u}	$2m'm'$	[100]
								Q_y, Q_{3v}	G_{zx}, G_{4u}^α	T_{zx}, T_{4u}^α	M_y, M_{3v}	$m'2m'$	[100]
E_2	2	−1	−1	−2	0	0	E_2^+	$Q_v, Q_{4u}^{\beta 1}, Q_{4u}^{\beta 2}$	G_{xyz}	T_{xyz}	$M_v, M_{4u}^{\beta 1}, M_{4u}^{\beta 2}$	$m'm'm'$	[100]
								$Q_{xy}, Q_{4v}^{\beta 1}, Q_{4v}^{\beta 2}$	G_z^β	T_z^β	$M_{xy}, M_{4v}^{\beta 1}, M_{4v}^{\beta 2}$	$2/m'$	[001]
							E_2^-	Q_{xyz}	$G_v, G_{4u}^{\beta 1}, G_{4u}^{\beta 2}$	$T_v, T_{4u}^{\beta 1}, T_{4u}^{\beta 2}$	M_{xyz}	222	[100]
								Q_z^β	$G_{xy}, G_{4v}^{\beta 1}, G_{4v}^{\beta 2}$	$T_{xy}, T_{4v}^{\beta 1}, T_{4v}^{\beta 2}$	M_z^β	$m'm'2$	[100]

Table C.38: IRREPs of four types of multipoles in $6/m'mm$. The superscript "±" of IRREP stands for the parity with respect to the antiunitary operation $\mathcal{A}=\theta I$.

	E	$2C_6$	$2C_3$	C_2	$3\sigma_y$	$3\sigma_x$	IRREP	E	ET	MT	M	MPG	P. axis
A_1	1	1	1	1	1	1	A_1^+	Q_0, Q_u, Q_{40}		T_z, T_z^α		$6/m'mm$	[001]
							A_1^-	Q_z, Q_z^α		T_0, T_u, T_{40}		$6mm$	[001]
A_2	1	1	1	1	−1	−1	A_2^+		G_z, G_z^α		M_0, M_u, M_{40}	$6/m'$	[001]
							A_2^-		G_0, G_u, G_{40}		M_z, M_z^α	$62'2'$	[001]
B_1	1	−1	1	−1	1	−1	B_1^+	Q_{4a}	G_{3a}	T_{3b}	M_{4b}	$\bar{3}'m$	[001]
							B_1^-	Q_{3b}	G_{4b}	T_{4a}	M_{3a}	$\bar{6}'2'm$	[001]
B_2	1	−1	1	−1	−1	1	B_2^+	Q_{4b}	G_{3b}	T_{3a}	M_{4a}	$\bar{3}'m$	[001]
							B_2^-	Q_{3a}	G_{4a}	T_{4b}	M_{3b}	$\bar{6}'m2'$	[001]
E_1	2	1	−1	−2	0	0	E_1^+	Q_{yz}, Q_{4v}^α	G_x, G_{3u}	T_y, T_{3v}	M_{zx}, M_{4u}^α	$2'/m$	[100]
								Q_{zx}, Q_{4u}^α	G_y, G_{3v}	T_x, T_{3u}	M_{yz}, M_{4v}^α	$2'/m$	[010]
							E_1^-	Q_y, Q_{3v}	G_{zx}, G_{4u}^α	T_{yz}, T_{4v}^α	M_x, M_{3u}	$m2'm'$	[100]
								Q_x, Q_{3u}	G_{yz}, G_{4v}^α	T_{zx}, T_{4u}^α	M_y, M_{3v}	$2'mm'$	[100]
E_2	2	−1	−1	−2	0	0	E_2^+	$Q_v, Q_{4u}^{\beta 1}, Q_{4u}^{\beta 2}$	G_{xyz}	T_z^β	$M_{xy}, M_{4v}^{\beta 1}, M_{4v}^{\beta 2}$	mmm'	[001]
								$Q_{xy}, Q_{4v}^{\beta 1}, Q_{4v}^{\beta 2}$	G_z^β	T_{xyz}	$M_v, M_{4u}^{\beta 1}, M_{4u}^{\beta 2}$	$2/m'$	[001]
							E_2^-	Q_z^β	$G_{xy}, G_{4v}^{\beta 1}, G_{4v}^{\beta 2}$	$T_v, T_{4u}^{\beta 1}, T_{4u}^{\beta 2}$	M_{xyz}	$mm2$	[100]
								Q_{xyz}	$G_v, G_{4u}^{\beta 1}, G_{4u}^{\beta 2}$	$T_{xy}, T_{4v}^{\beta 1}, T_{4v}^{\beta 2}$	M_z^β	$2'2'2$	[100]

Table C.39: IRREPs of four types of multipoles in $6'/mmm'$. The superscript "$\pm$" of IRREP stands for the parity with respect to the antiunitary operation $\mathcal{A}=\theta I$.

	E	$2IC_6$	$2C_3$	σ_h	$3C_{2y}$	$3\sigma_x$	IRREP	E	ET	MT	M	MPG	P. axis
A_1'	1	1	1	1	1	1	$A_1'^+$	Q_0, Q_u, Q_{40}		T_{3b}	M_{4b}	$6'/mmm'$	[001]
							$A_1'^-$	Q_{3b}	G_{4b}	T_0, T_u, T_{40}		$\bar{6}m2$	[001]
A_2'	1	1	1	1	-1	-1	$A_2'^+$		G_z, G_z^α	T_{3a}	M_{4a}	$6'/m$	[001]
							$A_2'^-$	Q_{3a}	G_{4a}		M_z, M_z^α	$\bar{6}2'm'$	[001]
A_1''	1	-1	1	-1	1	-1	$A_1''^+$	Q_{4b}	G_{3b}		M_0, M_u, M_{40}	$\bar{3}'m'$	[001]
							$A_1''^-$		G_0, G_u, G_{40}	T_{4b}	M_{3b}	$6'2'2$	[001]
A_2''	1	-1	1	-1	-1	1	$A_2''^+$	Q_{4a}	G_{3a}	T_z, T_z^α		$\bar{3}'m$	[001]
							$A_2''^-$	Q_z, Q_z^α		T_{4a}	M_{3a}	$6'mm'$	[001]
E''	2	1	-1	-2	0	0	E''^+	Q_{yz}, Q_{4v}^α	G_x, G_{3u}	T_z^β	$M_{xy}, M_{4v}^{\beta 1}, M_{4v}^{\beta 2}$	$2'/m$	[100]
								Q_{zx}, Q_{4u}^α	G_y, G_{3v}	T_{xyz}	$M_v, M_{4u}^{\beta 1}, M_{4u}^{\beta 2}$	$2/m'$	[010]
							E''^-	Q_z^β	$G_{xy}, G_{4v}^{\beta 1}, G_{4v}^{\beta 2}$	T_{yz}, T_{4v}^α	M_x, M_{3u}	$mm'2'$	[100]
								Q_{xyz}	$G_v, G_{4u}^{\beta 1}, G_{4u}^{\beta 2}$	T_{zx}, T_{4u}^α	M_y, M_{3v}	$2'22'$	[100]
E'	2	-1	-1	-2	0	0	E'^+	$Q_v, Q_{4u}^{\beta 1}, Q_{4u}^{\beta 2}$	G_{xyz}	T_y, T_{3v}	M_{zx}, M_{4u}^α	$mm'm$	[100]
								$Q_{xy}, Q_{4v}^{\beta 1}, Q_{4v}^{\beta 2}$	G_z^β	T_x, T_{3u}	$M_{yz}, M_{4v}^\alpha,$	$2'/m$	[001]
							E'^-	Q_y, Q_{3v}	G_{zx}, G_{4u}^α	$T_v, T_{4u}^{\beta 1}, T_{4u}^{\beta 2}$	M_{xyz}	$m2m$	[100]
								Q_x, Q_{3u}	G_{yz}, G_{4v}^α	$T_{xy}, T_{4v}^{\beta 1}, T_{4v}^{\beta 2}$	M_z^β	$2'm'm$	[100]

Table C.40: IRREPs of four types of multipoles in $6/mm'm'$. The superscript "±" of IRREP stands for the parity with respect to the antiunitary operation $\mathcal{A}=\theta C_{2x}$.

E	C_6	C_3	C_2	C_3^2	C_6^5	I	IC_6	IC_3	σ_h	IC_3^2	IC_6^5	IRREP	E	ET	MT	M	MPG	P. axis
A_g 1	1	1	1	1	1	1	1	1	1	1	1	A_g^+	Q_0, Q_u, Q_{40}			M_z, M_z^α	$6/mm'm'$	[001]
												A_g^-		G_z, G_z^α	T_0, T_u, T_{40}		$6/m$	[001]
B_g 1	−1	1	−1	1	−1	1	−1	1	−1	1	−1	B_g^+	Q_{4a}	G_{3a}	T_{4b}	M_{3b}	$\bar{3}m'$	[001]
												B_g^-	Q_{4b}	G_{3b}	T_{4a}	M_{3a}	$\bar{3}m'$	[001]
E_{1g} 1	$-\omega$	ω^2	−1	ω	$-\omega^2$	1	$-\omega$	ω^2	−1	ω	$-\omega^2$	$E_{1g}^{(1)+}$	Q_{yz}, Q_{4v}^α	G_x, G_{3u}			$2'/m'$	[100]
1	$-\omega^2$	ω	−1	ω^2	$-\omega$	1	$-\omega^2$	ω	−1	ω^2	$-\omega$	$E_{1g}^{(2)+}$	Q_{zx}, Q_{4u}^α	G_y, G_{3v}			$2'/m'$	[010]
												$E_{1g}^{(1)-}$			T_{yz}, T_{4v}^α	M_x, M_{3u}	$2'/m'$	[010]
												$E_{1g}^{(2)-}$			T_{zx}, T_{4u}^α	M_y, M_{3v}	$2'/m'$	[100]
E_{2g} 1	ω	ω^2	1	ω	ω^2	1	ω	ω^2	1	ω	ω^2	$E_{2g}^{(1)+}$	Q_v $Q_{4u}^{\beta 1}, Q_{4u}^{\beta 2}$	G_{xyz}			$m'm'm$	[100]
1	ω^2	ω	1	ω^2	ω	1	ω^2	ω	1	ω^2	ω	$E_{2g}^{(2)+}$	Q_{xy}, $Q_{4v}^{\beta 1}, Q_{4v}^{\beta 2}$	G_z^β			$2/m$	[001]
												$E_{2g}^{(1)-}$			T_v, $T_{4u}^{\beta 1}, T_{4u}^{\beta 2}$	M_{xyz}	$2/m$	[001]
												$E_{2g}^{(2)-}$			T_{xy}, $T_{4v}^{\beta 1}, T_{4v}^{\beta 2}$	M_z^β	$m'm'm$	[100]
A_u 1	1	1	1	1	1	−1	−1	−1	−1	−1	−1	A_u^+		G_0, G_u, G_{40}	T_z, T_z^α		$62'2'$	[001]
												A_u^-	Q_z, Q_z^α			M_0, M_u, M_{40}	$6m'm'$	[001]
B_u 1	−1	1	−1	1	−1	−1	1	−1	1	−1	1	B_u^+	Q_{3a}	G_{4a}	T_{3b}	M_{4b}	$\bar{6}2'm'$	[001]
												B_u^-	Q_{3b}	G_{4b}	T_{3a}	M_{4a}	$\bar{6}m'2'$	[001]
E_{1u} 1	$-\omega$	ω^2	−1	ω	$-\omega^2$	−1	ω	$-\omega^2$	1	$-\omega$	ω^2	$E_{1u}^{(1)+}$	Q_x, Q_{3u}	G_{yz}, G_{4v}^α			$2'm'm$	[100]
1	$-\omega^2$	ω	−1	ω^2	$-\omega$	−1	ω^2	$-\omega$	1	$-\omega^2$	ω	$E_{1u}^{(2)+}$	Q_y, Q_{3v}	G_{zx}, G_{4u}^α			$m'2'm$	[100]
												$E_{1u}^{(1)-}$			T_x, T_{3u}	M_{yz}, M_{4v}^α	$m'2'm$	[100]
												$E_{1u}^{(2)-}$			T_y, T_{3v}	M_{zx}, M_{4u}^α	$2'm'm$	[100]
E_{2u} 1	ω	ω^2	1	ω	ω^2	−1	$-\omega$	$-\omega^2$	−1	$-\omega$	$-\omega^2$	$E_{2u}^{(1)+}$	Q_{xyz}	G_v, $G_{4u}^{\beta 1}, G_{4u}^{\beta 2}$			$2'2'2$	[100]
1	ω^2	ω	1	ω^2	ω	−1	$-\omega^2$	$-\omega$	−1	$-\omega^2$	$-\omega$	$E_{2u}^{(2)+}$	Q_z^β	G_{xy}, $G_{4v}^{\beta 1}, G_{4v}^{\beta 2}$			$m'm'2$	[100]
												$E_{2u}^{(1)-}$			T_{xyz}	M_v, $M_{4u}^{\beta 1}, M_{4u}^{\beta 2}$	$m'm'2$	[100]
												$E_{2u}^{(2)-}$			T_z^β	M_{xy}, $M_{4v}^{\beta 1}, M_{4v}^{\beta 2}$	$2'2'2$	[100]

$\omega=\exp(-2\pi i/3)$

Table C.41: IRREPs of four types of multipoles in $6'/m'mm'$. The superscript "±" of IRREP stands for the parity with respect to the antiunitary operation $\mathcal{A}=\theta C_2$.

	E	$2C_3$	$3C_{2x}$	I	$2IC_3$	$3\sigma_x$	IRREP	E	ET	MT	M	MPG	P. axis
A_{1g}	1	1	1	1	1	1	A_{1g}^+	Q_0, Q_u, Q_{40}		T_{4a}	M_{3a}	$6'/m'mm'$	[001]
							A_{1g}^-	Q_{4a}	G_{3a}	T_0, T_u, T_{40}		$\bar{3}m$	[001]
A_{2g}	1	1	−1	1	1	−1	A_{2g}^+		G_z, G_z^α	T_{4b}	M_{3b}	$6'/m'$	[001]
							A_{2g}^-	Q_{4b}	G_{3b}		M_z, M_z^α	$\bar{3}m'$	[001]
E_g	2	−1	0	2	−1	0	E_g^+	Q_{xy}	G_z^β	T_{zx}, T_{4u}^α	M_y, M_{3v}	$2'/m'$	[001]
								$Q_{4v}^{\beta 1}, Q_{4v}^{\beta 2}$					
								Q_v	G_{xyz}	T_{yz}, T_{4v}^α	M_x, M_{3u}	$mm'm'$	[100]
								$Q_{4u}^{\beta 1}, Q_{4u}^{\beta 2}$					
							E_g^-	Q_{yz}, Q_{4v}^α	G_x, G_{3u}	T_v	M_{xyz}	$2/m$	[100]
										$T_{4u}^{\beta 1}, T_{4u}^{\beta 2}$			
								Q_{zx}, Q_{4u}^α	G_y, G_{3v}	T_{xy}	M_z^β	$2'/m'$	[010]
										$T_{4v}^{\beta 1}, T_{4v}^{\beta 2}$			
A_{1u}	1	1	1	−1	−1	−1	A_{1u}^+		G_0, G_u, G_{40}	T_{3a}	M_{4a}	$6'22'$	[001]
							A_{1u}^-	Q_{3a}	G_{4a}		M_0, M_u, M_{40}	$\bar{6}'2m'$	[001]
A_{2u}	1	1	−1	−1	−1	1	A_{2u}^+	Q_z, Q_z^α		T_{3b}	M_{4b}	$6'mm'$	[001]
							A_{2u}^-	Q_{3b}	G_{4b}	T_z, T_z^α		$\bar{6}'m2'$	[001]
E_u	2	−1	0	−2	1	0	E_u^+	Q_z^β	G_{xy}	T_y, T_{3v}	M_{zx}, M_{4u}^α	$mm'2'$	[100]
									$G_{4v}^{\beta 1}, G_{4v}^{\beta 2}$				
								Q_{xyz}	G_v	T_x, T_{3u}	M_{yz}, M_{4v}^α	$22'2'$	[100]
									$G_{4u}^{\beta 1}, G_{4u}^{\beta 2}$				
							E_u^-	Q_x, Q_{3u}	G_{yz}, G_{4v}^α	T_{xyz}	M_v	$2m'm'$	[100]
											$M_{4u}^{\beta 1}, M_{4u}^{\beta 2}$		
								Q_y, Q_{3v}	G_{zx}, G_{4u}^α	T_z^β	M_{xy}	$m2'm'$	[100]
											$M_{4v}^{\beta 1}, M_{4v}^{\beta 2}$		

Table C.42: IRREPs of four types of multipoles in $62'2'$. The superscript "$\pm$" of IRREP stands for the parity with respect to the antiunitary operation $\mathcal{A}=\theta C_{2x}$.

	E	C_6	C_3	C_2	C_3^2	C_6^5	IRREP	E	ET	MT	M	MPG	P. axis
A	1	1	1	1	1	1	A^+	Q_0, Q_u, Q_{40}	G_0, G_u, G_{40}	T_z, T_z^α	M_z, M_z^α	$62'2'$	[001]
							A^-	Q_z, Q_z^α	G_z, G_z^α	T_0, T_u, T_{40}	M_0, M_u, M_{40}	6	[001]
B	1	-1	1	-1	1	-1	B^+	Q_{3a}, Q_{4a}	G_{3a}, G_{4a}	T_{3b}, T_{4b}	M_{3b}, M_{4b}	$32'$	[001]
							B^-	Q_{3b}, Q_{4b}	G_{3b}, G_{4b}	T_{3a}, T_{4a}	M_{3a}, M_{4a}	$32'$	[001]
E_1	1	$-\omega$	ω^2	-1	ω	$-\omega^2$	$E_1^{(1)+}$	$Q_x, Q_{yz}, Q_{3u}, Q_{4v}^\alpha$	$G_x, G_{yz}, G_{3u}, G_{4v}^\alpha$			$2'$	[100]
	1	$-\omega^2$	ω	-1	ω^2	$-\omega$	$E_1^{(2)+}$	$Q_y, Q_{zx}, Q_{3v}, Q_{4u}^\alpha$	$G_y, G_{zx}, G_{3v}, Q_{4u}^\alpha$			$2'$	[010]
							$E_1^{(1)-}$			$T_x, T_{yz}, T_{3u}, T_{4v}^\alpha$	$M_x, M_{yz}, M_{3u}, M_{4v}^\alpha$	$2'$	[010]
							$E_1^{(2)-}$			$T_y, T_{zx}, T_{3v}, T_{4u}^\alpha$	$M_y, M_{zx}, M_{3v}, M_{4u}^\alpha$	$2'$	[100]
E_2	1	ω	ω^2	1	ω	ω^2	$E_2^{(1)+}$	$Q_v, Q_{xyz}, Q_{4u}^{\beta1}, Q_{4u}^{\beta2}$	$G_v, G_{xyz}, G_{4u}^{\beta1}, G_{4u}^{\beta2}$			$2'2'2$	[100]
	1	ω^2	ω	1	ω^2	ω	$E_2^{(2)+}$	$Q_{xy}, Q_z^\beta, Q_{4v}^{\beta1}, Q_{4v}^{\beta2}$	$G_{xy}, G_z^\beta, G_{4v}^{\beta1}, G_{4v}^{\beta2}$			2	[001]
							$E_2^{(1)-}$			$T_v, T_{xyz}, T_{4u}^{\beta1}, T_{4u}^{\beta2}$	$M_v, M_{xyz}, M_{4u}^{\beta1}, M_{4u}^{\beta2}$	2	[001]
							$E_2^{(2)-}$			$T_{xy}, T_z^\beta, T_{4v}^{\beta1}, T_{4v}^{\beta2}$	$M_{xy}, M_z^\beta, M_{4v}^{\beta1}, M_{4v}^{\beta2}$	$2'2'2$	[100]

$\omega=\exp(-2\pi i/3)$

Table C.43: IRREPs of four types of multipoles in $6'22'$. The superscript "$\pm$" of IRREP stands for the parity with respect to the antiunitary operation $\mathcal{A}=\theta C_2$.

	E	$2C_3$	$3C_{2x}$	IRREP	E	ET	MT	M	MPG	P. axis
A_1	1	1	1	A_1^+	Q_0, Q_u, Q_{40}	G_0, G_u, G_{40}	T_{3a}, T_{4a}	M_{3a}, M_{4a}	$6'22'$	[001]
				A_1^-	Q_{3a}, Q_{4a}	G_{3a}, G_{4a}	T_0, T_u, T_{40}	M_0, M_u, M_{40}	32	[001]
A_2	1	1	-1	A_2^+	Q_z, Q_z^α	G_z, G_z^α	T_{3b}, T_{4b}	M_{3b}, M_{4b}	$6'$	[001]
				A_2^-	Q_{3b}, Q_{4b}	G_{3b}, G_{4b}	T_z, T_z^α	M_z, M_z^α	$32'$	[001]
E	2	-1	0	E^+	$Q_{xy}, Q_z^\beta, Q_{4v}^{\beta1}, Q_{4v}^{\beta2}$	$G_{xy}, G_z^\beta, G_{4v}^{\beta1}, G_{4v}^{\beta2}$	$T_y, T_{zx}, T_{3v}, T_{4u}^\alpha$	$M_y, M_{zx}, M_{3v}, M_{4u}^\alpha$	$2'$	[001]
					$Q_v, Q_{xyz}, Q_{4u}^{\beta1}, Q_{4u}^{\beta2}$	$G_v, G_{xyz}, G_{4u}^{\beta1}, G_{4u}^{\beta2}$	$T_x, T_{yz}, T_{3u}, T_{4v}^\alpha$	$M_x, M_{yz}, M_{3u}, M_{4v}^\alpha$	$22'2'$	[100]
				E^-	$Q_x, Q_{yz}, Q_{3u}, Q_{4v}^\alpha$	$G_x, G_{yz}, G_{3u}, G_{4v}^\alpha$	$T_v, T_{xyz}, T_{4u}^{\beta1}, T_{4u}^{\beta2}$	$M_v, M_{xyz}, M_{4u}^{\beta1}, M_{4u}^{\beta2}$	2	[100]
					$Q_y, Q_{zx}, Q_{3v}, Q_{4u}^\alpha$	$G_y, G_{zx}, G_{3v}, G_{4u}^\alpha$	$T_{xy}, T_z^\beta, T_{4v}^{\beta1}, T_{4v}^{\beta2}$	$M_{xy}, M_z^\beta, M_{4v}^{\beta1}, M_{4v}^{\beta2}$	$2'$	[010]

Table C.44: IRREPs of four types of multipoles in $\bar{6}'m'2$. The superscript "±" of IRREP stands for the parity with respect to the antiunitary operation $\mathcal{A}=\theta\sigma_h$.

	E	$2C_3$	$3C_{2y}$	IRREP	E	ET	MT	M	MPG	P. axis
A_1	1	1	1	A_1^+	$Q_0, Q_u,$ Q_{3b}, Q_{40}	G_{4b}	T_{4b}	$M_0, M_u,$ M_{3b}, M_{40}	$\bar{6}'m'2$	[001]
				A_1^-	Q_{4b}	$G_0, G_u,$ G_{3b}, G_{40}	$T_0, T_u,$ T_{3b}, T_{40}	M_{4b}	32	[001]
A_2	1	1	−1	A_2^+	Q_{3a}	G_z, G_z^α, G_{4a}	T_z, T_z^α, T_{4a}	M_{3a}	$\bar{6}'$	[001]
				A_2^-	Q_z, Q_z^α, Q_{4a}	G_{3a}	T_{3a}	M_z, M_z^α, M_{4a}	$3m'$	[001]
E	2	−1	0	E^+	$Q_x, Q_{xy}, Q_{3u},$ $Q_{4v}^{\beta1}, Q_{4v}^{\beta2}$	$G_{yz},$ G_z^β, G_{4v}^α	$T_{yz},$ T_z^β, T_{4v}^α	$M_x, M_{xy}, M_{3u},$ $M_{4v}^{\beta1}, M_{4v}^{\beta2}$	m'	[001]
					Q_y, Q_v, Q_{3v} $Q_{4u}^{\beta1}, Q_{4u}^{\beta2}$	$G_{zx},$ G_{xyz}, G_{4u}^α	$T_{zx},$ T_{xyz}, T_{4u}^α	$M_x, M_v, M_{3v},$ $M_{4u}^{\beta1}, M_{4u}^{\beta2}$	$m'2m'$	[100]
				E^-	$Q_{yz},$ Q_z^β, Q_{4v}^α	G_x, G_{xy}, G_{3u} $G_{4v}^{\beta1}, G_{4v}^{\beta2}$	$T_x, T_{xy}, T_{3u},$ $T_{4v}^{\beta1}, T_{4v}^{\beta2}$	$M_{yz},$ M_z^β, M_{4v}^α	m'	[100]
					$Q_{zx},$ $Q_{xyz}, Q_{4u}^\alpha,$	$G_y, G_v, G_{3v},$ $G_{4u}^{\beta1}, G_{4u}^{\beta2}$	$T_y, T_v, T_{3v},$ $T_{4u}^{\beta1}, T_{4u}^{\beta2}$	$M_{zx},$ M_{xyz}, M_{4u}^α	2	[010]

Table C.45: IRREPs of four types of multipoles in $\bar{6}'m2'$. The superscript "±" of IRREP stands for the parity with respect to the antiunitary operation $\mathcal{A}=\theta\sigma_h$.

	E	$2C_3$	$3\sigma_x$	IRREP	E	ET	MT	M	MPG	P. axis
A_1	1	1	1	A_1^+	$Q_0, Q_u,$ Q_{3b}, Q_{40}	G_{4b}	T_z, T_z^α, T_{4a}	M_{3a}	$\bar{6}'m2'$	[001]
				A_1^-	Q_z, Q_z^α, Q_{4a}	G_{3a}	$T_0, T_u,$ T_{3b}, T_{40}	M_{4b}	$3m$	[001]
A_2	1	1	−1	A_2^+	Q_{3a}	G_z, G_z^α, G_{4a}	T_{4b}	$M_0, M_u,$ M_{3b}, M_{40}	$\bar{6}'$	[001]
				A_2^-	Q_{4b}	$G_0, G_u,$ G_{3b}, G_{40}	T_{3a}	M_z, M_z^α, M_{4a}	$32'$	[001]
E	2	−1	0	E^+	$Q_x, Q_{xy}, Q_{3u},$ $Q_{4v}^{\beta1}, Q_{4v}^{\beta2}$	$G_{yz},$ G_z^β, G_{4v}^α	$T_{zx},$ T_{xyz}, T_{4u}^α	$M_y, M_v, M_{3v},$ $M_{4u}^{\beta1}, M_{4u}^{\beta2}$	m'	[001]
					Q_y, Q_v, Q_{3v} $Q_{4u}^{\beta1}, Q_{4u}^{\beta2}$	$G_{zx},$ G_{xyz}, G_{4u}^α	$T_{yz},$ T_z^β, T_{4v}^α	$M_x, M_{xy}, M_{3u},$ $M_{4v}^{\beta1}, M_{4v}^{\beta2}$	$m2'm'$	[100]
				E^-	$Q_{yz},$ Q_z^β, Q_{4v}^α	G_x, G_{xy}, G_{3u} $G_{4v}^{\beta1}, G_{4v}^{\beta2}$	T_y, T_v, T_{3v} $T_{4u}^{\beta1}, T_{4u}^{\beta2}$	$M_{zx},$ M_{xyz}, M_{4u}^α	m	[100]
					$Q_{zx},$ $Q_{xyz}, Q_{4u}^\alpha,$	G_y, G_v, G_{3v} $G_{4u}^{\beta1}, G_{4u}^{\beta2}$	T_x, T_{xy}, T_{3u} $T_{4v}^{\beta1}, T_{4v}^{\beta2}$	$M_{yz},$ M_z^β, M_{4v}^α	$2'$	[010]

Table C.46: IRREPs of four types of multipoles in $\bar{6}m'2'$. The superscript "±" of IRREP stands for the parity with respect to the antiunitary operation $\mathcal{A}=\theta C_{2y}$.

	E	IC_6	C_3	σ_h	C_3^2	IC_6^5	IRREP	E	ET	MT	M	MPG	P. axis
A′	1	1	1	1	1	1	A′$^{+}$	Q_0, Q_u, Q_{3b}, Q_{40}	G_{4b}	T_{3a}	M_z, M_z^α, M_{4a}	$\bar{6}m'2'$	[001]
							A′$^{-}$	Q_{3a}	G_z, G_z^α, G_{4a}	T_0, T_u, T_{3b}, T_{40}	M_{4b}	$\bar{6}$	[001]
A″	1	−1	1	−1	1	−1	A″$^{+}$	Q_{4b}	G_0, G_u, G_{3b}, G_{40}	T_z, T_z^α, T_{4a}	M_{3a}	$32'$	[001]
							A″$^{-}$	Q_z, Q_z^α, Q_{4a}	G_{3a}	T_{4b}	M_0, M_u, M_{3b}, M_{40}	$3m'$	[001]
E′	1	ω	ω^2	1	ω	ω^2	E′$^{(1)+}$	$Q_v, Q_{4u}^{\beta1}, Q_{4u}^{\beta2}$	G_{xyz}	T_x, T_{3u}	M_{yz}, M_{4v}^α	$m'2'm$	[100]
	1	ω^2	ω	1	ω^2	ω	E′$^{(2)+}$	$Q_{xy}, Q_{4v}^{\beta1}, Q_{4v}^{\beta2}$	G_z^β	T_y, T_{3v}	M_{zx}, M_{4u}^α	m	[001]
							E′$^{(1)-}$	Q_x, Q_{3u}	G_{yz}, G_{4v}^α	$T_v, T_{4u}^{\beta1}, T_{4u}^{\beta2}$	M_{xyz}	m	[001]
							E′$^{(2)-}$	Q_y, Q_{3v}	G_{zx}, G_{4u}^α	$T_{xy}, T_{4v}^{\beta1}, T_{4v}^{\beta2}$	M_z^β	$m'2'm$	[100]
E″	1	$-\omega$	ω^2	−1	ω	$-\omega^2$	E″$^{(1)+}$	Q_{xyz}	$G_v, G_{4u}^{\beta1}, G_{4u}^{\beta2}$	T_{yz}, T_{4v}^α	M_x, M_{3u}	$2'$	[010]
	1	$-\omega^2$	ω	−1	ω^2	$-\omega$	E″$^{(2)+}$	Q_z^β	$G_{xy}, G_{4v}^{\beta1}, G_{4v}^{\beta2}$	T_{zx}, T_{4u}^α	M_y, M_{3v}	m'	[100]
							E″$^{(1)-}$	Q_{yz}, Q_{4v}^α	G_x, G_{3u}	T_{xyz}	$M_v, M_{4u}^{\beta1}, M_{4u}^{\beta2}$	m'	[100]
							E″$^{(2)-}$	Q_{zx}, Q_{4u}^α	G_y, G_{3v}	T_z^β	$M_{xy}, M_{4v}^{\beta1}, M_{4v}^{\beta2}$	$2'$	[010]

ω=exp($-2\pi i/3$)

Table C.47: IRREPs of four types of multipoles in $6'mm'$. The superscript "±" of IRREP stands for the parity with respect to the antiunitary operation $\mathcal{A}=\theta C_2$.

	E	$2C_3$	$3\sigma_x$	IRREP	E	ET	MT	M	MPG	P. axis
A_1	1	1	1	A_1^+	$Q_0, Q_z, Q_u, Q_z^\alpha, Q_{40}$		T_{3a}, T_{4b}	M_{3b}, M_{4a}	$6'mm'$	[001]
				A_1^-	Q_{3a}, Q_{4b}	G_{3b}, G_{4a}	$T_0, T_z, T_u, T_z^\alpha, T_{40}$		$3m$	[001]
A_2	1	1	−1	A_2^+		$G_0, G_z, G_u, G_z^\alpha, G_{40}$	T_{3b}, T_{4a}	M_{3a}, M_{4b}	$6'$	[001]
				A_2^-	Q_{3b}, Q_{4a}	G_{3a}, G_{4b}		$M_0, M_z, M_u, M_z^\alpha, M_{40}$	$3m'$	[001]
E	2	−1	0	E^+	$Q_{xy}, Q_{xyz}, Q_{4v}^{\beta1}, Q_{4v}^{\beta2}$	$G_v, G_z^\beta, G_{4u}^{\beta1}, G_{4u}^{\beta2}$	$T_x, T_{zx}, T_{3u}, T_{4u}^\alpha$	$M_y, M_{yz}, M_{3v}, M_{4v}^\alpha$	$2'$	[001]
					$Q_v, Q_z^\beta, Q_{4u}^{\beta1}, Q_{4u}^{\beta2}$	$G_{xy}, G_{xyz}, G_{4v}^{\beta1}, G_{4v}^{\beta2}$	$T_y, T_{yz}, T_{3v}, T_{4v}^\alpha$	$M_x, M_{zx}, M_{3u}, M_{4u}^\alpha$	$mm'2'$	[100]
				E^-	$Q_y, Q_{yz}, Q_{3v}, Q_{4v}^\alpha$	$G_x, G_{zx}, G_{3u}, G_{4u}^\alpha$	$T_v, T_z^\beta, T_{4u}^{\beta1}, T_{4u}^{\beta2}$	$M_{xy}, M_{xyz}, M_{4v}^{\beta1}, M_{4v}^{\beta2}$	m	[100]
					$Q_x, Q_{zx}, Q_{3u}, Q_{4u}^\alpha,$	$G_y, G_{yz}, G_{3v}, G_{4v}^\alpha$	$T_{xy}, T_{xyz}, T_{4v}^{\beta1}, T_{4v}^{\beta2}$	$M_v, M_z^\beta, M_{4u}^{\beta1}, M_{4u}^{\beta2}$	m'	[010]

Table C.48: IRREPs of four types of multipoles in $6m'm'$. The superscript "±" of IRREP stands for the parity with respect to the antiunitary operation $\mathcal{A}=\theta\sigma_x$.

	E	C_6	C_3	C_2	C_3^2	C_6^5	IRREP	E	ET	MT	M	MPG	P. axis
A	1	1	1	1	1	1	A^+	$Q_0, Q_z, Q_u,$ Q_z^α, Q_{40}			$M_0, M_z, M_u,$ M_z^α, M_{40}	$6m'm'$	[001]
							A^-		$G_0, G_z, G_u,$ G_z^α, G_{40}	$T_0, T_z, T_u,$ T_z^α, T_{40}		6	[001]
B	1	−1	1	−1	1	−1	B^+	Q_{3b}, Q_{4a}	G_{3a}, G_{4b}	T_{3a}, T_{4b}	M_{3b}, M_{4a}	$3m'$	[001]
							B^-	Q_{3a}, Q_{4b}	G_{3b}, G_{4a}	T_{3b}, T_{4a}	M_{3a}, M_{4b}	$3m'$	[001]
E_1	1	$-\omega$	ω^2	−1	ω	$-\omega^2$	$E_1^{(1)+}$	Q_{yz}, Q_{4v}^α	G_x, G_{3u}	T_x, T_{3u}	M_{yz}, M_{4v}^α	m'	[100]
	1	$-\omega^2$	ω	−1	ω^2	$-\omega$	$E_1^{(2)+}$	Q_{zx}, Q_{4u}^α	G_y, G_{3v}	T_y, T_{3v}	M_{zx}, M_{4u}^α	m'	[010]
							$E_1^{(1)-}$	Q_x, Q_{3u}	G_{yz}, G_{4v}^α	T_{yz}, T_{4v}^α	M_x, M_{3u}	m'	[010]
							$E_1^{(2)-}$	Q_y, Q_{3v}	G_{zx}, G_{4u}^α	T_{zx}, T_{4u}^α	M_y, M_{3v}	m'	[100]
E_2	1	ω	ω^2	1	ω	ω^2	$E_2^{(1)+}$	$Q_v, Q_{4u}^{\beta 1}, Q_{4u}^{\beta 2}$	G_{xyz}	T_{xyz}	$M_v, M_{4u}^{\beta 1}, M_{4u}^{\beta 2}$	$m'm'2$	[100]
	1	ω^2	ω	1	ω^2	ω	$E_2^{(2)+}$	$Q_{xy}, Q_{4v}^{\beta 1}, Q_{4v}^{\beta 2}$	G_z^β	T_z^β	$M_{xy}, M_{4v}^{\beta 1}, M_{4v}^{\beta 2}$	2	[001]
							$E_2^{(1)-}$	Q_{xyz}	$G_v, G_{4u}^{\beta 1}, G_{4u}^{\beta 2}$	$T_v, T_{4u}^{\beta 1}, T_{4u}^{\beta 2}$	M_{xyz}	2	[001]
							$E_2^{(2)-}$	Q_z^β	$G_{xy}, G_{4v}^{\beta 1}, G_{4v}^{\beta 2}$	$T_{xy}, T_{4v}^{\beta 1}, T_{4v}^{\beta 2}$	M_z^β	$m'm'2$	[100]

ω=exp($-2\pi i/3$)

Table C.49: IRREPs of four types of multipoles in $6'/m$. The superscript "±" of IRREP stands for the parity with respect to the antiunitary operation $\mathcal{A}=\theta I$.

	E	IC_6	C_3	σ_h	C_3^2	IC_6^5	IRREP	E	ET	MT	M	MPG	P. axis
A′	1	1	1	1	1	1	A'^+	$Q_0, Q_u,$ Q_{40}	G_z, G_z^α	T_{3a}, T_{3b}	M_{4a}, M_{4b}	$6'/m$	[001]
							A'^-	Q_{3a}, Q_{3b}	G_{4a}, G_{4b}	$T_0, T_u,$ T_{40}	M_z, M_z^α	$\bar{6}$	[001]
A″	1	−1	1	−1	1	−1	A''^+	Q_{4a}, Q_{4b}	G_{3a}, G_{3b}	T_z, T_z^α	$M_0, M_u,$ M_{40}	$\bar{3}'$	[001]
							A''^-	Q_z, Q_z^α	$G_0, G_u,$ G_{40}	T_{4a}, T_{4b}	M_{3a}, M_{3b}	6	[001]
E′	1	ω	ω^2	1	ω	ω^2	E′	$Q_v, Q_{4u}^{\beta 1}, Q_{4u}^{\beta 2}$	G_{xyz}	T_y, T_{3v}	M_{zx}, M_{4u}^α	$2'/m$	[001]
	1	ω^2	ω	1	ω^2	ω		$Q_{xy}, Q_{4v}^{\beta 1}, Q_{4v}^{\beta 2}$	G_z^β	T_x, T_{3u}	M_{yz}, M_{4v}^α	$2'/m$	[001]
								Q_y, Q_{3v}	G_{zx}, G_{4u}^α	$T_v, T_{4u}^{\beta 1}, T_{4u}^{\beta 2}$	M_{xyz}	m	[001]
								Q_x, Q_{3u}	G_{yz}, G_{4v}^α	$T_{xy}, T_{4v}^{\beta 1}, T_{4v}^{\beta 2}$	M_z^β	m	[001]
E″	1	$-\omega$	ω^2	−1	ω	$-\omega^2$	E″	Q_{yz}, Q_{4v}^α	G_x, G_{3u}	T_z^β	$M_{xy}, M_{4v}^{\beta 1}, M_{4v}^{\beta 2}$	$\bar{1}'$	—
	1	$-\omega^2$	ω	−1	ω^2	$-\omega$		Q_{zx}, Q_{4u}^α	G_y, G_{3v}	T_{xyz}	$M_v, M_{4u}^{\beta 1}, M_{4u}^{\beta 2}$	$\bar{1}'$	—
								Q_z^β	$G_{xy}, G_{4v}^{\beta 1}, G_{4v}^{\beta 2}$	T_{yz}, T_{4v}^α	M_x, M_{3u}	$2'$	[001]
								Q_{xyz}	$G_v, G_{4u}^{\beta 1}, G_{4u}^{\beta 2}$	T_{zx}, T_{4u}^α	M_y, M_{3v}	$2'$	[001]

ω=exp($-2\pi i/3$)

Table C.50: IRREPs of four types of multipoles in $6/m'$. The superscript "±" of IRREP stands for the parity with respect to the antiunitary operation $\mathcal{A}=\theta I$.

	E	C_6	C_3	C_2	C_3^2	C_6^5	IRREP	E	ET	MT	M	MPG	P. axis
A	1	1	1	1	1	1	A^+	Q_0, Q_u, Q_{40}	G_z, G_z^α	T_z, T_z^α	M_0, M_u, M_{40}	$6/m'$	[001]
							A^-	Q_z, Q_z^α	G_0, G_u, G_{40}	T_0, T_u, T_{40}	M_z, M_z^α	6	[001]
B	1	−1	1	−1	1	−1	B^+	Q_{4a}, Q_{4b}	G_{3a}, G_{3b}	T_{3a}, T_{3b}	M_{4a}, M_{4b}	$\bar{3}'$	[001]
							B^-	Q_{3a}, Q_{3b}	G_{4a}, G_{4b}	T_{4a}, T_{4b}	M_{3a}, M_{3b}	$\bar{6}'$	[001]
E_1	1	$-\omega$	ω^2	−1	ω	$-\omega^2$	E_1	Q_{yz}, Q_{4v}^α	G_x, G_{3u}	T_x, T_{3u}	M_{yz}, M_{4v}^α	$\bar{1}'$	—
								Q_{zx}, Q_{4u}^α	G_y, G_{3v}	T_y, T_{3v}	M_{zx}, M_{4u}^α	$\bar{1}'$	—
	1	$-\omega^2$	ω	−1	ω^2	$-\omega$		Q_x, Q_{3u}	G_{yz}, G_{4v}^α	T_{yz}, T_{4v}^α	M_x, M_{3u}	m'	[001]
								Q_y, Q_{3v}	G_{zx}, G_{4u}^α	T_{zx}, T_{4u}^α	M_y, M_{3v}	m'	[001]
E_2	1	ω	ω^2	1	ω	ω^2	E_2	$Q_v, Q_{4u}^{\beta 1}, Q_{4u}^{\beta 2}$	G_{xyz}	T_{xyz}	$M_v, M_{4u}^{\beta 1}, M_{4u}^{\beta 2}$	$2/m'$	[001]
								$Q_{xy}, Q_{4v}^{\beta 1}, Q_{4v}^{\beta 2}$	G_z^β	T_z^β	$M_{xy}, M_{4v}^{\beta 1}, M_{4v}^{\beta 2}$	$2/m'$	[001]
	1	ω^2	ω	1	ω^2	ω		Q_{xyz}	$G_v, G_{4u}^{\beta 1}, G_{4u}^{\beta 2}$	$T_v, T_{4u}^{\beta 1}, T_{4u}^{\beta 2}$	M_{xyz}	2	[001]
								Q_z^β	$G_{xy}, G_{4v}^{\beta 1}, G_{4v}^{\beta 2}$	$T_{xy}, T_{4v}^{\beta 1}, T_{4v}^{\beta 2}$	M_z^β	2	[001]

$\omega=\exp(-2\pi i/3)$

Table C.51: IRREPs of four types of multipoles in $6'/m'$. The superscript "±" of IRREP stands for the parity with respect to the antiunitary operation $\mathcal{A}=\theta C_2$.

	E	C_3	C_3^2	I	IC_3	IC_3^2	IRREP	E	ET	MT	M	MPG	P. axis
A_g	1	1	1	1	1	1	A_g^+	Q_0, Q_u, Q_{40}	G_z, G_z^α	T_{4a}, T_{4b}	M_{3a}, M_{3b}	$6'/m'$	[001]
							A_g^-	Q_{4a}, Q_{4b}	G_{3a}, G_{3b}	T_0, T_u, T_{40}	M_z, M_z^α	$\bar{3}$	[001]
E_g	1	ω	ω^2	1	ω	ω^2	E_g	Q_{yz}, Q_{4v}^α	G_x, G_{3u}	$T_v, T_{4u}^{\beta 1}, T_{4u}^{\beta 2}$	M_{xyz}	$\bar{1}$	—
	1	ω^2	ω	1	ω^2	ω		Q_{zx}, Q_{4u}^α	G_y, G_{3v}	$T_{xy}, T_{4v}^{\beta 1}, T_{4v}^{\beta 2}$	M_z^β	$\bar{1}$	—
								$Q_v, Q_{4u}^{\beta 1}, Q_{4u}^{\beta 2}$	G_{xyz}	T_{yz}, T_{4v}^α	M_x, M_{3u}	$2'/m'$	[001]
								$Q_{xy}, Q_{4v}^{\beta 1}, Q_{4v}^{\beta 2}$	G_z^β	$T_{zx}, T_{4u}^\alpha,$	M_y, M_{3v}	$2'/m'$	[001]
A_u	1	1	1	−1	−1	−1	A_u^+	Q_z, Q_z^α	G_0, G_u, G_{40}	T_{3a}, T_{3b}	M_{4a}, M_{4b}	$6'$	[001]
							A_u^-	Q_{3a}, Q_{3b}	G_{4a}, G_{4b}	T_z, T_z^α	M_0, M_u, M_{40}	$\bar{6}'$	[001]
E_u	1	ω	ω^2	−1	$-\omega$	$-\omega^2$	E_u	Q_x, Q_{3u}	G_{yz}, G_{4v}^α	T_{xyz}	$M_v, M_{4u}^{\beta 1}, M_{4u}^{\beta 2}$	m'	[001]
	1	ω^2	ω	−1	$-\omega^2$	$-\omega$		Q_y, Q_{3v}	G_{zx}, G_{4u}^α	T_z^β	$M_{xy}, M_{4v}^{\beta 1}, M_{4v}^{\beta 2}$		
								$Q_{xyz},$	$G_v, G_{4u}^{\beta 1}, G_{4u}^{\beta 2}$	T_x, T_{3u}	M_{yz}, M_{4v}^α	$2'$	[001]
								Q_z^β	$G_{xy}, G_{4v}^{\beta 1}, G_{4v}^{\beta 2}$	T_y, T_{3v}	M_{zx}, M_{4u}^α		

$\omega=\exp(-2\pi i/3)$

Table C.52: IRREPs of four types of multipoles in $\bar{6}'$. The superscript "±" of IRREP stands for the parity with respect to the antiunitary operation $\mathcal{A}=\theta\sigma_h$.

E	C_3	C_3^2	IRREP	E	ET	MT	M	MPG	P. axis
A 1	1	1	A^+	$Q_0, Q_u,$	$G_z, G_z^\alpha,$	$T_z, T_z^\alpha,$	$M_0, M_u,$	$\bar{6}'$	[001]
				Q_{3a}, Q_{3b}, Q_{40}	G_{4a}, G_{4b}	T_{4a}, T_{4b}	M_{3a}, M_{3b}, M_{40}		
			A^-	$Q_z, Q_z^\alpha,$	$G_0, G_u,$	$T_0, T_u,$	$M_z, M_z^\alpha,$	3	[001]
				Q_{4a}, Q_{4b}	G_{3a}, G_{3b}, G_{40}	T_{3a}, T_{3b}, T_{40}	M_{4a}, M_{4b}		
E 1	ω	ω^2	E	$Q_x, Q_v, Q_{3u},$	$G_{yz}, G_{xyz}, G_{4v}^\alpha$	$T_{yz}, T_{xyz}, T_{4v}^\alpha$	$M_x, M_v, M_{3u},$	m'	[001]
1	ω^2	ω		$Q_{4u}^{\beta 1}, Q_{4u}^{\beta 2}$			$M_{4u}^{\beta 1}, M_{4u}^{\beta 2}$		
				$Q_y, Q_{xy}, Q_{3v},$	$G_{zx}, G_z^\beta, G_{4u}^\alpha$	$T_{zx}, T_z^\beta, T_{4u}^\alpha$	$M_y, M_{xy}, M_{3v},$		
				$Q_{4v}^{\beta 1}, Q_{4v}^{\beta 2}$			$M_{4v}^{\beta 1}, M_{4v}^{\beta 2}$		
				$Q_{yz}, Q_{xyz}, Q_{4v}^\alpha$	$G_x, G_v, G_{3u},$	$T_x, T_v, T_{3u},$	$M_{yz}, M_{xyz}, M_{4v}^\alpha$	1	—
					$G_{4u}^{\beta 1}, G_{4u}^{\beta 2}$	$T_{4u}^{\beta 1}, T_{4u}^{\beta 2}$			
				$Q_{zx}, Q_z^\beta, Q_{4u}^\alpha$	$G_y, G_{xy}, G_{3v},$	$T_y, T_{xy}, T_{3v},$	$M_{zx}, M_z^\beta, M_{4u}^\alpha$		
					$G_{4v}^{\beta 1}, G_{4v}^{\beta 2}$	$T_{4v}^{\beta 1}, T_{4v}^{\beta 2}$			

$\omega=\exp(-2\pi i/3)$

Table C.53: IRREPs of four types of multipoles in $6'$. The superscript "±" of IRREP stands for the parity with respect to the antiunitary operation $\mathcal{A}=\theta C_2$.

E	C_3	C_3^2	IRREP	E	ET	MT	M	MPG	P. axis
A 1	1	1	A^+	$Q_0, Q_z, Q_u,$	G_0, G_z, G_u	$T_{3a}, T_{3b},$	$M_{3a}, M_{3b},$	$6'$	[001]
				Q_z^α, Q_{40}	G_z^α, G_{40}	T_{4a}, T_{4b}	M_{4a}, M_{4b}		
			A^-	$Q_{3a}, Q_{3b},$	$G_{3a}, G_{3b},$	$T_0, T_z, T_u,$	$M_0, M_z, M_u,$	3	[001]
				Q_{4a}, Q_{4b}	G_{4a}, G_{4b}	T_z^α, T_{40}	M_z^α, M_{40}		
E 1	ω	ω^2	E	$Q_v, Q_{xyz}, Q_{4u}^{\beta 1}, Q_{4u}^{\beta 2}$	$G_v, G_{xyz}, G_{4u}^{\beta 1}, G_{4u}^{\beta 2}$	$T_x, T_{yz}, T_{3u}, T_{4v}^\alpha$	$M_x, M_{yz}, M_{3u}, M_{4v}^\alpha$	$2'$	[001]
1	ω^2	ω		$Q_{xy}, Q_z^\beta, Q_{4v}^{\beta 1}, Q_{4v}^{\beta 2}$	$G_{xy}, G_z^\beta, G_{4v}^{\beta 1}, G_{4v}^{\beta 2}$	$T_y, T_{zx}, T_{3v}, T_{4u}^\alpha$	$M_y, M_{zx}, M_{3v}, M_{4u}^\alpha$		
				$Q_x, Q_{yz}, Q_{3u}, Q_{4v}^\alpha$	$G_x, G_{yz}, G_{3u}, G_{4v}^\alpha$	$T_v, T_{xyz}, T_{4u}^{\beta 1}, T_{4u}^{\beta 2}$	$M_v, M_{xyz}, M_{4u}^{\beta 1}, M_{4u}^{\beta 2}$	1	—
				$Q_y, Q_{zx}, Q_{3v}, Q_{4u}^\alpha$	$G_y, G_{zx}, G_{3v}, G_{4u}^\alpha$	$T_{xy}, T_z^\beta, T_{4v}^{\beta 1}, T_{4v}^{\beta 2}$	$M_{xy}, M_z^\beta, M_{4v}^{\beta 1}, M_{4v}^{\beta 2}$		

$\omega=\exp(-2\pi i/3)$

Table C.54: IRREPs of four types of multipoles in $\bar{3}'m'$. The superscript "±" of IRREP stands for the parity with respect to the antiunitary operation $\mathcal{A}=\theta I$.

	E	$2C_3$	$3C_{2y}$	IRREP	E	ET	MT	M	MPG	P. axis
A_1	1	1	1	A_1^+	$Q_0, Q_u,$ Q_{40}, Q_{4b}	G_{3b}	T_{3b}	$M_0, M_u,$ M_{40}, M_{4b}	$\bar{3}'m'$	[001]
				A_1^-	Q_{3b}	$G_0, G_u,$ G_{40}, G_{4b}	$T_0, T_u,$ T_{40}, T_{4b}	M_{3b}	32	[001]
A_2	1	1	−1	A_2^+	Q_{4a}	G_z, G_z^α, G_{3a}	T_z, T_z^α, T_{3a}	M_{4a}	$\bar{3}'$	[001]
				A_2^-	Q_z, Q_z^α, Q_{3a}	G_{4a}	T_{4a}	M_z, M_z^α, M_{3a}	$3m'$	[001]
E	2	−1	0	E^+	$Q_{yz}, Q_{xy},$ $Q_{4v}^\alpha, Q_{4v}^{\beta 1}, Q_{4v}^{\beta 2}$	G_x, G_{3u}, G_z^β	T_x, T_{3u}, T_z^β	$M_{yz}, M_{xy},$ $M_{4v}^\alpha, M_{4v}^{\beta 1}, M_{4v}^{\beta 2}$	$\bar{1}'$	—
					$Q_{zx}, Q_v,$ $Q_{4u}^\alpha, Q_{4u}^{\beta 1}, Q_{4u}^{\beta 2}$	G_y, G_{3v}, G_{xyz}	T_y, T_{3v}, T_{xyz}	$M_{zx}, M_v,$ $M_{4u}^\alpha, M_{4u}^{\beta 1}, M_{4u}^{\beta 2}$	$2/m'$	[010]
				E^-	Q_x, Q_{3u}, Q_z^β	$G_{yz}, G_{xy},$ $G_{4v}^\alpha, G_{4v}^{\beta 1}, G_{4v}^{\beta 2}$	$T_{yz}, T_{xy},$ $T_{4v}^\alpha, T_{4v}^{\beta 1}, T_{4v}^{\beta 2}$	M_x, M_{3u}, M_z^β	m'	[010]
					Q_y, Q_{3v}, Q_{xyz}	$G_{zx}, G_v,$ $G_{4u}^\alpha, G_{4u}^{\beta 1}, G_{4u}^{\beta 2}$	$T_{zx}, T_v,$ $T_{4u}^\alpha, T_{4u}^{\beta 1}, T_{4u}^{\beta 2}$	M_y, M_{3v}, M_{xyz}	2	[010]

Table C.55: IRREPs of four types of multipoles in $\bar{3}'m$. The superscript "±" of IRREP stands for the parity with respect to the antiunitary operation $\mathcal{A}=\theta I$.

	E	$2C_3$	$3\sigma_y$	IRREP	E	ET	MT	M	MPG	P. axis
A_1	1	1	1	A_1^+	$Q_0, Q_u,$ Q_{40}, Q_{4b}	G_{3b}	T_z, T_z^α, T_{3a}	M_{4a}	$\bar{3}'m$	[001]
				A_1^-	Q_z, Q_z^α, Q_{3a}	G_{4a}	$T_0, T_u,$ T_{40}, T_{4b}	M_{3b}	$3m$	[001]
A_2	1	1	−1	A_2^+	Q_{4a}	G_z, G_z^α, G_{3a}	T_{3b}	$M_0, M_u,$ M_{40}, M_{4b}	$\bar{3}'$	[001]
				A_2^-	Q_{3b}	$G_0, G_u,$ G_{40}, G_{4b}	T_{4a}	M_z, M_z^α, M_{3a}	$32'$	[001]
E	2	−1	0	E^+	$Q_{yz}, Q_{xy},$ $Q_{4v}^\alpha, Q_{4v}^{\beta 1}, Q_{4v}^{\beta 2}$	G_x, G_{3u}, G_z^β	T_y, T_{3v}, T_{xyz}	$M_{zx}, M_v,$ $M_{4u}^\alpha, M_{4u}^{\beta 1}, M_{4u}^{\beta 2}$	$\bar{1}'$	—
					Q_{zx}, Q_v $Q_{4u}^\alpha, Q_{4u}^{\beta 1}, Q_{4u}^{\beta 2}$	G_y, G_{3v}, G_{xyz}	T_x, T_{3u}, T_z^β	$M_{yz}, M_{xy},$ $M_{4v}^\alpha, M_{4v}^{\beta 1}, M_{4v}^{\beta 2}$	$2'/m$	[010]
				E^-	Q_y, Q_{3v}, Q_{xyz}	$G_{zx}, G_v,$ $G_{4u}^\alpha, G_{4u}^{\beta 1}, G_{4u}^{\beta 2}$	$T_{yz}, T_{xy},$ $T_{4v}^\alpha, T_{4v}^{\beta 1}, T_{4v}^{\beta 2}$	M_x, M_{3u}, M_z^β	$2'$	[010]
					Q_x, Q_{3u}, Q_z^β	$G_{yz}, G_{xy},$ $G_{4v}^\alpha, G_{4v}^{\beta 1}, G_{4v}^{\beta 2}$	$T_{zx}, T_v,$ $T_{4u}^\alpha, T_{4u}^{\beta 1}, T_{4u}^{\beta 2}$	M_y, M_{3v}, M_{xyz}	m	[010]

Table C.56: IRREPs of four types of multipoles in $\bar{3}m'$. The superscript "±" of IRREP stands for the parity with respect to the antiunitary operation $\mathcal{A}=\theta C_2'$.

	E	C_3	C_3^2	I	IC_3	IC_3^2	IRREP	E	ET	MT	M	MPG	P. axis
A_g	1	1	1	1	1	1	A_g^+	Q_0, Q_u, Q_{40}, Q_{4b}	G_{3b}	T_{4a}	M_z, M_z^α, M_{3a}	$\bar{3}m'$	[001]
							A_g^-	Q_{4a}	G_z, G_z^α, G_{3a}	T_0, T_u, T_{40}, T_{4b}	M_{3b}	$\bar{3}$	[001]
E_g	1	ω	ω^2	1	ω	ω^2	$E_g^{(1)+}$	$Q_{yz}, Q_{xy}, Q_{4v}^\alpha, Q_{4v}^{\beta 1}, Q_{4v}^{\beta 2}$	G_x, G_{3u}, G_z^β			$\bar{1}$	—
	1	ω^2	ω	1	ω^2	ω	$E_g^{(2)+}$	$Q_{zx}, Q_v, Q_{4u}^\alpha, Q_{4u}^{\beta 1}, Q_{4u}^{\beta 2}$	G_y, G_{3v}, G_{xyz}			$2'/m'$	[010]
							$E_g^{(1)-}$			$T_{yz}, T_{xy}, T_{4v}^\alpha, T_{4v}^{\beta 1}, T_{4v}^{\beta 2}$	M_x, M_{3u}, M_z^β	$2'/m'$	[010]
							$E_g^{(2)-}$			$T_{zx}, T_v, T_{4u}^\alpha, T_{4u}^{\beta 1}, T_{4u}^{\beta 2}$	M_y, M_{3v}, M_{xyz}	$\bar{1}$	—
A_u	1	1	1	-1	-1	-1	A_u^+	Q_{3b}	G_0, G_u, G_{40}, G_{4b}	T_z, T_z^α, T_{3a}	M_{4a}	$32'$	[001]
							A_u^-	Q_z, Q_z^α, Q_{3a}	G_{4a}	T_{3b}	M_0, M_u, M_{40}, M_{4b}	$3m'$	[001]
E_u	1	ω	ω^2	-1	$-\omega$	$-\omega^2$	$E_u^{(1)+}$	Q_x, Q_{3u}, Q_z^β	$G_{yz}, G_{xy}, G_{4v}^\alpha, G_{4v}^{\beta 1}, G_{4v}^{\beta 2}$			m'	[010]
	1	ω^2	ω	-1	$-\omega^2$	$-\omega$	$E_u^{(2)+}$	Q_y, Q_{3v}, Q_{xyz}	$G_{zx}, G_v, G_{4u}^\alpha, G_{4u}^{\beta 1}, G_{4u}^{\beta 2}$			$2'$	[010]
							$E_u^{(1)-}$			T_x, T_{3u}, T_z^β	$M_{yz}, M_{xy}, M_{4v}^\alpha, M_{4v}^{\beta 1}, M_{4v}^{\beta 2}$	$2'$	[010]
							$E_u^{(2)-}$			T_y, T_{3v}, T_{xyz}	$M_{zx}, M_v, M_{4u}^\alpha, M_{4u}^{\beta 1}, M_{4u}^{\beta 2}$	m'	[010]

$\omega=\exp(-2\pi i/3)$

Table C.57: IRREPs of four types of multipoles in $32'$. The superscript "±" of IRREP stands for the parity with respect to the antiunitary operation $\mathcal{A}=\theta C_2'$.

	E	C_3	C_3^2	IRREP	E	ET	MT	M	MPG	P. axis
A	1	1	1	A^+	$Q_0, Q_u, Q_{3b}, Q_{40}, Q_{4b}$	$G_0, G_u, G_{3b}, G_{40}, G_{4b}$	$T_z, T_z^\alpha, T_{3a}, T_{4a}$	$M_z, M_z^\alpha, M_{3a}, M_{4a}$	$32'$	[001]
				A^-	$Q_z, Q_z^\alpha, Q_{3a}, Q_{4a}$	$G_z, G_z^\alpha, G_{3a}, G_{4a}$	$T_0, T_u, T_{3b}, T_{40}, T_{4b}$	$M_0, M_u, M_{3b}, M_{40}, M_{4b}$	3	[001]
E	1	ω	ω^2	$E^{(1)+}$	$Q_x, Q_{yz}, Q_{xy}, Q_{3u}, Q_z^\beta, Q_{4v}^\alpha, Q_{4v}^{\beta 1}, Q_{4v}^{\beta 2}$	$G_x, G_{yz}, G_{xy}, G_{3u}, G_z^\beta, G_{4v}^\alpha, G_{4v}^{\beta 1}, G_{4v}^{\beta 2}$			1	—
	1	ω^2	ω	$E^{(2)+}$	$Q_y, Q_{zx}, Q_v, Q_{3v}, Q_{xyz}, Q_{4u}^\alpha, Q_{4u}^{\beta 1}, Q_{4u}^{\beta 2}$	$G_y, G_{zx}, G_v, G_{3v}, G_{xyz}, G_{4u}^\alpha, G_{4u}^{\beta 1}, G_{4u}^{\beta 2}$			$2'$	[010]
				$E^{(1)-}$			$T_x, T_{yz}, T_{xy}, T_{3u}, T_z^\beta, T_{4v}^\alpha, T_{4v}^{\beta 1}, T_{4v}^{\beta 2}$	$M_x, M_{yz}, M_{xy}, M_{3u}, M_z^\beta, M_{4v}^\alpha, M_{4v}^{\beta 1}, M_{4v}^{\beta 2}$	$2'$	[010]
				$E^{(2)-}$			$T_y, T_{zx}, T_v, T_{3v}, T_{xyz}, T_{4u}^\alpha, T_{4u}^{\beta 1}, T_{4u}^{\beta 2}$	$M_y, M_{zx}, M_v, M_{3v}, M_{xyz}, M_{4u}^\alpha, M_{4u}^{\beta 1}, M_{4u}^{\beta 2}$	1	—

$\omega=\exp(-2\pi i/3)$

Table C.58: IRREPs of four types of multipoles in $\bar{3}'$. The superscript "±" of IRREP stands for the parity with respect to the antiunitary operation $\mathcal{A}=\theta I$.

E	C_3	C_3^2	IRREP	E	ET	MT	M	MPG	P. axis
A 1	1	1	A^+	$Q_0, Q_u,$ Q_{40}, Q_{4a}, Q_{4b}	$G_z, G_z^\alpha, G_{3a}, G_{3b}$	$T_z, T_z^\alpha, T_{3a}, T_{3b}$	$M_0, M_u,$ M_{40}, M_{4a}, M_{4b}	$\bar{3}'$	[001]
			A^-	$Q_z, Q_z^\alpha, Q_{3a}, Q_{3b}$	$G_0, G_u,$ G_{40}, G_{4a}, G_{4b}	$T_0, T_u,$ T_{40}, T_{4a}, T_{4b}	$M_z, M_z^\alpha, M_{3a}, M_{3b}$	3	[001]
E 1	ω	ω^2	E	$Q_{yz}, Q_{xy},$ $Q_{4v}^\alpha, Q_{4v}^{\beta 1}, Q_{4v}^{\beta 2}$	G_x, G_{3u}, G_z^β	T_x, T_{3u}, T_z^β	$M_{yz}, M_{xy},$ $M_{4v}^\alpha, M_{4v}^{\beta 1}, M_{4v}^{\beta 2}$	$\bar{1}'$	—
1	ω^2	ω		$Q_{zx}, Q_v,$ $Q_{4u}^\alpha, Q_{4u}^{\beta 1}, Q_{4u}^{\beta 2}$	G_y, G_{3v}, G_{xyz}	T_y, T_{3v}, T_{xyz}	$M_{zx}, M_v,$ $M_{4u}^\alpha, M_{4u}^{\beta 1}, M_{4u}^{\beta 2}$		
				Q_x, Q_{3u}, Q_z^β	$G_{yz}, G_{xy},$ $G_{4v}^\alpha, G_{4v}^{\beta 1}, G_{4v}^{\beta 2}$	$T_{yz}, T_{xy},$ $T_{4v}^\alpha, T_{4v}^{\beta 1}, T_{4v}^{\beta 2}$	M_x, M_{3u}, M_z^β	1	—
				Q_y, Q_{3v}, Q_{xyz}	$G_{zx}, G_v,$ $G_{4u}^\alpha, G_{4u}^{\beta 1}, G_{4u}^{\beta 2}$	$T_{zx}, T_v,$ $T_{4u}^\alpha, T_{4u}^{\beta 1}, T_{4u}^{\beta 2}$	M_y, M_{3v}, M_{xyz}		

$\omega=\exp(-2\pi i/3)$

Table C.59: IRREPs of four types of multipoles in $3m'$. The superscript "±" of IRREP stands for the parity with respect to the antiunitary operation $\mathcal{A}=\theta\sigma_v$.

E	C_3	C_3^2	IRREP	E	ET	MT	M	MPG	P. axis
A 1	1	1	A^+	$Q_0, Q_z, Q_u,$ $Q_z^\alpha, Q_{3a}, Q_{40}, Q_{4b}$	G_{3b}, G_{4a}	T_{3a}, T_{4a}	$M_0, M_z, M_u,$ $M_z^\alpha, M_{3a}, M_{40}, M_{4b}$	$3m'$	[001]
			A^-	Q_{3b}, Q_{4a}	$G_0, G_z, G_u,$ $G_z^\alpha, G_{3a}, G_{40}, G_{4b}$	T_0, T_z, T_u $T_z^\alpha, T_{3b}, T_{40}, T_{4b}$	M_{3b}, M_{4a}	3	[001]
E 1	ω	ω^2	$E^{(1)+}$	$Q_{yz}, Q_{xy},$ $Q_{4v}^\alpha, Q_{4v}^{\beta 1}, Q_{4v}^{\beta 2}$	G_x, G_{3u}, G_z^β	T_x, T_{3u}, T_z^β	$M_{yz}, M_{xy},$ $M_{4v}^\alpha, M_{4v}^{\beta 1}, M_{4v}^{\beta 2}$	1	—
1	ω^2	ω	$E^{(2)+}$	$Q_{zx}, Q_v,$ $Q_{4u}^\alpha, Q_{4u}^{\beta 1}, Q_{4u}^{\beta 2}$	G_y, G_{3v}, G_{xyz}	T_y, T_{3v}, T_{xyz}	$M_{zx}, M_v,$ $M_{4u}^\alpha, M_{4u}^{\beta 1}, M_{4u}^{\beta 2}$	m'	[010]
			$E^{(1)-}$	Q_x, Q_{3u}, Q_z^β	$G_{yz}, G_{xy},$ $G_{4v}^\alpha, G_{4v}^{\beta 1}, G_{4v}^{\beta 2}$	$T_{yz}, T_{xy},$ $T_{4v}^\alpha, T_{4v}^{\beta 1}, T_{4v}^{\beta 2}$	M_x, M_{3u}, M_z^β	m'	[010]
			$E^{(2)-}$	Q_y, Q_{3v}, Q_{xyz}	$G_{zx}, G_v,$ $G_{4u}^\alpha, G_{4u}^{\beta 1}, G_{4u}^{\beta 2}$	$T_{zx}, T_v,$ $T_{4u}^\alpha, T_{4u}^{\beta 1}, T_{4u}^{\beta 2}$	M_y, M_{3v}, M_{xyz}	1	—

$\omega=\exp(-2\pi i/3)$

Table C.60: IRREPs of four types of multipoles in $4/m'm'm'$. The superscript "±" of IRREP stands for the parity with respect to the antiunitary operation $\mathcal{A}=\theta I$.

	E	$2C_4$	C_4^2	$2C_2'$	$2C_2''$	IRREP	E	ET	MT	M	MPG	P. axis
A_1	1	1	1	1	1	A_1^+	$Q_0, Q_u,$ Q_4, Q_{4u}			$M_0, M_u,$ M_4, M_{4u}	$4/m'm'm'$	[001]
						A_1^-		$G_0, G_u,$ G_4, G_{4u}	$T_0, T_u,$ T_4, T_{4u}		422	[001]
A_2	1	1	1	−1	−1	A_2^+	Q_{4z}^α	$G_z, G_z^\alpha,$	T_z, T_z^α	M_{4z}^α	$4/m'$	[001]
						A_2^-	Q_z, Q_z^α	G_{4z}^α	T_{4z}^α	M_z, M_z^α	$4m'm'$	[001]
B_1	1	−1	1	1	−1	B_1^+	Q_v, Q_{4v}	G_{xyz}	T_{xyz}	M_v, M_{4v}	$m'm'm'$	[100]
						B_1^-	Q_{xyz}	G_v, G_{4v}	T_v, T_{4v}	M_{xyz}	$\bar{4}'2m'$	[001]
B_2	1	−1	1	−1	1	B_2^+	Q_{xy}, Q_{4z}^β	G_z^β	T_z^β	M_{xy}, M_{4z}^β	$m'm'm'$	[110]
						B_2^-	Q_z^β	G_{xy}, G_{4z}^β	T_{xy}, T_{4z}^β	M_z^β	$\bar{4}'m'2$	[001]
E	2	0	−2	0	0	E^+	$Q_{yz},$ $Q_{4x}^\alpha, Q_{4x}^\beta$	$G_x,$ G_x^α, G_x^β	$T_x,$ T_x^α, T_x^β	$M_{yz},$ $M_{4x}^\alpha, M_{4x}^\beta$	$2/m'$	[100]
							$Q_{zx},$ $Q_{4y}^\alpha, Q_{4y}^\beta$	$G_y,$ G_y^α, G_y^β	$T_y,$ T_y^α, T_y^β	$M_{zx},$ $M_{4y}^\alpha, M_{4y}^\beta$	$2/m'$	[010]
						E^-	$Q_x,$ Q_x^α, Q_x^β	$G_{yz},$ $G_{4x}^\alpha, G_{4x}^\beta$	$T_{yz},$ $T_{4x}^\alpha, T_{4x}^\beta$	$M_x,$ M_x^α, M_x^β	$2m'm'$	[100]
							$Q_y,$ Q_y^α, Q_y^β	$G_{zx},$ $G_{4y}^\alpha, G_{4y}^\beta$	$T_{zx},$ $T_{4y}^\alpha, T_{4y}^\beta$	$M_y,$ M_y^α, M_y^β	$m'2m'$	[100]

Table C.61: IRREPs of four types of multipoles in $4'/m'm'm$. The superscript "±" of IRREP stands for the parity with respect to the antiunitary operation $\mathcal{A}=\theta I$.

	E	$2IC_4$	C_4^2	$2C_2'$	$2\sigma_d$	IRREP	E	ET	MT	M	MPG	P. axis
A_1	1	1	1	1	1	A_1^+	$Q_0, Q_u,$ Q_4, Q_{4u}		T_{xyz}	M_v, M_{4v}	$4'/m'm'm$	[001]
						A_1^-	Q_{xyz}	G_v, G_{4v}	$T_0, T_u,$ T_4, T_{4u}		$\bar{4}2m$	[001]
A_2	1	1	1	−1	−1	A_2^+	Q_{4z}^α	G_z, G_z^α	T_z^β	M_{xy}, M_{4z}^β	$4'/m'$	[001]
						A_2^-	Q_z^β	G_{xy}, G_{4z}^β	T_{4z}^α	M_z, M_z^α	$\bar{4}m'2'$	[001]
B_1	1	−1	1	1	−1	B_1^+	Q_v, Q_{4v}	G_{xyz}		$M_0, M_u,$ M_4, M_{4u}	$m'm'm'$	[100]
						B_1^-		$G_0, G_u,$ G_4, G_{4u}	T_v, T_{4v}	M_{xyz}	$4'22'$	[001]
B_2	1	−1	1	−1	1	B_2^+	Q_{xy}, Q_{4z}^β	G_z^β	T_z, T_z^α	M_{4z}^α	mmm'	[110]
						B_2^-	Q_z, Q_z^α	G_{4z}^α	T_{xy}, T_{4z}^β	M_z^β	$4'm'm$	[001]
E	2	0	−2	0	0	E^+	$Q_{yz},$ $Q_{4x}^\alpha, Q_{4x}^\beta$	$G_x,$ G_x^α, G_x^β	$T_x,$ T_x^α, T_x^β	$M_{yz},$ $M_{4x}^\alpha, M_{4x}^\beta$	$2/m'$	[100]
							$Q_{zx},$ $Q_{4y}^\alpha, Q_{4y}^\beta$	$G_y,$ G_y^α, G_y^β	$T_y,$ T_y^α, T_y^β	$M_{zx},$ $M_{4y}^\alpha, M_{4y}^\beta$	$2/m'$	[010]
						E^-	$Q_x,$ Q_x^α, Q_x^β	$G_{yz},$ $G_{4x}^\alpha, G_{4x}^\beta$	$T_{yz},$ $T_{4x}^\alpha, T_{4x}^\beta$	$M_x,$ M_x^α, M_x^β	$2m'm'$	[100]
							$Q_y,$ Q_y^α, Q_y^β	$G_{zx},$ $G_{4y}^\alpha, G_{4y}^\beta$	$T_{zx},$ $T_{4y}^\alpha, T_{4y}^\beta$	$M_y,$ M_y^α, M_y^β	$m'2m'$	[100]

Table C.62: IRREPs of four types of multipoles in $4/m'mm$. The superscript "±" of IRREP stands for the parity with respect to the antiunitary operation $\mathcal{A}=\theta I$.

	E	$2C_4$	C_4^2	$2\sigma_v$	$2\sigma_d$	IRREP	E	ET	MT	M	MPG	P. axis
A_1	1	1	1	1	1	A_1^+	$Q_0, Q_u,$ Q_4, Q_{4u}		T_z, T_z^α	M_{4z}^α	$4/m'mm$	[001]
						A_1^-	Q_z, Q_z^α	G_{4z}^α	$T_0, T_u,$ T_4, T_{4u}		$4mm$	[001]
A_2	1	1	1	−1	−1	A_2^+	Q_{4z}^α	G_z, G_z^α		$M_0, M_u,$ M_4, M_{4u}	$4/m'$	[001]
						A_2^-		$G_0, G_u,$ G_4, G_{4u}	T_{4z}^α	M_z, M_z^α	$42'2'$	[001]
B_1	1	−1	1	1	−1	B_1^+	Q_v, Q_{4v}	G_{xyz}	T_z^β	M_{xy}, M_{4z}^β	mmm'	[100]
						B_1^-	Q_z^β	G_{xy}, G_{4z}^β	T_v, T_{4v}	M_{xyz}	$\bar{4}'m2'$	[001]
B_2	1	−1	1	−1	1	B_2^+	Q_{xy}, Q_{4z}^β	G_z^β	T_{xyz}	M_v, M_{4v}	mmm'	[110]
						B_2^-	Q_{xyz}	G_v, G_{4v}	T_{xy}, T_{4z}^β	M_z^β	$\bar{4}'2'm$	[001]
E	2	0	−2	0	0	E^+	$Q_{yz},$ $Q_{4x}^\alpha, Q_{4x}^\beta$	$G_x,$ G_x^α, G_x^β	$T_y,$ T_y^α, T_y^β	$M_{zx},$ $M_{4y}^\alpha, M_{4y}^\beta$	$2'/m$	[100]
							$Q_{zx},$ $Q_{4y}^\alpha, Q_{4y}^\beta$	$G_y,$ G_y^α, G_y^β	$T_x,$ T_x^α, T_x^β	$M_{yz},$ $M_{4x}^\alpha, M_{4x}^\beta$	$2'/m$	[010]
						E^-	$Q_x,$ Q_x^α, Q_x^β	$G_{yz},$ $G_{4x}^\alpha, G_{4x}^\beta$	$T_{zx},$ $T_{4y}^\alpha, T_{4y}^\beta$	$M_y,$ M_y^α, M_y^β	$2'mm'$	[100]
							$Q_y,$ Q_y^α, Q_y^β	$G_{zx},$ $G_{4y}^\alpha, G_{4y}^\beta$	$T_{yz},$ $T_{4x}^\alpha, T_{4x}^\beta$	$M_x,$ M_x^α, M_x^β	$m2'm'$	[100]

Table C.63: IRREPs of four types of multipoles in $4/mm'm'$. The superscript "±" of IRREP stands for the parity with respect to the antiunitary operation $\mathcal{A}=\theta C_2'$ (about [100] axis).

	E	C_4	C_4^2	C_4^3	I	$2IC_4$	σ_h	IC_4^3	IRREP	E	ET	MT	M	MPG	P. axis
A_g	1	1	1	1	1	1	1	1	A_g^+	$Q_0, Q_u,$ Q_4, Q_{4u}		T_{4z}^α	M_z, M_z^α	$4/mm'm'$	[001]
									A_g^-	Q_{4z}^α	G_z, G_z^α	$T_0, T_u,$ T_4, T_{4u}		$4/m$	[001]
B_g	1	-1	1	-1	1	-1	1	-1	B_g^+	Q_v, Q_{4v}	G_{xyz}	T_{xy}, T_{4z}^β	M_z^β	$m'm'm$	[100]
									B_g^-	Q_{xy}, Q_{4z}^β	G_z^β	T_v, T_{4v}	M_{xyz}	$m'm'm$	[110]
E_g	1	$-i$	-1	i	1	$-i$	-1	i	$E_g^{(1)+}$	$Q_{yz},$ $Q_{4x}^\alpha, Q_{4x}^\beta$	$G_x,$ G_x^α, G_x^β			$2'/m'$	[100]
	1	i	-1	$-i$	1	i	-1	$-i$	$E_g^{(2)+}$	$Q_{zx},$ $Q_{4y}^\alpha, Q_{4y}^\beta$	$G_y,$ G_y^α, G_y^β			$2'/m'$	[010]
									$E_g^{(1)-}$			$T_{yz},$ $T_{4x}^\alpha, T_{4x}^\beta$	$M_x,$ M_x^α, M_x^β	$2'/m'$	[010]
									$E_g^{(2)-}$			$T_{zx},$ $T_{4y}^\alpha, T_{4y}^\beta$	$M_y,$ M_y^α, M_y^β	$2'/m'$	[100]
A_u	1	1	1	1	-1	-1	-1	-1	A_u^+		G_0, G_u G_4, G_{4u}	T_z, T_z^α	M_{4z}^α	$42'2'$	[001]
									A_u^-	Q_z, Q_z^α	G_{4z}^α		$M_0, M_u,$ M_4, M_{4u}	$4m'm'$	[001]
B_u	1	-1	1	-1	-1	1	-1	1	B_u^+	Q_{xyz}	G_v, G_{4v}	T_z^β	M_{xy}, M_{4z}^β	$\bar{4}2'm'$	[001]
									B_u^-	Q_z^β	G_{xy}, G_{4z}^β	T_{xyz}	M_v, M_{4v}	$\bar{4}m'2'$	[001]
E_u	1	$-i$	-1	i	-1	i	1	$-i$	$E_u^{(1)+}$	$Q_x,$ Q_x^α, Q_x^β	$G_{yz},$ $G_{4x}^\alpha, G_{4x}^\beta$			$2'm'm$	[100]
	1	i	-1	$-i$	-1	$-i$	1	i	$E_u^{(2)+}$	$Q_y,$ Q_y^α, Q_y^β	$G_{zx},$ $G_{4y}^\alpha, G_{4y}^\beta$			$m'2'm$	[100]
									$E_u^{(1)-}$			$T_x,$ T_x^α, T_x^β	$M_{yz},$ $M_{4x}^\alpha, M_{4x}^\beta$	$m'2'm$	[100]
									$E_u^{(2)-}$			$T_y,$ T_y^α, T_y^β	M_{zx} $M_{4y}^\alpha, M_{4y}^\beta$	$2'm'm$	[100]

Table C.64: IRREPs of four types of multipoles in $4'/mmm'$. The superscript "±" of IRREP stands for the parity with respect to the antiunitary operation $\mathcal{A}=\theta C_2''$ (about [110] axis).

	E	C_{2z}	C_{2y}	C_{2x}	I	σ_z	σ_y	σ_x	IRREP	E	ET	MT	M	MPG	P. axis
A_g	1	1	1	1	1	1	1	1	A_g^+	$Q_0, Q_u,$ Q_4, Q_{4u}		T_v, T_{4v}	M_{xyz}	$4'/mmm'$	[001]
									A_g^-	Q_v, Q_{4v}	G_{xyz}	$T_0, T_u,$ T_4, T_{4u}		mmm	[100]
B_{1g}	1	1	−1	−1	1	1	−1	−1	B_{1g}^+	Q_{xy}, Q_{4z}^β	G_z^β	T_{4z}^α	M_z, M_z^α	$m'm'm$	[110]
									B_{1g}^-	Q_{4z}^α	G_z, G_z^α	T_{xy}, T_{4z}^β	M_z^β	$4'/m$	[001]
B_{2g}	1	−1	1	−1	1	−1	1	−1	B_{2g}	$Q_{zx},$ $Q_{4y}^\alpha, Q_{4y}^\beta$	$G_y,$ G_y^α, G_y^β	$T_{zx},$ $T_{4y}^\alpha, T_{4y}^\beta$	$M_y,$ M_y^α, M_y^β	$2/m$	[010]
B_{3g}	1	−1	−1	1	1	−1	−1	1		$Q_{yz},$ $Q_{4x}^\alpha, Q_{4x}^\beta$	$G_x,$ G_x^α, G_x^β	$T_{yz},$ $T_{4x}^\alpha, T_{4x}^\beta$	$M_x,$ M_x^α, M_x^β	$2/m$	[100]
A_u	1	1	1	1	−1	−1	−1	−1	A_u^+		$G_0, G_u,$ G_4, G_{4u}	T_{xyz}	M_v, M_{4v}	$4'22'$	[001]
									A_u^-	Q_{xyz}	G_v, G_{4v}		$M_0, M_u,$ M_4, M_{4u}	$\bar{4}'2m'$	[001]
B_{1u}	1	1	−1	−1	−1	−1	1	1	B_{1u}^+	Q_z^β	G_{xy}, G_{4z}^β	T_z, T_z^α	M_{4z}^α	$\bar{4}'m2'$	[001]
									B_{1g}^-	Q_z, Q_z^α	G_{4z}^α	T_z^β	M_{xy}, M_{4z}^β	$4'mm'$	[001]
B_{2u}	1	−1	1	−1	−1	1	−1	1	B_{2u}	$Q_y,$ Q_y^α, Q_y^β	$G_{zx},$ $G_{4y}^\alpha, G_{4y}^\beta$	$T_y,$ T_y^α, T_y^β	$M_{zx},$ $M_{4y}^\alpha, M_{4y}^\beta$	$m2m$	[100]
B_{3u}	1	−1	−1	1	−1	1	1	−1		$Q_x,$ Q_x^α, Q_x^β	$G_{yz},$ $G_{4x}^\alpha, G_{4x}^\beta$	$T_x,$ T_x^α, T_x^β	$M_{yz},$ $M_{4x}^\alpha, M_{4x}^\beta$	$2mm$	[100]

Table C.65: IRREPs of four types of multipoles in $42'2'$. The superscript "±" of IRREP stands for the parity with respect to the antiunitary operation $\mathcal{A}=\theta C_2'$ (about [100] axis).

	E	C_4	C_4^2	C_4^3	IRREP	E	ET	MT	M	MPG	P. axis
A	1	1	1	1	A^+	$Q_0, Q_u,$ Q_4, Q_{4u}	$G_0, G_u,$ G_4, G_{4u}	$T_z,$ $T_z^\alpha, T_{4z}^\alpha$	$M_z,$ $M_z^\alpha, M_{4z}^\alpha$	$42'2'$	[001]
					A^-	$Q_z,$ $Q_z^\alpha, Q_{4z}^\alpha$	$G_z,$ $G_z^\alpha, G_{4z}^\alpha$	$T_0, T_u,$ T_4, T_{4u}	$M_0, M_u,$ M_4, M_{4u}	4	[001]
B	1	−1	1	−1	B^+	$Q_v,$ Q_{xyz}, Q_{4v}	$G_v,$ G_{xyz}, G_{4v}	$T_{xy},$ T_z^β, T_{4z}^β	$M_{xy},$ M_z^β, M_{4z}^β	$2'2'2$	[100]
					B^-	Q_{xy} Q_z^β, Q_{4z}^β	G_{xy} G_z^β, G_{4z}^β	$T_v,$ T_{xyz}, T_{4v}	$M_v,$ M_{xyz}, M_{4v}	$2'2'2$	[110]
E	1	$-i$	−1	i	$E^{(1)+}$	$Q_x, Q_{yz}, Q_{4x}^\alpha, Q_x^\beta,$ $Q_{4x}^\alpha, Q_{4x}^\beta$	$G_x, G_{yz}, G_{4x}^\alpha, G_x^\beta,$ $G_{4x}^\alpha, G_{4x}^\beta$			$2'$	[100]
	1	i	−1	$-i$	$E^{(2)+}$	$Q_y, Q_{zx}, Q_{4y}^\alpha, Q_y^\beta,$ $Q_{4y}^\alpha, Q_{4y}^\beta$	$G_y, G_{zx}, G_{4y}^\alpha, G_y^\beta,$ $G_{4y}^\alpha, G_{4y}^\beta$			$2'$	[010]
					$E^{(1)-}$			$T_x, T_{yz}, T_{4x}^\alpha, T_x^\beta,$ $T_{4x}^\alpha, T_{4x}^\beta$	$M_x, M_{yz}, M_{4x}^\alpha, M_x^\beta,$ $M_{4x}^\alpha, M_{4x}^\beta$	$2'$	[010]
					$E^{(2)-}$			$T_y, T_{zx}, T_{4y}^\alpha, T_y^\beta,$ $T_{4y}^\alpha, T_{4y}^\beta$	$M_y, M_{zx}, M_{4y}^\alpha, M_y^\beta,$ $M_{4y}^\alpha, M_{4y}^\beta$	$2'$	[100]

Table C.66: IRREPs of four types of multipoles in $4'22'$. The superscript "$\pm$" of IRREP stands for the parity with respect to the antiunitary operation $\mathcal{A}=\theta C_2''$ (about [110] axis).

	E	C_{2z}	C_{2y}	C_{2x}	IRREP	E	ET	MT	M	MPG	P. axis
A	1	1	1	1	A^+	$Q_0, Q_u,$	$G_0, G_u,$	$T_v,$	$M_v,$	$4'22'$	[001]
						Q_4, Q_{4u}	G_4, G_{4u}	T_{xyz}, T_{4v}	M_{xyz}, M_{4v}		
					A^-	$Q_v,$	$G_v,$	$T_0, T_u,$	$M_0, M_u,$	222	[100]
						Q_{xyz}, Q_{4v}	G_{xyz}, G_{4v}	T_4, T_{4u}	M_4, M_{4u}		
B_1	1	1	-1	-1	B_1^+	$Q_{xy},$	$G_{xy},$	$T_z,$	$M_z,$	$2'2'2$	[110]
						Q_z^β, Q_{4z}^β	G_z^β, G_{4z}^β	$T_z^\alpha, T_{4z}^\alpha$	$M_z^\alpha, M_{4z}^\alpha$		
					B_1^-	$Q_z,$	$G_z,$	T_{xy}	$M_{xy},$	$4'$	[001]
						$Q_z^\alpha, Q_{4z}^\alpha$	$G_z^\alpha, G_{4z}^\alpha$	T_z^β, T_{4z}^β	M_z^β, M_{4z}^β		
B_2	1	-1	1	-1	B_2	$Q_x, Q_{yz}, Q_x^\alpha,$	$G_x, G_{yz}, G_x^\alpha,$	$T_x, T_{yz}, T_x^\alpha,$	$M_x, M_{yz}, M_x^\alpha,$	2	[100]
						$Q_x^\beta, Q_{4x}^\alpha, Q_{4x}^\beta$	$G_x^\beta, G_{4x}^\alpha, G_{4x}^\beta$	$T_x^\beta, T_{4x}^\alpha, T_{4x}^\beta$	$M_x^\beta, M_{4x}^\alpha, M_{4x}^\beta$		
B_3	1	-1	-1	1		$Q_y, Q_{yz}, Q_y^\alpha,$	$G_y, G_{zx}, G_y^\alpha,$	$T_y, T_{zx}, T_y^\alpha,$	$M_y, M_{zx}, M_y^\alpha,$	2	[010]
						$Q_y^\beta, Q_{4y}^\alpha, Q_{4y}^\beta$	$G_y^\beta, G_{4y}^\alpha, G_{4y}^\beta$	$T_y^\beta, T_{4y}^\alpha, T_{4y}^\beta$	$M_y^\beta, M_{4y}^\alpha, M_{4y}^\beta$		

Table C.67: IRREPs of four types of multipoles in $\bar{4}2'm'$. The superscript "$\pm$" of IRREP stands for the parity with respect to the antiunitary operation $\mathcal{A}=\theta C_2'$ (about [100] axis).

	E	IC_4	C_4^2	IC_4^3	IRREP	E	ET	MT	M	MPG	P. axis
A	1	1	1	1	A^+	$Q_0, Q_u,$	G_v, G_{4v}	T_z^β, T_{4z}^α	$M_z, M_{xy},$	$\bar{4}2'm'$	[001]
						Q_{xyz}, Q_4, Q_{4u}			M_z^α, M_{4z}^β		
					A^-	Q_z^β, Q_{4z}^α	$G_z, G_{xy},$	$T_0, T_u,$	M_v, M_{4v}	$\bar{4}$	[001]
							G_z^α, G_{4z}^β	T_{xyz}, T_4, T_{4u}			
B	1	-1	1	-1	B^+	Q_v, Q_{4v}	$G_0, G_u,$	$T_z, T_{xy},$	M_z^β, M_{4z}^α	$2'2'2$	[100]
							G_{xyz}, G_4, G_{4u}	T_z^α, T_{4z}^β			
					B^-	$Q_z, Q_{xy},$	G_z^β, G_{4z}^α	T_v, T_{4v}	$M_0, M_u,$	$m'm'2$	[110]
						Q_z^α, Q_{4z}^β			M_{xyz}, M_4, M_{4u}		
E	1	$-i$	-1	i	$E^{(1)+}$	$Q_x, Q_{yz}, Q_x^\alpha, Q_x^\beta,$	$G_x, G_{yz}, G_x^\alpha, G_x^\beta,$			$2'$	[100]
						$Q_{4x}^\alpha, Q_{4x}^\beta$	$G_{4x}^\alpha, G_{4x}^\beta$				
	1	i	-1	$-i$	$E^{(2)+}$	$Q_y, Q_{zx}, Q_y^\alpha, Q_y^\beta,$	$G_y, G_{zx}, G_y^\alpha, G_y^\beta,$			$2'$	[010]
						$Q_{4y}^\alpha, Q_{4y}^\beta$	$G_{4y}^\alpha, G_{4y}^\beta$				
					$E^{(1)-}$			$T_x, T_{yz}, T_x^\alpha, T_x^\beta,$	$M_x, M_{yz}, M_x^\alpha, M_x^\beta,$	$2'$	[010]
								$T_{4x}^\alpha, T_{4x}^\beta$	$M_{4x}^\alpha, M_{4x}^\beta$		
					$E^{(2)-}$			$T_y, T_{zx}, T_y^\alpha, T_y^\beta,$	$M_y, M_{zx}, M_y^\alpha, M_y^\beta,$	$2'$	[100]
								$T_{4y}^\alpha, T_{4y}^\beta$	$M_{4y}^\alpha, M_{4y}^\beta$		

Table C.68: IRREPs of four types of multipoles in $\bar{4}'2m'$. The superscript "±" of IRREP stands for the parity with respect to the antiunitary operation $\mathcal{A}=\theta\sigma_d$ ($\sigma_d \perp [110]$).

	E	C_{2z}	C_{2y}	C_{2x}	IRREP	E	ET	MT	M	MPG	P. axis
A	1	1	1	1	A^+	$Q_0, Q_u,$ Q_{xyz}, Q_4, Q_{4u}	G_v, G_{4v}	T_v, T_{4v}	$M_0, M_u,$ M_{xyz}, M_4, M_{4u}	$\bar{4}'2m'$	[001]
					A^-	Q_v, Q_{4v}	$G_0, G_u,$ G_{xyz}, G_4, G_{4u}	$T_0, T_u,$ T_{xyz}, T_4, T_{4u}	M_v, M_{4v}	222	[100]
B_1	1	1	−1	−1	B_1^+	$Q_z, Q_{xy},$ Q_z^α, Q_{4z}^β	G_z^β, G_{4z}^α	T_z^β, T_{4z}^α	$M_z, M_{xy},$ M_z^α, M_{4z}^β	$m'm'2$	[110]
					B_1^-	Q_z^β, Q_{4z}^α	$G_z, G_{xy},$ G_z^α, G_{4z}^β	$T_z, T_{xy},$ T_z^α, T_{4z}^β	M_z^β, M_{4z}^α	$\bar{4}'$	[001]
B_2	1	−1	1	−1	B_2	$Q_y, Q_{zx}, Q_y^\alpha,$ $Q_y^\beta, Q_{4y}^\alpha, Q_{4y}^\beta$	$G_y, G_{zx}, G_y^\alpha,$ $G_y^\beta, G_{4y}^\alpha, G_{4y}^\beta$	$T_y, T_{zx}, T_y^\alpha,$ $T_y^\beta, T_{4y}^\alpha, T_{4y}^\beta$	$M_y, M_{zx}, M_y^\alpha,$ $M_y^\beta, M_{4y}^\alpha, M_{4y}^\beta$	2	[010]
B_3	1	−1	−1	1		$Q_x, Q_{yz}, Q_x^\alpha,$ $Q_x^\beta, Q_{4x}^\alpha, Q_{4x}^\beta$	$G_x, G_{yz}, G_x^\alpha,$ $G_x^\beta, G_{4x}^\alpha, G_{4x}^\beta$	$T_x, T_{yz}, T_x^\alpha,$ $T_x^\beta, T_{4x}^\alpha, T_{4x}^\beta$	$M_x, M_{yz}, M_x^\alpha,$ $M_x^\beta, M_{4x}^\alpha, M_{4x}^\beta$	2	[100]

Table C.69: IRREPs of four types of multipoles in $\bar{4}'m2'$. The superscript "±" of IRREP stands for the parity with respect to the antiunitary operation $\mathcal{A}=\theta C_2''$ (about [110] axis).

	E	C_{2z}	σ_y	σ_x	IRREP	E	ET	MT	M	MPG	P. axis
A_1	1	1	1	1	A_1^+	$Q_0, Q_u,$ Q_z^β, Q_4, Q_{4u}	G_{xy}, G_{4z}^β	$T_z, T_v,$ T_z^α, T_{4v}	M_{xyz}, M_{4z}^α	$\bar{4}'m2'$	[001]
					A_1^-	$Q_z, Q_v,$ Q_z^α, Q_{4v}	G_{xyz}, G_{4z}^α	$T_0, T_u,$ T_z^β, T_4, T_{4u}	M_{xy}, M_{4z}^β	$mm2$	[100]
A_2	1	1	−1	−1	A_2^+	Q_{xy}, Q_{4z}^β	$G_0, G_u,$ G_z^β, G_4, G_{4u}	T_{xyz}, T_{4z}^α	$M_z, M_v,$ M_z^α, M_{4v}	$2'2'2$	[110]
					A_2^-	Q_{xyz}, Q_{4z}^α	$G_z, G_v,$ G_z^α, G_{4v}	T_{xy}, T_{4z}^β	$M_0, M_u,$ M_z^β, M_4, M_{4u}	$\bar{4}'$	[001]
B_1	1	−1	1	−1	B_1	$Q_x, Q_{zx}, Q_x^\alpha,$ $Q_x^\beta, Q_{4y}^\alpha, Q_{4y}^\beta$	$G_y, G_{yz}, G_y^\alpha,$ $G_y^\beta, G_{4x}^\alpha, G_{4x}^\beta$	$T_x, T_{zx}, T_x^\alpha,$ $T_x^\beta, T_{4y}^\alpha, T_{4y}^\beta$	$M_y, M_{yz}, M_y^\alpha,$ $M_y^\beta, M_{4x}^\alpha, M_{4x}^\beta$	m	[010]
B_2	1	−1	−1	1		$Q_y, Q_{yz}, Q_y^\alpha,$ $Q_y^\beta, Q_{4x}^\alpha, Q_{4x}^\beta$	$G_x, G_{zx}, G_x^\alpha,$ $G_x^\beta, G_{4y}^\alpha, G_{4y}^\beta$	$T_y, T_{yz}, T_y^\alpha,$ $T_y^\beta, T_{4x}^\alpha, T_{4x}^\beta$	$M_x, M_{zx}, M_x^\alpha,$ $M_x^\beta, M_{4y}^\alpha, M_{4y}^\beta$	m	[100]

Table C.70: IRREPs of four types of multipoles in $4m'm'$. The superscript "±" of IRREP stands for the parity with respect to the antiunitary operation $\mathcal{A}=\theta\sigma_v$ ($\sigma_v \perp [100]$).

	E	C_4	C_4^2	C_4^3	IRREP	E	ET	MT	M	MPG	P. axis
A	1	1	1	1	A^+	$Q_0, Q_z, Q_u,$ Q_z^α, Q_4, Q_{4u}	G_{4z}^α	T_{4z}^α	$M_0, M_z, M_u,$ M_z^α, M_4, M_{4u}	$4m'm'$	[001]
					A^-	Q_{4z}^α	$G_0, G_z, G_u,$ G_z^α, G_4, G_{4u}	$T_0, T_z, T_u,$ T_z^α, T_4, T_{4u}	M_{4z}^α	4	[001]
B	1	−1	1	−1	B^+	$Q_v,$ Q_z^β, Q_{4v}	$G_{xy},$ G_{xyz}, G_{4z}^β	$T_{xy},$ T_{xyz}, T_{4z}^β	$M_v,$ M_z^β, M_{4v}	$m'm'2$	[100]
					B^-	$Q_{xy},$ Q_{xyz}, Q_{4z}^β	$G_v,$ G_z^β, G_{4v}	$T_v,$ T_z^β, T_{4v}	$M_{xy},$ M_{xyz}, M_{4z}^β	$m'm'2$	[110]
E	1	$-i$	−1	i	$E^{(1)+}$	$Q_{yz}, Q_{4x}^\alpha, Q_{4x}^\beta$	$G_x, G_x^\alpha, G_x^\beta$	$T_x, T_x^\alpha, T_x^\beta$	$M_{yz}, M_{4x}^\alpha, M_{4x}^\beta$	m'	[100]
	1	i	−1	$-i$	$E^{(2)+}$	$Q_{zx}, Q_{4y}^\alpha, Q_{4y}^\beta$	$G_y, G_y^\alpha, G_y^\beta$	$T_y, T_y^\alpha, T_y^\beta$	$M_{zx}, M_{4y}^\alpha, M_{4y}^\beta$	m'	[010]
					$E^{(1)-}$	$Q_x, Q_x^\alpha, Q_x^\beta$	$G_{yz}, G_{4x}^\alpha, G_{4x}^\beta$	$T_{yz}, T_{4x}^\alpha, T_{4x}^\beta$	$M_x, M_x^\alpha, M_x^\beta$	m'	[010]
					$E^{(2)-}$	$Q_y, Q_y^\alpha, Q_y^\beta$	$G_{zx}, G_{4y}^\alpha, G_{4y}^\beta$	$T_{zx}, T_{4y}^\alpha, T_{4y}^\beta$	$M_y, M_y^\alpha, M_y^\beta$	m'	[100]

Table C.71: IRREPs of four types of multipoles in $4'mm'$. The superscript "±" of IRREP stands for the parity with respect to the antiunitary operation $\mathcal{A}=\theta\sigma_d$ ($\sigma_d \perp [110]$).

	E	C_{2z}	σ_y	σ_x	IRREP	E	ET	MT	M	MPG	P. axis
A_1	1	1	1	1	A_1^+	$Q_0, Q_z, Q_u,$ Q_z^α, Q_4, Q_{4u}	G_{4z}^α	$T_v,$ T_z^β, T_{4v}	$M_{xy},$ M_{xyz}, M_{4z}^β	$4'mm'$	[001]
					A_1^-	$Q_v,$ Q_z^β, Q_{4v}	$G_{xy},$ G_{xyz}, G_{4z}^β	$T_0, T_z, T_u,$ T_z^α, T_4, T_{4u}	M_{4z}^α	$mm2$	[100]
A_2	1	1	−1	−1	A_2^+	$Q_{xy},$ Q_{xyz}, Q_{4z}^β	$G_v,$ G_z^β, G_{4z}^β	T_{4z}^α	$M_0, M_z, M_u,$ M_z^α, M_4, M_{4u}	$m'm'2$	[110]
					A_2^-	Q_{4z}^α	$G_0, G_z, G_u,$ G_z^α, G_4, G_{4u}	$T_{xy},$ T_{xyz}, T_{4z}^β	$M_v,$ M_z^β, M_{4v}	$4'$	[001]
B_1	1	−1	1	−1	B_1	$Q_x, Q_{zx}, Q_x^\alpha,$ $Q_x^\beta, Q_{4y}^\alpha, Q_{4y}^\beta$	$G_y, G_{yz}, G_y^\alpha,$ $G_y^\beta, G_{4x}^\alpha, G_{4x}^\beta$	$T_x, T_{zx}, T_x^\alpha,$ $T_x^\beta, T_{4y}^\alpha, T_{4y}^\beta$	$M_y, M_{yz}, M_y^\alpha,$ $M_y^\beta, M_{4x}^\alpha, M_{4x}^\beta$	m	[010]
B_2	1	−1	−1	1		$Q_y, Q_{yz}, Q_y^\alpha,$ $Q_y^\beta, Q_{4x}^\alpha, Q_{4x}^\beta$	$G_x, G_{zx}, G_x^\alpha,$ $G_x^\beta, G_{4y}^\alpha, G_{4y}^\beta$	$T_y, T_{yz}, T_y^\alpha,$ $T_y^\beta, T_{4x}^\alpha, T_{4x}^\beta$	$M_x, M_{zx}, M_x^\alpha,$ $M_x^\beta, M_{4y}^\alpha, M_{4y}^\beta$	m	[100]

Table C.72: IRREPs of four types of multipoles in $4'/m'$. The superscript "±" of IRREP stands for the parity with respect to the antiunitary operation $\mathcal{A}=\theta I$.

	E	IC_4	C_4^2	IC_4^3	IRREP	E	ET	MT	M	MPG	P. axis
A	1	1	1	1	A^+	$Q_0, Q_u,$ $Q_4, Q_{4u}, Q_{4z}^\alpha$	G_z, G_z^α	T_{xyz}, T_z^β	$M_v, M_{xy},$ M_{4v}, M_{4z}^β	$4'/m'$	[001]
					A^-	Q_{xyz}, Q_z^β	$G_v, G_{xy},$ G_{4v}, G_{4z}^β	$T_0, T_u,$ $T_4, T_{4u}, T_{4z}^\alpha$	M_z, M_z^α	$\bar{4}$	[001]
B	1	−1	1	−1	B^+	$Q_v, Q_{xy},$ Q_{4v}, Q_{4z}^β	G_{xyz}, G_z^β	T_z, T_z^α	$M_0, M_u,$ $M_4, M_{4u}, M_{4z}^\alpha$	$2/m'$	[001]
					B^-	Q_z, Q_z^α	$G_0, G_u,$ $G_4, G_{4u}, G_{4z}^\alpha$	$T_v, T_{xy},$ T_{4v}, T_{4z}^β	M_{xyz}, M_z^β	$4'$	[001]
E	1	$-i$	−1	i	E	$Q_{yz}, Q_{4x}^\alpha, Q_{4x}^\beta$	$G_x, G_x^\alpha, G_x^\beta$	$T_x, T_x^\alpha, T_x^\beta$	$M_{yz}, M_{4x}^\alpha, M_{4x}^\beta$	$\bar{1}'$	—
	1	i	−1	$-i$		$Q_{zx}, Q_{4y}^\alpha, Q_{4y}^\beta$	$G_y, G_y^\alpha, G_y^\beta$	$T_y, T_y^\alpha, T_y^\beta$	$M_{zx}, M_{4y}^\alpha, M_{4y}^\beta$	$\bar{1}'$	—
						$Q_x, Q_x^\alpha, Q_x^\beta$	$G_{yz}, G_{4x}^\alpha, G_{4x}^\beta$	$T_{yz}, T_{4x}^\alpha, T_{4x}^\beta$	$M_x, M_x^\alpha, M_x^\beta$	m'	[001]
						$Q_y, Q_y^\alpha, Q_y^\beta$	$G_{zx}, G_{4y}^\alpha, G_{4y}^\beta$	$T_{zx}, T_{4y}^\alpha, T_{4y}^\beta$	$M_y, M_y^\alpha, M_y^\beta$	m'	[001]

Table C.73: IRREPs of four types of multipoles in $4/m'$. The superscript "±" of IRREP stands for the parity with respect to the antiunitary operation $\mathcal{A}=\theta I$.

	E	C_4	C_4^2	C_4^3	IRREP	E	ET	MT	M	MPG	P. axis
A	1	1	1	1	A^+	$Q_0, Q_u,$ $Q_4, Q_{4u}, Q_{4z}^\alpha$	G_z, G_z^α	T_z, T_z^α	$M_0, M_u,$ $M_4, M_{4u}, M_{4z}^\alpha$	$4/m'$	[001]
					A^-	Q_z, Q_z^α	$G_0, G_u,$ $G_4, G_{4u}, G_{4z}^\alpha$	$T_0, T_u,$ $T_4, T_{4u}, T_{4z}^\alpha$	M_z, M_z^α	4	[001]
B	1	−1	1	−1	B^+	$Q_v, Q_{xy},$ Q_{4v}, Q_{4z}^β	G_{xyz}, G_z^β	T_{xyz}, T_z^β	$M_v, M_{xy},$ M_{4v}, M_{4z}^β	$2/m'$	[001]
					B^-	Q_{xyz}, Q_z^β	$G_v, G_{xy},$ G_{4v}, G_{4z}^β	$T_v, T_{xy},$ T_{4v}, T_{4z}^β	M_{xyz}, M_z^β	$\bar{4}'$	[001]
E	1	$-i$	−1	i	E	$Q_{yz}, Q_{4x}^\alpha, Q_{4x}^\beta$	$G_x, G_x^\alpha, G_x^\beta$	$T_x, T_x^\alpha, T_x^\beta$	$M_{yz}, M_{4x}^\alpha, M_{4x}^\beta$	$\bar{1}'$	—
	1	i	−1	$-i$		$Q_{zx}, Q_{4y}^\alpha, Q_{4y}^\beta$	$G_y, G_y^\alpha, G_y^\beta$	$T_y, T_y^\alpha, T_y^\beta$	$M_{zx}, M_{4y}^\alpha, M_{4y}^\beta$	$\bar{1}'$	—
						$Q_x, Q_x^\alpha, Q_x^\beta$	$G_{yz}, G_{4x}^\alpha, G_{4x}^\beta$	$T_{yz}, T_{4x}^\alpha, T_{4x}^\beta$	$M_x, M_x^\alpha, M_x^\beta$	m'	[001]
						$Q_y, Q_y^\alpha, Q_y^\beta$	$G_{zx}, G_{4y}^\alpha, G_{4y}^\beta$	$T_{zx}, T_{4y}^\alpha, T_{4y}^\beta$	$M_y, M_y^\alpha, M_y^\beta$	m'	[001]

Table C.74: IRREPs of four types of multipoles in $4'/m$. The superscript "±" of IRREP stands for the parity with respect to the antiunitary operation $\mathcal{A}=\theta C_4$.

	E	C_{2z}	I	σ_z	IRREP	E	ET	MT	M	MPG	P. axis
A_g	1	1	1	1	A_g^+	$Q_0, Q_u,$ $Q_4, Q_{4u}, Q_{4z}^\alpha$	G_z, G_z^α	$T_v, T_{xy},$ T_{4v}, T_{4z}^β	M_{xyz}, M_z^β	$4'/m$	[001]
					A_g^-	$Q_v, Q_{xy},$ Q_{4v}, Q_{4z}^β	G_{xyz}, G_z^β	$T_0, T_u,$ $T_4, T_{4u}, T_{4z}^\alpha$	M_z, M_z^α	$2/m$	[001]
B_g	1	−1	1	−1	B_g	$Q_{yz}, Q_{4x}^\alpha, Q_{4x}^\beta$	$G_x, G_x^\alpha, G_x^\beta$	$T_{yz}, T_{4x}^\alpha, T_{4x}^\beta$	$M_x, M_x^\alpha, M_x^\beta$	$\bar{1}$	—
						$Q_{zx}, Q_{4y}^\alpha, Q_{4y}^\beta$	$G_y, G_y^\alpha, G_y^\beta$	$T_{zx}, T_{4y}^\alpha, T_{4y}^\beta$	$M_y, M_y^\alpha, M_y^\beta$	$\bar{1}$	—
A_u	1	1	−1	−1	A_u^+	Q_z, Q_z^α	$G_0, G_u,$ $G_4, G_{4u}, G_{4z}^\alpha$	T_{xyz}, T_z^β	$M_v, M_{xy},$ M_{4v}, M_{4z}^β	$4'$	[001]
					A_u^-	Q_{xyz}, Q_z^β	$G_v, G_{xy},$ G_{4v}, G_{4z}^β	T_z, T_z^α	$M_0, M_u,$ $M_4, M_{4u}, M_{4z}^\alpha$	$\bar{4}'$	[001]
B_u	1	−1	−1	1	B_u	$Q_x, Q_x^\alpha, Q_x^\beta$	$G_{yz}, G_{4x}^\alpha, G_{4x}^\beta$	$T_x, T_x^\alpha, T_x^\beta$	$M_{yz}, M_{4x}^\alpha, M_{4x}^\beta$	m	[001]
						$Q_y, Q_y^\alpha, Q_y^\beta$	$G_{zx}, G_{4y}^\alpha, G_{4y}^\beta$	$T_y, T_y^\alpha, T_y^\beta$	$M_{zx}, M_{4y}^\alpha, M_{4y}^\beta$	m	[001]

Table C.75: IRREPs of four types of multipoles in $\bar{4}'$. The superscript "±" of IRREP stands for the parity with respect to the antiunitary operation $\mathcal{A}=\theta I C_4$.

	E	C_{2z}	IRREP	E	ET	MT	M	MPG	P. axis
A	1	1	A^+	$Q_0, Q_u,$ $Q_{xyz}, Q_z^\beta,$ $Q_4, Q_{4u}, Q_{4z}^\alpha$	G_z, G_v, G_{xy} $G_z^\alpha, G_{4v}, G_{4z}^\beta$	$T_z, T_v, T_{xy},$ $T_z^\alpha, T_{4v}, T_{4z}^\beta$	$M_0, M_u,$ $M_{xyz}, M_z^\beta,$ $M_4, M_{4u}, M_{4z}^\alpha$	$\bar{4}'$	[001]
			A^-	$Q_z, Q_v, Q_{xy},$ $Q_z^\alpha, Q_{4v}, Q_{4z}^\beta$	$G_0, G_u,$ $G_{xyz}, G_z^\beta,$ $G_4, G_{4u}, G_{4z}^\alpha$	$T_0, T_u,$ $T_{xyz}, T_z^\beta,$ $T_4, T_{4u}, T_{4z}^\alpha$	$M_z, M_v, M_{xy},$ $M_z^\alpha, M_{4v}, M_{4z}^\beta$	2	[001]
B	1	−1	B	$Q_x, Q_{yz},$ $Q_x^\alpha, Q_x^\beta, Q_{4x}^\alpha, Q_{4x}^\beta$	$G_z, G_{yz},$ $G_x^\alpha, G_x^\beta, G_{4x}^\alpha, G_{4x}^\beta$	$T_x, T_{yz},$ $T_x^\alpha, T_x^\beta, T_{4x}^\alpha, T_{4x}^\beta$	$M_x, M_{yz},$ $M_x^\alpha, M_x^\beta, M_{4x}^\alpha, M_{4x}^\beta$	1	—
				$Q_y, Q_{zx},$ $Q_y^\alpha, Q_y^\beta, Q_{4y}^\alpha, Q_{4y}^\beta$	$G_y, G_{zx},$ $G_y^\alpha, G_y^\beta, G_{4y}^\alpha, G_{4y}^\beta$	$T_y, T_{zx},$ $T_y^\alpha, T_y^\beta, T_{4y}^\alpha, T_{4y}^\beta$	$M_y, M_{zx},$ $M_y^\alpha, M_y^\beta, M_{4y}^\alpha, M_{4y}^\beta$	1	—

Table C.76: IRREPs of four types of multipoles in $4'$. The superscript "$\pm$" of IRREP stands for the parity with respect to the antiunitary operation $\mathcal{A}=\theta C_4$.

	E	C_{2z}	IRREP	E	ET	MT	M	MPG	P. axis
A	1	1	A^+	$Q_0, Q_z,$	$G_0, G_z,$	$T_v, T_{xy},$	$M_v, M_{xy},$	$4'$	[001]
				$Q_u, Q_z^\alpha,$	$G_u, G_z^\alpha,$	$T_{xyz}, T_z^\beta,$	$M_{xyz}, M_z^\beta,$		
				$Q_4, Q_{4u}, Q_{4z}^\alpha$	$G_4, G_{4u}, G_{4z}^\alpha$	T_{4v}, T_{4z}^β	M_{4v}, M_{4z}^β		
			A^-	$Q_v, Q_{xy},$	$G_v, G_{xy},$	$T_0, T_z,$	$M_0, M_z,$	2	[001]
				$Q_{xyz}, Q_z^\beta,$	$G_{xyz}, G_z^\beta,$	$T_u, T_z^\alpha,$	$M_u, M_z^\alpha,$		
				Q_{4v}, Q_{4z}^β	G_{4v}, G_{4z}^β	$T_4, T_{4u}, T_{4z}^\alpha$	$M_4, M_{4u}, M_{4z}^\alpha$		
B	1	-1	B	$Q_x, Q_{yz},$	$G_x, G_{yz},$	$T_x, T_{yz},$	$M_x, M_{yz},$	1	—
				$Q_x^\alpha, Q_x^\beta, Q_{4x}^\alpha, Q_{4x}^\beta$	$G_x^\alpha, G_x^\beta, G_{4x}^\alpha, G_{4x}^\beta$	$T_x^\alpha, T_x^\beta, T_{4x}^\alpha, T_{4x}^\beta$	$M_x^\alpha, M_x^\beta, M_{4x}^\alpha, M_{4x}^\beta$		
				$Q_y, Q_{zx},$	$G_y, G_{zx},$	$T_y, T_{zx},$	$M_y, M_{zx},$	1	—
				$Q_y^\alpha, Q_y^\beta, Q_{4y}^\alpha, Q_{4y}^\beta$	$G_y^\alpha, G_y^\beta, G_{4y}^\alpha, G_{4y}^\beta$	$T_y^\alpha, T_y^\beta, T_{4y}^\alpha, T_{4y}^\beta$	$M_y^\alpha, M_y^\beta, M_{4y}^\alpha, M_{4y}^\beta$		

Table C.77: IRREPs of four types of multipoles in $m'm'm'$. The superscript "±" of IRREP stands for the parity with respect to the antiunitary operation $\mathcal{A}=\theta I$.

	E	C_{2z}	C_{2y}	C_{2x}	IRREP	E	ET	MT	M	MPG	P. axis
A	1	1	1	1	A^+	$Q_0, Q_u, Q_v,$ Q_4, Q_{4u}, Q_{4v}	G_{xyz}	T_{xyz}	$M_0, M_u, M_v,$ M_4, M_{4u}, M_{4v}	$m'm'm'$	[100]
					A^-	Q_{xyz}	$G_0, G_u, G_v,$ G_4, G_{4u}, G_{4v}	$T_0, T_u, T_v,$ T_4, T_{4u}, T_{4v}	M_{xyz}	222	[100]
B_1	1	1	−1	−1	B_1^+	$Q_{xy},$ $Q_{4z}^\alpha, Q_{4z}^\beta$	$G_z,$ G_z^α, G_z^β	$T_z,$ T_z^α, T_z^β	$M_{xy},$ $M_{4z}^\alpha, M_{4z}^\beta$	$2/m'$	[001]
					B_1^-	$Q_z,$ Q_z^α, Q_z^β	$G_{xy},$ $G_{4z}^\alpha, G_{4z}^\beta$	$T_{xy},$ $T_{4z}^\alpha, T_{4z}^\beta$	$M_z,$ M_z^α, M_z^β	$m'm'2$	[100]
B_2	1	−1	1	−1	B_2^+	$Q_{zx},$ $Q_{4y}^\alpha, Q_{4y}^\beta$	$G_y,$ G_y^α, G_y^β	$T_y,$ T_y^α, T_y^β	$M_{zx},$ $M_{4y}^\alpha, M_{4y}^\beta$	$2/m'$	[010]
					B_2^-	$Q_y,$ Q_y^α, Q_y^β	$G_{zx},$ $G_{4y}^\alpha, G_{4y}^\beta$	$T_{zx},$ $T_{4y}^\alpha, T_{4y}^\beta$	$M_y,$ M_y^α, M_y^β	$m'2m'$	[100]
B_3	1	−1	−1	1	B_3^+	$Q_{yz},$ $Q_{4x}^\alpha, Q_{4x}^\beta$	$G_x,$ G_x^α, G_x^β	$T_x,$ T_x^α, T_x^β	$M_{yz},$ $M_{4x}^\alpha, M_{4x}^\beta$	$2/m'$	[100]
					B_3^-	$Q_x,$ Q_x^α, Q_x^β	$G_{yz},$ $G_{4x}^\alpha, G_{4x}^\beta$	$T_{yz},$ $T_{4x}^\alpha, T_{4x}^\beta$	$M_x,$ M_x^α, M_x^β	$2m'm'$	[100]

Table C.78: IRREPs of four types of multipoles in $m'm'm$. The superscript "±" of IRREP stands for the parity with respect to the antiunitary operation $\mathcal{A}=\theta C_{2x}$.

	E	C_{2z}	I	σ_z	IRREP	E	ET	MT	M	MPG	P. axis
A_g	1	1	1	1	A_g^+	$Q_0, Q_u, Q_v,$ Q_4, Q_{4u}, Q_{4v}	G_{xyz}	$T_{xy},$ $T_{4z}^\alpha, T_{4z}^\beta$	$M_z,$ M_z^α, M_z^β	$m'm'm$	[100]
					A_g^-	Q_{xy} $Q_{4z}^\alpha, Q_{4z}^\beta$	G_z G_z^α, G_z^β	$T_0, T_u, T_v,$ T_4, T_{4u}, T_{4v}	M_{xyz}	$2/m$	[001]
B_g	1	−1	1	−1	B_g^+	$Q_{yz},$ $Q_{4x}^\alpha, Q_{4x}^\beta$	$G_x,$ G_x^α, G_x^β	$T_{zx},$ $T_{4y}^\alpha, T_{4y}^\beta$	$M_y,$ M_y^α, M_y^β	$2'/m'$	[100]
					B_g^-	$Q_{zx},$ $Q_{4y}^\alpha, Q_{4y}^\beta$	$G_y,$ G_y^α, G_y^β	$T_{yz},$ $T_{4x}^\alpha, T_{4x}^\beta,$	$M_x,$ M_x^α, M_x^β	$2'/m'$	[010]
A_u	1	1	−1	−1	A_u^+	Q_{xyz}	$G_0, G_u, G_v,$ G_4, G_{4u}, G_{4v}	$T_z,$ T_z^α, T_z^β	$M_{xy},$ $M_{4z}^\alpha, M_{4z}^\beta$	$2'2'2$	[100]
					A_u^-	$Q_z,$ Q_z^α, Q_z^β	$G_{xy},$ $G_{4z}^\alpha, G_{4z}^\beta$	T_{xyz}	$M_0, M_u, M_v,$ M_4, M_{4u}, M_{4v}	$m'm'2$	[100]
B_u	1	−1	−1	1	B_u^+	$Q_x,$ Q_x^α, Q_x^β	$G_{yz},$ $G_{4x}^\alpha, G_{4x}^\beta$	$T_y,$ T_y^α, T_y^β	$M_{zx},$ $M_{4y}^\alpha, M_{4y}^\beta$	$2'm'm$	[100]
					B_u^-	$Q_y,$ Q_y^α, Q_y^β	$G_{zx},$ $G_{4y}^\alpha, G_{4y}^\beta$	$T_x,$ T_x^α, T_x^β	$M_{yz},$ $M_{4x}^\alpha, M_{4x}^\beta$	$m'2'm$	[100]

Table C.79: IRREPs of four types of multipoles in mmm'. The superscript "±" of IRREP stands for the parity with respect to the antiunitary operation $\mathcal{A}=\theta I$.

	E	C_{2z}	σ_y	σ_x	IRREP	E	ET	MT	M	MPG	P. axis
A_1	1	1	1	1	A_1^+	$Q_0, Q_u, Q_v,$ Q_4, Q_{4u}, Q_{4v}	G_{xyz}	$T_z,$ T_z^α, T_z^β	$M_{xy},$ $M_{4z}^\alpha, M_{4z}^\beta$	mmm'	[100]
					A_1^-	$Q_z,$ Q_z^α, Q_z^β	$G_{xy},$ $G_{4z}^\alpha, G_{4z}^\beta$	$T_0, T_u, T_v,$ T_4, T_{4u}, T_{4v}	M_{xyz}	$mm2$	[100]
A_2	1	1	−1	−1	A_2^+	$Q_{xy},$ $Q_{4z}^\alpha, Q_{4z}^\beta$	$G_z,$ G_z^α, G_z^β	T_{xyz}	$M_0, M_u, M_v,$ M_4, M_{4u}, M_{4v}	$2/m'$	[001]
					A_2^-	Q_{xyz}	$G_0, G_u, G_v,$ G_4, G_{4u}, G_{4v}	$T_{xy},$ $T_{4z}^\alpha, T_{4z}^\beta$	$M_z,$ M_z^α, M_z^β	$2'2'2$	[100]
B_1	1	−1	1	−1	B_1^+	$Q_{zx},$ $Q_{4y}^\alpha, Q_{4y}^\beta$	$G_y,$ G_y^α, G_y^β	$T_x,$ T_x^α, T_x^β	$M_{yz},$ $M_{4x}^\alpha, M_{4x}^\beta$	$2'/m$	[010]
					B_1^-	Q_x Q_x^α, Q_x^β	G_{yz} $G_{4x}^\alpha, G_{4x}^\beta$	T_{zx} $T_{4y}^\alpha, T_{4y}^\beta$	M_y M_y^β, M_y^β	$2'mm'$	[100]
B_2	1	−1	−1	1	B_2^+	$Q_{yz},$ $Q_{4x}^\alpha, Q_{4x}^\beta$	$G_x,$ G_x^α, G_x^β	$T_y,$ T_y^α, T_y^β	$M_{zx},$ $M_{4y}^\alpha, M_{4y}^\beta$	$2'/m$	[100]
					B_2^-	$Q_y,$ Q_y^α, Q_y^β	$G_{zx},$ $G_{4y}^\alpha, G_{4y}^\beta$	$T_{yz},$ $T_{4x}^\alpha, T_{4x}^\beta$	$M_x,$ M_x^α, M_x^β	$m2'm'$	[100]

Table C.80: IRREPs of four types of multipoles in $2'2'2$. The superscript "±" of IRREP stands for the parity with respect to the antiunitary operation $\mathcal{A}=\theta C_{2x}$.

	E	C_{2z}	IRREP	E	ET	MT	M	MPG	P. axis
A	1	1	A^+	$Q_0, Q_u, Q_v,$ $Q_{xyz}, Q_4, Q_{4u}, Q_{4v}$	$G_0, G_u, G_v,$ $G_{xyz}, G_4, G_{4u}, G_{4v}$	$T_z, T_{xy}, T_z^\alpha, T_z^\beta,$ $T_{4z}^\alpha, T_{4z}^\beta$	$M_z, M_{xy}, M_z^\alpha, M_z^\beta,$ $M_{4z}^\alpha, M_{4z}^\beta$	$2'2'2$	[100]
			A^-	$Q_z, Q_{xy}, Q_z^\alpha, Q_z^\beta,$ $Q_{4z}^\alpha, Q_{4z}^\beta$	$G_z, G_{xy}, G_z^\alpha, G_z^\beta,$ $G_{4z}^\alpha, G_{4z}^\beta$	$T_0, T_u, T_v,$ $T_{xyz}, T_4, T_{4u}, T_{4v}$	$M_0, M_u, M_v,$ $M_{xyz}, M_4, M_{4u}, M_{4v}$	2	[001]
B	1	−1	B^+	$Q_x, Q_{yz}, Q_x^\alpha, Q_x^\beta,$ $Q_{4x}^\alpha, Q_{4x}^\beta$	$G_x, G_{yz}, G_x^\alpha, G_x^\beta,$ $G_{4x}^\alpha, G_{4x}^\beta$	$T_y, T_{zx}, T_y^\alpha, T_y^\beta,$ $T_{4y}^\alpha, T_{4y}^\beta$	$M_y, M_{zx}, M_y^\alpha, M_y^\beta,$ $M_{4y}^\alpha, M_{4y}^\beta$	$2'$	[100]
			B^-	$Q_y, Q_{zx}, Q_y^\alpha, Q_y^\beta,$ $Q_{4y}^\alpha, Q_{4y}^\beta$	$G_y, G_{zx}, G_y^\alpha, G_y^\beta,$ $G_{4y}^\alpha, G_{4y}^\beta$	$T_x, T_{yz}, T_x^\alpha, T_x^\beta,$ $T_{4x}^\alpha, T_{4x}^\beta$	$M_x, M_{yz}, M_x^\alpha, M_x^\beta,$ $M_{4x}^\alpha, M_{4x}^\beta$	$2'$	[010]

Table C.81: IRREPs of four types of multipoles in $m'm'2$. The superscript "±" of IRREP stands for the parity with respect to the antiunitary operation $\mathcal{A}=\theta\sigma_x$.

	E	C_{2z}	IRREP	E	ET	MT	M	MPG	P. axis
A	1	1	A^+	$Q_0, Q_z, Q_u, Q_v,$ $Q_z^\alpha, Q_z^\beta,$ Q_4, Q_{4u}, Q_{4v}	$G_{xy}, G_{xyz},$ $G_{4z}^\alpha, G_{4z}^\beta$	$T_{xy}, T_{xyz},$ $T_{4z}^\alpha, T_{4z}^\beta$	$M_0, M_z, M_u, M_v,$ $M_z^\alpha, M_z^\beta,$ M_4, M_{4u}, M_{4v}	$m'm'2$	[100]
			A^-	$Q_{xy}, Q_{xyz},$ $Q_{4z}^\alpha, Q_{4z}^\beta$	$G_0, G_z, G_u, G_v,$ $G_z^\alpha, G_z^\beta,$ G_4, G_{4u}, G_{4v}	$T_0, T_z, T_u, T_v,$ $T_z^\alpha, T_z^\beta,$ T_4, T_{4u}, T_{4v}	$M_{xy}, M_{xyz},$ $M_{4z}^\alpha, M_{4z}^\beta$	2	[001]
B	1	−1	B^+	$Q_y, Q_{yz}, Q_y^\alpha, Q_y^\beta,$ $Q_{4x}^\alpha, Q_{4x}^\beta$	$G_x, G_{zx}, G_x^\alpha, G_x^\beta,$ $G_{4y}^\alpha, G_{4y}^\beta$	$T_x, T_{zx}, T_x^\alpha, T_x^\beta,$ $T_{4y}^\alpha, T_{4y}^\beta$	$M_y, M_{yz}, M_y^\alpha, M_y^\beta,$ $M_{4x}^\alpha, M_{4x}^\beta$	m'	[100]
			B^-	$Q_x, Q_{zx}, Q_x^\alpha, Q_x^\beta,$ $Q_{4y}^\alpha, Q_{4y}^\beta$	$G_y, G_{yz}, G_y^\alpha, G_y^\beta,$ $G_{4x}^\alpha, G_{4x}^\beta$	$T_y, T_{yz}, T_y^\alpha, T_y^\beta,$ $T_{4x}^\alpha, T_{4x}^\beta$	$M_x, M_{zx}, M_x^\alpha, M_x^\beta,$ $M_{4y}^\alpha, M_{4y}^\beta$	m'	[010]

Table C.82: IRREPs of four types of multipoles in $m'm2'$. The superscript "$\pm$" of IRREP stands for the parity with respect to the antiunitary operation $\mathcal{A}=\theta C_{2z}$.

	E	σ_y	IRREP	E	ET	MT	M	MPG	P. axis
A′	1	1	A′$^+$	Q_0, Q_z, Q_u, Q_v	G_{xy}, G_{xyz},	T_x, T_{zx},	M_y, M_{yz},	$m'm2'$	[010]
				Q_z^α, Q_z^β,	$G_{4z}^\alpha, G_{4z}^\beta$	$T_x^\alpha, T_x^\beta, T_{4y}^\alpha, T_{4y}^\beta$	$M_y^\alpha, M_y^\beta, M_{4x}^\alpha, M_{4x}^\beta$		
				Q_4, Q_{4u}, Q_{4v}					
			A′$^-$	Q_x, Q_{zx},	G_y, G_{yz},	T_0, T_z, T_u, T_v,	M_{xy}, M_{xyz},	m	[010]
				$Q_x^\alpha, Q_x^\beta, Q_{4y}^\alpha, Q_{4y}^\beta$	$G_y^\alpha, G_y^\beta, G_{4x}^\alpha, G_{4x}^\beta$	T_z^α, T_z^β,	$M_{4z}^\alpha, M_{4z}^\beta$		
						T_4, T_{4u}, T_{4v}			
A″	1	−1	A″$^+$	Q_{xy}, Q_{xyz},	G_0, G_z, G_u, G_v,	T_y, T_{yz},	M_x, M_{zx},	$2'$	[001]
				$Q_{4z}^\alpha, Q_{4z}^\beta$	G_z^α, G_z^β,	$T_y^\alpha, T_y^\beta, T_{4x}^\alpha, T_{4x}^\beta$	$M_x^\alpha, M_x^\beta, M_{4y}^\alpha, M_{4y}^\beta$		
					G_4, G_{4u}, G_{4v}				
			A″$^-$	Q_y, Q_{yz},	G_x, G_{zx},	T_{xy}, T_{xyz},	M_0, M_z, M_u, M_v,	m'	[100]
				$Q_y^\alpha, Q_y^\beta, Q_{4x}^\alpha, Q_{4x}^\beta$	$G_x^\alpha, G_x^\beta, G_{4y}^\alpha, G_{4y}^\beta$	$T_{4z}^\alpha, T_{4z}^\beta$	M_z^α, M_z^β		
							M_4, M_{4u}, M_{4v}		

Table C.83: IRREPs of four types of multipoles in $2'/m$. The superscript "±" of IRREP stands for the parity with respect to the antiunitary operation $\mathcal{A}=\theta I$.

E	σ_y	IRREP	E	ET	MT	M	MPG	P. axis
A′ 1	1	A′$^{+}$	Q_0, Q_u, Q_v, Q_{zx}, Q_4, Q_{4u}, Q_{4v}, $Q^{\alpha}_{4y}, Q^{\beta}_{4y}$	G_y, $G_{xyz}, G^{\alpha}_{y}, G^{\beta}_{y}$	T_x, T_z, $T^{\alpha}_{x}, T^{\alpha}_{z}, T^{\beta}_{x}, T^{\beta}_{z}$	M_{yz}, M_{xy}, $M^{\alpha}_{4x}, M^{\alpha}_{4z}, M^{\beta}_{4x}, M^{\beta}_{4z}$	$2'/m$	[010]
		A′$^{-}$	Q_x, Q_z, $Q^{\alpha}_{x}, Q^{\alpha}_{z}, Q^{\beta}_{x}, Q^{\beta}_{z}$	G_{yz}, G_{xy}, $G^{\alpha}_{4x}, G^{\alpha}_{4z}, G^{\beta}_{4x}, G^{\beta}_{4z}$	T_0, T_u, T_v, T_{zx}, T_4, T_{4u}, T_{4v}, $T^{\alpha}_{4y}, T^{\beta}_{4y}$	M_y, $M_{xyz}, M^{\alpha}_{y}, M^{\beta}_{y}$	m	[010]
A″ 1	−1	A″$^{+}$	Q_{yz}, Q_{xy}, $Q^{\alpha}_{4x}, Q^{\alpha}_{4z}, Q^{\beta}_{4x}, Q^{\beta}_{4z}$	G_x, G_z, $G^{\alpha}_{x}, G^{\alpha}_{z}, G^{\beta}_{x}, G^{\beta}_{z}$	T_y, $T_{xyz}, T^{\alpha}_{y}, T^{\beta}_{y}$	M_0, M_u, M_v, M_{zx}, M_4, M_{4u}, M_{4v}, $M^{\alpha}_{4y}, M^{\beta}_{4y}$	$\bar{1}'$	—
		A″$^{-}$	Q_y, $Q_{xyz}, Q^{\alpha}_{y}, Q^{\beta}_{y}$	G_0, G_u, G_v, G_{zx}, G_4, G_{4u}, G_{4v}, $G^{\alpha}_{4y}, G^{\beta}_{4y}$	T_{yz}, T_{xy}, $T^{\alpha}_{4x}, T^{\alpha}_{4z}, T^{\beta}_{4x}, T^{\beta}_{4z}$	M_x, M_z, $M^{\alpha}_{x}, M^{\alpha}_{z}, M^{\beta}_{x}, M^{\beta}_{z}$	m'	[010]

Table C.84: IRREPs of four types of multipoles in $2'/m'$. The superscript "±" of IRREP stands for the parity with respect to the antiunitary operation $\mathcal{A}=\theta C_2$.

E	I	IRREP	E	ET	MT	M	MPG	P. axis
A_g 1	1	A_g^{+}	Q_0, Q_u, Q_v, Q_{zx}, Q_4, Q_{4u}, Q_{4v}, $Q^{\alpha}_{4y}, Q^{\beta}_{4y}$	G_y, $G_{xyz}, G^{\alpha}_{y}, G^{\beta}_{y}$	T_{yz}, T_{xy}, $T^{\alpha}_{4x}, T^{\alpha}_{4z}, T^{\beta}_{4x}, T^{\beta}_{4z}$	M_x, M_z, $M^{\alpha}_{x}, M^{\alpha}_{z}, M^{\beta}_{x}, M^{\beta}_{z}$	$2'/m'$	[010]
		A_g^{-}	Q_{yz}, Q_{xy}, $Q^{\alpha}_{4x}, Q^{\alpha}_{4z}, Q^{\beta}_{4x}, Q^{\beta}_{4z}$	G_x, G_z, $G^{\alpha}_{x}, G^{\alpha}_{z}, G^{\beta}_{x}, G^{\beta}_{z}$	T_0, T_u, T_v, T_{zx}, T_4, T_{4u}, T_{4v}, $T^{\alpha}_{4y}, T^{\beta}_{4y}$	M_y, $M_{xyz}, M^{\alpha}_{y}, M^{\beta}_{y}$	$\bar{1}$	—
A_u 1	−1	A_u^{+}	Q_y, $Q_{xyz}, Q^{\alpha}_{y}, Q^{\beta}_{y}$	G_0, G_u, G_v, G_{zx}, G_4, G_{4u}, G_{4v}, $G^{\alpha}_{4y}, G^{\beta}_{4y}$	T_x, T_z, $T^{\alpha}_{x}, T^{\alpha}_{z}, T^{\beta}_{x}, T^{\beta}_{z}$	M_{yz}, M_{xy}, $M^{\alpha}_{4x}, M^{\alpha}_{4z}, M^{\beta}_{4x}, M^{\beta}_{4z}$	$2'$	[010]
		A_u^{-}	Q_x, Q_z, $Q^{\alpha}_{x}, Q^{\alpha}_{z}, Q^{\beta}_{x}, Q^{\beta}_{z}$	G_{yz}, G_{xy}, $G^{\alpha}_{4x}, G^{\alpha}_{4z}, G^{\beta}_{4x}, G^{\beta}_{4z}$	T_y, $T_{xyz}, T^{\alpha}_{y}, T^{\beta}_{y}$	M_0, M_u, M_v, M_{zx}, M_4, M_{4u}, M_{4v}, $M^{\alpha}_{4y}, M^{\beta}_{4y}$	m'	[010]

Table C.85: IRREPs of four types of multipoles in $2/m'$. The superscript "±" of IRREP stands for the parity with respect to the antiunitary operation $\mathcal{A}=\theta I$.

E	C_{2y}	IRREP	E	ET	MT	M	MPG	P. axis
A 1	1	A^{+}	Q_0, Q_u, Q_v, Q_{zx}, Q_4, Q_{4u}, Q_{4v}, $Q^{\alpha}_{4y}, Q^{\beta}_{4y}$	G_y, $G_{xyz}, G^{\alpha}_{y}, G^{\beta}_{y}$	T_y, $T_{xyz}, T^{\alpha}_{y}, T^{\beta}_{y}$	M_0, M_u, M_v, M_{zx}, M_4, M_{4u}, M_{4v}, $M^{\alpha}_{4y}, M^{\beta}_{4y}$	$2/m'$	[010]
		A^{-}	Q_y, $Q_{xyz}, Q^{\alpha}_{y}, Q^{\beta}_{y}$	G_0, G_u, G_v, G_{zx}, G_4, G_{4u}, G_{4v}, $G^{\alpha}_{4y}, G^{\beta}_{4y}$	T_0, T_u, T_v, T_{zx}, T_4, T_{4u}, T_{4v}, $T^{\alpha}_{4y}, T^{\beta}_{4y}$	M_y, $M_{xyz}, M^{\alpha}_{y}, M^{\beta}_{y}$	2	[010]
B 1	−1	B^{+}	Q_{yz}, Q_{xy}, $Q^{\alpha}_{4x}, Q^{\alpha}_{4z}, Q^{\beta}_{4x}, Q^{\beta}_{4z}$	G_x, G_z, $G^{\alpha}_{x}, G^{\alpha}_{z}, G^{\beta}_{x}, G^{\beta}_{z}$	T_x, T_z, $T^{\alpha}_{x}, T^{\alpha}_{z}, T^{\beta}_{x}, T^{\beta}_{z}$	M_{yz}, M_{xy}, $M^{\alpha}_{4x}, M^{\alpha}_{4z}, M^{\beta}_{4x}, M^{\beta}_{4z}$	$\bar{1}'$	—
		B^{-}	Q_x, Q_z, $Q^{\alpha}_{x}, Q^{\alpha}_{z}, Q^{\beta}_{x}, Q^{\beta}_{z}$	G_{yz}, G_{xy}, $G^{\alpha}_{4x}, G^{\alpha}_{4z}, G^{\beta}_{4x}, G^{\beta}_{4z}$	T_{yz}, T_{xy}, $T^{\alpha}_{4x}, T^{\alpha}_{4z}, T^{\beta}_{4x}, T^{\beta}_{4z}$	M_x, M_z, $M^{\alpha}_{x}, M^{\alpha}_{z}, M^{\beta}_{x}, M^{\beta}_{z}$	m'	[010]

Table C.86: IRREPs of four types of multipoles in m'. The superscript "±" of IRREP stands for the parity with respect to the antiunitary operation $\mathcal{A}=\theta\sigma$.

	E	IRREP	E	ET	MT	M	MPG	P. axis
A	1	A^+	$Q_0, Q_x, Q_z,$ $Q_u, Q_v, Q_{zx},$ $Q_x^\alpha, Q_z^\alpha, Q_x^\beta, Q_z^\beta,$ $Q_4, Q_{4u}, Q_{4v},$ $Q_{4y}^\alpha, Q_{4y}^\beta$	$G_y, G_{yz}, G_{xy},$ $G_{xyz}, G_y^\alpha, G_y^\beta,$ $G_{4x}^\alpha, G_{4z}^\alpha, G_{4x}^\beta, G_{4z}^\beta$	$T_y, T_{yz}, T_{xy},$ $T_{xyz}, T_y^\alpha, T_y^\beta,$ $T_{4x}^\alpha, T_{4z}^\alpha, T_{4x}^\beta, T_{4z}^\beta$	$M_0, M_x, M_z,$ $M_u, M_v, M_{zx},$ $M_x^\alpha, M_z^\alpha, M_x^\beta, M_z^\beta,$ $M_4, M_{4u}, M_{4v},$ $M_{4y}^\alpha, M_{4y}^\beta$	m'	[010]
		A^-	$Q_y, Q_{yz}, Q_{xy},$ $Q_{xyz}, Q_y^\alpha, Q_y^\beta,$ $Q_{4x}^\alpha, Q_{4z}^\alpha, Q_{4x}^\beta, Q_{4z}^\beta$	$G_0, G_x, G_z,$ $G_u, G_v, G_{zx},$ $G_x^\alpha, G_z^\alpha, G_x^\beta, G_z^\beta,$ $G_4, G_{4u}, G_{4v},$ $G_{4y}^\alpha, G_{4y}^\beta$	$T_0, T_x, T_z,$ $T_u, T_v, T_{zx},$ $T_x^\alpha, T_z^\alpha, T_x^\beta, T_z^\beta,$ $T_4, T_{4u}, T_{4v},$ $T_{4y}^\alpha, T_{4y}^\beta$	$M_y, M_{yz}, M_{xy},$ $M_{xyz}, M_y^\alpha, M_y^\beta,$ $M_{4x}^\alpha, M_{4z}^\alpha, M_{4x}^\beta, M_{4z}^\beta$	1	—

Table C.87: IRREPs of four types of multipoles in $2'$. The superscript "±" of IRREP stands for the parity with respect to the antiunitary operation $\mathcal{A}=\theta C_2$.

	E	IRREP	E	ET	MT	M	MPG	P. axis
A	1	A^+	$Q_0, Q_y,$ $Q_u, Q_v, Q_{zx},$ $Q_{xyz}, Q_y^\alpha, Q_y^\beta,$ $Q_4, Q_{4u}, Q_{4v},$ $Q_{4y}^\alpha, Q_{4y}^\beta$	$G_0, G_y,$ $G_u, G_v, G_{zx},$ $G_{xyz}, G_y^\alpha, G_y^\beta,$ $G_4, G_{4u}, G_{4v},$ $G_{4y}^\alpha, G_{4y}^\beta$	$T_x, T_z, T_{yz}, T_{xy},$ $T_x^\alpha, T_z^\alpha, T_x^\beta, T_z^\beta,$ $T_{4x}^\alpha, T_{4z}^\alpha, T_{4x}^\beta, T_{4z}^\beta$	$M_x, M_z, M_{yz}, M_{xy},$ $M_x^\alpha, M_z^\alpha, M_x^\beta, M_z^\beta,$ $M_{4x}^\alpha, M_{4z}^\alpha, M_{4x}^\beta, M_{4z}^\beta$	$2'$	[010]
		A^-	$Q_x, Q_z, Q_{yz}, Q_{xy},$ $Q_x^\alpha, Q_z^\alpha, Q_x^\beta, Q_z^\beta,$ $Q_{4x}^\alpha, Q_{4z}^\alpha, Q_{4x}^\beta, Q_{4z}^\beta$	$G_x, G_z, G_{yz}, G_{xy},$ $G_x^\alpha, G_z^\alpha, G_x^\beta, G_z^\beta,$ $G_{4x}^\alpha, G_{4z}^\alpha, G_{4x}^\beta, G_{4z}^\beta$	$T_0, T_y,$ $T_u, T_v, T_{zx},$ $T_{xyz}, T_y^\alpha, T_y^\beta,$ $T_4, T_{4u}, T_{4v},$ $T_{4y}^\alpha, T_{4y}^\beta$	$M_0, M_y,$ $M_u, M_v, M_{zx},$ $M_{xyz}, M_y^\alpha, M_y^\beta,$ $M_4, M_{4u}, M_{4v},$ $M_{4y}^\alpha, M_{4y}^\beta$	1	—

Table C.88: IRREPs of four types of multipoles in $\bar{1}'$. The superscript "±" of IRREP stands for the parity with respect to the antiunitary operation $\mathcal{A}=\theta I$.

	E	IRREP	E	ET	MT	M	MPG	P. axis
A	1	A^+	$Q_0,$ $Q_u, Q_v, Q_{yz}, Q_{zx}, Q_{xy},$ $Q_4, Q_{4u}, Q_{4v},$ $Q_{4x}^\alpha, Q_{4y}^\alpha, Q_{4z}^\alpha,$ $Q_{4x}^\beta, Q_{4y}^\beta, Q_{4z}^\beta$	$G_x, G_y, G_z,$ $G_{xyz}, G_x^\alpha, G_y^\alpha, G_z^\alpha,$ $G_x^\beta, G_y^\beta, G_z^\beta$	$T_x, T_y, T_z,$ $T_{xyz}, T_x^\alpha, T_y^\alpha, T_z^\alpha,$ $T_x^\beta, T_y^\beta, T_z^\beta$	$M_0,$ $M_u, M_v, M_{yz}, M_{zx}, M_{xy},$ $M_4, M_{4u}, M_{4v},$ $M_{4x}^\alpha, M_{4y}^\alpha, M_{4z}^\alpha,$ $M_{4x}^\beta, M_{4y}^\beta, M_{4z}^\beta$	$\bar{1}'$	—
		A^-	$Q_x, Q_y, Q_z,$ $Q_{xyz}, Q_x^\alpha, Q_y^\alpha, Q_z^\alpha,$ $Q_x^\beta, Q_y^\beta, Q_z^\beta$	$G_0,$ $G_u, G_v, G_{yz}, G_{zx}, G_{xy},$ $G_4, G_{4u}, G_{4v},$ $G_{4x}^\alpha, G_{4y}^\alpha, G_{4z}^\alpha,$ $G_{4x}^\beta, G_{4y}^\beta, G_{4z}^\beta$	$T_0,$ $T_u, T_v, T_{yz}, T_{zx}, T_{xy},$ $T_4, T_{4u}, T_{4v},$ $T_{4x}^\alpha, T_{4y}^\alpha, T_{4z}^\alpha,$ $T_{4x}^\beta, T_{4y}^\beta, T_{4z}^\beta$	$M_x, M_y, M_z,$ $M_{xyz}, M_x^\alpha, M_y^\alpha, M_z^\alpha,$ $M_x^\beta, M_y^\beta, M_z^\beta$	1	—

Appendix D

Laue and Magnetic Laue Groups

The correspondence between Laue groups and magnetic point groups is summarized in Table D.1. The correspondence between magnetic Laue groups and magnetic point groups is also listed for the case with the $\mathcal{T}$ and/or $\mathcal{PT}$ symmetries in Table D.2 and for the case without the $\mathcal{PT}$ symmetry in Table D.3.

Table D.1: Laue group (LG) and the corresponding gray point group (GPG), crystallographic point group (CPG), and black-and-white point group (BWPG).

LG	GPG	CPG	BWPG
$m\bar{3}m$	$m\bar{3}m1'$	$m\bar{3}m$	$m'\bar{3}'m'$, $m\bar{3}m'$, $m'\bar{3}'m$
	$4321'$	432	$4'32'$
	$\bar{4}3m1'$	$\bar{4}3m$	$\bar{4}'3m'$
$m\bar{3}$	$m\bar{3}1'$, $231'$	$m\bar{3}$, 23	$\bar{m}'\bar{3}'$
$4/mmm$	$4/mmm1'$	$4/mmm$	$4/m'm'm'$, $4/mm'm'$, $4'/m'm'm$, $4'/mm'm$, $4/m'mm$
	$4221'$	422	$42'2'$, $4'22'$
	$\bar{4}2m1'$	$\bar{4}2m$	$\bar{4}2'm'$, $\bar{4}'2m'$, $\bar{4}'2'm$
	$4mm1'$	$4mm$	$4m'm'$, $4'm'm$
$4/m$	$4/m1'$	$4/m$	$4'/m'$, $4/m'$, $4'/m$
	$41'$, $\bar{4}1'$	4, $\bar{4}$	$4'$, $\bar{4}'$
mmm	$mmm1'$	mmm	$m'm'm'$, $m'm'm$, $m'mm$
	$2221'$	222	$2'2'2$
	$mm21'$	$mm2$	$m'm'2$, $m'm2'$
$2/m$	$2/m1'$	$2/m$	$2'/m'$, $2/m'$, $2'/m$
	$21'$, $m1'$	2, m	$2'$, m'
$\bar{1}$	$\bar{1}1'$, $11'$	$\bar{1}$, 1	$\bar{1}'$
$6/mmm$	$6/mmm1'$	$6/mmm$	$6/m'm'm'$, $6/mm'm'$, $6'/m'mm'$, $6'/mmm'$, $6/m'mm$
	$6221'$	622	$62'2'$, $6'22'$
	$\bar{6}m21'$	$\bar{6}m2$	$\bar{6}m'2'$, $\bar{6}'m2'$, $\bar{6}'m'2$
	$6mm1'$	$6mm$	$6m'm'$, $6'mm'$
$6/m$	$6/m1'$	$6/m$	$6'/m'$, $6/m'$, $6'/m$
	$61'$, $\bar{6}1'$	6, $\bar{6}$	$6'$, $\bar{6}'$
$\bar{3}m$	$\bar{3}m1'$	$\bar{3}m$	$\bar{3}m'$, $\bar{3}'m'$, $\bar{3}'m$
	$321'$	32	$32'$
	$3m1'$	$3m$	$3m'$
$\bar{3}$	$\bar{3}1'$, $31'$	$\bar{3}$, 3	$\bar{3}'$

Table D.2: Magnetic Laue group (MLG) for gray point group (GPG) and the $\mathcal{PT}$-symmetric black-and-white point group (BWPG).

MLG	GPG	BWPG
$m\bar{3}m1'$	$m\bar{3}m1'$, $4321'$, $\bar{4}3m1'$	$m'\bar{3}'m', m'\bar{3}'m$
$m\bar{3}1'$	$m\bar{3}1'$, $231'$	$m'\bar{3}'$
$4/mmm1'$	$4/mmm1'$, $4221'$, $\bar{4}2m1'$, $4mm1'$	$4/m'm'm', 4'/m'm'm, 4/m'mm$
$4/m1'$	$4/m1'$, $41'$, $\bar{4}1'$	$4'/m', 4/m'$
$mmm1'$	$mmm1'$, $2221'$, $mm21'$	$m'm'm', m'mm$
$2/m1'$	$2/m1'$, $21'$, $m1'$	$2'/m, 2/m'$
$\bar{1}1'$	$\bar{1}1'$, $11'$	$\bar{1}'$
$6/mmm1'$	$6/mmm1'$, $6221'$, $\bar{6}m21'$, $6mm1'$	$6/m'm'm', 6'/mmm', 6/m'mm$
$6/m1'$	$6/m1'$, $61'$, $\bar{6}1'$	$6'/m, 6/m'$
$\bar{3}m1'$	$\bar{3}m1'$, $321'$, $3m1'$	$\bar{3}'m', \bar{3}'m$
$\bar{3}1'$	$\bar{3}1'$, $31'$	$\bar{3}'$

Table D.3: Magnetic Laue group (MLG) for crystallographic point group (CPG) and the $\mathcal{PT}$-breaking black-and-white point group (BWPG).

MLG	CPG
$m\bar{3}m$	$m\bar{3}m$, 432, $\bar{4}3m$
$m\bar{3}$	$m\bar{3}$, 23
$4/mmm$	$4/mmm$, 422, $\bar{4}2m$, $4mm$
$4/m$	$4/m$, 4, $\bar{4}$
mmm	mmm, 222, $mm2$
$2/m$	$2/m$, 2, m
$\bar{1}$	$\bar{1}$, 1
$6/mmm$	$6/mmm$, 622, $\bar{6}m2$, $6mm$
$6/m$	$6/m$, 6, $\bar{6}$
$\bar{3}m$	$\bar{3}m$, 32, $3m$
$\bar{3}$	$\bar{3}$, 3

MLG	BWPG
$m\bar{3}m'$	$m\bar{3}m'$, $4'32'$, $\bar{4}'3m'$
$4/mm'm'$	$4/mm'm'$, $42'2'$, $\bar{4}2'm'$, $4m'm'$
$4'/mm'm$	$4'/mm'm$, $4'22'$, $\bar{4}'2m'$, $\bar{4}'2'm$, $4'm'm$
$4'/m$	$4'/m$, $4'$, $\bar{4}'$
$m'm'm$	$m'm'm$, $2'2'2$, $m'm'2$, $m'm2'$
$2'/m'$	$2'/m'$, $2'$, m'
$6/mm'm'$	$6/mm'm'$, $62'2'$, $\bar{6}m'2'$, $6m'm'$
$6'/m'mm'$	$6'/m'mm'$, $6'22'$, $\bar{6}'m2'$, $\bar{6}'m'2$, $6'mm'$
$6'/m'$	$6'/m'$, $6'$, $\bar{6}'$
$\bar{3}m'$	$\bar{3}m'$, $32'$, $3m'$

Appendix E

Relation between Multipoles and Response Tensors

E.1 Derivation of Multipoles in Response Tensors

We present the correspondence between response tensor components and multipoles in detail. The rank-2 tensors are shown in Secs. E.1.1 and E.1.2, the rank-3 tensors in Secs. E.1.3 and E.1.4, and the rank-4 tensors in Secs. E.1.5 and E.1.6.

E.1.1 $\chi^{[1\times1]}$

We decompose the rank-2 tensor $\chi^{[1\times1]}$ into the monopole, dipole, and quadrupole components, which are given as

$$\chi^{\mathrm{M}(1\times1)}=\frac{1}{3}\sum_{i}\chi^{[1\times1]}_{i;i}, \tag{E.1}$$

$$\chi^{\mathrm{D}(1\times1)}_{i}=\frac{1}{2}\sum_{jk}\epsilon_{ijk}\chi^{[1\times1]}_{j;k}, \tag{E.2}$$

$$\chi^{\mathrm{Q}(1\times1)}_{ij}=\frac{1}{2}\left(\chi^{[1\times1]}_{i;j}+\chi^{[1\times1]}_{j;i}\right)=\chi^{\mathrm{Q}(1\times1)}_{ji}, \tag{E.3}$$

respectively, where $i,j=x,y,z$. ϵ_{ijk} is the totally antisymmetric tensor (Levi-Civita symbol). The superscript of $\chi^{\mathrm{X}(l_B\times l_F)}$ (X=M, D, Q) represents the ranks of the response (output), l_B, and the external field (input), l_F, in terms of the spherical tensors. By using Eqs. (E.1)–(E.3), the tensor components represented by multipoles in Eq. (2.25) are

expressed as

$$X_0 = \chi^{\mathrm{M}(1\times1)}, \tag{E.4}$$

$$(Y_x, Y_y, Y_z) = (\chi_x^{\mathrm{D}(1\times1)}, \chi_y^{\mathrm{D}(1\times1)}, \chi_z^{\mathrm{D}(1\times1)}), \tag{E.5}$$

$$X_u = \frac{1}{6}\left(3\chi_{zz}^{\mathrm{Q}(1\times1)} - \sum_i \chi_{ii}^{\mathrm{Q}(1\times1)}\right),$$

$$X_v = \frac{1}{2}\left(\chi_{xx}^{\mathrm{Q}(1\times1)} - \chi_{yy}^{\mathrm{Q}(1\times1)}\right),$$

$$(X_{yz}, X_{zx}, X_{xy}) = (\chi_{yz}^{\mathrm{Q}(1\times1)}, \chi_{zx}^{\mathrm{Q}(1\times1)}, \chi_{xy}^{\mathrm{Q}(1\times1)}). \tag{E.6}$$

E.1.2 $\chi^{[0\times2]}$

The tensor components represented by monopole and quadrupole in $\chi^{[0\times2]}$ of Eq. (2.26) have the following forms:

$$X_0 = \frac{1}{3}\left(\chi_{0;xx}^{[0\times2]} + \chi_{0;yy}^{[0\times2]} + \chi_{0;zz}^{[0\times2]}\right), \tag{E.7}$$

$$X_u = \frac{1}{6}\left(3\chi_{0;zz}^{[0\times2]} - \sum_i \chi_{0;ii}^{[0\times2]}\right),$$

$$X_v = \frac{1}{2}\left(\chi_{0;xx}^{[0\times2]} - \chi_{0;yy}^{[0\times2]}\right),$$

$$(X_{yz}, X_{zx}, X_{xy}) = (\chi_{0;yz}^{[0\times2]}, \chi_{0;zx}^{[0\times2]}, \chi_{0;xy}^{[0\times2]}). \tag{E.8}$$

E.1.3 $\chi^{[1\times2]}$

$\chi^{[1\times2]}$ consists of the dipole, quadrupole, and octupole components, which are represented by $\chi_{i;jk}^{[1\times2]} (= \chi_{i;kj}^{[1\times2]})$ as follows:

$$\chi_i^{\mathrm{D}(1\times0)} = \frac{1}{3}\sum_j \chi_{i;jj}^{[1\times2]}, \tag{E.9}$$

$$\chi_i^{\mathrm{D}(1\times2)} = \sum_j \left(\frac{1}{3}\chi_{i;jj}^{[1\times2]} - \chi_{j;ij}^{[1\times2]}\right), \tag{E.10}$$

$$\chi_{ij}^{\mathrm{Q}(1\times2)} = \frac{1}{2}\sum_{kl}\left(\epsilon_{ikl}\chi_{k;lj}^{[1\times2]} + \epsilon_{jkl}\chi_{k;li}^{[1\times2]}\right) = \chi_{ji}^{\mathrm{Q}(1\times2)}, \tag{E.11}$$

$$\chi_{ijk}^{\mathrm{O}(1\times2)} = \frac{1}{3}\left(\chi_{i;jk}^{[1\times2]} + \chi_{j;ki}^{[1\times2]} + \chi_{k;ij}^{[1\times2]}\right) = \chi_{jki}^{\mathrm{O}(1\times2)} = \chi_{jik}^{\mathrm{O}(1\times2)}. \tag{E.12}$$

It is noted that there are two dipole components in $\chi^{[1\times2]}$, as the symmetric tensor field $F^{[2]} = (F_{xx}, F_{yy}, F_{zz}, F_{yz}, F_{zx}, F_{xy})$ is decomposed into the components with $l_F = 0$ and with $l_F = 2$. The $l_F = 0$ component in $F^{[2]}$ leads to $\chi_i^{\mathrm{D}(1\times0)}$ in Eq. (E.9), whereas the $l_F = 2$ component in $F^{[2]}$ leads to $\chi_i^{\mathrm{D}(1\times2)}$, $\chi_{ij}^{\mathrm{Q}(1\times2)}$, and $\chi_{ijk}^{\mathrm{O}(1\times2)}$ in Eqs. (E.10)–(E.12).

The corresponding multipoles in Eq. (E.49) are expressed by $\chi_i^{\mathrm{D}(1\times0)}$, $\chi_i^{\mathrm{D}(1\times2)}$, $\chi_{ij}^{\mathrm{Q}(1\times2)}$, and $\chi_{ijk}^{\mathrm{O}(1\times2)}$ in Eqs. (E.9)–(E.12) as

$$(X_x,X_y,X_z)=\frac{1}{15}(5\chi_x^{\mathrm{D}(1\times0)}-2\chi_x^{\mathrm{D}(1\times2)},5\chi_y^{\mathrm{D}(1\times0)}-2\chi_y^{\mathrm{D}(1\times2)},5\chi_z^{\mathrm{D}(1\times0)}-2\chi_z^{\mathrm{D}(1\times2)}), \tag{E.13}$$

$$(X'_x,X'_y,X'_z)=\frac{1}{6}(2\chi_x^{\mathrm{D}(1\times0)}+\chi_x^{\mathrm{D}(1\times2)},2\chi_y^{\mathrm{D}(1\times0)}+\chi_y^{\mathrm{D}(1\times2)},2\chi_z^{\mathrm{D}(1\times0)}+\chi_z^{\mathrm{D}(1\times2)}), \tag{E.14}$$

$$\begin{aligned}
Y_u&=\frac{1}{6}\left(3\chi_{zz}^{\mathrm{Q}(1\times2)}-\sum_i\chi_{ii}^{\mathrm{Q}(1\times2)}\right),\\
Y_v&=\frac{1}{6}\left(\chi_{xx}^{\mathrm{Q}(1\times2)}-\chi_{yy}^{\mathrm{Q}(1\times2)}\right),\\
(Y_{yz},Y_{zx},Y_{xy})&=\frac{1}{3}(\chi_{yz}^{\mathrm{Q}(1\times2)},\chi_{zx}^{\mathrm{Q}(1\times2)},\chi_{xy}^{\mathrm{Q}(1\times2)}),
\end{aligned} \tag{E.15}$$

$$\begin{aligned}
X_{xyz}&=\chi_{xyz}^{\mathrm{O}(1\times2)},\\
(X_x^\alpha,X_y^\alpha,X_z^\alpha)&=\frac{1}{20}\left(5\chi_{xxx}^{\mathrm{O}(1\times2)}-3\sum_i\chi_{xii}^{\mathrm{O}(1\times2)},5\chi_{yyy}^{\mathrm{O}(1\times2)}-3\sum_i\chi_{yii}^{\mathrm{O}(1\times2)},5\chi_{zzz}^{\mathrm{O}(1\times2)}-3\sum_i\chi_{zii}^{\mathrm{O}(1\times2)}\right),\\
(X_x^\beta,X_y^\beta,X_z^\beta)&=\frac{1}{4}\left(\chi_{xyy}^{\mathrm{O}(1\times2)}-\chi_{zzx}^{\mathrm{O}(1\times2)},\chi_{yzz}^{\mathrm{O}(1\times2)}-\chi_{xxy}^{\mathrm{O}(1\times2)},\chi_{zxx}^{\mathrm{O}(1\times2)}-\chi_{yyz}^{\mathrm{O}(1\times2)}\right).
\end{aligned} \tag{E.16}$$

E.1.4 $\chi^{[0\times3]}$

The multipoles in Eq. (2.28) are represented by $\chi_{0;ijk}^{[0\times3]}$, which is totally symmetric for the permutation of i, j, and k, as follows:

$$\begin{aligned}
(X_x,X_y,X_z)&=\frac{1}{5}\left(\sum_i\chi_{0;xii}^{[0\times3]},\sum_i\chi_{0;yii}^{[0\times3]},\sum_i\chi_{0;zii}^{[0\times3]}\right),\\
X_{xyz}&=\chi_{0;xyz}^{[0\times3]},\\
(X_x^\alpha,X_y^\alpha,X_z^\alpha)&=\frac{1}{10}\left(5\chi_{0;xxx}^{[0\times3]}-3\sum_i\chi_{0;xii}^{[0\times3]},5\chi_{0;yyy}^{[0\times3]}-3\sum_i\chi_{0;yii}^{[0\times3]},5\chi_{0;zzz}^{[0\times3]}-3\sum_i\chi_{0;zii}^{[0\times3]}\right),\\
(X_x^\beta,X_y^\beta,X_z^\beta)&=\frac{1}{2}\left(\chi_{0;xyy}^{[0\times3]}-\chi_{0;zzx}^{[0\times3]},\chi_{0;yzz}^{[0\times3]}-\chi_{0;xxy}^{[0\times3]},\chi_{0;zxx}^{[0\times3]}-\chi_{0;yyz}^{[0\times3]}\right).
\end{aligned} \tag{E.17, E.18}$$

E.1.5 $\chi^{[1\times3]}$

The monopole, dipole, quadrupole, octupole, and hexadecapole components of $\chi^{[1\times3]}$ are represented by $\chi_{i;jkl}^{[1\times3]}$, which is totally symmetric with respect to the permutation of j, k,

and l. Those components are

$$\chi^{\mathrm{M}(1\times1)}=\frac{1}{3}\sum_{ij}\chi^{[1\times3]}_{i;ijj}, \tag{E.19}$$

$$\chi^{\mathrm{D}(1\times1)}_{i}=\frac{1}{2}\sum_{jkl}\epsilon_{ijk}\chi^{[1\times3]}_{j;kll}, \tag{E.20}$$

$$\chi^{\mathrm{Q}(1\times1)}_{ij}=\frac{1}{6}\sum_{k}\left(\chi^{[1\times3]}_{i;jkk}+\chi^{[1\times3]}_{j;ikk}\right)=\chi^{\mathrm{Q}(1\times1)}_{ji}, \tag{E.21}$$

$$\chi^{\mathrm{Q}(1\times3)}_{ij}=\frac{1}{2}\sum_{k}\left[\left(\chi^{[1\times3]}_{k;ijk}+\chi^{[1\times3]}_{k;jik}\right)-\frac{2}{5}\left(\chi^{[1\times3]}_{i;jkk}+\chi^{[1\times3]}_{j;ikk}\right)\right]=\chi^{\mathrm{Q}(1\times3)}_{ji}, \tag{E.22}$$

$$\chi^{\mathrm{O}(1\times3)}_{ijk}=\frac{1}{6}\sum_{lm}\left(\epsilon_{klm}\chi^{[1\times3]}_{l;ijm}+\epsilon_{ilm}\chi^{[1\times3]}_{l;jkm}+\epsilon_{jlm}\chi^{[1\times3]}_{l;kim}\right)=\chi^{\mathrm{O}(1\times3)}_{jki}=\chi^{\mathrm{O}(1\times3)}_{jik}, \tag{E.23}$$

$$\chi^{\mathrm{H}(1\times3)}_{ijkl}=\frac{1}{4}\left(\chi^{[1\times3]}_{i;jkl}+\chi^{[1\times3]}_{j;kli}+\chi^{[1\times3]}_{k;lij}+\chi^{[1\times3]}_{l;ijk}\right)=\chi^{\mathrm{H}(1\times3)}_{jkli}=\chi^{\mathrm{H}(1\times3)}_{jikl}. \tag{E.24}$$

The field $F^{[3]}=(F_{xxx},F_{yyy},F_{zzz},F_{yyz},F_{zzx},F_{xxy},F_{yzz},F_{zxx},F_{xyy},F_{xyz})$ is decomposed into the $l_F=1$ and $l_F=3$ components. The $l_F=1$ field in $F^{[3]}$ leads to the monopole, dipole, and quadrupole components, $\chi^{\mathrm{M}(1\times1)}$, $\chi^{\mathrm{D}(1\times1)}$, and $\chi^{\mathrm{Q}(1\times1)}$, whereas the $l_F=3$ field in $F^{[3]}$ results in the quadrupole, octupole, and hexadecapole components, $\chi^{\mathrm{Q}(1\times3)}$, $\chi^{\mathrm{O}(1\times3)}$, and $\chi^{\mathrm{H}(1\times3)}$.

By using Eqs. (E.19)–(E.24), the multipoles in Eq. (2.29) are shown as

$$X_0=\frac{1}{5}\chi^{\mathrm{M}(1\times1)}, \tag{E.25}$$

$$(Y_x,Y_y,Y_z)=\frac{1}{5}\left(\chi_x^{\mathrm{D}(1\times1)},\chi_y^{\mathrm{D}(1\times1)},\chi_z^{\mathrm{D}(1\times1)}\right), \tag{E.26}$$

$$X_u=\frac{1}{42}\left(3\chi_{zz}^{\mathrm{Q}(1\times3)}-\sum_i\chi_{ii}^{\mathrm{Q}(1\times3)}\right),$$

$$X_v=\frac{1}{42}\left(\chi_{xx}^{\mathrm{Q}(1\times3)}-\chi_{yy}^{\mathrm{Q}(1\times3)}\right),$$

$$(X_{yz},X_{zx},X_{xy})=\frac{1}{21}\left(\chi_{yz}^{\mathrm{Q}(1\times3)},\chi_{zx}^{\mathrm{Q}(1\times3)},\chi_{xy}^{\mathrm{Q}(1\times3)}\right), \tag{E.27}$$

$$X'_u=\frac{1}{10}\left(3\chi_{zz}^{\mathrm{Q}(1\times1)}-\sum_i\chi_{ii}^{\mathrm{Q}(1\times1)}\right),$$

$$X'_v=\frac{3}{10}\left(\chi_{xx}^{\mathrm{Q}(1\times1)}-\chi_{yy}^{\mathrm{Q}(1\times1)}\right),$$

$$(X'_{yz},X'_{zx},X'_{xy})=\frac{3}{5}\left(\chi_{yz}^{\mathrm{Q}(1\times1)},\chi_{zx}^{\mathrm{Q}(1\times1)},\chi_{xy}^{\mathrm{Q}(1\times1)}\right), \tag{E.28}$$

$$Y_{xyz}=\chi_{xyz}^{\mathrm{O}(1\times3)},$$

$$(Y_x^\alpha,Y_y^\alpha,Y_z^\alpha)=\frac{1}{20}\left(5\chi_{xxx}^{\mathrm{O}(1\times3)}-3\sum_i\chi_{xii}^{\mathrm{O}(1\times3)},5\chi_{yyy}^{\mathrm{O}(1\times3)}-3\sum_i\chi_{yii}^{\mathrm{O}(1\times3)},5\chi_{zzz}^{\mathrm{O}(1\times3)}-3\sum_i\chi_{zii}^{\mathrm{O}(1\times3)}\right),$$

$$(Y_x^\beta,Y_y^\beta,Y_z^\beta)=\frac{1}{4}\left(\chi_{xyy}^{\mathrm{O}(1\times3)}-\chi_{zzx}^{\mathrm{O}(1\times3)},\chi_{yzz}^{\mathrm{O}(1\times3)}-\chi_{xxy}^{\mathrm{O}(1\times3)},\chi_{zxx}^{\mathrm{O}(1\times3)}-\chi_{yyz}^{\mathrm{O}(1\times3)}\right), \tag{E.29}$$

$$X_4=\frac{1}{15}\left[\sum_i\chi_{iiii}^{\mathrm{H}(1\times3)}-3\left(\chi_{yyzz}^{\mathrm{H}(1\times3)}+\chi_{zzxx}^{\mathrm{H}(1\times3)}+\chi_{xxyy}^{\mathrm{H}(1\times3)}\right)\right],$$

$$X_{4u}=\frac{1}{42}\left[3\chi_{zzzz}^{\mathrm{H}(1\times3)}-\sum_i\chi_{iiii}^{\mathrm{H}(1\times3)}+6\left(2\chi_{xxyy}^{\mathrm{H}(1\times3)}-\chi_{yyzz}^{\mathrm{H}(1\times3)}-\chi_{zzxx}^{\mathrm{H}(1\times3)}\right)\right],$$

$$X_{4v}=\frac{1}{14}\left[\chi_{xxxx}^{\mathrm{H}(1\times3)}-\chi_{yyyy}^{\mathrm{H}(1\times3)}+6\left(\chi_{yyzz}^{\mathrm{H}(1\times3)}-\chi_{zzxx}^{\mathrm{H}(1\times3)}\right)\right],$$

$$(X_{4x}^\alpha,X_{4y}^\alpha,X_{4z}^\alpha)=\frac{1}{2}\left(\chi_{yyyz}^{\mathrm{H}(1\times3)}-\chi_{yzzz}^{\mathrm{H}(1\times3)},\chi_{zzzx}^{\mathrm{H}(1\times3)}-\chi_{zxxx}^{\mathrm{H}(1\times3)},\chi_{xxxy}^{\mathrm{H}(1\times3)}-\chi_{xyyy}^{\mathrm{H}(1\times3)}\right),$$

$$(X_{4x}^\beta,X_{4y}^\beta,X_{4y}^\beta)=\frac{1}{14}\left(7\chi_{xxyz}^{\mathrm{H}(1\times3)}-\sum_i\chi_{iiyz}^{\mathrm{H}(1\times3)},7\chi_{yyzx}^{\mathrm{H}(1\times3)}-\sum_i\chi_{iizx}^{\mathrm{H}(1\times3)},7\chi_{zzxy}^{\mathrm{H}(1\times3)}-\sum_i\chi_{iixy}^{\mathrm{H}(1\times3)}\right). \tag{E.30}$$

For notational simplicity, we set

$$\begin{aligned}
(\tilde{X}_u,\tilde{X}'_u)&\equiv(X_u+X'_u,4X_u-X'_u),\ \ \tilde{X}''_u\equiv\tilde{X}_u-\tilde{X}'_u,\\
(\tilde{X}_v,\tilde{X}'_v)&\equiv(3X_v+X'_v,2X_v-X'_v),\ \ \tilde{X}''_v\equiv\tilde{X}_v+2\tilde{X}'_v,\\
(\tilde{X}_{yz},\tilde{X}'_{yz})&\equiv(2X_{yz}-X'_{yz},8X_{yz}+X'_{yz}),(\text{cyclic}).
\end{aligned} \tag{E.31}$$

E.1.6 $\chi^{[2\times2]}$

For the rank-4 tensor

$$\chi^{[2\times2]}=\begin{pmatrix}\chi_{ll} & \chi_{lt}\\ \chi_{tl} & \chi_{tt}\end{pmatrix}, \tag{E.32}$$

consisting of the following 3×3 tensors

$$\chi_{ll}=\begin{pmatrix}\chi^{[2\times2]}_{xx;xx} & \chi^{[2\times2]}_{xx;yy} & \chi^{[2\times2]}_{xx;zz}\\ \chi^{[2\times2]}_{yy;xx} & \chi^{[2\times2]}_{yy;yy} & \chi^{[2\times2]}_{yy;zz}\\ \chi^{[2\times2]}_{zz;xx} & \chi^{[2\times2]}_{zz;yy} & \chi^{[2\times2]}_{zz;zz}\end{pmatrix},\ \chi_{lt}=\begin{pmatrix}\chi^{[2\times2]}_{xx;yz} & \chi^{[2\times2]}_{xx;zx} & \chi^{[2\times2]}_{xx;xy}\\ \chi^{[2\times2]}_{yy;yz} & \chi^{[2\times2]}_{yy;zx} & \chi^{[2\times2]}_{yy;xy}\\ \chi^{[2\times2]}_{zz;yz} & \chi^{[2\times2]}_{zz;zx} & \chi^{[2\times2]}_{zz;xy}\end{pmatrix},$$
$$\chi_{tl}=\begin{pmatrix}\chi^{[2\times2]}_{yz;xx} & \chi^{[2\times2]}_{yz;yy} & \chi^{[2\times2]}_{yz;zz}\\ \chi^{[2\times2]}_{zx;xx} & \chi^{[2\times2]}_{zx;yy} & \chi^{[2\times2]}_{zx;zz}\\ \chi^{[2\times2]}_{xy;xx} & \chi^{[2\times2]}_{xy;yy} & \chi^{[2\times2]}_{xy;zz}\end{pmatrix},\ \chi_{tt}=\begin{pmatrix}\chi^{[2\times2]}_{yz;yz} & \chi^{[2\times2]}_{yz;zx} & \chi^{[2\times2]}_{yz;xy}\\ \chi^{[2\times2]}_{zx;yz} & \chi^{[2\times2]}_{zx;zx} & \chi^{[2\times2]}_{zx;xy}\\ \chi^{[2\times2]}_{xy;yz} & \chi^{[2\times2]}_{xy;zx} & \chi^{[2\times2]}_{xy;xy}\end{pmatrix}, \tag{E.33}$$

the monopole, dipole, quadrupole, octupole, and hexadecapole components are expressed by using the tensor component $\chi^{[2\times2]}_{ij;kl}(=\chi^{[2\times2]}_{ji;kl}=\chi^{[2\times2]}_{ij;lk})$ as

$$\chi^{\mathrm{M}(0\times0)}=\frac{1}{3}\sum_{ij}\chi^{[2\times2]}_{ii;jj}, \tag{E.34}$$
$$\chi^{\mathrm{Q}(0\times2,\pm)}_{ij}=\frac{1}{6}\sum_{k}\left(\chi^{[2\times2]}_{kk;ij}\pm\chi^{[2\times2]}_{ij;kk}\right), \tag{E.35}$$
$$\chi^{\mathrm{M}(2\times2)}=\frac{1}{3}\sum_{ij}\left(\chi^{[2\times2]}_{ij;ji}-\frac{1}{3}\chi^{[2\times2]}_{ii;jj}\right), \tag{E.36}$$
$$\chi^{\mathrm{D}(2\times2)}_{i}=\frac{1}{2}\sum_{jkl}\epsilon_{ijk}\chi^{[2\times2]}_{lj;kl}, \tag{E.37}$$
$$\chi^{\mathrm{Q}(2\times2)}_{ij}=\frac{1}{2}\sum_{k}\left[\left(\chi^{[2\times2]}_{ik;kj}+\chi^{[2\times2]}_{jk;ki}\right)-\frac{2}{3}\left(\chi^{[2\times2]}_{ij;kk}+\chi^{[2\times2]}_{kk;ij}\right)\right]=\chi^{\mathrm{Q}(2\times2)}_{ji}, \tag{E.38}$$
$$\begin{aligned}\chi^{\mathrm{O}(2\times2)}_{ijk}&=\frac{1}{6}\sum_{lm}\left(\epsilon_{ilm}\chi^{[2\times2]}_{jl;mk}+\epsilon_{jlm}\chi^{[2\times2]}_{kl;mi}+\epsilon_{klm}\chi^{[2\times2]}_{il;mj}+\epsilon_{ilm}\chi^{[2\times2]}_{kl;mj}+\epsilon_{jlm}\chi^{[2\times2]}_{il;mk}+\epsilon_{klm}\chi^{[2\times2]}_{jl;mi}\right)\\ &=\chi^{\mathrm{O}(2\times2)}_{jki}=\chi^{\mathrm{O}(2\times2)}_{jik},\end{aligned} \tag{E.39}$$
$$\chi^{\mathrm{H}(2\times2)}_{ijkl}=\frac{1}{6}\left(\chi^{[2\times2]}_{ij;kl}+\chi^{[2\times2]}_{ik;jl}+\chi^{[2\times2]}_{il;kj}+\chi^{[2\times2]}_{kj;il}+\chi^{[2\times2]}_{lj;ki}+\chi^{[2\times2]}_{kl;ij}\right)=\chi^{\mathrm{H}(2\times2)}_{jkli}=\chi^{\mathrm{H}(2\times2)}_{jikl}. \tag{E.40}$$

Since both $B^{[2]}=(B_{xx},B_{yy},B_{zz},B_{yz},B_{zx},B_{xy})$ and $F^{[2]}=(F_{xx},F_{yy},F_{zz},F_{yz},F_{zx},F_{xy})$ contain $l_B,l_F=0,2$ components, there are two types of monopole components $\chi^{\mathrm{M}(0\times0)}$ and $\chi^{\mathrm{M}(2\times2)}$ and three types of quadrupole components $\chi^{\mathrm{Q}(0\times2,\pm)}_{ij}$ and $\chi^{\mathrm{Q}(2\times2)}_{ij}$. By using

Eqs. (E.34)–(E.40), the multipoles in Eqs. (2.31)–(2.34) are represented as

$$X_0=\frac{1}{10}\chi^{\mathrm{M}(2\times2)},\ \ X_0'=\frac{1}{3}\chi^{\mathrm{M}(0\times0)}, \tag{E.41}$$

$$(Y_x,Y_y,Y_z)=\frac{1}{5}\left(\chi_x^{\mathrm{D}(2\times2)},\chi_y^{\mathrm{D}(2\times2)},\chi_z^{\mathrm{D}(2\times2)}\right), \tag{E.42}$$

$$\begin{aligned}
X_u&=\frac{1}{42}\left(3\chi_{zz}^{\mathrm{Q}(2\times2)}-\sum_i\chi_{ii}^{\mathrm{Q}(2\times2)}\right),\\
X_v&=\frac{1}{14}\left(\chi_{xx}^{\mathrm{Q}(2\times2)}-\chi_{yy}^{\mathrm{Q}(2\times2)}\right),\\
(X_{yz},X_{zx},X_{xy})&=\frac{1}{7}\left(\chi_{yz}^{\mathrm{Q}(2\times2)},\chi_{zx}^{\mathrm{Q}(2\times2)},\chi_{xy}^{\mathrm{Q}(2\times2)}\right),
\end{aligned} \tag{E.43}$$

$$\begin{aligned}
X_u^{(\pm)}&=\frac{1}{6}\left(3\chi_{zz}^{\mathrm{Q}(0\times2,\pm)}-\sum_i\chi_{ii}^{\mathrm{Q}(0\times2,\pm)}\right),\\
X_v^{(\pm)}&=\frac{1}{2}\left(\chi_{xx}^{\mathrm{Q}(0\times2,\pm)}-\chi_{yy}^{\mathrm{Q}(0\times2,\pm)}\right),\\
(X_{yz}^{(\pm)},X_{zx}^{(\pm)},X_{xy}^{(\pm)})&=\left(\chi_{yz}^{\mathrm{Q}(0\times2,\pm)},\chi_{zx}^{\mathrm{Q}(0\times2,\pm)},\chi_{xy}^{\mathrm{Q}(0\times2,\pm)}\right),
\end{aligned} \tag{E.44}$$

$$\begin{aligned}
Y_{xyz}&=\chi_{xyz}^{\mathrm{O}(2\times2)},\\
(Y_x^\alpha,Y_y^\alpha,Y_z^\alpha)&=\frac{1}{20}\left(5\chi_{xxx}^{\mathrm{O}(2\times2)}-3\sum_i\chi_{xii}^{\mathrm{O}(2\times2)},5\chi_{yyy}^{\mathrm{O}(2\times2)}-3\sum_i\chi_{yii}^{\mathrm{O}(2\times2)},5\chi_{zzz}^{\mathrm{O}(2\times2)}-3\sum_i\chi_{zii}^{\mathrm{O}(2\times2)}\right),\\
(Y_x^\beta,Y_y^\beta,Y_z^\beta)&=\frac{1}{4}\left(\chi_{xyy}^{\mathrm{O}(2\times2)}-\chi_{zzx}^{\mathrm{O}(2\times2)},\chi_{yzz}^{\mathrm{O}(2\times2)}-\chi_{xxy}^{\mathrm{O}(2\times2)},\chi_{zxx}^{\mathrm{O}(2\times2)}-\chi_{yyz}^{\mathrm{O}(2\times2)}\right),
\end{aligned} \tag{E.45}$$

$$\begin{aligned}
X_4&=\frac{1}{6}\left(\sum_i\chi_{iiii}^{\mathrm{H}(2\times2)}-\frac{3}{5}\sum_{ij}\chi_{iijj}^{\mathrm{H}(2\times2)}\right),\\
X_{4u}&=\frac{1}{6}\left[\left(3\chi_{zzzz}^{\mathrm{H}(2\times2)}-\sum_i\chi_{iiii}^{\mathrm{H}(2\times2)}\right)-\frac{6}{7}\sum_i\left(2\chi_{iizz}^{\mathrm{H}(2\times2)}-\chi_{iixx}^{\mathrm{H}(2\times2)}-\chi_{iiyy}^{\mathrm{H}(2\times2)}\right)\right],\\
X_{4v}&=\frac{1}{2}\left[\chi_{xxxx}^{\mathrm{H}(2\times2)}-\chi_{yyyy}^{\mathrm{H}(2\times2)}-\frac{6}{7}\sum_i\left(\chi_{iixx}^{\mathrm{H}(2\times2)}-\chi_{iiyy}^{\mathrm{H}(2\times2)}\right)\right],\\
(X_{4x}^\alpha,X_{4y}^\alpha,X_{4z}^\alpha)&=\frac{1}{2}\left(\chi_{yyyz}^{\mathrm{H}(2\times2)}-\chi_{yzzz}^{\mathrm{H}(2\times2)},\chi_{zzzx}^{\mathrm{H}(2\times2)}-\chi_{zxxx}^{\mathrm{H}(2\times2)},\chi_{xxxy}^{\mathrm{H}(2\times2)}-\chi_{xyyy}^{\mathrm{H}(2\times2)}\right),\\
(X_{4x}^\beta,X_{4y}^\beta,X_{4z}^\beta)&=\frac{1}{2}\left(6\chi_{xxyz}^{\mathrm{H}(2\times2)}-\frac{1}{7}\sum_i\chi_{yzii}^{\mathrm{H}(2\times2)},6\chi_{yyzx}^{\mathrm{H}(2\times2)}-\frac{1}{7}\sum_i\chi_{zxii}^{\mathrm{H}(2\times2)},6\chi_{zzxy}^{\mathrm{H}(2\times2)}-\frac{1}{7}\sum_i\chi_{xyii}^{\mathrm{H}(2\times2)}\right).
\end{aligned} \tag{E.46}$$

We use the notation

$$\begin{aligned}
(\tilde{X}_0,\tilde{X}_0')&\equiv(4X_0+X_0',-2X_0+X_0'),\\
(\tilde{X}_u,\tilde{X}_u^{(\pm)})&\equiv(-4X_u-2X_u^{(+)},-4X_u+X_u^{(+)}\pm3X_u^{(-)}),\ \ \tilde{X}_u'\equiv-\tilde{X}_u^{(+)}-\tilde{X}_u^{(-)},\\
(\tilde{X}_v,\tilde{X}_v^{(\pm)})&\equiv(4X_v+2X_v^{(+)},-4X_v+X_v^{(+)}\pm X_v^{(-)}),\\
(\tilde{X}_{yz}^{(\pm)},\tilde{X}_{yz}'^{(\pm)})&\equiv(-4X_{yz}+X_{yz}^{(+)}\pm X_{yz}^{(-)},2X_{yz}+X_{yz}^{(+)}\pm X_{yz}^{(-)}),(\text{cyclic}),
\end{aligned} \tag{E.47}$$

for simplicity.

E.2 Tensor Expression in Hexagonal/Trigonal System

In the hexagonal and trigonal systems, it is convenient to use the tesseral harmonics to describe multipoles rather than the cubic harmonics. Since the tesseral harmonics have the different functional form from the cubic harmonics for the rank $l \geq 3$ (See Appendix A), we show the rank-3 and -4 response tensors in the hexagonal and trigonal systems as

$$\chi^{[0\times3]} = \begin{pmatrix} 3X_x+X_{3a}-3X_{3u} \\ 3X_y-X_{3b}-3X_{3v} \\ 3X_z+2X_z^\alpha \\ X_z-X_z^\alpha-X_z^\beta \\ X_x+4X_{3u} \\ X_y+X_{3b}-X_{3v} \\ X_y+4X_{3v} \\ X_z-X_z^\alpha+X_z^\beta \\ X_x-X_{3a}-X_{3u} \\ X_{xyz} \end{pmatrix}^{\mathrm{T}}, \tag{E.48}$$

$$\chi^{[1\times2]} = \begin{pmatrix} 3X_x+X_{3a}-3X_{3u} & 2(X_y'-Y_{zx})+X_y+X_{3b}-X_{3v} & 2(X_z'+Y_{xy})+X_z-X_z^\alpha+X_z^\beta \\ 2(X_x'+Y_{yz})+X_x-X_{3a}-X_{3u} & 3X_y-X_{3b}-3X_{3v} & 2(X_z'-Y_{xy})+X_z-X_z^\alpha-X_z^\beta \\ 2(X_x'-Y_{yz})+X_x+4X_{3u} & 2(X_y'+Y_{zx})+X_y+4X_{3v} & 3(X_z+X_z^\alpha) \\ Y_u+Y_v+X_{xyz} & -X_z'+Y_{xy}+X_z-X_z^\alpha-X_z^\beta & -X_y'-Y_{zx}+X_y+4X_{3v} \\ -X_z'-Y_{xy}+X_z-X_z^\alpha+X_z^\beta & -Y_u+Y_v+X_{xyz} & -X_x'+Y_{yz}+X_x+4X_{3u} \\ -X_y'+Y_{zx}+X_y+X_{3b}-X_{3v} & -X_x'-Y_{yz}+X_x-X_{3a}-X_{3u} & -2Y_v+X_{xyz} \end{pmatrix}^{\mathrm{T}}. \tag{E.49}$$

$$\chi^{[1\times3]} = \begin{pmatrix} 3(X_0-\tilde{X}_u+\tilde{X}_v)+3X_{40}+X_{4u}^{\beta1}-X_{4u}^{\beta2} & 3(-Y_z-\tilde{X}_{xy}+Y_z^\alpha-Y_z^\beta)+X_{4v}^{\beta1}-X_{4v}^{\beta2} & 3(Y_y-\tilde{X}_{zx}+Y_{3b}-Y_{3v})+X_{4b}-3X_{4u}^\alpha \\ 3(Y_z-\tilde{X}_{xy}-Y_z^\alpha-Y_z^\beta)-X_{4v}^{\beta1}-X_{4v}^{\beta2} & 3(X_0-\tilde{X}_u-\tilde{X}_v)+3X_{40}+X_{4u}^{\beta1}+X_{4u}^{\beta2} & 3(-Y_x-\tilde{X}_{yz}+Y_{3a}+Y_{3u})-X_{4a}-3X_{4v}^\alpha \\ -3(Y_y+\tilde{X}_{zx}+4Y_{3v})+4X_{4u}^\alpha & 3(Y_x-\tilde{X}_{yz}+4Y_{3u})+4X_{4v}^\alpha & 3(X_0+2\tilde{X}_u)+8X_{40} \\ -Y_y-\tilde{X}_{zx}+Y_{3b}+11Y_{3v}-X_{4b}-X_{4u}^\alpha & Y_x+\tilde{X}_{yz}'-Y_{3a}-Y_{3u}-X_{4a}-3X_{4v}^\alpha & X_0+\tilde{X}_u''-5X_v-Y_{xyz}-4X_{40}-X_{4u}^{\beta2} \\ X_0+\tilde{X}_u'-\tilde{X}_v'-Y_{xyz}-4X_{40}+X_{4u}^{\beta2} & -Y_z-\tilde{X}_{xy}-4Y_z^\alpha+2Y_z^\beta+2X_{4v}^{\beta2} & Y_y+\tilde{X}_{zx}'+4Y_{3v}+4X_{4u}^\alpha \\ Y_z+\tilde{X}_{xy}'-Y_z^\alpha+Y_z^\beta+X_{4v}^{\beta1}-X_{4v}^{\beta2} & X_0-\tilde{X}_u+\tilde{X}_v''-Y_{xyz}+X_{40}-X_{4u}^{\beta1} & -Y_x-\tilde{X}_{yz}-3Y_{3a}+Y_{3u}+X_{4a}-X_{4v}^\alpha \\ Y_z-\tilde{X}_{xy}+4Y_z^\alpha+2Y_z^\beta+2X_{4v}^{\beta2} & X_0+\tilde{X}_u'+\tilde{X}_v'+Y_{xyz}-4X_{40}-X_{4u}^{\beta2} & -Y_x+\tilde{X}_{yz}'-4Y_{3u}+4X_{4v}^\alpha \\ -Y_y+\tilde{X}_{zx}'-Y_{3b}+Y_{3v}+X_{4b}-3X_{4u}^\alpha & Y_x-\tilde{X}_{yz}+Y_{3a}-11Y_{3u}+X_{4a}-X_{4v}^\alpha & X_0+\tilde{X}_u''+5X_v+Y_{xyz}-4X_{40}+X_{4u}^{\beta2} \\ X_0-\tilde{X}_u-\tilde{X}_v''+Y_{xyz}+X_{40}-X_{4u}^{\beta1} & -Y_z+\tilde{X}_{xy}'+Y_z^\alpha+Y_z^\beta-X_{4v}^{\beta1}-X_{4v}^{\beta2} & Y_y-\tilde{X}_{zx}-3Y_{3b}-Y_{3v}-X_{4b}-X_{4u}^\alpha \\ 5X_{yz}+Y_{3a}+5Y_{3u}+X_{4a}-X_{4v}^\alpha & 5X_{zx}+Y_{3b}-5Y_{3v}-X_{4b}-X_{4u}^\alpha & 5X_{xy}-2Y_z^\beta+2X_{4v}^{\beta2} \end{pmatrix}^{\mathrm{T}}, \tag{E.50}$$

$$\chi^{[2\times2]} = \begin{pmatrix} \chi_{ll} & \chi_{lt} \\ \chi_{tl} & \chi_{tt} \end{pmatrix}, \tag{E.51}$$

$$\chi_{ll}=\begin{pmatrix} \tilde{X}_0+\tilde{X}_u+\tilde{X}_v+3X_{40}+X_{4u}^{\beta 1}-X_{4u}^{\beta 2} & \tilde{X}_0'+\tilde{X}_u'-2\tilde{X}_v^{(-)}+Y_{xyz}+X_{40}-X_{4u}^{\beta 1} & \tilde{X}_0'+\tilde{X}_u^{(+)}+\tilde{X}_v^{(-)}-Y_{xyz}-4X_{40}+X_{4u}^{\beta 2} \\ \tilde{X}_0'+\tilde{X}_u'+2\tilde{X}_v^{(-)}-Y_{xyz}+X_{40}-X_{4u}^{\beta 1} & \tilde{X}_0+\tilde{X}_u-\tilde{X}_v+3X_{40}+X_{4u}^{\beta 1}+X_{4u}^{\beta 2} & \tilde{X}_0'+\tilde{X}_u^{(+)}-\tilde{X}_v^{(-)}+Y_{xyz}-4X_{40}-X_{4u}^{\beta 2} \\ \tilde{X}_0'+\tilde{X}_u^{(-)}+\tilde{X}_v^{(+)}+Y_{xyz}-4X_{40}+X_{4u}^{\beta 2} & \tilde{X}_0'+\tilde{X}_u^{(-)}-\tilde{X}_v^{(+)}-Y_{xyz}-4X_{40}-X_{4u}^{\beta 2} & \tilde{X}_0-2\tilde{X}_u+8X_{40} \end{pmatrix}, \tag{E.52}$$

$$\chi_{lt}=\begin{pmatrix} \tilde{X}_{yz}^{(+)}+Y_{3a}+5Y_{3u}+X_{4a}-X_{4v}^{\alpha} & -2Y_y+\tilde{X}_{zx}'^{(+)}-Y_{3b}+Y_{3v}+X_{4b}-3X_{4u}^{\alpha} & 2Y_z+\tilde{X}_{xy}'^{(+)}-Y_z^{\alpha}+Y_z^{\beta}+X_{4v}^{\beta 1}-X_{4v}^{\beta 2} \\ 2Y_x+\tilde{X}_{yz}'^{(+)}-Y_{3a}-Y_{3u}-X_{4a}-3X_{4v}^{\alpha} & \tilde{X}_{zx}^{(+)}+Y_{3b}-5Y_{3v}-X_{4b}-X_{4u}^{\alpha} & -2Y_z+\tilde{X}_{xy}'^{(+)}+Y_z^{\alpha}+Y_z^{\beta}-X_{4v}^{\beta 1}-X_{4v}^{\beta 2} \\ -2Y_x+\tilde{X}_{yz}'^{(+)}-4Y_{3u}+4X_{4v}^{\alpha} & 2Y_y+\tilde{X}_{zx}'^{(+)}+4Y_{3v}+4X_{4u}^{\alpha} & \tilde{X}_{xy}^{(+)}-2Y_z^{\beta}+2X_{4v}^{\beta 2} \end{pmatrix}, \tag{E.53}$$

$$\chi_{tl}=\begin{pmatrix} \tilde{X}_{yz}^{(-)}-Y_{3a}-5Y_{3u}+X_{4a}-X_{4v}^{\alpha} & -2Y_x+\tilde{X}_{yz}'^{(-)}+Y_{3a}+Y_{3u}-X_{4a}-3X_{4v}^{\alpha} & 2Y_x+\tilde{X}_{yz}'^{(-)}+4Y_{3u}+4X_{4v}^{\alpha} \\ 2Y_y+\tilde{X}_{zx}'^{(-)}+Y_{3b}-Y_{3v}+X_{4b}-3X_{4u}^{\alpha} & \tilde{X}_{zx}^{(-)}-Y_{3b}+5Y_{3v}-X_{4b}-X_{4u}^{\alpha} & -2Y_y+\tilde{X}_{zx}'^{(-)}-4Y_{3v}+4X_{4u}^{\alpha} \\ -2Y_z+\tilde{X}_{xy}'^{(-)}+Y_z^{\alpha}-Y_z^{\beta}+X_{4v}^{\beta 1}-X_{4v}^{\beta 2} & 2Y_z+\tilde{X}_{xy}'^{(-)}-Y_z^{\alpha}-Y_z^{\beta}-X_{4v}^{\beta 1}-X_{4v}^{\beta 2} & \tilde{X}_{xy}^{(-)}+2Y_z^{\beta}+2X_{4v}^{\beta 2} \end{pmatrix}, \tag{E.54}$$

$$\chi_{tt}=\begin{pmatrix} 3X_0+3X_u-3X_v-4X_{40}-X_{4u}^{\beta 2} & -Y_z+3X_{xy}-2Y_z^{\alpha}+2X_{4v}^{\beta 2} & Y_y+3X_{zx}-Y_{3b}-3Y_{3v}-X_{4b}-X_{4u}^{\alpha} \\ Y_z+3X_{xy}+2Y_z^{\alpha}+2X_{4v}^{\beta 2} & 3X_0+3X_u+3X_v-4X_{40}+X_{4u}^{\beta 2} & -Y_x+3X_{yz}-Y_{3a}+3Y_{3u}+X_{4a}-X_{4v}^{\alpha} \\ -Y_y+3X_{zx}+Y_{3b}+3Y_{3v}-X_{4b}-X_{4u}^{\alpha} & Y_x+3X_{yz}+Y_{3a}-3Y_{3u}+X_{4a}-X_{4v}^{\alpha} & 3X_0-6X_u+X_{40}-X_{4u}^{\beta 1} \end{pmatrix}, \tag{E.55}$$

where the following relations with respect to the octupoles and hecadecapoles are used as

$$\begin{gathered} Y_{3a}=\frac{1}{4}(5Y_x^{\alpha}-3Y_x^{\beta}),\ Y_{3b}=-\frac{1}{4}(5Y_y^{\alpha}+3Y_y^{\beta}),\ Y_{3u}=-\frac{1}{4}(Y_x^{\alpha}+Y_x^{\beta}),\ Y_{3v}=-\frac{1}{4}(Y_y^{\alpha}-Y_y^{\beta}), \\ X_{40}=\frac{1}{4}(X_4+X_{4u}),\ X_{4u}^{\alpha}=\frac{1}{4}(X_{4y}^{\alpha}-X_{4y}^{\beta}),\ X_{4v}^{\alpha}=-\frac{1}{4}(X_{4x}^{\alpha}+X_{4x}^{\beta}),\ X_{4u}^{\beta 1}=\frac{1}{4}(5X_4-7X_{4u}), \\ X_{4v}^{\beta 1}=X_{4z}^{\alpha},\ X_{4u}^{\beta 2}=-X_{4v},\ X_{4v}^{\beta 2}=X_{4z}^{\beta},\ X_{4a}=-\frac{1}{4}(X_{4x}^{\alpha}-7X_{4x}^{\beta}),\ X_{4b}=-\frac{1}{4}(X_{4y}^{\alpha}+7X_{4y}^{\beta}), \end{gathered} \tag{E.56}$$

in $\chi^{[0\times 3]}$, $\chi^{[1\times 3]}$ and $\chi^{[2\times 2]}$, while

$$X_{3a}=\frac{1}{4}(5X_x^{\alpha}-3X_x^{\beta}),\ X_{3b}=-\frac{1}{4}(5X_y^{\alpha}+3X_y^{\beta}),\ X_{3u}=-\frac{1}{4}(X_x^{\alpha}+X_x^{\beta}),\ X_{3v}=-\frac{1}{4}(X_y^{\alpha}-X_y^{\beta}), \tag{E.57}$$

in $\chi^{[1\times 2]}$.

Appendix F

Other NMR Spectra

F.1 Field-Swept NMR Spectra

We show the field-swept NMR spectra for the resonance frequency $\omega=1.1\gamma$ at the [001] and [100] magnetic fields. We set $\gamma=1$ and the coupling constant as well as that in Secs. 4.6.4 and 4.6.5. Figures F.1(a)–F.1(c) show the spectra in the [001] magnetic field, whereas Figs. F.1(d)–F.1(f) show those in the [100] magnetic field. The results show a similar tendency in the cases of the frequency-swept spectra in Figs. 4.14 and 4.15.

F.2 [110]-Field NMR Spectra

We show the effective hyperfine fields and NMR spectra in the case of the [110] magnetic field in the Q_v- and Q_u-type AFQ states and M_x-type AFM state. The hyperfine field Hamiltonian is given by

$$\begin{aligned}\tilde{\mathcal{H}}^{[110]}_{\rm para}=&\left(\tilde{c}^{\rm e,1}_{x,y}Q^{\rm (c)}_u+\tilde{c}^{\rm e,2}_{x,y}Q^{\rm (c)}_{xy}\right)\left(\hat{I}_x+\hat{I}_y\right)\\&+\left[\tilde{c}^{\rm e,1}_{u}Q^{\rm (c)}_{xy}+\tilde{c}^{\rm e,2}_{u}\left(M^{\rm (c)}_x+M^{\rm (c)}_y\right)\right]\hat{I}_u+\left[\tilde{c}^{\rm e,1}_{xy}Q^{\rm (c)}_u+\tilde{c}^{\rm e,2}_{xy}\left(M^{\rm (c)}_x+M^{\rm (c)}_y\right)\right]\hat{I}_{xy},\end{aligned}\tag{F.1}$$

$$\begin{aligned}\tilde{\mathcal{H}}^{\rm o[110]}_{\rm order}=&\tilde{c}^{\rm o,1}_{x,y}G^{\rm (c)}_{xy}\left(\hat{I}_x+\hat{I}_y\right)+\left[\tilde{c}^{\rm o,2}_{x,y}\left(T^{\rm (c)}_x-T^{\rm (c)}_y\right)+\tilde{c}^{\rm o,3}_{x,y}Q^{\rm (c)}_z+\tilde{c}^{\rm o,4}_{x,y}G^{\rm (c)}_v\right]\left(\hat{I}_x-\hat{I}_y\right)+\tilde{c}^{\rm o}_z\left(Q^{\rm (c)}_x-Q^{\rm (c)}_y\right)\hat{I}_z\\&+\tilde{c}^{\rm o}_u\left(T^{\rm (c)}_x+T^{\rm (c)}_y\right)\hat{I}_u+\left[\tilde{c}^{\rm o,1}_{v}G^{\rm (c)}_v+\tilde{c}^{\rm o,2}_{v}\left(T^{\rm (c)}_x-T^{\rm (c)}_y\right)\right]\hat{I}_v\\&+\left[\tilde{c}^{\rm o,1}_{yz,zx}M^{\rm (c)}_u+\tilde{c}^{\rm o,2}_{yz,zx}M^{\rm (c)}_{xy}\right]\left(\hat{I}_{yz}-\hat{I}_{zx}\right)+\left[\tilde{c}^{\rm o,3}_{yz,zx}\left(Q^{\rm (c)}_x-Q^{\rm (c)}_y\right)+\tilde{c}^{\rm o,4}_{yz,zx}M^{\rm (c)}_v\right]\left(\hat{I}_{yz}+\hat{I}_{zx}\right)\\&+\left[\tilde{c}^{\rm o,1}_{xy}G^{\rm (c)}_{xy}+\tilde{c}^{\rm o,2}_{xy}\left(T^{\rm (c)}_x+T^{\rm (c)}_y\right)\right]\hat{I}_{xy},\end{aligned}\tag{F.2}$$

$$\begin{aligned}\tilde{\mathcal{H}}^{\rm e[110]}_{\rm order}=&\left[\tilde{c}^{\rm e,3}_{x,y}\left(M^{\rm (c)}_x-M^{\rm (c)}_y\right)+\tilde{c}^{\rm e,4}_{x,y}Q^{\rm (c)}_v\right]\left(\hat{I}_x-\hat{I}_y\right)+\left[\tilde{c}^{\rm e,1}_{z}\left(Q^{\rm (c)}_{yz}+Q^{\rm (c)}_{zx}\right)+\tilde{c}^{\rm e,2}_{z}M^{\rm (c)}_{xyz}\right]\hat{I}_z\\&+\tilde{c}^{\rm e}_v\left(M^{\rm (c)}_x-M^{\rm (c)}_y\right)\hat{I}_v+\tilde{c}^{\rm e,1}_{yz,zx}M^{\beta\rm (c)}_z\left(\hat{I}_{yz}-\hat{I}_{zx}\right)\\&+\left[\tilde{c}^{\rm e,2}_{yz,zx}\left(Q^{\rm (c)}_{yz}+Q^{\rm (c)}_{zx}\right)+\tilde{c}^{\rm e,3}_{yz,zx}M^{\rm (c)}_z+\tilde{c}^{\rm e,4}_{yz,zx}M^{\rm (c)}_{xyz}\right]\left(\hat{I}_{yz}+\hat{I}_{zx}\right).\end{aligned}\tag{F.3}$$

We set the coupling constants as $c^{\rm e}_u=c_{\rm Q}=0.13$, $c^{\rm o}_{x,y}=0.3$, and the others are set to be 0.02 for simplicity.

Figures F.2(a)–F.2(c) show the frequency-swept NMR spectra for the magnetic field $|\boldsymbol{H}^{\rm (n)}|=1$, whereas Figs. F.2(d)–F.2(f) are the field-swept NMR spectra for the resonance

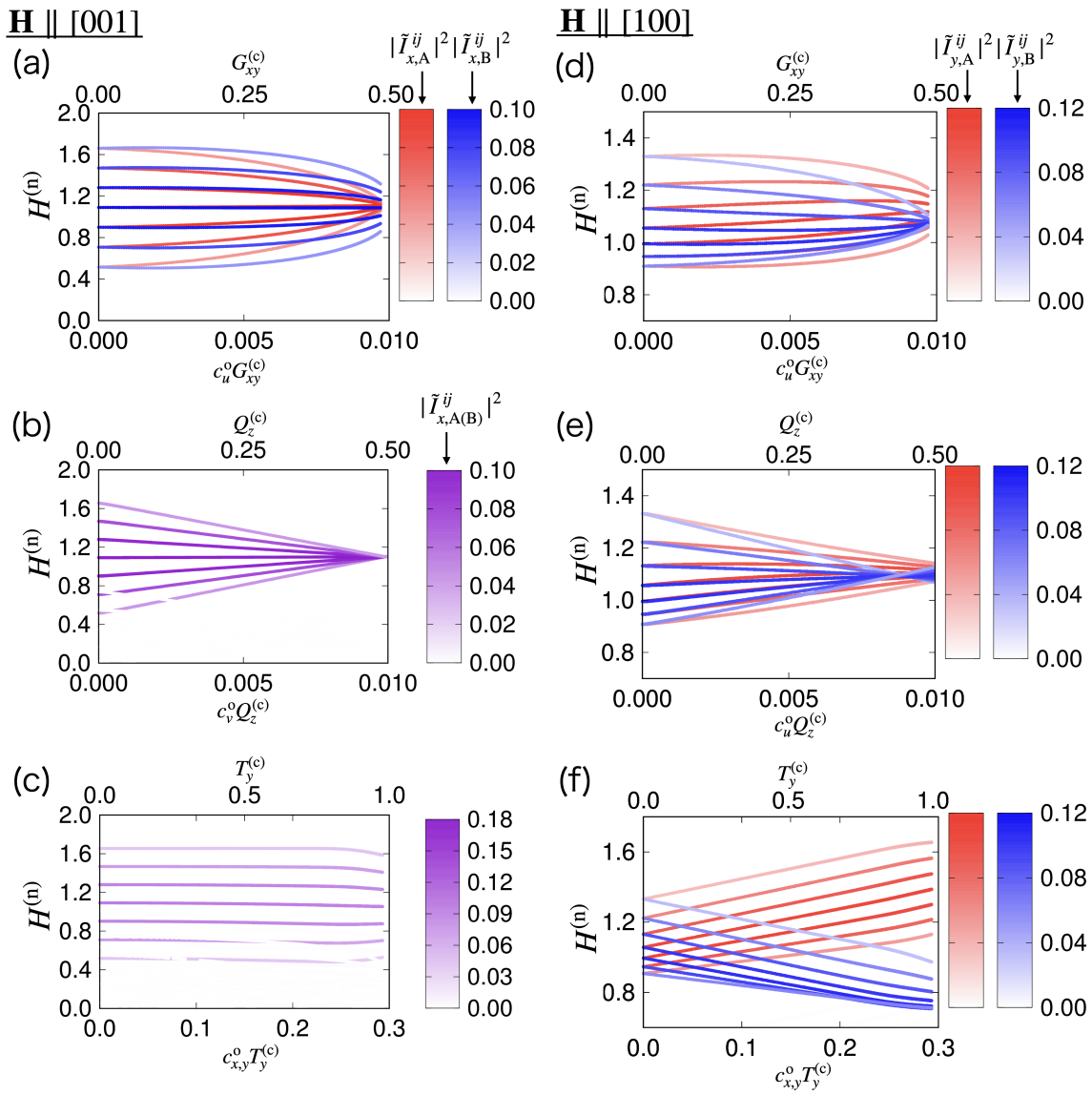

Figure F.1: The odd-parity multipole dependences of the field-swept NMR spectra at the (a–c) [001] magnetic field and (d–f) [100] magnetic field. The data are for the (a,d) Q_v-type AFQ, (b,e) Q_u-type AFQ, and (c,f) M_x-type AFM states. The color scales represent the intensities with (a–c) $\left|\tilde{I}_{x,\mathrm{A(B)}}^{ij}\right|^2$ and (d–f) $\left|\tilde{I}_{y,\mathrm{A(B)}}^{ij}\right|^2$. The coupling constants are $c_u^{\mathrm{o}}=c_v^{\mathrm{o}}=c=0.02$ in the AFQ states and $c_{x,y}^{\mathrm{o}}=c=0.3$ in the AFM state. Other coupling constants are set to be $c'=0.02$.

frequency $\omega=1.1\gamma$, where γ is set to be 1. The intensity of the spectra is calculated by $\left|\tilde{I}_{[\bar{1}10],\mathrm{A(B)}}^{ij}\right|^2$ for $I_{[\bar{1}10]}=(I_x-I_y)/2$.

In the Q_v-type AFQ [Figs. F.2(a) and F.2(d)] and M_x-type AFM states [Figs. F.2(d) and F.2(f)], the splittings in the [110] field show a similar tendency to those in the [100] field in Sec. 4.6.5. Their splittings are dominantly characterized by $G_{xy}^{(c)}$ and $T_y^{(c)}$, respectively. On the other hand, in the Q_u-type AFQ state in Figs. F.2(b) and F.2(e), there are no spectral splittings in contrast to the result under the [100] field in Sec. 4.6.5. The

reason why no splittings occur under the [110] field is attributed to the difference of the site symmetry at Co site. As the present site symmetry is $2'22'$, which is different from $2'mm'$ in the [100] direction, there is no coupling between odd-parity $Q_z^{(c)}$ and any of I_x+I_y, I_u, and I_{xy} in Eq. (F.2).

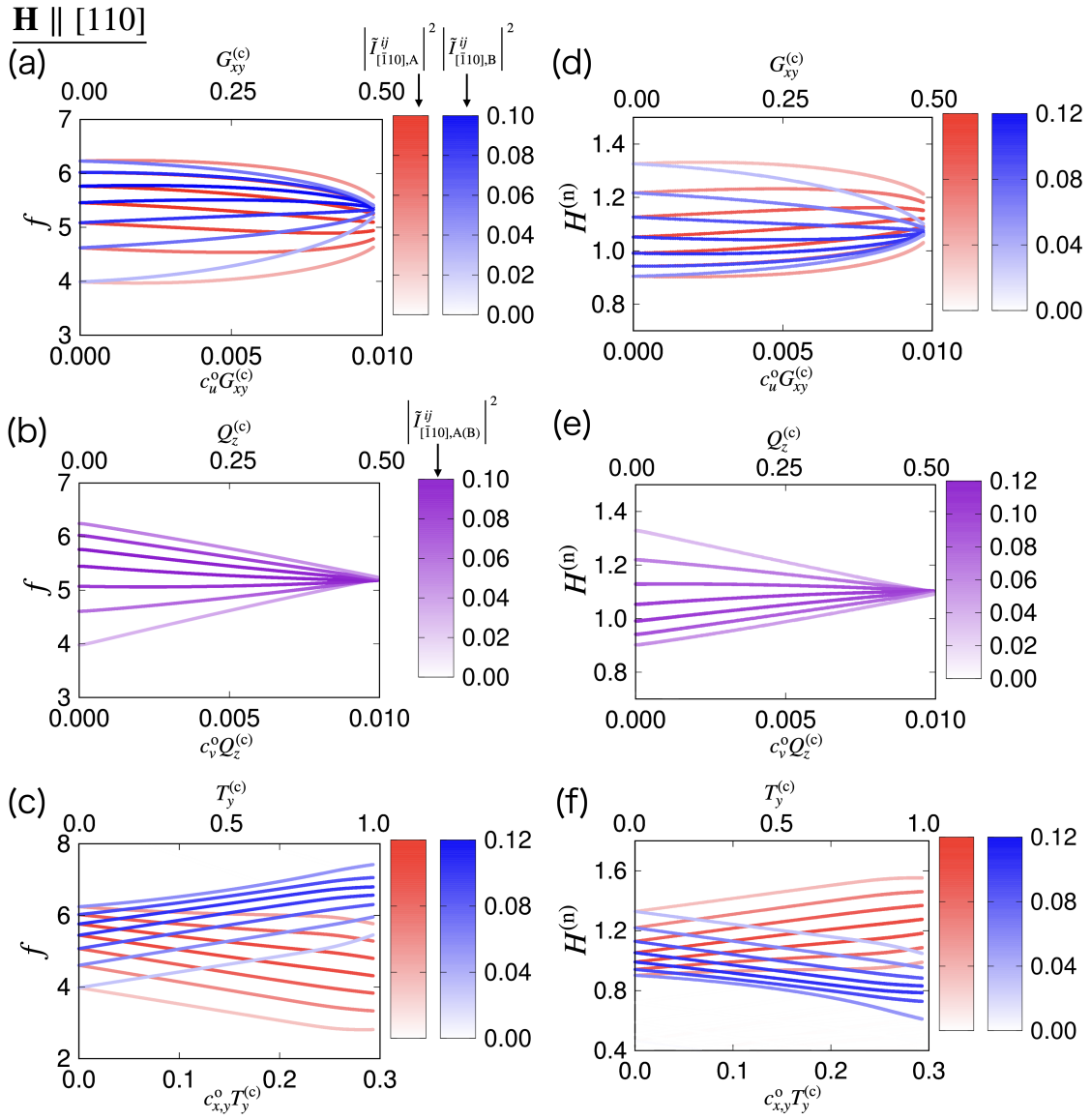

Figure F.2: The odd-parity multipole dependences of the (a–c) frequency-swept NMR spectra and (d–f) field-swept NMR spectra under the [110] magnetic field. The data are for the (a,d) Q_v-type AFQ, (b,e) Q_u-type AFQ, and (c,f) M_x-type AFM states. The color scales represent the intensities with $\left|\tilde{I}^{ij}_{[\bar{1}10],\mathrm{A(B)}}\right|^2$. The coupling constants are c^{o}_u=c^{o}_v=0.02 in the AFQ states and $c^{\mathrm{o}}_{x,y}$=0.3 in the AFM state. Other coupling constants are set to be c'=0.02.

F.3 Spectral Splittings for $\Gamma_7^{(1)}$-$\Gamma_7^{(2)}$ Levels

The different low-energy crystal-field levels activate different types of odd-parity multipole orderings. In this appendix, we show the expected sublattice-dependent splittings in NQR and NMR spectra by supposing the low-energy CEF level consisting of the two Γ_7 doublets [202]. In this case, other two multipole orderings become possible: Q_{4z}^{α}-type antiferroic E hexadecapole ordering (AFH) with the odd-parity ET quadrupole G_u and M_{5u}-type antiferroic M triacontadipole ordering (AFT) with the MT dipole T_z, where the functional forms of Q_{4z}^{α} and M_{5u} are shown in Ref. [39].

By performing a similar procedure in Secs. 4.6.2–4.6.5, the presence or absence of the sublattice-dependent spectral splittings in NQR and NMR is obtained. The results are summarized in Table F.1. The common multipoles appearing in both the two Γ_7 doublets and Γ_6-Γ_7 doublets, T_x, T_y, M_u, Q_z, Q_x, and Q_y, give the same result in Table 4.9. Note that electric toroidal quadrupole G_v, G_{xy} and magnetic quadrupole M_v, M_{xy} are not activated within the low-energy crystal-field levels unless the first-excited state is Γ_6 doublet.

Table F.1: The sublattice-dependent NQR and NMR splittings in the AFM, AFQ, AFH, and AFT states under the six field directions [001], [100], [110], $\perp$[001], $\perp$[010], and $\perp$[$\bar{1}$10], when the crystal-field first-excited state is Γ_7 doublet. The local multipoles (LMP) at Ce site and cluster odd-parity multipoles (OPMP) are shown in second and third columns, respectively. The mark ✓ represents the presence of the sublattice-dependent splittings.

			NQR	NMR					
	LMP	OPMP	—	$\boldsymbol{H}_{\parallel[001]}$	$\boldsymbol{H}_{\parallel[100]}$	$\boldsymbol{H}_{\parallel[110]}$	$\boldsymbol{H}_{\perp[001]}$	$\boldsymbol{H}_{\perp[010]}$	$\boldsymbol{H}_{\perp[\bar{1}10]}$
AFM	M_x	T_y	—	—	✓	✓	✓	✓	✓
	M_y	T_x	—	—	—	✓	✓	—	✓
	M_z	M_u	—	—	—	—	—	✓	—
AFQ	Q_u	Q_z	—	—	✓	—	✓	✓	—
	Q_{yz}	Q_y	—	—	—	—	—	—	✓
	Q_{zx}	Q_x	—	—	—	—	—	✓	✓
AFH	Q_{4z}^{α}	G_u	—	—	—	✓	✓	—	✓
AFT	M_{5u}	T_z	—	—	—	—	—	—	✓

Reference

[1] L. D. Landau and E. M. Lifshitz: *The Classical Theory of Fields, 4th ed.* (Butterworth-Heinemann, Oxford, 1 1980).

[2] J. D. Jackson: *Classical Electrodynamics, Third Edition* (John Wiley and Sons, Inc., 1 1999).

[3] R. J. Blin-Stoyle, Rev. Mod. Phys. **28**, 75 (1956).

[4] I. B. Zel'dovich, Sov. Phys. J. Exp. Theor. Phys. **6**, 1184 (1958).

[5] V. V. Flambaum and D. W. Murray, Phys. Rev. C **56**, 1641 (1997).

[6] S. Kruk and Y. Kivshar, ACS Photonics **4**, 2638 (2017).

[7] A. D. Utyushev, V. I. Zakomirnyi, and I. L. Rasskazov, Rev. Phys. **6**, 100051 (2021).

[8] K. Koshelev and Y. Kivshar, ACS Photonics **8**, 102 (2021).

[9] I. I. Smalyukh, Annu. Rev. Condens. Matter Phys. **9**, 207 (2018).

[10] B. Senyuk, J. Aplinc, M. Ravnik, and I. I. Smalyukh, Nat. Commun. **10**, 1 (2019).

[11] H. Kusunose, J. Phys. Soc. Jpn. **77**, 064710 (2008).

[12] S. Hayami and H. Kusunose, J. Phys. Soc. Jpn. **87**, 033709 (2018).

[13] H. Kusunose, R. Oiwa, and S. Hayami, J. Phys. Soc. Jpn. **89**, 104704 (2020).

[14] Y. Kuramoto, H. Kusunose, and A. Kiss, J. Phys. Soc. Jpn. **78**, 072001 (2009).

[15] P. Santini, S. Carretta, G. Amoretti, R. Caciuffo, N. Magnani, and G. H. Lander, Rev. Mod. Phys. **81**, 807 (2009).

[16] M.-T. Suzuki, H. Ikeda, and P. M. Oppeneer, J. Phys. Soc. Jpn. **87**, 041008 (2018).

[17] M. Takigawa, H. Yasuoka, T. Tanaka, and Y. Ishizawa, J. Phys. Soc. Jpn. **52**, 728 (1983).

[18] B. Lüthi, S. Blumenröder, B. Hillebrands, E. Zirngiebl, G. Güntherodt, and K. Winzer, Z. Phys. **58**, 31 (1984).

[19] J. Effantin, J. Rossat-Mignod, P. Burlet, H. Bartholin, S. Kunii, and T. Kasuya, J. Magn. Magn. Mater. **47-48**, 145 (1985).

[20] W. Erkelens, L. Regnault, P. Burlet, J. Rossat-Mignod, S. Kunii, and T. Kasuya, J. Magn. Magn. Mater. **63-64**, 61 (1987).

[21] S. Nakamura, T. Goto, S. Kunii, K. Iwashita, and A. Tamaki, J. Phys. Soc. Jpn. **63**, 623 (1994).

[22] O. Sakai, R. Shiina, H. Shiba, and P. Thalmeier, J. Phys. Soc. Jpn. **66**, 3005 (1997).

[23] R. Shiina, H. Shiba, and P. Thalmeier, J. Phys. Soc. Jpn. **66**, 1741 (1997).

[24] R. Shiina, O. Sakai, H. Shiba, and P. Thalmeier, J. Phys. Soc. Jpn. **67**, 941 (1998).

[25] P. Santini and G. Amoretti, Phys. Rev. Lett. **85**, 2188 (2000).

[26] J. A. Paixão, C. Detlefs, M. J. Longfield, R. Caciuffo, P. Santini, N. Bernhoeft, J. Rebizant, and G. H. Lander, Phys. Rev. Lett. **89**, 187202 (2002).

[27] O. Sakai, R. Shiina, and H. Shiba, J. Phys. Soc. Jpn. **74**, 457 (2005).

[28] Y. Tokunaga, D. Aoki, Y. Homma, S. Kambe, H. Sakai, S. Ikeda, T. Fujimoto, R. E. Walstedt, H. Yasuoka, E. Yamamoto, A. Nakamura, and Y. Shiokawa, Phys. Rev. Lett. **97**, 257601 (2006).

[29] N. Magnani, S. Carretta, R. Caciuffo, P. Santini, G. Amoretti, A. Hiess, J. Rebizant, and G. H. Lander, Phys. Rev. B **78**, 104425 (2008).

[30] M.-T. Suzuki, N. Magnani, and P. M. Oppeneer, Phys. Rev. B **82**, 241103(R) (2010).

[31] Y. Kuramoto, J. Otsuki, A. Kiss, and H. Kusunose, Prog. of Theor. Phys. Suppl. **160**, 134 (2005).

[32] T. Maehira and T. Hotta, J. Phys. Soc. Jpn. **75**, 262 (2006).

[33] M. Yatsushiro and S. Hayami, J. Phys. Soc. Jpn. **88**, 054708 (2019).

[34] M.-T. Suzuki, T. Koretsune, M. Ochi, and R. Arita, Phys. Rev. B **95**, 094406 (2017).

[35] M.-T. Suzuki, T. Nomoto, R. Arita, Y. Yanagi, S. Hayami, and H. Kusunose, Phs. Rev. B **99**, 174407 (2019).

[36] S. Hayami, Y. Yanagi, H. Kusunose, and Y. Motome, Phys. Rev. Lett. **122**, 147602 (2019).

[37] S. Hayami, Y. Yanagi, and H. Kusunose, Phys. Rev. B **102**, 144441 (2020).

[38] H. Watanabe and Y. Yanase, Phys. Rev. B **96**, 064432 (2017).

[39] S. Hayami, M. Yatsushiro, Y. Yanagi, and H. Kusunose, Phys. Rev. B **98**, 165110 (2018).

[40] H. Watanabe and Y. Yanase, Phys. Rev. B **98**, 245129 (2018).

[41] S. Hayami, Y. Yanagi, and H. Kusunose, J. Phys. Soc. Jpn. **88**, 123702 (2019).

[42] S. Hayami, Y. Yanagi, and H. Kusunose, Phys. Rev. B **101**, 220403(R) (2020).

[43] C. Schwartz, Phys. Rev. **97**, 380 (1955).

[44] J. M. Blatt and V. F. Weisskopf: *Theoretical Nuclear Physics* (Dover Publications, New York, 1991).

[45] V. Dubovik and A. Cheshkov, Sov. J. Part. Nucl. **5**, 318 (1974).

[46] S. Nanz: *Toroidal Multipole Moments in Classical Electrodynamics: An Analysis of Their Emergence and Physical Significance* (Springer, 2016).

[47] R. G. Barrera, G. A. Estevez, and J. Giraldo, **6**, 287 (1985).

[48] V. Dubovik, L. Tosunyan, and V. Tugushev, Zh. Eksp. Teor. Fiz. **90**, 590 (1986).

[49] V. Dubovik and V. Tugushev, Phys. Rep. **187**, 145 (1990).

[50] M. T. Hutchings, Solid State Phys. **16**, 227 (1964).

[51] S. Watanabe and K. Miyake, J. Phys. Soc. Jpn. **88**, 033701 (2019).

[52] D. Jérome, T. Rice, and W. Kohn, Phys. Rev. **158**, 462 (1967).

[53] B. I. Halperin and T. M. Rice, Rev. Mod. Phys. **40**, 755 (1968).

[54] J. Kuneš, J. Phys. Condens. Matter **27**, 333201 (2015).

[55] J. Kuneš and P. Augustinský, Phys. Rev. B **90**, 235112 (2014).

[56] T. Kaneko and Y. Ohta, Phys. Rev. B **94**, 125127 (2016).

[57] T. Yamaguchi, K. Sugimoto, and Y. Ohta, Physica B Condens. Matter **536**, 37 (2017).

[58] N. A. Spaldin, M. Fiebig, and M. Mostovoy, J. Phys. Condens. Matter **20**, 434203 (2008).

[59] S. Hayami, H. Kusunose, and Y. Motome, J. Phys. Condens. Matter **28**, 395601 (2016).

[60] S. Nakatsuji, N. Kiyohara, and T. Higo, Nature **527**, 212 (2015).

[61] T. Arima, J. Phys. Soc. Jpn. **82**, 013705 (2013).

[62] A. S. Patri, A. Sakai, S. Lee, A. Paramekanti, S. Nakatsuji, and Y. B. Kim, Nat. Commun. **10**, 4092 (2019).

[63] Y. F. Popov, A. Kadomtseva, D. Belov, G. Vorob'ev, and A. Zvezdin, J. Exp. Theor. Phys. Lett. **69**, 330 (1999).

[64] Y. F. Popov, A. Kadomtseva, G. Vorob'ev, V. Timofeeva, D. Ustinin, A. Zvezdin, and M. Tegeranchi, J. Exp. Theor. Phys. **87**, 146 (1998).

[65] T.-h. Arima, J.-H. Jung, M. Matsubara, M. Kubota, J.-P. He, Y. Kaneko, and Y. Tokura, J. Phys. Soc. Jpn. **74**, 1419 (2005).

[66] B. B. Van Aken, J.-P. Rivera, H. Schmid, and M. Fiebig, Nature **449**, 702 (2007).

[67] A. S. Zimmermann, D. Meier, and M. Fiebig, Nat. Commun. **5**, 4796 (2014).

[68] P. Toledano, D. D. Khalyavin, and L. C. Chapon, Phys. Rev. B **84**, 094421 (2011).

[69] S. Hayami, H. Kusunose, and Y. Motome, Phys. Rev. B **90**, 024432 (2014).

[70] S. Hayami, H. Kusunose, and Y. Motome, J. Phys.: Conf. Ser. **592**, 012101 (2015).

[71] H. Saito, K. Uenishi, N. Miura, C. Tabata, H. Hidaka, T. Yanagisawa, and H. Amitsuka, J. Phys. Soc. Jpn. **87**, 033702 (2018).

[72] M. Shinozaki, G. Motoyama, T. Mutou, S. Nishigori, A. Yamaguchi, K. Fujiwara, K. Miyoshi, and A. Sumiyama, JPS Conf. Proc. **30**, 011189 (2020).

[73] M. Shinozaki, G. Motoyama, M. Tsubouchi, M. Sezaki, J. Gouchi, S. Nishigori, T. Mutou, A. Yamaguchi, K. Fujiwara, K. Miyoshi, and Y. Uwatoko, J. Phys. Soc. Jpn. **89**, 033703 (2020).

[74] N. D. Khanh, N. Abe, H. Sagayama, A. Nakao, T. Hanashima, R. Kiyanagi, Y. Tokunaga, and T. Arima, Phys. Rev. B **93**, 075117 (2016).

[75] N. D. Khanh, N. Abe, S. Kimura, Y. Tokunaga, and T. Arima, Phys. Rev. B **96**, 094434 (2017).

[76] Y. Yanagi, S. Hayami, and H. Kusunose, Physica B Condens. Matter **536**, 107 (2018).

[77] Y. Yanagi, S. Hayami, and H. Kusunose, Phys. Rev. B **97**, 020404(R) (2018).

[78] S. Hayami, H. Kusunose, and Y. Motome, Phys. Rev. B **97**, 024414 (2018).

[79] Y. Shiomi, H. Watanabe, H. Masuda, H. Takahashi, Y. Yanase, and S. Ishiwata, Phys. Rev. Lett. **122**, 127207 (2019).

[80] I. Affleck and J. B. Marston, Phys. Rev. B **37**, 3774 (1988).

[81] C. Nayak, Phys. Rev. B **62**, 4880 (2000).

[82] S. Chakravarty, R. B. Laughlin, D. K. Morr, and C. Nayak, Phys. Rev. B **63**, 094503 (2001).

[83] A. Allais, J. Bauer, and S. Sachdev, Phys. Rev. B **90**, 155114 (2014).

[84] C. M. Varma, Phys. Rev. B **73**, 155113 (2006).

[85] A. Shekhter and C. M. Varma, Phys. Rev. B **80**, 214501 (2009).

[86] L. Zhao, D. Torchinsky, H. Chu, V. Ivanov, R. Lifshitz, R. Flint, T. Qi, G. Cao, and D. Hsieh, Nat. Phys. **12**, 32 (2016).

[87] H. Murayama, K. Ishida, R. Kurihara, T. Ono, Y. Sato, Y. Kasahara, H. Watanabe, Y. Yanase, G. Cao, Y. Mizukami, T. Shibauchi, Y. Matsuda, and S. Kasahara, Phys. Rev. X **11**, 011021 (2021).

[88] S. Hayami and H. Kusunose, Phys. Rev. B **104**, 045117 (2021).

[89] M. Naka, S. Hayami, H. Kusunose, Y. Yanagi, Y. Motome, and H. Seo, Nat. Commun. **10**, 4305 (2019).

[90] S. Hayami, Y. Yanagi, M. Naka, H. Seo, Y. Motome, and H. Kusunose, JPS Conf. Proc. **30**, 011149 (2020).

[91] M. Lee, E. S. Choi, X. Huang, J. Ma, C. R. Dela Cruz, M. Matsuda, W. Tian, Z. L. Dun, S. Dong, and H. D. Zhou, Phys. Rev. B **90**, 224402 (2014).

[92] R. Birss: *Symmetry and magnetism* (Selected topics in solid state physics. North-Holland Pub. Co., 1964), Selected topics in solid state physics.

[93] H. Grimmer, Acta Crystallogr. A **47**, 226 (1991).

[94] H. Grimmer, Acta Crystallogr. A **75**, 409 (2019).

[95] S. V. Gallego, J. Etxebarria, L. Elcoro, E. S. Tasci, and J. M. Perez-Mato, Acta Cryst. A **75**, 438 (2019).

[96] F. Neumann and O. Meyer: *Vorlesungen über die Theorie der Elasticität der festen Körper und des Lichtäthers: gehalten an der Universität Königsberg* (Number 5 in Franz Neumann. B.G. Teubner, 1885), number 5 in Franz Neumann.

[97] P. Curie, J. Phys. Theor. Appl. **3**, 393 (1894).

[98] S. Hayami and H. Kusunose, Phys. Rev. B **103**, L180407 (2021).

[99] C. Ederer and N. A. Spaldin, Phys. Rev. B **76**, 214404 (2007).

[100] M. Matsumoto, K. Chimata, and M. Koga, J. Phys. Soc. Jpn. **86**, 034704 (2017).

[101] M. Yatsushiro and S. Hayami, J. Phys. Soc. Jpn. **89**, 013703 (2020).

[102] Y. Gao, Front. Phys. **14**, 33404 (2019).

[103] Q. Ma, A. G. Grushin, and K. S. Burch, Nat. Mater. , (2021).

[104] M. Yatsushiro, H. Kusunose, and S. Hayami, Phys. Rev. B **104**, 054412 (2021).

[105] N. Nagaosa, J. Sinova, S. Onoda, A. H. MacDonald, and N. P. Ong, Rev. Mod. Phys. **82**, 1539 (2010).

[106] D. Xiao, M.-C. Chang, and Q. Niu, Rev. Mod. Phys. **82**, 1959 (2010).

[107] M. Gradhand, D. Fedorov, F. Pientka, P. Zahn, I. Mertig, and B. Györffy, J. Phys. Condens. Matter **24**, 213202 (2012).

[108] L. Smejkal, A. H. MacDonald, J. Sinova, S. Nakatsuji, and T. Jungwirth, arXiv: 2107.03321 , (2021).

[109] D. Khomskii, Physics **2**, 20 (2009).

[110] K. Wang, J.-M. Liu, and Z. Ren, Adv. Phys. **58**, 321 (2009).

[111] S. Dong, J.-M. Liu, S.-W. Cheong, and Z. Ren, Adv. Phys. **64**, 519 (2015).

[112] N. A. Spaldin and R. Ramesh, Nat. Mater. **18**, 203 (2019).

[113] M. Fiebig, J. Phys. D **38**, R123 (2005).

[114] W. Eerenstein, N. Mathur, and J. F. Scott, Nature **442**, 759 (2006).

[115] Y. Tokura and N. Nagaosa, Nat. Commun. **9**, 3740 (2018).

[116] A. Shubnikov: *Symmetry and Antisymmetry of Finite Figures* (USSR Press, Moscow, 1951).

[117] B. Tavger and V. Zaitsev, Soviet Phys. JETP **3**, 430 (1956).

[118] N. Belov, N. Neronova, and T. Smirnova, Phys. Crystallogr **2**, 311 (1957).

[119] W. Opechowski and R. Guccione: *Magnetism, edited by G.T. Rado and H. Suhl, Vol. 2A, ch. 3* (New York: Academic Press, 1965).

[120] D. B. Litvin: *Magnetic Group Tables* (International Union of Crystallography, 2013).

[121] E. Wigner. Group Theory (Translated from the German by GRIFFIN JJ) Chap. 26, 1959.

[122] C. Bradley and A. Cracknell: *The mathematical theory of symmetry in solids: representation theory for point groups and space groups* (Oxford University Press, 2009).

[123] V. Heine: *Group theory in quantum mechanics: an introduction to its present usage* (Courier Corporation, 2007).

[124] E. P. Wigner: *The collected works of Eugene Paul Wigner: Historical, philosophical, and socio-political papers. Historical and Biographical Reflections and Syntheses* (Springer Science & Business Media, 2013).

[125] J. O. Dimmock, J. Math. Phys. **4**, 1307 (1963).

[126] J. Dimmock and R. Wheeler, J. Phys. Chem. Solids **23**, 729 (1962).

[127] A. P. Cracknell, Prog. Theor. Phys. **35**, 196 (1966).

[128] A. Cracknell and K. Wong, Aust. J. Phys. **20**, 173 (1967).

[129] C. Bradley and B. Davies, Rev. Mod. Phys. **40**, 359 (1968).

[130] T. Inui, Y. Tanabe, and Y. Onodera: *Group Theory and Its Applications in Physics* (Springer-Verlag, 1990).

[131] G. Karavaev, SOVIET PHYSICS SOLID STATE, USSR **6**, 2943 (1965).

[132] A. P. Cracknell, Advances in Physics **17**, 367 (1968).

[133] A. Andreev and I. Grishchuk, Sov. Phys. JETP **60**, 267 (1984).

[134] N. Papanicolaou, Nucl. Phys. B. **305**, 367 (1988).

[135] H. H. Chen and P. M. Levy, Phys. Rev. Lett. **27**, 1383 (1971).

[136] C. Lacroix, P. Mendels, and F. Mila: *Introduction to Frustrated Magnetism: Materials, Experiments, Theory (Chap. 13)* (Springer, New York, 2011).

[137] V. Wadhawan: *Introduction to ferroic materials* (CRC press, 2000).

[138] K. Aizu, Phys. Rev. **146**, 423 (1966).

[139] K. Aizu, J. Phys. Soc. Jpn. **27**, 387 (1969).

[140] K. Aizu, Phs. Rev. B **2**, 754 (1970).

[141] D. B. Litvin, Acta Cryst. A **64**, 316 (2008).

[142] J. Hlinka, J. Privratska, P. Ondrejkovic, and V. Janovec, Phys. Rev. Lett. **116**, 177602 (2016).

[143] S.-W. Cheong, D. Talbayev, V. Kiryukhin, and A. Saxena, npj Quantum Mater. **3**, 19 (2018).

[144] H. Schmid, Ferroelectrics **162**, 317 (1994).

[145] H. Schmid, Ferroelectrics **221**, 9 (1999).

[146] H. Schmid, J. Phys. Condens. Matter **20**, 434201 (2008).

[147] M. Yatsushiro and S. Hayami, Phys. Rev. B **102**, 195147 (2020).

[148] R. Oiwa and H. Kusunose, J. Phys. Soc. Jpn. **91**, 014701 (2022).

[149] S. Shtrikman and H. Thomas, Solid State Commun. **3**, 147 (1965).

[150] W. H. Kleiner, Phys. Rev. **142**, 318 (1966).

[151] W. H. Kleiner, Phys. Rev. **153**, 726 (1967).

[152] W. H. Kleiner, Phys. Rev. **182**, 705 (1969).

[153] H.-D. Butzal and R. Birss, Phys. A: Stat. Mech. Appl. **114**, 518 (1982).

[154] H. Grimmer, Acta Cryst. A **49**, 763 (1993).

[155] H. Grimmer, Ferroelectrics **161**, 181 (1994).

[156] M. Seemann, D. Ködderitzsch, S. Wimmer, and H. Ebert, Phys. Rev. B **92**, 155138 (2015).

[157] J. Železný, Y. Zhang, C. Felser, and B. Yan, Phys. Rev. Lett. **119**, 187204 (2017).

[158] A. Mook, R. R. Neumann, A. Johansson, J. Henk, and I. Mertig, Phys. Rev. Research **2**, 023065 (2020).

[159] S. Wimmer, K. Chadova, M. Seemann, D. Ködderitzsch, and H. Ebert, Phys. Rev. B **94**, 054415 (2016).

[160] R. Kubo, J. Phys. Soc. Jpn. **12**, 570 (1957).

[161] J. E. Sipe and E. Ghahramani, Phys. Rev. B **48**, 11705 (1993).

[162] J. E. Sipe and A. I. Shkrebtii, Phys. Rev. B **61**, 5337 (2000).

[163] C. Aversa and J. E. Sipe, Phys. Rev. B **52**, 14636 (1995).

[164] H. Watanabe and Y. Yanase, Phys. Rev. X **11**, 011001 (2021).

[165] S. V. Gallego, J. M. Perez-Mato, L. Elcoro, E. S. Tasci, R. M. Hanson, K. Momma, M. I. Aroyo, and G. Madariaga, J. Appl. Crystallogr. **49**, 1750 (2016).

[166] M. Yatsushiro, R. Oiwa, H. Kusunose, and S. Hayami, arXiv:2109.14132 , (2021).

[167] A. A. Gorbatsevich and Y. V. Kopaev, Ferroelectrics **161**, 321 (1994).

[168] Y. V. Kopaev, Phys.-Uspekhi **52**, 1111 (2009).

[169] A. Oyamadaa, T. Inoharaa, E. Yamamotob, and Y. Hagab, Prog. Nucl. Sci. Techn. **5**, 128 (2018).

[170] H. Watanabe and Y. Yanase, Phys. Rev. Research **2**, 043081 (2020).

[171] Y. Yanase, J. Phys. Soc. Jpn. **83**, 014703 (2014).

[172] Y. Gao, D. Vanderbilt, and D. Xiao, Phys. Rev. B **97**, 134423 (2018).

[173] Y. Gao and D. Xiao, Phys. Rev. B **98**, 060402(R) (2018).

[174] A. Shitade, H. Watanabe, and Y. Yanase, Phys. Rev. B **98**, 020407(R) (2018).

[175] F. Thöle and N. A. Spaldin, Philos. Trans. R. Soc. A **376**, 20170450 (2018).

[176] F. Thöle, A. Keliri, and N. A. Spaldin, J. Appl. Phys. **127**, 213905 (2020).

[177] C. Wang, Y. Gao, and D. Xiao, Phys. Rev. Lett. **127**, 277201 (2021).

[178] H. Liu, J. Zhao, Y.-X. Huang, W. Wu, X.-L. Sheng, C. Xiao, and S. A. Yang, Phys. Rev. Lett. **127**, 277202 (2021).

[179] D. Maruyama, M. Sigrist, and Y. Yanase, J. Phys. Soc. of Jpn. **81**, 034702 (2012).

[180] S. Hayami, H. Kusunose, and Y. Motome, J. Phys. Soc. Jpn. **84**, 064717 (2015).

[181] T. Ideue, K. Hamamoto, S. Koshikawa, M. Ezawa, S. Shimizu, Y. Kaneko, Y. Tokura, N. Nagaosa, and Y. Iwasa, Nat. Phys. **13**, 578 (2017).

[182] A. I. Tursina, S. N. Nesterenko, E. V. Murashova, I. V. Chernyshev, H. Noël, and Y. D. Seropegin, Acta Cryst. E **61**, i12 (2005).

[183] H. Kato, R. Kobayashi, T. Takesaka, T. Nishioka, M. Matsumura, K. Kaneko, and N. Metoki, J. Phys. Soc. Jpn. **80**, 073701 (2011).

[184] S. Suzuki, K. Takubo, K. Kuga, W. Higemoto, T. U. Ito, T. Tomita, Y. Shimura, Y. Matsumoto, C. Bareille, H. Wadati, S. Shin, and S. Nakatsuji, Phys. Rev. Research **3**, 023140 (2021).

[185] V. Barthem, C. Colin, H. Mayaffre, M.-H. Julien, and D. Givord, Nat. Commun. **4**, 2892 (2013).

[186] G. Will, W. Schäfer, F. Pfeiffer, F. Elf, and J. Etourneau, J. LESS-COMMN MET. **82**, 349 (1981).

[187] G. Will and W. Schäfer, J. LESS-COMMN MET **67**, 31 (1979).

[188] P. Wadley, V. Hills, M. R. Shahedkhah, K. W. Edmonds, R. P. Campion, V. Novák, B. Ouladdiaf, D. Khalyavin, S. Langridge, V. Saidl, P. Nemec, A. W. Rushforth, B. L. Gallagher, S. S. Dhesi, F. Maccherozzi, J. Železný, and J. Jungwirth, Sci Rep **5**, 17079 (2015).

[189] C. Wang, Y. Gao, and D. Xiao, arXiv:2106.12695 , (2021).

[190] S. A. J. Kimber, A. H. Hill, Y.-Z. Zhang, H. O. Jeschke, R. Valentí, C. Ritter, I. Schellenberg, W. Hermes, R. Pöttgen, and D. N. Argyriou, Phys. Rev. B **82**, 100412(R) (2010).

[191] N. Emery, E. J. Wildman, J. M. S. Skakle, A. C. Mclaughlin, R. I. Smith, and A. N. Fitch, Phys. Rev. B **83**, 144429 (2011).

[192] W. Bao, Q.-Z. Huang, G.-F. Chen, D.-M. Wang, J.-B. He, and Y.-M. Qiu, Chin. Phys. Lett. **28**, 086104 (2011).

[193] V. Y. Pomjakushin, E. V. Pomjakushina, A. Krzton-Maziopa, K. Conder, and Z. Shermadini, J. Condens. Matter Phys. **23**, 156003 (2011).

[194] A. F. May, M. A. McGuire, H. Cao, I. Sergueev, C. Cantoni, B. C. Chakoumakos, D. S. Parker, and B. C. Sales, Phys. Rev. Lett. **109**, 077003 (2012).

[195] M. Yatsushiro and S. Hayami, JPS Conf. Proc. **30**, 011151 (2020).

[196] R. Welter, G. Venturini, E. Ressouche, and B. Malaman, J. Alloys Compd. **210**, 279 (1994).

[197] B. Chevalier, S. F. Matar, J. S. Marcos, and J. R. Fernandez, Physica B Condens. Matter **378**, 795 (2006).

[198] E. Lengyel, M. Nicklas, N. Caroca-Canales, and C. Geibel, Phys. Rev. B **88**, 155137 (2013).

[199] H. Tanida, Y. Muro, and T. Matsumura, J. Phys. Soc. Jpn. **87**, 023705 (2018).

[200] H. Tanida, K. Mitsumoto, Y. Muro, T. Fukuhara, Y. Kawamura, A. Kondo, K. Kindo, Y. Matsumoto, T. Namiki, T. Kuwai, and T. Matsumura, J. Phys. Soc. Jpn. **88**, 054716 (2019).

[201] Y. Kawamura, H. Tanida, R. Ueda, J. Hayashi, K. Takeda, and C. Sekine, J. Phys. Soc. Jpn. **89**, 054702 (2020).

[202] S. E. Nikitin, D. G. Franco, J. Kwon, R. Bewley, A. Podlesnyak, A. Hoser, M. M. Koza, C. Geibel, and O. Stockert, Phys. Rev. B **101**, 214426 (2020).

[203] H. Tanida, K. Mitsumoto, Y. Muro, T. Fukuhara, Y. Kawamura, A. Kondo, K. Kindo, Y. Matsumoto, T. Namiki, T. Kuwai, and T. Matsumura, JPS Conf. Proc. **30**, 011156 (2020).

[204] S. Chandra, A. Khatun, and R. Jannat, Solid State Commun , 113953 (2020).

[205] M. Manago, H. Kotegawa, H. Tou, H. Harima, and H. Tanida, J. Phys. Soc. Jpn. **90**, 023702 (2021).

[206] O. Bodak, E. Gladyshevskii, and P. Kripyakevich, J. Struct. Chem **11**, 283 (1970).

[207] E. Matsuoka, J. Kitagawa, K. Ohoyama, H. Yoshizawa, and M. Ishikawa, J. Condens. Matter Phys. **13**, 11009 (2001).

[208] Y. Kawarasaki, T. Matsumura, M. Sera, and A. Ochiai, J. Phys. Soc. Jpn. **80**, 023713 (2011).

[209] H. Yamauchi, H. Onodera, K. Ohoyama, T. Onimaru, M. Kosaka, M. Ohashi, and Y. Yamaguchi, J. Phys. Soc. Jpn. **68**, 2057 (1999).

[210] K. Mitsumoto, K. Tanaka, and H. Tanida, International Conference on Strongly Correlated Electron Systems 2019 , Fr-A-32 (2019).

[211] Y. Kawamura, S. Kishida, M. Tsukagoshi, H. Tanida, H. Nakao, and T. Matsumura, JPS 2021 Autumn Meeting , 20pH2-1 (2021).

[212] K. Hanzawa and T. Kasuya, J. Phys. Soc. Jpn. **53**, 1809 (1984).

[213] K. Kugel and D. Khomskii, Zh. Eksp. Teor. Fiz **64**, 1429 (1973).

[214] S. Hayami, H. Kusunose, and Y. Motome, J. Phys. Soc. Jpn. **85**, 053705 (2016).

[215] T. Das and E. Hahn: *Solid State Physics Supplement, Vol 1* (Academic Press, 1958).

[216] O. Sakai, R. Shiina, H. Shiba, and P. Thalmeier, J. Phys. Soc. Jpn. **68**, 1364 (1999).